



HAL
open science

Stereodivergent synthesis by means of chirally-amplified supramolecular catalysts

Ahmad Hammoud

► **To cite this version:**

Ahmad Hammoud. Stereodivergent synthesis by means of chirally-amplified supramolecular catalysts. Catalysis. Sorbonne Université, 2021. English. NNT : 2021SORUS026 . tel-03470166

HAL Id: tel-03470166

<https://theses.hal.science/tel-03470166v1>

Submitted on 8 Dec 2021

HAL is a multi-disciplinary open access archive for the deposit and dissemination of scientific research documents, whether they are published or not. The documents may come from teaching and research institutions in France or abroad, or from public or private research centers.

L'archive ouverte pluridisciplinaire **HAL**, est destinée au dépôt et à la diffusion de documents scientifiques de niveau recherche, publiés ou non, émanant des établissements d'enseignement et de recherche français ou étrangers, des laboratoires publics ou privés.

Sorbonne Université

École doctorale de physique et chimie de matériaux (ED 397).

Institut Parisien de Chimie Moléculaire / Equipe de Chimie des Polymères (UMR 8232)

Stereodivergent synthesis by means of chirally-amplified supramolecular catalysts

Par Ahmad HAMMOUD

Thèse de doctorat de Physique et Chimie des Matériaux

Dirigée par Matthieu RAYNAL

Présentée et soutenue publiquement le 21 Mai 2021

Devant un jury composé de :

M. Olivier Riant	Professeur Université Catholique de Louvain	Rapporteur
M. David Leboeuf	Chargé de Recherche Université de Strasbourg	Rapporteur
M. Lionel Magna	Chargé de Projet IFP Energies Nouvelles	Examineur
Mme. Corinne Aubert	Directrice de Recherche Sorbonne Université	Examinatrice
M. Matthieu Raynal	Chargé de Recherche	Directeur de thèse

Acknowledgments

First of all, I would like to thank Prof. Olivier Riant, and Dr. David Lebœuf for agreeing to be the reviewers of this thesis. I also thank Dr. Lionel Magna, and Dr. Corinne Aubert for their agreement to be part of the thesis jury. My thanks also go to Matthieu Raynal, my supervisor during those three years, and to Laurent Bouteiller, the Boss of our team, and the director of the Lab.

Those three years of my life journey have been such amazing, which allowed me to learn a lot about science in general and chemistry in particular. Most importantly, I had the opportunity to work with great mind scientists whose exchanges have always led me in the right direction.

Again, I'm so grateful to Matthieu who has always been there to help, guide and supervise me during my PhD. I have learned a lot from him, inside the lab, and during the period of redaction.

I also thank the members of the ANR project "AbsoluCat": Virginie Mouriès-Mansuy and Louis Fensterbank. I have also a thought for the trainees whom I had the pleasure of supervising: Gauthier Thevenet, Amal Lakhal, and Cassandre Bories.

Further thanks go to the team members, I would start with my office mates: Danilo Nunes, the multifunctional guy that prevented me from quitting smoking, thanks to coffee/cigarette breaks. Quentin Sallembien, the French ambassador of wine and lamps. Dorian Rabaud, the movie/series director and the cheese killer. Oceane Fort, the light weight champion in boxing, and the great photographer. Khaled Bilal, the Egyptian pharoah. Richard, Adrian (Tommy), Mayte, Pamela, Yan li, Benjamin, Sandrine, Ludovic, Lydia, Fanny, Francois, Jutta, Martine, Cecile, and Brigitte are not forgotten for sure, they were all like a big family to me. A very BIG thanks goes to a very special person in this lab! A person who was not only a colleague but more a great friend! For sure, you all knew whom I am talking about! she is the GREAT guitarist Laura Luiz, my official French teacher, and my all-time friend and supporter. I would also like to thank Annie Colin, Arnaud Voituriez, David Kreher, and Lydia Sosa Vargas who agreed to be members of my CST. I also have a thought for the service members of analysis whether it is NMR (Claire Troufflard), chiral GC/HPLC (Omar Khaled), or Chiral HPLC (Nicolas Vanthuylene). I'm

also grateful to my friends outside the Lab: Mouhamad Mouazen, Aladine Merhe, Moustafa Zmerli, Alain M, Daniel M, Mark, Ahmed Abramovic, Esti, Ali Assy, Ghaydaa, S. Saker, I. Ashek, Mike, A. Hijjawi, A. Ghourabi, Huss HS, and Nabil Mroweh. Finally, many thanks to my parents who have supported me for 28 years and allowed me to reach my thesis. I warmly thank my brother, the guy who always had my back, and my lovely sisters, nieces and nephews.

Table of Contents

Acknowledgments.....	2
Chapter I : Stereodivergence in asymmetric catalysis: towards selecting the configuration of consecutively formed stereogenic centers in a single pot catalytic process.	10
I.1. General introduction:.....	11
I.2. Examples of stereodivergent strategies.....	13
I.2.a. Stereodivergency in concerted reactions.....	13
I.2.a.i. By tuning the substrate structure.	14
I.2.a.ii. By catalyst redesign.....	16
I.2.a.iii. By changing the reaction conditions.....	18
I.2.a.iv. By changing the ligand.	19
I.2.a.v. By changing the metal cation.....	20
I.2.b. Case of stereodivergent dual catalysis.	21
I.2.c. Case of cascade (sequential) catalysis.	24
I.2.d. Conclusion.....	27
I.3. Enantiodivergency by means of switchable asymmetric catalysts.....	28
I.3.a. Light.	29
I.3.b. Redox potential.....	31
I.3.c. Temperature.	33
I.3.d. Combined heat and light stimuli.....	35
I.3.e. Helical polymers as scaffolds for switchable catalysis.....	40
I.3.e.i. Switchable helical covalent catalysts.	42
I.3.e.ii. Switchable helical supramolecular catalyst.	46
I.4. In situ control of product configuration by means of switchable asymmetric catalysts.....	54
I.4.a. With two (pseudo) <i>enantiomeric</i> catalysts.	54
I.4.b. By two catalysts anchored on the rotating arm of a substrate.	55
I.4.c. With a single asymmetric catalyst.	58
I.5. Description and objectives of the project.....	61
I.6. References.....	63

Chapter II : Phosphine-containing BTA ligands with various aryl groups on the phosphorous atom: Synthesis, characterization, assembly behavior, and implementation in asymmetric copper-catalyzed hydrosilylation of 1-(4-nitrophenyl)ethanone.	71
II.1. Introduction:	72
II.1.a. Synthesis and importance of BTAs.	72
II.1.b. Helical BTA ligands for asymmetric reactions.....	75
II.1.c. Role of the ligand structure in catalyst design.	79
II.1.d. Designing a new set of phosphine-containing BTA ligands.	83
II.2. Synthesis of a new set of phosphine-containing BTA ligands.....	84
II.2.a. General retrosynthetic route.....	84
II.2.b. Synthesis of 4-P(Mesityl) ₂ -aniline, 4-P(Ph) ₂ -aniline, and 4-P(Xylyl) ₂ -aniline via protocol I.....	86
II.2.c. Synthesis of new 4-P(Ar) ₂ -aniline derivatives via protocol II.	90
II.2.c.i. Issues with the purity and stability of some PAr ₂ Cl precursors:.....	90
II.2.c.ii. Attempted synthesis of some PAr ₂ Cl precursors.	92
II.2.c.iii. Synthesis of new phosphinoaniline derivatives via protocol II.	93
II.2.d. Synthesis of the BTA ligands.	95
II.2.e. Table of comparison between protocol I and II for the synthesis of BTA-pPPH ₂ ...	96
II.3. Structural characterization of the (S&S) co-assemblies by SANS and FT-IR analyses....	96
II.4. Implementation in copper-catalyzed hydrosilylation of 1-(4-nitrophenyl)ethenone .	101
II.5. Conclusion.	106
II.6. Annex.....	107
II.6.a. Experimental procedures.....	109
II.6.b. Synthesis of the BTA ligands.	115
II.6.c. NMR data.	135
II.6.d. Selected chiral GC analyses:	165
II.7. References.....	168
Chapter III Copper-catalyzed hydro-functionalization reactions with sergeants-and-soldiers type helical BTA catalysts : Hydroamination of styrene and cascade hydrosilylation/hydroamination of enone derivatives.	174
III.1. Introduction.....	175
III.1.a. Hydrosilylation of unsaturated substrates by phosphine copper hydride catalysts....	175

III.1.b.	Regioselectivity issues in hydrosilylation reactions.....	177
III.1.c.	Asymmetric copper catalyzed hydroamination for the preparation of chiral amines.....	180
III.1.d.	Content of this chapter.....	184
III.2.	Copper-catalyzed hydroamination of styrene with sergeants-and-soldiers type helical BTA catalysts.	184
III.2.a.	Probing the stability of the co-assemblies.....	185
III.2.b.	BTA-pPPH ₂ as ligand for the copper-catalyzed HA of styrene.....	186
III.2.c.	Screening of different BTA ligands with [Cu(OAc) ₂ .xH ₂ O] as metal precursor in the HA of styrene.	191
III.2.d.	Optimization for BTA-P(DTF) ₂ ligand: Cu(OAc) ₂ .H ₂ O versus Cu(II)-i-butyrate as a metal precursor.	193
III.3.	Hydrosilylation/hydroamination cascade process on “enone” substrates.	194
III.3.a.	Hydrosilylation of benzylideneacetone, and cascade of (<i>E</i>)-3-methyl-4-phenylbut-3-en-2-one.	194
III.3.b.	Evaluation of hydrosilylation and cascade reaction on (<i>E</i>)-1,4-diphenylbut-3-en-1-one and derivatives.	197
III.4.	Conclusion.....	198
III.5.	Annex.....	199
III.5.a.	General experimental procedure for catalysis.	200
III.5.b.	Supplementary figures.....	202
III.5.b.i.	FT-IR analysis.	202
III.5.b.ii.	¹ H NMR analysis of the kinetic study of styrene Hydroamination in toluene-d ₈	203
III.5.b.iii.	¹ H NMR analysis of hydrosilylation and cascade of enone derivatives in CDCl ₃	212
III.5.c.	Selected HPLC traces.....	214
III.5.d.	Synthesis of substrates.	216
III.5.e.	¹ H NMR of substrates.....	218
III.5.f.	¹ H NMR and HRMS of Product-1.....	220
III.6.	References.....	221
Chapter IV	: Enantio and diastereoselective cascade reaction with supramolecular and chirally-amplified helical catalyst: towards stereodivergency.	227

IV.1. Introduction.....	228
IV.2. Hydrosilylation of different vinyl acetophenone derivatives with supramolecular helical BTA catalysts.	231
IV.2.a. Hydrosilylation of 4-VPnone and 4- <i>E</i> -MeVPnone.....	232
IV.2.b. Hydrosilylation of 3-VPnone and 3-MeVPnone.....	233
IV.2.b.i. Substrate : 3-VPnone.....	233
IV.2.b.ii. Substrates : 3- <i>E</i> -MeVPnone and 3- <i>Z</i> -MeVPnone.	237
IV.2.c. Hydrosilylation of Substrate : 4-VBPnone.	238
IV.2.d. Conclusion.....	238
IV.3. Preliminary tests for the cascade hydrosilylation/hydroamination reaction of 3-VPnone, 3-MeVPnone and 4-MeVPnone.....	239
IV.3.a. Evaluation of the cascade process for 3-VPnone.	239
IV.3.b. Evaluation of the cascade process on 3- <i>E</i> -MeVPnone and 3- <i>Z</i> -MeVPnone.	242
IV.3.c. Evaluation of the cascade process for 4- <i>E</i> -MeVPnone.....	244
IV.4. Cascade hydrosilylation/hydroamination of 3-VPnone : optimization of reaction conditions.....	245
IV.4.a. Order of addition of the amine electrophile and influence of the reaction temperature.	246
IV.4.b. Screening of different metal precursors.....	247
IV.4.c. Optimization of the conditions with Cu(II)- <i>i</i> -butyrate.....	248
IV.5. Applying the catalytic switch.	250
IV.6. Probing the chirality amplification properties by Circular Dichroism.....	251
IV.6.a. CD analyses for probing the diluted majority rule effects.....	251
IV.6.a.i. In MCH.	253
IV.6.a.ii. In toluene.....	254
IV.6.b. Probing chirality amplification effects in catalysis in presence of BTA cyclohex as an additive.	255
IV.6.c. Probing the stereochemical switch capability of the catalyst.....	258
IV.6.c.i. Applying the catalytic switch in presence of BTA cyclohex additive.	259
IV.7. Conclusion.....	261
IV.8. Annex.....	263
IV.8.a. Materials preparation and methods.....	263

IV.8.b.	General procedures for catalysis.	265
IV.8.c.	Preparation of solutions for CD analyses.....	269
IV.8.d.	Supplementary figures.....	271
IV.8.e.	Synthesis of substrates.	281
IV.8.f.	Analytical chiral HPLC separation for compound 3-APnol.....	282
IV.8.g.	Formulas for determining ee ₁ , ee ₂ , ee _{tot} , and dr.....	290
IV.8.h.	Selected HPLC spectrums.....	292
IV.8.i.	Selected crude ¹ H NMR analyses of some catalytic experiments in CDCl ₃	305
IV.8.j.	¹ H NMR data of substrates.	311
IV.8.k.	¹ H NMR, ¹³ C NMR, and HRMS of 3-APnol:	314
IV.9.	References.....	316
Conclusions.	318
Resumé.	326

Abbreviations

BAr _F : tetrakis(3,5-bistrifluoromethylphenyl)borate	MR: majority-rules
BTA: benzene-1,3,5-tricarboxamide	NMR: nuclear magnetic resonance
BTA alkyl: N,N',N''-trialkylbenzene-1,3,5-tricarboxamides	PE: petroleum ether
CD: circular dichroism	PPh ₂ : diphenylphosphine
DABCO: 1,4-diazabicyclo[2.2.2]octane	PQX : poly(quinoxaline-2,3-diyl)
DCM: dichloromethane	SANS: small angle neutron scattering
DIBAL-H: diisobutylaluminium hydride	S&S: sergeants-and-soldiers
DI: diisocyanide	THF: tetrahydrofuran
DMAP: 4-dimethylaminopyridine	TrMA: triphenylmethyl methacrylate
DP _n : degree of polymerization	
EDC.HCl: N-(3-dimethylaminopropyl)-N'-ethylcarbodiimide	
EDG: electron donating group	
EWG: electron withdrawing group	
<i>ee</i> : enantiomeric excess	
FT-IR: fourier-transform infrared	
HA: hydroamination	
HRMS: high-resolution mass spectrometry	
HS: hydrosilylation	
MCH: methylcyclohexane	

Chapter I : Stereodivergence in asymmetric catalysis: towards selecting the configuration of consecutively formed stereogenic centers in a single pot catalytic process.

Abstract: A stereodivergent process is the process which provides access to any given stereoisomer of a product with multiple stereocenters from the same set of starting materials. However, one-pot stereodivergent catalysis using a single catalyst has not been achieved despite the fundamental interest and practical advantages of such an approach. The objective of this thesis is therefore to develop a stereodivergent approach by exploiting the chirality amplification and the dynamic properties of switchable helical BTA catalysts. A cascade hydrosilylation/hydroamination reaction will thus be implemented in order to access all the possible stereoisomers of an amino alcohol. Importantly, all stereoisomers should be obtained in a unique way that has no precedent in the literature.

I.1. General introduction:

Biological activity^[1] of any drug candidate is affected and altered by its configuration. For this reason, regulatory agencies require the evaluation of the therapeutic as well as toxicological properties of all stereoisomers of a drug candidate during the drug discovery. Polypharmacology deals with the property of drugs to react and respond to more than one biological target in the body^[2], eventually leading to side effects (Figure I-1).

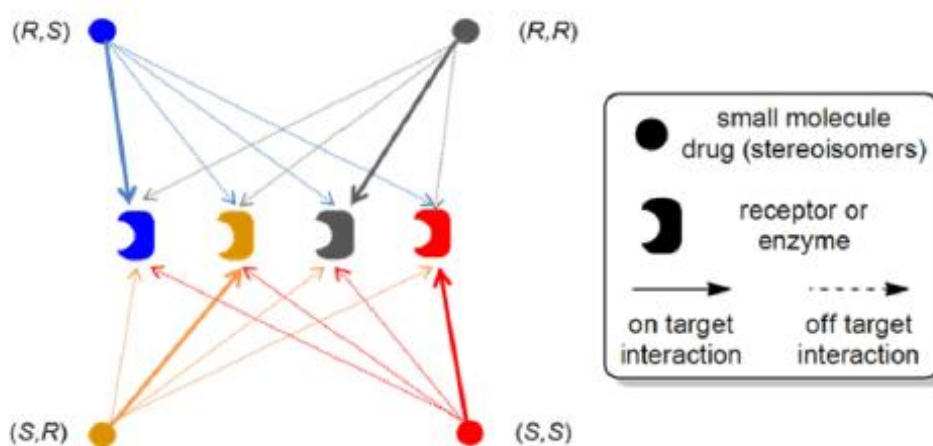


Figure I-1 General schematic drawing showing polypharmacology of drug stereoisomers. Adapted from reference^[2].

Thus, the configuration of a drug candidate can modulate its activity towards different targets in the body, which can result in an improved therapeutic profile^[3]. Stereodivergent synthesis can play a very important role in this field by enabling access to all stereoisomers of a drug candidate and thus maximizing on-target interactions with the desired enzyme or receptor. However, a complete and decisive control of the configuration of all stereogenic centers within the same molecule by means of a catalyzed reaction remains a challenge^[4,5]. This is because the enantiomers of a well-designed catalyst will favor the formation of a pair of stereoisomers, whilst the other stereoisomers will not be accessible. In the context of asymmetric synthesis, a stereodivergent process is the method that allows to access any given stereoisomer of a product with multiple stereocenters from the same set of starting materials. Ideally, such a process would use the same set of catalysts (apart from their configuration) and reaction

conditions to access the various stereoisomers. Metal-catalyzed and organocatalyzed processes are the main strategies employed in stereodivergent catalysis (Figure I-2).

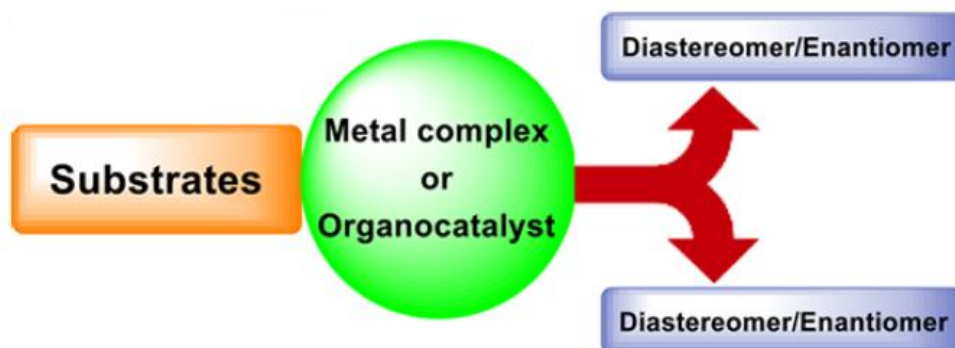
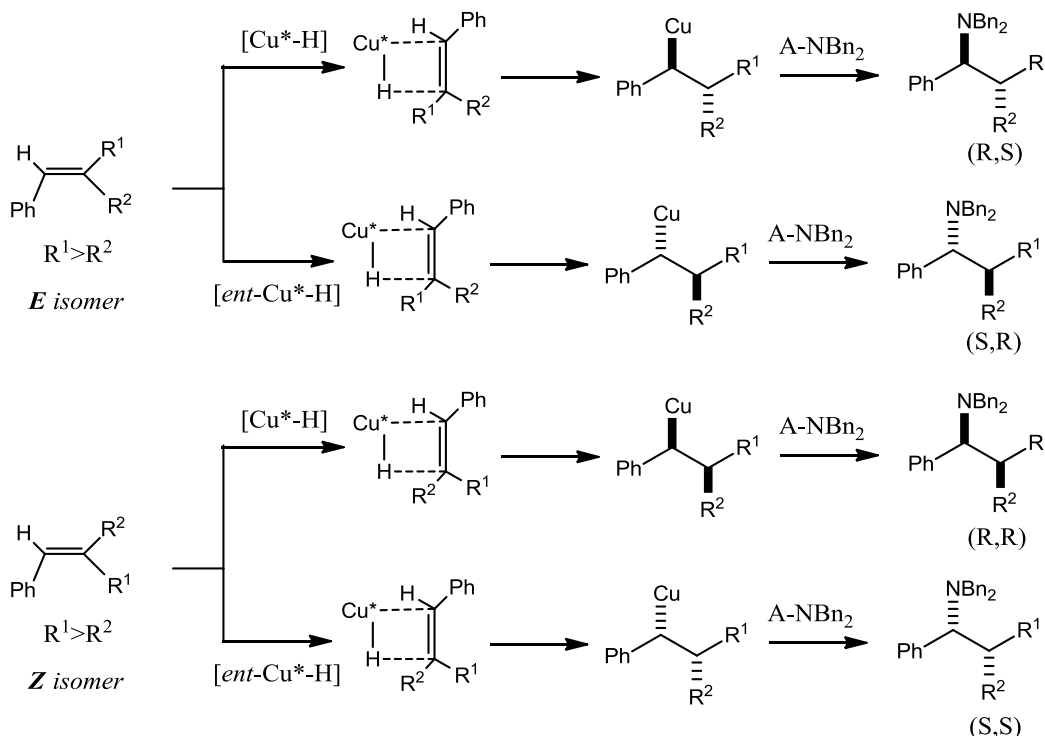


Figure I-2 Metal-catalyzed and organocatalyzed processes are the main strategies in stereodivergent catalysis.



Scheme I-1 Syn-facial addition of Cu-H to the olefin lead to stereospecific reaction with respect to the olefin geometry.

Most stereodivergent processes developed to date rely on chemical intuition and serendipity. Thus, predictability of reaction outcome is one of the biggest challenges to make stereodivergency of more general applicability.

One specific case for which stereodivergency can be predictably achieved concerns the nucleophilic insertion of an organometallic compound into an alkene. If the insertion is the enantio-determining step in the catalytic cycle and occurs with facial selectivity, all possible stereoisomers will be accessed by selecting the *E* and *Z* configuration of the alkene (Scheme I-1). In the given example, the addition of the alkyl-Cu nucleophile to the amine electrophile (represented as A-NBn₂) occurs with retention of configuration.

In the first part of the Chapter, we will describe a few stereodivergent strategies ranked as follows:

1. Stereodivergent methods that arise through fine tuning of the catalyst structure or by optimizing the reaction conditions for concerted reactions (section **I.2.a**).
2. Predictable stereodivergency in dual catalysis employing two enantiopure catalysts (section **I.2.b**).
3. Predictable stereodivergency in cascade reactions (section **I.2.c**).

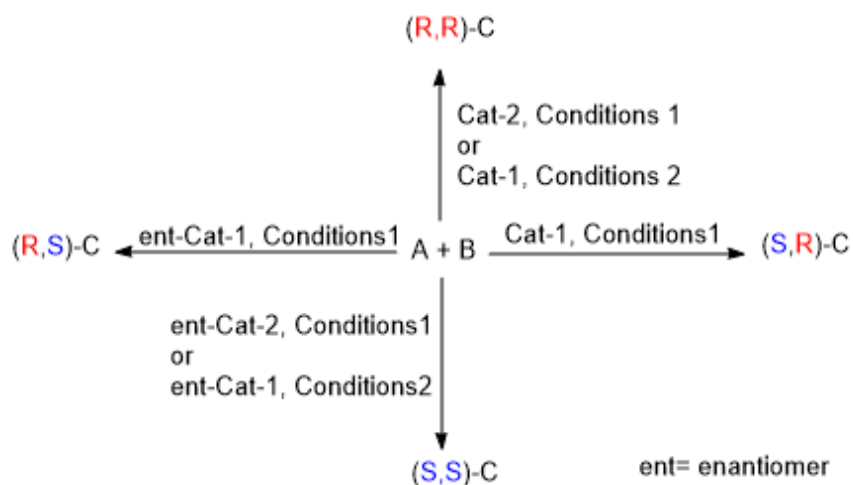
The second part of this Chapter will deal with a specific class of catalysts for which the enantiomeric state can be switched allowing both enantiomers of the product to be obtained with the same catalyst. We will then see in the third part that these switchable asymmetric catalysts have not been yet efficiently exploited in stereodivergent processes. Finally, the objectives of the thesis will be presented in the last part.

I.2. Examples of stereodivergent strategies.

I.2.a. Stereodivergency in concerted reactions.

Stereodivergent methods might arise through fine tuning of the catalyst structure or by optimizing reaction conditions (Scheme I-2). Instead of using separate reactions and starting compounds to prepare each diastereomer, a simpler strategy could be followed based on the utilization of the same starting material with a small variation in reaction conditions, or/and small changes in the structure of reagents, to obtain each stereoisomer individually. Structural modifications of the ligand or the metal in the case of metal complexes or of the organocatalyst are crucial for developing efficient stereodivergent catalysis notably in the context of concerted reactions. In addition, these processes could be affected by changing reaction conditions such

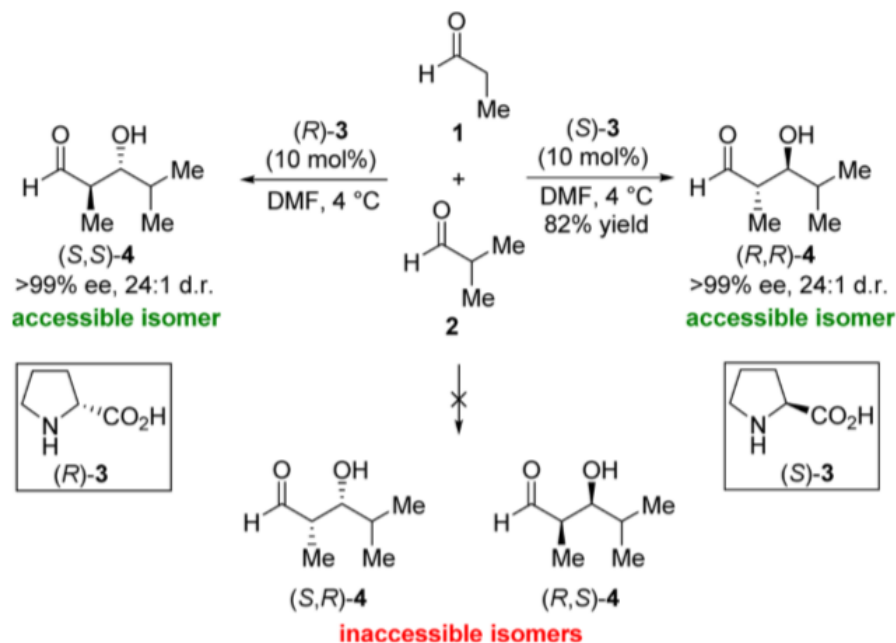
as solvent, temperature, pressure, and additives, especially Lewis and Brønsted acids or bases. In the case of metal catalysis, not only the ligand could be modified but also the metallic precursor, either by using different metal precursors or by varying the ligand-to-metal ratio. A few examples will be mentioned in the following part.



Scheme I-2 Concept of stereodivergent catalyst in the case of a concerted mechanism leading to the formation of two stereogenic centers. Adapted from reference^[6].

I.2.a.i. By tuning the substrate structure.

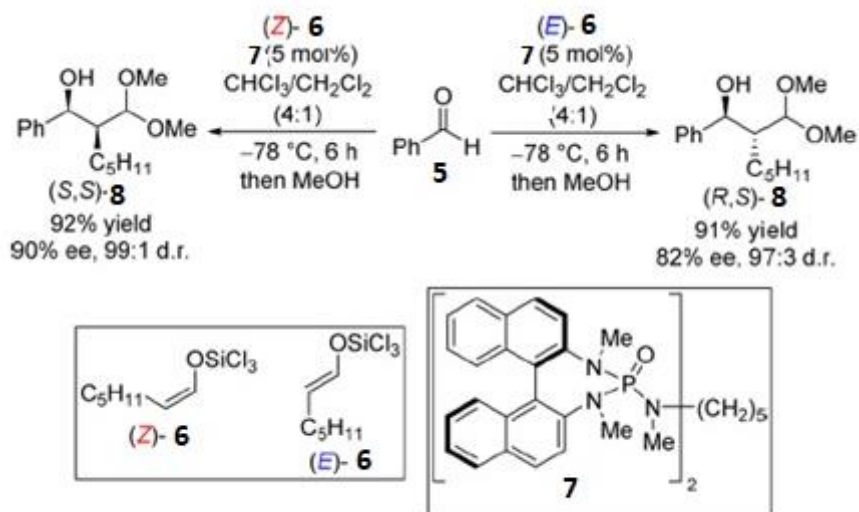
A lot of examples in literature proceeded through a concerted mechanism in which a single catalyst leads to the formation of two or more stereogenic centers. The aldol reaction is a prototypical example of such reactions. Northrup and MacMillan^[7] devised the proline-catalyzed cross-aldol reaction between propionaldehyde **1** and isobutyraldehyde **2** (Scheme I-3). *Anti*-aldol products (*R,R*)-**4** and (*S,S*)-**4** were obtained with high enantiomeric excess (*ee*>99%) and diastereomeric ratio (*dr*= 24:1) by using (*S*)-proline or (*R*)-proline, respectively. However, the corresponding *syn*-isomers cannot be prepared through this method because the catalyst privileged a pair of enantiomers over the other. *Syn*-isomers were obtained as reported by Hofferberth and Brückner^[8] through a fully different synthetic route which considerably burdens the access to the four stereoisomers of this aldol product. A lot of common asymmetric transformations suffer from this limited access to diastereoisomers^[9].



Scheme I-3 Proline-catalyzed direct cross-aldol reaction of aldehydes. Adapted from reference^[7].

A drastically more efficient strategy was reported, which relies on the nature of the substrate. Usually, when the structure of the substrates is changed to achieve stereodivergency, the transformations are called pseudo-diastereodivergent^[9].

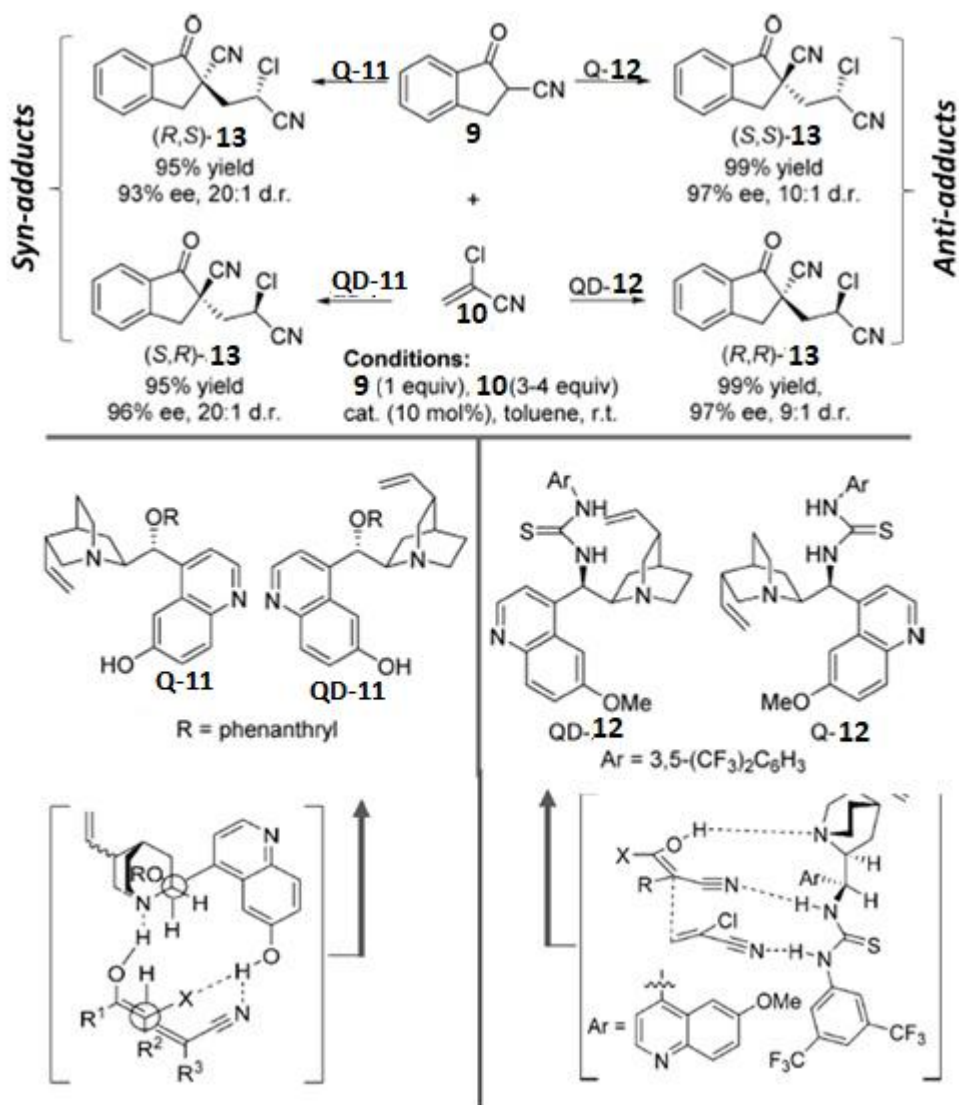
It is well established that controlling the configuration of an enolate or enolate equivalent (carbonyl, imine) involved in conjugate addition reactions can be used to influence diastereoselectivity^[11]. A striking example is the phosphoramidate-catalyzed addition of trichlorosilyl enolates to aldehydes reported by Denmark *et al.* (Scheme I-4)^[10]. The two isomers of enolates **6** were obtained from the corresponding stereo defined trimethylsilyl enol ethers derived from heptanal. (*E*)-**6** and (*Z*)-**6** react with benzaldehyde **5** in presence of 1,1'-binaphthyl-2,2'-diamine-derived phosphoramidate (*S,S*)-**7** to afford the *anti* and the *syn* adducts respectively ((*R,S*)-**8**, (*S,S*)-**8**). Even though the scope of the aldehydes that can be transformed with satisfying enantioselectivities is limited, this strategy demonstrated that a relatively simple stereodivergent route can emerge through tuning of the substrate structure.



Scheme I-4 Phosphoramidate-catalyzed cross-aldol reaction. Adapted from reference^[10].

I.2.a.ii. By catalyst redesign.

The following strategy demonstrates the possibility of developing stereodivergent transformations by changing the nature of the functional groups anchored to the catalyst. Deng and co-workers^[12] reported the cinchona alkaloid derivative-catalyzed conjugate 1,4-addition of (*rac*)- α -cyanoketones **9** to α -chloroacrylonitriles **10** (Scheme I-5, Above). A preliminary result documented on the highly *syn* selective synthesis of (*R,S*)-**13** and (*S,R*)-**13** when the reaction is catalyzed by the pseudo-enantiomeric phenanthryl-protected alkaloids **Q-11** and **QD-11** as the bifunctional catalysts^[12]. These *syn* adducts were obtained in very high yield (up to 99%), very high enantiomeric excess (up to 96%) and a dr value of 20:1. As rationalized by the transition-state model illustrated in Scheme I-5 (bottom left), a network of hydrogen-bonding interactions established between the cinchona catalyst **Q-11** and the substrates dictates the preferential formation of the *syn* adducts. This led the authors to hypothesize that a different selectivity could be obtained by changing the position of the hydrogen-bond donor and hydrogen-bond acceptor in the catalyst. **Q-12** was designed for which the alkoxy-phenanthryl group was replaced by a thiourea moiety and the hydroxyl group on the quinoline was methylated. A complementary sense of diastereoselectivity with respect to that promoted by **Q-11** was indeed observed, *i.e.* the *anti*-adducts were obtained selectively with a very high yield (99%), up to 97% *ee* and 9:1 dr.



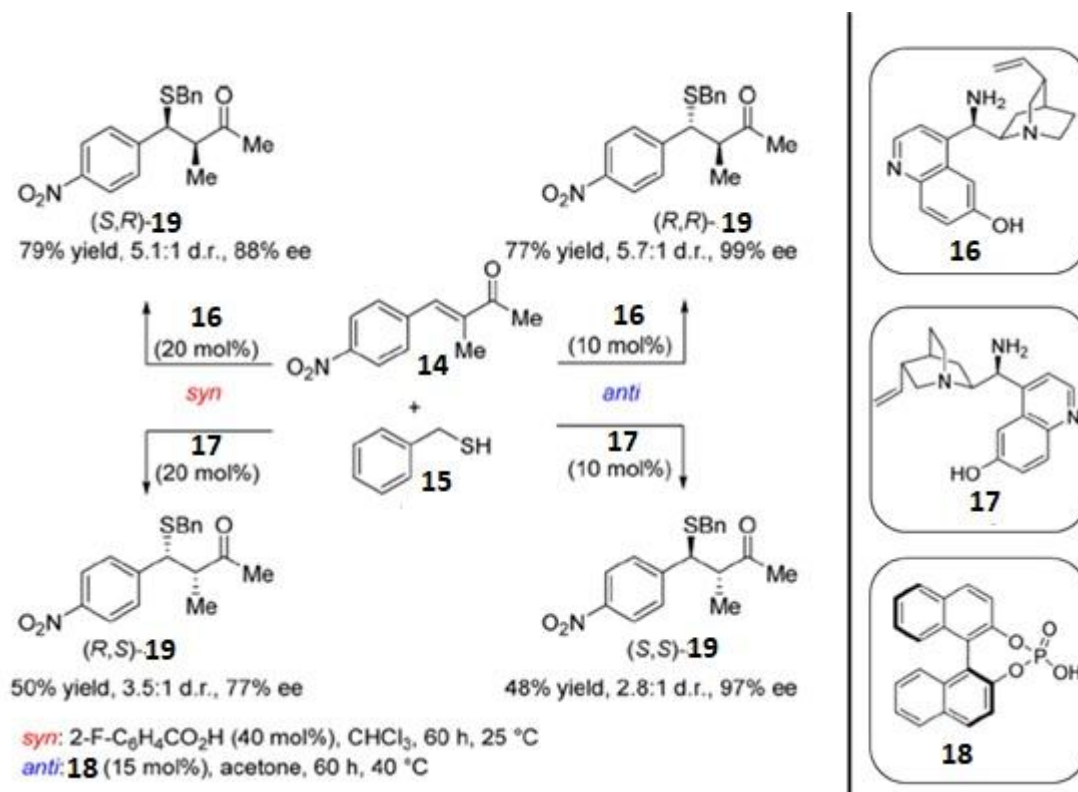
Scheme I-5 Above: Stereodivergent conjugate addition of α -cyanoketones to α -chloroacrylonitriles. Below: proposed transition state models for accessing both the *syn* and the *anti*-adducts using **Q-11/Q-12** catalysts and their corresponding enantiomers **QD-11/QD-12**. Adapted from reference^[12].

These results implied that the switch of the sense of diastereoselectivity between the two reactions catalyzed by **Q-11** and **Q-12**, respectively, arises from a reversal of the face of the Michael donor **9** being exposed to the Michael acceptor **10**. The stereochemical outcome (*anti*-adducts) of the asymmetric tandem reaction catalyzed by **Q-12** can thus be rationalized by the transition-state model shown in Scheme I-5 (bottom right^[13]), in which the assumed enolic Michael donor **9** approaches the Michael acceptor **10** with its *Si* face. In short, **Q-11** (and its pseudo enantiomer **QD-11**) provided the *syn* adducts (*RS* and *SR*), while **Q-12** (and its pseudo-

enantiomer **QD-12**) provided the *anti*-ones (*RR* and *SS*). All four stereoisomers of adduct **13** were prepared with high stereoselectivity (93–99% *ee*, 9:1–20:1 *dr*) simply by selecting the appropriate cinchona derivative (**Q-11/QD-11** and **Q-12/QD-12**).

I.2.a.iii. By changing the reaction conditions.

Another way to alter the sense of diastereoselectivity implemented by a catalyst is by means of additives, co-catalysts or through solvent effects. Secondary amine and weak acids are usually combined to activate carbonyl compounds through iminium type catalysis. Melchiorre and co-workers^[14] combined two catalysts to control the diastereoselectivity of the asymmetric 1,4-addition of benzylthiol **15** to α,β -unsaturated ketone **14** (Scheme I-6).



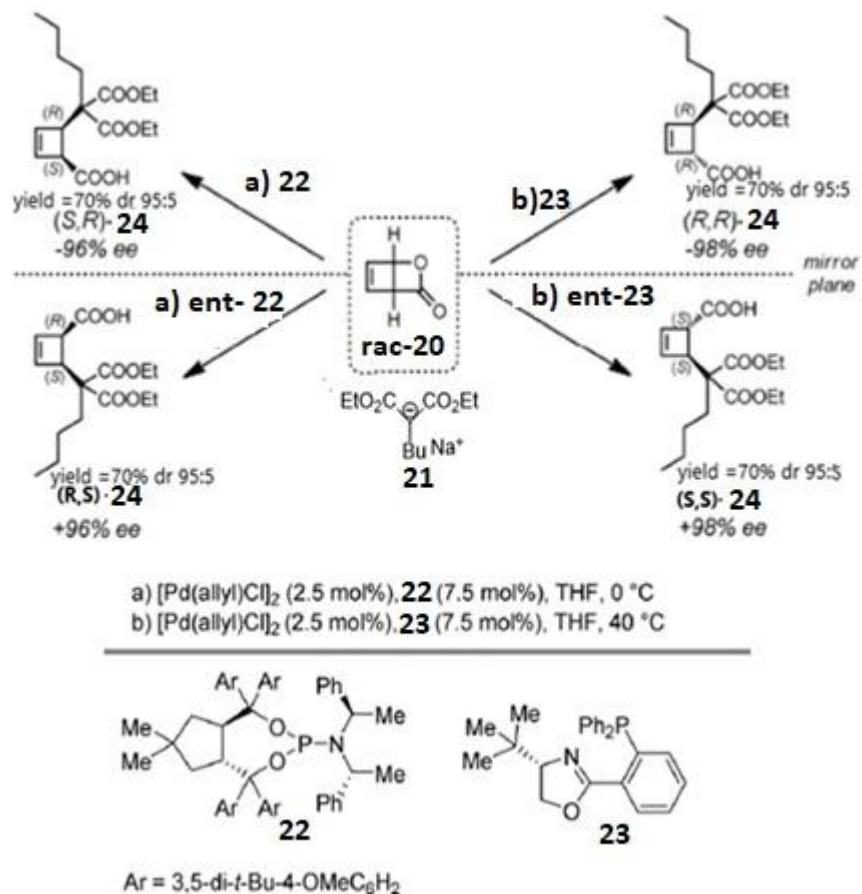
Scheme I-6 Stereodivergent, amine-catalyzed 1,4-addition of thiols to α,β -unsaturated ketones. Adapted from reference^[14].

Cinchona alkaloid **16** combined with 2-fluorobenzoic acid in chloroform provided the *syn* isomer (*S,R*)-**19**. However, the *anti*-stereoisomer (*R,R*)-**19** was favored when the 1,4-addition was performed in acetone in the presence chiral phosphoric acid **18** instead of 2-fluorobenzoic acid (Scheme I-6). The remaining two stereoisomers were synthesized using **17**, the pseudo-

enantiomeric catalyst of **16** (Scheme I-6). The authors proposed that the different selectivities stem from the distinct geometries of the iminium ion intermediates generated by the use of different acids and solvents. The judicious choice of a designer acidic additive and the reaction medium switches the sense of the catalyst's diastereoselection, but the choice merely relies on serendipity. Further mechanistic investigations should be undertaken to understand the origin of the stereodivergent behavior at the molecular level.

I.2.a.iv. By changing the ligand.

Cyclobutene derivatives were synthesized by a new method developed by Maulide and co-workers^[15] through palladium-catalyzed allylic substitution of racemic lactone **20** with malonate derivatives **21** (Scheme I-7). More specifically, the *cis* isomer of cyclobutene (*S,R*)-**24** was obtained in 96% *ee* and >95:5 *dr*^[15] using the phosphoramidite ligand **22** (Scheme I-7). The *trans*-isomer (*R,R*)-**24** was obtained with equally impressive stereoselectivity when phosphine-oxazoline ligand **23** was used instead of **22** (Scheme I-7). The authors proposed that this selectivity arises from a change in the reaction mechanism triggered by the ligand. The formation of *trans*-**24** with the Pd/**23** catalyst system is particularly unusual as it is thought to occur through ionization of lactone **20** by Pd with retention of configuration (instead of inversion as classically observed in Tsuji-Trost reaction). This method represents a deracemization process (*i.e.* the full conversion of a chiral racemic starting material into a single enantioenriched product) in which the product has more than one stereogenic element. The ability to prepare selectively all possible stereoisomers of the final product is achieved by changing the ligand and tuning of the reaction conditions, leading the authors to propose the name "diastereodivergent deracemization". Indeed, the four stereoisomers of **24** can be obtained with excellent optical purity and yields of 70% despite the racemic nature of the lactone substrate (Scheme I-7).

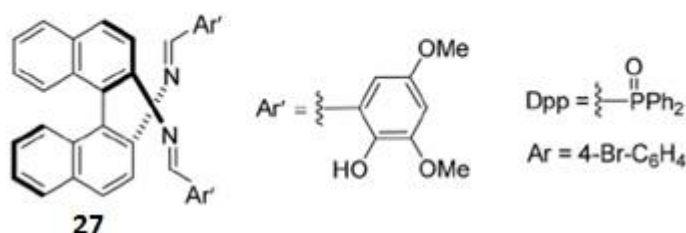
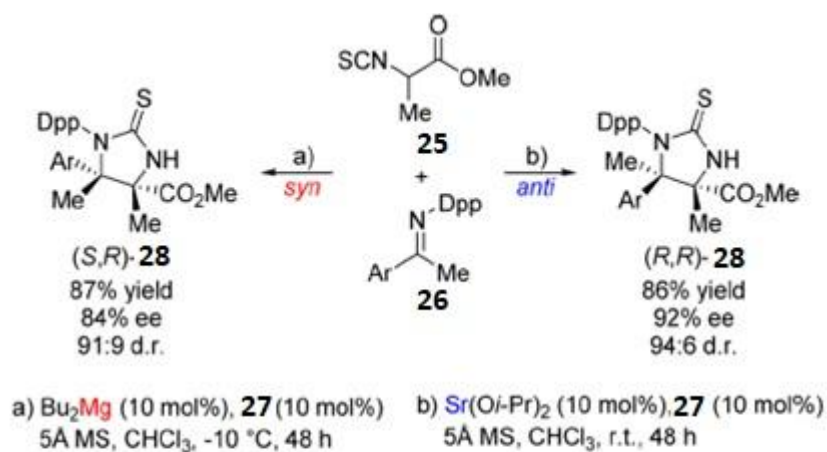


Scheme I-7 Stereodivergent Pd-catalyzed synthesis of cyclobutene derivatives. Adapted from reference^[15].

I.2.a.v. By changing the metal cation.

Changing the nature of the metal cation coordinated to a ligand is another way to achieve stereodivergency. An example on this strategy is illustrated by Shibasaki and co-workers^[16] who developed a stereodivergent method for the addition of isothiocyanato esters **25** to ketimines **26** catalyzed by diimine alkaline earth metals (Scheme I-8, **Mg** or **Sr**). The metal cation used here controls the stereochemical outcomes of the reactions induced by chiral ligand **27**. Magnesium cation furnished the *syn*-isomer (*S,R*)-**28**, while strontium cation proceeded with *anti*-selectivity to give (*R,R*)-**28** (Scheme I-8)^[16]. These Sr and Mg catalytic systems were not applicable to other ketimines, such as aryl ethyl ketimines and aliphatic ketimines, because of their lower reactivity. The α -ethyl- α -isothiocyanato ester also showed much lower reactivity

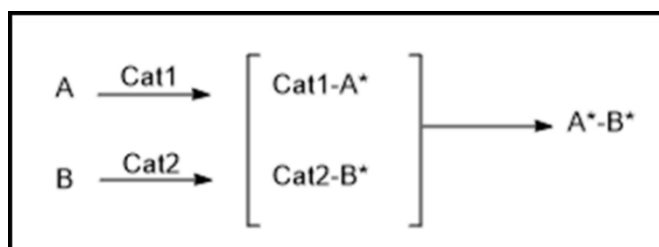
and stereoselectivity than the α -methyl- α -isothiocyanato ester, this could be attributed to the severe steric hindrance in the construction of vicinal tetrasubstituted carbon stereocenters.



Scheme I-8 Stereodivergent *Mannich*-type reaction. Adapted from reference^[16].

I.2.b. Case of stereodivergent dual catalysis.

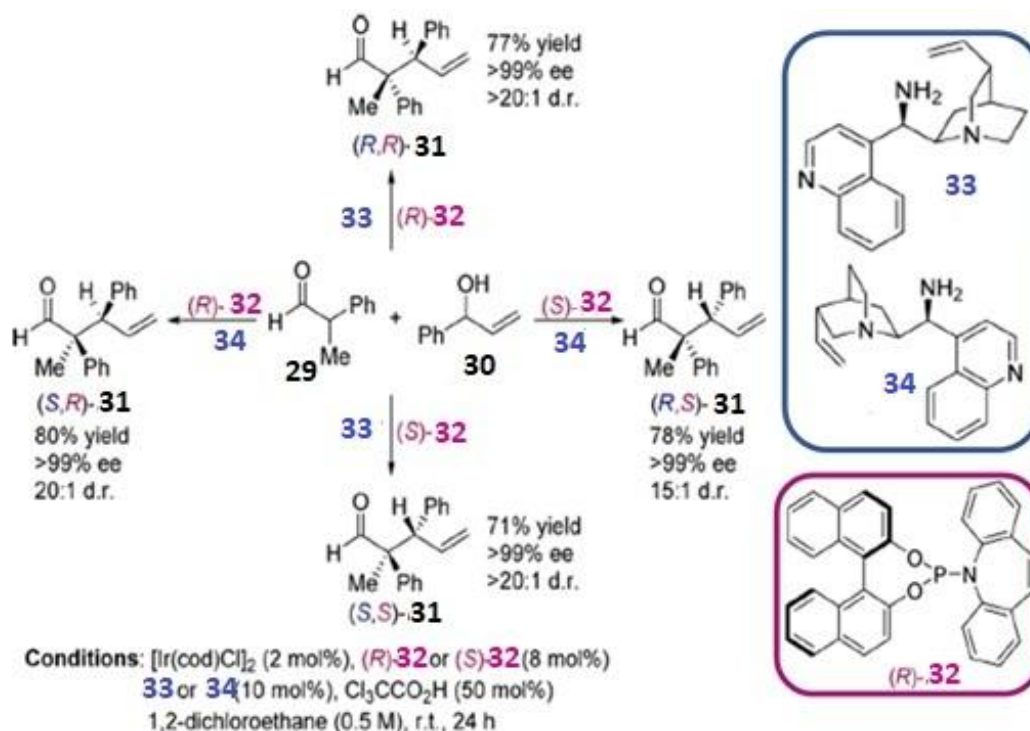
Dual catalysis (also referred to as synergistic or cooperative catalysis) corresponds to the concerted reaction of two “activated substrates”, each of them being activated by two distinct catalysts.



Scheme I-9 Concept of dual catalysis.

Stereodivergency in the context of dual catalysis is achieved when two chiral catalysts activate independently and simultaneously both reaction partners, thus the respective catalyst can fully control the configuration of the stereocenter originated from the fragment it activates. In such

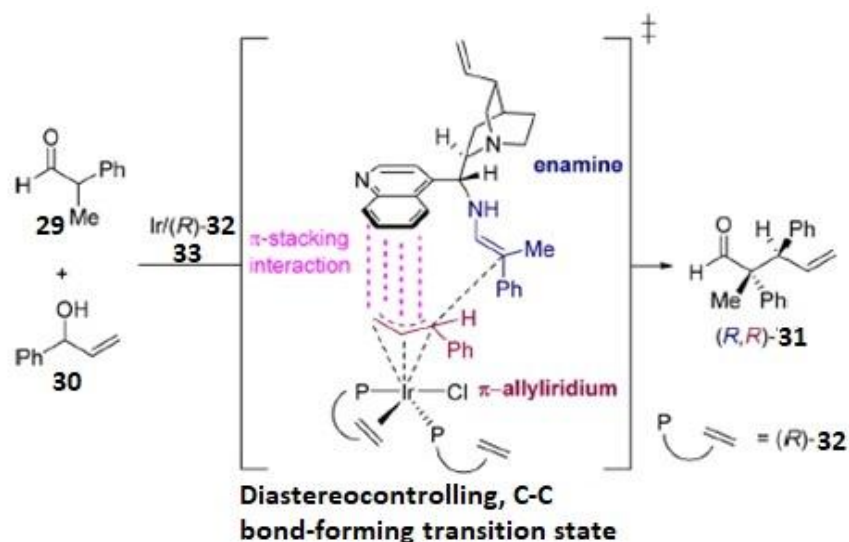
a case, the chiral product A*-B* is formed directly from the reaction of the resulting activated intermediates (**Cat**¹-A* and **Cat**²-B*, Scheme I-9). Since the two stereocenters are formed at the same time, then the mechanism of this strategy is very close to concerted a mechanism, but unlike the aforementioned examples each chiral catalyst activates the prochiral centers chemo-selectively. Successful application of this approach was demonstrated in the α -allylation of branched aldehydes^[17-21] (Scheme I-10).



Scheme I-10 Stereodivergent dual Ir/primary amine-catalyzed α -allylation of hydratropaldehyde. Adapted from reference^[22].

An iridium complex of a chiral phosphoramidite ligand **32** and a cinchona alkaloid derivative **34** were used to activate the allylic alcohol **30** and the aldehyde **29**, respectively. Trichloroacetic acid (Cl_3CCO_2) plays the role of the promoter. All four stereoisomers of **31** were accessed in good yields (71–80%) and in excellent enantio- and diastereoselectivities (>99% *ee*, 15:1 to >20:1 dr) (Scheme I-10). The appropriate combination of the enantiomer ligand **32** and of the pseudo enantiomers of cinchona amine **33/34** allowed to control the configuration of the two stereogenic centers in **31**. Achieving a high degree of stereodivergence was due to the use of two catalysts that are capable of shielding opposite diastereo-faces of their respective

substrates, in turn allowing the two coupling partners to come together in a harmonic stereocontrolled fashion. It is very important to mention that both enantiomers of allylic alcohol **30** yielded a single diastereomer when a given enantiomer of ligand **32** was used. The configuration at the β -carbon of product **31** was therefore set during or after the formation of the π -allyl species. However, transition-state modeling showed that the diastereoselectivity of the reaction was set during the C–C bond-forming step. The transition state was well stabilized through a π - π stacking interaction coming from the quinoline ring with the phenyl ring of the π -allyl-iridium^[22] as illustrated in Scheme I-11. This model accurately predicted the formation of (*R,R*)-**31** as the major product stereoisomer when (*R*)-**32** and **33** were used as catalysts. The minimization of matched and mismatched effects was anticipated to be a challenge for this approach. However, the operation of an outer sphere mechanism in which the stereocontrol elements are positioned opposite the reactive diastereofaces for each reactant allows two independent catalysts with a high degree of local diastereofacial differentiation to participate in a single transition state.



Scheme I-11 Schematic, simplified representation of the computed transition state leading to formation of (*R,R*)-**31**. Adapted from reference^[22].

The scope of the dual Ir/amine-catalyzed α -allylation was subsequently expanded to include linear aldehydes^[23]. Importantly, the concept of stereodivergent dual catalysis can be extended

to other reactions that unite two reactive fragments, such as the Diels–Alder reaction, and thus offers numerous opportunities for further development.

I.2.c. Case of cascade (sequential) catalysis.

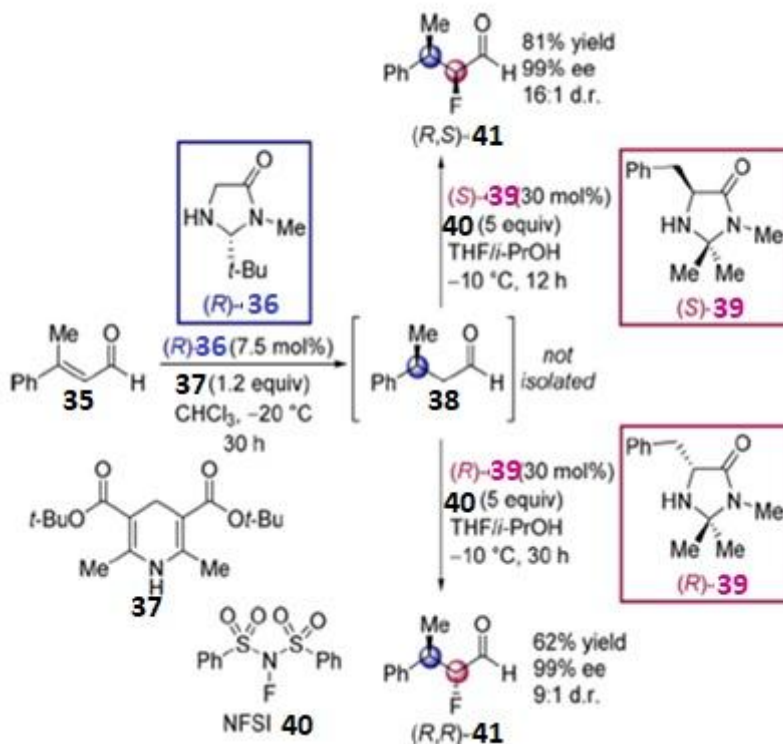
For a catalytic cascade, a catalyst is required for at least one step during the sequence of consecutive transformations. For a stereodivergent cascade reaction, two or more stereogenic centers are formed successively.



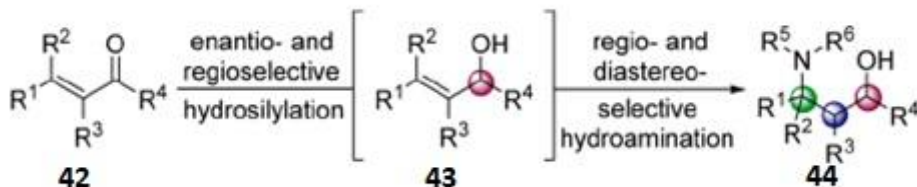
Scheme I-12 Schematic representation of the concept of cascade catalysis.

As shown in Scheme I-12, a sequential operation of two or more catalysts in a cascade reaction includes first the generation of chiral intermediate **B*** from a reaction of **A** catalyzed by **Cat1**. The second catalyst **Cat2** is ready to activate **B*** after the completion of the first reaction to give the chiral final product **B*-C***. The main challenge in this process, lies in the second step after the generation of the first chiral center. The configuration of the stereogenic center formed in the second step could be affected by the chiral bias induced by the stereogenic center generated in the first step. In this case, it would be impossible to have access to all possible stereoisomers of certain products through the cascade process. To overcome this challenge, the enantiodiscrimination event must be controlled exclusively by the catalyst. Such examples of stereodivergent cascade reactions occurring under catalyst control are presented below. MacMillan and co-workers^[24] implemented a strategy for the stereodivergent formal α -hydrofluorination of enals by means of a combination of two chiral secondary amine catalysts (Scheme I-13). The first step consists of the 1,4-reduction of the chiral α,β -unsaturated iminium ion generated from the reaction of enal **35** and amine catalyst (**R**)-**36**. Activation of aldehyde intermediate **38** by an amine catalyst **39** in the second step led to an enamine which reacts with an electrophilic fluorination reagent, NFSI (**40**), to yield **41**. Along this route, two diastereomers are accessible for which the configuration of each stereogenic center is controlled by different catalysts. Diastereomers (**R,S**)-**41** and (**R,R**)-**41** were obtained with excellent enantioselectivities

and dr. ratios by simply changing the configuration of catalyst **39**, used in the second step. The two other stereoisomers of **41** could in principle be accessed by using catalyst (**S**)-**36** in the first step but this was not demonstrated. Conceptually, this result demonstrates that cascade catalysis pathways, which proceed through an iminium/enamine sequence, can be readily modulated to provide almost perfect diastereo- and enantioselective outcome.



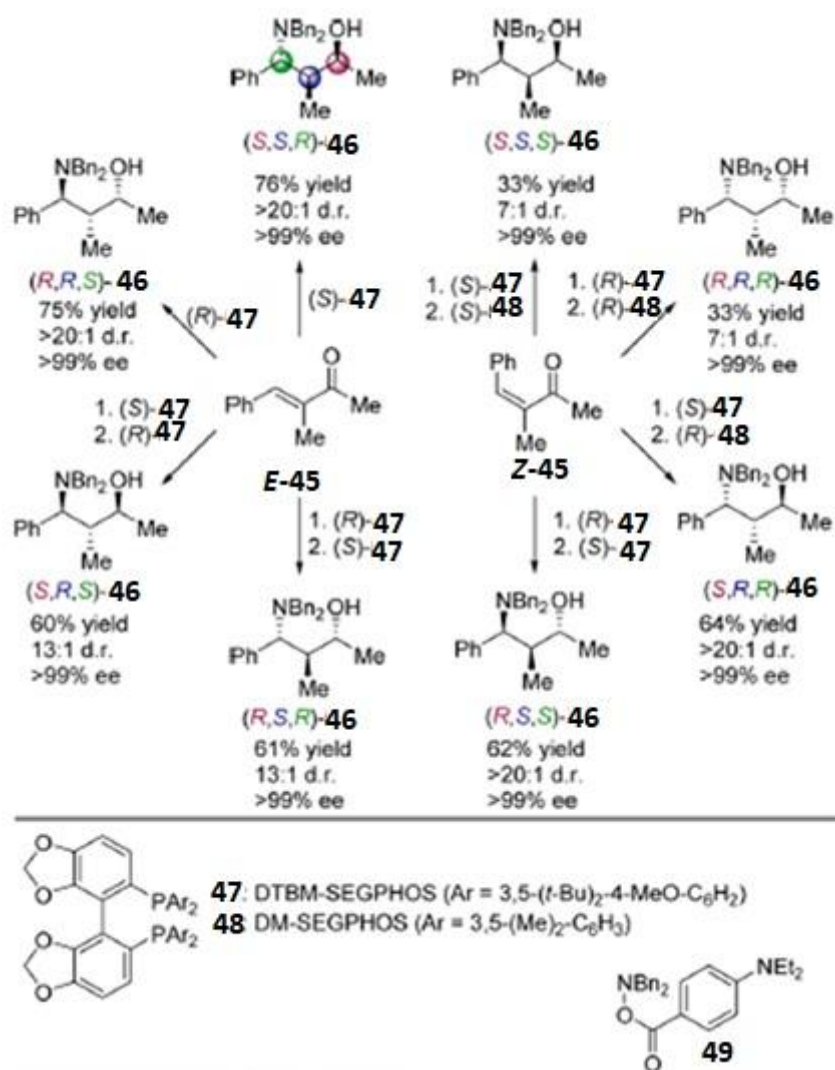
Scheme I-13 Strategy of cycle-specific amine catalysis in formal hydrofluorination of enals. Adapted from reference^[24].



Scheme I-14 Cascade-catalysis strategy for synthesis of 1,3-aminoalcohols. Adapted from reference^[25].

In 2016, Buchwald and coworkers^[25] introduced a similar approach for accessing all possible stereoisomers of a set of 1,3-amino alcohols from various enones through organometallic catalysis.

The cascade reaction consists of an asymmetric copper-catalyzed hydrosilylation of the carbonyl group leading to allylic alcohol **43** followed by catalyst controlled diastereoselective hydroamination of the double bond of **43** leading to amino alcohol **44** (Scheme I-14)^[25]. Both steps involve a diphosphine copper hydride complex as the active species.



Scheme I-15 Synthesis of the eight stereoisomers of amino alcohol **46**. Conditions for synthesis of (*R,S,S*)-**46**: Hydrosilylation step: Cu(OAc)₂ (5 mol%), (*R*)-**47** (5.5 mol%), (MeO)₂MeSiH (3.0 equiv), THF, -78°C, 24 h, 91% yield. Hydroamination step: Cu(OAc)₂ (5 mol%), (*S*)-**47** (5.5 mol%), (MeO)₂MeSiH (5.0 equiv), **49** (2 equiv), THF, 55°C, 70 h, 68% yield^[25].

The cascade hydrosilylation/hydroamination transformation of enone **45** into amino-alcohol **46** is shown in Scheme I-15. This method provides an access to all possible eight stereoisomers of amino alcohol **46** starting from either (*E*)-**45** or (*Z*)-**45** (Scheme I-15), thanks to the selectivity of both steps being catalyst-controlled and to the *syn*-facial nature of the hydroamination process (Scheme I-1). All stereoisomers are generated through the appropriate choice of substrate geometry (*E* or *Z*) and ligand enantiomer (*R* or *S*) even though in some cases slightly different ligands must be employed (DTBM-SEGPHOS **47** and DM-SEGPHOS **48**, see Scheme I-15). This approach offers the advantage to employ Cu catalyst system for both steps. The limitation is the necessity to isolate the intermediate allylic alcohols when the stereodivergence requires the use of ligand enantiomers coordinated on Cu.

I.2.d. Conclusion.

	Formation of the stereogenic centers	Number of catalysts	Predictability
Concerted pathway	≈ simultaneously	≥1	-
Dual catalysis	≈ simultaneously	2	+
Cascade catalysis	sequentially	≥1	+

Briefly, several elegant strategies for achieving diastereodivergency in asymmetric synthesis and catalysis have been developed and significant progress was made. These strategies have been developed for both organocatalyzed and metal-catalyzed reactions. In the context of reactions occurring through a concerted pathway involving a single chiral catalyst, reversal of diastereoselectivity has been mostly achieved by serendipity through ligand or metal atom redesign, or modulation of the reaction conditions. The scope of these approaches is presently quite limited but progress in modelling of the catalytic system will undoubtedly lead to more

predictable design. Conversely, new stereodivergent approaches relying on dual catalysis or cascade reactions have recently emerged, which yield all possible stereoisomers in a predictable manner and, as such, hold promise for a higher degree of generality. Among all of the developed strategies, a cascade reaction relying on the same type of organometallic species to construct successive stereogenic centers is particularly attractive. A future challenge in this domain would be to design stereodivergent cascade reaction which is truly one-pot, *i.e.* that a single, stimuli-responsive catalyst allows to get all possible stereoisomers.

I.3. Enantiodivergency by means of switchable asymmetric catalysts.

Hard work, persistence, and patience are not the only factors necessary to foster progress in science and push its limits. Additional factors must be embedded to drive science properly towards innovation and novelty. These complementary factors are imagination and knowledge. For any future scientific development, while knowledge provides the necessary input, imagination reflects the potentiality of the output. This has notably been reflected by 2016 Nobel prize awarded to Jean-Pierre Sauvage, J. Fraser Stoddart, and Bernard (Ben) Feringa for the development of artificial molecular machines. *i.e.* synthetic molecules able to perform various stimuli-responsive and controlled tasks^[26–30]. Nature comprises a huge library of smart biological machines for conducting infinite parallel processes with an extraordinary level of proficiency. Inspiration from enzymes have led to the design of stimuli-controlled catalysts. Initially, these artificial switchable catalysts have been designed to respond rapidly to an external stimulus such as light, pH, redox event, metal-ion coordination, temperature, heat or any other physicochemical trigger, in order to control the rate of the reaction, classically between “on” and “off” states. Controlling the reaction rate is the most common type of ‘control’ achieved by switchable catalysis, which is, switching the catalysis ‘on’ (upregulation) and ‘off’ (downregulation) in response to an applied stimulus. More recently, it has been envisaged to switch the enantioselectivity of the catalyst through reversal of its configuration by means of a suitable stimulus.

Many applications are targeted for a such class of catalysts: (i) enantiodivergent process in which both enantiomers of a product are obtained using reagents from a single chiral source, thus avoiding the otherwise needed access to catalyst enantiomers, (ii) reversible control of the

tacticity during polymerization reactions allowing the preparation of multi stereo-block copolymers out of reach with conventional catalysts and (iii) stereodivergent cascade reactions for which the switchable nature of the catalyst allows all stereoisomers to be accessed in a truly one pot manner (Figure I-3). However, despite their potential applications in asymmetric catalysis, switchable enantioselective catalysts only start to emerge. In this section, a selection of switchable asymmetric catalysts which allow a predictable control of the configuration of a stereogenic center will be presented according to the nature of the stereochemical trigger.

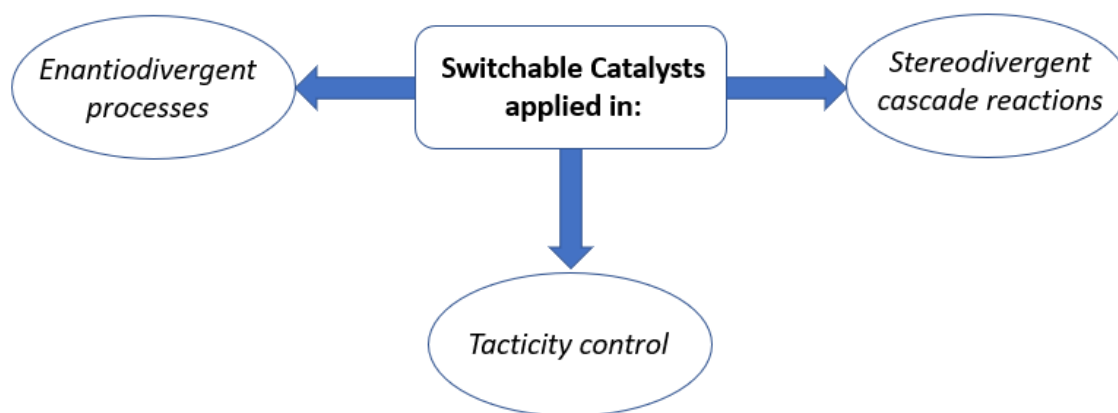


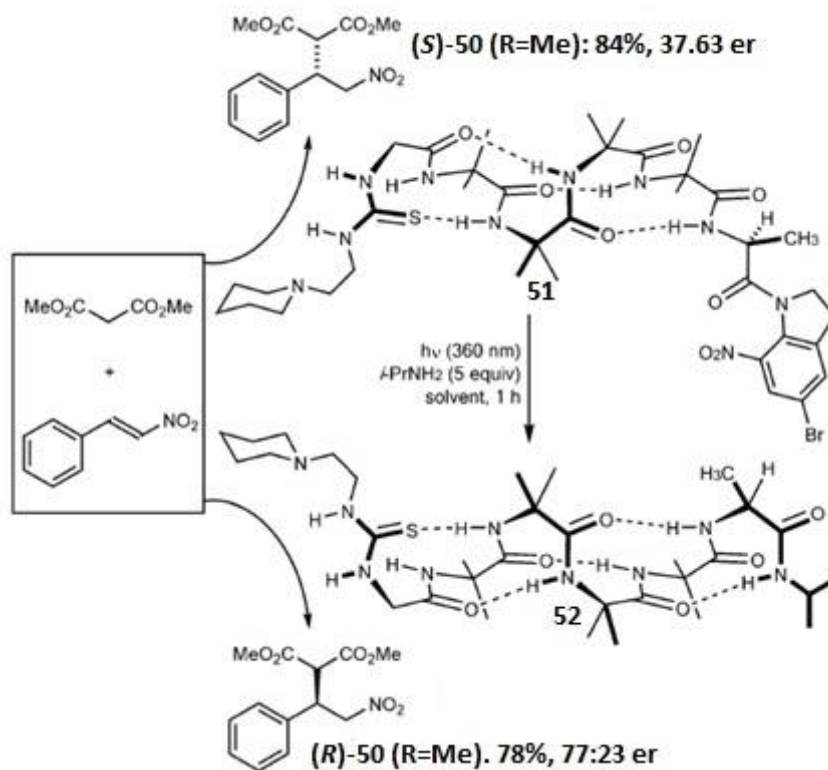
Figure I-3 Targeted applications for switchable asymmetric catalysts.

I.3.a. Light.

Using light as a stimulus is advantageous because of its non-aggressive nature, its modularity (appropriate choice of desired wavelength depending on the chromophoric unit) and its ease of operation. Light induced switching of either activity or selectivity of a chemical reaction is based on the controlled perturbation at the catalytic site(s) through some sorts of cooperative, steric (blocking/shielding) or electronic effects^[31]. This can be done through two different ways, either by incorporating a photoresponsive function within the catalyst or by using an additive that has photochemical properties. However, the design of switchable enantioselective catalysts with light as the only trigger is a challenge. An interesting example has been reported by Clayden and coworkers^[32] in 2016 which utilizes a small change in the conformation of a foldamer to invert its configuration.

The conformers of an Aib (2-aminoisobutyric acid) foldamer **51** are desymmetrised by attachment to an alanine terminus, causing imbalance in the groups of the two-interconverting

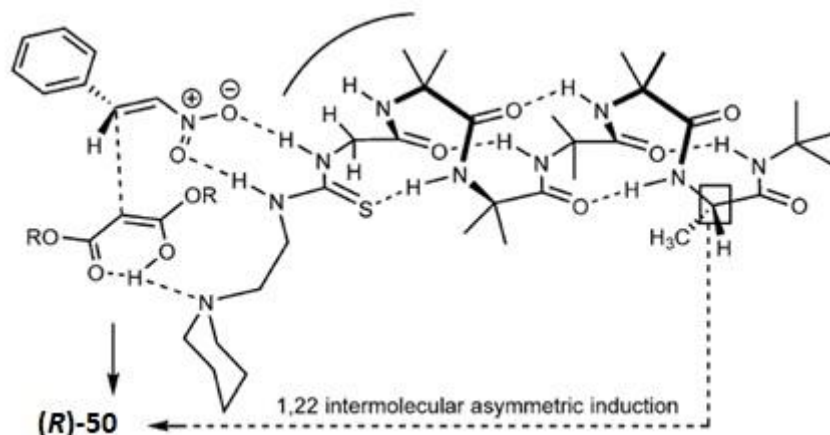
helical-sense conformers (**51**, Scheme I-16). Variable-temperature ^{13}C NMR analyses of **51** showed that it is preferentially left-handed (72:28) at 25 °C in THF. Compound **51** is also equipped with a reactive O-acyl nitronate group at its C terminus which is cleaved upon irradiation at 360 nm for 1h in THF- d_8 in the presence of an excess of iso-propylamine.



Scheme I-16 Photochemical refolding of a catalytic foldamer with consequent inversion of the sense of asymmetric induction. Adapted from reference^[32].

The formed secondary amine has an additional NH group which engaged in the H-bond network. As a consequence, **52** adopts a *P* helical sense with a 99:1 helical ratio. The authors assumed that this helical inversion is a result of introducing a new hydrogen bond donor at the C terminus of the oligomer, inducing the formation of new β -turn (as shown for **52**) in place of the extended structure at the C terminus of **51**, and thus the global reversal of the helical-sense preference. Catalyst **51** was subsequently engaged in the Michael addition reaction between dimethylmalonate and nitrostyrene and the Michael adduct (**S**)-**50** was obtained in 37:63 er (Scheme I-16).

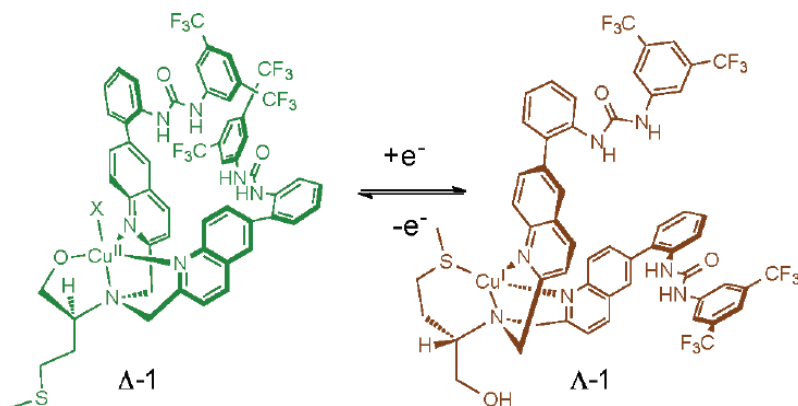
The catalyst was then irradiated at 360 nm in the presence of iso-propylamine, converting the tertiary amide into a secondary amide and inducing the helix to switch into a left-handed conformation. As expected, catalyst **52** provided (*R*)-**50** as a preferentially-formed enantiomer in 77:23 er. The induced switch of enantioselectivity demonstrates that insertion of a single hydrogen bond at a remote site in a refoldable molecule is sufficient to induce a global conformational switch and that was translated in the stereochemical outcome of the catalytic reaction. The authors proposed a transition state (Scheme I-17) in which the malonate bound to the piperidine function, located at the *N* terminus of the *P* helix, attacks on the less sterically hindered lower face of the nitrostyrene bound to thiourea. The preferential formation of (*R*)-**50** involves a remote 1,22 intermolecular asymmetric induction, *i.e.* induction from groups separated by 22 atoms. A limitation of this system for further application is that the stereochemical switch is irreversible.



Scheme I-17 Proposed model for remote asymmetric induction by a light-triggered switchable asymmetric catalyst. Adapted from reference^[32].

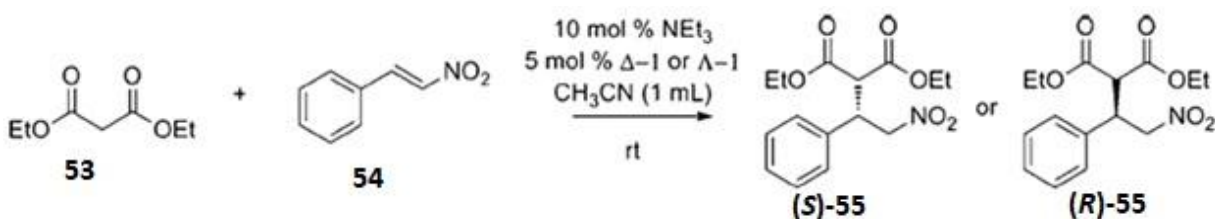
I.3.b. Redox potential.

Redox-switchable catalysts have been studied for different chemical processes such as polymerization, hydrogenation, isomerization, ring closing metathesis reactions, *etc*^[31,33]. Redox potential is a suitable trigger for modulating the reaction rate, the substrate selectivity^[34,35] and more scarcely the product stereochemistry^[35,36]. In 2012, Canary and co-workers^[37] synthesized a redox-switchable catalyst derived from *L*-methioninol and bearing catalytic urea groups (**1**, Scheme I-18).



Scheme I-18 Redox-triggered switching between Δ -1 and Λ -1. Adapted from reference^[37].

Upon one-electron oxidation or reduction of copper metal, an inner sphere ligand rearrangement takes place between the alcoholate and thioether coordination moieties. This rearrangement is related to the relative orientation of two quinoline rings which is behind the generation of right (Δ , Cu^{2+})- or left (Λ , Cu^+)-handed orientations according to exciton-coupled circular dichroism analysis (Scheme I-18). The authors examined the possibility of using the appended urea catalytic moieties of **1** as promoters of the enantioselective addition of diethyl malonate **53** to trans- β -nitrostyrene **54** (Scheme I-19). Here, the copper ion serves to modulate the asymmetric orientation of the catalytic groups without being involved directly in the catalytic event.



Scheme I-19 Asymmetric conjugate addition reaction catalyzed by redox-switchable catalyst **1**. Adapted from reference^[37].

The catalytic behavior of Δ -1 was assessed in the Michael addition of diethyl malonate **53** to trans- β -nitrostyrene **54** with a 5 mol% catalytic loading of **1** and 10 mol% of NEt_3 serving as co-catalyst (Scheme I-19). The Michael adduct (**S**)-**55** was formed in 72% *ee*. The same reaction, using 5 mol % of Λ -1 as the catalyst, generated (**R**)-**55** with a similar *ee* (70%). The exact

mechanism of this catalytic process is not known since the urea groups are capable of binding both reactants, so it is not really known whether one or both urea groups are involved in the transition state. The same group^[38] conducted more mechanistic and kinetic studies assisted with some molecular modelling and crystal structure data. The authors suggested that one urea group binds and activates a nitrostyrene molecule in a chiral cleft during the stereo-determining step. Malonate attack likely occurs on just one face of the nitrostyrene as shown in Figure I-4 affording the conjugate addition product.

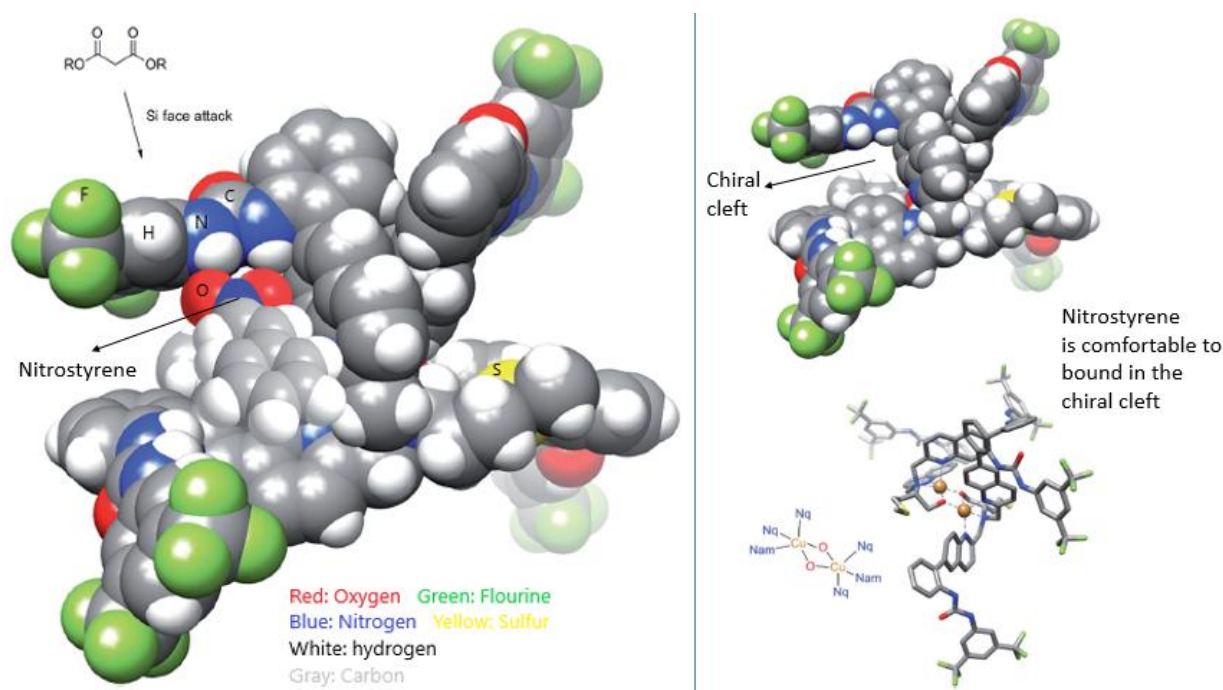


Figure I-4 Model of catalyst showing hindered attack at *Re* face of hydrogen-bonded *trans*- β -nitrostyrene (left). The space filling (top) and stick (bottom) molecular structure of Δ -1(right). The crystal structure of Δ -1 exists as a dimer with a bis(μ -alkoxo)dicopper(II) bridge connecting the monomers. Adapted from reference^[38].

The mirrored-image chiral cleft is formed upon catalyst reconfiguration leading to a nearly mirror image transition state. The use of the same catalyst for the sequential transformation of two malonates, through in situ reduction or oxidation of the catalyst, is described in part **I.3.d**.

I.3.c. Temperature.

Most asymmetric reactions show a modulation of their enantioselectivity with temperature which obeys the differential Eyring equation. Inversion of the stereochemical outcome of

asymmetric catalyst with temperature is not a rare phenomenon. Unusual temperature dependence profiles have multiple origins (change in enthalpy/entropy contributions, in the nature of the enantio-discriminating step, etc...) which makes temperature a hardly predictable trigger.



Scheme I-20 Selectivity controlled by temperature^[39].

In 2015, Trapp and coworkers^[39] reported a diastereomeric rhodium(I) catalyst that is stereochemically flexible and inverts its enantioselectivity through temperature modulation (Scheme I-20). The flexibility of this system comes from the tropos 2,2'-bis(diphenylphosphino) biphenyl (BIPHEP) ligand, which was modified with binding sites to attach readily available chiral auxiliaries. Upon binding of these auxiliaries, a pair of diastereomeric ligands is formed at room temperature (Figure I-5). Through these bounded chiral auxiliaries, chiral information is transferred to the stereochemically flexible chiral axis of the tropos biphenyl, which in turn, changes the diastereomeric ratio and shifts it away from the 1:1 equilibrium (Figure I-5B). In presence of the chiral auxiliary (*S*)-naproxen, the ratio of the ligand diastereoisomer (R_{ax},SS)-**2**/ (S_{ax},SS) -**57** reaches a 61:39 ratio at room temperature. This pair of diastereomeric ligands bounds to the rhodium atom with the equilibrium ratio of the isomers being unaltered, *i.e.* (R_{ax},SS) -**58**/ (S_{ax},SS) -**58** ratio is also of 61:39 (Figure I-5C). The equilibrium ratio of the metal-fixed diastereomeric catalysts can be modified by changing the temperature, and heating to 70 °C provides the previously minor isomer (S_{ax},SS) -**58** in a purity greater than 99%. Upon cooling, the diastereomeric ratio is frozen. Using this strategy both enantiomers of the hydrogenation product are obtained by using (R_{ax},SS) -**58**/ (S_{ax},SS) -**58** in a 61:39 ratio or pure (S_{ax},SS) -**58**.

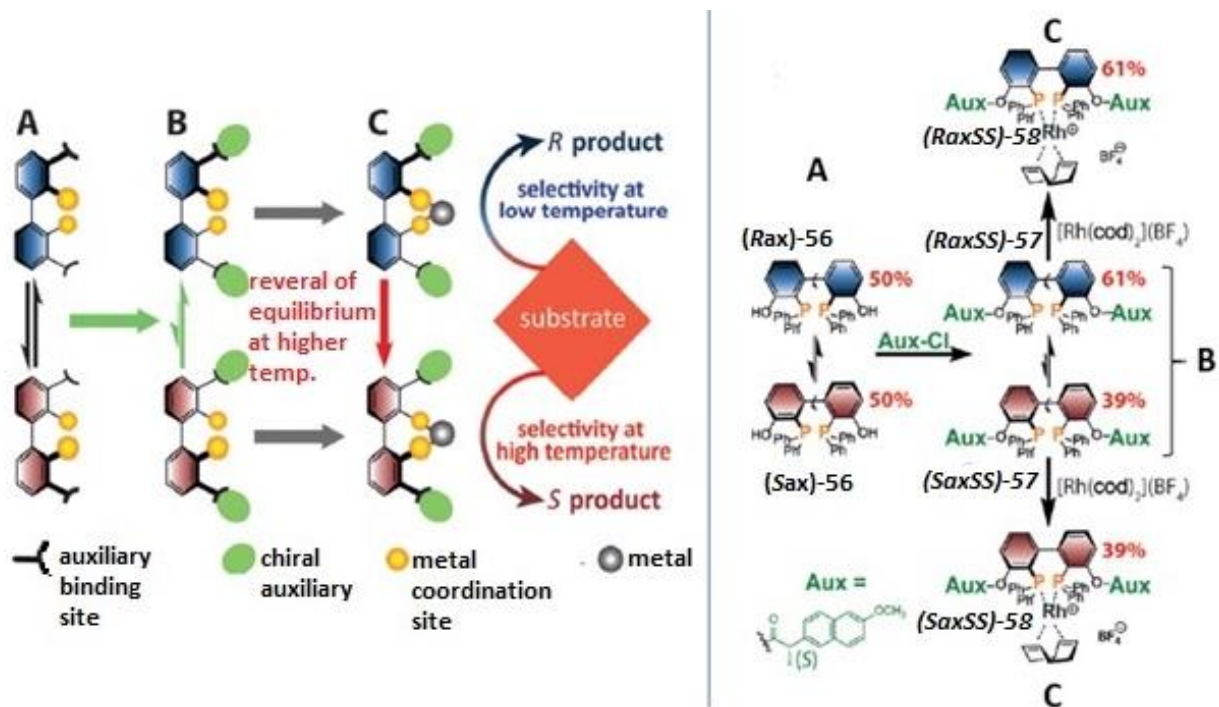


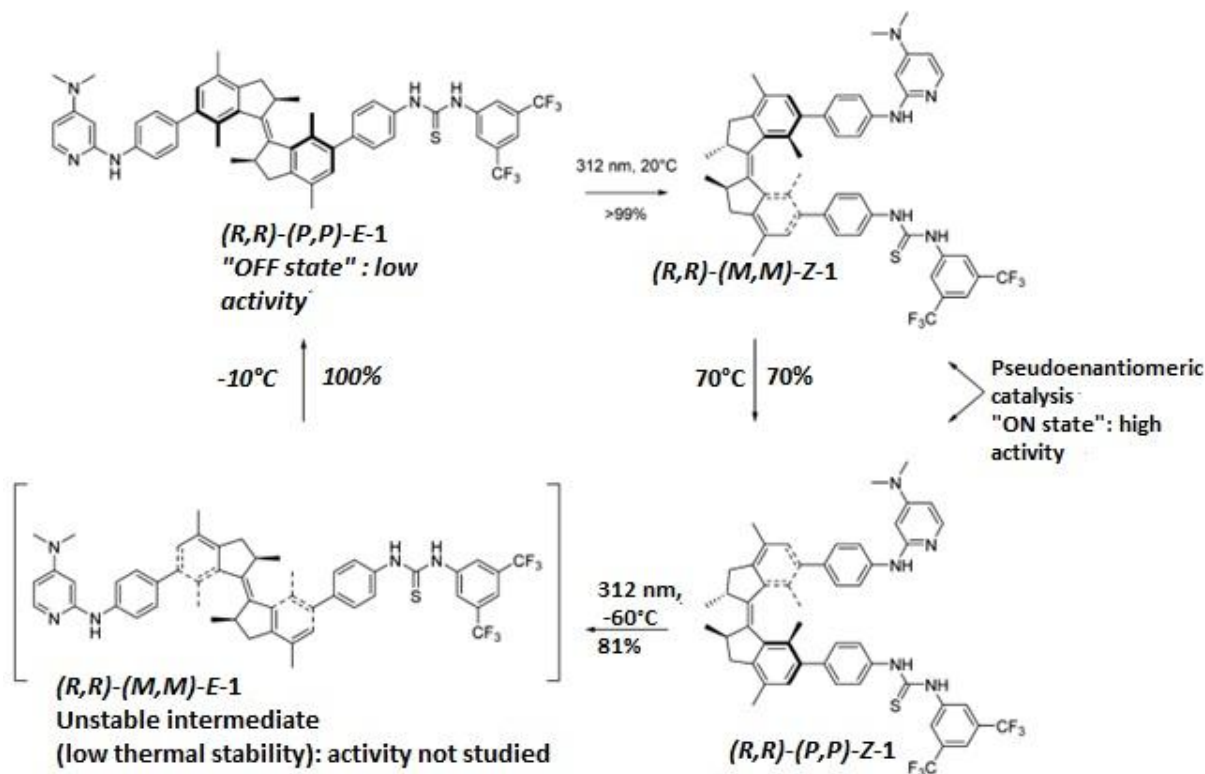
Figure I-5 Design of a bidirectional enantioselective catalyst that switches enantioselectivity as a function of the temperature. Adapted from reference^[39].

The temperature-controlled bidirectional enantioselectivity of the flexible Rh(I) catalyst $(R_{ax},SS)-58/(S_{ax},SS)-58$ is possible without any separation of the diastereomers. The predictable nature of this system comes from the fact the stereoselectivity of the reaction inverts when the catalyst changes its configuration. However, the temperature at which the switch occurs is hard to predict and the system loses its flexibility upon rhodium binding which makes this approach troublesome for sequential reactions.

I.3.d. Combined heat and light stimuli.

Synthetic molecular motors have emerged in the last two decades and those built on axially chiral hindered alkenes proved particularly powerful. Unidirectional rotation around the alkene double bond is triggered by a succession of light and heat stimuli. In 2011, a textbook example of a dynamic chiral switchable catalyst was described by Wang and Feringa^[40]. They designed and synthesized chiral molecular motor **1**, and used it as a switchable chiral organocatalyst (Scheme I-21) in the sulfa-Michael addition of thiophenol to α,β -unsaturated ketones (Scheme I-22 A). The upper and bottom parts of the molecular motor are functionalized by a thiourea and a Brønsted basic DMAP moieties expected to act cooperatively in the sulfa-Michael

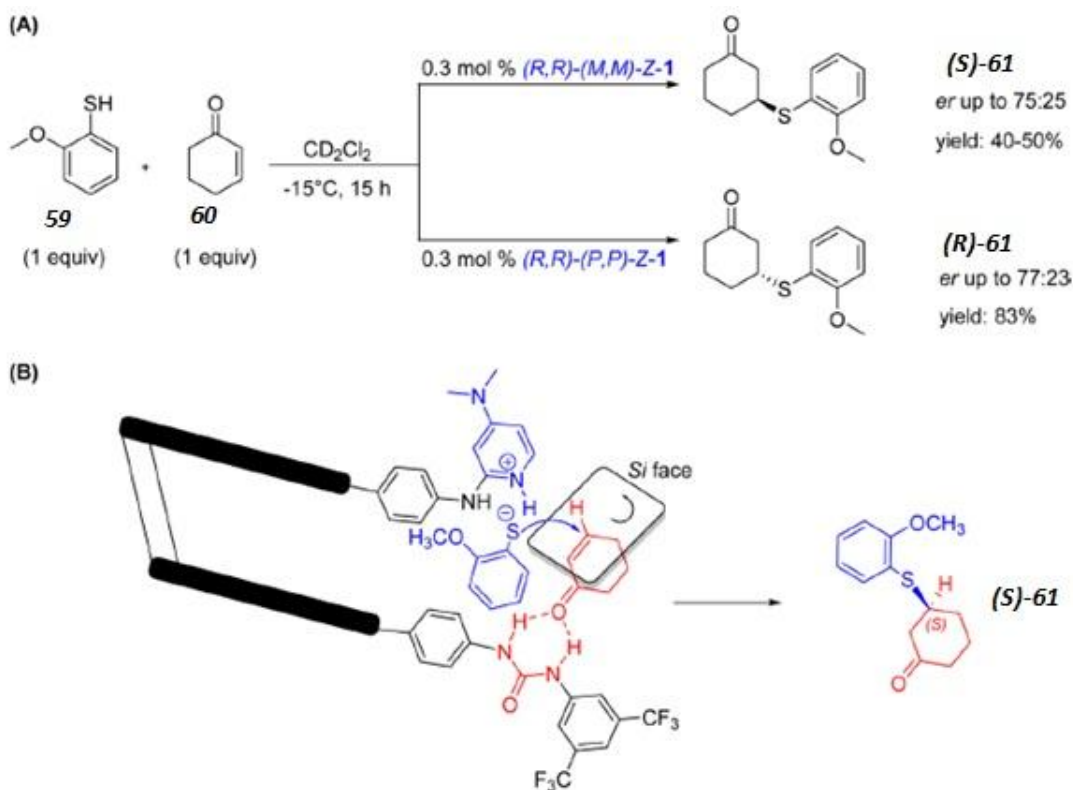
addition. The chiral crowded alkene moiety in the molecular motor can move through a unidirectional rotatory cycle with a series of two photo-isomerizations and two thermal-isomerizations (Scheme I-21).



Scheme I-21 Light- and heat-driven switchable asymmetric catalyst **1**. Adapted from reference^[40].

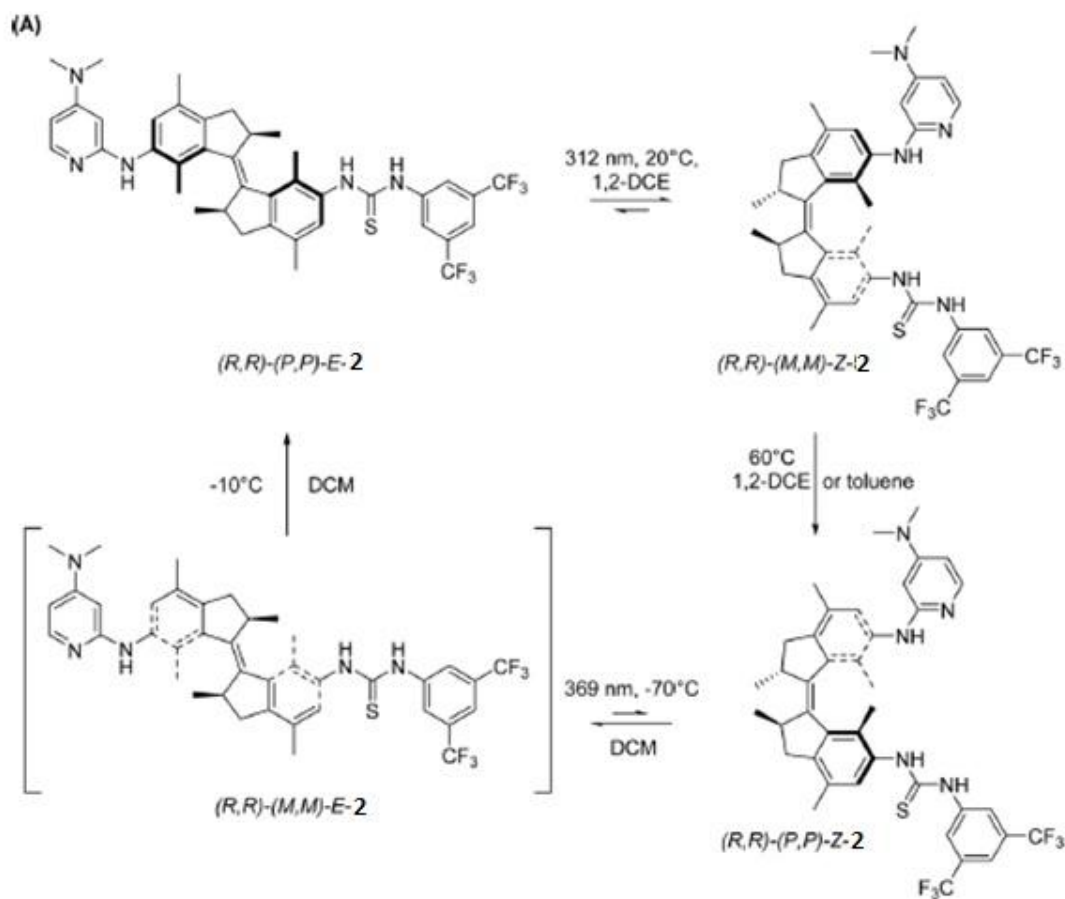
This rotation impacts the relative orientations of the two catalytic moieties. In particular, irradiation (312 nm) at 20 °C of **(R,R)-(P,P)-E-1** lead to a *E*-*Z* photoisomerization and a *P* to *M* helix inversion which eventually gives pure **(R,R)-(M,M)-Z-1**. In this isomer, the two catalytic moieties are brought closer to each other. A thermal helix inversion at 70 °C gives the **(R,R)-(P,P)-Z-1** isomer, while maintaining the two moieties in close proximity. The original structure **(R,R)-(P,P)-E-1** was regenerated by a photochemical step followed by thermal isomerization passing through the intermediate **(R,R)-(M,M)-E-1**, which was not tested in catalysis because of its low thermal stability. Huge effort has been implemented for studying and characterizing all the steps of this 360° rotation cycle of molecular motor **1** by chiral HPLC, circular dichroism (CD), UV-vis, and ¹H NMR spectroscopy. Chiral molecular motor **(R,R)-(P,P)-E-1** has been used

as an organocatalyst for the sulfa-Michael addition of thiophenol to α,β -unsaturated ketones and provided the Michael adduct **61** as a racemic mixture in very low yield (7%) as expected given the distant positions of the two catalytic moieties. Conversely, **(R,R)-(M,M)-Z-1** furnished **(S)-61** in 50% yield with an enantiomeric ratio (er) up to 75:25 as a probable result of the cooperative activation of the nucleophile and electrophile by the catalytic moieties and the establishment of a well-defined transition state as a result of the proximity between these catalytic sites (Scheme I-22 A).



Scheme I-22 (A) Control of the enantioselectivity of a sulfa-Michael addition employing switchable chiral catalyst **1** and (B) Plausible ternary complex Involved in the mechanism of thiol addition to enone. Adapted from reference^[40].

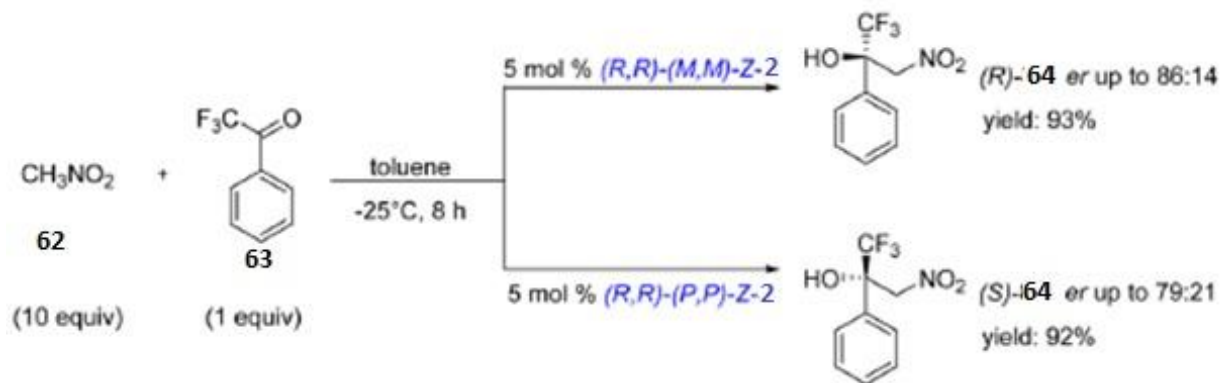
By using the **Z** isomer of opposite helicity, **(R,R)-(P,P)-Z-1**, the reaction was even faster, giving a higher yield (83%) and exhibiting a similar degree of enantioselectivity (er up to 77:23) but in favor of opposite enantiomer **(R)-61** (Scheme I-22 A). The authors proposed that the absolute stereochemistry of product **61** is determined by the helicity of the catalyst according to the stereochemical model shown in Scheme I-22B.



Scheme I-23 Light- and heat-driven chiral switchable catalyst **2**. Adapted from reference^[41].

Later on, the same group^[41] modified the design of their system and developed a new molecular motor-based dynamic organocatalyst **2** (Scheme I-23) which was able to accelerate the Henry addition of nitromethane to trifluoroacetophenone, with high control of the enantioinduction (Scheme I-24).

The aforementioned catalyst **1** (Scheme I-21) was found to be poorly efficient in this Henry reaction both in terms of activity and stereoselectivity. This new design of catalyst **2** (Scheme I-23) was obtained by removing the phenyl spacers between the stator and the catalytic moieties in order to get the two functionalities closer in the *Z* isomers.



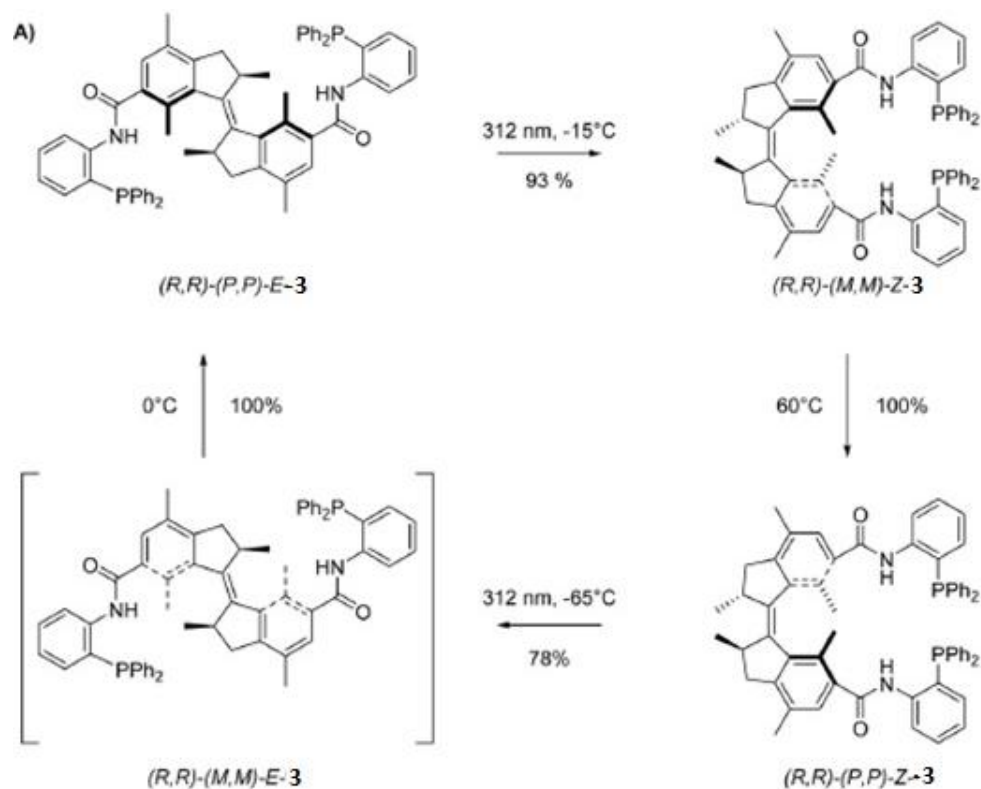
Scheme I-24 Control of the enantioselectivity of a Henry reaction employing chiral switchable catalyst. Adapted from reference^[41].

The same type of isomerization steps as for **1** were required to obtain its 360° rotation. The two Z-states of catalyst **2** were indeed effective in catalysis, affording the corresponding products with opposite enantioselectivity (er up to 86:14 for **(R)-64** and er up to 79:21 for **(S)-64**) in excellent yields (93% for **(R)-64** and 92% for **(S)-64** (Scheme I-24).

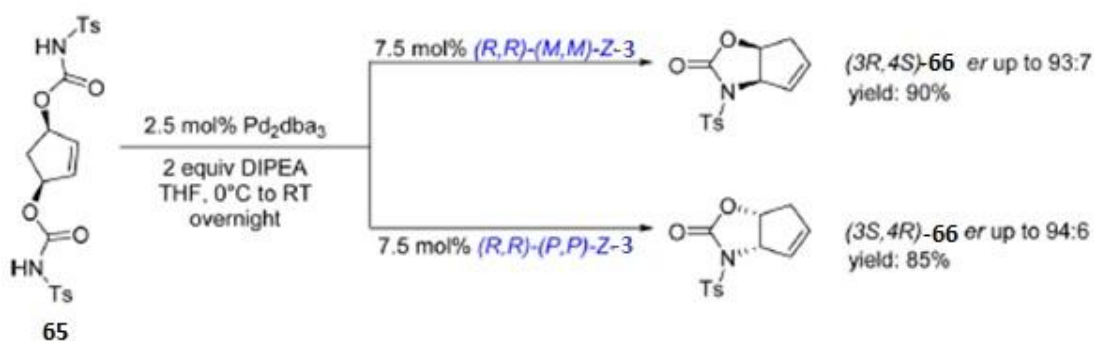
A switchable asymmetric organometallic catalyst was built on the same strategy. The rotary molecular motor system **3** is C_2 -symmetric since both sides of the alkene are substituted by diphenylphosphine groups (Scheme I-25)^[41]. Thanks to light and heat, helicity and geometry of **3** were modified to furnish a switchable ligand that exhibited excellent selectivity in the Pd-catalyzed desymmetrization reaction of meso-biscarbamate (Scheme I-26).

Using the two isolated Z states of molecule **3**, product **66** was obtained with excellent stereo-control, up to 93:7 er for **(3R,4S)-66**, and up to 94:6 er for the opposite enantiomer **(3S,4R)-66** (Scheme I-26). A stepwise control over the helicity of the bisphosphine ligand and spatial distance between these two phosphine groups are achieved by the photochemical and thermal isomerization during unidirectional rotation around the motor central double bond. These results highlight the proof-of-principle of multistage dynamically tunable and responsive chiral ligands at the molecular level. However, the dynamicity of the system is lost when Pd is coordinated to the Z forms of the ligand probably because the formation of a chelate complex prevents any further rotation of the motor double bond. These molecular motors hold promise in the design of asymmetric catalysts with predictable control of the enantioselectivity, despite

the current limitations of the slow interconversion process between the pseudo-enantiomeric states which precludes their potential implementation in cascade reactions.



Scheme I-25 Light- and heat-driven switchable chiral ligand **3**. Adapted from reference^[41].



Scheme I-26 Control of the enantioselectivity of a Pd-catalyzed desymmetrization reaction using switchable chiral ligand **3**. Adapted from reference^[41].

I.3.e. Helical polymers as scaffolds for switchable catalysis.

The α -helix^[42] conformation of proteins and the DNA double helix structure^[43] are key structural elements of biomolecules. Intensive endeavors have been devoted for mimicking

these helical structures with synthetic macromolecules. This resulted in the development of a variety of helical polymers with interesting properties for a wide range of applications^[44].

These helical polymers are distinguished in two main classes. First class encompasses static helical polymers characterized by a fixed helical sense, *i.e.* the sense of rotation can't interconvert. Within this class, the handedness of the helix is controlled by the chirality of the side chains, or by stereo-elements present the main chain. The second main class consists of dynamic and/or stimuli-responsive helical polymers which may undergo a dramatic change in morphology, structure, shape, or function in presence of a suitable trigger^[45]. These polymers become helical under specific reaction conditions and can interconvert to adopt opposite handedness.

The first helical covalent polymers were constructed from vinyl monomers but they lost their helical conformation in solution. Poly-triphenylmethyl methacrylate (poly-TrMA) and polyisocyanates were found to maintain a stable helical conformation in solution^[46]. In the case of poly-(TrMA), the conformation stability was increased by incorporating bulky groups on the lateral chains of the polymers. However, it has been demonstrated by some subsequent studies that introducing bulkiness in the monomer side chain is not a general requirement to get configurationally stable helical polymers^[47].

In 1990, the group of Lehn^[48] synthesized the first supramolecular polymer in the liquid crystalline phase, which consists of two monomers bearing complementary uracil and 2,6-diaminopyridine groups. Later on, long one-dimensional supramolecular polymers were characterized in solution and those derived from the ureido-pyrimidinone^[49] form particularly strong assemblies thanks to self-complementary 4-fold hydrogen bonding interactions. In addition, a range of monomers with a disk-like shape were found to form hydrogen-bonded helical polymers in many states, including in solution^[45]. Macroscopic properties of these assemblies resemble that of covalent polymers but with additional stimuli-responsive features relative to their dynamic nature.

The possibility of controlling the chirality of the main chain of helical polymers by different mechanisms is a particularly fascinating feature of this class of molecules. Single handed helices

can be obtained not only from homopolymers of enantiopure monomers (Figure I-6A) but also from copolymers consisting of a mixture of enantiopure monomers (called the “sergeants”) and achiral monomers (called the “soldiers”). The so-called “sergeants-and-soldiers” (S&S) effect^[50] arises when the sergeants that are present in minority can impose their chiral bias on the excess of soldiers resulting in the control of the sense of rotation of the helix (Figure I-6B). The same explanation is also valid for a non-racemic (*i.e.* scalemic) mixture of enantiomeric monomers in which the major enantiomer controls the main helicity (Figure I-6C). This second effect is referred to as “majority-rules” (MR)^[50]. Combining the sergeants and-soldiers and majority-rules effects is possible in the case of terpolymers composed of achiral monomers and a scalemic mixture of enantiopure co-monomers, and such effect is named as “diluted majority-rules” (Figure I-6D).

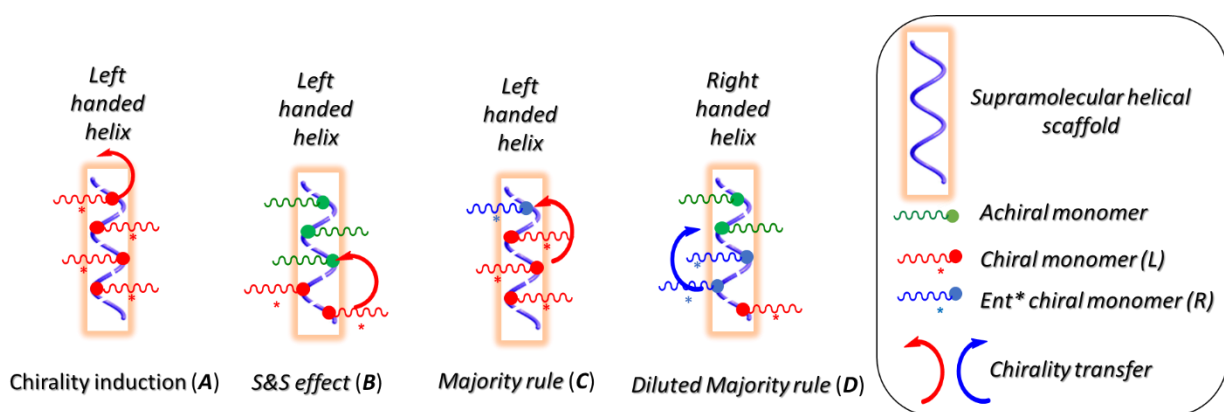


Figure I-6 controlling the chirality of the main chain of helical polymers by different mechanisms.

Other amplification mechanisms that do not rely on chiral co-monomers exist, *e.g.* by means of chiral solvents and physical fields^[51]. Chirality amplification through the S&S, MR and diluted MR effects is not restricted to covalent polymers, since many supramolecular polymers adopting a helical structure also display chirality amplification^[52].

I.3.e.i. Switchable helical covalent catalysts.

The backbone of poly(quinoxaline)s (PQXs) is flexible and as such a preferred handedness can be induced, amplified and inverted by several means. Bidirectional induction was achieved by modifying the structure of the soldier^[53], of the sergeant^[54], by controlling the sequence of the

monomers^[53], or by the solvent^[55–63]. In the present context, the latter approach is particularly remarkable. Indeed, PQXs bearing chiral (*R*)-2-butoxymethyl side chains can possess pure and opposite handedness in CHCl₃ and 1,1,2-trichloroethane (TCE) respectively.

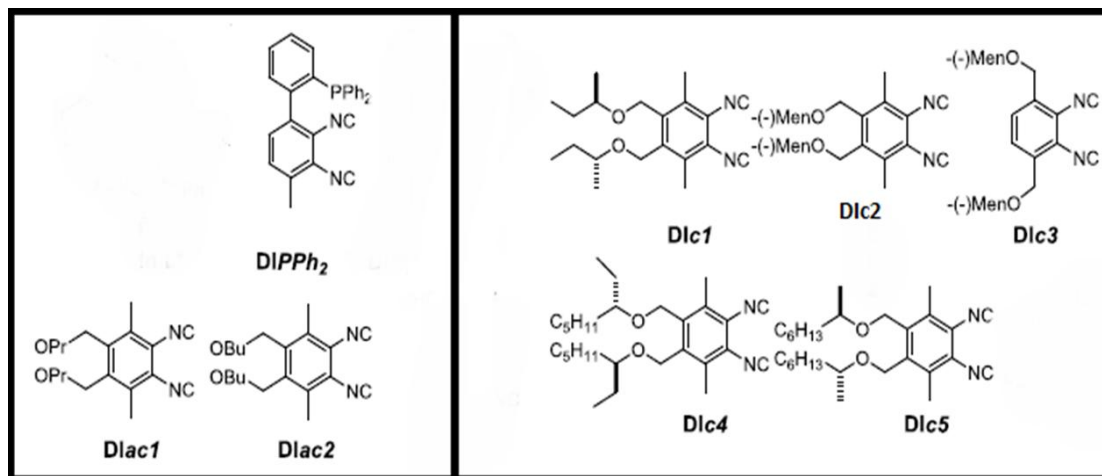


Figure I-7 Chemical structures of the **DI** monomers used to prepare PQX ligands.

Thus, Suginome and co-workers decided to exploit this feature in asymmetric catalytic reactions and for this purpose synthesized switchable PQX ligands by copolymerization of an achiral phosphine-functionalized monomer **DIPPh₂** and a monomer bearing a (*R*)-2-butoxymethyl side chain (**Dlc1**) (Figure I-7). Heating a solution of the synthesized (*P*)-helical ligands in TCE/THF or TCE/toluene leads to inverting the helicity state into (*M*)-helix. This inversion of handedness of PQXs ligands was harvested in a range of catalytic reactions^[55,56,58–60,62] allowing a highly enantioselective production of both enantiomers of the products (Figure I-8). Improved levels of chirality amplification were reported for **DI** sergeants having a (–)-menthol moiety located at the 6- and 7-positions (**Dlc2**) or at the 5- and 8-positions (**Dlc3**) of the quinoxaline ring (Figure I-8). CD spectroscopy analyses revealed that polymers incorporating **Dlc2** or **Dlc3** adopt opposite handedness even though these sergeants possess the same chiral moiety. The PQX ligand, **poly-(DIPPh₂⁵⁰-co-Diac1⁷⁵⁰-co-Dlc2²⁰⁰)**, with only 20% of sergeant units, adopted a pure (*P*)-helical conformation and provided the (*S*) hydrosilylation product with 95% *ee*. Consistently with the CD data, the (*R*)-hydrosilylation product was the main enantiomer when the reaction was conducted with the PQX ligands containing **Dlc3** sergeants (Figure I-8). The particularly fascinating point in this new class of enantiodivergent catalyst is that the configuration of the

product is related to the sense of rotation of the helices. In addition, the S&S effect was intensively studied in this class of polymers.

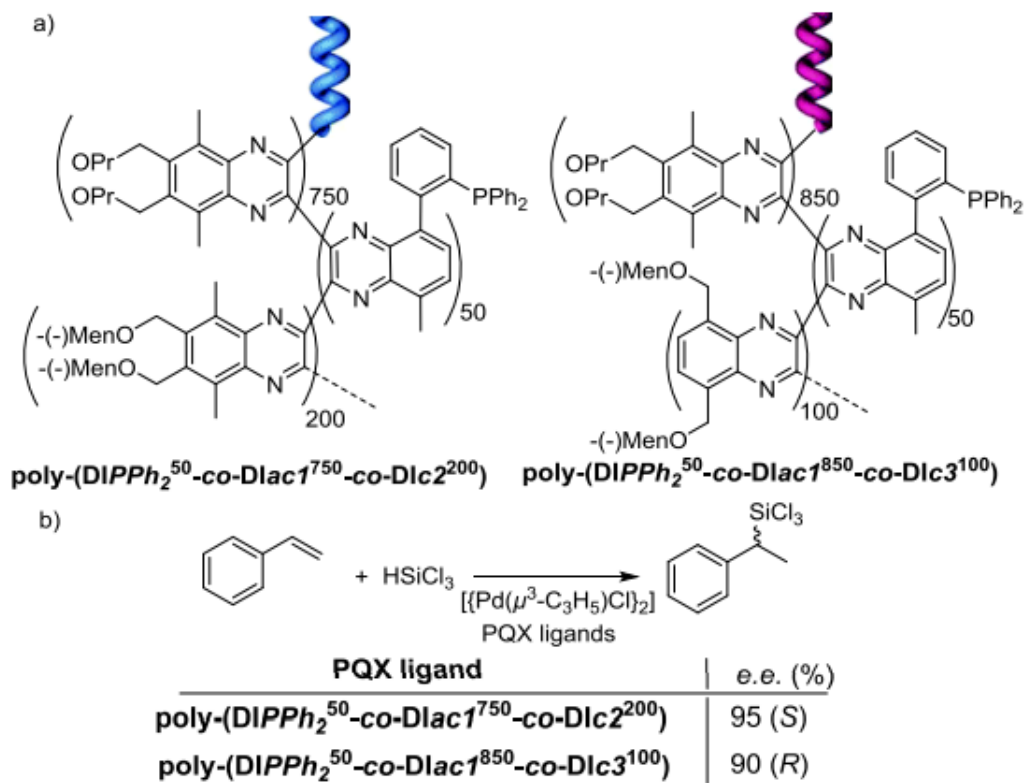
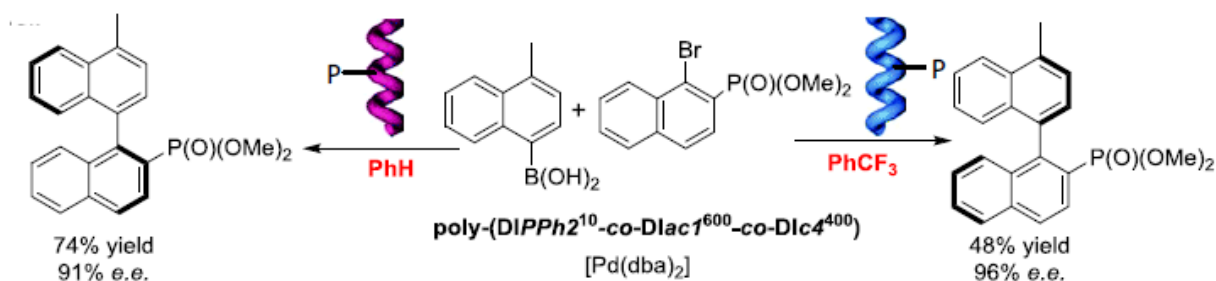
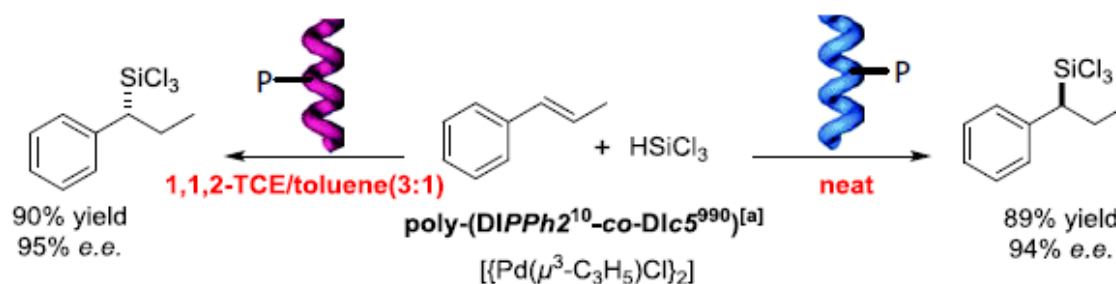


Figure I-8 Asymmetric palladium-catalyzed hydrosilylation of styrene with PDX ligands derived from (-)-menthol^[63]. a) Structure of the PDX ligands. b) Result obtained in the hydrosilylation reaction^[63].

Concerning S&S-type PDXs, it has been shown that in order to get solvent-induced reversal of selectivity, the nature of the soldier is a crucial parameter. For example, poly-(**DIc4**⁵-co-**DIac2**¹⁰⁰) adopted exclusively a (*P*)-helical conformation in various aromatic solvents. Conversely, poly-(**DIc4**⁵-co-**DIac1**¹⁰⁰), which contains the same sergeants but a different soldier, exhibited a (*M*)-helical conformation in benzene and (*P*)-helical one in PhCF₃^[64].



Scheme I-27 Selectivity-switchable S&S-type-PQX ligands triggered by the solvent. DIc5 is a mixture of the *d*, *l*, and *meso* isomers in a ratio of 38.8: 15.8: 45.4



Scheme I-28 Selectivity-switchable PQX ligands triggered by the solvent. [a] DIc5 is a mixture of the *d*, *l*, and *meso* isomers in a ratio of 38.8 : 15.8 : 45.4, respectively.

This particularly intriguing feature of the latter PQX polymer was exploited in catalysis by incorporating a few **DIPPh₂** units. **Poly-(DIPPh₂¹⁰-co-DIac¹⁶⁰⁰-co-DIc⁴⁴⁰⁰)**, was found to be a highly efficient ligand for the palladium-catalyzed Suzuki-Miyaura reaction furnishing the two enantiomers in benzene and in PhCF₃ with excellent enantioselectivities (Scheme I-27).

Thanks to chirality amplification effects, it was possible to get single-handed PQX copolymers even though synthesized from non-optimally pure materials. For example, **poly-(DIPPh₂¹¹⁰-co-DIc⁹⁹⁰)**, with **DIc5** being present as a mixture of the *d*, *l* and *meso* isomers, forms pure (*M*) and (*P*) helices in 1,1,2-TCE/toluene (3:1) and neat, respectively. In the palladium-catalyzed hydrosilylation of methyl styrene, both enantiomers were obtained with satisfactory yields and selectivities (Scheme I-28).

In summary, helically chiral PQXs serve as highly enantioselective ligands in asymmetric hydrosilylation of styrene and asymmetric Suzuki–Miyaura coupling reactions. In addition to the easy reuse of the chiral catalyst, reversible conformational change of the polymer backbone was applied to switch the enantio-induction direction in asymmetric catalysis in a predictable

manner. On the other hand, this system suffers from some drawbacks related to the use of different solvents in order to switch the selectivity of the catalyst. Besides, the dynamicity in this system is locked upon coordination of ligands to the catalytic metal centers. Thus, when the metal complex is formed, it will not be possible to invert its configuration. This last point impedes the application of PQXs as stereodivergent catalysts, *e.g.* in the framework of asymmetric cascade reactions.

***I.3.e.ii.* Switchable helical supramolecular catalyst.**

A lot of efforts have been implemented for controlling the handedness and generating single-handed supramolecular helical polymers especially by means of S&S and MR effects^[52,65,66]. One of the most popular and famous building blocks in the domain of supramolecular polymers is benzene-1,3,5-tricarboxamide (BTA), which consists of three alkyl amide functions connected through their carbon atom to the central aromatic ring.

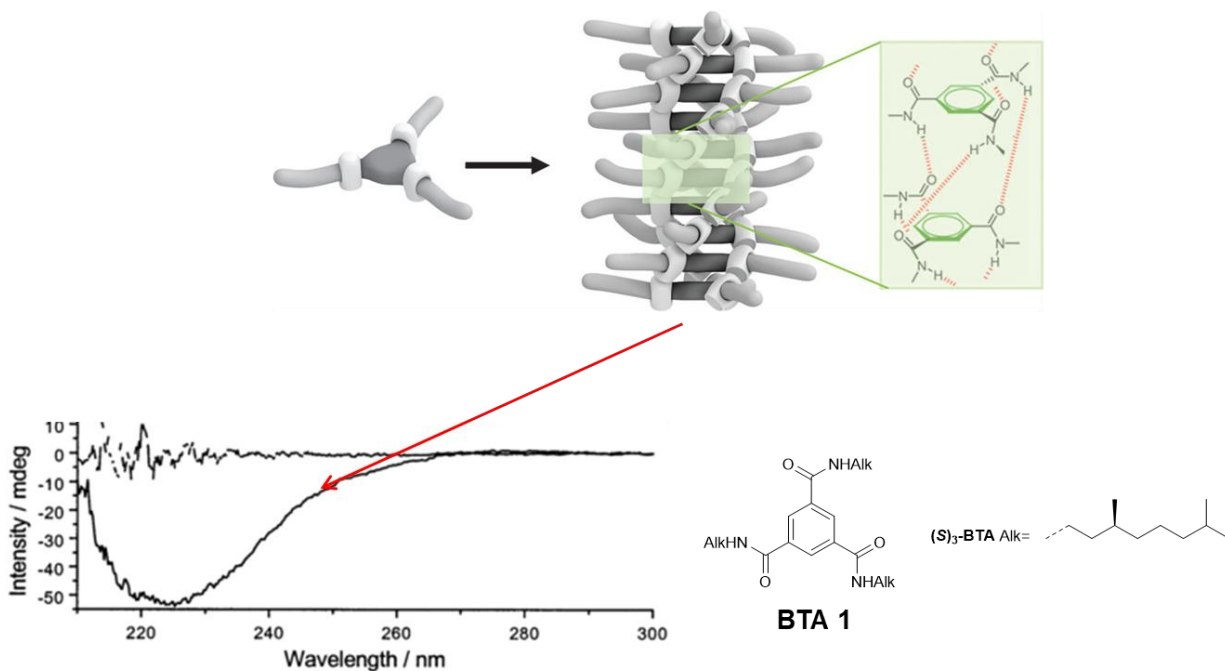


Figure I-9 Chemical structure of enantiopure **BTA 1** and its CD spectra in heptane ($6.5 \cdot 10^{-5}$ M) at 10°C (intensity = -55 mdeg) and at 90°C ($-10 < \text{intensity} < 10$ mdeg). Adapted from references^[67,68].

The main driving forces for the formation of BTA helices are π - π stacking and hydrogen-bonding interactions (Figure I-9). Additionally, these BTAs can be easily modified and functionalized with

different groups to impart the formed assemblies with new properties. By incorporating chiral side chains, helices with a preferred handedness are obtained^[67]. As shown in Figure I-9, a negative Cotton effect can be detected at 225 nm in the CD spectrum of **BTA 1** in heptane, which means that helix formed by the BTA monomers possesses a preferential handedness. An efficient transfer of chirality is taking place between the stereogenic center in the side chain of the monomers and the main chain helicity of the stacks. Further studies established that stacks of **BTA 1** are preferentially right-handed^[69] and that their structure in solution is similar to the one established in the crystalline state for a related BTA molecule^[70]. Disassembly of these supramolecular helices^[68] was achieved by increasing the temperature to 90°C as shown by the CD-silent spectrum obtained at this temperature (Figure I-9).

The assembly properties of this class of monomers can be controlled by the stereochemistry of an enantiopure monomer. This effect was notably demonstrated for BTA derived from amino esters (ester BTAs). The heterochiral BTA derived from valine (**BTA (S,S,R)-Val**, Figure I-10a) as well as a racemic mixture of monomers derived from (*rac*)-valine are able to form long rods in cyclohexane, while the homochiral analogue **BTA (S)-Val** assembles only into dimers at the same concentration as demonstrated by a range of analyses including FT-IR^[71] (Figure I-10b, and c). So, incorporating stereogenic centers with opposite configuration in the same monomer triggers the formation of stable helical structures. This is related to a subtle difference in the relative energy of the dimeric and helical assemblies which co-exist in solution for this class of monomers. Another important feature is the possibility to form co-assemblies by mixing ester BTAs and alkyl BTAs^[72,73]. Only the groups of Liu^[75–77] and Raynal^[72,78–80] have reported asymmetric catalytic reactions whose enantioselectivity is solely controlled by the helicity of the supramolecular polymers. The ability of benzene-1,3,5-tricarboxamide (BTA) molecules^[67] to assemble in a helical manner in apolar solvents was notably exploited to control the handedness of supramolecular helical BTA catalysts.

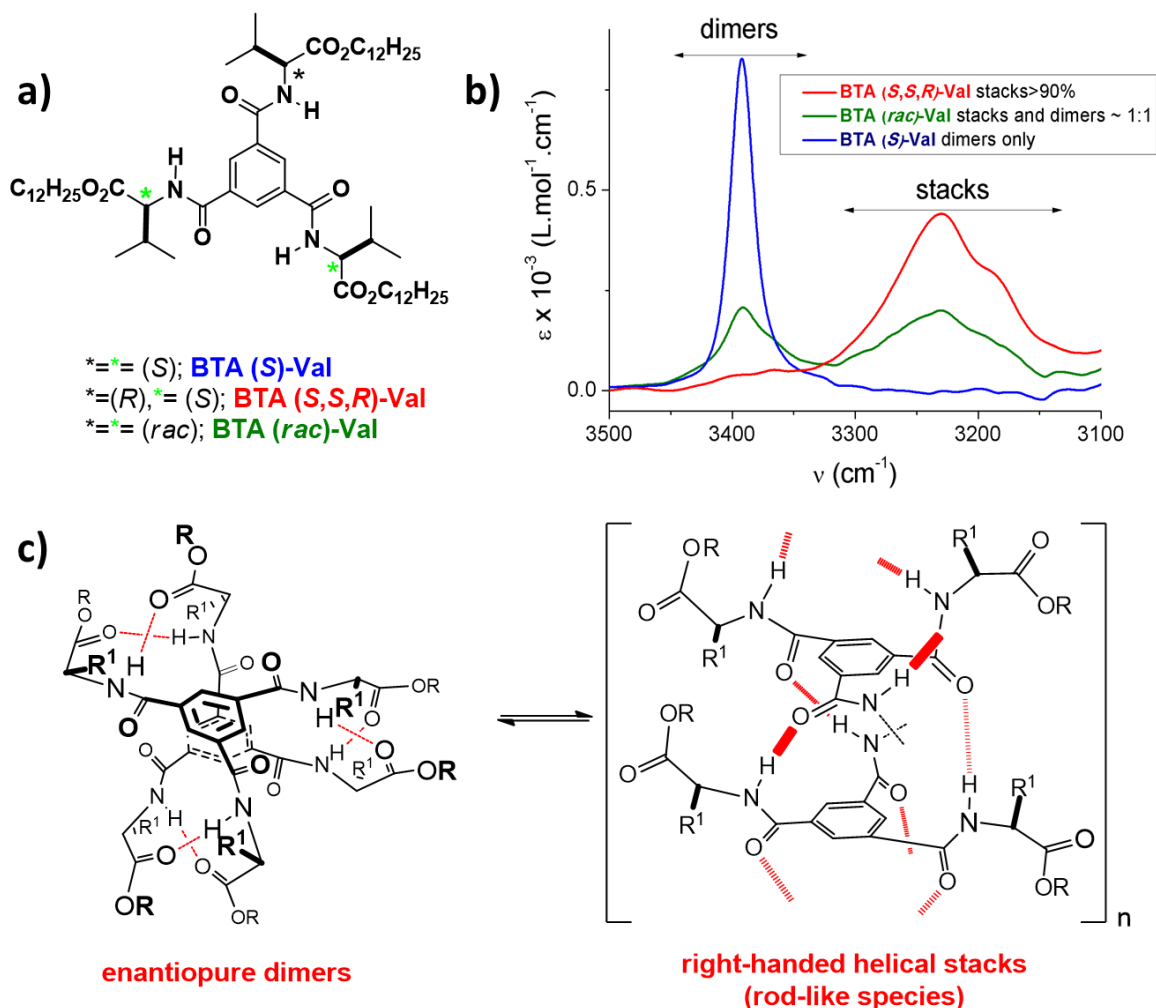


Figure I-10 **a)** Chemical structure of BTA-Val monomers and **b)** their FT-IR spectra. **BTA (rac)-Val** were obtained by synthesis with racemic valine and thus consists of a mixture of **BTA (S,S,R)-Val** (37.5%), **BTA (R,R,S)-Val** (37.5%), **BTA (S)-Val** (12.5%) and **BTA (R)-Val** (12.5%). **c)** Molecular structures of the enantiopure rod-like and dimeric hydrogen-bonded species formed by BTAs derived from (S) α -amino esters^[73,74] (ester BTAs, bottom). Adapted from reference^[71].

The combination of the achiral ligand **BTA-mPPh2** and the enantiopure but phosphorus-free BTA comonomer ^H**BTA(S)**, in a 1:1.25 ratio, proved to be modestly selective for the rhodium-catalyzed hydrogenation of dimethyl itaconate (31% *ee*, Figure I-11)^[78]. However, the same reaction performed with ^{Me}**BTAm-PPh2**, an analogue of **BTAm-PPh2** for which the alkyl amide functions have been methylated, showed no selectivity under the same conditions (Figure I-11).

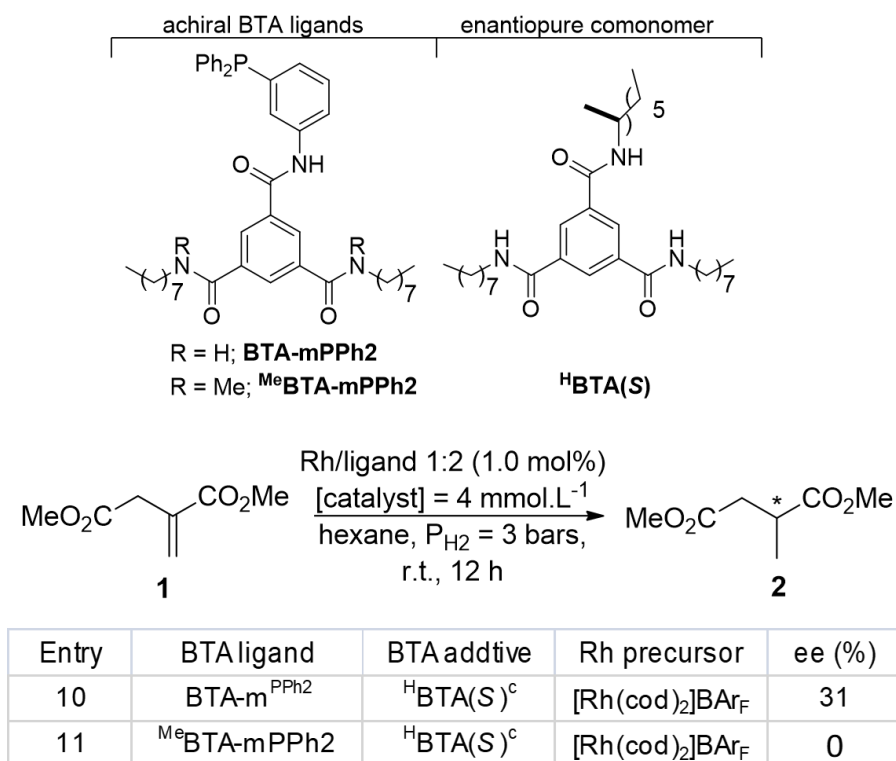


Figure I-11 Structure and nomenclature of the BTA derivatives. Asymmetric hydrogenation of dimethyl itaconate **1** with mixtures of BTA ligand, [Rh(cod)₂]BAR_F, and ^HBTA(S) (2.5 mol%). Conversion 100%. Adapted from reference^[78].

This demonstrates that the observed enantioselectivity arises from the helical co-assembly formed between **BTA-m-PPh2** and ^H**BTA(S)**. Thus, ^H**BTA(S)** in these catalytic co-assemblies plays the role of the sergeant.

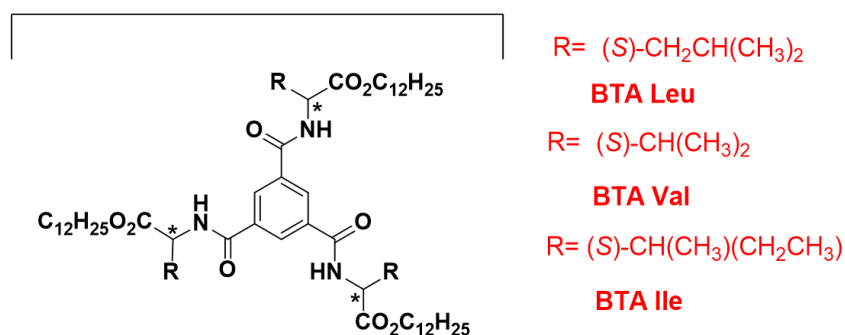


Figure I-12 Structures of ester BTAs. Adapted from reference^[74].

Ester BTAs^[71,73,74] (see Figure I-12) were found to be better sergeants than ^H**BTA(S)**. The selectivity of the reaction for mixtures of **BTA-m-PPh2** and various **ester BTAs** (1:1.25 ratio) in

the asymmetric hydrogenation of dimethyl itaconate **1** was found to be satisfactory with **BTA Leu** (74% *ee*), **BTA Val** (85% *ee*) and **BTA Ile** (85% *ee*)^[74]. Further studies showed that the quantity of **BTA Ile** can be decreased in the corresponding S&S-type mixture without deteriorating the selectivity. More precisely, one molecule of sergeant was sufficient to impose its chiral bias to four achiral ligands (or two rhodium catalytic centers) (Figure I-13).

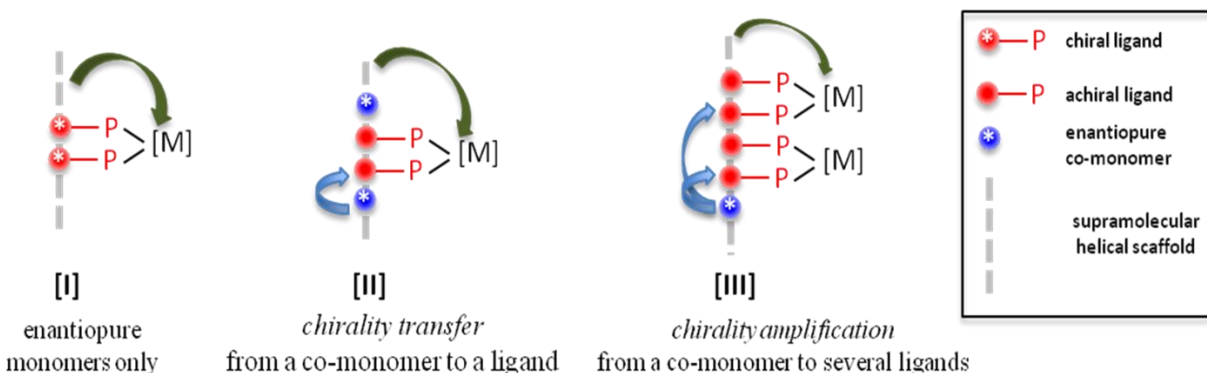


Figure I-13 Possible strategies [I]–[III] for the construction of supramolecular helices supporting catalytic metal centers. Arrows illustrate the chirality transfers. Adapted from reference^[72].

Later, mixtures of related BTA monomers were evaluated in the copper-catalyzed hydrosilylation of 4-nitroacetophenone^[80]. Here, the combination of **BTA_p-PPh₂** and the enantiopure BTA derived from cyclohexyl-alanine, **BTA Cha** (1.1 equiv.), displayed the highest selectivity (54% *ee* at room temperature) (Figure I-14). Importantly in these reactions, the major enantiomer and the selectivity of the catalytic reaction are related to the handedness and the optical purity of the co-assemblies, respectively. This offers the possibility to control the direction of the reaction by changing the sense of rotation of the helices similarly to what is observed for PQX ligands.

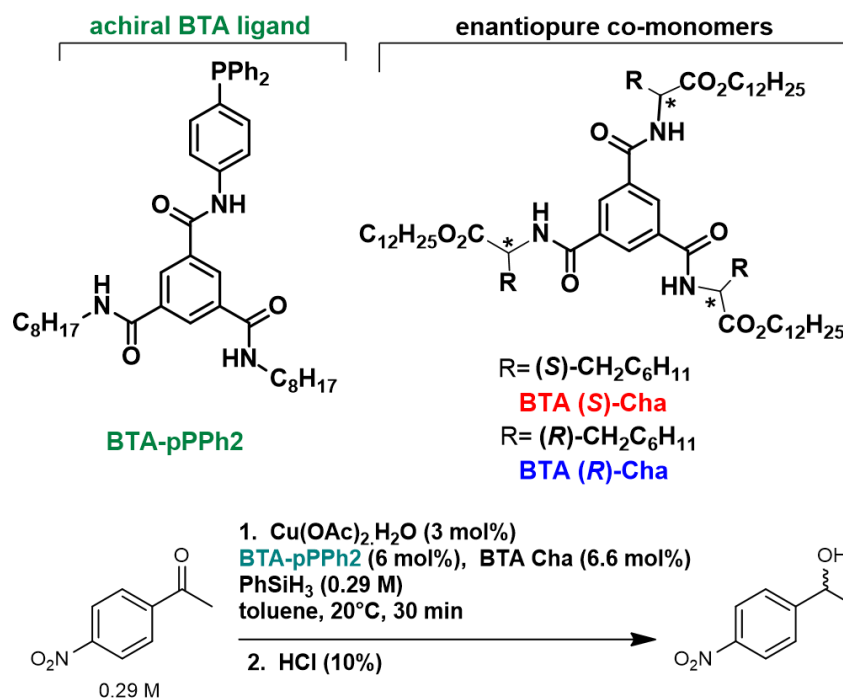


Figure I-14 Above: Structures of **BTA-pPPh2** and **BTA Cha**. Below: The copper-catalyzed hydrosilylation of 4-nitroacetophenone. Adapted from reference^[80].

Towards this objective, a dynamic supramolecular helical catalyst capable of switching its selectivity in real time was designed. The sense of rotation of the helices was controlled by the composition of the monomers present in the assemblies^[80]. The helical BTA catalyst is composed of **BTA-pPPh2** and a scalemic mixture of enantiopure co-monomers, the handedness of the system is decided by the nature of the chiral co-monomer present in excess. The composition and thus the handedness of the co-assemblies is varied by simple addition of enantiopure co-monomers (Figure I-15). Thanks to chirality amplification properties, though the diluted MR effect, both helices are expected to be single-handed.

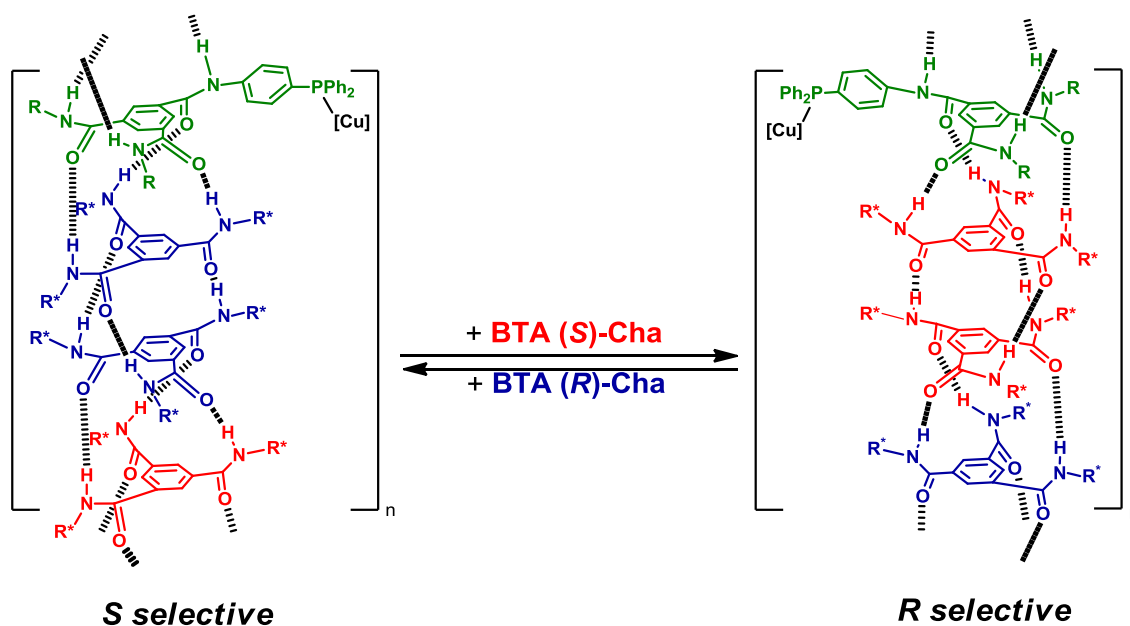


Figure I-15 Real-time control of the enantioselectivity of a supramolecular metal catalyst. The outcome of the catalytic reaction and the structure of the BTA assemblies were correlated according to various spectroscopic and scattering analyses. Adapted from reference^[80].

For demonstrating the dynamicity of the helical BTA catalyst^[80], the authors first decided to switch its selectivity in situ in a procedure involving sequential additions of 4-nitroacetophenone and PhSiH_3 . The reaction was started with a scalemic mixture biased in favor of **BTA (S)-Cha** (+33% *ee*, run 1). After 15 minutes, complete conversion of the substrate was achieved leading to the formation of (*R*)-1-(4-nitro)phenylethanol with 53% *ee*. Then **BTA (R)-Cha** was added in order to invert the enantiomeric bias in the mixture (-33% *ee* in favor of **BTA (R)-Cha**, run 2) and thus the handedness of the co-assemblies. The same protocol was reproduced in order to get 4 successive runs corresponding to three switches of the selectivity. The full inversion of the selectivity observed for each consecutive run confirms that the enantiomeric state of the catalyst can be completely switched in situ (Figure I-16). In addition, thanks to the chirally-amplified nature of the helical scaffold, the selectivity of the different run (54% *ee* on average) is close to the optimal selectivity (63% *ee*) achievable under these experimental conditions. This constitutes a unique example of an enantiodivergent catalyst for which the direction of a one-pot reaction can be controlled in real time (part I.3).

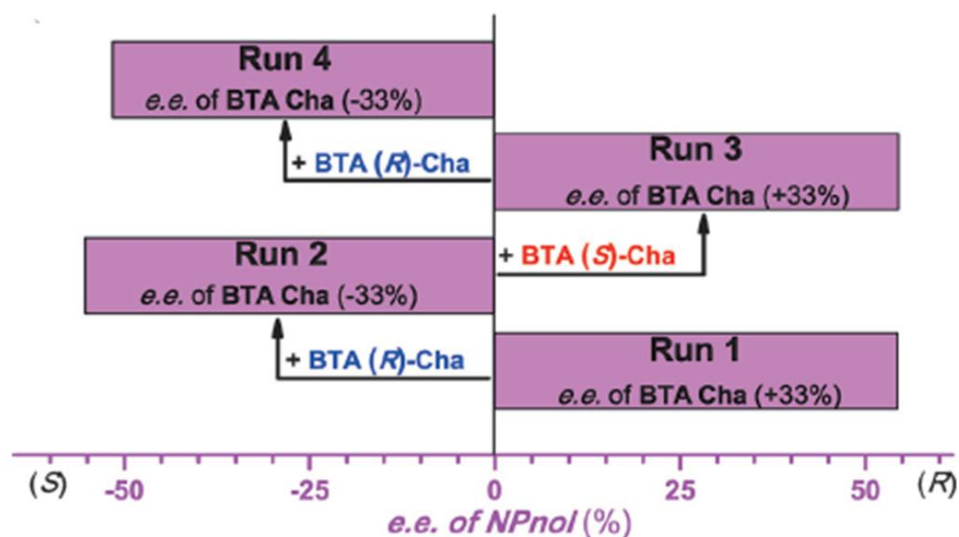
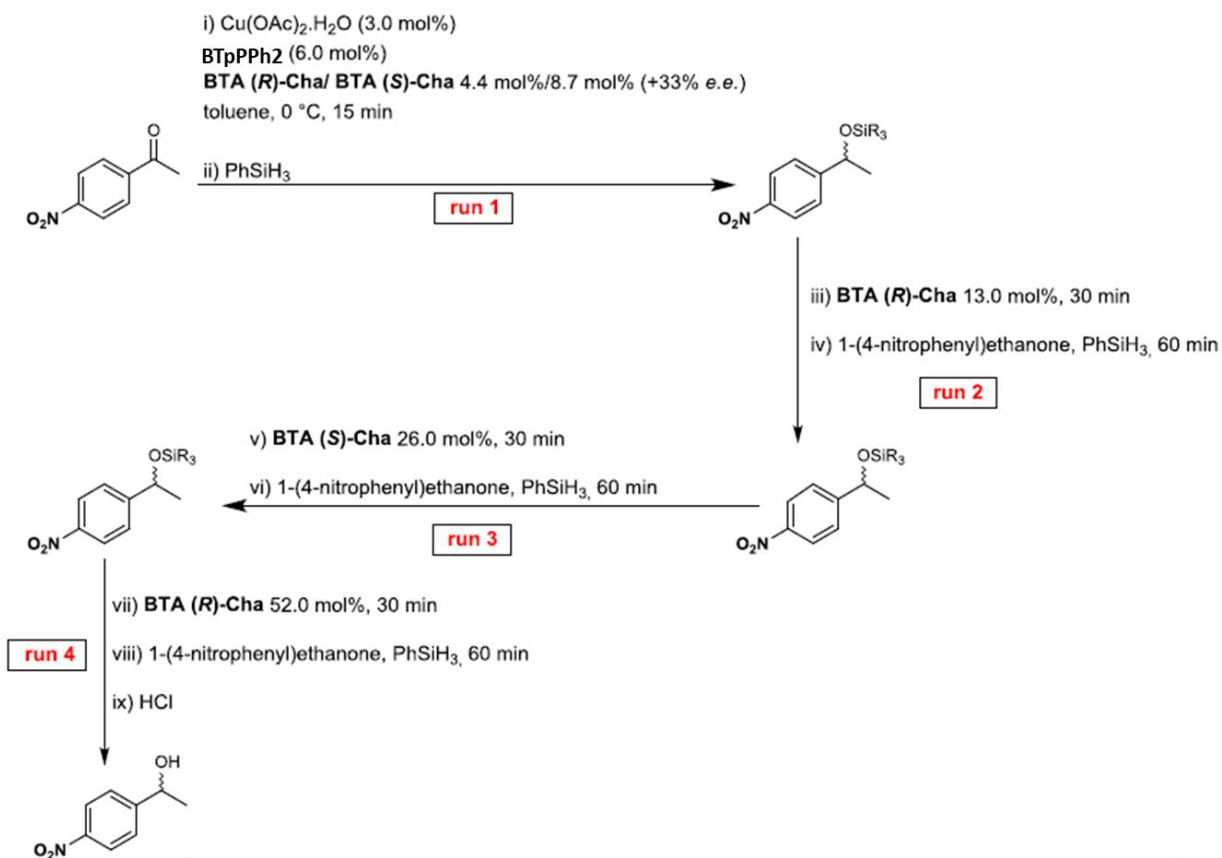


Figure I-16 Reaction conditions: 1-(4-nitrophenyl)ethanone (4×100 mol% = 400 mol% in total), $\text{Cu}(\text{OAc})_2 \cdot \text{H}_2\text{O}$ (3.0 mol%), **BTA-pPPh₂** (6.0 mol%), **BTA (R)-Cha/BTA (S)-Cha** (33% ee), PhSiH_3 (200 mol% for run 1 and then 100 mol% for run 2, run 3 and run 4 = 500 mol% in total), toluene, 0 °C. Conversion >99% was obtained for all runs as determined by GC and ^1H NMR analyses. Adapted from reference^[80].

I.4. In situ control of product configuration by means of switchable asymmetric catalysts.

We will discuss in this part the rare examples of switchable asymmetric catalysts that have been applied in the context of achieving stereodivergency, *i.e.* the control of the configuration of consecutively formed stereogenic centers.

I.4.a. With two (pseudo) enantiomeric catalysts.

An interesting approach that has been also explored by Leigh and coworkers^[81] includes the possibility of controlling the activity of two orthogonal and switchable asymmetric catalysts. A complementary pair of enantioselective catalysts was designed and synthesized by varying the position of the light-triggered switching unit present in their framework (*E* or *Z*). As a consequence, for the same conditions employed, one catalyst could be switched ON while the other one is switched OFF.

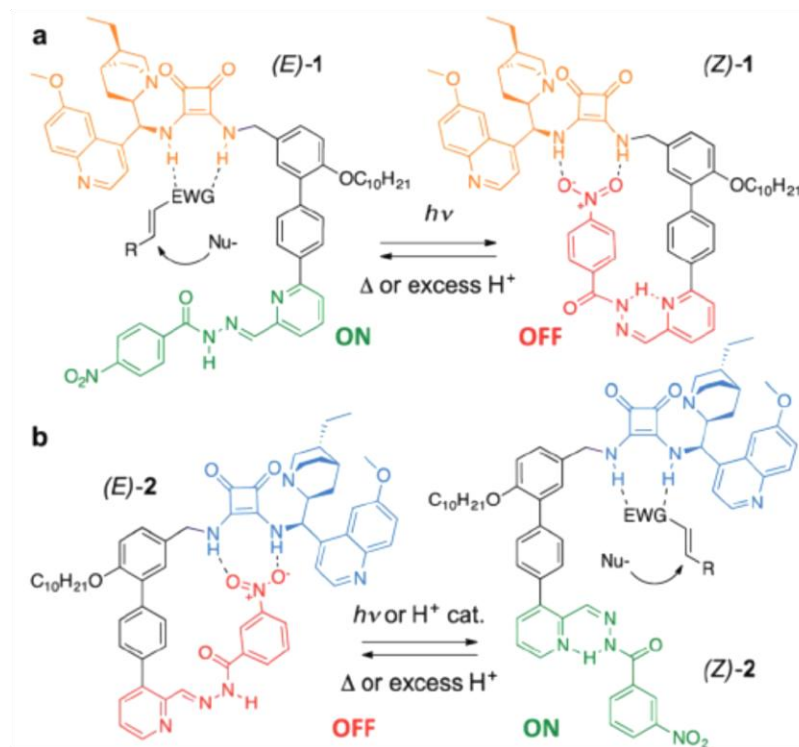


Figure I-17 A pair of enantioselective switchable bifunctional organocatalysts^[81].

Each catalyst contains a bifunctional cinchona alkaloid-squaramide motif as the active center, accompanied with a nitrobenzene moiety as a hydrogen bond acceptor (Figure I-17). The *E/Z*

isomerisation of a pyridyl-acyl hydrazone linker is used to switch the activity ON/OFF. For catalyst (**E**)-1, the active state (ON) is converted to the inactive state OFF (**Z**)-1 by operating the switch with UV light which leads to the binding of the squaramide by the nitro group (Figure I-17a). Catalyst (**E**)-2 is inactive and turns to the ON state when the same stimulus is used since in that case the isomerisation process forces the nitro group to point out away from the squaramide unit (Figure I-17b). Various stimuli (light, heat, or pH) can be used to switch between the two states giving ON:OFF ratios of up to 98:2 and 1:99. The catalysts were first evaluated individually. In their ON states, each catalyst promotes Michael additions with an enantiomeric ratio (er) of up to 95:5 and conversions between 70%-95%. The OFF states also catalyze the reaction to some extent, since a given amount of the complementary catalyst is present after the switching event, but the activity is significantly lower. This strategy developed for the complementary pair of switchable enantioselective catalysts is highly attractive if it could be utilized for both catalysts at the same time in the same reaction vessel so that the enantioselectivity of products can be controlled by switching OFF one catalyst while the same stimulus switches the pseudo-enantiomer ON. Unfortunately, when mixed together, the switchable organocatalysts remain inactive whatever the applied stimulus is. It is mentioned in literature that bifunctional cinchona-squaramide catalysts have an affinity to aggregate, and it appears that for those two catalysts, the OFF state of one of them binds to the ON state of the other catalyst, preventing catalysis by either state of either member of the catalyst pair. This inhibiting association between the catalysts must be taken into consideration for future designs of complementary pairs of switchable enantioselective catalysts.

I.4.b. By two catalysts anchored on the rotating arm of a substrate.

In 2017, Leigh and coworkers designed and developed an artificial molecular machine^[82] with two pseudo enantiomeric sites separated by a dynamic connector accompanied with an arm to hold the substrate and move it sequentially between the two chiral catalytic sites.

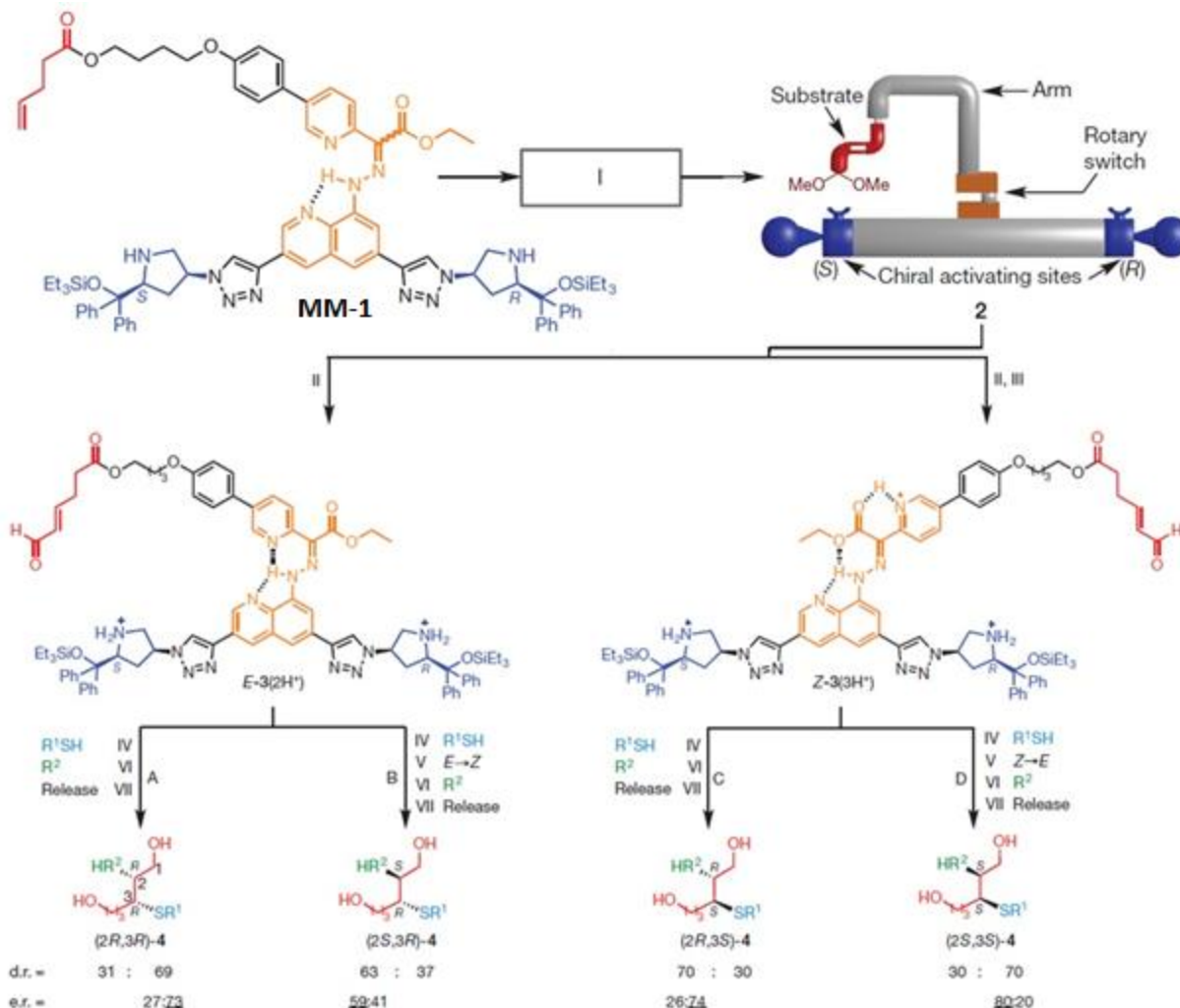


Figure I-18 Molecular structure of **MM-1** and schematic representation of the molecular machine components. Programmable stereodivergent synthesis of all possible stereoisomers of **4** from a one-pot tandem iminium–enamine promoted reaction sequence by molecular machine. Reagents and conditions: II, CF₃COOH (2.2 equiv.), room temperature, 10 min, CD₂Cl₂ (1 mM); III (*E* → *Z*), CF₃COOH (3.0 equiv.), room temperature, 5 h, CD₂Cl₂ (1 mM); IV, R¹SH (100 equiv.), 0 °C, 30–41 h, CD₂Cl₂ (1 mM); V (*E* → *Z*), CF₃COOH (6.0 equiv.), 0 °C, 20 h, CD₂Cl₂ (1 mM); V (*Z* → *E*), Et₃N (7.0 equiv.), 120 μl CD₃CN, 0 °C, 6 h, CD₂Cl₂ (1 mM); VI, R² (200 equiv.), 0 °C, 24 h, CD₂Cl₂ (1 mM); VII, NaBH₄, MeOH, 0 °C, 2 h, CD₂Cl₂ (1 mM), then LiAlH₄, THF, –78 °C to room temperature, 1 h. Stages II–VI are carried out as a one-pot sequence. R¹ = (CH₂)₂(CF₂)₇CF₃. R² = H₂C=C(SO₂Ph)₂. Program sequences are as follows. **A**: I, II, IV, VI, VII; **B**: I, II, IV, V, VI, VII; **C**: I, II, III, IV, VI, VII; **D**: I, II, III, IV, V, VI, VII. Adapted from reference^[82].

The design of **MM-1** relies on pyridyl-acyl hydrazone switch appended with a rotating arm serving to anchor the substrate and a bottom part composed of the two pseudo-enantiomeric catalysts. A terminal alkene in the upper part of **MM-1** is responsible for the covalent

attachment of an α,β -unsaturated aldehyde substrate through a metathesis reaction which can be activated by the two prolinol silyl ethers present in the bottom part (Figure I-18)^[82]. When the rotary switch is steered, the substrate gets closer to one of the active sites it was steered towards. In consequence, the stereochemical outcome of a tandem transformation will depend on the position of the arm at each stage. In this regard, the molecular motor can be selectively controlled through different sequences of inputs, since the hydrazone configuration can be varied from 4:1 *E*:*Z* to 1:9 *E*:*Z* under the conditions of machine operation.

The envisaged cascade reaction with this molecular machine was related to the stereodivergent strategy developed by MacMillan and co-workers for the formal α -hydrofluorination of enals mentioned in Figure I-13^[24], except that in the present case all stereoisomers are expected to be obtained in a one-pot protocol. The cascade reaction consists here in the 1,4-addition of a thiol to the iminium activated enal followed by 1,2-addition of the electrophile $\text{H}_2\text{C}=\text{C}(\text{SO}_2\text{Ph})_2$ to the enamine intermediate. Four programs were conducted which consist in the anchoring of the substrate, performing the iminium-catalyzed step, switching between the *E* and *Z* isomers when needed, performing the enamine-catalyzed step and releasing the product from the molecular machine. The obtained results are summarized in Table I-1.

Program	Initial configuration state	Switch	Final configuration state	Stereoisomer obtained	ee (%)	dr (%)
A	<i>E</i> , (<i>S</i>)	-	<i>E</i> , (<i>S</i>)	(2 <i>R</i> , 3 <i>R</i>), <i>syn</i>	46	2.7
B	<i>E</i> , (<i>S</i>)	<i>E</i> → <i>Z</i>	<i>Z</i> , (<i>R</i>)	(2 <i>S</i> , 3 <i>R</i>), <i>anti</i>	18	1.7
C	<i>Z</i> , (<i>R</i>)	-	<i>Z</i> , (<i>R</i>)	(2 <i>R</i> , 3 <i>S</i>), <i>syn</i>	48	2.8
D	<i>Z</i> , (<i>R</i>)	<i>Z</i> → <i>E</i>	<i>E</i> , (<i>S</i>)	(2 <i>S</i> , 3 <i>S</i>), <i>anti</i>	60	2.8

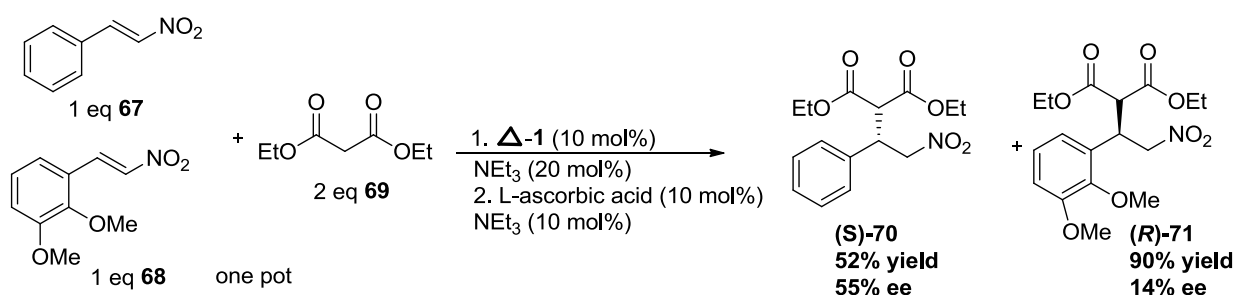
Table I-1 Result of the cascade reaction for the four states of the molecular machine.

The four programs yield the four stereoisomers as the major products albeit with modest enantio- and diastereoselectivities notably in the case of program **B**. Further looking at the configuration of the stereoisomers, it appears that the configuration of the first created stereogenic center, the C3 center, is related to the configuration of the amine catalyst, as it was expected. However, the configuration of the second generated center, the C2 center, depends on both the configuration at C3 and the configuration *E*/*Z* of the hydrazone switch. Accordingly,

when the switch is in the *E* configuration (programs **A** and **D**) the addition of R² to C2 occurs *syn* to the substituent at C3, whereas the *anti* diastereoisomer is generated when the switch is in the *Z* state (programs **B** and **C**). This contrasting behavior of the two configurational states of the machine presumably results from the temporarily formed macrocyclic intermediates produced upon enamine formation having different conformations, sizes and shapes on the different sides of the machine. This effect and the non-ideal ratio of *Z* and *E* isomers translates into an imperfect stereodivergent process. Obviously, designing a stereodivergent catalytic molecular machine for which the substrate and catalysts are coupled in the same framework is a challenge.

I.4.c. With a single asymmetric catalyst.

In 2015, Canary and coworkers utilized the redox-switchable catalyst^[83] mentioned in Part **I.3.b** to control the stereochemical outcome during the transformation of 1:1 mixture of two substrates. The stereochemical switch was achieved in situ, depending on the oxidation state of the catalyst during the course of the reaction. Two nitrostyrene reactants with different reactivities were engaged with the same Michael donor. The first dynamic reaction was performed using *L*-ascorbic acid to reduce Δ -1 to Λ -1 during the course of the reaction (Scheme I-29).

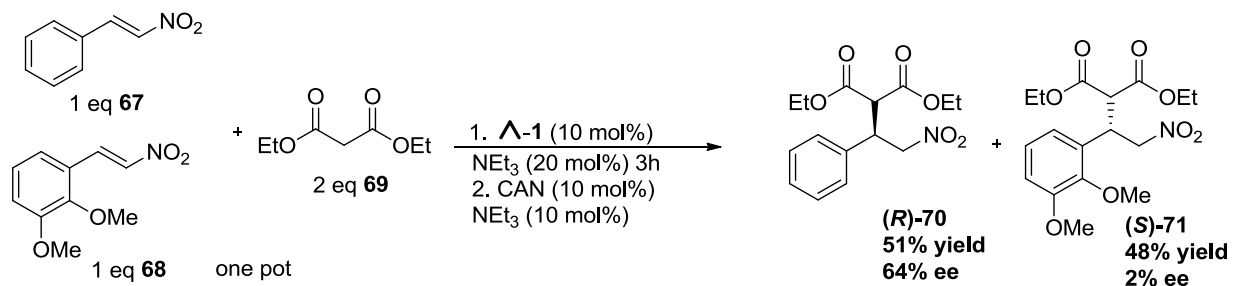


Scheme I-29 Dynamic catalysis performed with the ambidextrous catalyst. The in situ reduction of the catalyst leads to chiral products with opposite absolute configurations [(**S**)-**70** and (**R**)-**71**]^[83].

Kinetic studies indicated that nitrostyrene **67** was mostly consumed after three hours in the presence of Δ -1 and triethylamine. The reactants were added to the flask and allowed to react for three hours before 10 mol% of *L*-ascorbic acid was added to reduce the catalyst. The reduction was monitored qualitatively by a color change of the solution from green (Δ -1) to

yellow (**A-1**). As hypothesized, the products were obtained in the opposite absolute stereochemistry, albeit with lower enantiomeric excess notably for the product formed in second step. The (**S**)-**70** product was obtained in 55% *ee*, and the (**R**)-**71** product was obtained in 14% *ee* (Scheme I-29).

The reaction was also performed in the opposite direction, using **A-1** which was oxidized by CAN after three hours (Scheme I-30). Nitroalkane (**R**)-**70** was obtained in 64% *ee* while the (**S**)-**71** product was attained with only 2% *ee*. The yield of both addition products was low, possibly due to side reactions with CAN. This is considered as a limitation for this approach. It appears that all four permutations of possible stereochemical products in the reaction can be obtained with some degree of selectivity, but still this system suffers from drawbacks related to the low yields obtained and low enantiomeric excess values, especially for products obtained after the switch.



Scheme I-30 Dynamic catalysis upon oxidation of **A-1** to obtain products of opposite absolute configuration [(**R**)-**70** and (**S**)-**71**]^[83].

Another approach was explored based on the aforementioned switchable BTA helical catalysts^[80]. This time, the catalyst has been also evaluated in the copper-catalyzed hydrosilylation reaction of a 1:1 mixture of two different substrates with different reactivities (4-nitro-acetophenone, **NPnone**, and 4-biphenyl-acetophenone, **PPnone**) (Figure I-19).

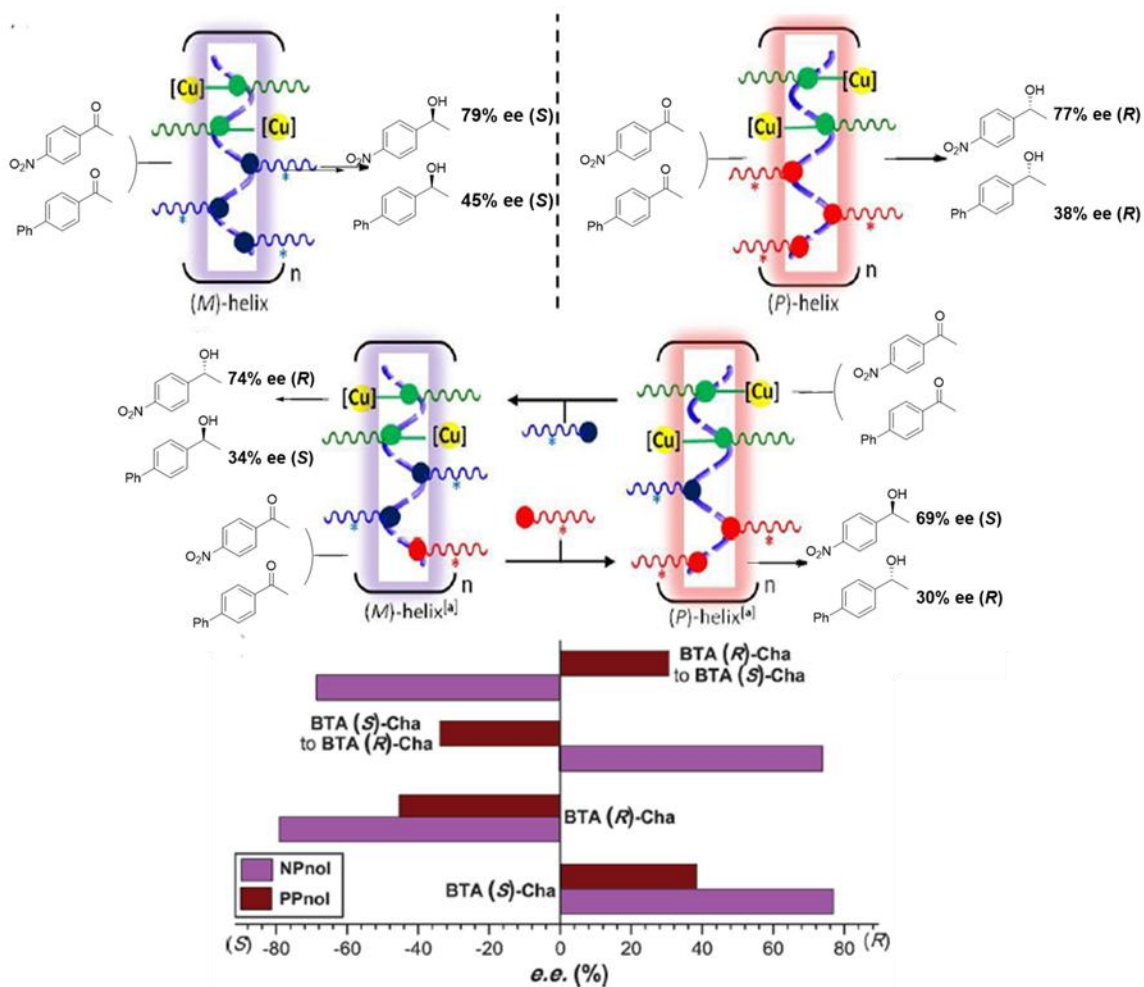


Figure I-19 Copper-catalyzed hydrosilylation of a 1:1 mixture of NPnone and PPnone by switchable BTA helical catalysts. For the selectivity inverting experiments, 20.0 mol% of BTA Cha was added during the reaction. Adapted from reference^[80].

The authors performed two experiments with enantiopure co-monomers (**BTA (S)-Cha** and **BTA (R)-Cha**) and two selectivity-inverting experiments starting with a scalemic mixture of enantiopure co-monomers (+60%ee → -60%ee and -60%ee → +60%ee). As expected, 1-(4-nitrophenyl)-ethanol (**NPnol**), and 1-(4-biphenyl)ethanol (**PPnol**) were obtained with the same preferred configuration, that is, predominantly (*R*) or (*S*), when the reaction was conducted with a single enantiomer of the BTA co-monomer (Figure I-19). More precisely, the experiment performed in the presence of **BTA (S)-Cha** (respectively **BTA (R)-Cha**) provided the alcohols with optimal selectivities: +77%/+38% ee (respectively -79%/-45% ee) for **NPnol** and **PPnol**. In contrast, the alcohols were obtained with an opposite preferred configuration, for example,

one is predominantly (*R*) whilst the other is predominantly (*S*), when the enantiomer in excess in the co-assemblies was changed during the course of the catalytic reaction (Figure I-19). Any combination of the enantiomers is thus obtained in a one-pot procedure without significant diminishing of the catalyst selectivity thanks to chirality amplification through the diluted MR effect.

The aforementioned approaches constitute interesting strategies to control the configuration of consecutively formed stereogenic centers but achieving stereodivergency in one-pot process with a single catalyst has not been accomplished yet.

I.5. Description and objectives of the project.

As mentioned above, controlling the formation of multiple stereogenic centers in terms of both relative and absolute configuration remains a big challenge for chemists. Thus, developing new and efficient approaches towards stereodivergent synthesis is essential. Among the existing strategies, asymmetric cascade reactions are attractive for developing diastereodivergent methods and controlling the stereoselectivity in a predictable manner. Buchwald and coworkers have introduced a fully stereodivergent approach for accessing all possible stereoisomers of a set of 1,3-amino alcohols via a two-step copper-catalyzed cascade reaction. This method was presented in Scheme I-15. Readily available enols or enals were hydrosilylated to produce allylic alcohols in the first step and addition of an amine electrophile reagent in the second step promotes the formation of the amino alcohol. This strategy is fully stereodivergent, the stereogenic centers are not created at the same time, thanks to the sequential addition of reagents. A limitation of this approach is that the allylic alcohol intermediate must be isolated in order to access the stereoisomers that require a different configuration of the catalyst for the two steps of the cascade reaction. Our overview of the state-of-the-art indicates that one-pot stereodivergent catalysis by means of a single catalyst has not been achieved despite the fundamental interest and practical advantages of such an approach.

In parallel, helical BTA supramolecular catalysts have shown their efficiency in asymmetric catalysis, and high levels of enantioselectivity have been obtained when BTA catalysts have been employed in rhodium-catalyzed hydrogenation and copper-catalyzed hydrosilylation

reactions^[72,80,84]. Importantly, the configuration of the product in these reactions is related to the handedness of the helical assemblies. The dynamic nature of the assemblies was exploited to switch and tune the selectivity of consecutive catalytic reactions by designing a dynamic catalytic system capable of switching its selectivity in real time by addition of an excess of a chiral co-monomer^[80]. The selectivity-switchable capability of this catalytic system has been also evaluated in the copper-catalyzed hydrosilylation reaction of a 1:1 mixture of two different substrates^[80].

Inspired by these two precedents, the final objective of my thesis is to develop a stereodivergent approach by exploiting the dynamic properties of the switchable helical BTA catalysts in order to access all possible stereoisomers of an amino alcohol in a one-pot manner (Figure I-20).

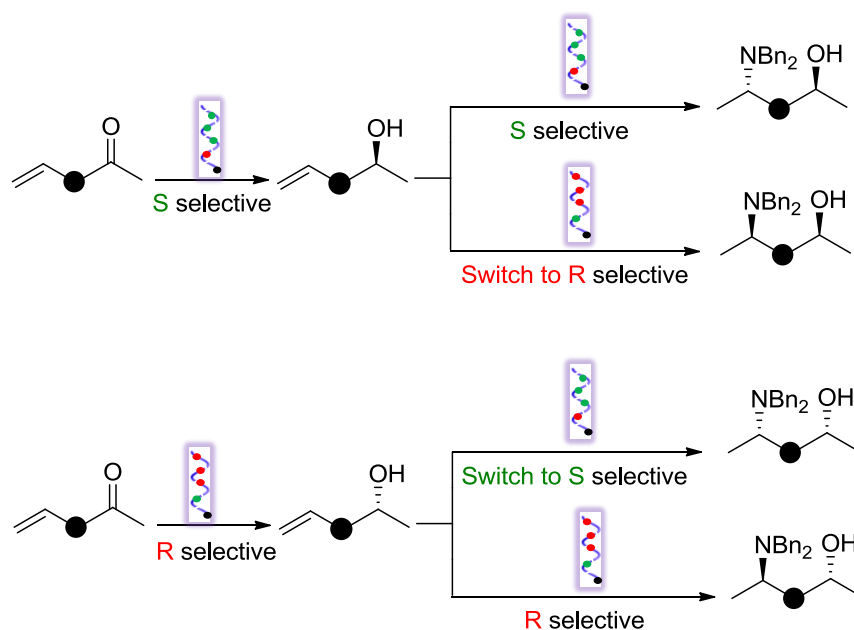


Figure I-20 Targeted one-pot copper-hydride catalyzed hydrosilylation and hydroamination of readily available enones.

Considering the efficiency of the BTA helical catalyst in the copper-catalyzed hydrosilylation of acetophenone derivatives, a hydrosilylation/hydroamination cascade reaction similar to the one developed by Buchwald is reported. Starting by a model substrate bearing two functionalities (carbonyl and vinyl), we expect that the copper-catalyzed reaction in presence of

silane precursor at room temperature will reduce selectively the carbonyl functionality to generate the chiral allylic alcohol species. The same copper catalyst will then be engaged in the hydroamination of the vinyl moiety in presence of an amine electrophile. Thanks to the diluted MR effect, the handedness of the helices will be switched or not in order to access the four stereoisomers (Figure I-20).

The challenges associated with the main objective of the thesis can be summarized as follows:

1. BTA co-assemblies that are efficient for the copper-catalyzed hydroamination reactions have to be developed. It is anticipated here that the BTA ligand has to be re-designed in order to get a better control of the coordination sphere of the copper complexes. Indeed, copper-catalyzed hydroamination proceeds efficiently for a limited number of phosphine ligands, notably those bearing substituents at the 3, 4, and 5 positions of the aryl rings connected to the P atom^[85–92]. For this purpose, a novel class of phosphine-containing BTA ligands has been synthesized, characterized, and evaluated in a reaction of reference (**Chapter II**).
2. This new set of ligands was tested in the hydroamination of styrene as well as for the hydrosilylation/hydroamination cascade of different enones (**Chapter III**).
3. The aforementioned concept was implemented in hydrosilylation/hydroamination cascade reaction starting from vinyl acetophenone derivatives (**Chapter IV**). Herein, a particular attention will be paid to the challenges associated with our concept: i) the independent reactivity of the vinyl and ketone functions, ii) the sequential transformation of these two functions, iii) the chirality amplification properties of the helical catalyst, and iv) the rapidity of the stereochemical switch.

I.6. References.

- [1] C. G. Wermuth, *The Practice of Medicinal Chemistry*, Academic Press, **2015**.
- [2] A. Anighoro, J. Bajorath, G. Rastelli, *J. Med. Chem.* **2014**, *57*, 7874–7887.
- [3] J. U. Peters, *J. Med. Chem.* **2013**, *56*, 8955–8971.

- [4] H. Yamamoto, A. Pfaltz, E. N. Jacobsen, *Comprehensive Asymmetric Catalysis*, Springer-Verlag Berlin Heidelberg, **1999**.
- [5] E. Carreira, H. Yamamoto, *Comprehensive Chirality - 1st Edition*, Elsevier Science, **2012**.
- [6] S. Krautwald, E. M. Carreira, *J. Am. Chem. Soc.* **2017**, *139*, 5627–5639.
- [7] A. B. Northrup, D. W. C. MacMillan, *J. Am. Chem. Soc.* **2002**, *124*, 6798–6799.
- [8] M. L. Hofferberth, R. Brückner, *Angew. Chem. Int. Ed.* **2014**, *53*, 7328–7334.
- [9] C. John, G. Zhao, M. Bihani, *Adv. Synth. Catal.* **2017**, *359*, 534–575.
- [10] S. E. Denmark, S. K. Ghosh, *Angew. Chem. Int. Ed.* **2001**, *40*, 4759–4762.
- [11] E. M. C. Lisbet Kvaerno, *Classics in Stereoselective Synthesis*, Angewandte Chemie International Edition, **2009**.
- [12] Y. Wang, X. Liu, L. Deng, *J. Am. Chem. Soc.* **2006**, *128*, 3928–3930.
- [13] B. Wang, F. Wu, Y. Wang, X. Liu, L. Deng, *J. Am. Chem. Soc.* **2007**, *129*, 768–769.
- [14] X. Tian, C. Cassani, Y. Liu, A. Moran, A. Urakawa, P. Galzerano, E. Arceo, P. Melchiorre, *J. Am. Chem. Soc.* **2011**, *133*, 17934–17941.
- [15] N. Maulide, M. Luparia, *Angew. Chem. Int. Ed.* **2011**, *50*, 12631–12635.
- [16] G. Lu, T. Yoshino, H. Morimoto, S. Matsunaga, M. Shibasaki, *Angew. Chem. Int. Ed.* **2011**, *50*, 4382–4385.
- [17] J. Y. Hamilton, D. Sarlah, E. M. Carreira, *J. Am. Chem. Soc.* **2014**, *136*, 3006–3009.
- [18] J. Y. Hamilton, D. Sarlah, E. M. Carreira, *Angew Chem Int Ed* **2013**, *52*, 7532–7535.
- [19] M. A. Schafroth, D. Sarlah, S. Krautwald, E. M. Carreira, *J. Am. Chem. Soc.* **2012**, *134*, 20276–20278.
- [20] C. Defieber, M. A. Ariger, P. Moriel, E. M. Carreira, *Angew. Chem. Int. Ed.* **2007**, *46*, 3139–3143.
- [21] O. F. Jeker, A. G. Kravina, E. M. Carreira, *Angew Chem Int Ed* **2013**, *52*, 12166–12169.
- [22] B. Bhaskararao, R. B. Sunoj, *J. Am. Chem. Soc.* **2015**, *137*, 15712–15722.

- [23] S. Krautwald, M. A. Schafroth, D. Sarlah, E. M. Carreira, *J. Am. Chem. Soc.* **2014**, *136*, 3020–3023.
- [24] Y. Huang, A. M. Walji, C. H. Larsen, D. W. C. MacMillan, *J. Am. Chem. Soc.* **2005**, *127*, 15051–15053.
- [25] S. L. Shi, Z. L. Wong, S. L. Buchwald, *Nature* **2016**, *532*, 353–356.
- [26] Q. Zhang, D.-H. Qu, *ChemPhysChem* **2016**, *17*, 1759–1768.
- [27] S. Erbas-Cakmak, D. A. Leigh, C. T. McTernan, A. L. Nussbaumer, *Chem. Rev.* **2015**, *115*, 10081–10206.
- [28] J. P. Sauvage, *Angew. Chem. Int. Ed.* **2017**, *56*, 11080–11093.
- [29] J. F. Stoddart, *Angew. Chem. Int. Ed.* **2017**, *56*, 11094–11125.
- [30] C. Cheng, J. F. Stoddart, *ChemPhysChem* **2016**, *17*, 1780–1793.
- [31] V. Blanco, D. A. Leigh, V. Marcos, *Chem. Soc. Rev.* **2015**, *44*, 5341–5370.
- [32] B. A. F. Le Bailly, L. Byrne, J. Clayden, *Angew. Chem. Int. Ed.* **2016**, *55*, 2132–2136.
- [33] A. J. Teator, D. N. Lastovickova, C. W. Bielawski, *Chem. Rev.* **2016**, *116*, 1969–1992.
- [34] D. N. Lastovickova, H. Shao, G. Lu, P. Liu, C. W. Bielawski, *Chem. – Eur. J.* **2017**, *23*, 5994–6000.
- [35] A. J. Teator, C. W. Bielawski, *J. Polym. Sci. Part Polym. Chem.* **2017**, *55*, 2949–2960.
- [36] G. Romanazzi, L. Degennar, P. Mastrorilli, R. Luisi, *ACS Catal.* **2017**, *7*, 4100–4114.
- [37] S. Mortezaei, N. R. Catarineu, X. Duan, C. Hu, J. W. Canary, *Chem. Sci.* **2015**, *6*, 5904–5912.
- [38] S. Mortezaei, N. R. Catarineu, J. W. Canary, *J. Am. Chem. Soc.* **2012**, *134*, 8054–8057.
- [39] G. Storch, O. Trapp, *Angew. Chem. Int. Ed.* **2015**, *54*, 3580–3586.
- [40] J. Wang, B. L. Feringa, *Science* **2011**, *331*, 1429–1432.
- [41] D. Zhao, T. M. Neubauer, B. L. Feringa, *Nat. Commun.* **2015**, *6*, 6652.
- [42] L. Pauling, R. B. Corey, H. R. Branson, *Proc. Natl. Acad. Sci.* **1951**, *37*, 205–211.

- [43] J. D. Watson, F. H. C. Crick, *Nature* **1953**, *171*, 737–738.
- [44] E. Yashima, K. Maeda, H. Iida, Y. Furusho, K. Nagai, *Chem. Rev.* **2009**, *109*, 6102–6211.
- [45] B. Jeong, A. Gutowska, *Trends Biotechnol.* **2002**, *20*, 305–311.
- [46] Y. Okamoto, K. Suzuki, K. Ohta, K. Hatada, H. Yuki, *J. Am. Chem. Soc.* **1979**, *101*, 4763–4765.
- [47] E. Yashima, K. Maeda, H. Iida, Y. Furusho, K. Nagai, *Chem. Rev.* **2009**, *109*, 6102–6211.
- [48] C. Fouquey, J.-M. Lehn, A.-M. Levelut, *Adv. Mater.* **1990**, *2*, 254–257.
- [49] M. M. L. Nieuwenhuizen, T. F. A. de Greef, R. L. J. van der Bruggen, J. M. J. Paulusse, W. P. J. Appel, M. M. J. Smulders, R. P. Sijbesma, E. W. Meijer, *Chem. – Eur. J.* **2010**, *16*, 1601–1612.
- [50] M. M. Green, M. P. Reidy, R. J. Johnson, G. Darling, D. J. O’Leary, G. Willson, *J. Am. Chem. Soc.* **1989**, *111*, 6452–6454.
- [51] J. Kim, J. Lee, W. Y. Kim, H. Kim, S. Lee, H. C. Lee, Y. S. Lee, M. Seo, S. Y. Kim, *Nat. Commun.* **2015**, *6*, 6959.
- [52] E. Yashima, N. Ousaka, D. Taura, K. Shimomura, T. Ikai, K. Maeda, *Chem. Rev.* **2016**, *116*, 13752–13990.
- [53] Y. Nagata, T. Nishikawa, M. Suginome, *J. Am. Chem. Soc.* **2015**, *137*, 4070–4073.
- [54] Y. Nagata, T. Yamada, T. Adachi, Y. Akai, T. Yamamoto, M. Suginome, *J. Am. Chem. Soc.* **2013**, *135*, 10104–10113.
- [55] T. Yamamoto, R. Murakami, M. Suginome, *J. Am. Chem. Soc.* **2017**, *139*, 2557–2560.
- [56] Y. Nagata, T. Nishikawa, M. Suginome, *J. Am. Chem. Soc.* **2014**, *135*, 5901–15904.
- [57] T. Yamada, Y. Nagata, M. Suginome, *Chem. Commun.* **2010**, *46*, 4914–4916.
- [58] T. Yamamoto, Y. Akai, Y. Nagata, M. Suginome, *Angew. Chem. Int. Ed.* **2011**, *50*, 8844–8847.

- [59] T. Yamamoto, T. Yamada, Y. Nagata, M. Suginome, *J. Am. Chem. Soc.* **2010**, *132*, 7899–7901.
- [60] Y. Akai, T. Yamamoto, Y. Nagata, T. Ohmura, M. Suginome, *J. Am. Chem. Soc.* **2012**, *134*, 11092–11095.
- [61] T. Yamamoto, T. Adachi, M. Suginome, *ACS Macro Lett.* **2013**, *2*, 790–793.
- [62] Y. Akai, L. Konnert, T. Yamamoto, M. Suginome, *Chem. Commun.* **2015**, *51*, 7211–7214.
- [63] Y. Nagata, T. Nishikawa, M. Suginome, *Chem. Commun.* **2018**, *54*, 6867–6870.
- [64] Y. Nagata, T. Nishikawa, M. Suginome, *ACS Macro Lett.* **2016**, *5*, 519–522.
- [65] A. R. A. Palmans, E. W. Meijer, *Angew. Chem. Int. Ed.* **2007**, *46*, 8948–8968.
- [66] M. Liu, L. Zhang, T. Wang, *Chem. Rev.* **2015**, *115*, 7304–7397.
- [67] S. Cantekin, T. F. A. de Greef, A. R. A. Palmans, *Chem. Soc. Rev.* **2012**, *41*, 6125.
- [68] L. Brunsveld, A. P. H. J. Schenning, M. a. C. Broeren, H. M. Janssen, J. a. J. M. Vekemans, E. W. Meijer, *Chem. Lett.* **2000**, *29*, 292–293.
- [69] M. M. J. Smulders, T. Buffeteau, D. Cavagnat, M. Wolffs, A. P. H. J. Schenning, E. W. Meijer, *Chirality* **2008**, *20*, 1016–1022.
- [70] M. P. Lightfoot, F. S. Mair, R. G. Pritchard, J. E. Warren, *Chem. Commun.* **1999**, 1945–1946.
- [71] X. Caumes, A. Baldi, G. Gontard, P. Brocorens, R. Lazzaroni, N. Vanthuyne, C. Troufflard, M. Raynal, L. Bouteiller, *Chem. Commun.* **2016**, *52*, 13369–13372.
- [72] A. Desmarchelier, X. Caumes, M. Raynal, A. Vidal-Ferran, P. W. N. M. van Leeuwen, L. Bouteiller, *J. Am. Chem. Soc.* **2016**, *138*, 4908–4916.
- [73] A. Desmarchelier, M. Raynal, P. Brocorens, N. Vanthuyne, L. Bouteiller, *Chem. Commun.* **2015**, *51*, 7397–7400.
- [74] A. Desmarchelier, B. G. Alvarenga, X. Caumes, L. Dubreucq, C. Troufflard, M. Tessier, N. Vanthuyne, J. Idé, T. Maistriaux, D. Beljonne, P. Brocorens, R. Lazzaroni, M. Raynal, L. Bouteiller, *Soft Matter* **2016**, *12*, 7824–7838.

- [75] C. Yuan, J. Jiang, H. Sun, D. Wang, Y. Hu, M. Liu, *ChemCatChem* **2018**, *10*, 2190–2194.
- [76] J. Jiang, Y. Meng, L. Zhang, M. Liu, *J. Am. Chem. Soc.* **2016**, *138*, 15629–15635.
- [77] Q. Jin, L. Zhang, H. Cao, T. Wang, X. Zhu, J. Jiang, M. Liu, *Langmuir* **2011**, *27*, 13847–13853.
- [78] M. Raynal, F. Portier, P. W. N. M. van Leeuwen, L. Bouteiller, *J. Am. Chem. Soc.* **2013**, *135*, 17687–17690.
- [79] M. Raynal, P. Ballester, A. Vidal-Ferran, P. W. N. M. van Leeuwen, *Chem Soc Rev* **2014**, *43*, 1660–1733.
- [80] J. M. Zimbron, X. Caumes, Y. Li, C. M. Thomas, M. Raynal, L. Bouteiller, *Angew. Chem. Int. Ed.* **2017**, *56*, 14016–14019.
- [81] G. De Bo, D. A. Leigh, C. T. McTernan, S. Wang, *Chem. Sci.* **2017**, *8*, 7077–7081.
- [82] S. Kassem, A. T. L. Lee, D. A. Leigh, V. Marcos, L. I. Palmer, S. Pisano, *Nature* **2017**, *549*, 374–378.
- [83] S. Mortezaei, N. R. Catarineu, J. W. Canary, *Tetrahedron Lett.* **2016**, *57*, 459–462.
- [84] Y. Li, A. Hammoud, L. Bouteiller, M. Raynal, *J. Am. Chem. Soc.* **2020**, *142*, 5676–5688.
- [85] S. Zhu, N. Niljianskul, S. L. Buchwald, *Nat. Chem.* **2016**, *8*, 144–150.
- [86] S. Ichikawa, S. Zhu, S. L. Buchwald, *Angew. Chem. Int. Ed.* **2018**, *57*, 8714–8718.
- [87] S. L. Shi, S. L. Buchwald, *Nat. Chem.* **2015**, *7*, 38–44.
- [88] Y. Miki, K. Hirano, T. Satoh, M. Miura, *Angew. Chem. Int. Ed.* **2013**, *52*, 10830–10834.
- [89] S. Tobisch, *Chem. Eur. J.* **2016**, *22*, 8290–8300.
- [90] D. Niu, S. L. Buchwald, *J. Am. Chem. Soc.* **2015**, *137*, 9716–9721.
- [91] J. S. Bandar, M. T. Pirnot, S. L. Buchwald, *J. Am. Chem. Soc.* **2015**, *137*, 14812–14818.
- [92] A. A. Thomas, K. Speck, I. Kevlishvili, Z. Lu, P. Liu, S. L. Buchwald, *J. Am. Chem. Soc.* **2018**, *140*, 13976–13984.

Chapter II : Phosphine-containing BTA ligands with various aryl groups on the phosphorous atom: Synthesis, characterization, assembly behavior, and implementation in asymmetric copper-catalyzed hydrosilylation of 1-(4-nitrophenyl)ethanone.

Abstract: The synthesis of nine new phosphine-containing BTA ligands is disclosed. These newly designed BTA ligands differ from the previously employed **BTA-pPPh₂** ligand by the nature of the substituents present on the aryl groups attached to the phosphorous atom. These ligands present different electronic and steric properties. The design of these BTA ligands also considered the possible ligand substrate interactions which might arise in the transition state of the copper-catalyzed hydroamination reaction. Accordingly, electron-donating and electron-withdrawing groups were introduced at the 3- and 5- positions of the aryl groups. A common synthetic route was followed by means of a three-step synthetic procedure, which allowed obtaining the final BTA ligands on hundreds of mg or gram scale. These newly designed BTA ligands were implemented in the copper-catalyzed hydrosilylation of 1-(4-nitrophenyl)ethanone in presence of very limited amount of **BTA Cha** as chiral co-monomer (0.5%). Significant selectivity was displayed (up to 90% ee) when **BTA-P(Xylyl)₂** was employed in presence of **BTA cyclohex** in the catalytic mixture.

II.1. Introduction:

II.1.a. Synthesis and importance of BTAs.

The design and the synthesis of functional molecules that grow into one-dimensional superstructures led to the emergence of the supramolecular polymer field. These polymers constitute ordered structures which possess tunable properties arising from the non-covalent interactions between the constituting parts^[1]. Benzene-1,3,5-

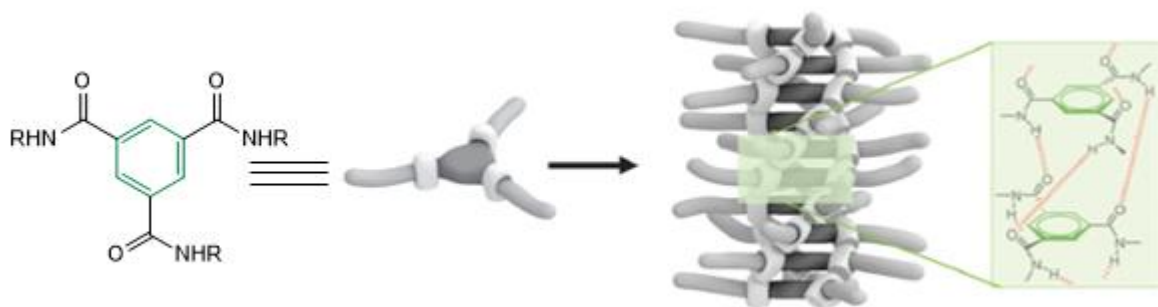
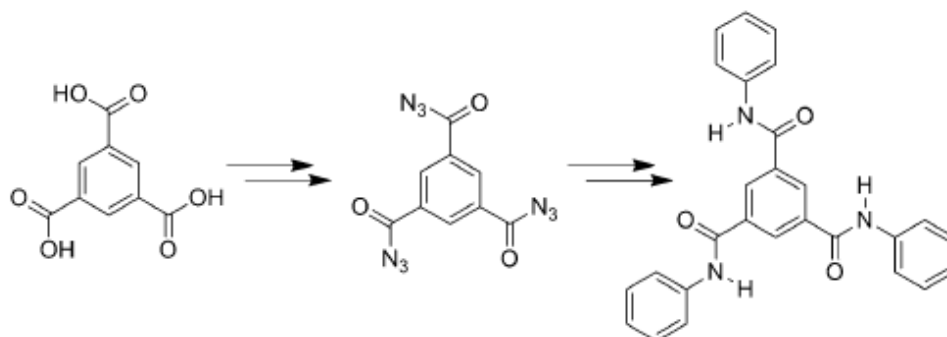


Figure II-1 General structures of benzene-1,3,5-tricarboxamide, and their self-assembly into helical one-dimensional aggregates, which are stabilized by threefold intermolecular H-bonding.

tricarboxamides abbreviated as BTAs are found in a distinguishable design comprising three C=O-centered amide moieties responsible for providing a hydrogen bond donor/acceptor platform, connected on the 1,3,5 positions of a benzene core involved in π - π stacking interactions (Figure II-1)^[2]. Under selected conditions, these weak interactions promote the growth of the monomers into one-dimensional supramolecular polymers, which attracted a lot of attention in the last two decades. The **R** groups attached to the periphery of the amide functionality can be aliphatic or aromatic, polar or apolar, charged or neutral, chiral or achiral. When these **R** groups are identical, then the BTA molecule possesses a C_3 axis of symmetry. The first symmetrical BTA (sBTA) molecule was synthesized and reported in 1915 by Curtius^[3] (Scheme II-1) by utilizing benzene-1,3,5-tricarboxylic acid (trimesic acid) as the starting material to furnish later a tri-ester, which is used to generate an explosive triacyl triazide. The latter is treated with aniline to form a triphenyl substituted BTA as shown in Scheme II-1. Because this method requires utilization of highly explosive intermediates, it was restricted to a small-scale preparation. For this reason, Rohm and Haas patented in 1956 the preparation of the tris-

(vinylxyethyl) BTA analogue, via an amidation reaction between trimethyl benzene-1,3,5-tricarboxylate and 2-vinylxyethylamine^[4].

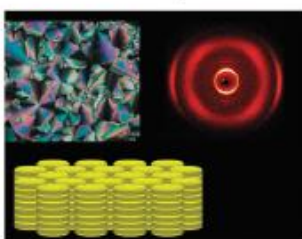


Scheme II-1 Synthesis of the first BTA molecule by Curtius. Adapted from reference^[3].

But, also this method suffered from some drawbacks, since the amidation reaction requires high reaction temperature and long reaction time^[4]. Another synthetic route relies on treating trimesic acid with highly reactive thionyl chloride to obtain the acid chloride precursor, which is later reacted with an amine at room temperature to yield tris(*ortho*-nitrophenyl) BTA more efficiently^[5]. Meanwhile, the most common synthetic strategy to prepare C=O-centered BTAs relies on a straightforward route based on reacting trimesoyl chloride with the appropriate amine in presence of a base^[6,7]. Nevertheless, appropriate coupling agents are still often used to directly functionalize a trimesic acid precursor with the appropriate amine to furnish the desired sBTAs^[8].

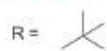
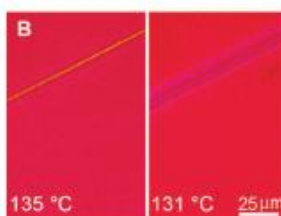
sBTA structures have been synthesized with different **R** groups, such as alkyl^[9], aryl^[10], pyridyl^[11], bipyridyl^[12], porphyrinyl^[13], triphenyl^[14], oligo(*p*-phenylenevinylene)^[15], amino acid^[16], dipeptide^[17], oligopeptide^[18], oligo(ethyleneoxy)^[19], and benzocrown ethers^[20]. These BTA derivatives have found applications in a wide range of domains including organogels, hydrogels, liquid crystals, nanostructured materials, MRI contrast reagents, nucleating agents for polymers, metal complexation reagents and microcapsules for drug delivery (Figure II-2)^[2].

B. Thermotropic LC's

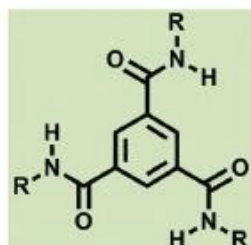
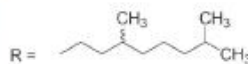


R = C₆H₁₃ to C₁₈H₃₇

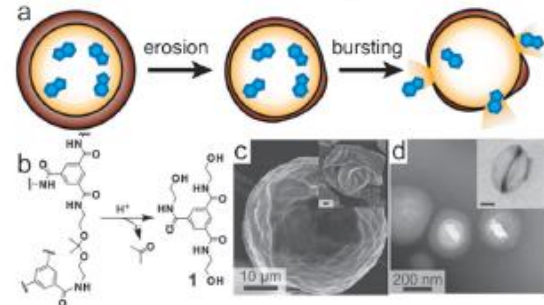
A. Nucleating agents for *i*PP



C. Organogels



E. Microcapsules



D. MRI contrast agents

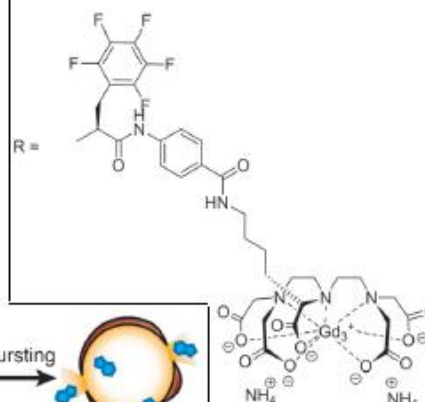
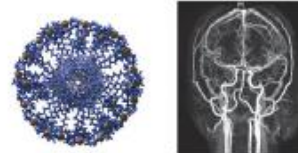
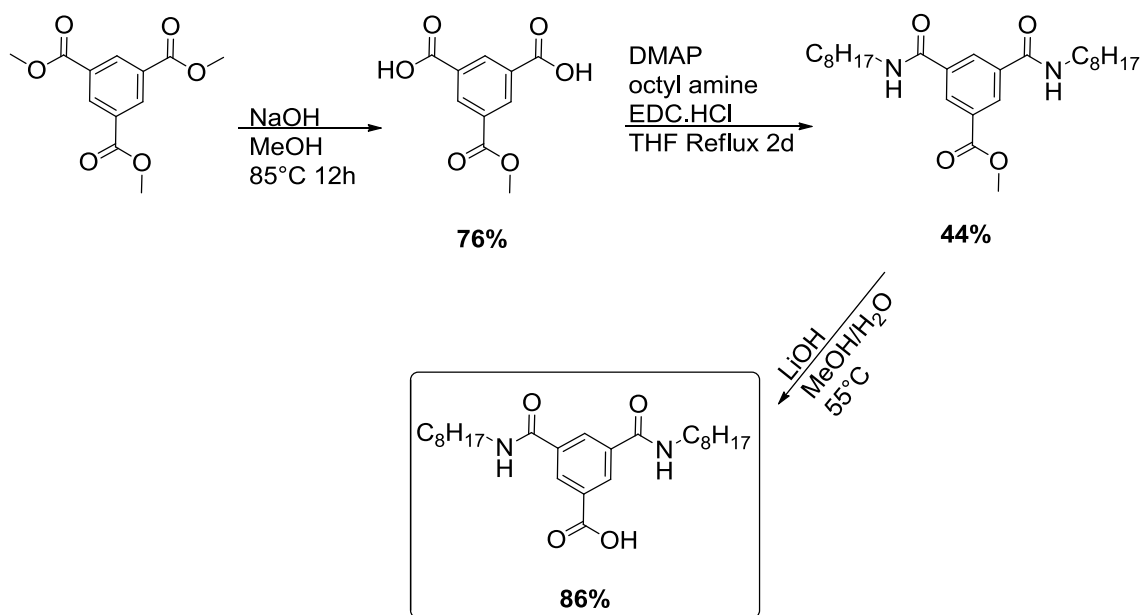


Figure II-2 An overview of the application areas for BTAs. Different side chains attached to the BTAs result in different properties^[2].

In short, C₃-symmetric BTA monomers are easily prepared through direct functionalization of benzene-1,3,5-tricarboxylic acid or its acyl chloride derivative, and have found numerous applications in various fields of chemical sciences. On the other hand, breaking the C₃-symmetry of BTAs is highly desired to improve the solubility of the BTA monomers and to construct functional BTA assemblies. C₂-symmetric BTA monomers have notably been used in organic solvents as assembling ligands for performing asymmetric reactions^[21–25], as building blocks for the design of hierarchical structures^[26], and as pendant units to trigger the folding or self-assembly of polymer chains^[27–30]. For example, telechelic polymers such as poly(ethylene butylene), end-capped with BTAs, were used for soft rubbery materials^[31] because of the thermoplastic elastomeric behavior they possess, while poly(methacrylate)s with pendant BTA units have been used as nanoreactors for efficient catalysis^[32]. These desymmetrised BTAs (*dB*TAs) are obtained through the incomplete hydrolysis of trimethyl benzene-1,3,5-

tricarboxylate^[31], the partial esterification of trimesic acid^[33] or the stoichiometrically biased addition of alkyl amines to trimesoyl chloride^[34,35]; all of these routes are somewhat lengthy but each step is achieved with a reasonable yield^[36]. The route starting by the incomplete hydrolysis of trimethyl benzene-1,3,5-tricarboxylate has been depicted by Meijer and co-workers^[37] and later by our group^[24] for the preparation of *dBTA*s on the gram scale (Scheme II-2). Hydrolysis of this abundant and cheap starting material in methanol at 85°C for 12 h in presence of 2 equivalents sodium hydroxide yield 76% of 5-(methoxycarbonyl)isophthalic acid.



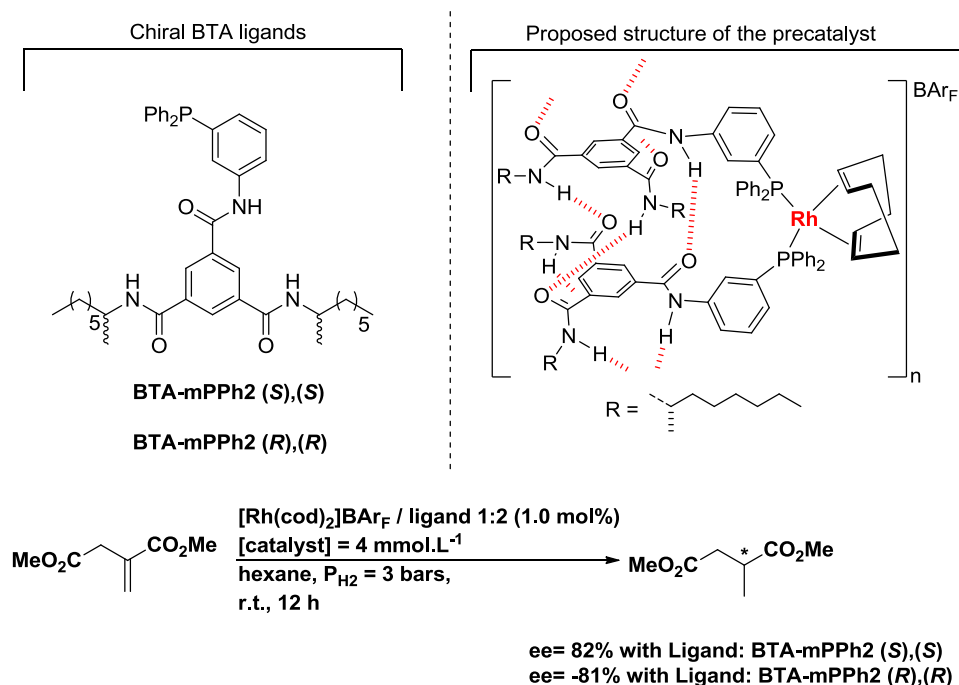
Scheme II-2 Synthesis of 3,5-bis(octylcarbamoyl)benzoic acid. Adapted from reference^[37].

This diacid is coupled with 2 equivalents of octylamine in THF in presence of DMAP and EDC·HCl at reflux temperature for 2 days to yield 44% of the corresponding diester. Its hydrolysis yields 3,5-bis(octylcarbamoyl)benzoic acid which can then be functionalized with the desired functional amine.

II.1.b. Helical BTA ligands for asymmetric reactions.

In 2013^[35], our group exploited the idea of modifying BTA structures, to design supramolecular catalysts based on BTA units. These supramolecular polymers appeared as promising scaffolds in catalysis for several reasons. First because of their **tunability**: the composition of supramolecular polymers can be easily modified by simply mixing complementary monomers.

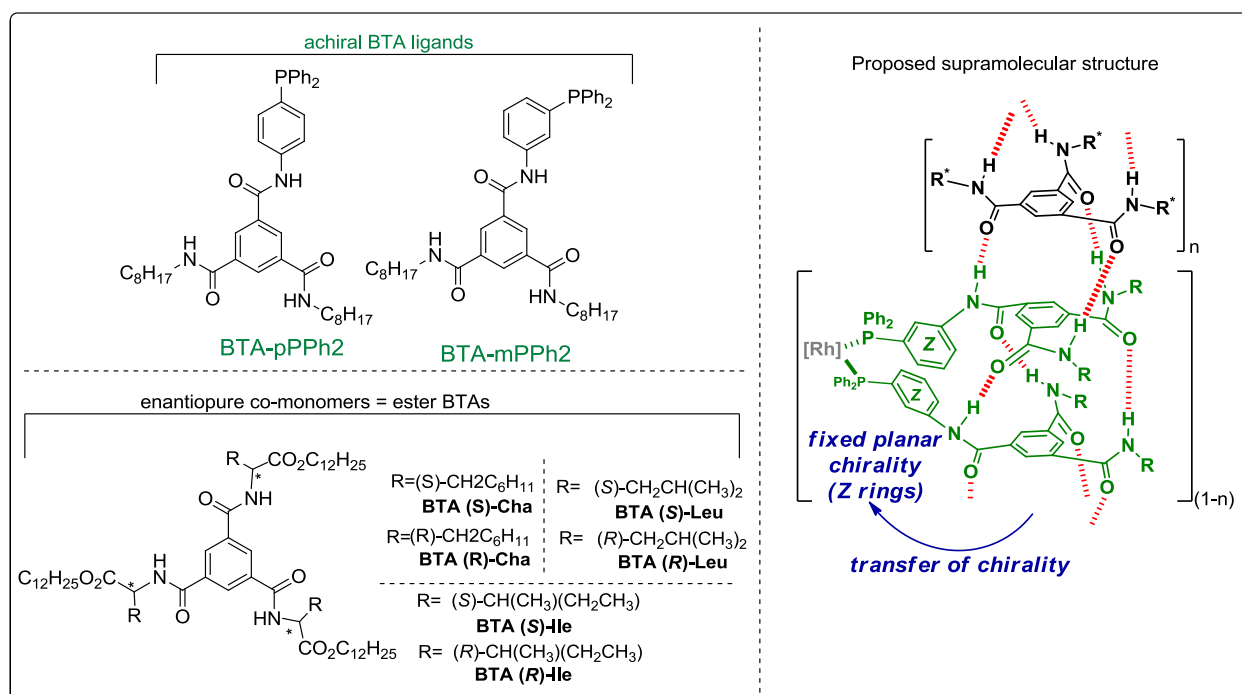
Secondly, because of their **chiral properties**: **1)** The induction of chirality from chiral building blocks to a supramolecular structure has been applied for construction of efficient asymmetric catalysts. **2)** Chirality amplification phenomenon which allow the formation of homochiral BTA helices even though constituted of non-optically pure monomers. Chirality amplification effects are particularly attractive in catalysis when a small number of chiral BTA molecules can impose their chirality to a larger number of catalytic centers. Hence, combining the above-mentioned properties would give rise to highly dynamic supramolecular BTA systems.



Scheme II-3 Chiral BTA ligands utilized for the rhodium-catalyzed hydrogenation of dimethyl itaconate. Proposed structure for the pre-catalyst derived from BTA-mPPh2 (S),(S). n , the degree of polymerization, depends on the reaction conditions; it is probably high in hexane, giving rise to a selective catalyst^[35].

These supramolecular catalysts were derived from BTA units by introducing a diphenylphosphine functionality (PPh_2) at the “*meta*” position of a phenylene linker which plays the role of a rigid connector between the introduced PPh_2 and amide functions (Scheme II-3). The introduced (PPh_2) functionality is able to coordinate to “soft” metal centers. These phosphine-containing BTA ligands were used as a chiral scaffold for the rhodium-catalyzed asymmetric hydrogenation of dimethyl itaconate^[35] (Scheme II-3). The aim was to transfer

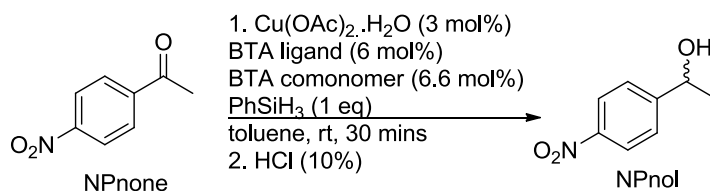
chirality from the helical supramolecular polymer formed by the BTAs to the catalytic rhodium center. The catalytic species were prepared by simply mixing the BTA ligand and the rhodium precursor in DCM. Evaporation of the DCM and suspension in hexane of the yellow solid gave the pre-catalysts used for the hydrogenation of dimethyl itaconate (Scheme II-3). With **BTA-mPPh₂ (S),(S)**, good selectivity was obtained (82% *ee*) even though the chiral centers are located 12 atoms away from the metal center. Opposite selectivity was obtained with the enantiomer of this BTA ligand (**BTA-mPPh₂ (R),(R)**, -81% *ee*). Control experiments and analytical data confirm that the selectivity stems from the formation of helically-biased supramolecular assemblies, not from dissociated chiral BTA ligands.



Scheme II-4 Left: structures of achiral BTA ligands, and of enantiopure chiral BTA ester co-monomers. Right: Proposed supramolecular **structure** for the catalysts and postulated mechanism for the chirality transfer^[38].

Later on, in 2016^[38] the possibility of applying the chiral amplification properties of BTA assemblies in asymmetric catalysis was exploited. In that context, a BTA ligand with achiral side chains was explored in presence of complementary ligand-free enantiopure monomers. Catalytic tests were performed with mixtures composed of **BTA-mPPh₂** ligand (see Scheme II-4

for ligand structure), a rhodium metal precursor, and an ester BTA for the same reaction^[38]. Ester BTAs were chosen as chiral co-monomers since they are derived from an important accessible chiral pool, and can be straightforwardly prepared in two synthetic steps. Hydrogen-bonded co-assemblies formed by the ester BTA co-monomer (**BTA Ile**, see Scheme II-4 for structure) and the intrinsically achiral catalytic rhodium catalyst, induced a chirality transfer providing the hydrogenation product with up to 85% *ee*. The amount of the BTA co-monomer (**BTA Ile**, the “sergeant”) can be decreased to one-fourth that of the ligand (the “soldier”) without deteriorating the selectivity of the reaction. It was the first example of the sergeants-and-soldiers effect in supramolecular helices applied to asymmetric catalysis. **BTA-mPPh₂**, but also **BTA-pPPh₂**, *i.e.* the BTA ligand with a PPh₂ moiety attached at the “*para*” position of the phenylene linker, were screened in the copper-catalyzed hydrosilylation of acetophenone derivatives^[24] (Scheme II-4).



Entry	BTA ligand	BTA co-monomer	ee (%)
1	BTA-pPPh₂ (S),(S)	none	48 %
2	BTA-mPPh₂ (S),(S)	none	25%
3	BTA-pPPh₂	BTA (S)-Cha	60%
4	BTA-mPPh₂	BTA (R)-Cha	11%
5	BTA-pPPh₂	BTA (S)-Leu	53%

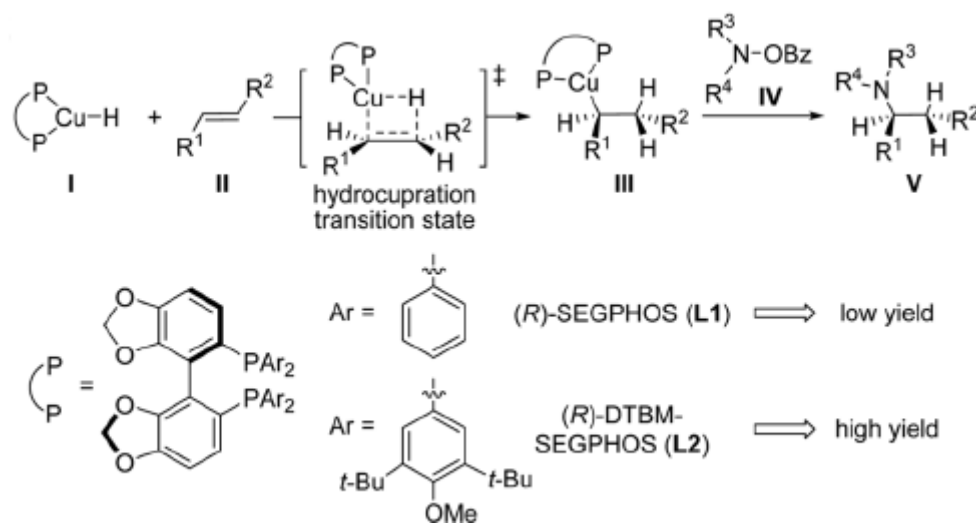
Table II-1 Reaction scheme of the hydrosilylation of 1-(4-nitrophenyl)ethanone (0.17 mmol, 0.3 M), Cu(OAc)₂·H₂O (3 mol%), BTA ligand (6 mol%), BTA comonomer (6.6 mol%), PhSiH₃ (1.0 eq), toluene (570 μL), room temperature, 30 min^[24].

These scaffolds were formed by mixing an achiral BTA ligand coordinated to copper metal with an enantiopure comonomer (“sergeants-and-soldiers”-type mixtures). When comparing the selectivity displayed by the chiral ligands **BTA-mPPh₂ (S),(S)** (25% *ee*) and **BTA-pPPh₂ (S),(S)** (48% *ee*) (entries 1, and 2: Table II-1), it clearly appears that the “*para*” position of the

phosphine relative to the linker had a great influence on the selectivity of the catalytic reaction. Furthermore, achiral **BTA-pPPh2** ligand was also superior to the achiral **BTA-mPPh2** in reactions conducted with an enantiopure co-monomer **BTA Cha** (entries 3, and 4, Table II-1). Higher reaction selectivity (60% *ee*) was obtained when **BTA-pPPh2** was employed as a ligand. It is suspected that the coordination sphere of the Cu is affected by the relative positions of the PPh₂ unit in the supramolecular helices. The location of the PPh₂ unit at the para position of the phenylene linker appears more suitable for generating a suitable chiral environment to the coordinated Cu-H species^[39].

II.1.c. Role of the ligand structure in catalyst design.

The successful outcome of transition-metal catalysis can largely be assigned to the development of structurally diverse ancillary ligands with tunable electronic and steric properties. Modifying the functional groups surrounding the binding site of any ligand has a huge impact on the performance of the catalyst in terms of efficiency and stereochemical outcome. These ligands act as templates that regulate reactions occurring in the coordination sphere of a metal ion^[40].



Scheme II-5 Ligand effects on reactivity of CuH-catalyzed hydroamination of unactivated olefins^[41].

A simplified mechanistic scheme of the copper-catalyzed hydroamination of olefins is shown in Scheme II-5.

Cu-H species **I** insert into the double bond of the olefin **II** via a hydrocupration transition state and yield an enantioenriched alkyl copper intermediate **III**. Up to now, this step has been established as the enantio-determining step^[41]. Afterwards, stereoretentive addition of amine electrophile **IV** into the formed alkyl copper furnishes the amine product **V** and a copper(I) benzoate intermediate that is subsequently reconverted to the CuH catalyst **I**. Non-activated aliphatic olefins were found to be challenging because of the slow rate of hydrocupration step with most Cu-H catalysts. It has been shown that only copper catalysts generated from bulky bidentate phosphine ligands (e.g., **DTBM-SEGPHOS (L2)** in Scheme II-5) are capable of facilitating the hydrocupration of these non-activated olefins^[41]. Cu-H catalysts coordinated to bulky bidentate phosphine ligands, such as **DTBM-SEGPHOS (L2)**, proved to be particularly efficient for these reactions. It was determined that dispersion interactions between the bulky tert-butyl groups attached on 3- and 5- positions of PAryl₂ and the substrate, greatly stabilize the hydrocupration transition state, thus significantly accelerating the overall rate of the reaction^[41].

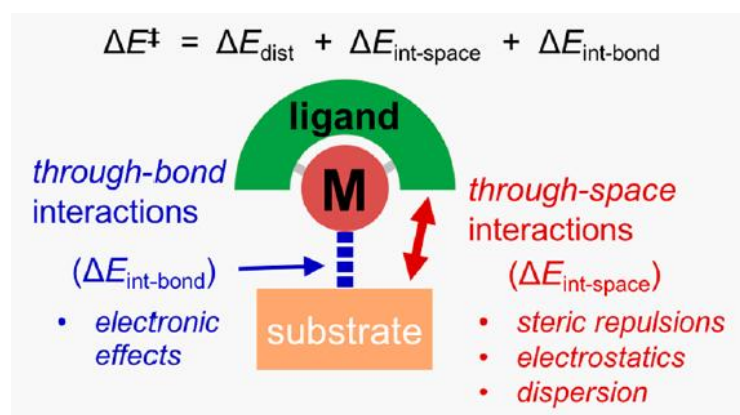


Figure II-3 Ligand-substrate interaction model to dissect activation energies, and study the origin of reactivity in hydrocupration. Through-space and through-bond interactions in transition metal catalysis^[42].

Furthermore, the authors employed energy decomposition analysis methods (Figure II-3), and were able to estimate and predict the individual energy contributions for the steric, electronic, and dispersion effects that constitute the hydrocupration barrier. They found that, the through space London dispersion interactions, electrostatic interactions, and through bond inductive effects of electron withdrawing substituents, all participate in lowering the energy barrier for

hydrocupration step^[42]. Thus, they decided first to modify the **DTBM-SEGPHOS (L2)** ligand by installing *i*-C₃F₇ moieties (Figure II-4a, **L3**). The resulting ligand *i*-C₃F₇-SEGPHOS (**L3**) was capable of providing a 61-fold rate increase compared to reactions carried with the **DTBM-SEGPHOS (L2)** in the hydroamination of non-activated terminal olefins^[42]. However, only a short burst of reactivity was observed. This suggests that the **L3Cu-H** complex, although an active catalyst, was not stable under the reaction conditions. This catalyst decomposition is most likely the consequence of the diminished Lewis basicity of the phosphorus atoms in **L3**, due to the electron-withdrawing nature of the *i*-C₃F₇ substituents which results in weaker binding to the copper center.

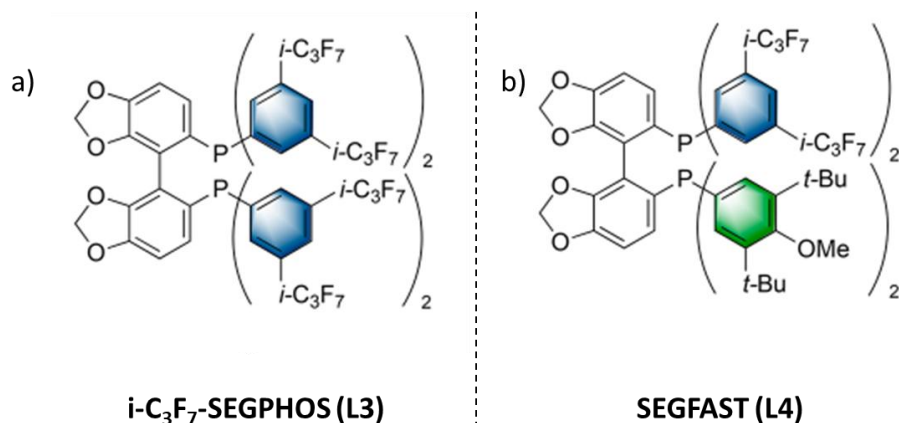


Figure II-4 **SEGPHOS** derivatives for the Cu-H catalyzed hydroamination reaction of non-activated terminal olefins. a) *i*-C₃F₇-SEGPHOS (**L3**), *i*-C₃F₇ moieties improves catalyst reactivity. b) **SEGFAST (L4)**, DTBM groups improve the stability of the catalyst, while *i*-C₃F₇ moieties improve its reactivity^[42].

To harness the increased reactivity observed using the *i*-C₃F₇ substituents without sacrificing the stability of the resulting complex, the authors decided to exchange one **PC₆H₃(*i*-C₃F₇)₂** substituent for a more electron-donating group in order to stabilize the resulting copper complex. Thus, they synthesized a new ligand **SEGFAST** (Figure II-4b, **L4**), which was also capable of providing a 62-fold rate increase compared to reactions carried with the **DTBM-SEGPHOS (L2)**^[42] in the hydroamination of non-activated terminal olefins^[42], and no detectable catalyst decomposition was observed. Both stability and reactivity of the catalyst were improved with **L4** through tuning of attractive noncovalent ligand–substrate interactions and of the electronic nature of the Cu center, respectively.

Recently, Hartwig and coworkers^[43] reported the incorporation of even larger substituents based on heavy main-group elements to enhance dispersion interactions. The authors prepared the chiral biaryl bisphosphine ligand (**TMG-SYNPHOS**) containing 3,5-bis(trimethylgermyl)phenyl groups on phosphorus and applied this ligand in the enantioselective copper-catalyzed hydroboration reaction of 1,1-disubstituted alkenes. The formed copper catalyst, was able to catalyze the hydroboration of 1,1-disubstituted alkenes with high levels of enantioselectivity (94:6 er), even when the two substituents on the alkene were both primary alkyl groups. Computational studies revealed that the enantioselectivity and catalytic efficiency of the germyl-substituted ligands are higher than that of the silyl and tert-butyl-substituted analogues because of attractive dispersion interactions between the bulky trimethylgermyl groups on the ancillary ligand and the alkene substrate (Figure II-5).

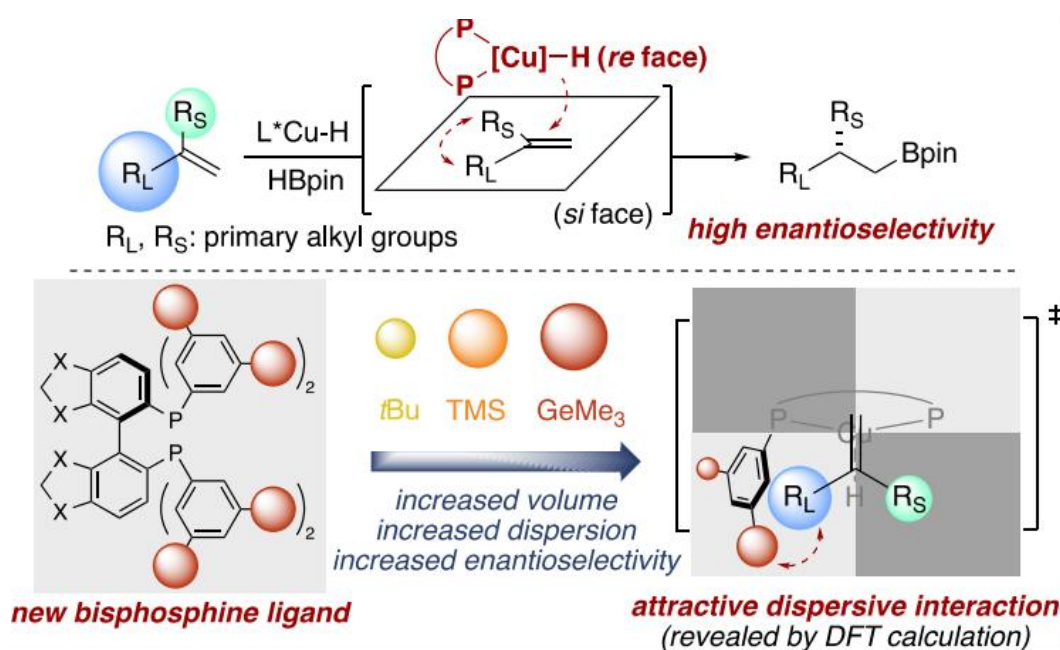
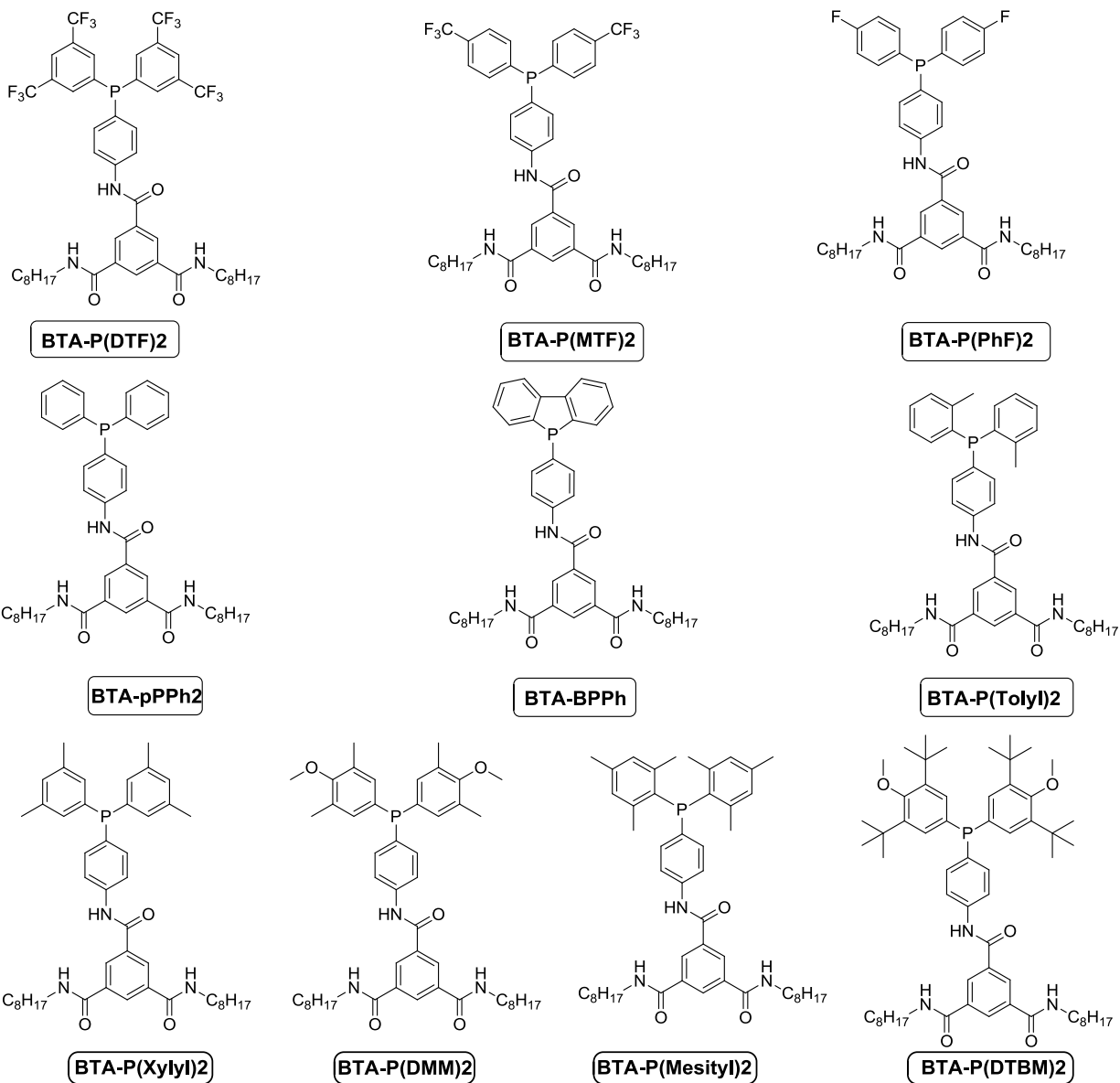


Figure II-5 New bisphosphine ligands developed by Hartwig based on incorporating large substituents for enhancing dispersion effects and thus improving overall reactivity in the hydroboration of alkenes^[43].

Obviously, the through bond-interactions mainly dominated by the electronic effects of the ligand have a huge impact on improving the reactivity of metal catalyzed reactions. In addition, through-space interactions expressed by dispersion interactions occurring between the bulky groups attached on 3- and 5- positions of the $PAryl_2$ and the substrate, could contribute

significantly in accelerating the overall rate of the reaction, notably in the case of reactions catalyzed by phosphine Cu-H species. These combined interactions are an important element of design for developing new efficient ligands for Cu-H catalysis.

II.1.d. Designing a new set of phosphine-containing BTA ligands.

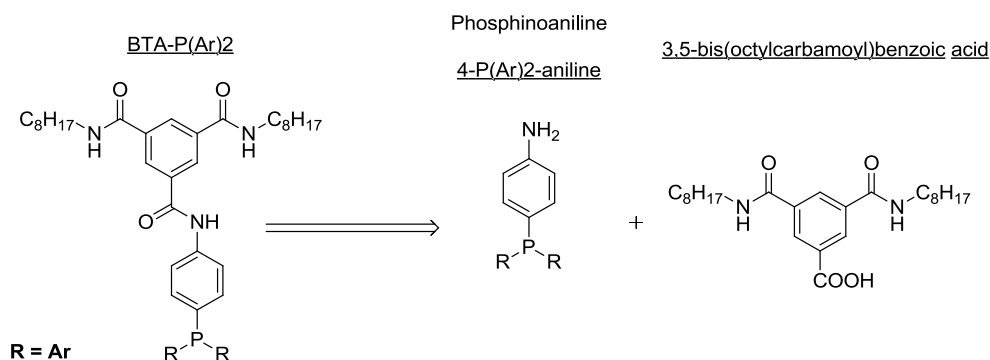


Scheme II-6 Chemical structure of the newly designed phosphine-containing BTA ligands. The ligands are approximately ranked according to their electronic nature: from the less electron rich on the upper left to the more electron rich to the bottom right. Obviously, steric effects are likely to play a key role in the coordination behavior of ligand with o-substituted aryl rings such as BTA-P(TolyI)2 and BTA-P(MesityI)2.

As demonstrated in section **II.1.b**, phosphine-containing BTA ligands, where diphenylphosphine (PPh₂) moiety is attached on the “para” position of the phenylene linker are more selective than those with a meta-linker for the copper-catalyzed hydrosilylation of **NPnone**. For this reason, “para” substitution on the phenylene linker was preferred for the design of our family of BTA ligands. Likewise, by considering the possibility of promoting catalyst-substrate interactions (through dispersion) during the hydrocupration step, most phosphine-containing BTA ligands will be modified at the **3,5** positions of phosphine-bound aryl groups (ex: **BTA-P(DTF)2**, **BTA-P(Xylyl)2**, **BTA-P(DMM)2**, and **BTA-P(DTBM)2**, Scheme II-6). Some other BTAs will be modified exclusively at the position **4** (ex: **BTA-P(MTF)2**, **BTA-P(Phf)2**), or position **2** (ex: **BTA-P(Tolyl)2**, **BTA-P(BPPh)**), or **2,4,6** positions (**BTA-P(Mesityl)2**). Steric effects are likely to play an important role in the cases of **BTA-P(Tolyl)2** and **BTA-P(Mesityl)2**. In order to tune the electronic properties of the ligand, EDGs and EWGs will be introduced on the phosphine aryl ring. In addition to these expected effects, the added groups on the aryl moieties, can highly affect the solubility of the ligands, and more importantly it can have a huge impact on the assembly formation mechanism, which is essential for inducing and improving chirality amplification effects. Thus, these added groups could have a huge impact on all aspects of the catalytic process (reactivity, selectivity for the catalytic part and chirality amplification for the supramolecular part). All synthesized BTA ligands are shown in Scheme II-6).

II.2. Synthesis of a new set of phosphine-containing BTA ligands

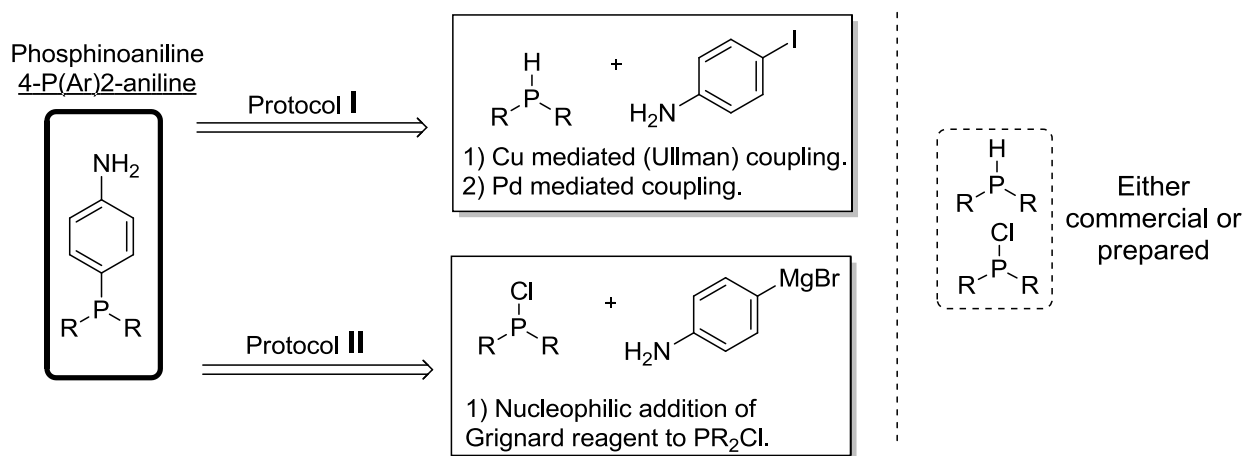
II.2.a. General retrosynthetic route.



Scheme II-7 General retro-synthetic method that divides the BTA ligand into two main fragments.

Fixing a unique synthetic route for furnishing all phosphine-containing BTA ligands presented in Scheme II-6 on a **gram scale** is highly essential. A retro-synthetic route was applied by cutting the BTA ligand into two main fragments, the phosphinoaniline fragment (**4-P(Ar)₂-aniline**), and the 3,5-bis(octylcarbamoyl)benzoic acid fragment (Scheme II-7). The latter compound is obtained through an efficient published procedure^[37] as shown in Scheme II-2.

For accessing different families of **4-P(Ar)₂-aniline** fragments, two protocols could be followed (**I** and **II**, Scheme II-8).

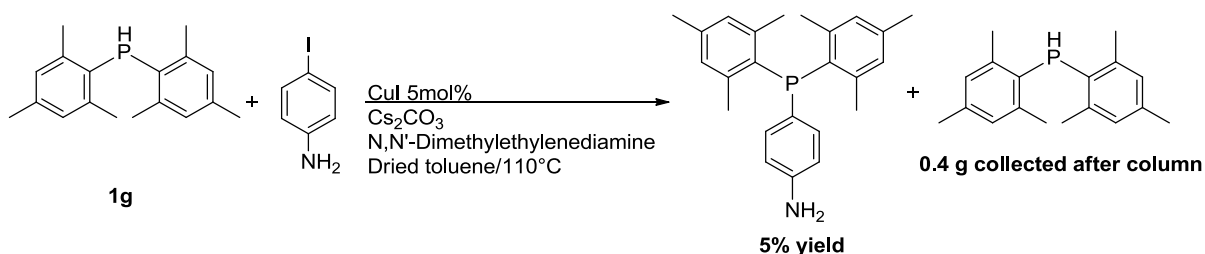


Scheme II-8 Two different protocols envisaged for accessing different families of phosphinoaniline fragments.

Protocol **I** is inspired from two procedures reported in literature. The first procedure is copper-mediated coupling (Ullman type) used for the synthesis of 4-(dicyclohexylphosphino)aniline^[44] (**4-P(Cyclohex)₂-aniline**), and the second procedure is a palladium-mediated coupling used for the synthesis of 4-(diphenylphosphino)aniline^[45] (**4-P(Ph)₂-aniline**) (Scheme II-8, **I**). The copper method was previously utilized by our group for the synthesis of **4-P(Ph)₂-aniline**, required for preparing **BTA-pPPPh₂**^[24]. Protocol **II** consists of a nucleophilic addition of Grignard reagent to PAr₂Cl precursor (Scheme II-8, **II**), inspired from a reported procedure used for the synthesis of 3-diphenylphosphinoaniline^[46] (**3-P(Ph)₂-aniline**). This procedure was previously followed by our group for the synthesis of **3-P(Ph)₂-aniline** required for preparing **BTA-mPPPh₂**^[38].

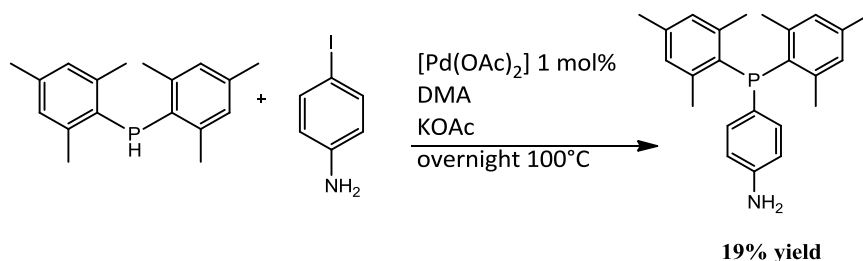
II.2.b. Synthesis of 4-P(Mesityl)2-aniline, 4-P(Ph)2-aniline, and 4-P(Xylyl)2-aniline via protocol I¹.

4-P(Mesityl)2-aniline: We attempted to synthesize 4-(dimesitylphosphino)aniline (**4-P(Mesityl)2-aniline**), through copper-mediated cross-coupling reaction between dimesitylphosphine and 4-iodoaniline (Scheme II-9). This coupling was carried out in presence of Cs₂CO₃, and N,N'-dimethylethylenediamine at 110°C in toluene for 13 h. The reaction provided the desired product in very low yield (5%). This low yield could be attributed to the low reactivity of the dimesitylphosphine since a significant amount of it was recovered after the reaction. The methyl groups at 2,4,6-positions of the aryl group impose some steric hindrance effects which lower the reactivity of the phosphine.



Scheme II-9 Copper-mediated cross coupling reaction for the synthesis of 4-P(Mesityl)2-aniline.

Considering the low yield in **4-P(Mesityl)2-aniline** by means of the Cu reaction, we envisioned to use the Pd cross-coupling process^[45] in presence of palladium acetate and KOAc, in DMA at 100°C. **4-P(Mesityl)2-aniline** was obtained in *ca.* 19% yield (Scheme II-10).

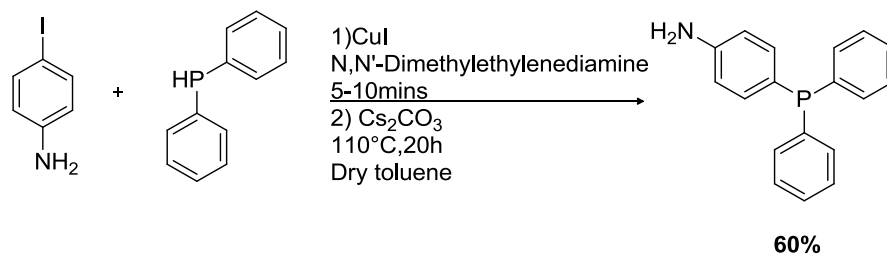


Scheme II-10 Palladium-mediated cross coupling reaction for the synthesis of 4-P(Mesityl)2-aniline.

¹ For experimental procedures (see Annex, subsection II.6.a).

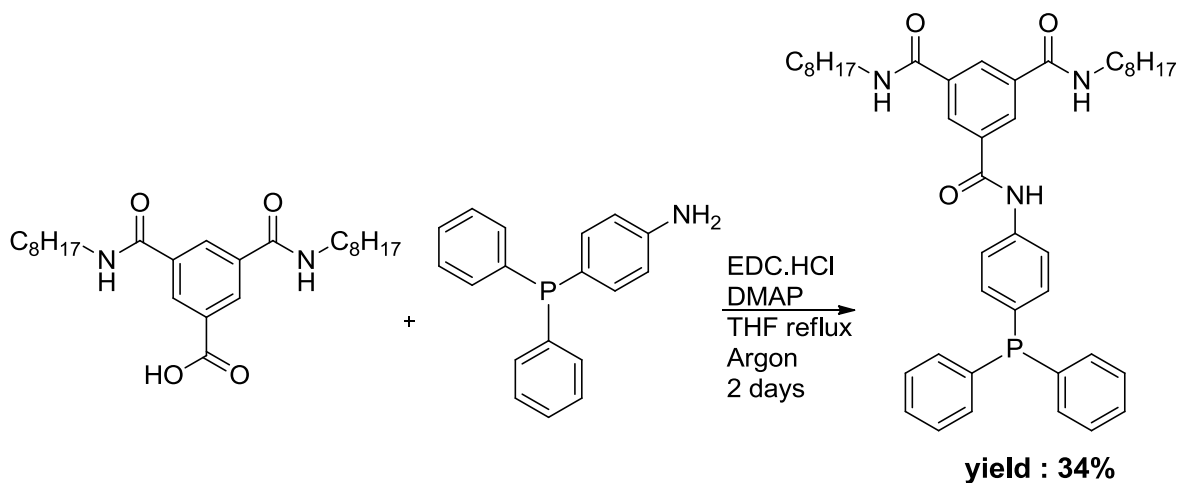
This low yield is again attributed to the low reactivity of dimesitylphosphine. The quantity of **4-P(Mesityl)2-aniline** obtained through this protocol was too low to engage in the subsequent step, *i.e.* the amide bond coupling reaction with bis(octylcarbamoyl)benzoic acid.

4-P(Ph)2-aniline: Again, through the copper-mediated cross-coupling reaction, we attempted to synthesize the classical **4-P(Ph)2-aniline**. The reaction between diphenylphosphine and 4-iodoaniline provided **4-P(Ph)2-aniline** in 60% yield (Scheme II-11).



Scheme II-11 Copper-mediated cross coupling reaction for the synthesis of **4-P(Ph)2-aniline**.

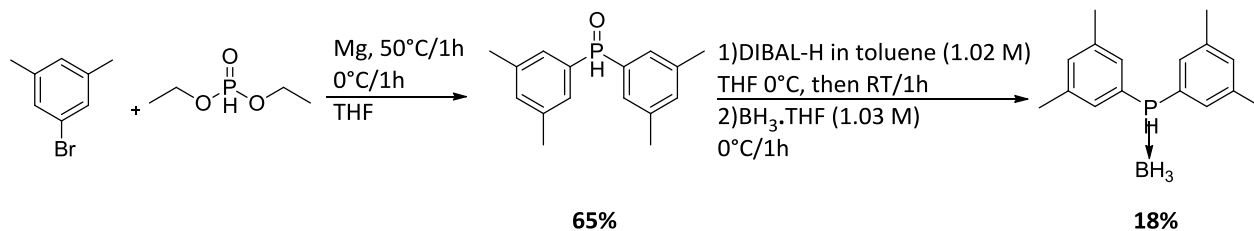
Obviously, the yield is higher than that obtained for **4-P(Mesityl)2-aniline** (5%) due the higher reactivity of **P(Ph)₂Cl** precursor. The obtained quantity was enough to engage in the subsequent step, *i.e.* the amide bond coupling reaction with bis(octylcarbamoyl)benzoic acid (Scheme II-12).



Scheme II-12 Amide bond forming reaction between **4-P(Ph)2-aniline** and bis(octylcarbamoyl)benzoic acid for the synthesis of **BTA-pPPh2**.

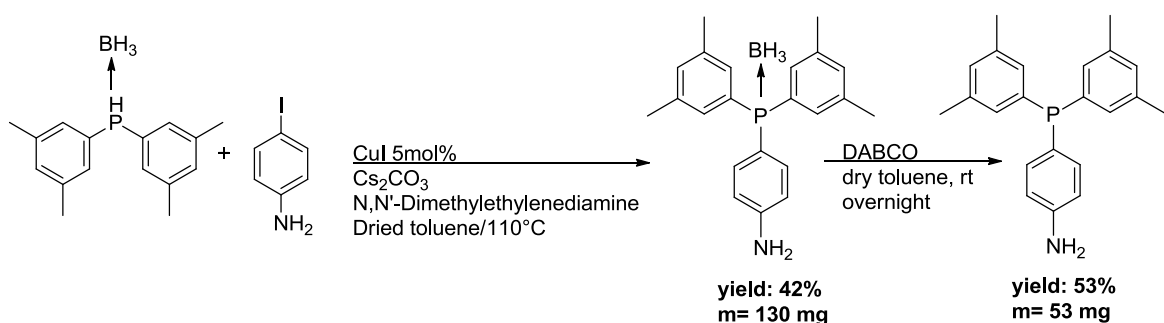
The final coupling reaction in THF in presence of EDC.HCl and DMAP at reflux temperature for 2 days provided **BTA-pPPh2** in 34% yield.

4-P(Xylyl)2-aniline: We investigated the possibility of constructing the whole scaffold of **4-P(Xylyl)2-aniline** through cheap and abundant starting materials. First, we attempted to synthesize bis(3,5-dimethylphenyl)phosphine by following a two-step procedure reported by Nakamura and coworkers^[47]. This procedure was used to synthesize the phosphine-borane adduct bis(3,5-dimethylphenyl)phosphine-BH₃ (Scheme II-13) as a stable precursor of the phosphine.



Scheme II-13 A synthetic route towards the synthesis of phosphine-borane adduct bis(3,5-dimethylphenyl)phosphine-BH₃^[47].

Following a reaction between 1-bromo-3,5-dimethyl benzene (5.0 g) and (EtO)₂POH in THF in presence of Mg turnings, bis(3,5-dimethylphenyl) phosphine oxide was obtained in 65% yield after purification by flash column chromatography over silica. A higher yield (≥96%) was reported in the original publication^[47], probably because the reaction was performed on a higher scale. The second step consists of reducing the phosphine oxide moiety to phosphine using DIBAL-H, and afterwards protecting the formed phosphine functionality (PH) as a borane adduct (BH₃) by the addition of a 1.06 M solution of BH₃.THF. A very poor yield was obtained for the final product (18%) compared to the reported one (78%), and this could be maybe attributed to the purity of reducing agent engaged in our reaction. However, the borane adduct was engaged in the synthesis of the corresponding phosphinoaniline (**4-P(Xylyl)2-aniline**) (Scheme II-14).



Scheme II-14 Copper mediated coupling for the synthesis of 4-P(Xylyl)₂-aniline-borane adduct^[47], followed by a deprotection step to release the borane (inspired from reference^[48]).

The copper-mediated coupling yielded 42% of **4-P(Xylyl)₂-aniline-borane** adduct (Scheme II-14). This yield is lower than that obtained with diphenylphosphine (60%) but still allows the isolation of a reasonable quantity of the corresponding phosphine aniline under the form of its borane adduct. Releasing the borane adduct was performed in toluene in presence of DABCO according to a modified procedure reported by Taylor and co-workers^[48]. Unfortunately, **4-P(Xylyl)₂-aniline** was obtained in a low yield (53%), and the quantity collected was too low to engage in the subsequent step.

In conclusion, the preparation of **4-P(Ar)₂-aniline** compounds through metal-mediated coupling reaction between diarylphosphine and 4-iodoaniline suffers from two main limitations: **1)** Usually this reaction is not scalable, which prevents obtaining the desired product on gram scale. **2)** Some aniline might form (by de-iodination) during the catalytic reaction, which complicates the purification process and reduces the isolated yields. Thus, protocol I was not investigated further for the synthesis of phosphinoaniline derivatives.

II.2.c. Synthesis of new 4-P(Ar)₂-aniline derivatives via protocol II.

II.2.c.i. Issues with the purity and stability of some PAr₂Cl precursors:

Before starting to investigate protocol II, the purity and stability of the commercial PAr₂Cl precursors were checked by NMR analyses. It was found that some PAr₂Cl precursors were sensitive to high temperature, and able to oxidize/hydrolyze in THF (solvent previously used for conducting nucleophilic addition with the Grignard reagent^[46]).

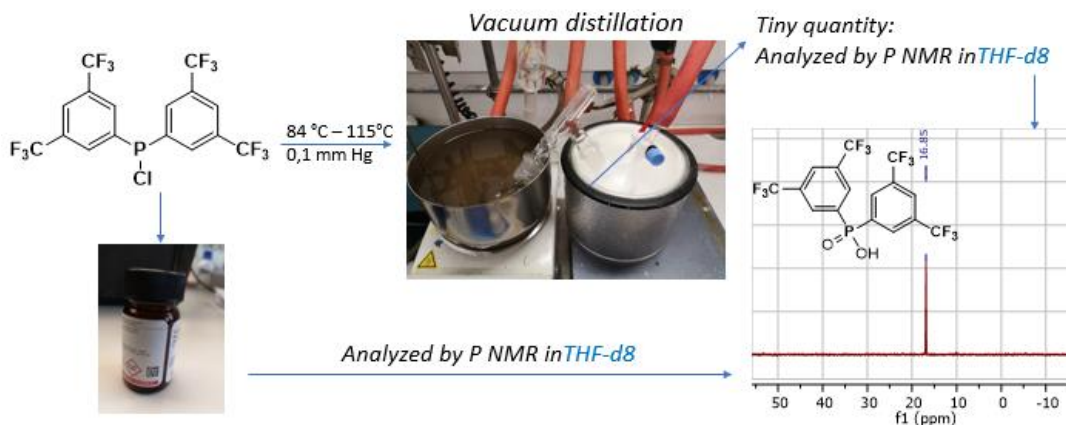


Figure II-6 $^{31}\text{P}\{^1\text{H}\}$ NMR analyses of the as received and distilled commercial P(DTF)₂-Cl in THF-d₈ show the presence of the oxidized species (16.85 ppm).

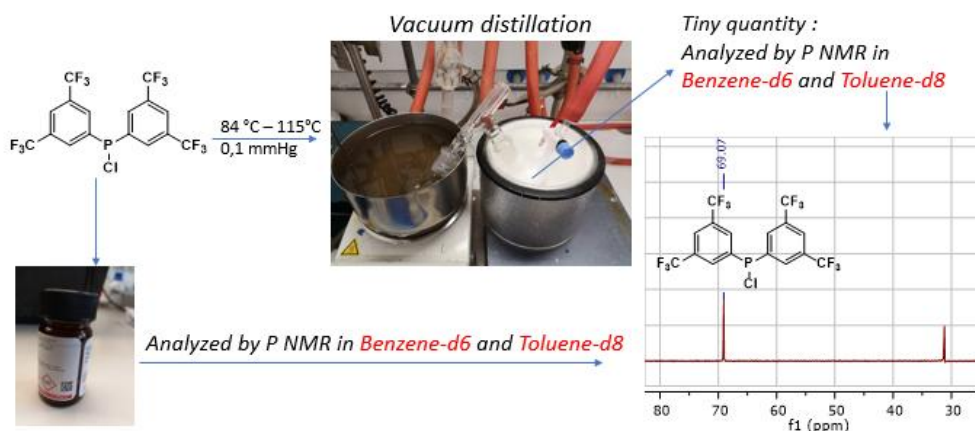


Figure II-7 $^{31}\text{P}\{^1\text{H}\}$ NMR analyses of the as received and distilled commercial P(DTF)₂-Cl in toluene-d₈ or benzene-d₆ (69.07 ppm)².

² The proportion of the oxidized species with respect to the expected product was the same before and after distillation.

This instability was confirmed by $^{31}\text{P}\{^1\text{H}\}$ NMR analysis conducted on the following chlorophosphine precursor: bis(3,5-bis(trifluoromethyl)phenyl)chlorophosphine (**P(DTF)₂Cl**). The $^{31}\text{P}\{^1\text{H}\}$ NMR of both the as received and distilled commercial precursor in THF-*d*₈ was consistent with $^{31}\text{P}\{^1\text{H}\}$ NMR of the diarylphosphinic acid (chemical shift at 16.85 ppm) (Figure II-6). However, the $^{31}\text{P}\{^1\text{H}\}$ NMR in toluene-*d*₈ or benzene-*d*₆ gave the expected $^{31}\text{P}\{^1\text{H}\}$ NMR peak signal (69.07 ppm) of **P(DTF)₂Cl** (Figure II-7) with an estimated purity of 67% (Table II-2).

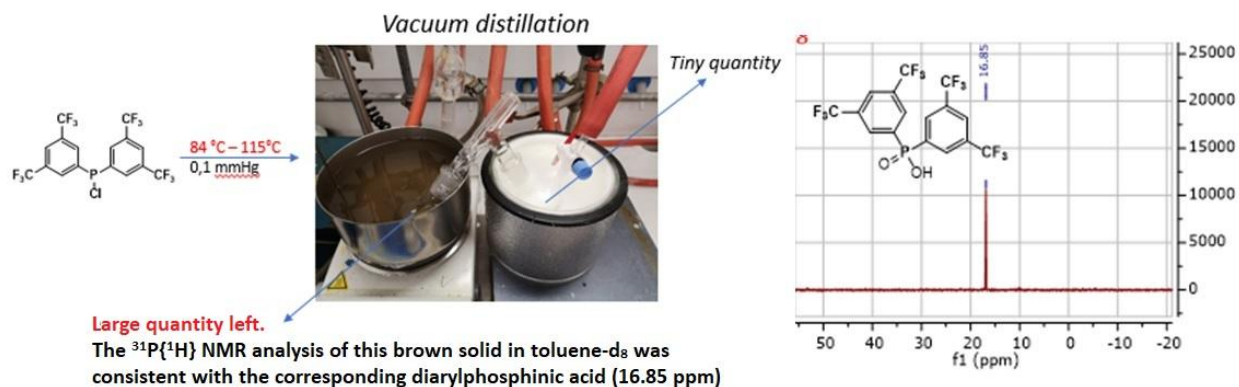


Figure II-8 $^{31}\text{P}\{^1\text{H}\}$ NMR analyses in toluene-*d*₈ for the large quantity left undistilled shows that the **P-(DTF)₂Cl** is oxidized into diarylphosphinic acid.

Additionally, it was noticed that when the distillation process (heating above 84°C) was stopped, a large quantity of this commercial **P(DTF)₂Cl** precursor was left undistilled in the form of a brown solid. The $^{31}\text{P}\{^1\text{H}\}$ NMR analysis of this brown solid in toluene-*d*₈ was consistent with the corresponding diarylphosphinic acid (16.85 ppm) (Figure II-8). Clearly, **P-(DTF)₂Cl** is unstable in THF, and prone to oxidation/hydrolysis at high temperature ($\geq 84^\circ\text{C}$).

Commercial PAR₂Cl precursors	Sigma Aldrich purity %	Alfa Aesar purity %	Expected $^{31}\text{P}\{^1\text{H}\}$ NMR (ppm) in CDCl_3
P-(DTF) ₂ Cl	≈40-60 %	≈67%	68.9
P-(Xyllyl) ₂ Cl	≈50-65%	≈81%	84.6
P-(DTBM) ₂ Cl	0%	≈77%	86.1
P-(BPPh)Cl	≈30%	-	68.1
P-(DMM) ₂ Cl	0%	-	85.3
P-(Mesityl) ₂ Cl	≈75%	-	85.5

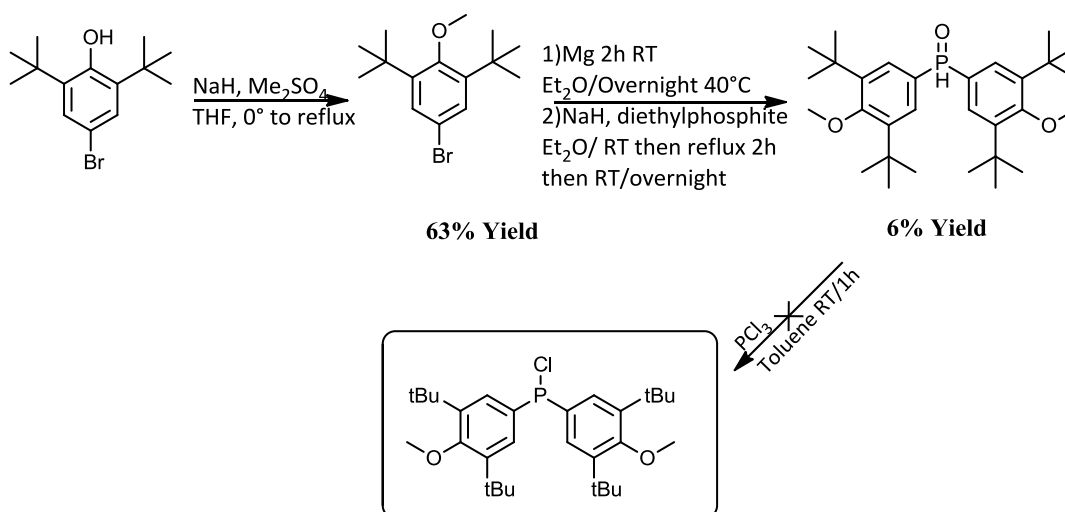
Table II-2 Purity of commercial **PAR₂Cl** precursors have been estimated according to ^1H NMR and $^{31}\text{P}\{^1\text{H}\}$ NMR analyses in toluene-*d*₈. Note: New samples of P-(DTBM)₂Cl and P-(DMM)₂Cl were sent to us by Sigma-Aldrich but we did not determine the purity of these new batches.

Besides, it has been noticed by NMR spectroscopy that different commercially available (PAr_2Cl) precursors (Sigma Aldrich, and Alfa Aesar) are either totally impure ($\text{P}(\text{-DTBM})_2\text{Cl}$ and $\text{P}(\text{-DMM})_2\text{Cl}$) or of moderate purity when analyzed as received in toluene- d_8 (see Table II-2 for the purity of PAr_2Cl precursors).

For the reasons mentioned above, and for the aim of having a modular synthetic approach which doesn't rely on the purity of commercially available starting materials, we decided to synthesize some PAr_2Cl precursors.

II.2.c.ii. Attempted synthesis of some PAr_2Cl precursors³.

We chose to prepare bis(3,5-di-*tert*-butyl-4-methoxyphenyl)chlorophosphine ($\text{P}(\text{-DTBM})_2\text{Cl}$) by combining different modified procedures (Scheme II-15) in one synthetic route. The first step of the proposed synthetic route was adapted from a procedure reported by Breit and coworkers^[49]. The alcohol functionality of bromo-2,6-di-*tert*-butyl phenol was methylated using sodium hydride (60% in mineral oil) suspended in THF in presence of dimethyl sulfate. The methylated product was obtained in *ca.* 63% yield. Afterwards, the corresponding Grignard reagent was formed by addition of magnesium turnings into a solution of 1-bromo-3,5-di-*tert*-butyl-4-methoxybenzene in THF according to a modified procedure reported by Hayashi and coworkers^[50].



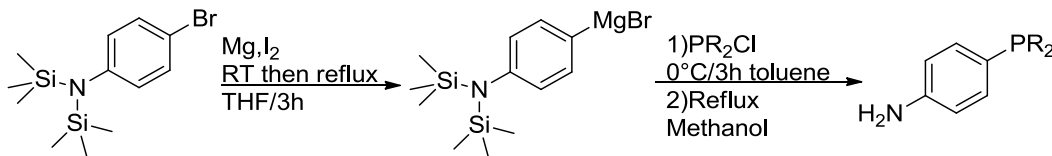
Scheme II-15 Proposed synthetic route towards the synthesis of $\text{P}(\text{-DTBM})_2\text{Cl}$ precursor.

³ For experimental procedures (see Annex, subsection II.6.a).

Then a solution of deprotonated diethyl phosphite was slowly added to the Grignard suspension to give rise to bis-(3,5-di-tert-butyl-4-methoxyphenyl) phosphine oxide, albeit in very poor yield (6%). The phosphine oxide moiety was reduced into the corresponding phosphine chloride by adapting a procedure reported by Liu and coworkers^[51]. This transformation completely failed and no traces of the desired **P-(DTBM)₂Cl** compound could be detected by ³¹P NMR.

Synthesis of **PAR₂Cl** precursors is a multi-step and tedious process and they are only intermediates in our synthetic route towards BTA ligands. We decided finally to proceed with the commercially available (**PAR₂Cl**) precursors we have in hand even though their purity was not perfect. The synthesis of the **4-P(Ar)₂-aniline** fragments was performed by adapting the protocol II reported by Piet van Leeuwen et al^[46].

II.2.c.iii. Synthesis of new phosphinoaniline derivatives via protocol II⁴.



Scheme II-16 General synthetic route for the synthesis of diverse 4-(diarylphosphino)aniline fragments.

This proposed synthetic route (Scheme II-16) was followed to prepare **4-P(Ph)₂-aniline**. The Grignard reagent is formed in situ by mixing 4-bromo-N,N-bis(trimethylsilyl)aniline and magnesium turnings in THF with a chip of Iodine. The addition of **P-(Ph)₂Cl** in THF to the previously prepared Grignard reagent under inert atmosphere yields the TMS-protected **4-P(Ph)₂-aniline** fragment, which is engaged in the next step without purification. The free amine was generated by refluxing the TMS-protected **4-P(Ph)₂-aniline** intermediate in MeOH, thereof yielding **4-P(Ph)₂-aniline** in 43% yield after purification on flash column chromatography over silica.

This modified protocol has been also adapted for the synthesis of all other **4-P(Ar)₂-anilines**. Reaction time for each step has been adapted according to the reactivity of each **PAR₂Cl**

⁴ For experimental procedures (see Annex, subsection II.6.b).

precursor used (estimated by monitoring the reactions by $^{31}\text{P}\{^1\text{H}\}$ NMR spectroscopy). Better yields were obtained when toluene was used instead of THF as a solvent for the nucleophilic addition step between the Grignard reagent and **PAR₂Cl** precursor (Table II-3).

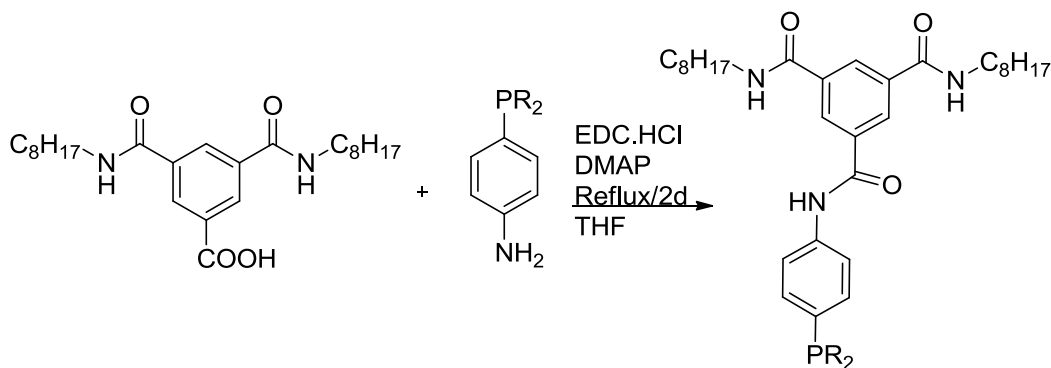
4-(diarylphosphino)aniline	Mass obtained (g)	$^{31}\text{P}\{^1\text{H}\}$ NMR (ppm) in CDCl_3	Yield %	Purity %
4-P(DTF)2-aniline ^[a]	2.12	-4.7 ^[a]	52	>95
4-P(MTF)2-aniline ^[c]	0.50	-6.5 ^[b]	52	>95
4-P(PhF)2-aniline ^[c]	0.40	-8.7 ^[b]	11	>95
4-P(Ph)2-aniline	1.99	-6.6 ^[a]	43	>95
4-P(BPPh)-aniline	0.60	-11.2	53	>90
4-P(Tolyl)2-aniline	2.45	-22.5	44	>95
4-P(Xylyl)2-aniline	3.17	-6.5	60	>95
4-P(DMM)2-aniline	0.06	-8.5	6	50
4-P(Mesityl)2-aniline	0.50	-22.9	24	80
4-P(DTBM)2-aniline	0.70	-6.7 ^a	30	>95

Table II-3 Quantities obtained, $^{31}\text{P}\{^1\text{H}\}$ NMR shifts, yields and purity associated with different 4-P(Ar)2-aniline fragments formed. (a) $^{31}\text{P}\{^1\text{H}\}$ NMR in C_6D_6 . (b) $^{31}\text{P}\{^1\text{H}\}$ NMR in toluene- d_8 . (c) 4-(N,N-trimethylsilyl)₂-aniline magnesium bromide was bought from supplier instead of synthesized and used as received. The reason for the low yield in 4-P(PhF)2-aniline is not known. (d) The batch was prepared multiple times, and a yield of *ca.* 50% was obtained for all batches.

Although the yields were not satisfactory for all **4-P(Ar)2-aniline** derivatives (11-60%), we were able to get all except one product at the hundreds of mg and even g scale. The exception was **4-P(DMM)2-aniline** for which the low yield and purity can be probably explained by the low purity of the commercial **PAR₂Cl** precursor. All other **4-P(Ar)2-anilines** were obtained with high purity (>95%) except **4-P(Mesityl)2-aniline** (80%). The yield of the latter compound (24%) is similar to that obtained through the Pd route (19%) showcasing the special challenge associated with the reactivity of **P-(Mesityl)₂Cl**.

II.2.d. Synthesis of the BTA ligands⁵.

Finally, a last amide coupling reaction is required between both the **4-P(Ar)2-aniline** and 3,5-bis(octylcarbamoyl)benzoic acid in THF, in presence of DMAP and EDC·HCl at reflux temperature for two days to yield the desired phosphine-containing BTA ligands (Scheme II-17).



Scheme II-17 Final coupling step required for furnishing the final BTA ligand.

BTA-P(Ar)2	Mass obtained (g)	³¹ P{ ¹ H} NMR (ppm)	Yield %	Purity %
BTA-P(DTF)2	1.82	-5.6	74	>95
BTA-P(MTF)2	0.54	-7.3	67	>95
BTA-P(PhF)2	0.34	-10.2	46	>95
BTA-pPPPh2	1.90	-7.7	79	>95
BTA-P(BPPh)	0.89	-12.1	66	>95
BTA-P(Tolyl)2	1.24	-22.9	64	>95
BTA-P(Xylyl)2	1.00	-7.4	55	>95
BTA-P(DMM)2	0.03	-9.0	23	>95
BTA-P(Mesityl)2	0.12	-23.3	13	90
BTA-P(DTBM)2	0.60	-7.8	65	>95

Table II-4 Masses obtained, ³¹P{¹H} NMR shifts in DMSO-d₆, yields and purity of the BTA ligands.

All BTA ligands were obtained with acceptable yields (46-74%, Table II-4) except **BTA-P(DMM)2** and **BTA-P(Mesityl)2**. The low yields associated with **BTA-P(Mesityl)2** and **BTA-P(DMM)2** are attributed to the low purity of the corresponding **4-P(Ar)2-anilines** (<80% see Table II-3). The

⁵ For experimental procedures (see Annex, subsection II.6.b).

BTA ligands were characterized by ^1H NMR, $^{31}\text{P}\{^1\text{H}\}$ NMR, ^{13}C NMR, FT-IR and HRMS analyses (see the Annex) and satisfactory purity was observed in all cases (>95%, Table II-4).

In conclusion, we were able to obtain most of the BTA ligands on hundreds of mg or gram scale. The low yields associated with the two synthetic steps required for the formation of **BTA-P(DMM)2**, and **BTA-P(Mesityl)2** prevent their isolation in sufficient quantity. Further optimization should be carried on for improving the yields, by optimizing purification conditions, or even reaction conditions to obtain these two BTA ligands in higher amount.

II.2.e. Table of comparison between protocol I and II for the synthesis of BTA-pPPh2.

Protocol	Yield of 4-P(Ph)2-aniline (%)	Yield of BTA-pPPh2 (%)	Overall yield (%)
I (P-H starting material)	60	34	20
II (P-Cl starting material)	43	79	34

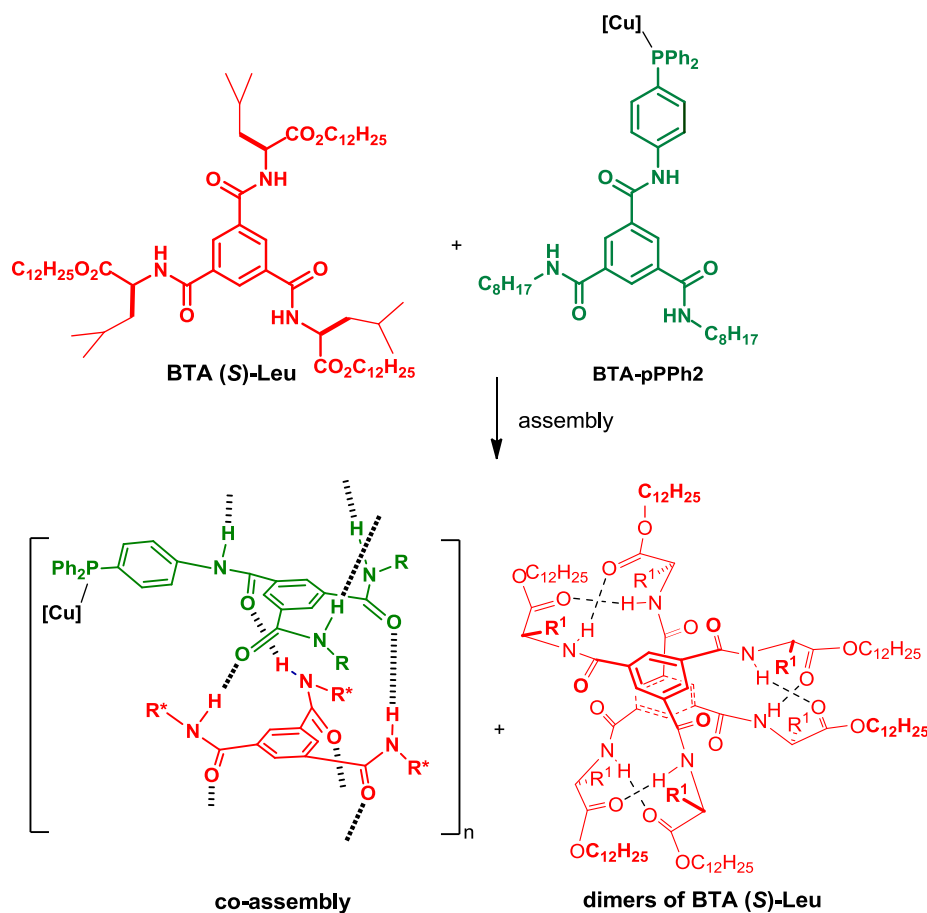
Table II-5 Comparison between protocol I and II for the synthesis of BTA-pPPh2.

Yield of **4-P(Ph)2-aniline** obtained via protocol I (60%, Table II-5) is higher than the one obtained via protocol II (43%, Table II-5). However, the amide coupling reaction performs better with a **4-P(Ph)2-aniline** obtained via protocol II, (79% versus 34%). The overall yield in **BTA-pPPh2** was eventually higher for protocol II.

II.3. Structural characterization of the (S&S) co-assemblies by SANS and FT-IR analyses

We performed SANS, and FT-IR analyses on the sergeants-and-soldiers (S&S) mixtures composed of some of the new BTA-P(Ar)2 ligands: **BTA-P(DTF)2**, **BTA-P(Xylyl)2**, **BTA-P(Tolyl)2**, **BTA-P(DTBM)2**, and **BTA-BPPH** (as soldier) and of **BTA Leu** (as sergeant) in order to unveil the structural features of the co-assemblies. Analyses have been performed without copper but its coordination to any of the selected BTA-P(Ar)2 ligands is not expected to significantly influence the structure of the co-assemblies as found previously in the case of **BTA-pPPh2/BTA Cha** mixtures^[52]. **BTA Leu** has been chosen as the sergeant for three reasons: 1) It is the main sergeant used in most catalytic experiments of this project especially in the cascade hydrosilylation/hydroamination reaction (**Chapter IV**). 2) **BTA Leu** improved the solubility of all

selected BTA-P(Ar)₂ ligands in toluene, since all BTA ligands except **BTA-pPPH2**, are poorly soluble on their own in this solvent. 3) The S&S-type mixture of **BTA-pPPH2/BTA Leu** has been well described by our lab previously^[53], and the obtained data would be used as reference for comparison with the newly studied mixtures. **BTA Leu** alone is known to self-assemble under the form of dimers^[38,54]. In the case of S&S-type mixture between **BTA-pPPH2** (5.8 mM) and **BTA Leu** (3.7 mM, $f_s^0 = 39\%$)^[53], the major part of the engaged **BTA Leu** molecules co-assembles **with BTA-pPPH2** into the helical stacks, as determined by SANS and FT-IR (Table II-6). The few sergeants that do not co-assemble are present in solution as dimers (Scheme II-18). The composition and structure of the helical BTA co-assemblies are particularly important parameters in the context of their implementation in catalysis.



Scheme II-18 Upon co-assembly, a fraction of BTA (S)-Leu molecules is incorporated into the co-assembly formed by BTA-pPPH₂, and a fraction is present as dimers^[53].

Accordingly, SANS data for the newly S&S-type mixtures (Figure II-9) in this study were modelled by a combination of rigid cylinders of infinite length and of spheres. The radius of the rigid cylinders was fixed to 12 Å and that of spheres to 11 Å. The adjustable parameter was the proportion of sergeants that co-assemble with **BTA-P(Ar)2** into cylinders (f_s^S = fraction of sergeants in stacks).

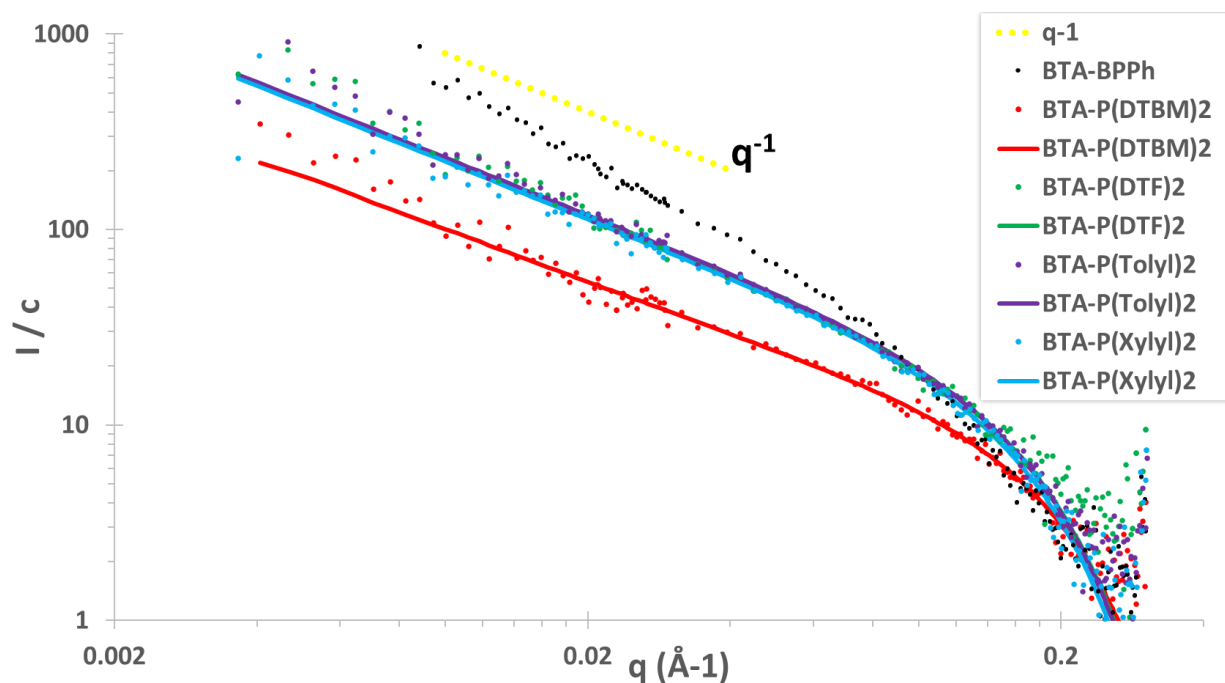


Figure II-9 Probing the influence of the soldier (BTA-P(Ar)2) on the properties and structure of the co-assemblies formed with **BTA Leu** by SANS. The S&S-type mixtures: Black: **BTA-BPPh** (3.33 g.L⁻¹, 4.82 mM) and **BTA Leu** (3.11 mM, f_s^0 = 39%), Red: **BTA-P(DTBM)2** (3.33 g.L⁻¹, 3.4 mM) and **BTA Leu** (3.11 mM, f_s^0 = 47%), Green: **BTA-P(DTF)2** (3.33 g.L⁻¹, 3.45 mM) and **BTA Leu** (3.11 mM, f_s^0 = 47%), Violet: **BTA-P(Tolyl)2** (3.33 g.L⁻¹, 4.63 mM) and **BTA Leu** (3.11 mM, f_s^0 = 40%), Blue: **BTA-P(Xylyl)2** (3.33 g.L⁻¹, 4.45 mM) and **BTA Leu** (3.11 mM, f_s^0 = 41%) in toluene-d₈. Analysis is shown on the full scattering vector range. Data are fitted as indicated in the caption of Table II-5.

The quality of the fits allowed an estimation of f_s^S values, which was compared to that deduced from FT-IR analyses through deconvolution of the ester C=O bands (Table II-6). The geometrical features of the co-assemblies as extracted from the SANS data differ significantly according to the nature of the soldier. Notably, the significant differences in scattered intensity at intermediate and low q values are a first indication of the different nature of the co-assemblies in terms of composition, structure and length (Figure II-9).

For S&S-type mixtures with **BTA-P(Tolyl)2**, **BTA-P(Xylyl)2**, and **BTA-P(DTF)2**, the fraction of sergeant incorporated in stack was found to be high (f_s^S -SANS > 25%) and similar to the one determined for **BTA-pPPh2** mixture (35%). On contrary, for **BTA-P(DTBM)2**, the fraction of incorporated **BTA Leu** is very low. Lastly, the scattering intensity of the SANS curve for **BTA-BPPH** mixture does not follow a q^{-1} dependence at intermediate and low q values which suggests the aggregation of rods, *i.e.* the formation of bundles (Figure II-9).

Soldier	$f_s^{0[c]}$ (%)	f_s^S -SANS ^[d] (%)	f_s^S -IR ^[e] (%)	Comment
BTA-pPPH2 ^[a]	39	35±4	36±1	S&S mixed in single rods of $l > 200\text{Å}$, S&S mixture of reference ^[53]
BTA-P(DTF)2 ^[b]	47	31	41	S&S mixed in single rods of $l > 200\text{Å}$
BTA-P(DTBM)2 ^[b]	47	0	8	Short rods with limited incorporation of BTA Leu
BTA-P(Tolyl)2 ^[b]	40	25	31	S&S mixed in single rods of $l > 200\text{Å}$
BTA-P(Xylyl)2 ^[b]	41	28	24	S&S mixed in single rods of $l > 200\text{Å}$.
BTA-BPPH ^[b]	39	nd	26	S&S mixed in aggregated rods, <i>i.e.</i> in bundles

Table II-6 Geometrical features of the co-assemblies determined by fitting the SANS data (BTA in stacks, f_s^S -SANS) and FT-IR data (f_s^S -IR) of S&S-type mixtures. [a] SANS data was modelled by a combination of rigid cylinders of finite length and of spheres, both objects with of radius of $11\pm 1\text{Å}$. [b] SANS data was modelled by a combination of rigid cylinders of infinite length ($r= 12\text{Å}$) and of spheres ($r= 11\text{Å}$). [c] Overall fraction of sergeants in stacks. [d] From SANS data, f_s^S : Fraction of sergeants in stacks = [sergeant in stacks] / ([BTA-P(Ar)2] + [sergeant in stacks]). $f_s^{Smax} = f_s^0$ (full co-assembly). [e] from FT-IR data.

FT-IR analyses are informative about the nature of the hydrogen-bonded species present in these S&S-type mixtures. Ester-bonded dimers formed by the sergeants and amide-bonded stacks formed upon co-assemblies can be distinguished, which allow for an independent determination of the f_s^S values (see Figure II-10 for the attribution of the bands corresponding to these 2 species). The different FT-IR signature of **BTA Leu** in dimers and stacks in the ester C=O region allows to estimate the fraction of incorporated **BTA Leu**. These f_s^S values are in good agreement with those determined by SANS analyses for **BTA-P(Tolyl)2**, and **BTA-P(Xylyl)2** mixtures and in fair agreement for **BTA-P(DTF)2**, and **BTA-P(DTBM)2** mixtures. Thus, FT-IR and

SANS analyses corroborate that **BTA Leu** efficiently co-assemble with **BTA-P(Tolyl)2**, **BTA-P(Xylyl)2** and **BTA-P(DTF)2** but not with **BTA-P(DTBM)2**.

FT-IR analyses allows determining that a significant amount of **BTA Leu** molecules (f_s^S -IR= 26%) are present in the aggregated rods for the **BTA-BPPH** mixture. In addition, according to frequencies of the amide N-H (FT-IR band), additional information can be deduced concerning the length of stacks. The large band present at 3400 cm^{-1} in the case of **BTA-P(DTBM)2/BTA Leu** mixture which signifies that free NH are present. The free NH component belongs to soldier **BTA-P(DTBM)2** molecules that are present as free monomers, and thus, it is an indication for short stacks in the **BTA-P(DTBM)2/BTA Leu** mixture.

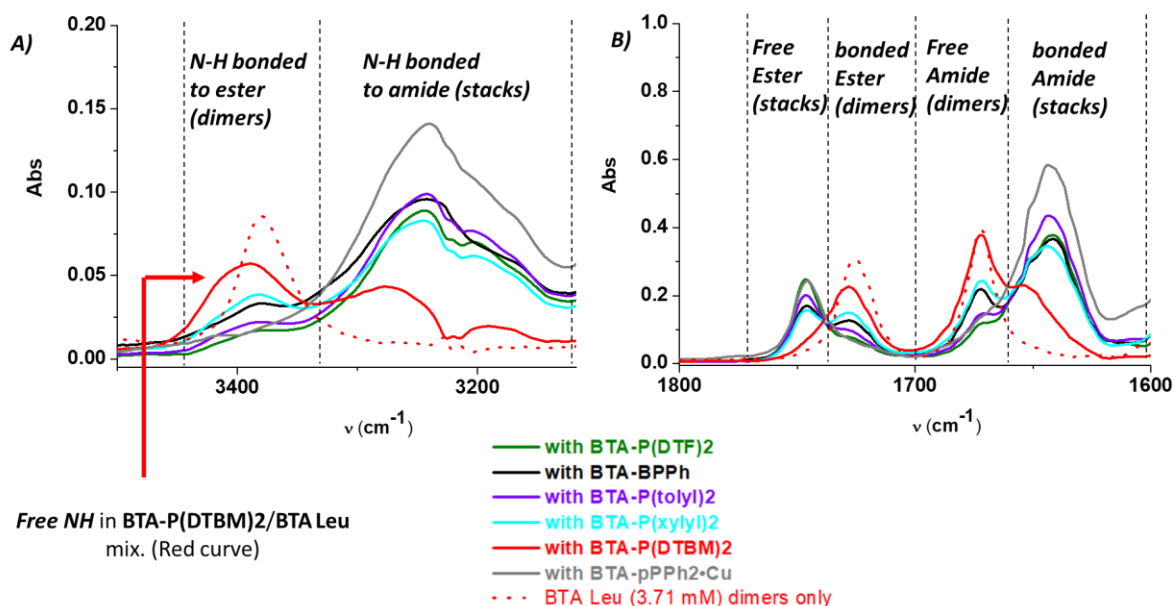


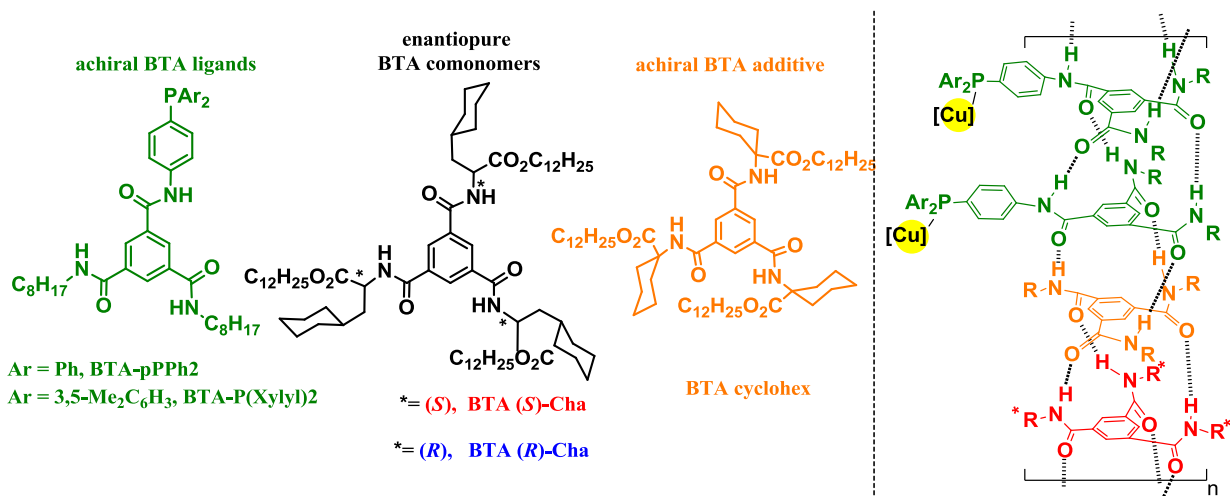
Figure II-10 Comparison of the FT-IR spectra of **BTA Leu** with FT-IR spectra for The S&S-type mixtures: **BTA-BPPH** (3.33 g.L^{-1} , 4.82 mM) and **BTA Leu** (3.11 mM , $f_s^0 = 39\%$), **BTA-P(DTBM)2** (3.33 g.L^{-1} , 3.4 mM) and **BTA Leu** (3.11 mM , $f_s^0 = 47\%$), **BTA-P(DTF)2** (3.33 g.L^{-1} , 3.45 mM) and **BTA Leu** (3.11 mM , $f_s^0 = 47\%$), **BTA-P(Tolyl)2** (3.33 g.L^{-1} , 4.63 mM) and **BTA Leu** (3.11 mM , $f_s^0 = 40\%$), **BTA-P(Xylyl)2** (3.33 g.L^{-1} , 4.45 mM) and **BTA Leu** (3.11 mM , $f_s^0 = 41\%$) in toluene at 293 K . **A)** Zoom of the N-H region. **B)** Zoom of the C=O region.

Combination of SANS and FT-IR data was thus used to estimate the structure of the supramolecular polymers in toluene- d_8 . According to the SANS data, **BTA-P(DTF)2**, **BTA-P(Xylyl)2**, and **BTA-P(tolyl)2** co-assemble with **BTA Leu** into long unaggregated rods whilst **BTA-BPPH** and **BTA Leu** are mixed into bundles. On contrary, only short rods were detected in the

mixture composed of **BTA-P(DTBM)2** and **BTA Leu** and the rods only incorporate a small fraction of **BTA Leu**. This preliminary investigation therefore reveals the important influence of the nature of the ligand on the co-assembly properties of the BTA ligands with **BTA Leu**.

II.4. Implementation in copper-catalyzed hydrosilylation of 1-(4-nitrophenyl)ethenone

BTA-pPPh2 ligand has been utilized extensively in the copper-catalyzed hydrosilylation of 1-(4-nitrophenyl)ethanone (**NPnone**). Initially, sergeants-and-soldiers mixtures composed of **BTA-pPPh2** and ester BTAs were evaluated in this reaction, and it was found that helical co-assemblies with an excess of **BTA (S)-Cha** relative to **BTA-pPPh2** provided 1-(4-nitrophenyl)ethanol (**NPnol**) with $54 \pm 2\%$ *ee* at 293 K. For the purpose of probing the degree of chirality amplification of this system through the S&S effect the amount of **BTA (S)-Cha** was varied (thesis of Yan Li^[55]).



Scheme II-19 Chemical structures of the BTA monomers used as S&S-type mixtures for the hydrosilylation reaction. Right: representation of the helical co-assemblies, preferentially right-handed, formed by mixing **BTA-P(Ar)2**, [Cu(OAc)₂·H₂O], **BTA (S)-Cha** and **BTA cyclohex**^[56].

For this S&S-type catalytic mixture, it was found that the enantioselectivity in **NPnol** increases nonlinearly with the fraction of **BTA (S)-Cha** present in the catalytic mixture ($0.1\% \text{ fs}^0 \leq 52\%$), but no plateau is reached ($|ee_{\text{max}}| = 57.6\%$, Figure II-11, black curve). It means that the S&S effect was weak in this initial system. So, it was decided to optimize his catalytic system by adding a second achiral BTA: **BTA cyclohex** (Scheme II-19). **BTA cyclohex** was selected as an

additive in this catalytic reaction, since the cyclohexyl group attached on the amino-ester α -carbon was expected to reduce the conformational freedom of the amide functions and thus to rigidify the hydrogen-bonded network between the complementary monomers in the co-assemblies^[57] where the chirality induction stems from. In the presence of **BTA cyclohex**, the S&S effect was improved by two orders of magnitude. In the presence of **BTA cyclohex** ($[\text{BTA-pPPH2}]/[\text{BTA cyclohex}] = 1$), a plateau of enantioselectivity is reached for $f_s^0 = 0.50\%$ of **BTA (S)-Cha**, $|ee_{\text{max}}| = 51.4\%$, and 98% of the plateau value is achieved with $f_s^0 = 0.25\%$, $|ee| = 50.4\%$, Figure II-11, red curve). This was in good agreement with the minimal fraction of **BTA (S)-Cha** required to obtain homochiral helices as probed by CD spectroscopy.

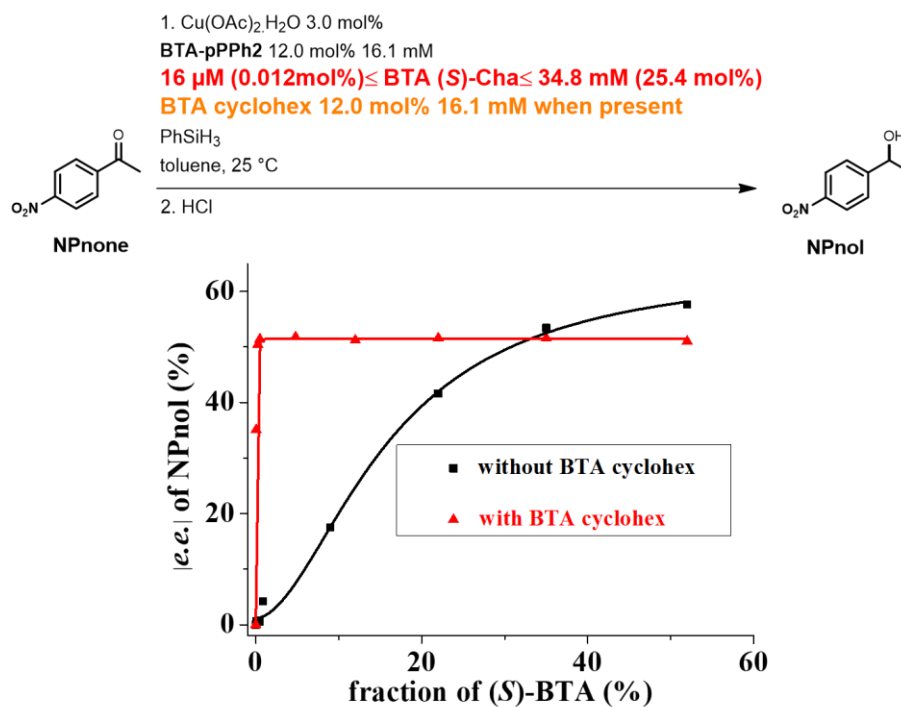
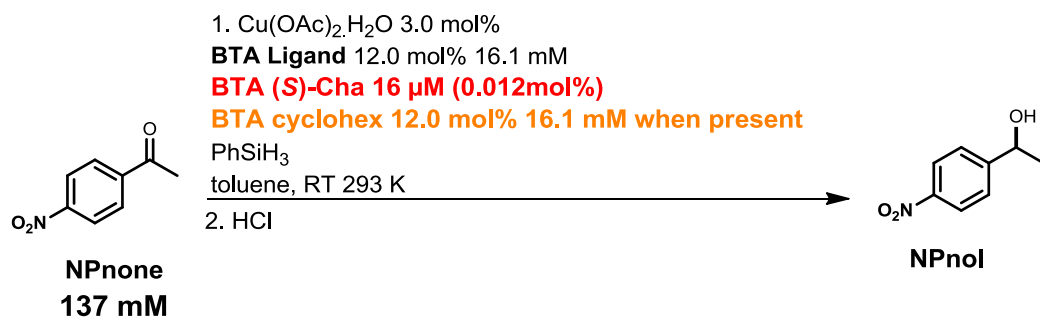


Figure II-11 Asymmetric catalysis with S&S and diluted MR type helical catalysts (293 K, toluene). Enantioselectivity in NPnol ($\pm 1\%$) versus the fraction of BTA (S)-Cha in the catalytic mixtures with and without BTA cyclohex^[56].

It was thus seen that amplification effects were hugely enhanced upon addition of a second achiral BTA monomer as an additive (**BTA cyclohex**), leading to a perfect control of the helicity by means of a remarkably low amount of sergeants (0.5%). One limitation of this ternary mixture, **BTA-pPPH2/BTA (S)-Cha/BTA cyclohex** is that the optimal selectivity is only of *ca.* 50%

ee. For the aim of improving the enantioselectivity of this catalytic system, we envisaged to vary

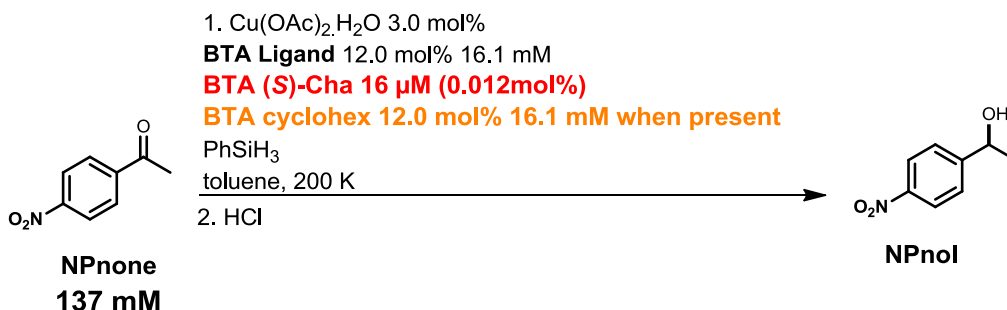


Entry	BTA ligand	[BTA cyclohex] (mM)	ee in NPhol (%)
1	BTA-pPPh2	-	0.5
2	BTA-pPPh2	16.1	-50.4
3	BTAP(Xylyl)2	-	-2
4	BTAP(Xylyl)2	16.1	-66.5
5	BTA-BPPh	-	0
6	BTA-BPPh	16.1	0
7	BTA-P(Mesityl)2	16.1	0
8	BTA-P(tolyl)2	-	-6.5
9	BTA-P(tolyl)2	16.1	0
10	BTA-P(DTF)2	-	-8.5
11	BTA-P(DTF)2	16.1	-69
12	BTA-P(DTBM)2	-	0
13	BTA-P(DTBM)2	16.1	-47.7

Table II-7 **Optimization of S&S-type catalytic experiments: composition and catalytic result for each mixture.** Catalytic loading in BTA (S)-Cha = [BTA (S)-Cha]/[NPhnone]. Conversion >99% was obtained for all catalytic experiments. The optical purity of NPhol was determined by GC analysis, ee are set as positive and negative when (S)-NPhol and (R)-NPhol are the majority enantiomers, respectively. Note: BTA-P(PhF)2, and BTA-P(MTF)2 were not tested for this investigation as they were not synthesized at the time of this screening. Likewise, BTA-P(DMM)2 was only tested at low temperature given its limited quantity.

the nature of the BTA ligand. For this purpose, the newly designed BTA ligands were tested under different conditions. As the aim was to improve the selectivity of the helical BTA catalyst operating with a very small fraction of sergeant, the following conditions were assessed: reaction temperature, and concentration of **NPhnone**. First, S&S mixtures of different BTA

ligands and **BTA (S)-Cha** were screened in the hydrosilylation of **NPnone** [137 Mm] in presence and absence of **BTA cyclohex** at RT in toluene. For catalytic results and reaction scheme, see Table II-7.



Entry	BTA ligand	[BTA cyclohex] (mM)	ee in NPnol (%)
1	BTA-pPPh2	-	-11
2	BTA-pPPh2	16.1	-80
3	BTAP(Xylyl)2	-	-2.5
4	BTAP(Xylyl)2	16.1	-90
5	BTAP(Xylyl)2	16.1	91 ^[a]
6	BTA-P(DTF)2	-	0 ^[b]
7	BTA-P(DTF)2	16.1	-65
8	BTA-P(DMM)2	-	0 ^[b]
9	BTA-P(DMM)2	16.1	-43 ^[b]

Table II-8 **Optimization of S&S-type catalytic experiments: composition and catalytic result for each mixture.** Catalytic loading in BTA (S)-Cha= [BTA (S)-Cha]/[NPnone]. Conversion >99% was obtained except otherwise noted. The optical purity of NPnol was determined by GC analysis, ee are set as positive and negative when (S)-NPnol and (R)-NPnol are the majority enantiomers, respectively. [a] **BTA (R)-Cha** was used instead of **BTA (S)-Cha**. [b] incomplete conversion.

BTA-BPPh, **BTA-P(Mesityl)2**, and **BTA-P(tolyl)2** provides no significant selectivity ($ee < 6\%$) for the hydrosilylation reaction even in presence of the BTA additive (entries 5, 6, 7, 8, and 9 Table II-7). **BTAP(Xylyl)2**: provides no selectivity in absence of additive (entry 3, Table II-7), but -67% ee when the additive is present which is higher than that obtained with **BTA-pPPh2** (entry 4, Table II-7). For **BTA-P(DTF)2** the selectivity is also markedly increased in presence of the additive from -8.5% ee to -69% ee. Finally, **BTA-P(DTBM)2** displays a similar catalytic behavior

as **BTA-pPPh2**. For the latter ligand, it is particularly remarkable that a significant degree of selectivity is obtained in presence of the additive since our aforementioned analytical data indicates that only short stacks were present in its absence. The additive has maybe here both the ability of removing the defects and of increasing the length of the assemblies.

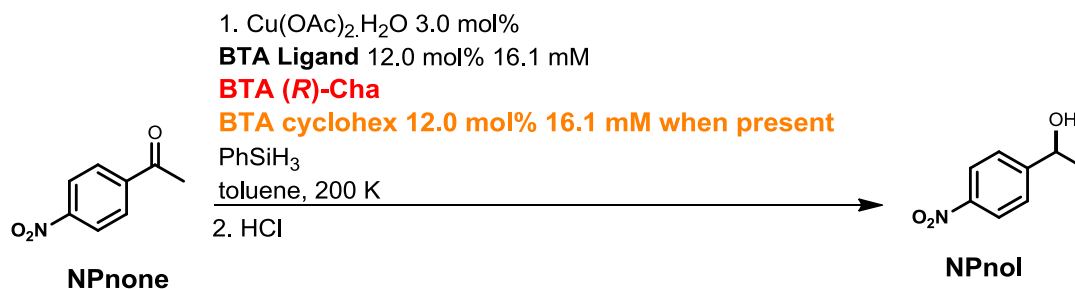
BTA-P(DTF)2 and **BTA-P(Xylyl)2** were selected for further investigation at lower temperature (200K) as well as **BTA-P(DMM)2** which was only investigated at 200K. Again, the mixtures were tested in presence and absence of the additive. For catalytic results and reactions scheme see (Table II-8).

The selectivity provided by **BTA-P(DMM)2** is lower than for that of the other ligands (entry 8 and 9, Table II-8). **BTA-P(DTF)2** showed no or little improvement in selectivity at lower temperatures, both in presence and absence of additive (entries 6 and 7, Table II-8), while for **BTAP(Xylyl)2**, upon addition of **BTA cyclohex**, the selectivity rises to -90% *ee* allowing both enantiomers of **NPnol** to be obtained with high levels of enantiopurity (entries 3, 4, and 5 Table II-8). The extent of selectivity that emerges with the additive in the case of **BTA-P(Xylyl)2** ($\Delta ee = 87\%$)^[56] is higher than that observed for the reference ligand **BTA-pPPh2** ($\Delta ee = 69\%$)^[56] under the same conditions.

Finally, the influence of the substrate loading was investigated for the optimized catalytic system, *i.e.* those embedding **BTAP(Xylyl)2**. The system remains active at remarkably low loadings in Cu and **BTA (S)-Cha** (0.38 mol % and 75 ppm, respectively) at the cost of a limited drop in enantioselectivity (74% *ee*, entry 3 Table II-9).

In conclusion, the structure of the phosphine BTA ligand showed a huge impact on the stereochemical outcome of the copper catalyzed hydrosilylation reaction of **NPnone**. The structure of the ligand not only influences the extent of enantioselectivity that can be provided in the catalytic reaction of reference but also affects the behavior of the catalytic system as a function of the temperature. Indeed, whilst for **BTA-pPPh2** and **BTA-P(Xylyl)2** the enantioselectivity of the reaction increases when the temperature is lower, for **BTA-P(DTF)2**, the temperature has no significant effect. In addition, a high selectivity was displayed (up to

90% *ee*) when **BTA-P(Xylyl)2** was employed as ligand despite the limited amount of sergeant (ppm levels relative to the substrate) present in the catalytic mixture.



Entry	BTA ligand	[NPnone] (mM)	BTA (R)-Cha loading in ppm	<i>ee</i> in NPnol (%)
1	BTAP(Xylyl)2	274	300	86
2	BTAP(Xylyl)2	548	150	83
3	BTAP(Xylyl)2	1096	75	74

Table II-9 **Optimization of S&S-type catalytic experiments: composition and catalytic result for each mixture.** Catalytic loading in BTA (S)-Cha= [BTA (S)-Cha]/[NPnone]. Conversion >99% was obtained. The optical purity of NPnol was determined by GC analysis.

II.5. Conclusion.

A new set of phosphine containing BTA ligands was designed by modifying the aryl groups around the phosphorous atom, leading to 9 new ligands with different electronic and steric properties. Electron-donating and electron-withdrawing groups were introduced at the 3- and 5- positions of the aryl group which may possibly favor ligand substrate interactions. These nine BTA ligands were synthesized according to a similar three-step synthetic procedure, and were obtained on hundreds of mg or gram scale with a high level of purity except for **BTA-P(DMM)2** and **BTA-P(Mesityl)2**. Further optimization could be carried out for improving these yields, either by optimizing purification conditions of starting materials, or by modifying the reaction conditions for obtaining the corresponding starting materials and intermediates with a higher purity.

SANS data combined with FT-IR analyses showed the ability of **BTA-P(DTF)2**, **BTA-P(Xylyl)2** and **BTA-P(Tolyl)2** to co-assemble with **BTA Leu** into unaggregated rods of length > 200 Å whilst for **BTA-BPPH** both monomers co-assemble into aggregated rods. On contrary, only short stacks

are detected for the mixture between **BTA-P(DTBM)2** and **BTA Leu**. The chiroptical properties of the S&S-mixture between **BTA-P(DTF)2** and **BTA Leu** will be probed in **Chapter IV**.

These newly designed BTA ligands were implemented in the copper-catalyzed hydrosilylation of 1-(4-nitrophenyl)ethenone in presence of a very limited amount of **BTA Cha** as chiral co-monomer. The BTA ligand structure has an important impact on the stereochemical outcome of this reaction. Significant selectivity was displayed (up to 90% *ee*) with **BTA-P(Xylyl)2** when an achiral additive is present in the catalytic mixture. This selectivity is significantly higher than that displayed by the reference ligand **BTA-pPPh2** showcasing the importance of the substitution on the aryl groups attached to the P atom of the BTA ligands.

II.6. Annex.

Materials preparation and methods:

Chlorodi-*o*-tolylphosphine, chlorobis(3,5-di-*tert*-butyl-4-methoxyphenyl)phosphine, 5-chloro-5H-benzo[*b*]phosphindole, chlorodimesitylphosphine, bis(4-methoxy-3,5-dimethylphenyl)chlorophosphine, bis(4-(trifluoromethyl)phenyl)chlorophosphine, bis(3,5-dimethylphenyl)chlorophosphine, bis(4-fluorophenyl)chlorophosphine, chlorodiphenylphosphine, bis(3,5-bis(trifluoromethyl)phenyl)chlorophosphine, bis(3,5-dimethylphenyl)phosphine, and dimesitylphosphine were obtained from Alfa Aesar, and/or Sigma-Aldrich and used as received. PAr_2Cl precursors are highly unstable and sensitive to air and oxygen, and must be stored under argon. 1-(4-nitrophenyl)ethanone (>98%), PhSiH_3 (>97%) and $[\text{Cu}(\text{OAc})_2 \cdot \text{H}_2\text{O}]$ (>99%) were purchased from Alfa Aesar. 4-bromo-*N,N*-bis(trimethylsilyl)aniline, (4-(bis(trimethylsilyl)amino)phenyl)magnesium bromide, and DMAP was acquired from Sigma Aldrich and were used without purification. EDC-HCl was purchased from Fluorochem. 3,5-bis(octylaminocarbonyl)-benzoic acid^[37], BTA (*S*)-Cha^[58] and BTA (*R*)-Cha^[58], and BTA cyclohex^[56] were synthesized and characterized according to reported procedures. BTA (*S*)-Cha and BTA (*R*)-Cha monomers used in this study have been purified by preparative HPLC. Dried solvents were obtained from an SPS solvent purification system (IT-Inc). NMR spectra were recorded on a Bruker Advance 400, 300 or 200 spectrometer and calibrated to the residual solvent peak: $\text{DMSO-}d_6$ (^1H : 2.50 ppm; ^{13}C : 39.52 ppm); CDCl_3 (^1H : 7.26 ppm; ^{13}C : 77.16 ppm). Acetone- d_6 (^1H :

2.05 ppm; ^{13}C : 29.84 ppm). Peaks are reported with their corresponding multiplicity (s: singlet; br s: broad singlet, d: doublet, t: triplet; q: quartet) and integration, and respective J coupling constants are given in Hertz. Exact mass measurements (HRMS) were obtained on TQ R30-10 HRMS spectrometer by ESI+ ionization and are reported in m/z for the major signal. FT-IR spectra for solids were recorded by reflection on a Ge probe (attenuated total reflectance (ATR) and the main bands were reported (w: weak, m: medium, s: strong, br: broad). Solution spectra were measured in CaF_2 cells and are corrected for air, solvent and cell absorption. Unless otherwise noted, chromatography-grade solvents were used as received. All inert atmosphere reactions were carried out under an argon or nitrogen atmosphere with standard Schlenk-line techniques.

Small-angle neutron scattering (SANS) analyses: SANS measurements were made at the LLB (Saclay, France) on the PA20 instrument, at three distance-wavelength combinations to cover the 2×10^{-3} to 0.3 \AA^{-1} q -range, where the scattering vector q is defined as usual, assuming elastic scattering, as $q = (4\pi/\lambda)\sin(\theta/2)$, where θ is the angle between incident and scattered beam. Data were corrected for the empty cell signal and the solute and solvent incoherent background. A light water standard was used to normalize the scattered intensities to cm^{-1} units. The data was fitted with the DANSE software SasView. SANS data was modelled by a combination of rigid cylinders of infinite length ($r = 12 \text{ \AA}$) and of spheres ($r = 11 \text{ \AA}$) except for **BTA-pPPh2/BTA Leu** mixture for which SANS data was modelled by a combination of rigid cylinders of finite length and of spheres, both objects with of radius of $11 \pm 1 \text{ \AA}$.

Fourier-Transform Infrared (FT-IR) analyses: FT-IR measurements were performed on a Nicolet iS10 spectrometer. Spectra of solutions in toluene were measured in 0.2 mm pathlength CaF_2 cells at 293 K and were corrected for air, solvent and cell absorption. Procedure for the simulation of the experimental FT-IR spectra: The concentration of dimers is extracted by fitting the ester carbonyl region of the experimental FT-IR spectrum ($1700\text{-}1800 \text{ cm}^{-1}$) with the individual spectra of **BTA Leu** (representative of sergeants in dimers, bonded ester CO, $\nu \approx 1725 \text{ cm}^{-1}$) and of **BTA Met**^[38,58] (reference for ester BTAs in stacks, free ester CO, $\nu \approx 1745 \text{ cm}^{-1}$).

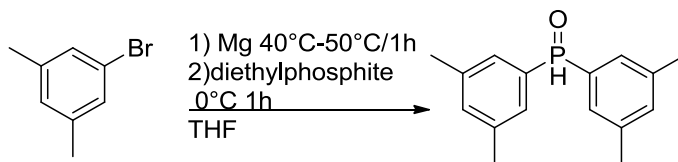
General procedure for the catalytic experiments.

In all catalytic experiments a pre-catalytic mixture composed of the ligand, the copper salt and the substrate was prepared as follows: a tube was loaded with $[\text{Cu}(\text{OAc})_2 \cdot \text{H}_2\text{O}]$ (0.5 mg, 2.55 μmol , 3.0 mol%) and **BTA-P(Ar)₂** (6.9 mg, 10.0 μmol , 12.0 mol%) in dry THF (500 μL) and the mixture was stirred for 30 minutes. The solvent was removed under vacuum and the tube was further put under vacuum (10^{-3} mbar) for 1 hour. Then 1-(4-nitrophenyl)ethanone (14.0 mg, 0.085 mmol, 100 mol%) was added before flushing the tube with argon for 10 seconds. Then, the desired amount of **BTA Cha** co-monomer with **BTA cyclohex** when present (10.9 mg, 10.0 μmol , 12.0 mol%) were added to the tube as well as dry toluene. The total solvent volume was set equal to 600 μL). The mixture was stirred for 15 min at room temperature, and then the solution was briefly heated to reflux. After cooling down to the desired temperature (293 K or 200 K), PhSiH_3 (21.0 μL , 0.17 mmol, 200 mol%) was added to the tube and the reaction mixture was stirred for 12 hours before being hydrolysed with aqueous HCl and analysed by ^1H NMR and chiral GC. For experiments mentioned in Table II-8, the amount of substrate was adapted.

Chiral GC analyses. The optical purity was determined by GC analysis: Chiral Cyclosil-B column, 30 m \times 250 μm \times 0.25 μm , inlet pressure = 12.6 psi. Injection temperature = 250°C; detector temperature = 300°C; column temperature = 145°C. Retention time: 17.9 min (1-(4-nitrophenyl)ethanone), 47.6 min ((*R*)-enantiomer), 49.9 min ((*S*)-enantiomer).

II.6.a. Experimental procedures.

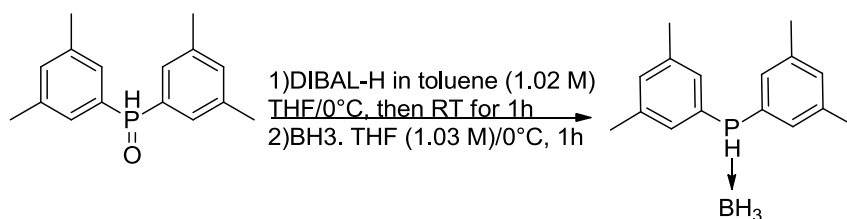
1) Synthesis of bis(3,5-dimethylphenyl)phosphine oxide



1-Bromo-3,5-dimethylbenzene (0.026 mole, 5.0 g, 3.5 equiv.) was slowly added to a suspension of Mg turnings (0.026 mole, 0.63 g, 3.5 equiv.) in THF (29 mL) while the internal temperature was maintained at 40–50 °C. The mixture was stirred at 40–50 °C for 1 h then cooled to 0 °C. Diethylphosphite (0.007 mole, 1.5 mL, 1 equiv.) was added over 30 min, and the mixture was stirred at 0°C for 1 h. The reaction was quenched with 6 M aq. HCl (10 mL) and the mixture was

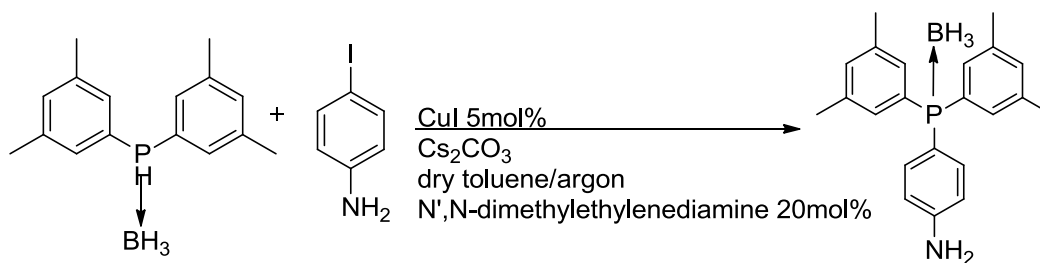
extracted with CH_2Cl_2 (10 mL \times 3) and washed with H_2O (10 mL \times 2). After evaporation under vacuum, the residue was purified by column chromatography on silica gel using hexane/ethyl acetate (1/2) to give bis-(3,5-dimethylphenyl)phosphine oxide as a pale-yellow solid (1.3 g, 65% yield). ^1H NMR (300 MHz, CDCl_3) δ (ppm) 8.03 (d, $J^{\text{P-H}} = 477\text{Hz}$, 1H), 7.42 (s, 2H), 7.37 (s, 2H) 7.26 (s, 2H), 2.43 (s, 12H).

2) Synthesis of bis(3,5-dimethylphenyl)phosphine-borane adduct



A solution of bis(3,5-dimethylphenyl)phosphine oxide (5.03 mmole, 1.3 g, 1 equiv.) in THF (26 mL) at 0°C was treated by slow addition of a 1.02 M solution of DIBAL-H in toluene (15.1 mmole, 14.8 mL, 3.0 equiv.). The mixture was stirred at room temperature for 1 h, cooled to 0°C , and a 1.06 M solution of $\text{BH}_3 \cdot \text{THF}$ in THF (10.1 mmole, 9.9 mL, 2 equiv.) was added. The resulting mixture was stirred at 0°C for 1 h and then the reaction was quenched with 36 mL of 2M aq. KOH. The mixture was extracted with toluene (20 mL \times 2) and successively washed with 2M aq KOH and H_2O . After evaporation of solvent under vacuum, the residue was purified by chromatography on silica gel by 90/10 hexane/ethyl acetate to give the title compound (0.23 g, 18% yield) as a white solid. ^1H NMR (400 MHz, CDCl_3) δ (ppm) 7.28 (s, 2H), 7.24 (s, 2H), 7.13 (s, 2H), 6.17 (dq, $J^{\text{P-H}} = 378$, $J^{\text{H-H}} = 6.9$ Hz, 1H), 2.33 (s, 12H), 0.56–1.47 (m, 3H, BH_3).

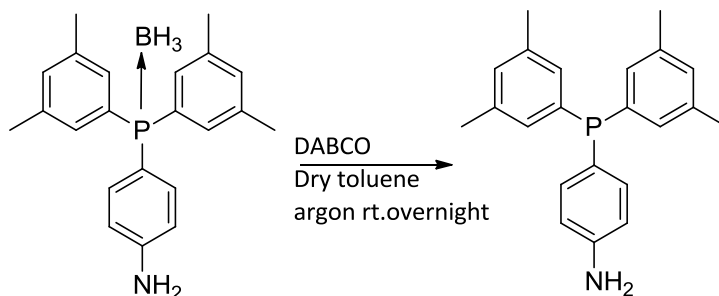
3) Synthesis of 4-(bis(3,5-dimethylphenyl)phosphino)aniline-Borane adduct



An oven-dried Schlenk tube was evacuated and refilled with argon three times and then charged with CuI (0.04 mmol, 7.6 mg, 0.05 equiv.) followed by anhydrous toluene, bis(3,5-

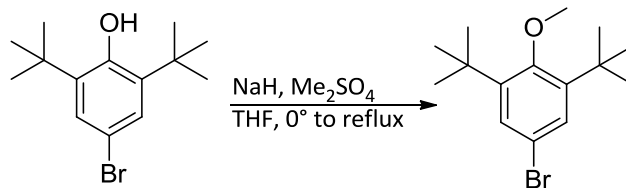
dimethylphenyl)phosphine-borane adduct (0.90 mmol, 0.23 g, 1 equiv.) and N,N'-dimethylethylenediamine (0.20 mmol, 21 mL, 0.22 equiv.). The colorless or slightly yellow solution was allowed to stir for 5-10 min. Then 4-Iodoaniline (0.82 mmol, 0.18 g, 0.91 equiv.) and Cs₂CO₃ (1.64 mmol, 0.53 g, 1.82 equiv.) were added at once followed by anhydrous toluene (1.15 mL). The Schlenk tube was sealed with a Teflon valve and the reaction mixture was stirred at 110 °C until all 4-Iodoaniline is consumed. The resulting suspension was diluted with water (2 mL) and extracted with ethyl acetate (4 × 4 mL). The combined organic phases were dried over MgSO₄, concentrated, and the residue was purified by flash chromatography on silica with ethyl acetate/hexane to provide the desired product (0.14 g, 42% yield). ¹H NMR (400 MHz, CDCl₃) δ (ppm) 7.18 (t, 2H), 6.96 (s, 2H), 6.92 (d, 4H), 6.68 (d, 2H), 3.78 (s, 2H), 2.27 (s, 12H), 1.48 – 0.79 (m, 3H, BH₃).

4) Synthesis of 4-(bis(3,5-dimethylphenyl)phosphino)aniline, releasing of the borane



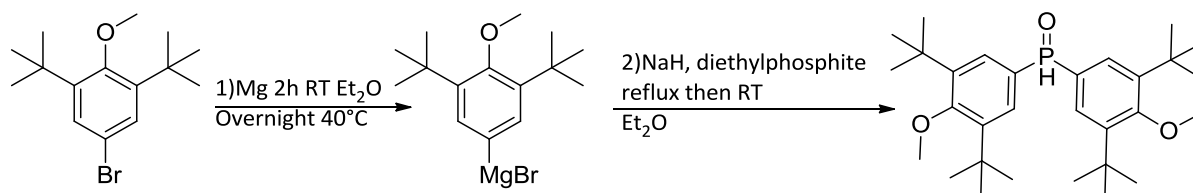
A solution of 4-(bis(3,5-dimethylphenyl)phosphino)aniline-Borane adduct (0.36 mmol, 0.13 g, 1 equiv.) and DABCO (1.08 mmol, 0.12 g, 3 equiv.), in 3 mL of dry toluene, was stirred under argon at room temperature overnight. The solvent was evaporated under vacuum, and the residue was purified by flash chromatography on silica with 3:1 petroleum ether/ethyl acetate to provide the desired product (53 mg, 53% yield). ¹H NMR (400 MHz, CDCl₃) δ (ppm) 7.18 (t, 2H), 6.94 (s, 2H), 6.93 (d, 4H), 6.69 (d, 2H), 3.78 (s, 2H), 2.28 (s, 12H). ³¹P{¹H} NMR (CDCl₃): δ (ppm) –6.48.

5) Synthesis of 2,6-di-*tert*-butyl-4-bromoanisole



NaH (60 % in mineral oil, 26.2 mmol, 0.63 g, 1.5 equiv.) was suspended in THF (60 mL) and cooled down to 0°C. A solution of 4-bromo-2,6-di-tert-butyl phenol (17.5 mmol, 5.0 g, 1 equiv.) in THF (15 mL) was slowly added via a dropping funnel. After complete addition, the reaction mixture was allowed to come to RT and stirred for one hour. The mixture was cooled down to 0 °C and dimethyl sulfate (19.3 mmol, 1.8 mL, 1.1 equiv.) was added. The reaction mixture was heated to reflux overnight. Then, distilled H₂O (50 mL) was carefully added at 0°C and the unclear mixture was allowed to come to RT. Additional distilled H₂O (75 mL) and Et₂O (250 mL) were added and the organic layer was extracted with Et₂O (2x 250 mL). The combined organic layers were washed with distilled H₂O (2x 100 mL) and brine (100 mL). The clear solution was dried over MgSO₄ and concentrated under reduced pressure. The crude product was purified via flash column chromatography on silica with hexanes to afford the product (3.3 g, 63% yield) as a colorless solid. ¹H NMR (300 MHz, CDCl₃) δ (ppm) 7.35 (s, 2H), 3.70 (s, 3H), 1.43 (s, 18H).

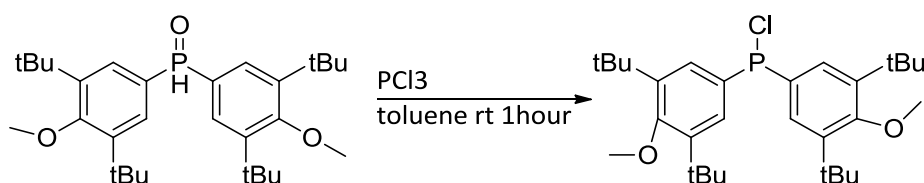
6) Synthesis of Bis(3,5-di-tert-butyl-4-methoxyphenyl)phosphine oxide



A two-necked 25 mL round-bottomed flask equipped with a reflux condenser, a dropping funnel, and a magnetic stirring bar was charged with Mg turnings (11.1 mmol, 0.26 g, 1 equiv.), evacuated while being heated by a heat-gun for 10 mins, and then back-filled with argon. Dry Et₂O (1.1 mL) was added through the dropping funnel. The dropping funnel was then charged with a solution of 2,6-di-tert-butyl-4-bromoanisole (DTBM-Br, 11.1 mmol, 3.3 g, 1 equiv.) in Et₂O (1.7 mL). Ten drops of the DTBM-Br solution were added, and the mixture was stirred until heat evolution and color changes to black. Then the rest of the DTBM-Br solution was added dropwise over 2.5 h. After the addition was complete, the dropping funnel was washed with

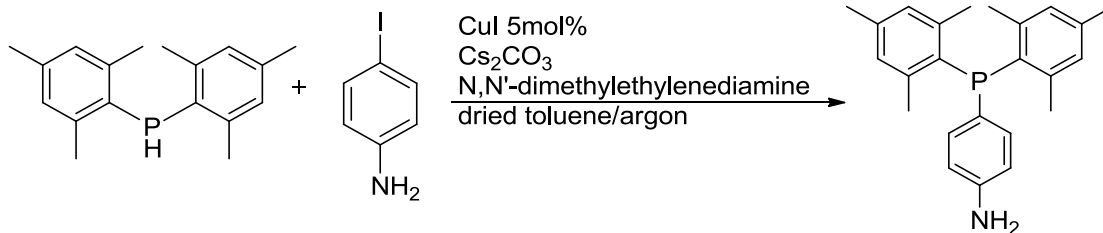
Et₂O (2.5 mL). The mixture was then stirred at 40 °C overnight. In the meanwhile, diethyl phosphite (5.53 mmol, 0.7 mL, 0.5 equiv.) was carefully added to a suspension of NaH (6.63 mmol, 0.16 g, 0.6 eq.) in THF (2 mL) and heated to reflux, until everything was dissolved. The solution of the deprotonated diethyl phosphite was then slowly added at RT to the Grignard suspension and the reaction mixture was heated to reflux for 1.5–2 h, then allowed to come to RT and stirred overnight. Then, H₂O (5 mL) and aq. HCl (1 N, 25 mL) were added. The aq. layer was separated and extracted with ethylacetate (3 x 25 mL). The combined organic layers were washed with brine, dried over MgSO₄ and concentrated under reduced pressure to give a white solid (0.165 g, 6% yield). ¹H NMR (400 MHz, CDCl₃) δ (ppm) 8.05 (d, *J*^{P-H} = 474.6 Hz, 1H), 7.57 (s, 2H), 7.53 (s, 22H), 3.72 (s, 6H), 1.43 (s, 36H). ³¹P{¹H} NMR (CDCl₃): δ 26.58.

7) Attempted synthesis of chlorobis(3,5-di-tert-butyl-4-methoxyphenyl)phosphine



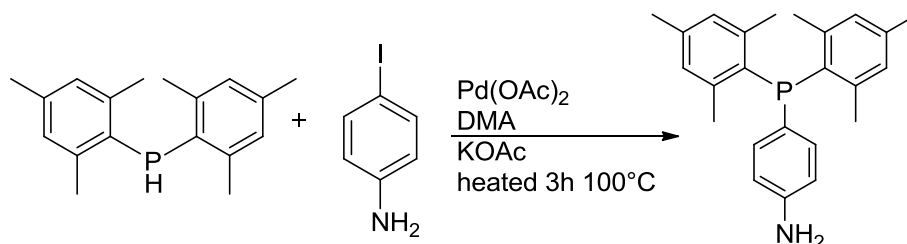
To a solution of Bis(3,5-di-tert-butyl-4-methoxyphenyl)phosphine oxide (0.34 mmol, 0.17 g, 1 equiv.) in toluene (20 mL), PCl₃ (0.34 mmol, 0.03 mL, 1 equiv.) was added slowly at 0-10 °C. The reaction mixture was stirred for 30 min at 0-10 °C. The solvent was removed under vacuum. The ³¹P{¹H} NMR (CDCl₃) of the crude mixture displayed 4 peaks at δ = 36.98, 25.17, 7.16 and -43.01 ppm. According to this data, we confirmed that the reaction did not proceed since the expected ³¹P{¹H} NMR signal (CDCl₃) of chlorobis(3,5-di-tert-butyl-4-methoxyphenyl)phosphine is δ = 86.14 ppm.

8) Synthesis of 4-(dimesitylphosphino)aniline by ***Ullman type coupling reaction***.



An oven-dried Schlenk tube was evacuated and refilled with argon three times and then charged with CuI (0.17 mmol, 0.032 g, 0.05 equiv.) followed by anhydrous toluene 3 mL, dimesitylphosphine (3.69 mmol, 1 g, 1 equiv.) and N,N'-dimethylethylenediamine (0.81 mmol, 88 mL, 0.2 equiv.). The colorless or slightly yellow solution was allowed to stir for 5-10 min. Then 4-Iodoaniline (3.36 mmol, 0.737 g, 0.91 equiv.) and Cs₂CO₃ (6.72 mmol, 2.18 g, 1.82 equiv.) were added at once followed by anhydrous toluene (3.8 mL). The Schlenk tube was sealed with a Teflon valve and the reaction mixture was stirred at 110 °C for the desired period of time. The resulting suspension was diluted with water (2 mL) and extracted with ethyl acetate (4 x 4 mL). The combined organic phases were dried over MgSO₄, concentrated, and the residue was purified by flash chromatography on silica with ethyl acetate/PE (25/75) to provide the desired product (65 mg, 5% yield). ¹H NMR (300 MHz, CDCl₃) δ (ppm) 7.25-7.15 (m, 2H), 6.82 (br s, 4H), 6.62 (t, J = 8.0 Hz, 2H), 3.69 (br s, 2H), 2.28 (s, 6H), 2.11 (s, 12H). ³¹P{¹H} NMR (300 MHz, CDCl₃) δ (ppm) -22.94.

9) Synthesis of 4-(dimesitylphosphino)aniline through ***palladium-mediated reaction***



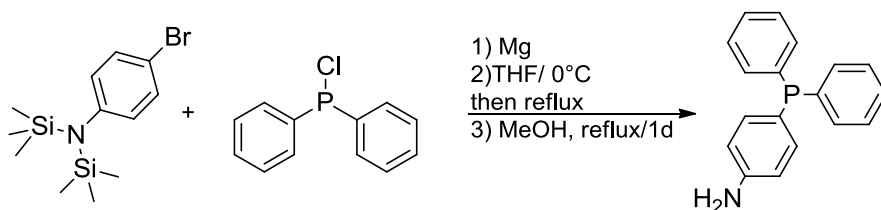
KOAc (1.78 mmol, 0.17 g, 1.2 equiv.) and Pd(OAc)₂ (0.00148 mmol, 0.33 mg, 0.001 equiv.) were added as solids to a solution of 4-Iodoaniline (1.48 mmol, 0.32 g, 1 equiv.) in 2 mL of dimethylacetamide (DMA). The suspension obtained was degassed in vacuum. After addition of dimesitylphosphine (1.48 mmol, 0.4 g, 1 equiv.), the mixtures were heated overnight. The reaction mixtures were poured into 50 mL of water and extracted with 50 mL CH₂Cl₂. The organic phase was washed with water (3 x 30 mL), dried over Na₂SO₄, evaporated under vacuum. The crude mixture was passed over a silica column using ethyl acetate/petroleum ether (25/75) to give the desired product (0.1 g, 19% yield). ¹H NMR (300 MHz, CDCl₃) δ (ppm) 7.25-7.15 (m, 2H), 6.82 (br s, 4H), 6.62 (t, J = 8.0 Hz, 2H), 3.69 (br s, 2H), 2.28 (s, 6H), 2.11 (s, 12H). ³¹P{¹H} NMR (300 MHz, CDCl₃) δ (ppm) -22.94.

II.6.b. Synthesis of the BTA ligands.

1) Synthesis of BTA-pPPh₂

The synthesis was previously reported by our group by adapting the Ullmann-type coupling reported in the literature^[44]. Here we have privileged the nucleophilic addition of a Grignard over chlorodiphenylphosphine since it allows to synthesize the corresponding 4-(diphenylphosphino)aniline on a larger scale.

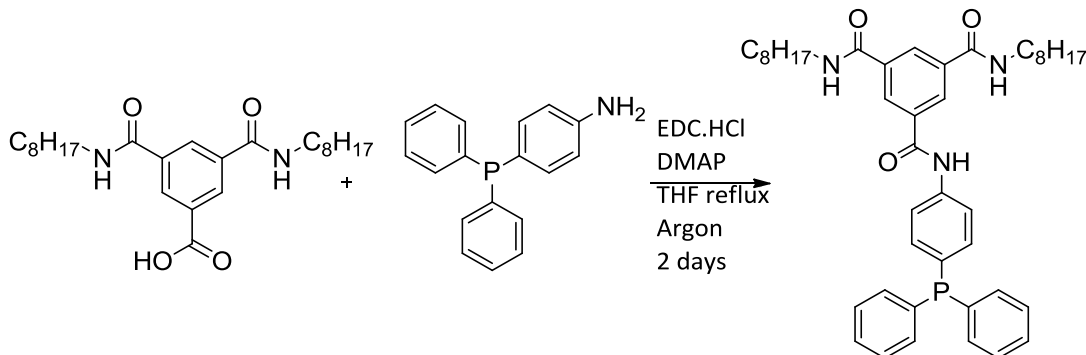
- Step 1: Synthesis of 4-(diphenylphosphino)aniline.



In a three-neck round-bottom flask equipped with a condenser under argon, 4-bromo-*N,N*-bis(trimethylsilyl)aniline (5.0 g, 15.8 mmol, 1.0 equiv.) in THF (16 mL) was added over 40 minutes to a well-stirred dispersion of magnesium turnings (0.46 g, 19.0 mmol, 1.2 equiv.) in THF (just enough to cover the magnesium turnings). Prior to starting the addition, magnesium turnings were activated with a small crystal of I₂ and a drop of 4-bromo-*N,N*-bis(trimethylsilyl)aniline. The reaction was stirred first at room temperature, then heated to 60°C for 3 h. After cooling the solution to room temperature with an ice bath, chlorodiphenylphosphine (4.2 g, 19.0 mmol, 1.2 equiv.) in THF (7.4 mL) was added slowly over 45 minutes. The reaction was monitored by ³¹P{¹H} NMR. The reaction mixture was stirred for 1 h at reflux temperature. The volatiles were removed under vacuum and the solid residue was extracted with dry Et₂O via a cannula to another three-neck round-bottom flask equipped with a special fritted funnel designed to perform filtrations under argon. Et₂O was removed under vacuum, the crude product was then dissolved in dry MeOH (22 mL) and the solution was stirred at reflux temperature for one day under argon. The solution was evaporated under vacuum, and the crude product was purified by flash column chromatography on silica gel, eluting with DCM/methanol 99:1–95:5 gradient, yielding 4-(diphenylphosphino)aniline (1.9 g, 6.85 mmol, 43% yield) as a light-yellow oil. ¹H NMR (300 MHz, C₆D₆) δ (ppm) 7.46 (td, J= 7.8, 1.6

Hz, 4H), 7.32 (t, 2H), 7.13-6.99 (m, 6H), 6.22 (dd, J= 8.6, 0.9 Hz, 2H), 2.77 (bs, 2H, NH₂). ³¹P{¹H} NMR (C₆D₆): δ (ppm) -6.55.

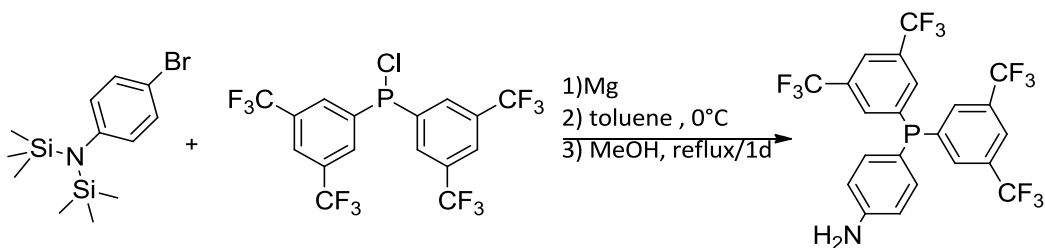
- Step 2: Synthesis of **BTA-pPPh₂**:



N-(3-Dimethylaminopropyl)-N'-ethylcarbodiimide hydrochloride (1.13 g, 5.9 mmol, 1.68 equiv.), DMAP (0.72 g, 5.9 mmol, 1.68 equiv.) and 4-diphenylphosphinoaniline (1.44 g, 5.2 mmol, 1.48 equiv.) were added to a solution of 3,5-bis(octylaminocarbonyl)-benzoic acid (1.50 g, 3.5 mmol, 1 equiv.) in dry THF (100 mL) in an oven-dried Schlenk flask under argon. The reaction mixture was refluxed for 2 days. After cooling to room temperature, the mixture was evaporated under vacuum and the crude product was purified by column chromatography on silica gel eluting with DCM/ethyl acetate (95/5 to 7/1) to yield **BTA-pPPh₂** (1.90 g, 79% yield) as a colorless solid. The product is stable in the solid state and stored at room temperature. ¹H NMR (300 MHz, DMSO-d₆) δ (ppm) 10.62 (s, 1H, ArNH), 8.68 (t, J= 5.6 Hz, 2H, CH₂NH), 8.45 (dd, J= 7.7, 1.6 Hz, 3H, CH_{arom.} BTA ring), 7.84 (d, J = 8.1 Hz, 2H, CH_{arom.} linker), 7.46-7.37 (m, 6H, CH_{arom.} PPh₂), 7.31-7.21 (m, 6H, 4× CH_{arom.} PPh₂ + 2× CH_{arom.} linker), 3.29-3.22 (m, 4H, CH₂NH), 1.61-1.47 (m, 4H, CH₂CH₂NH), 1.36-1.11 (m, 20H, CH₂), 0.90-0.79 (m, 6H, CH₃). ³¹P{¹H} NMR (DMSO-d₆) δ -7.7. ¹³C{¹H} NMR (DMSO-d₆) δ (ppm) 165.2, 165.0, 139.9, 137.0 (d, J = 11.4 Hz), 135.2, 135.1, 134.1 (d, J = 20.6 Hz), 133.1 (d, J = 19.4 Hz), 129.0, 128.9, 128.8, 128.7 (d, J = 6.8 Hz), 120.4 (d, J = 7.4 Hz), 39.6 (below the solvent peak), 31.3, 29.0, 28.8, 28.7, 26.5, 22.1, 13.9. HRMS: Calculated for C₄₃H₅₅N₃O₃P [M+H]⁺: 692.3976, found: 692.3973. The analytical data are in agreement with the published ones^[24].

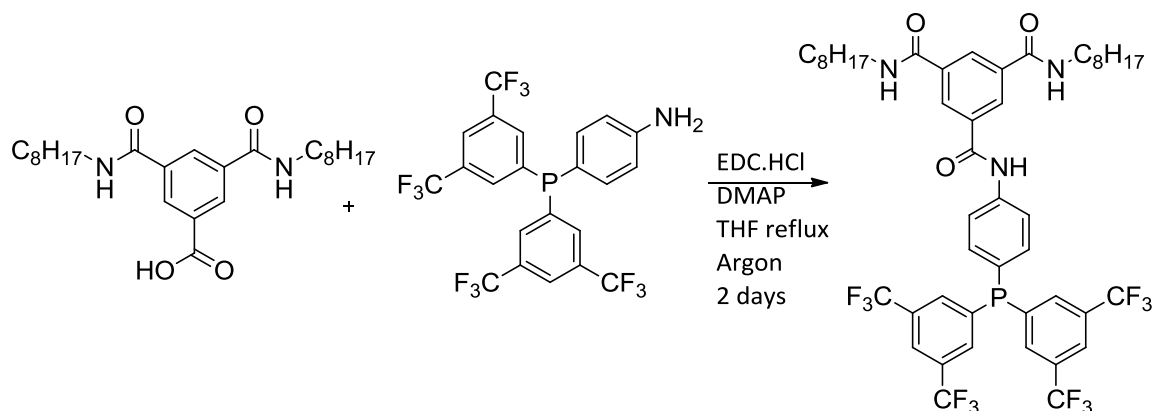
2) Synthesis of **BTA-P(DTF)2**

- Step 1: Synthesis of 4-(bis(3,5 bis(trifluoromethyl)phenyl)phosphino)aniline



In a three-neck round-bottom flask equipped with a condenser under argon, 4-bromo-*N,N*-bis(trimethylsilyl)aniline (2.33 g, 7.38 mmol, 1.0 equiv.) in THF (7.4 mL) was added over 40 minutes to a well-stirred dispersion of magnesium turnings (0.21 g, 8.86 mmol, 1.2 equiv.) in THF (just enough to cover the magnesium turnings). Prior to starting the addition, magnesium turnings were activated with a small crystal of I₂ and a drop of 4-bromo-*N,N*-bis(trimethylsilyl)aniline. The reaction was stirred first at room temperature, then heated to 60°C for 3 hours. THF was evaporated under vacuum and replaced by dry toluene. Bis(3,5-(trifluoromethyl)phenyl)chlorophosphine (4.0 g, 8.1 mmol, 1.1 equiv.) in dry toluene (7.4 mL) was added slowly over 45 minutes to the solution of 4-(*N,N*-trimethylsilyl)₂-aniline magnesium bromide while the reaction flask was cooled with in an ice bath. The reaction mixture was stirred at room temperature, and monitored by ³¹P{¹H} NMR which showed full consumption of Bis(3,5-(trifluoromethyl)phenyl)chlorophosphine after 1 h. The volatiles were removed under vacuum and the solid residue was extracted with dry Et₂O via a cannula to another three-neck round-bottom flask equipped with a special fritted funnel designed to perform filtrations under argon. Et₂O was removed under vacuum, the crude product was then dissolved in dry MeOH (22 mL) and the solution was stirred at reflux temperature for one day under argon. The solution was evaporated under vacuum, and the crude product was purified by flash column chromatography on silica gel, eluting with DCM/methanol 99:1–95:5 gradient yielding 4-(bis(3,5-bis(trifluoromethyl)phenyl)phosphino)aniline (2.12 g, 52% yield) as a yellow oil. ¹H NMR (300 MHz, C₆D₆) δ (ppm) 7.76 (s, 2H), 7.59 (d, J = 6.4 Hz, 4H), 7.08 (t, J = 8.5 Hz, 2H), 6.63 (d, J = 7.5 Hz, 2H), 3.88 (br s, 2H, NH₂). A signal is present at δ = 5.20 ppm for residual DCM. ³¹P{¹H} NMR (122 MHz, C₆D₆) δ (ppm) -4.69.

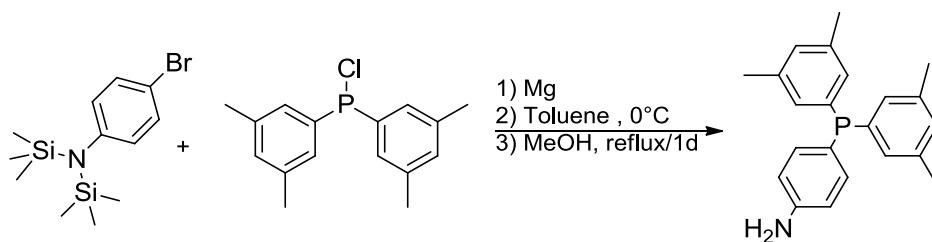
- Step 2: Synthesis of **BTA-P(DTF)2**



3,5-bis(octylaminocarbonyl)benzoic acid (1.1 g, 2.59 mmol, 1 equiv.) and dry THF (100 mL) were mixed in an oven-dried Schlenk flask under argon and then DMAP (0.46 g, 3.8 mmol, 1.46 equiv.), N-(3-Dimethylaminopropyl)-N'-ethylcarbodiimide hydrochloride (0.74 g, 3.8 mmol, 1.46 equiv.) and 4-(bis(3,5 bis(trifluoromethyl)phenyl)phosphino)aniline (2.0 g, 3.64 mmol, 1.40 equiv.) were added. The reaction mixture was refluxed for 2 days. After cooling to room temperature, the mixture was evaporated under vacuum and the crude product was purified by column chromatography on silica gel eluting with DCM/ethyl acetate (95/5 to 7/1) to yield **BTA-P(DTF)2** (1.82 g, 73% yield) as a white solid. The product is stable in the solid state and stored at room temperature. ^1H NMR (300 MHz, DMSO- d_6) δ (ppm) 10.74 (s, 1H, ArNH), δ 8.69 (t, J = 5.5 Hz, 2H, CH_2NH), 8.52 – 8.43 (m, 3H, CH_{arom} . BTA ring), 8.20 (s, 2H, CH_{arom} . PAR_2), 7.93 (m, 6H, $2 \times \text{CH}_{\text{arom}}$. linker + $4 \times \text{CH}_{\text{arom}}$. PAR_2), 7.52 (t, J = 8.4 Hz, 2H, $2 \times \text{CH}_{\text{arom}}$. linker), 3.29 (q, 4H, CH_2NH), 1.54 (q, J = 6.0, 5.5 Hz, 4H, $\text{CH}_2\text{CH}_2\text{NH}$), 1.28 (m, 20H, CH_2), 0.84 (t, 6H, CH_3). Signals are present at δ = 1.20, 1.97 and 4.06 ppm for residual ethyl acetate. $^{31}\text{P}\{^1\text{H}\}$ NMR (122 MHz, DMSO- d_6) δ (ppm) -5.55. $^{13}\text{C}\{^1\text{H}\}$ NMR (DMSO- d_6) δ (ppm) 165.72, 165.64, 141.81, 141.09, 140.90, 135.77 (d, J = 10.3 Hz), 135.55 (d, J = 9.2 Hz), 133.70, 133.49, 131.65 (d, J = 6.1 Hz), 131.33 (d, J = 5.8 Hz), 131.00 (d, J = 5.9 Hz), 130.67 (d, J = 5.8 Hz), 129.55, 129.30, 127.60, 127.39 (d, J = 9.4 Hz), 124.89, 123.65, 122.17, 121.34 (d, J = 8.5 Hz), 119.46, 31.71, 29.47, 29.21, 29.12, 26.97, 22.54, 14.36. FT-IR (ATR, cm^{-1}): 682 (s), 796 (m), 898 (m), 1112 (s), 1182 (m), 1272 (s), 1350 (m), 1525 (m), 1639 (m), 2854 (w), 2933 (w), 3080 (w), 3261 (bw).

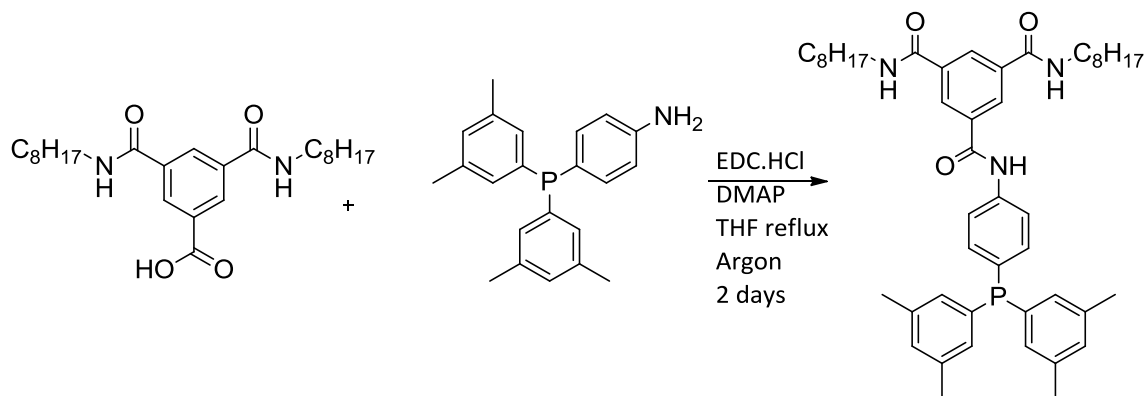
3) Synthesis of **BTA-P(Xylyl)2**

- Step 1: Synthesis of 4-(bis(3,5-dimethylphenyl)phosphino)aniline



In a three-neck round-bottom flask equipped with a condenser under argon, 4-bromo-N,N-bis(trimethylsilyl)aniline (5.0 g, 15.8 mmol, 1.0 equiv.) in THF (16 mL) was added over 40 minutes to a well-stirred dispersion of magnesium turnings (0.46 g, 19.0 mmol, 1.2 equiv.) in THF (just enough to cover the magnesium turnings). Prior to starting the addition, magnesium turnings were activated with a small crystal of I₂ and a drop of 4-bromo-N,N-bis(trimethylsilyl)aniline. The reaction was stirred first at room temperature, then heated to 60°C for 3 hours. THF was evaporated and replaced by dry toluene. Chlorobis(3,5-dimethylphenyl)phosphine (5.0 g, 18.1 mmol, 1.15 equiv.) in toluene (7.4 mL) was added over 15 minutes to the in situ generated toluene solution of 4-(N,N-trimethylsilyl)aniline magnesium bromide while the reaction flask was cooled with in an ice bath. The reaction mixture was stirred for 30 minutes. The reaction was monitored by ³¹P{¹H} NMR. The volatiles were removed under vacuum and the solid residue was extracted with dry Et₂O via a cannula to another three-neck round-bottom flask equipped with a special fritted funnel designed to perform filtrations under argon. Et₂O was removed under vacuum, the crude product was then dissolved in MeOH (22 mL) and the solution was stirred at reflux temperature for one day under argon. The solution was evaporated under vacuum, and the crude product was purified by flash column chromatography on silica gel, eluting with DCM/methanol 99:1–95:5 gradient yielding 4-(bis(3,5-dimethylphenyl)phosphino)aniline (3.17 g, 9.5 mmol, 60% yield) as a white solid. ¹H NMR (CDCl₃): δ (ppm) 7.17 (t, J = 8.0 Hz, 2H), 6.95 (s, 4H), 6.92 (s, 2H), 6.66 (d, ³J = 7.9 Hz, 2H), 3.75 (br s, 2H, NH₂), 2.27 (s, 12H). ³¹P{¹H} NMR (CDCl₃): δ (ppm) –6.48. ¹³C{¹H} (CDCl₃): δ (ppm) 147.16, 138.1 (d, J = 9.9 Hz), 137.8 (d, J = 7.1 Hz), 135.7 (d, J = 21.4 Hz), 131.2 (d, J = 19.2 Hz), 130.2, 125.1 (d, J = 6.6 Hz), 115.2 (d, J = 8.2 Hz), 21.4. HRMS (ESI, m/z): Calculated for C₂₂H₂₅NP, [M+H]⁺: 334.1720, found: 334.1719.

- Step 2: Synthesis of **BTA-P(Xylyl)2**:

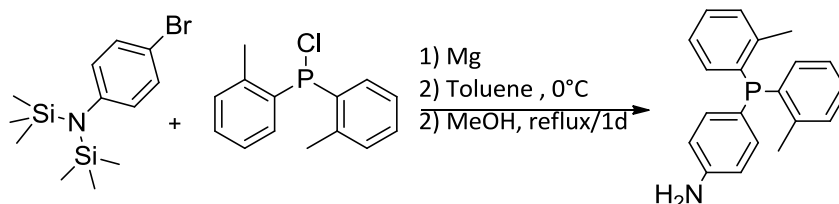


3,5-bis(octylaminocarbonyl)benzoic acid (1.0 g 2.5 mmol, 1.0 equiv.) was suspended in THF (100 mL) under argon and DMAP (0.45 g, 3.8 mmol, 1.5 equiv.), EDC·HCl (0.72 g, 3.8 mmol, 1.5 equiv.) and 4-((bis-(3,5-dimethyl-phenyl)phosphine)-aniline (1.0 g 3.0 mmol, 1.2 equiv.) were added to the flask. The reaction mixture was stirred at reflux temperature for two days under argon. Then the reaction mixture was cooled to room temperature, and the solvent was evaporated under vacuum. DCM was added to the residue, and the organic layer was washed three times with water. Organic layers were combined, dried over magnesium sulfate and evaporated under vacuum. The crude product was purified by flash column chromatography on silica gel, eluting with DCM/ethyl acetate 95:5–88:12 gradient yielding **BTA-P(Xylyl)2** (1.0 g, 1.4 mmol, 55% yield) as a white powder. The product is stable in the solid state and stored at room temperature. ^1H NMR (DMSO- d_6) δ (ppm) 10.60 (s, 1H, ArNH), 8.69 (t, J = 5.5 Hz, 2H, CH_2NH), 8.49-8.47 (m, 2H, CH_{arom} . BTA ring), 8.44-8.41 (m, 1H, BTA ring), 7.82 (d, J = 8.1 Hz, 2H, $2 \times \text{CH}_{\text{arom}}$. linker), 7.27 (t, J = 7.5 Hz, 2H, $2 \times \text{CH}_{\text{arom}}$. linker), 7.01 (s, 2H, $2 \times \text{CH}_{\text{arom}}$. PAR_2), 6.86 (d, J = 8.0 Hz, 4H, $4 \times \text{CH}_{\text{arom}}$. PAR_2), 3.28 (q, J = 7.5 Hz, 4H, CH_2NH), 2.22 (s, 12H, CH_3 xylyl), 1.63-1.46 (m, 4H, $\text{CH}_2\text{CH}_2\text{NH}$), 1.28-1.17 (m, 20H, CH_2), 0.85 (t, J = 6.9 Hz, 6H, CH_3). Signals are present at δ = 1.20, 1.97 and 4.06 ppm for residual ethyl acetate. $^{31}\text{P}\{^1\text{H}\}$ NMR (DMSO- d_6) δ (ppm) -7.42. $^{13}\text{C}\{^1\text{H}\}$ NMR (DMSO- d_6) δ (ppm) 165.18, 165.01, 139.63, 137.53 (d, J = 7.3 Hz), 136.83 (d, J = 11.0 Hz), 135.2, 133.99 (d, J = 20.5 Hz), 131.43 (d, J = 10.4 Hz), 130.77 (d, J = 19.7 Hz), 130.38, 128.92, 128.75, 120.30 (d, J = 7.3 Hz), 31.2, 29.0, 28.7, 28.6, 26.5, 22.1, 20.9, 13.9. HRMS (ESI, m/z): Calculated for $\text{C}_{47}\text{H}_{63}\text{N}_3\text{O}_3\text{P}$, $[\text{M}+\text{H}]^+$: 748.4602, found: 748.4602. FT-IR (ATR, cm^{-1}): 646 (m), 690 (s), 827 (m), 845 (m), 908 (w), 1093 (w), 1124 (w), 1186 (w), 1259 (m), 1290 (s), 1317 (s), 1394

(w), 1464 (m), 1497 (m), 1525 (s), 1555 (m), 1591 (s), 1633 (s), 2855 (m), 2922 (s), 3026 (w), 3086 (w), 3252 (br).

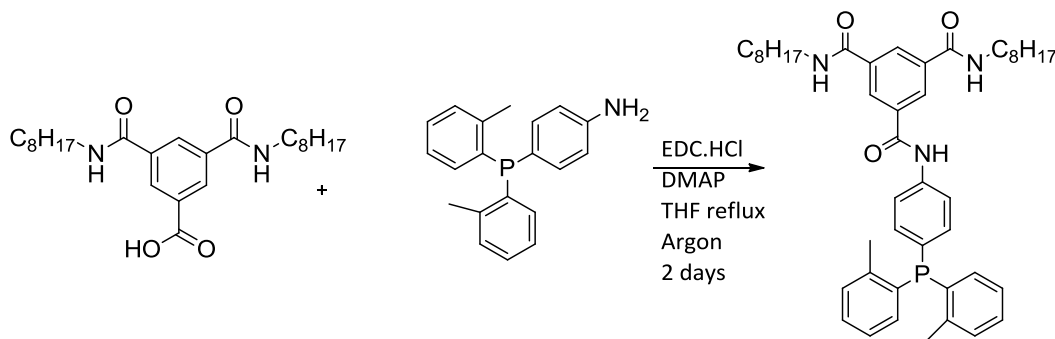
4) Synthesis of **BTA-P(Tolyl)₂**

- Step 1: Synthesis of 4-(di-*o*-tolylphosphino)aniline



In a three-neck round-bottom flask equipped with a condenser under argon, 4-bromo-N,N-bis(trimethylsilyl)aniline (5.78 g, 18.27 mmol, 1.0 equiv.) in THF (16 mL) was added over 40 minutes to a well-stirred dispersion of magnesium turnings (0.53 g, 21.93 mmol, 1.2 equiv.) in THF (just enough to cover the magnesium turnings). Prior to starting the addition, magnesium turnings were activated with a small crystal of I₂ and a drop of 4-bromo-N,N-bis(trimethylsilyl)aniline. The reaction was stirred first at room temperature, then heated to 60°C for 3 hours. THF was evaporated and replaced by dry toluene. Chlorodi-*o*-tolylphosphine (5.0 g, 20.1 mmol, 1.1 equiv.) in toluene (7.4 mL) was added over 15 minutes to the solution of 4-(N,N-trimethylsilyl)2-aniline magnesium bromide while the reaction flask was cooled with in an ice bath. The reaction mixture was stirred for 2 hours. The progress of the reaction was probed by ³¹P{¹H} NMR. The volatiles were removed under vacuum and the solid residue was extracted with dry Et₂O via a cannula to another three-neck round-bottom flask equipped with a special fritted funnel designed to perform filtrations under argon. Et₂O was removed under vacuum, the crude product was then dissolved in MeOH (22 mL) and the solution was stirred at reflux temperature for one day under argon. The solution was evaporated under vacuum, and the crude product was purified by flash column chromatography on silica gel, eluting with DCM/methanol 99:1–95:5 gradient, yielding 4-(di-*o*-tolylphosphino)aniline (2.45 g, 9.5 mmol, 44% yield) as a white powder. ¹H NMR (300 MHz, CDCl₃) δ (ppm) 7.25 (m, 4H), 7.17 – 7.05 (m, 4H), 6.81 (dd, J = 7.3, 4.4 Hz, 2H), 6.69 (d, J = 7.9 Hz, 2H), 3.79 (br s, 2H, NH₂), 2.41 (s, 6H). A signal is present at δ = 5.20 ppm for residual DCM. ³¹P{¹H} NMR (DMSO-d₆) δ (ppm) -22.46.

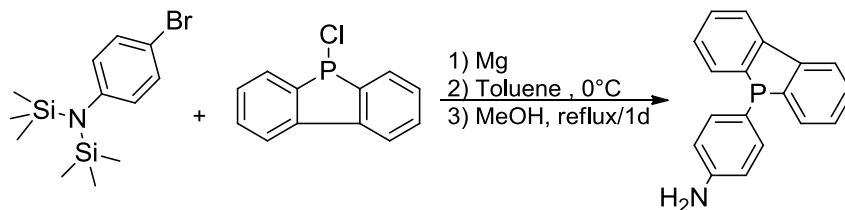
- Step 2: Synthesis of **BTA-P(Tolyl)2**



3,5-bis(octylaminocarbonyl)benzoic acid (1.15 g 2.72 mmol, 1.0 equiv.) was suspended in THF (100 mL) under argon and DMAP (0.5 g, 4.08 mmol, 1.5 equiv.), EDC·HCl (0.78 g, 4.08 mmol, 1.5 equiv.) and 4-(di-*o*-tolylphosphino)aniline (1.0 g, 0.27 mmol, 1.2 equiv.) were added to the flask. The reaction mixture was stirred at reflux temperature for two days under argon. Then the reaction mixture was cooled to room temperature, and the solvent was evaporated under vacuum. DCM was added to the residue, and the organic layer was washed three times with water. Organic layers were combined, dried over magnesium sulfate and evaporated under vacuum. The crude product was purified by flash column chromatography on silica gel, eluting with DCM/ethyl acetate 95:5–88:12 gradient, yielding **BTA-P(Tolyl)2** (1.24 g, 64% yield) as a white solid. The product is stable in the solid state and stored at room temperature. ^1H NMR (300 MHz, DMSO- d_6) δ (ppm) 10.64 (s, 1H, ArNH), 8.69 (t, $J = 5.4$ Hz, 2H, CH_2NH), 8.50 – 8.43 (m, 3H, $\text{CH}_{\text{arom. BTA ring}}$), 7.85 (d, $J = 7.9$ Hz, 2H, $2 \times \text{CH}_{\text{arom. linker}}$), 7.37 – 7.25 (m, 4H, $2 \times \text{CH}_{\text{arom. linker}} + 2 \times \text{CH}_{\text{arom. PAR}_2}$), 7.25 – 7.09 (m, 4H, $\text{CH}_{\text{arom. PAR}_2}$), 6.73 – 6.61 (m, 2H, $\text{CH}_{\text{arom. PAR}_2}$), 3.28 (q, 4H, CH_2NH), 2.31 (s, 6H, CH_3 toyl), 1.54 (q, $J = 6.5$ Hz, 4H, $\text{CH}_2\text{CH}_2\text{NH}$), 1.41 – 1.19 (m, 20H, CH_2), 0.93 – 0.77 (m, 6H, CH_3). $^{31}\text{P}\{^1\text{H}\}$ NMR (122 MHz, DMSO- d_6) δ (ppm) -22.99. $^{13}\text{C}\{^1\text{H}\}$ NMR (DMSO- d_6) δ (ppm) 165.69, 165.57, 142.11, 141.77, 140.50, 135.70 (d, $J = 2.6$ Hz), 135.44, 135.29, 135.15, 134.87, 132.53, 130.66 (d, $J = 4.5$ Hz), 129.30, 126.69, 120.98 (d, $J = 7.3$ Hz), 114.96, 31.73, 29.49, 29.18 (d, $J = 7.3$ Hz), 26.99, 22.56, 21.24, 20.97, 14.38. FT-IR (ATR, cm^{-1}): 644 (m), 717 (m), 744 (s), 829 (m), 1294 (s), 1450 (m), 1521 (s), 1587 (m), 1629 (s), 2856 (w), 2927 (m), 3053 (w), 3238 (bw).

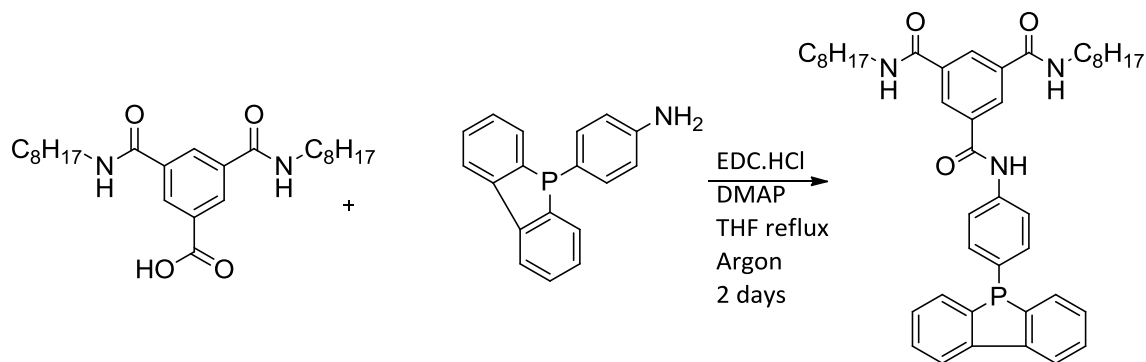
5) Synthesis of **BTA-BPPH**

- Step 1: Synthesis of 4-(5H-benzo[b]phosphindol-5-yl)aniline



In a three-neck round-bottom flask equipped with a condenser under argon, 4-bromo-N,N-bis(trimethylsilyl)aniline (1.31 g, 4.15 mmol, 1.0 equiv.) in THF (4.1 mL) was added over 40 minutes to a well-stirred dispersion of magnesium turnings (0.12 g, 4.98 mmol, 1.2 equiv.) in THF (just enough to cover the magnesium turnings). Prior to starting the addition, magnesium turnings were activated with a small crystal of I_2 and a drop of 4-bromo-N,N-bis(trimethylsilyl)aniline. The reaction was stirred first at room temperature, then heated to 60°C for 3 hours. THF was evaporated and replaced by dry toluene. 5-chloro-5H-benzo[b]phosphindole (1.0 g, 4.57 mmol, 1.1 equiv.) in toluene (4.1 mL) was added over 5 minutes to the solution of 4-(N,N-trimethylsilyl)₂-aniline magnesium bromide while the reaction flask was cooled with in an ice bath. The reaction mixture was stirred for 1 h. The reaction was monitored by $^{31}P\{^1H\}$ NMR. The volatiles were removed under vacuum and the solid residue was extracted with dry Et_2O via a cannula to another three-neck round-bottom flask equipped with a special fritted funnel designed to perform filtrations under argon. Et_2O was removed under vacuum, the crude product was then dissolved in MeOH (10 mL) and the solution was stirred at reflux temperature for one day under argon. The solution was evaporated under vacuum, and the crude product was purified by flash column chromatography on silica gel, eluting with DCM/methanol 99:1–95:5 gradient, yielding 4-(5H-benzo[b]phosphindol-5-yl)aniline (0.6 g, 53% yield) as a white powder. 1H NMR (300 MHz, $CDCl_3$) δ (ppm) 7.97 (d, J = 7.3 Hz, 2H), 7.70 – 7.65 (m, 2H), 7.47 (td, J = 7.6, 1.2 Hz, 2H), 7.33 (td, J = 7.4, 2.8, 1.0 Hz, 2H), 7.08 (t, J = 8.4 Hz, 2H), 6.55 (d, 2H), 3.73 (br s, 2H, NH_2). A signal is present at δ = 5.20 ppm for residual DCM. $^{31}P\{^1H\}$ NMR (122 MHz, $CDCl_3$) δ (ppm) -11.15.

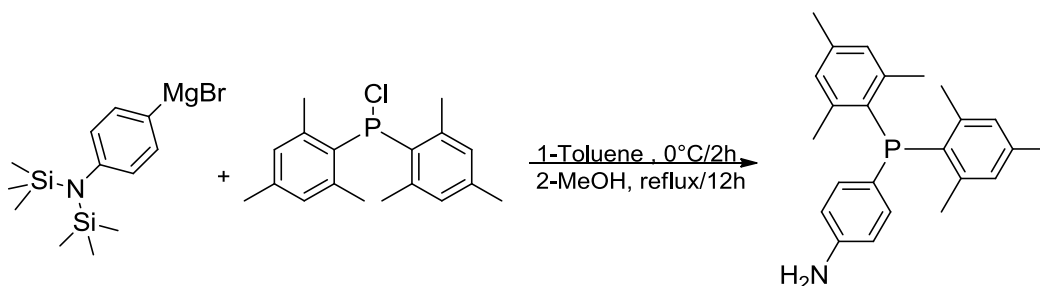
- Step 2: Synthesis of **BTA-BPPH**



3,5-bis(octylamino)carbonyl-benzoic acid (0.83 g, 1.98 mmol, 1.0 equiv.) was suspended in THF (83 mL) under argon and DMAP (0.36 g, 2.97 mmol, 1.5 equiv.), EDC-HCl (0.56 g, 2.97 mmol, 1.5 equiv.) and 4-(5H-benzo[b]phosphindol-5-yl)aniline (0.6 g, 2.17 mmol, 1.2 equiv.) were added to the flask. The reaction mixture was stirred at reflux temperature for two days under argon. Then the reaction mixture was cooled to room temperature, and the solvent was evaporated under vacuum. DCM was added to the residue, and the organic layer was washed three times with water. Organic layers were combined, dried over magnesium sulfate and evaporated under vacuum. The crude product was purified by flash column chromatography on silica gel, eluting with DCM/ethyl acetate 95:5–88:12 gradient, yielding **BTA-BPPH** (0.89 g, 66% yield) as a white solid. The product is stable in the solid state and stored at room temperature. ^1H NMR (300 MHz, DMSO- d_6) δ (ppm) 10.55 (s, 1H, ArNH), 8.67 (t, J = 5.7 Hz, 2H, CH_2NH), 8.43 (br s, 3H, $\text{CH}_{\text{arom. BTA ring}}$), 8.16 (d, J = 7.8 Hz, 2H, $\text{CH}_{\text{arom. PAR}_2}$), 7.80 (t, J = 5.7 Hz, 2H, $\text{CH}_{\text{arom. PAR}_2}$), 7.72 (d, J = 8.5 Hz, 2H, $\text{CH}_{\text{arom. linker}}$), 7.55 (t, J = 7.6 Hz, 2H, $\text{CH}_{\text{arom. linker}}$), 7.42 (td, J = 7.5, 3.6 Hz, 2H, $\text{CH}_{\text{arom. PAR}_2}$), 7.28 (t, J = 8.2 Hz, 2H, $\text{CH}_{\text{arom. PAR}_2}$), 3.28 (q, 4H, CH_2NH), 1.62 – 1.43 (m, 4H, $\text{CH}_2\text{CH}_2\text{NH}$), 1.34 – 1.20 (m, 20H), 0.94 – 0.77 (m, 6H). Signals are present at δ = 1.20, 1.97 and 4.06 ppm for residual ethyl acetate. $^{31}\text{P}\{^1\text{H}\}$ NMR (122 MHz, DMSO- d_6) δ (ppm) -12.14. $^{13}\text{C}\{^1\text{H}\}$ NMR (DMSO- d_6) δ (ppm) 165.67, 165.41, 143.51 (d, J = 2.8 Hz), 142.30 (d, J = 2.9 Hz), 140.63, 135.68, 135.54, 133.11, 132.91, 130.88, 130.67, 130.45, 130.27, 129.41, 129.22, 128.36, 128.29, 122.32, 121.06 (d, J = 7.8 Hz), 31.72, 29.46, 29.16 (d, J = 9.4 Hz), 26.96, 22.55, 14.40. FT-IR (ATR, cm^{-1}): 717 (s), 829 (m), 1182 (m), 1282 (s), 1438 (m), 1519 (s), 1631 (s), 2860 (m), 2929 (m), 3027 (w), 3259 (bw).

6) Synthesis of **BTA-P(Mesityl)2**

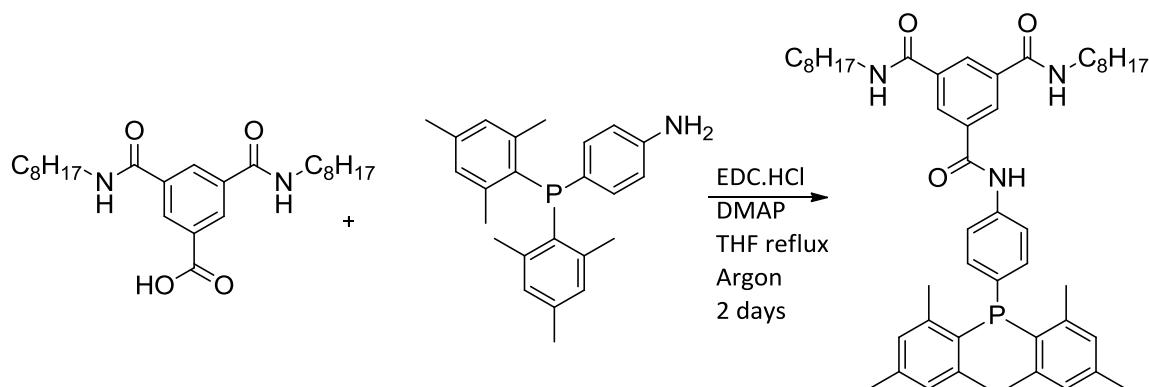
- Step 1: Synthesis of 4-(dimesitylphosphino)aniline



In a three-neck round-bottom flask equipped with a condenser under argon, 4-bromo-N,N-bis(trimethylsilyl)aniline (1.88 g, 5.96 mmol, 1.0 equiv.) in THF (6 mL) was added over 40 minutes to a well-stirred dispersion of magnesium turnings (0.17 g, 7.15 mmol, 1.2 equiv.) in THF (just enough to cover the magnesium turnings). Prior to starting the addition, magnesium turnings were activated with a small crystal of I_2 and a drop of 4-bromo-N,N-bis(trimethylsilyl)aniline. The reaction was stirred first at room temperature, then heated to 60°C for 3 hours. THF was evaporated and replaced by dry toluene. Chlorodimesitylphosphine (2.0 g, 6.56 mmol, 1.1 equiv.) in toluene (4.1 mL) was added over 15 minutes to the in situ generated toluene solution of 4-(N,N-trimethylsilyl)aniline magnesium bromide while the reaction flask was cooled with an ice. The reaction mixture was stirred at RT for overnight. The reaction was monitored by $^{31}P\{^1H\}$ NMR. The volatiles were removed under vacuum and the solid residue was extracted with dry Et_2O via a cannula to another three-neck round-bottom flask equipped with a special fritted funnel designed to perform filtrations under argon. Et_2O was removed under vacuum, the crude product was then dissolved in MeOH (20 mL) and the solution was stirred at reflux temperature for one day under argon. The solution was evaporated under vacuum, and the crude product was purified by flash column chromatography on silica gel, eluting with DCM/methanol 99:1–95:5 gradient yielding 4-(dimesitylphosphino)aniline (0.5 g, 24% yield). The purity of the compound is *ca.* 50% according to 1H NMR. 1H NMR (300 MHz, $CDCl_3$) δ (ppm) 7.25-7.15 (m, 2H), 6.82 (br s, 4H), 6.62 (t, $J = 8.0$ Hz, 2H), 3.69 (br s, 2H), 2.28 (s, 6H), 2.11 (s, 12H). An impurity (lacking the PAR_2 group) is found

together with the desired product with main signals at 7.00, 6.82 and 3.69 ppm. $^{31}\text{P}\{^1\text{H}\}$ NMR (300 MHz, CDCl_3) δ (ppm) -22.94.

- Step 2: Synthesis of **BTA-P(Mesityl)₂**

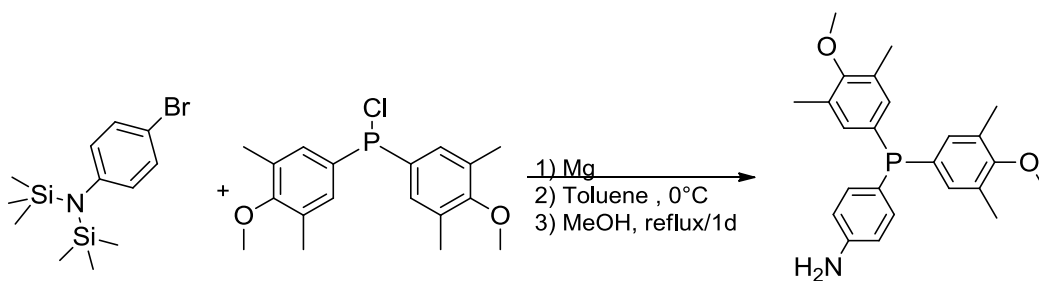


3,5-bis(octylamino)benzoic acid (0.52 g, 1.25 mmol, 1.0 equiv.) was suspended in THF (40 mL) under argon and DMAP (0.22 g, 1.88 mmol, 1.5 equiv.), EDC·HCl (0.36 g, 1.88 mmol, 1.5 equiv.) and 4-(dimesitylphosphino)aniline (0.5 g, \approx 50% pure, 1.38 mmol, 1.1 equiv.) were added to the flask. The reaction mixture was stirred at reflux temperature for two days under argon. Then the reaction mixture was cooled to room temperature, and the solvent was evaporated under vacuum. DCM was added to the residue, and the organic layer was washed three times with water. Organic layers were combined, dried over magnesium sulfate and evaporated under vacuum. The crude product was purified by flash column chromatography on silica gel, eluting with DCM/ethyl acetate 95:5–88:12 gradient, yielding **BTA-P(Mesityl)₂** (121 mg, 13% yield, *ca.* 90% purity). The product is stable in the solid state and stored at room temperature. ^1H NMR (300 MHz, DMSO-d_6) δ (ppm) 10.60 (s, 1H, ArNH), 8.69 (t, J = 5.6 Hz, 2H, CH_2NH), 8.51 – 8.39 (m, 3H, $\text{CH}_{\text{arom.}}$ BTA ring), 7.77 (d, J = 9.3 Hz, 1H, $\text{CH}_{\text{arom.}}$ linker), 7.30 (t, J = 9.6, 7.8 Hz, 2H, $\text{CH}_{\text{arom.}}$ linker), 6.87 (d, J = 18.0 Hz 4H, $\text{CH}_{\text{arom.}}$ PAR_2), 3.31 (q, 4H, CH_2NH), 2.23 (s, 6H, CH_3 mesityl), 2.04 (s, 12H, CH_3 mesityl), 1.64 – 1.47 (m, 4H, $\text{CH}_2\text{CH}_2\text{NH}$), 1.28 (d, 20H, CH_2), 0.87 (t, J = 5.8 Hz, 6H, CH_3). Signals are present at δ = 1.20, 1.97 and 4.06 ppm for residual ethyl acetate. An impurity (\approx 10%) is found together with the desired product with main signals at 10.41 ppm and in the aromatic region. $^{31}\text{P}\{^1\text{H}\}$ NMR (122 MHz, DMSO-d_6) δ (ppm) -23.27. $^{13}\text{C}\{^1\text{H}\}$ NMR (DMSO-d_6) δ (ppm) 142.66 (d, J = 2.9 Hz), 142.38, 142.17, 141.38, 141.25, 141.02

(d, $J = 2.5$ Hz), 138.15, 135.68, 135.64, 135.54, 131.69, 131.41, 131.26, 130.40, 130.37, 130.11, 129.86, 129.31, 129.20, 128.85, 120.43, 31.71, 29.45, 29.16 (d, $J = 7.1$ Hz), 26.96, 23.35 (d, $J = 4.5$ Hz), 23.05, 22.84, 22.55, 20.96, 20.92, 18.01, 14.38. FT-IR (ATR, cm^{-1}): 661 (s), 833 (m), 900 (m), 1110 (m), 1292 (s), 1450 (m), 1517 (s), 1589 (s), 1633 (s), 2852 (m), 292 (m), 3068 (w), 3259 (bw).

7) Synthesis of **BTA-P(DMM)2**

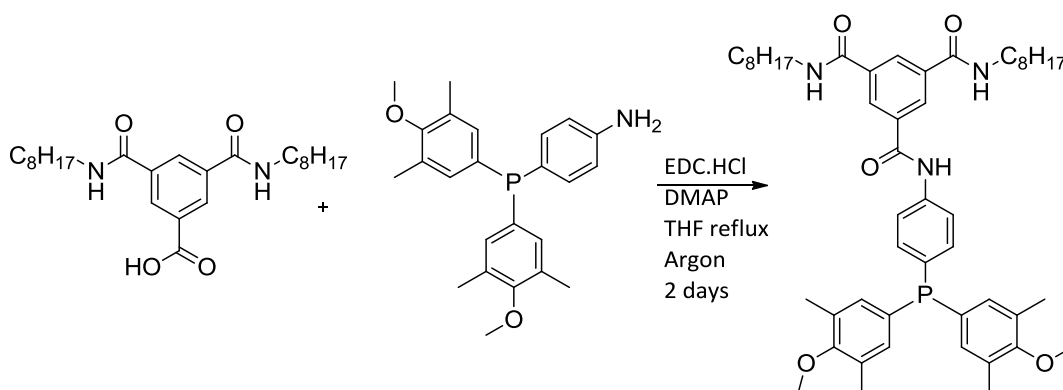
- Step 1: Synthesis of 4-(bis(4-methoxy-3,5-dimethylphenyl)phosphino)aniline



In a three-neck round-bottom flask equipped with a condenser under argon, 4-bromo-N,N-bis(trimethylsilyl)aniline (0.85 g, 2.69 mmol, 1.0 equiv.) in THF (2.7 mL) was added over 40 minutes to a well-stirred dispersion of magnesium turnings (80 mg, 3.23 mmol, 1.2 equiv.) in THF (just enough to cover the magnesium turnings). Prior to starting the addition, magnesium turnings were activated with a small crystal of I_2 and a drop of 4-bromo-N,N-bis(trimethylsilyl)aniline. The reaction was stirred first at room temperature, then heated to 60°C for 3 hours. THF was evaporated and replaced by dry toluene. bis(4-methoxy-3,5-dimethylphenyl)chlorophosphine (1.0 g, 2.96 mmol, 1.1 equiv.) in toluene (4.1 mL) was added over 15 minutes to the toluene solution of 4-(N,N-trimethylsilyl)₂-aniline magnesium bromide while the reaction flask was cooled with in an ice. The reaction mixture was stirred at RT for 4 h. The progress of the reaction was probed by $^{31}\text{P}\{^1\text{H}\}$ NMR. The volatiles were removed under vacuum and the solid residue was extracted with dry Et_2O via a cannula to another three-neck round-bottom flask equipped with a special fritted funnel designed to perform filtrations under argon. Et_2O was removed under vacuum, the crude product was then dissolved in MeOH (10 mL) and the solution was stirred at reflux temperature for one day under argon. The solution was evaporated under vacuum, and the crude product was purified by flash column

chromatography on silica gel, eluting with DCM/methanol 99:1–95:5 gradient, yielding 4-(bis(4-methoxy-3,5-dimethylphenyl)phosphino)aniline (60 mg, 6% yield, 60-70% purity). ^1H NMR (300 MHz, CDCl_3) δ (ppm) 7.15 (t, $J = 8.0$ Hz, 2H), 6.96 (d, $J = 7.7$ Hz, 4H), 6.68 (d, $J = 8.0$ Hz, 2H), 3.74 (s, 6H), 2.24 (s, 12H). $^{31}\text{P}\{^1\text{H}\}$ NMR (122 MHz, CDCl_3) δ (ppm) -8.50. An impurity ($\approx 30\text{-}40\%$) is found together with the desired product which might be the phosphine oxide ($\delta = 41.36$ ppm in $^{31}\text{P}\{^1\text{H}\}$ NMR).

- Step 2: Synthesis of **BTA-P(DMM)2**

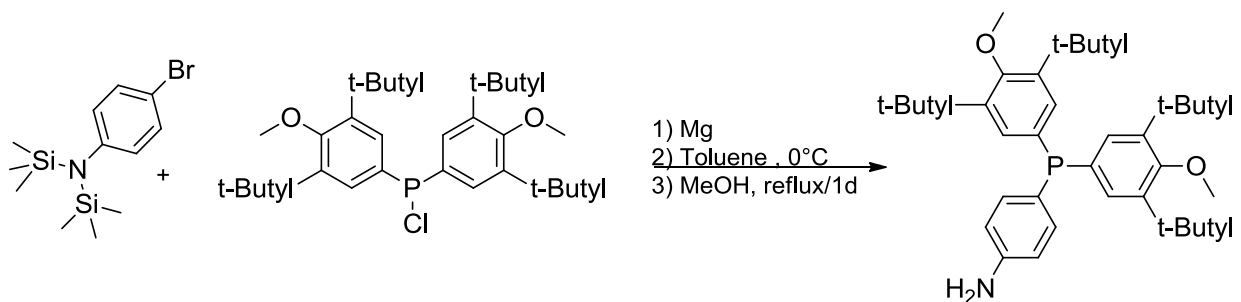


3,5-bis(octylamino)benzoic acid (64 mg, 0.15 mmol, 1.0 equiv.) was suspended in THF (6 mL) under argon and DMAP (28 mg, 0.26 mmol, 1.5 equiv.), EDC·HCl (43 mg, 0.26 mmol, 1.5 equiv.) and 4-(bis(4-methoxy-3,5-dimethylphenyl)phosphino)aniline (60 mg, 60-70% purity, 0.16 mmol, 1.1 equiv.) were added to the flask. The reaction mixture was stirred at reflux temperature for two days under argon. Then the reaction mixture was cooled to room temperature, and the solvent was evaporated under vacuum. DCM was added to the residue, and the organic layer was washed three times with water. Organic layers were combined, dried over magnesium sulfate and evaporated under vacuum. The crude product was purified by flash column chromatography on silica gel, eluting with DCM/ethyl acetate 95:5–88:12 gradient yielding **BTA-P(DMM)2** (27 mg, 23% yield). The product is stable in the solid state and stored at room temperature. ^1H NMR (300 MHz, DMSO-d_6) δ (ppm) 10.60 (s, 1H, ArNH), 8.70 (t, $J = 5.7$ Hz, 2H, CH_2NH), 8.55 – 8.40 (m, 3H, $\text{CH}_{\text{arom.}}$ BTA ring), 7.82 (d, $J = 8.4$ Hz, 2H, $\text{CH}_{\text{arom.}}$ linker), 7.26 (t, $J = 7.9$ Hz, 2H, $\text{CH}_{\text{arom.}}$ linker), 6.95 (d, $J = 7.7$ Hz, 4H, $\text{CH}_{\text{arom.}}$ PAR_2), 3.68 (s, 6H, OMe), 3.28 (q, 4H, CH_2NH), 2.20 (s, 12H, ArCH_3), 1.56 (qt, 4H, $\text{CH}_2\text{CH}_2\text{NH}$), 1.28 (m, 20H, CH_2), 0.86 (t, $J = 6.4$ Hz, 6H,

CH₃). Signals are present at δ = 1.20, 1.97 and 4.06 ppm for ethyl acetate. ³¹P{¹H} NMR (122 MHz, DMSO-d₆) δ (ppm) -9.03. FT-IR (ATR, cm⁻¹): 688 (s), 825 (m), 1010 (s), 1112 (s), 1217 (s), 1267 (s), 1467 (s), 1519 (s), 1637 (s), 2856 (m), 2927 (m), 3087 (w), 3242 (bw). Given the limited amount, the product was only characterized by ¹H NMR, ³¹P NMR and FT-IR.

8) Synthesis of **BTA-P(DTBM)2**

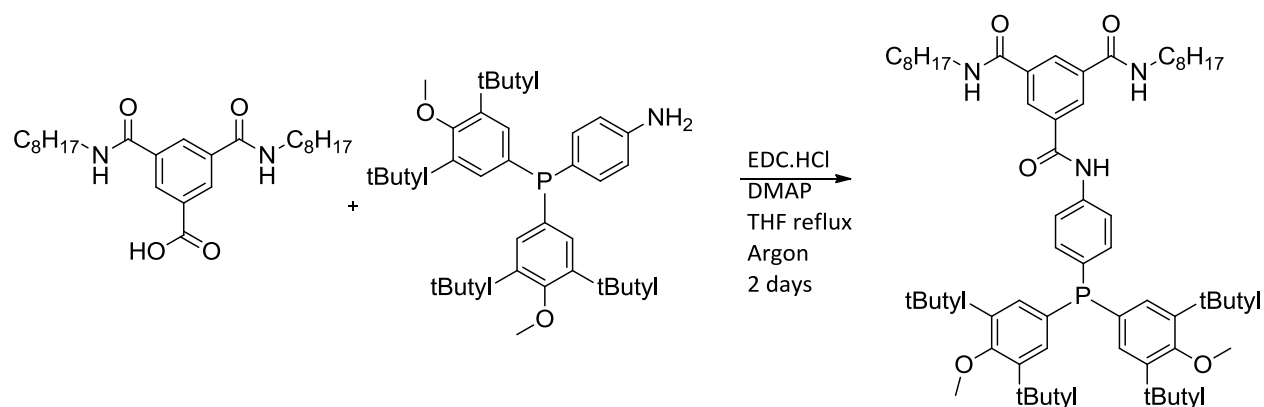
- Step 1: Synthesis of: 4-(bis(3,5-di-tert-butyl-4-methoxyphenyl)phosphino)aniline



In a three-neck round-bottom flask equipped with a condenser under argon, 4-bromo-N,N-bis(trimethylsilyl)aniline (1.3 g, 4.13 mmol, 1.0 equiv.) in THF (4.1 mL) was added over 40 minutes to a well-stirred dispersion of magnesium turnings (120 mg, 4.95 mmol, 1.2 equiv.) in THF (just enough to cover the magnesium turnings). Prior to starting the addition, magnesium turnings were activated with a small crystal of I₂ and a drop of 4-bromo-N,N-bis(trimethylsilyl)aniline. The reaction was stirred first at room temperature, then heated to 60°C for 3 hours. bis(3,5-di-tert-butyl-4-methoxyphenyl)chlorophosphine (2.5 g, 4.95 mmol, 1.2 equiv.) in THF (4.1 mL) was added over 15 minutes to the toluene solution of 4-(N,N-trimethylsilyl)₂-aniline magnesium bromide while the reaction flask was cooled with in an ice. The reaction mixture was stirred at RT for 1 h. The reaction was monitored by ³¹P{¹H} NMR. The volatiles were removed under vacuum and the solid residue was extracted with dry Et₂O via a cannula to another three-neck round-bottom flask equipped with a special fritted funnel designed to perform filtrations under argon. Et₂O was removed under vacuum, the crude product was then dissolved in MeOH (10 mL) and the solution was stirred at reflux temperature for one day under argon. The solution was evaporated under vacuum, and the crude product was purified by flash column chromatography on silica gel, eluting with DCM/methanol 99:1–95:5 gradient, yielding 4-(bis(3,5-di-tert-butyl-4-methoxyphenyl)phosphino)aniline (700 mg,

30% yield). ^1H NMR (300 MHz, C_6D_6) δ (ppm) 7.56 (d, J = 7.6 Hz, 4H), 7.47 (t, J = 7.8 Hz, 2H), 6.28 (d, J = 8.1 Hz, 2H), 3.39 (s, 6H), 2.74 (br s, 2H, NH_2), 1.39 (s, 36H). $^{31}\text{P}\{^1\text{H}\}$ NMR (122 MHz, C_6D_6) δ (ppm) -6.68.

- Step 2: Synthesis of **BTA-P(DTBM)2**

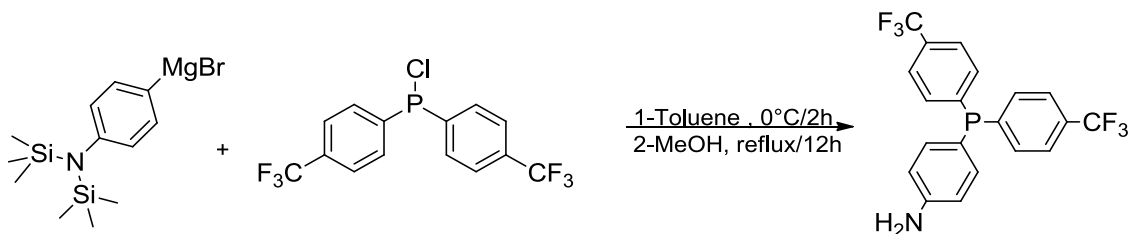


3,5-bis(octylamino)benzoic acid (400 mg, 0.96 mmol, 1.0 equiv.) was suspended in THF (30 mL) under argon and DMAP (170 mg, 1.4 mmol, 1.5 equiv.), EDC·HCl (260 mg, 1.4 mmol, 1.5 equiv.) and 4-(bis(3,5-di-tert-butyl-4-methoxyphenyl)phosphino)aniline (600 mg, 1.06 mmol, 1.1 equiv.) were added to the flask. The reaction mixture was stirred at reflux temperature for two days under argon. Then the reaction mixture was cooled to room temperature, and the solvent was evaporated under vacuum. DCM was added to the residue, and the organic layer was washed three times with water. Organic layers were combined, dried over magnesium sulfate and evaporated under vacuum. The crude product was purified by flash column chromatography on silica gel, eluting with DCM/ethyl acetate 95:5–88:12 gradient, yielding **BTA-P(DTBM)2** (600 mg, 65% yield). The product is stable in the solid state and stored at room temperature. ^1H NMR (300 MHz, DMSO-d_6) δ (ppm) 10.59 (s, 1H, ArNH), 8.69 (t, J = 5.5 Hz, 2H, CH_2NH), 8.47 (m, J = 11.8 Hz, 3H, $\text{CH}_{\text{arom. BTA ring}}$), 7.84 (d, J = 8.1 Hz, 2H, $\text{CH}_{\text{arom. linker}}$), 7.25 (t, J = 7.9 Hz, 2H, $\text{CH}_{\text{arom. linker}}$), 7.05 (d, J = 7.7 Hz, 4H, $\text{CH}_{\text{arom. PAr}_2}$), 3.64 (s, 6H, OMe of DTBM), 3.29 (d, J = 9.3 Hz, 4H, CH_2NH), 1.75–1.42 (m, 4H, $\text{CH}_2\text{CH}_2\text{NH}$), 1.41 – 1.12 (m, 56H, $10 \times \text{CH}_2 + 4 \times t\text{-Bu}$), 0.95 – 0.77 (m, 6H, CH_3). $^{31}\text{P}\{^1\text{H}\}$ NMR (122 MHz, DMSO-d_6) δ (ppm) -7.78. $^{13}\text{C}\{^1\text{H}\}$ NMR (DMSO-d_6) δ (ppm) 165.68, 165.44, 160.04, 143.56 (d, J = 6.7 Hz), 139.98, 135.67, 135.63, 134.19, 133.99, 132.97, 132.86, 132.02, 131.82, 131.18 (d, J = 9.1 Hz), 129.43, 129.24, 120.68 (d,

J= 7.1 Hz), 64.69, 35.88, 32.19, 32.05, 31.72, 29.47, 29.22, 29.13, 26.97, 22.56, 14.40. FT-IR (ATR, cm^{-1}): 692 (s), 825 (s), 881 (m), 1012 (s), 1116 (s), 1220 (s), 1292 (s), 1390 (s), 1531 (s), 1631 (s), 2856 (m), 2926 (s), 2954 (s), 3087 (w), 3247 (bw).

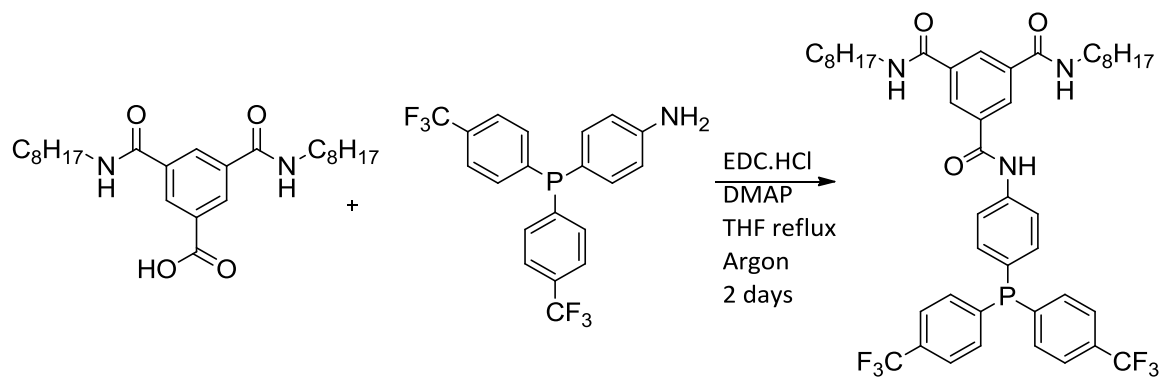
9) Synthesis of **BTA-P(MTF)2**

- Step 1: synthesis of 4-(bis(4-(trifluoromethyl)phenyl)phosphino)aniline



Bis(4-(trifluoromethyl)phenyl)chlorophosphine (2.8 mmol, 1.0 g, 1.2 equiv.) in dry toluene was added dropwise to a 1 M solution of (N-trimethylsilyl)₂-4-magnesiumbromide (2.34 mmol, 2.4 mL, 1 equiv.) at 0 °C. The reaction mixture was stirred for 2 hours at 0°C. The reaction was monitored by ³¹P{¹H} NMR. The volatiles were removed under vacuum and the solid residue was extracted with dry Et₂O via a cannula to another three-neck round-bottom flask equipped with a special fritted funnel designed to perform filtrations under argon. Et₂O was removed under vacuum, the crude product was then dissolved in MeOH (10 mL) and the solution was stirred at reflux temperature for one day under argon. The solution was evaporated under vacuum, and the crude product was purified by flash column chromatography on silica gel, eluting with DCM/methanol 99:1–95:5 gradient, yielding 4-(bis(4-(trifluoromethyl)phenyl)phosphino)aniline (500 mg, 52% yield). ¹H NMR (400 MHz, Toluene d₈) δ (ppm) 7.26 – 7.15 (m, 4H), 7.14 – 7.04 (m, 6H), 6.16 (d, J 8.0 Hz, 2H), 2.82 (br s, 2H, NH₂). ³¹P{¹H} NMR (122 MHz, C₆D₆) δ (ppm) -6.47.

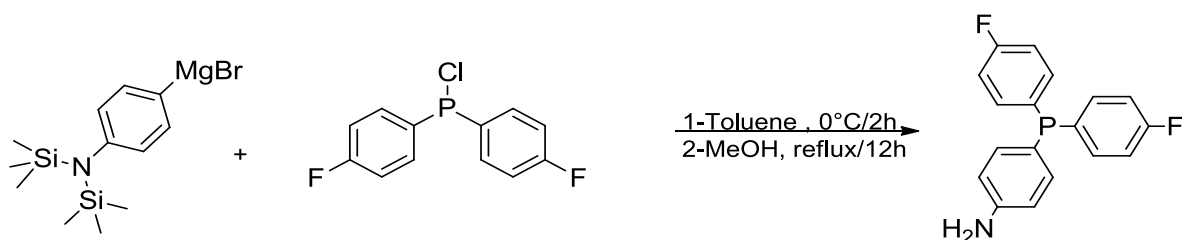
- Step 2: synthesis of **BTA-P(MTF)2**



3,5-bis(octylamino)carbonyl-benzoic acid (0.97 mmol, 417 mg, 1.0 equiv.) was suspended in THF (30 mL) under argon and DMAP (1.36 mmol, 166 mg, 1.5 equiv.), EDC·HCl (1.36 mmol, 260 mg, 1.5 equiv.) and 4-(bis(4-(trifluoromethyl)phenyl)phosphino)aniline (1.21 mmol, 500 mg, 1.1 equiv.) were added to the flask. The reaction mixture was stirred at reflux temperature for two days under argon. Then the reaction mixture was cooled to room temperature, and the solvent was evaporated under vacuum. DCM was added to the residue, and the organic layer was washed three times with water. Organic layers were combined, dried over magnesium sulfate and evaporated under vacuum. The crude product was purified by flash column chromatography on silica gel, eluting with DCM/ethyl acetate 95:5–88:12 gradient, yielding **BTA-P(MTF)₂** (543 mg, 67% yield). ¹H NMR (400 MHz, DMSO-d₆): δ (ppm) 10.69 (s, 1H, ArNH), 8.69 (t, J= 5.3 Hz, 2H, CH₂NH), 8.55 – 8.39 (m, 3H, CH_{arom.} BTA ring), 7.92 (d, J= 8.2 Hz, 2H, CH_{arom.} linker), 7.79 (d, J= 7.9 Hz, 4H, CH_{arom.} PAR₂), 7.48 (t, J= 7.4 Hz, 4H, CH_{arom.} PAR₂), 7.38 (t, J= 8.0 Hz, 2H, CH_{arom.} linker), 3.40 – 3.16 (m, 4H, CH₂NH), 1.61 – 1.47 (m, 4H, CH₂CH₂NH), 1.39 – 1.15 (m, 20H, CH₂), 0.84 (t, J= 6.1 Hz, 6H, CH₃). ³¹P{¹H} NMR (122 MHz, DMSO-d₆): δ (ppm) -7.32. ¹⁹F{¹H} NMR (122 MHz, DMSO-d₆): δ (ppm) -61.29. ¹³C{¹H} NMR (122 MHz, DMSO-d₆) δ (ppm) 165.66, 142.67, 142.52, 141.23, 135.71, 135.58, 135.34, 135.12, 134.24, 134.04, 129.98, 129.66, 129.48, 129.30, 128.98, 128.89, 128.60, 126.05, 126.02, 125.99, 125.95, 125.91, 125.89, 123.18, 121.16 (d, J= 8.2 Hz), 31.73, 29.48, 29.22, 29.13, 26.98, 22.56, 14.39.

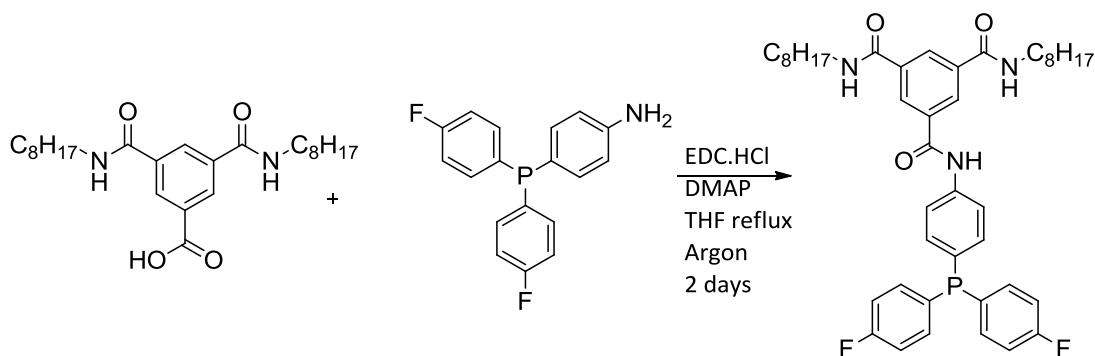
10) Synthesis of **BTA-P(PhF)₂**

- Step 1: synthesis of 4-(bis(4-fluorophenyl)phosphino)aniline



Bis(4-fluorophenyl)chlorophosphine (11.7 mmol, 3.0 g, 1.2 equiv.) in dry toluene was added dropwise to a 1 M solution of (N-trimethylsilyl)₂-4-magnesiumbromide (9.7 mL, 9.7 mmol, 1 equiv.) at 0 °C. The reaction mixture was stirred for 2 hours at 0°C. The reaction was monitored by ³¹P{¹H} NMR. The volatiles were removed under vacuum and the solid residue was extracted with dry Et₂O via a cannula to another three-neck round-bottom flask equipped with a special fritted funnel designed to perform filtrations under argon. Et₂O was removed under vacuum, the crude product was then dissolved in MeOH (10 mL) and the solution was stirred at reflux temperature for one day under argon. The solution was evaporated under vacuum, and the crude product was purified by flash column chromatography on silica gel, eluting with DCM/methanol 99:1–95:5 gradient, yielding 4-(bis(4-fluorophenyl)phosphino)aniline (400 mg, 11% yield) as a colorless solid. ¹H NMR (400 MHz, Toluene d-8): δ (ppm) 7.20 – 7.11 (m, 6H), 6.75 (t, *J* = 8.5 Hz, 4H), 6.22 (d, 2H), 2.86 (br s, 2H) ppm. A signal is present at δ = 4.35 ppm for residual DCM. ³¹P{¹H} NMR (122 MHz, toluene d-8) δ (ppm) = -8.74.

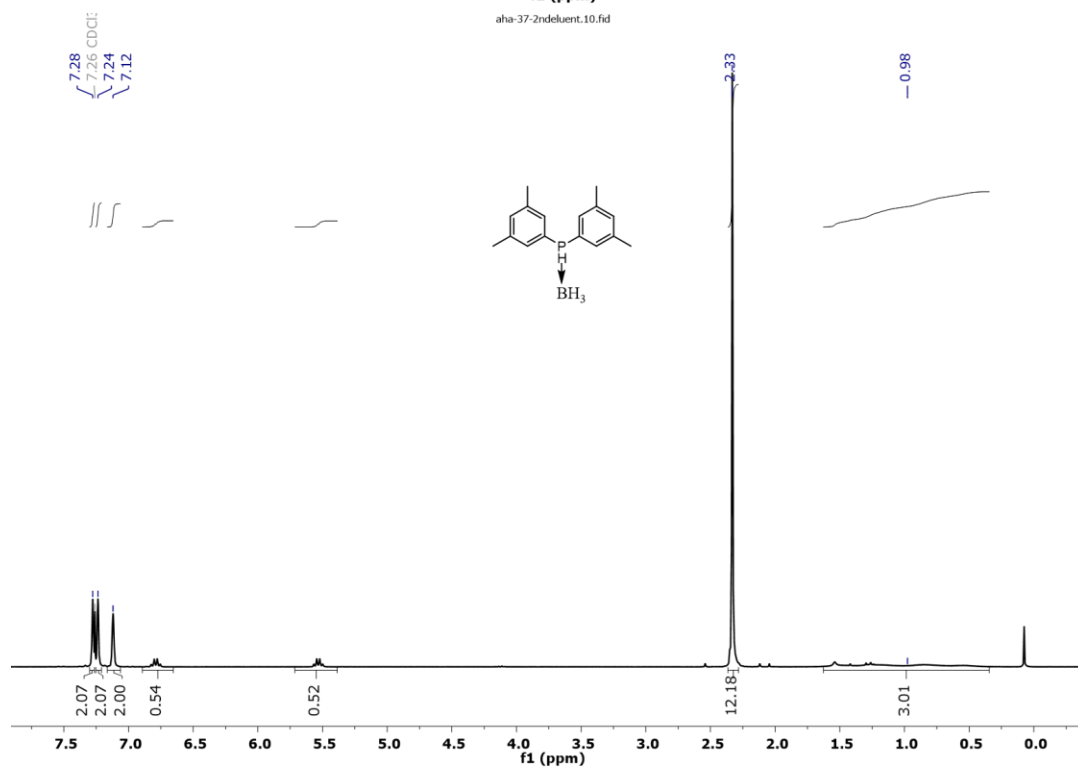
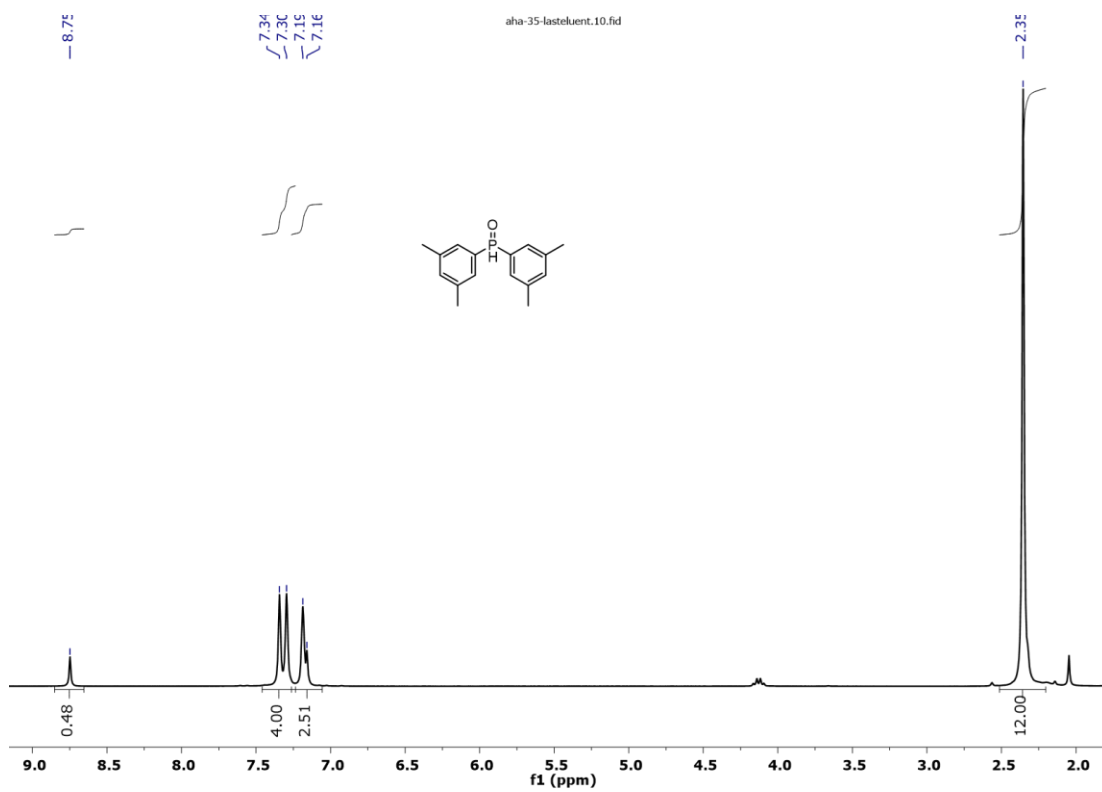
- Step 2: synthesis of **BTA-P(PhF)₂**

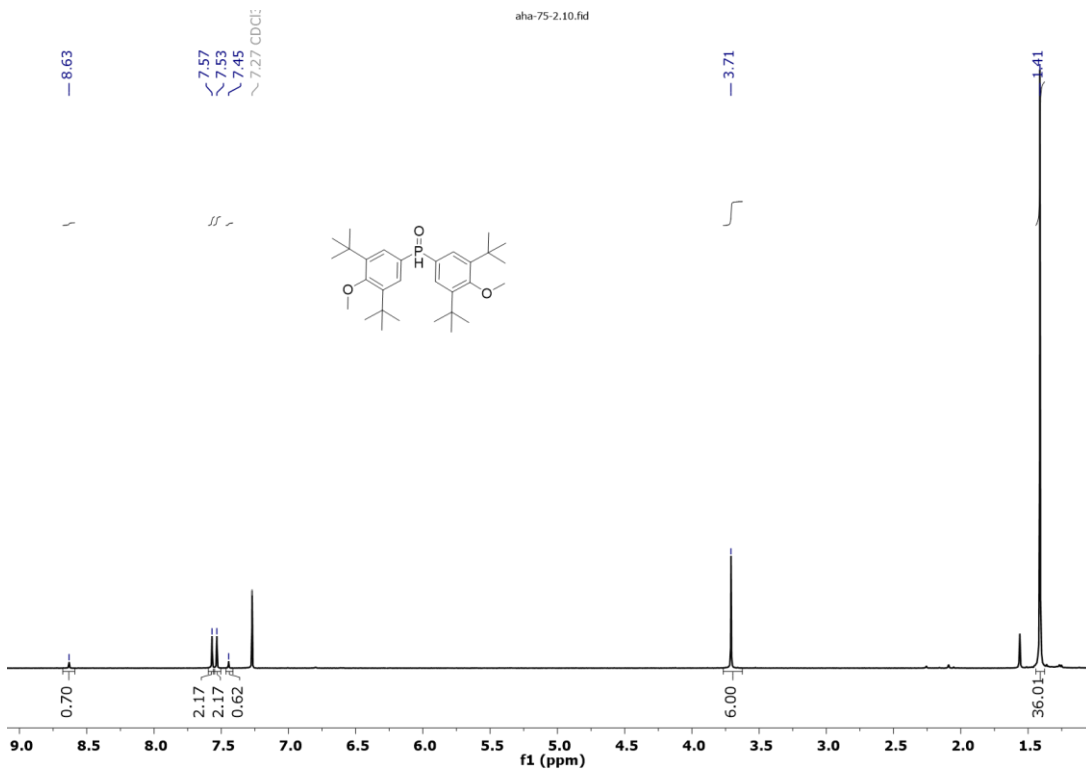
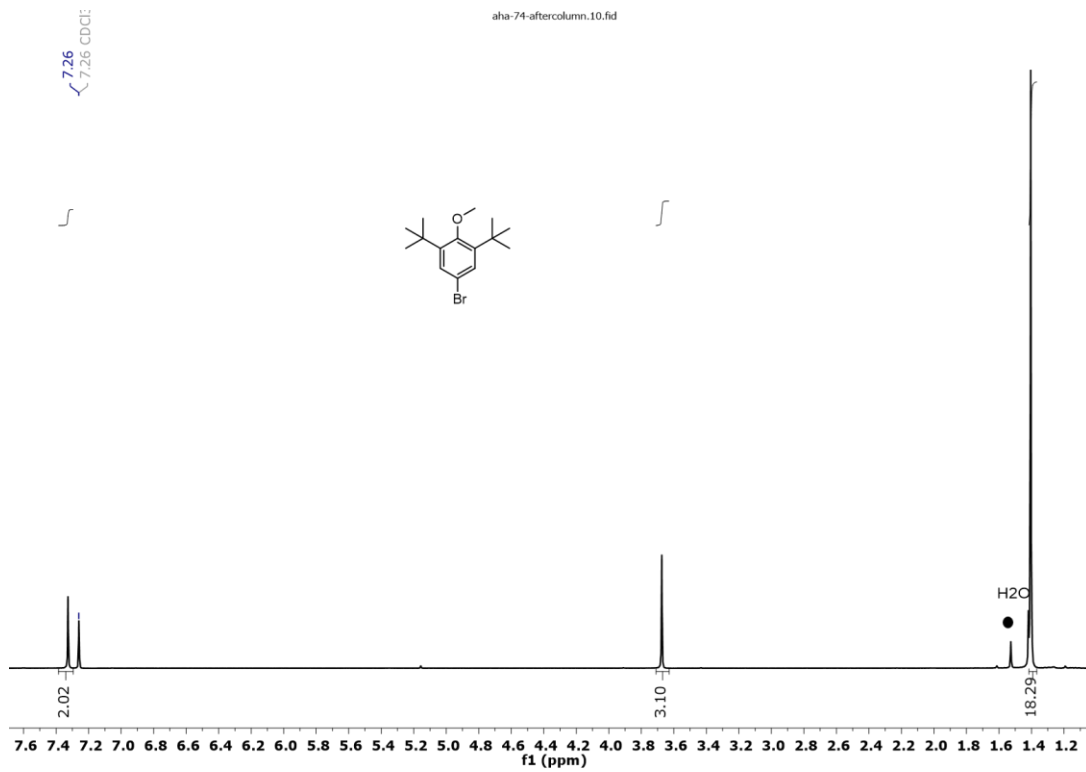


3,5-bis(octylaminocarbonyl)benzoic acid (1 mmol, 430 mg, 1.0 equiv.) was suspended in THF (30 mL) under argon and DMAP (1.43 mmol, 175 mg, 1.5 equiv.), EDC·HCl (1.43 mmol, 275 mg, 1.5 equiv.) and 4-(bis(4-fluorophenyl)phosphino)aniline (1.28 mmol, 400 mg, 1.1 equiv.) were

added to the flask. The reaction mixture was stirred at reflux temperature for two days under argon. Then the reaction mixture was cooled to room temperature, and the solvent was evaporated under vacuum. DCM was added to the residue, and the organic layer was washed three times with water. Organic layers were combined, dried over magnesium sulfate and evaporated under vacuum. The crude product was purified by flash column chromatography on silica gel, eluting with DCM/ethyl acetate 95:5–88:12 gradient, yielding **BTA-P(PhF)₂** (338 mg, 67% yield) as a colorless solid. ¹H NMR (400 MHz, DMSO-d₆) δ (ppm) 10.63 (s, 1H, ArNH), 8.69 (t, J = 5.6 Hz, 2H, CH₂NH), 8.53 – 8.40 (m, 3H, CH_{arom.} BTA ring), 7.85 (d, J= 8.2 Hz, 2H, CH_{arom.} linker), 7.44 – 7.10 (m, 10H, 2× CH_{arom.} linker + 8× CH_{arom.} PAr₂), 3.28 (dd, J= 11.7, 5.4 Hz, 4H, CH₂NH), 1.60 – 1.48 (m, 4H, CH₂CH₂NH), 1.45 – 1.07 (m, 20H, CH₂), 0.85 (t, J= 6.4 Hz, 6H, CH₃). ³¹P{¹H} NMR (122 MHz, DMSO-d₆) δ (ppm) -10.15. ¹⁹F{¹H} NMR (122 MHz, DMSO-d₆) δ (ppm) -112.23. ¹³C{¹H} NMR (122 MHz, DMSO-d₆) δ (ppm) 165.67, 165.56, 164.44, 161.98, 140.51, 135.95 (d, J= 8.2 Hz), 135.74 (d, J= 8.7 Hz), 134.41, 134.21, 129.44, 129.27, 120.97 (d, J= 7.1 Hz), 116.57 (d, J= 7.4 Hz), 116.36 (d, J= 7.4 Hz), 31.72, 29.47, 29.17 (d, J= 9.6 Hz), 26.97, 22.56, 14.41.

II.6.c. NMR data.

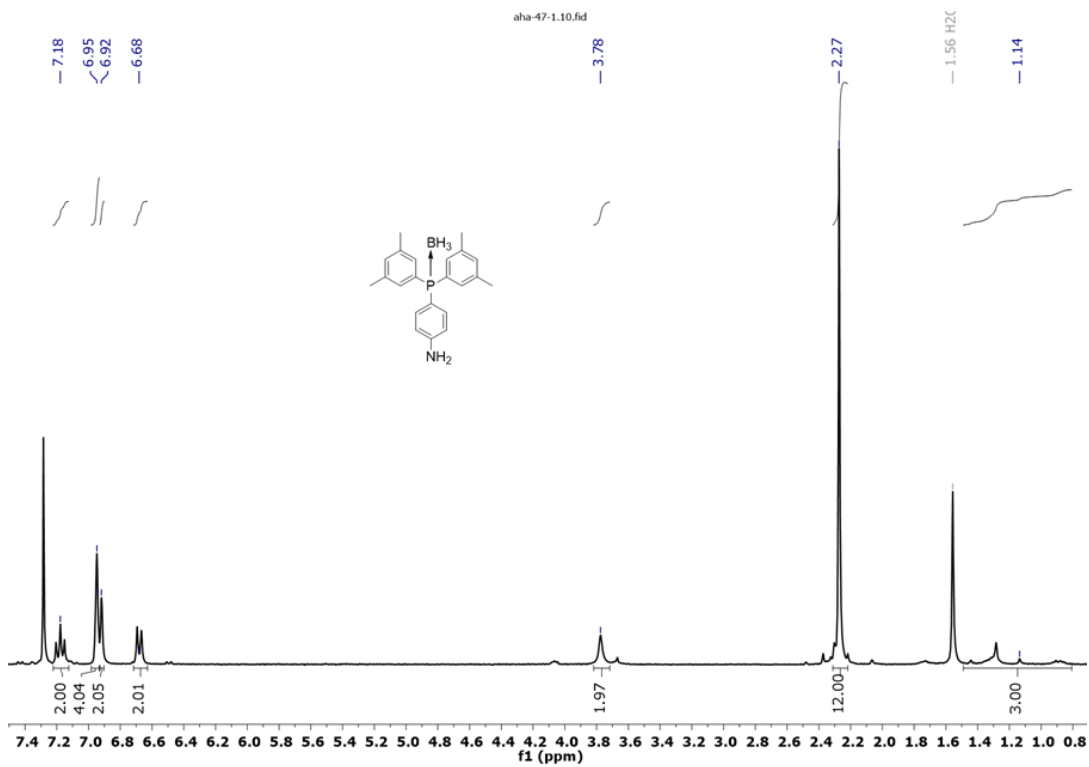
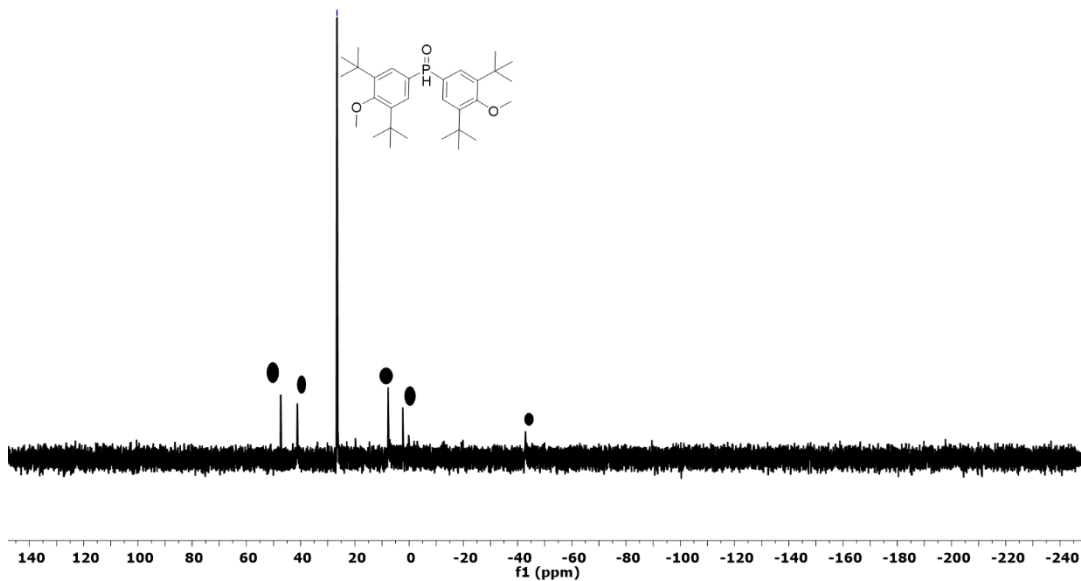


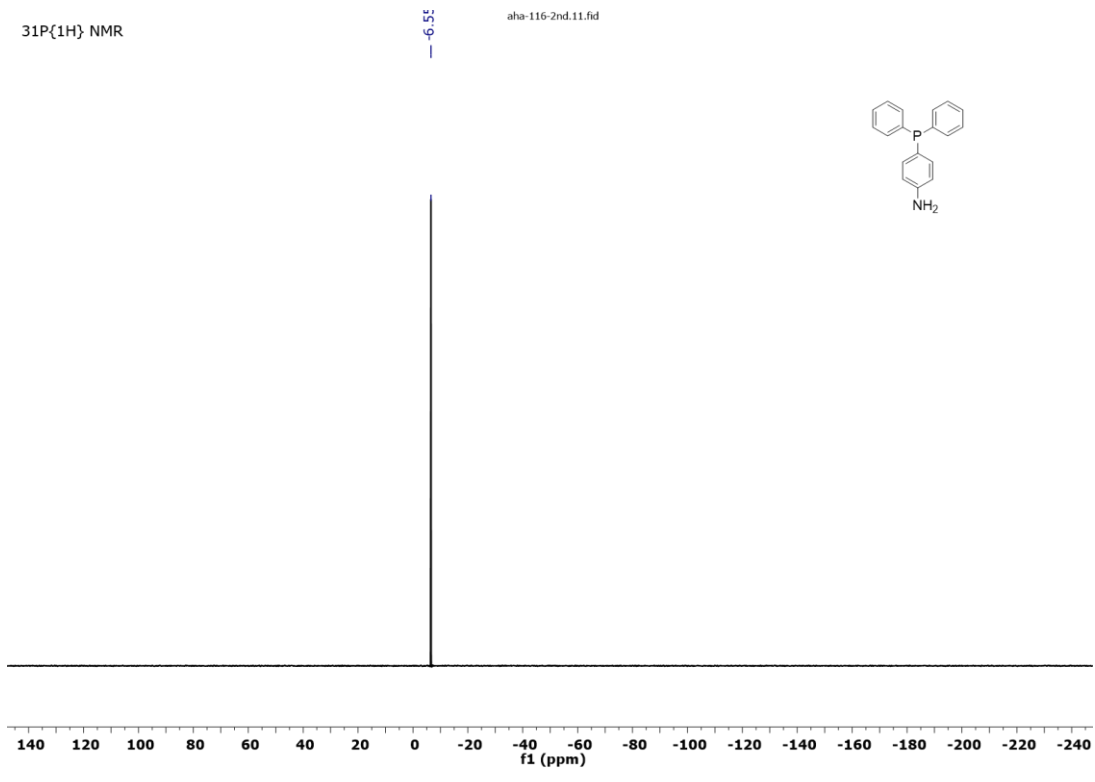
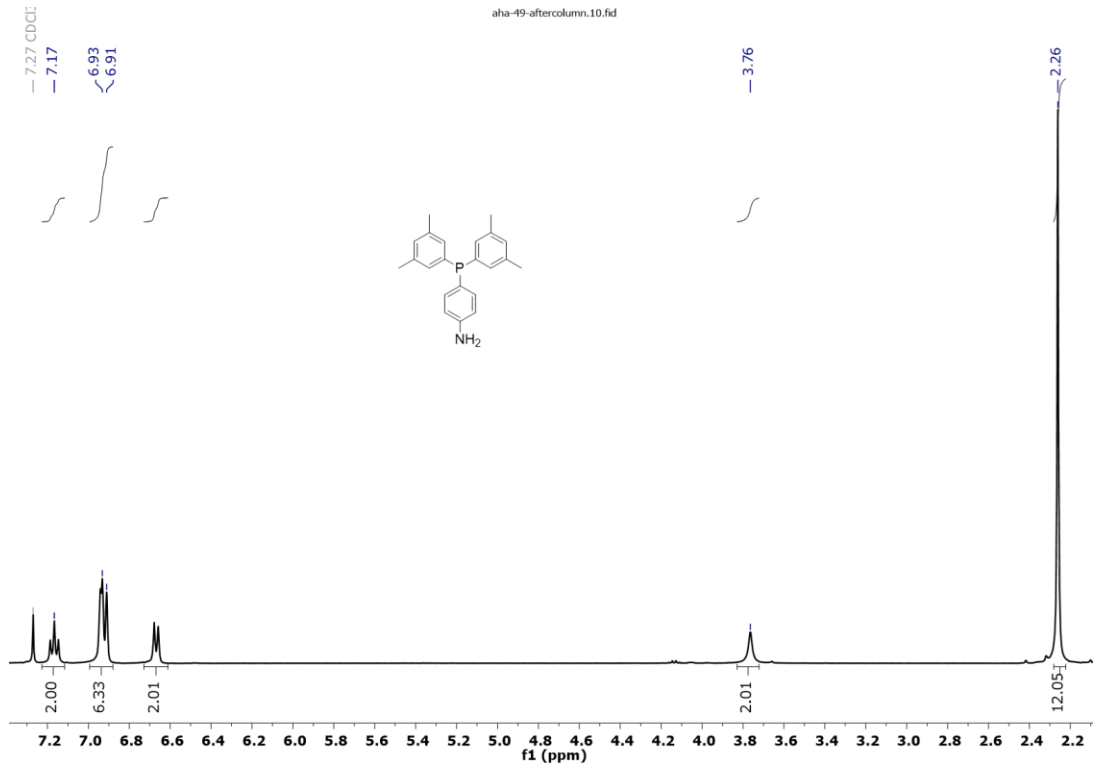


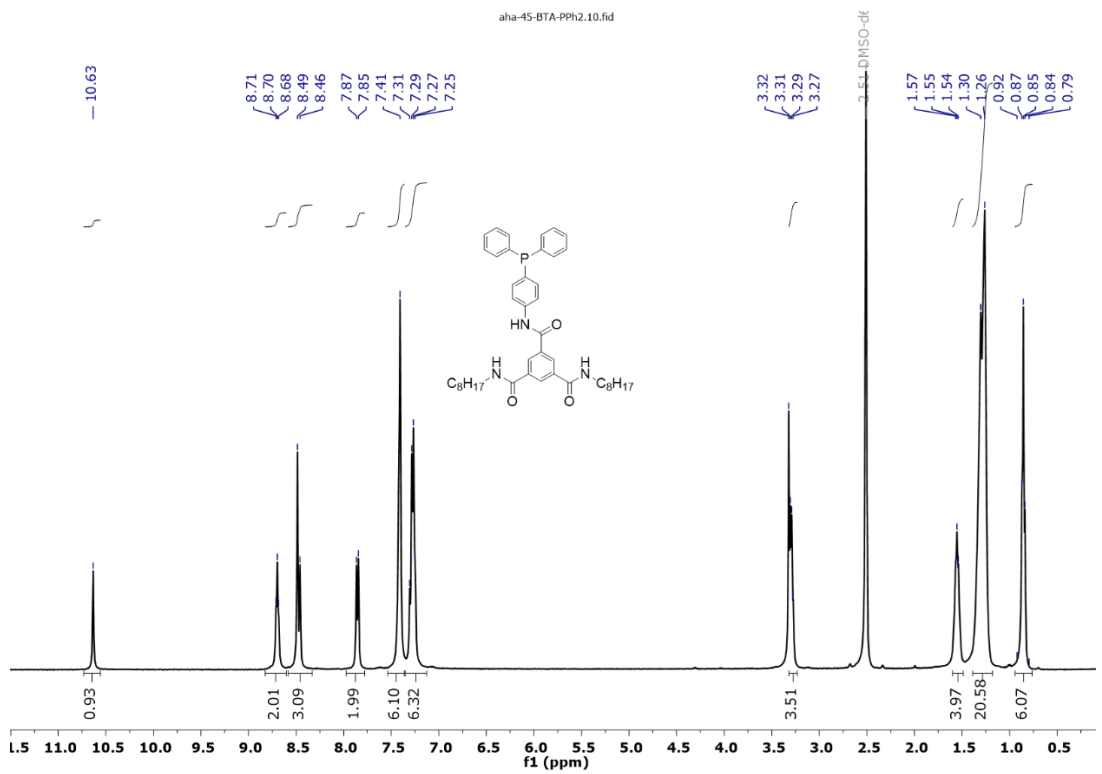
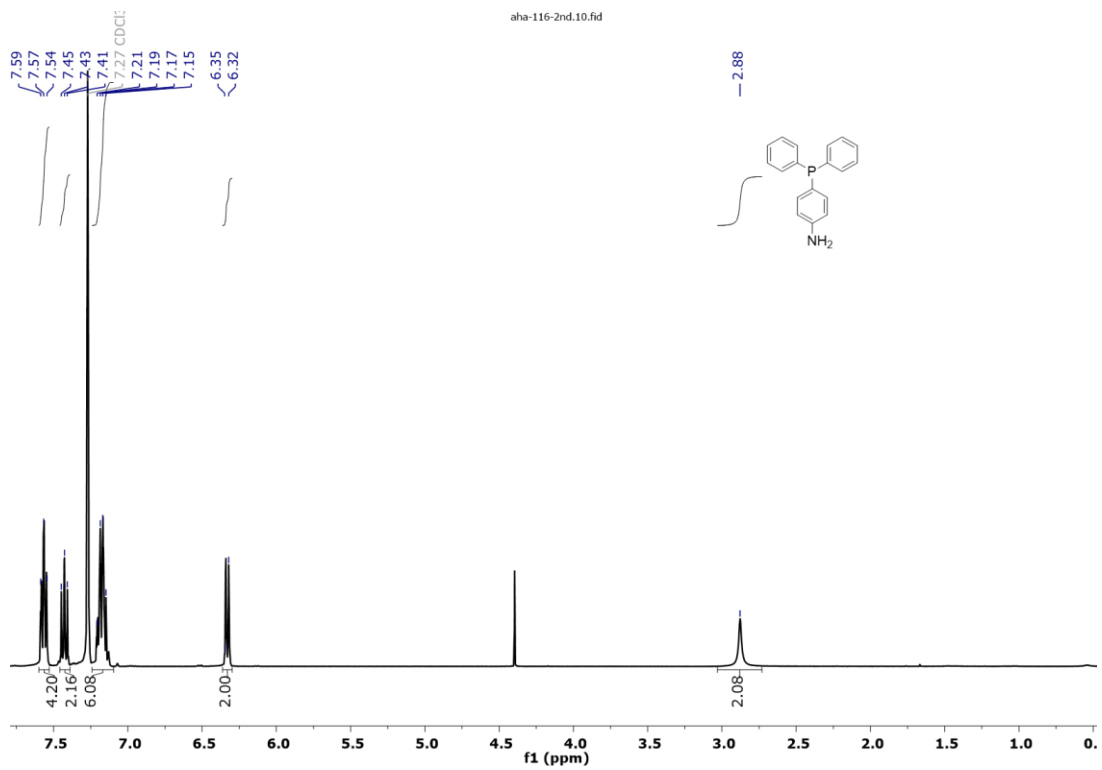
● Impurity

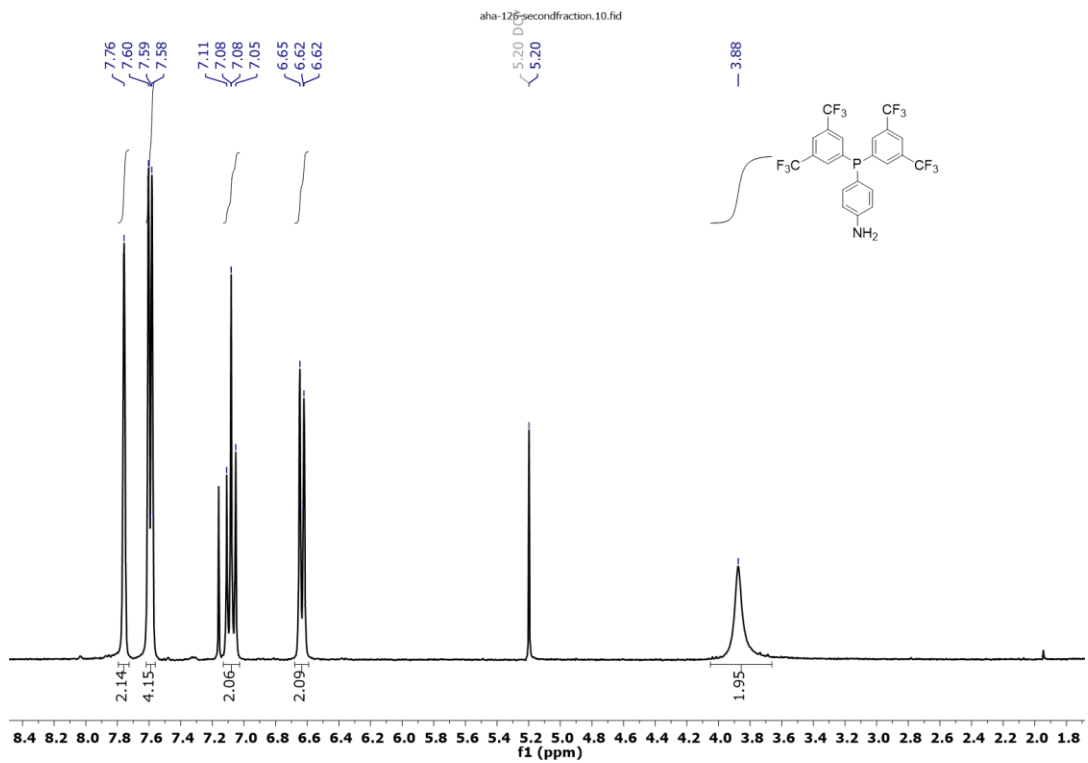
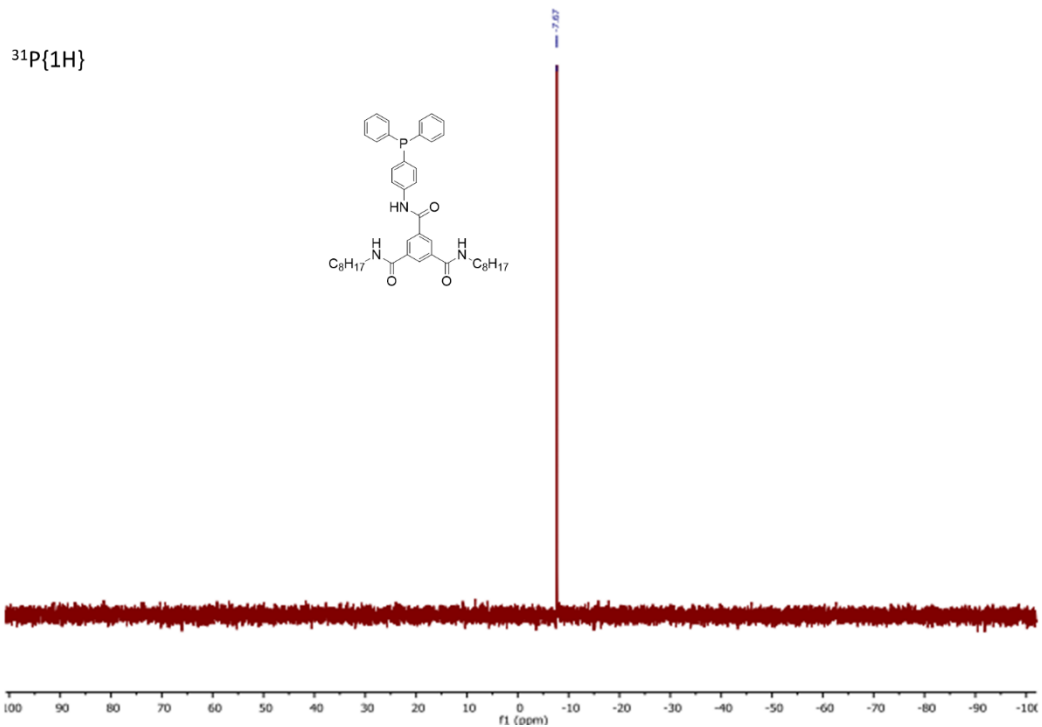
26.58

aha-76-product.11.fid





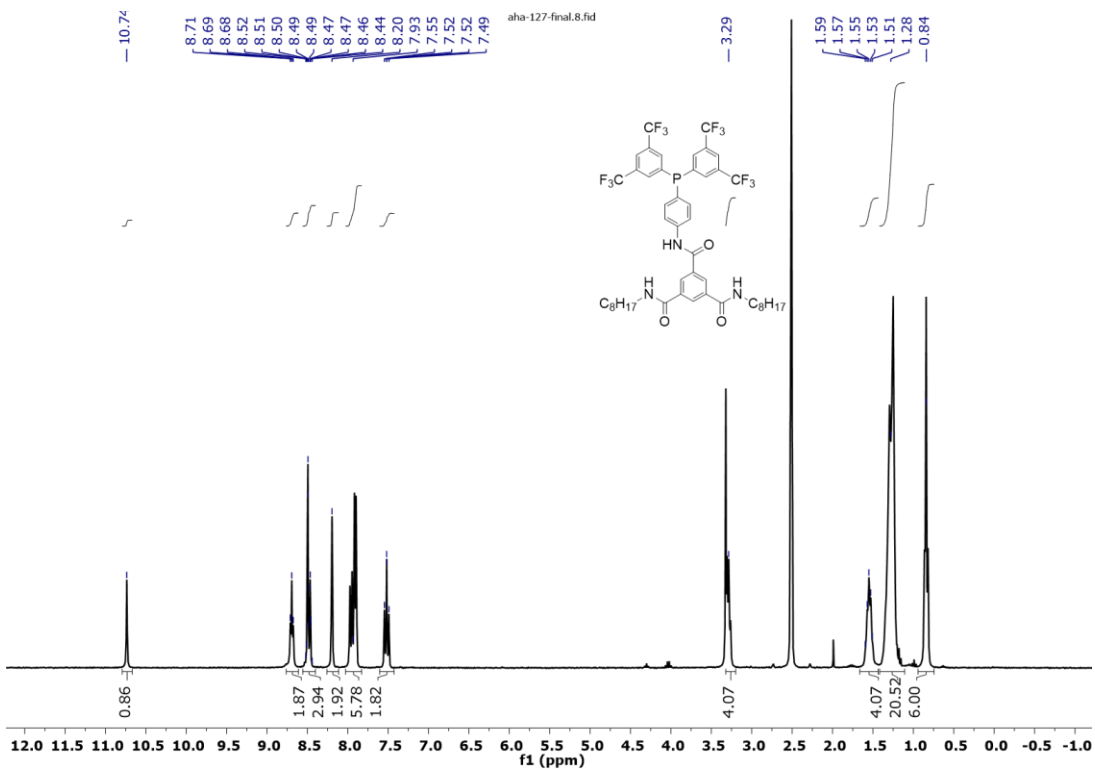
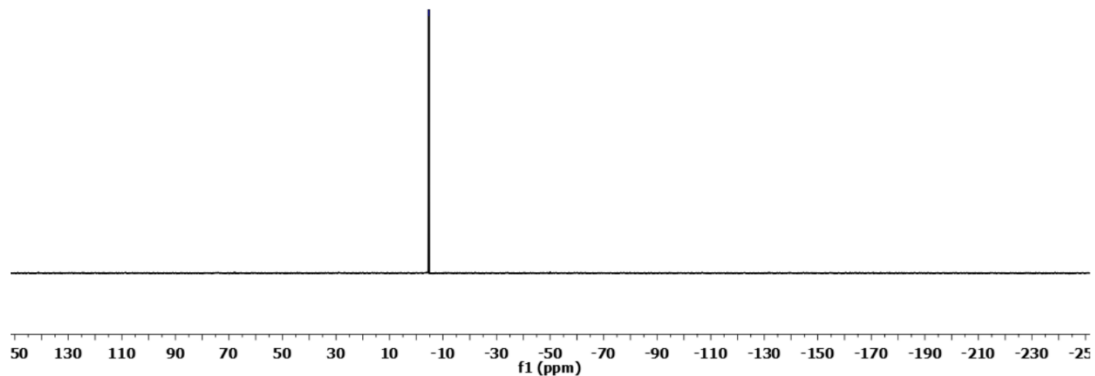
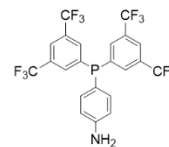


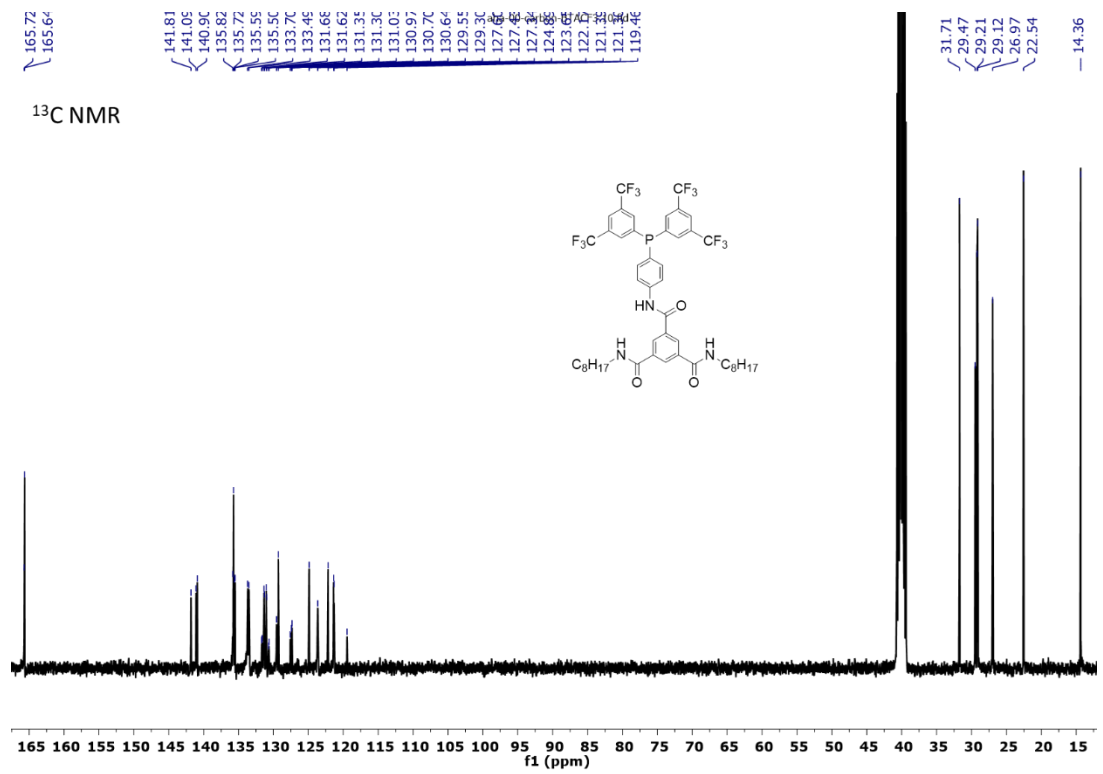
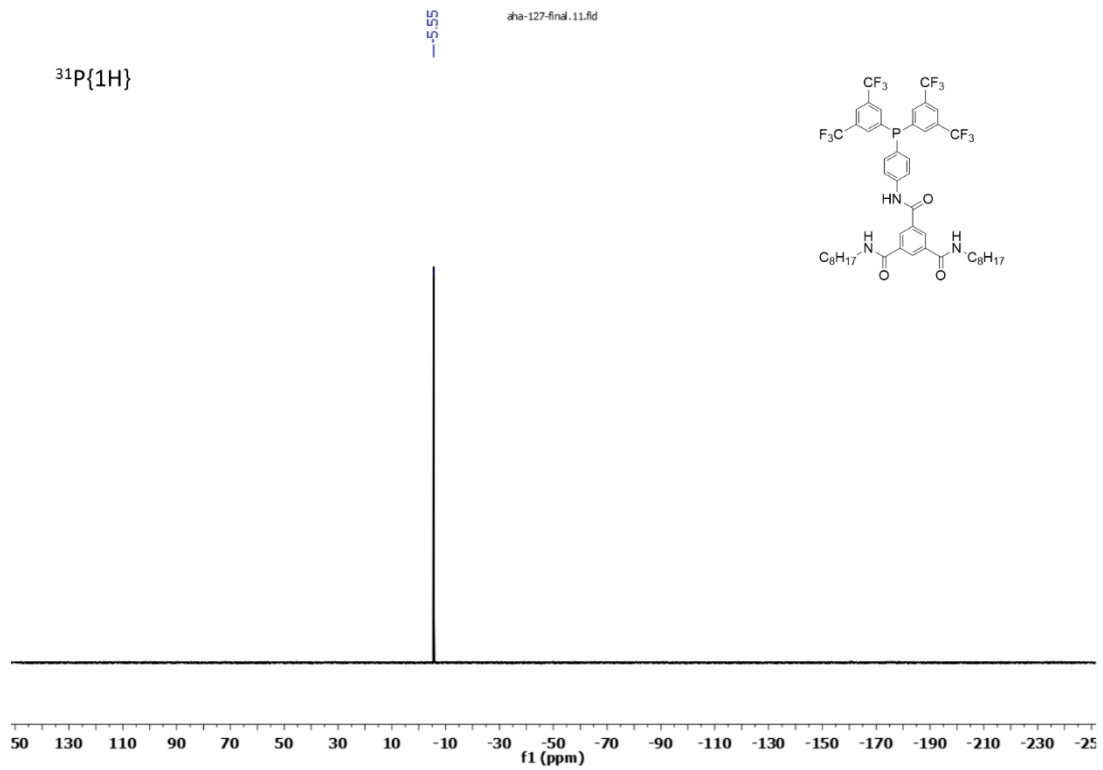


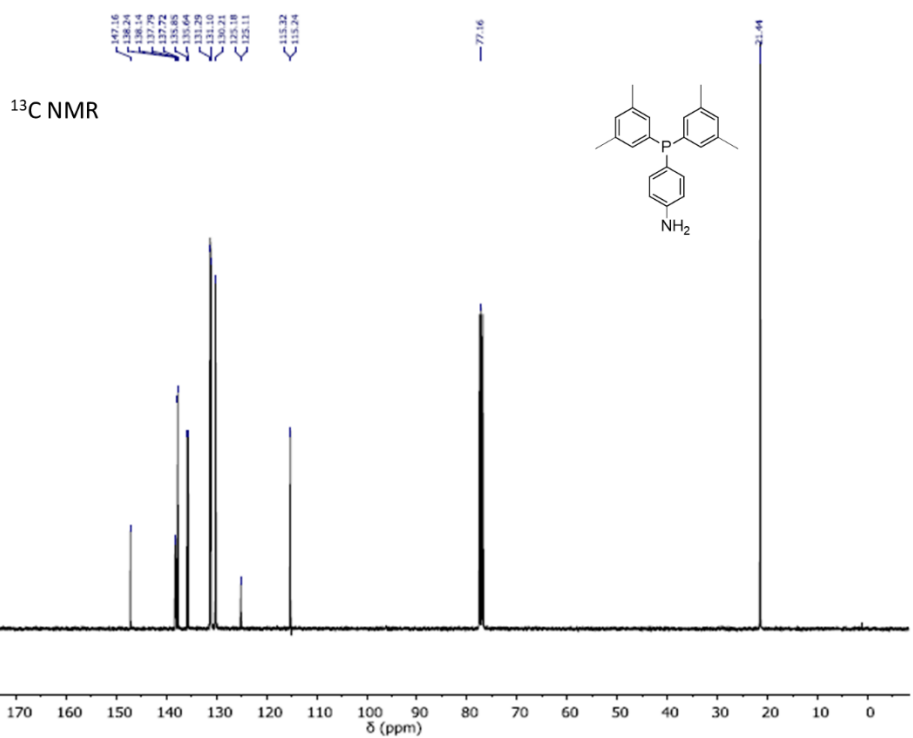
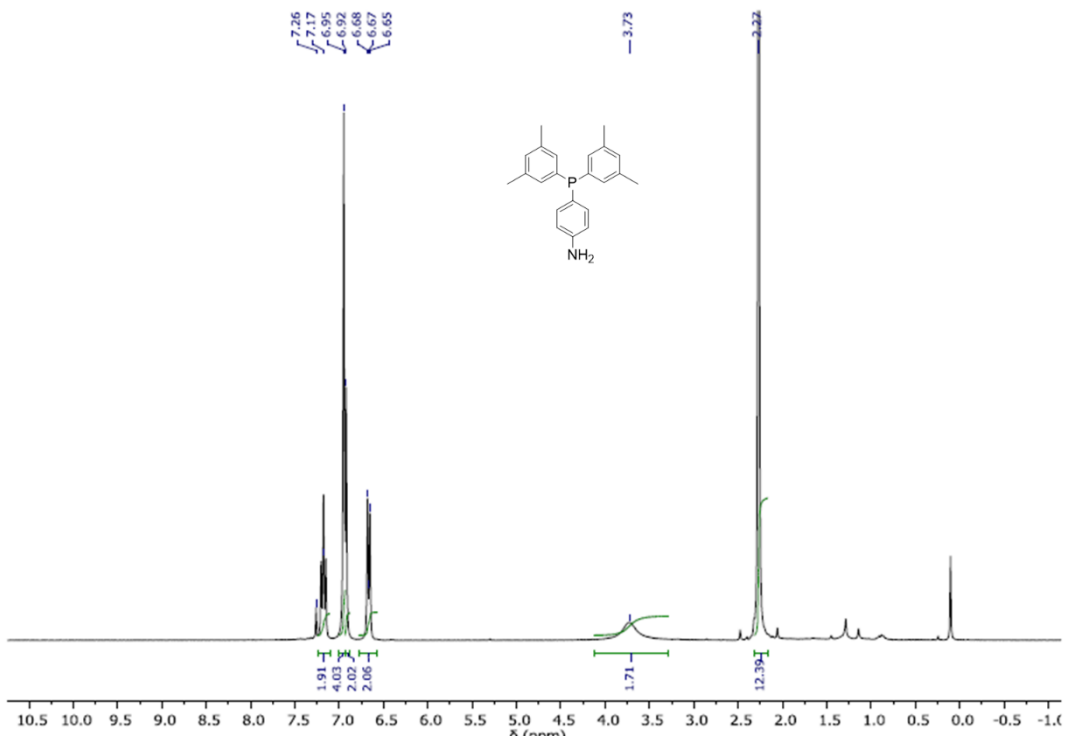
$^{31}\text{P}\{^1\text{H}\}$

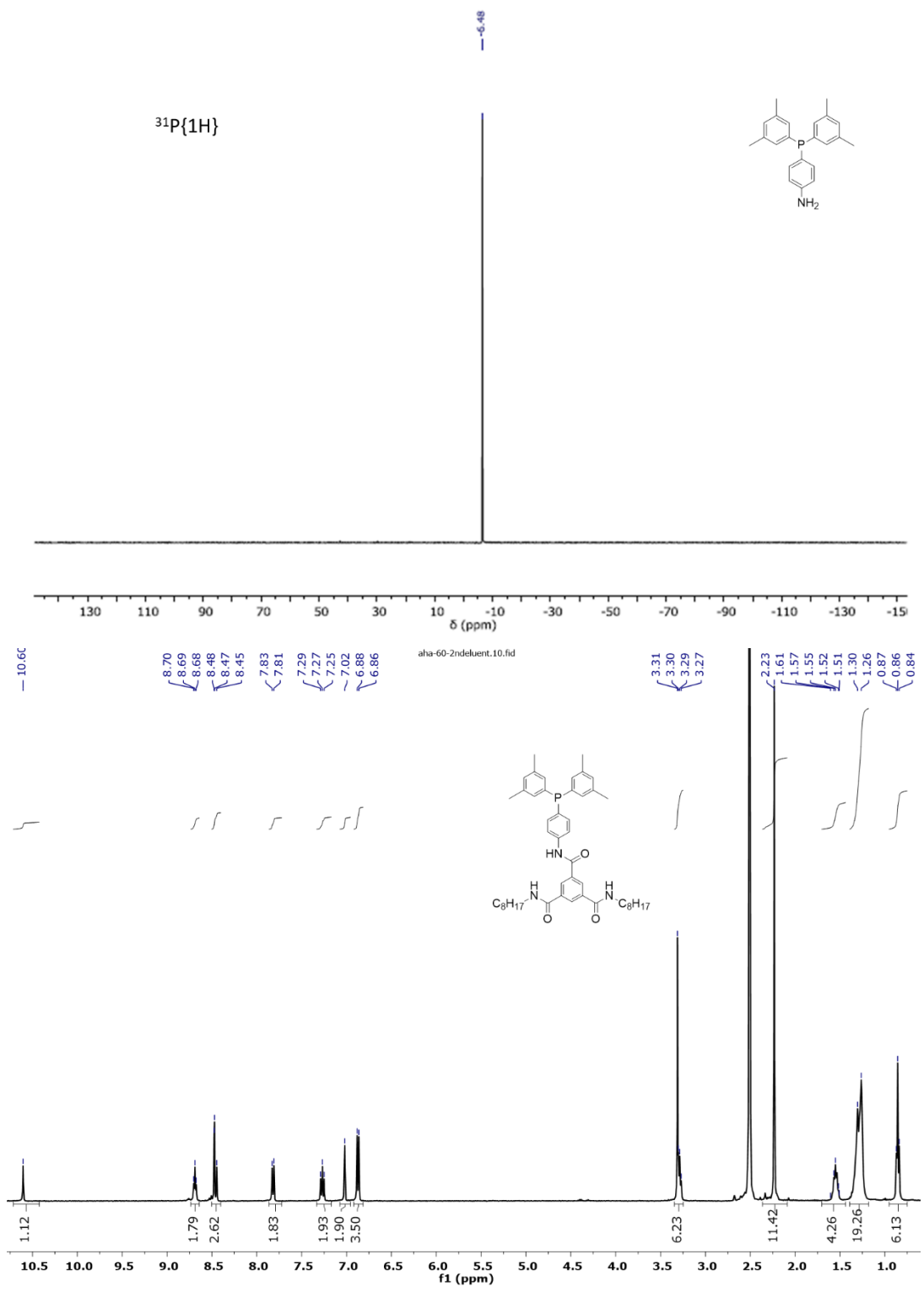
-4.69

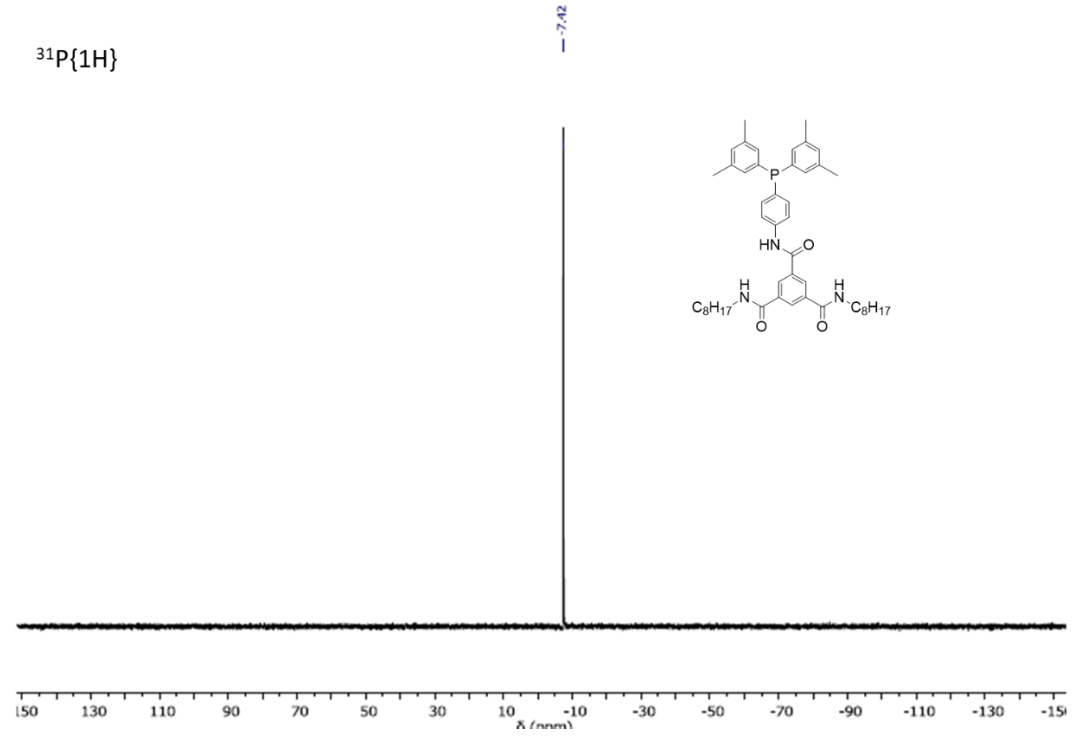
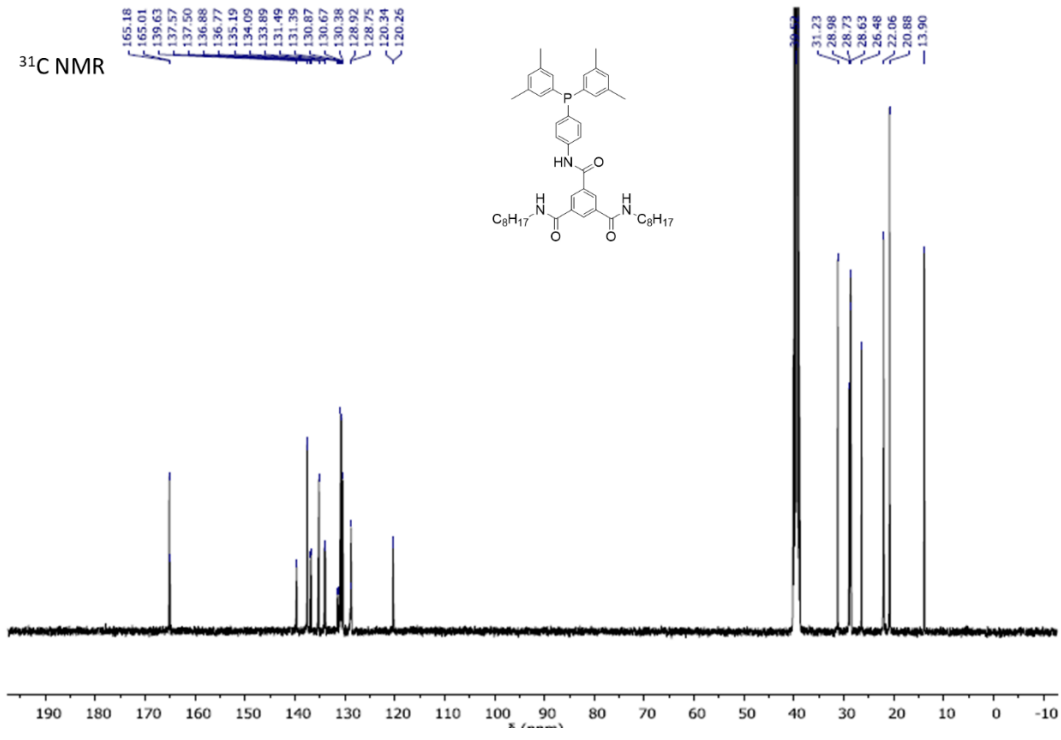
aha-126-secondfrac.11.fid

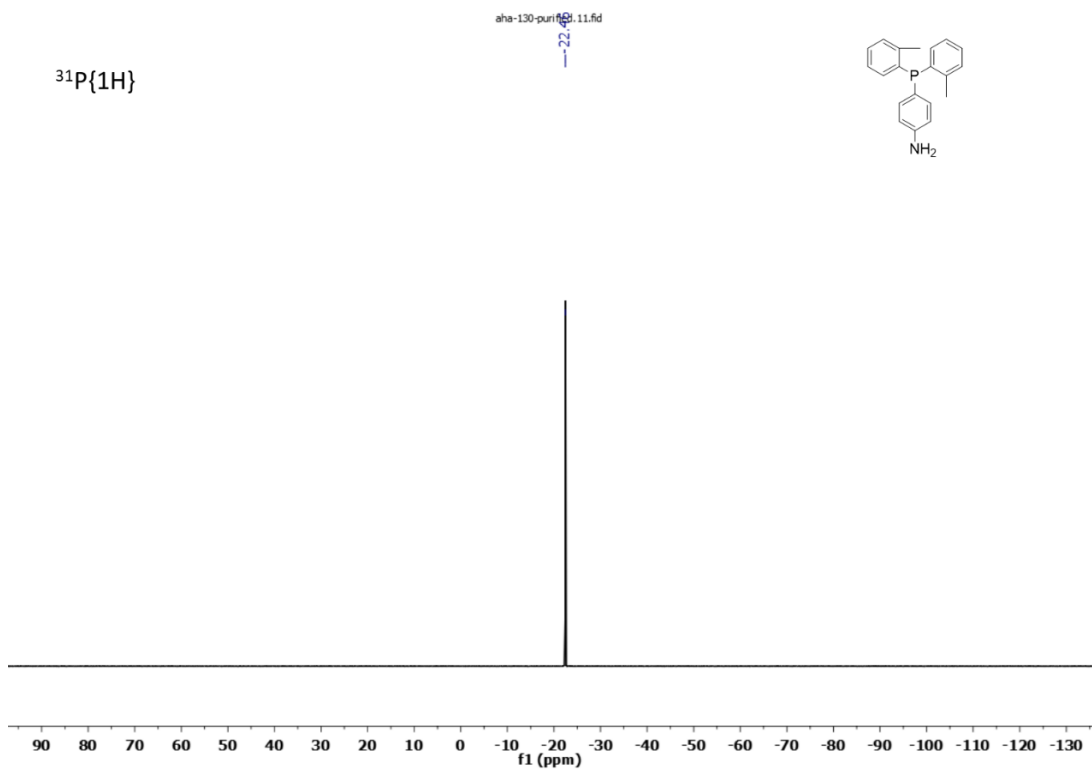
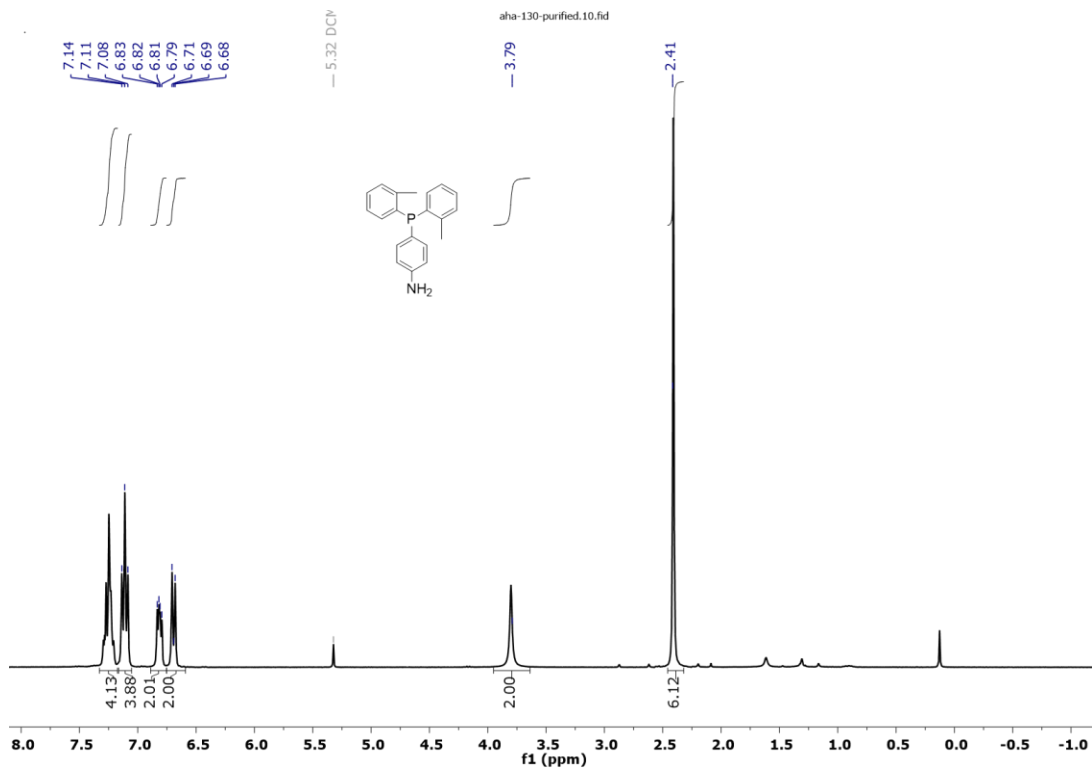


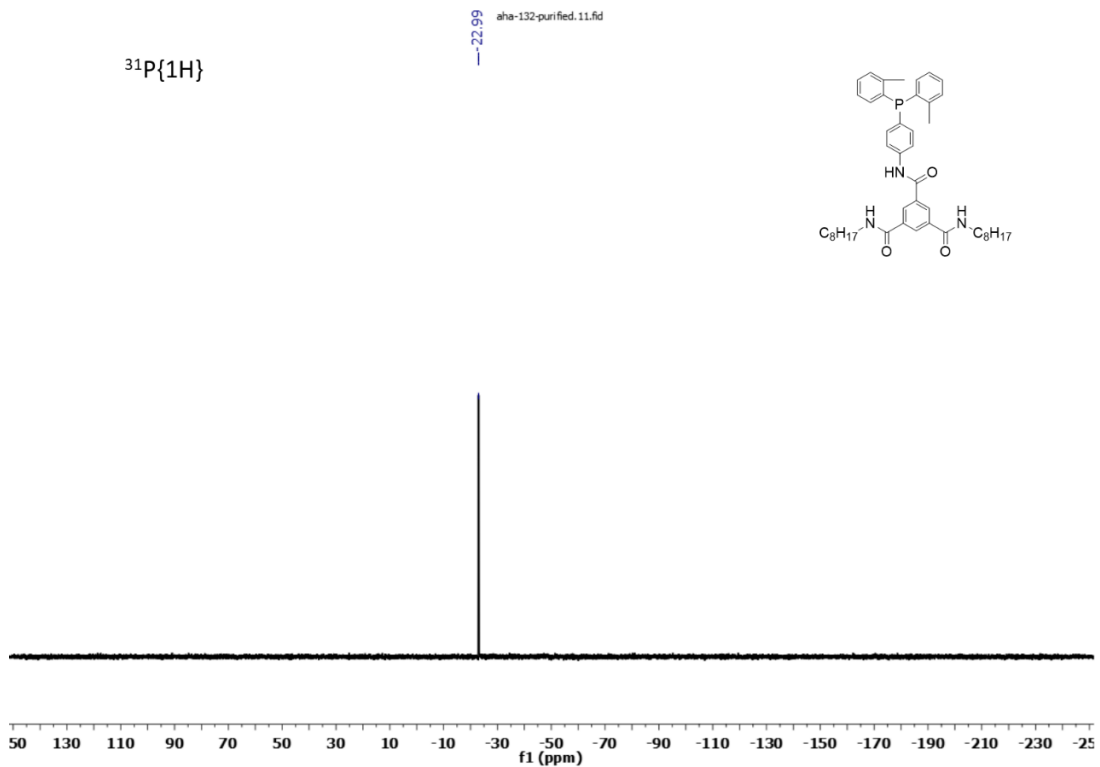
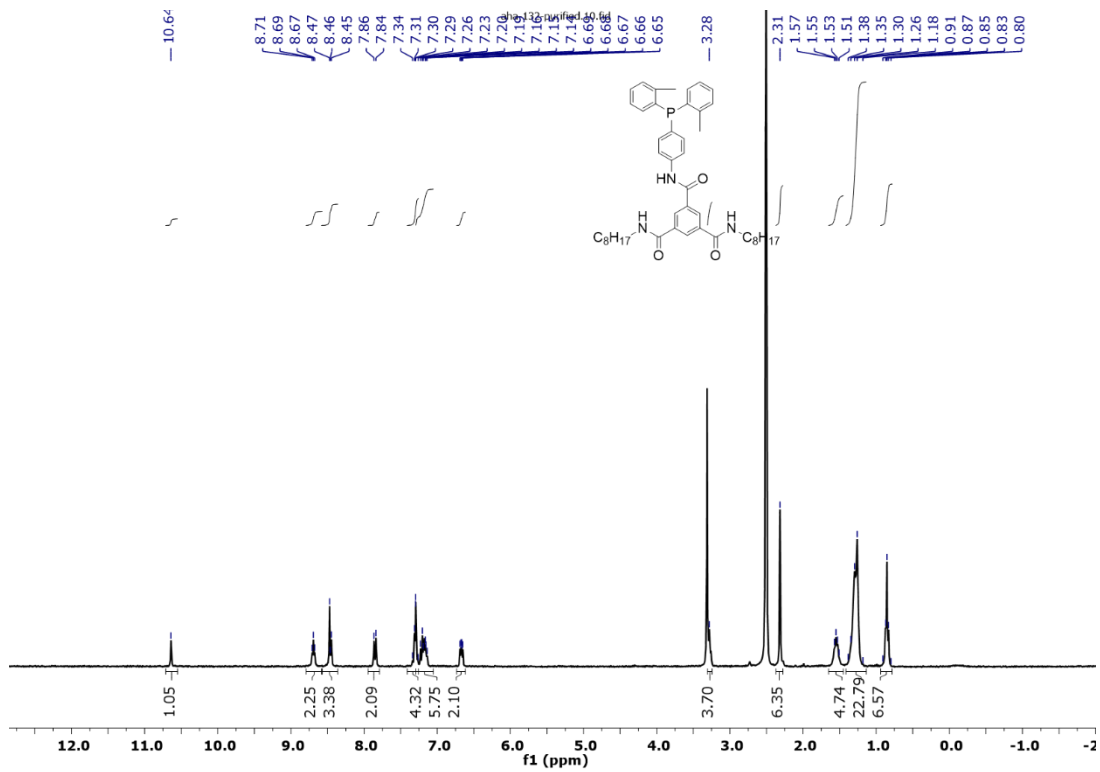


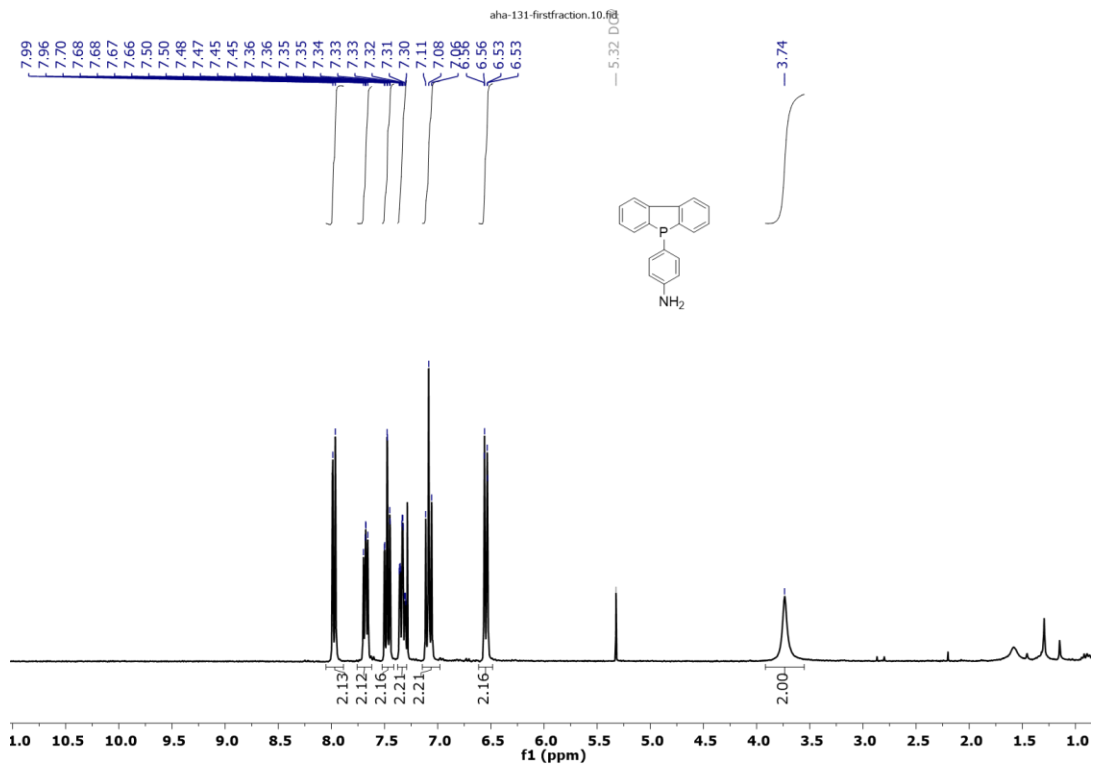
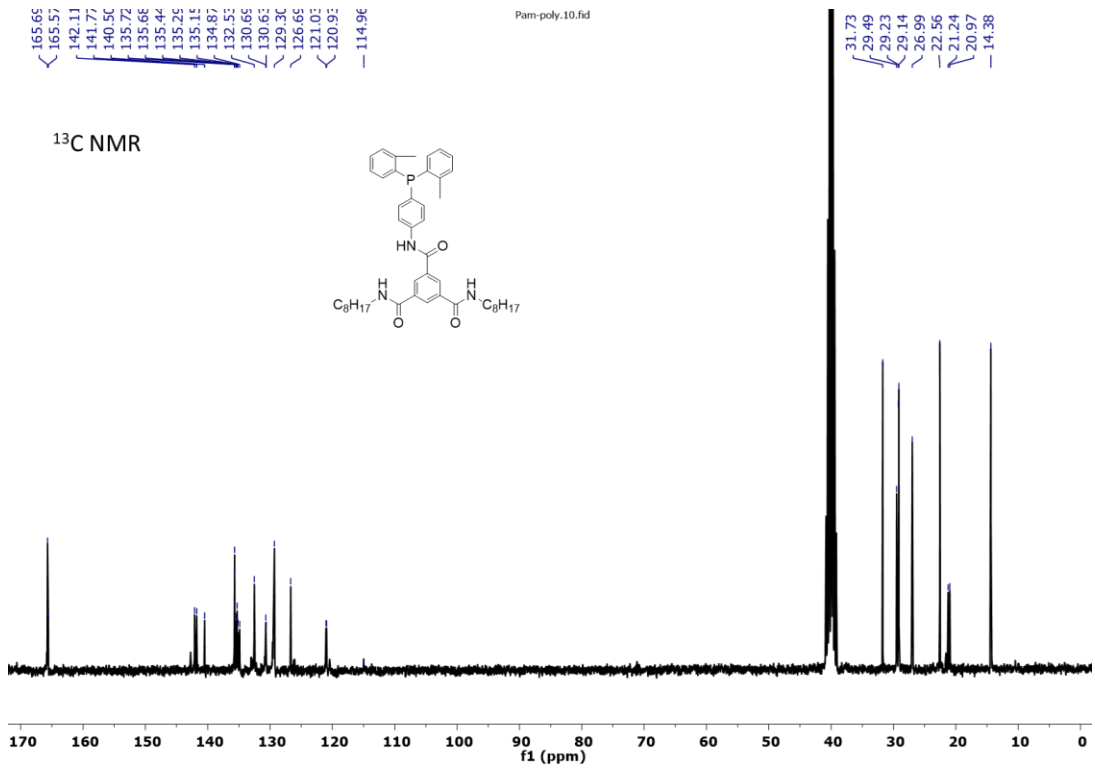






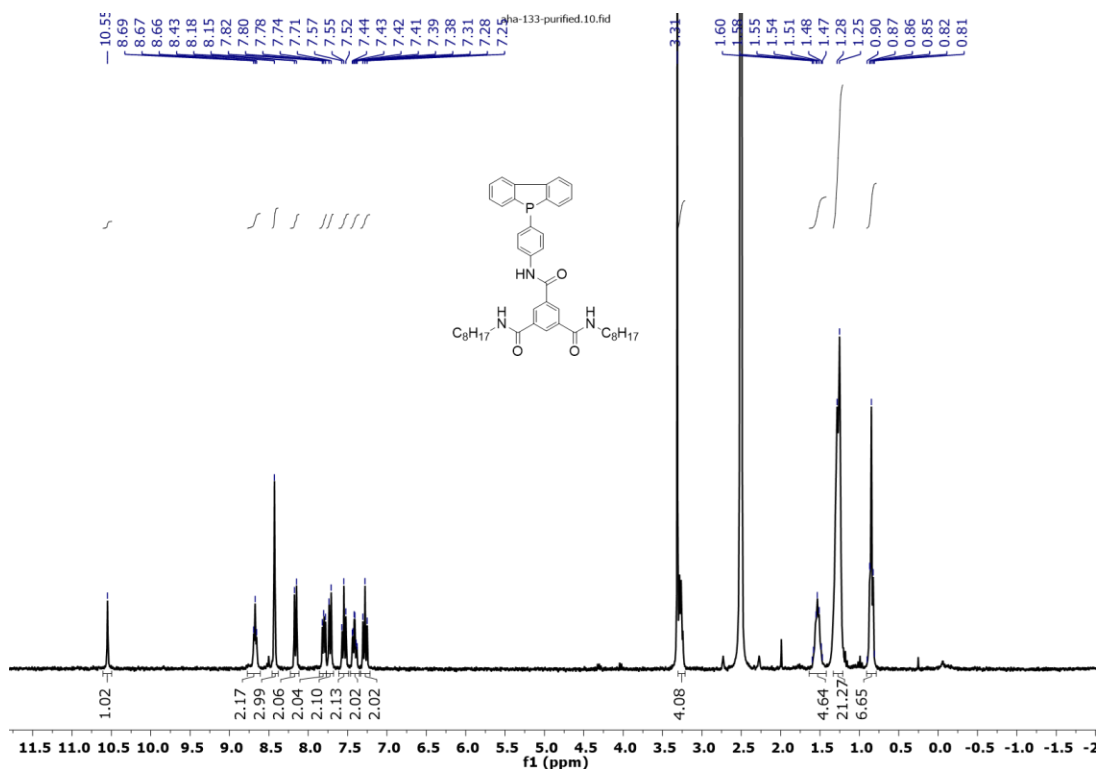
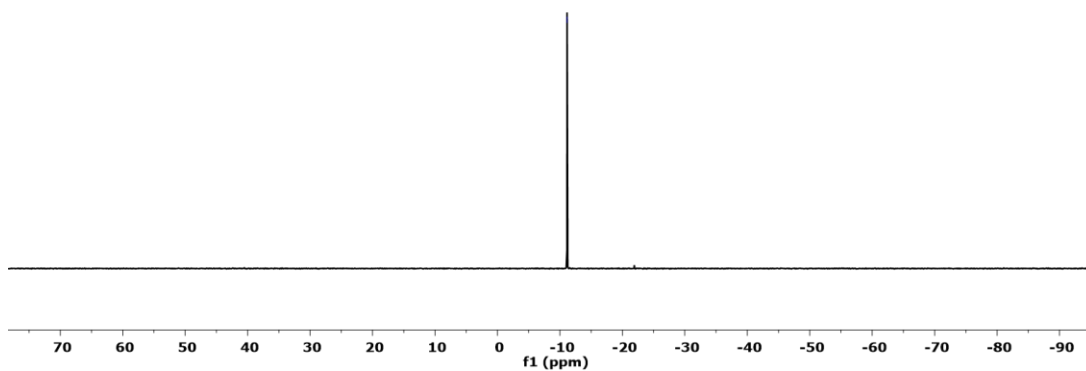
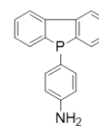


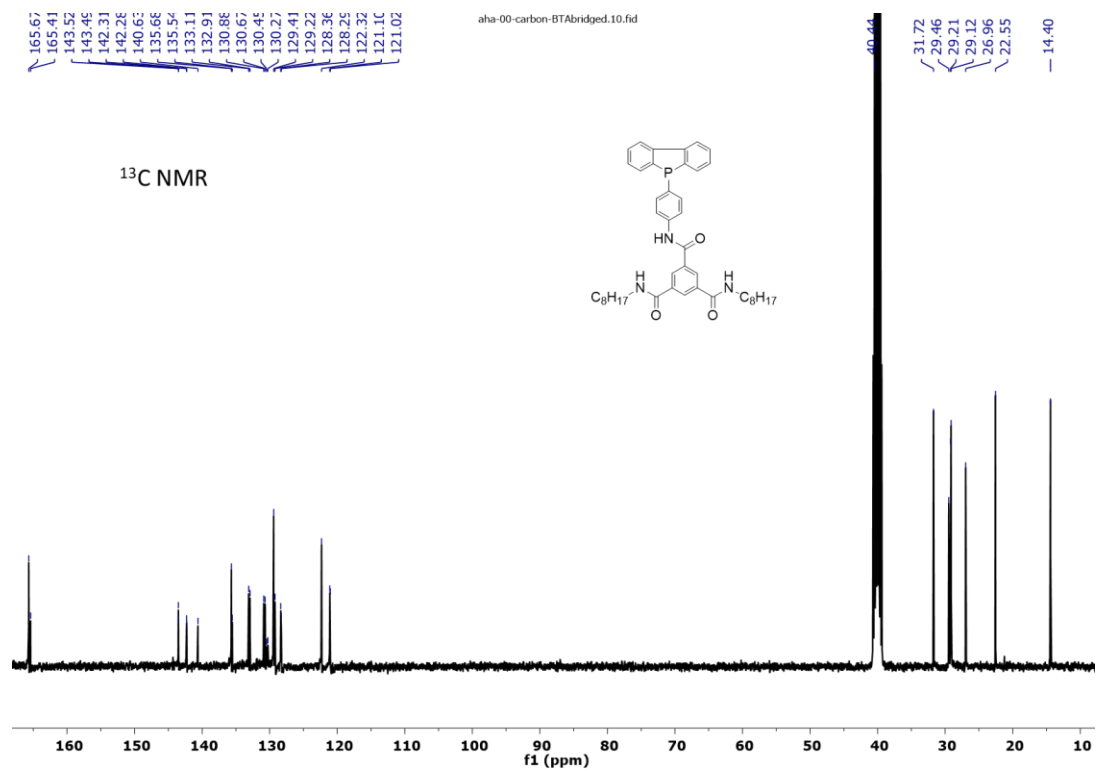
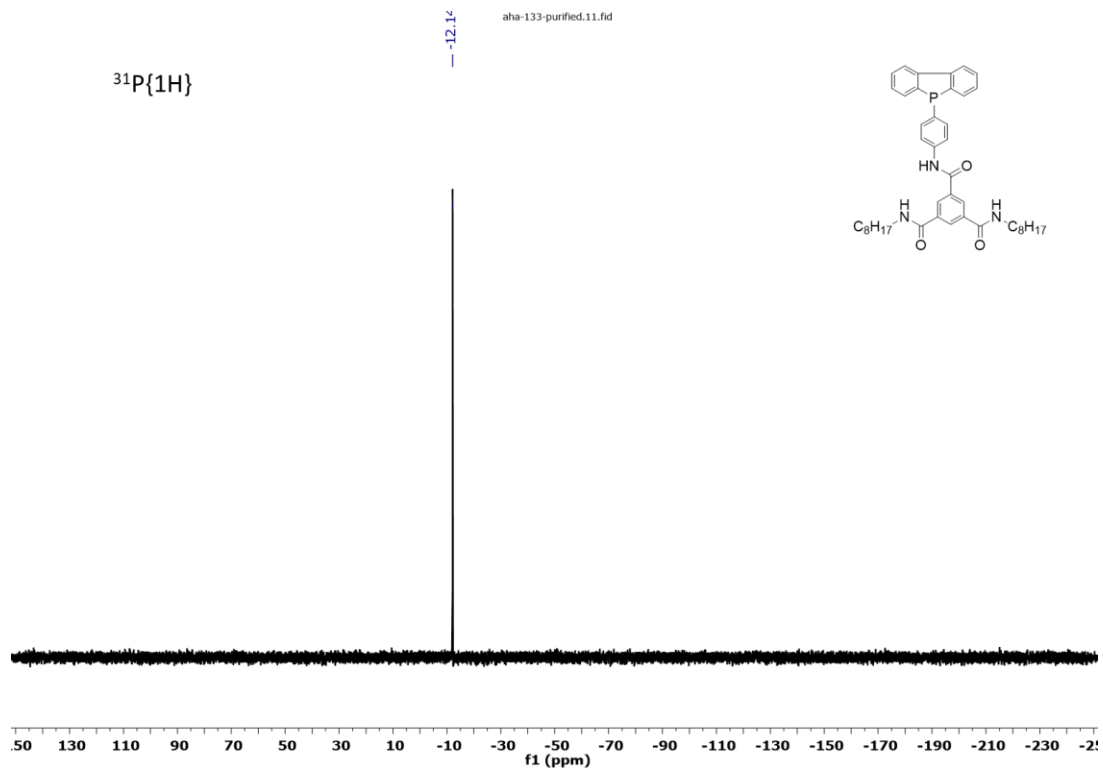


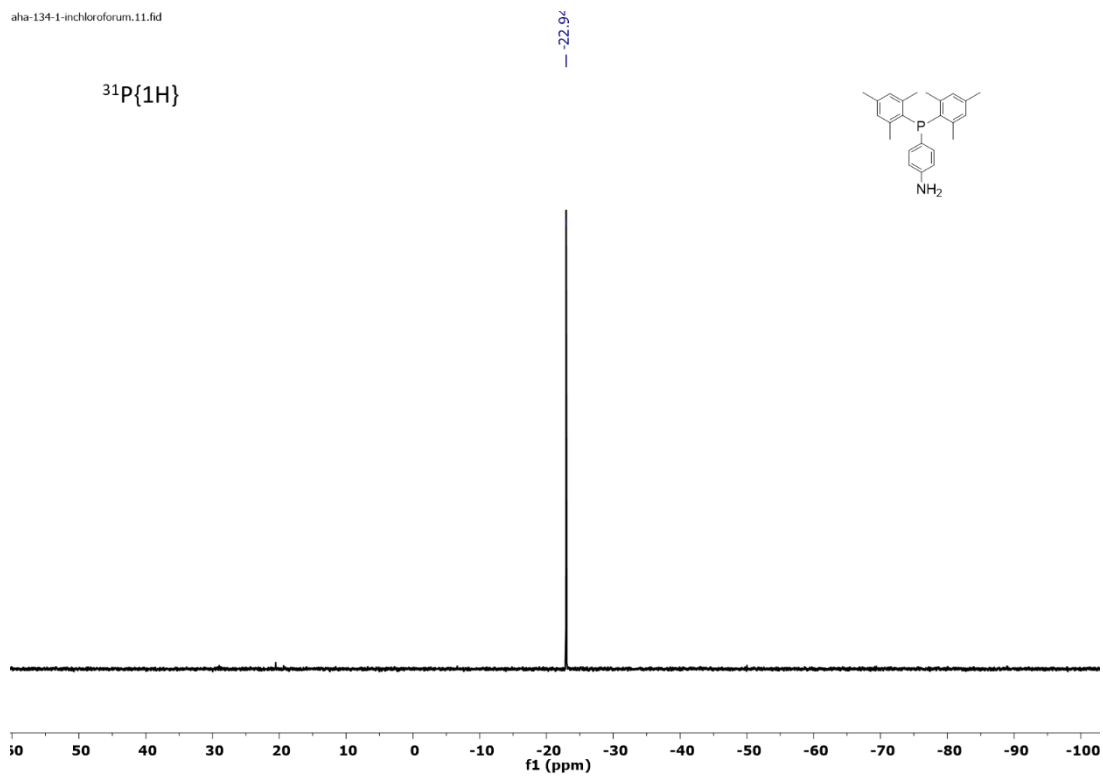
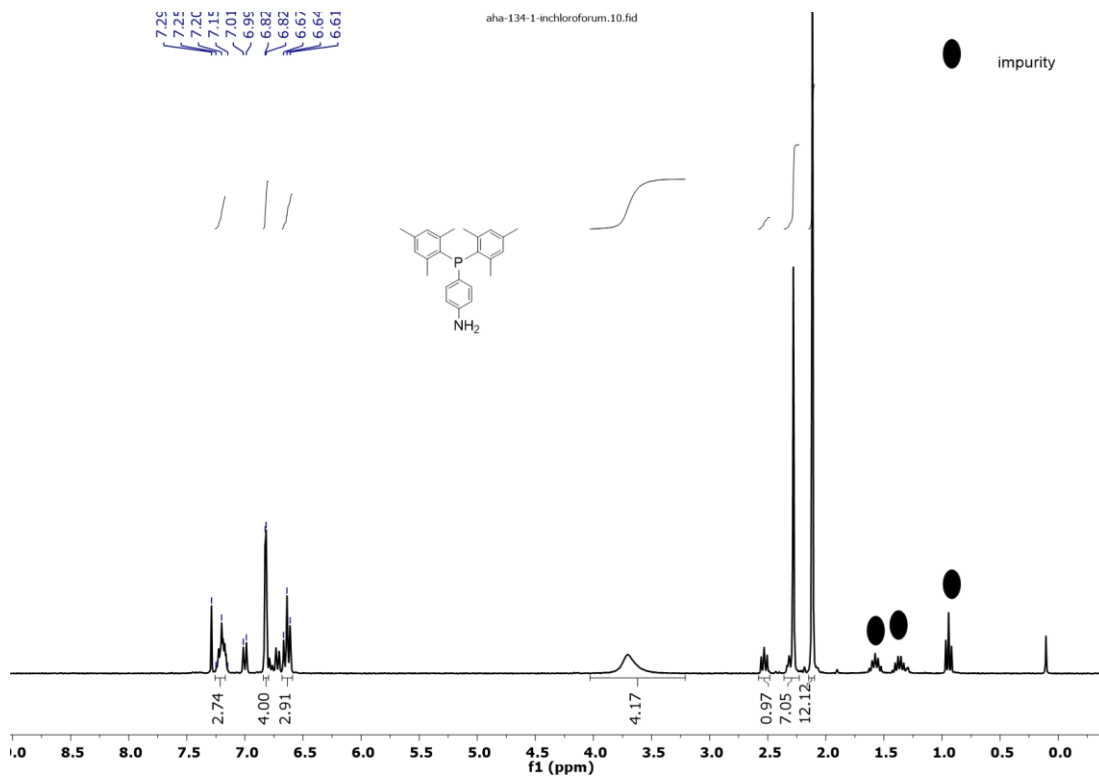


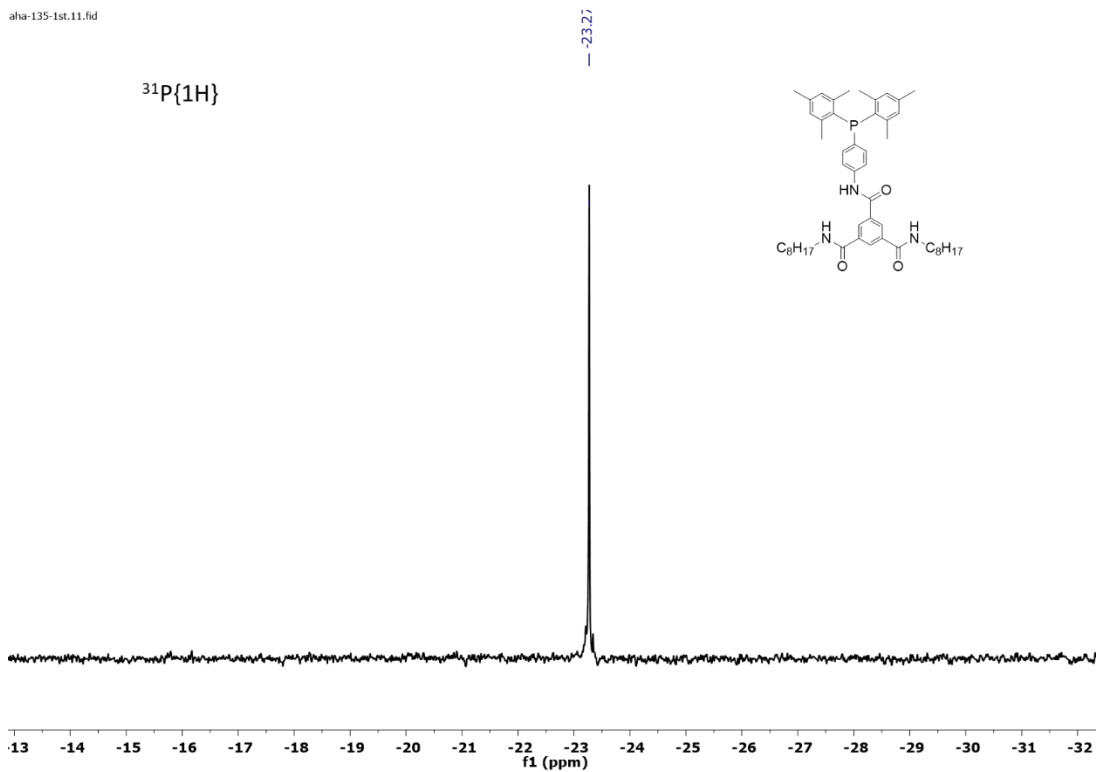
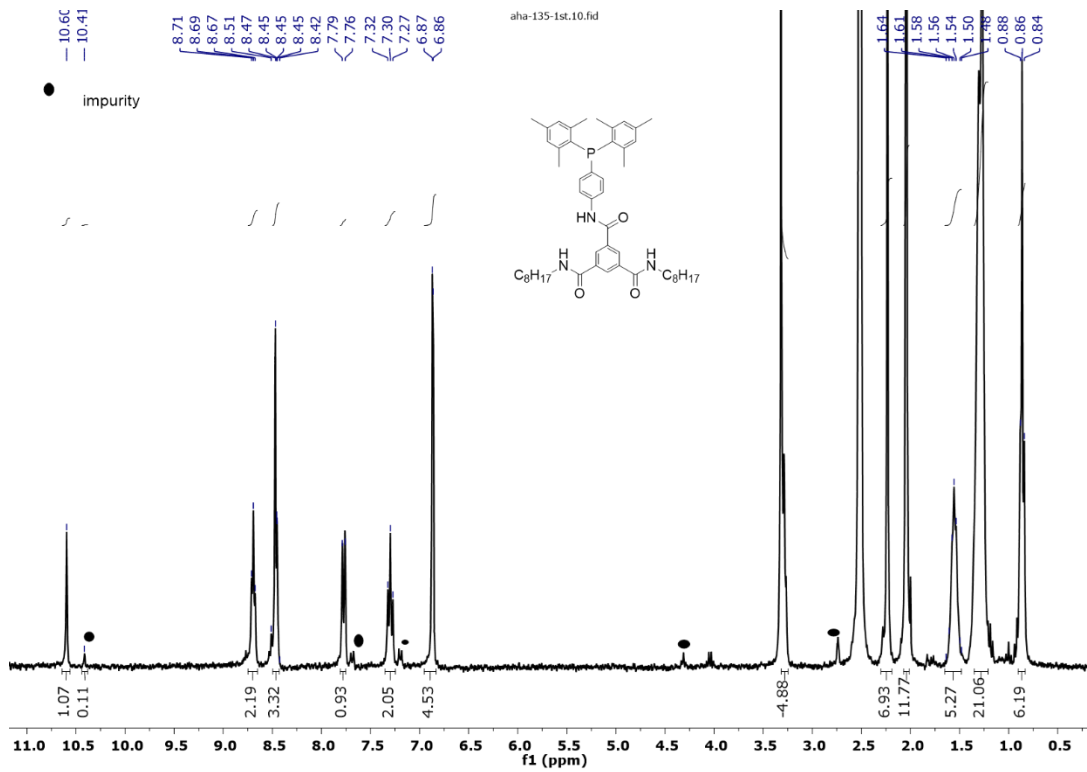
$^{31}\text{P}\{1\text{H}\}$

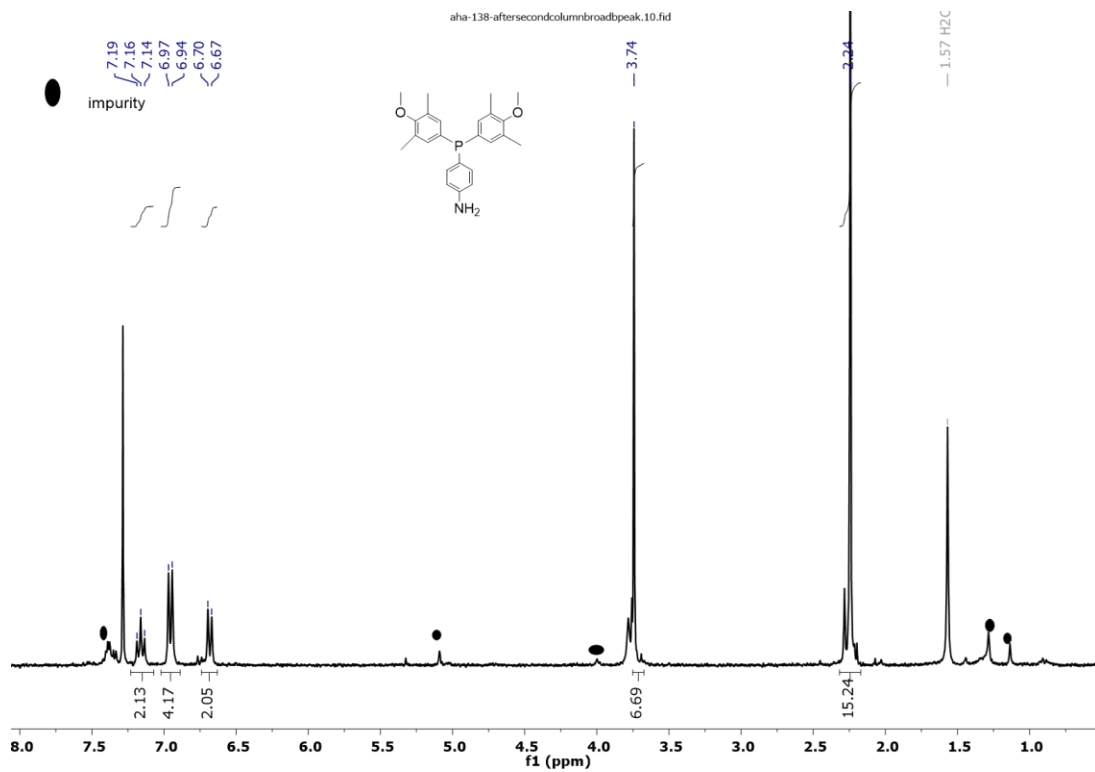
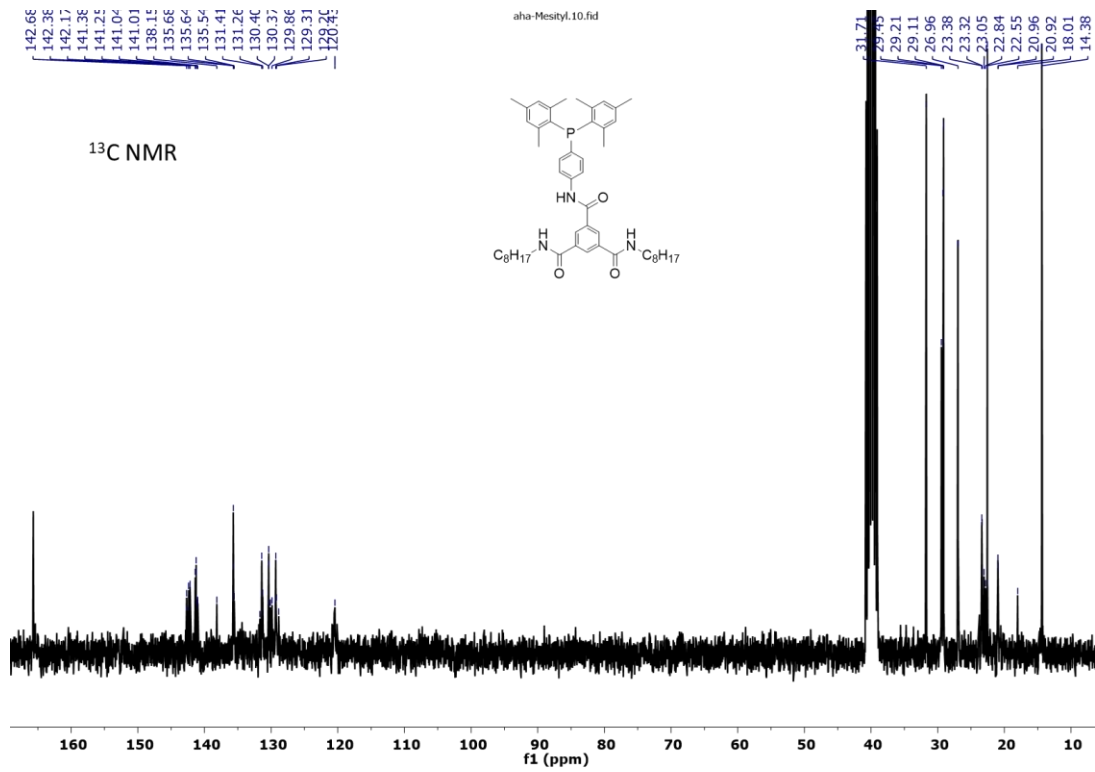
-11.15

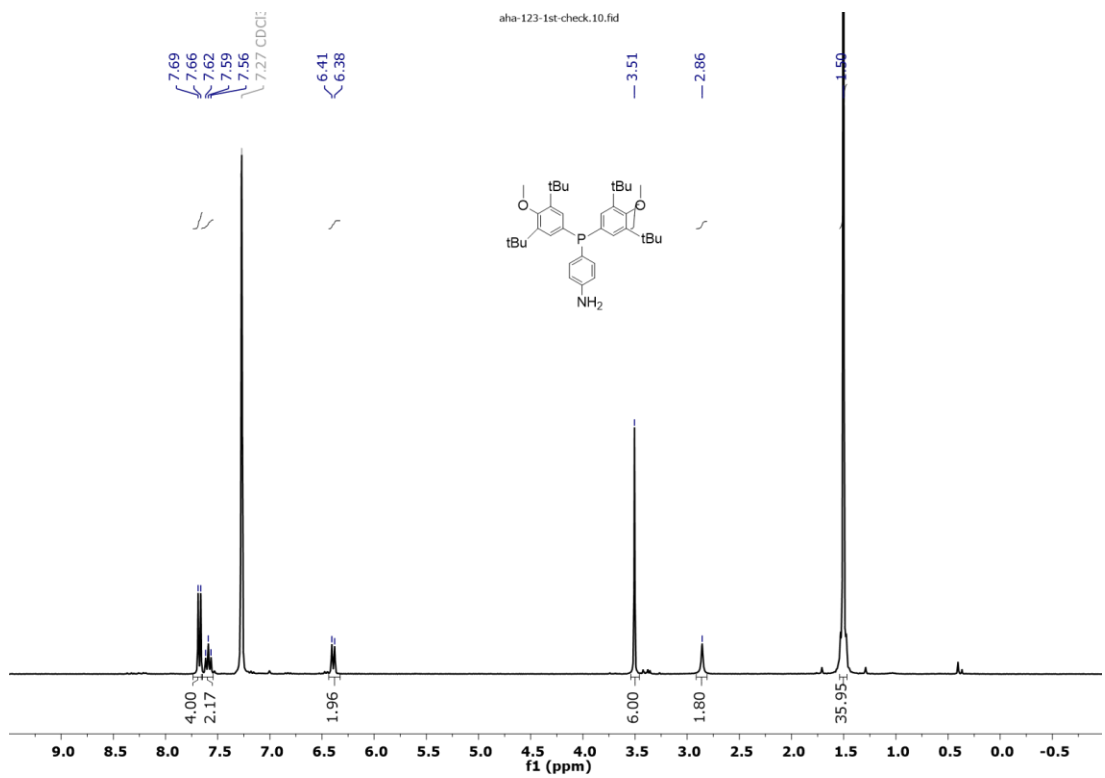
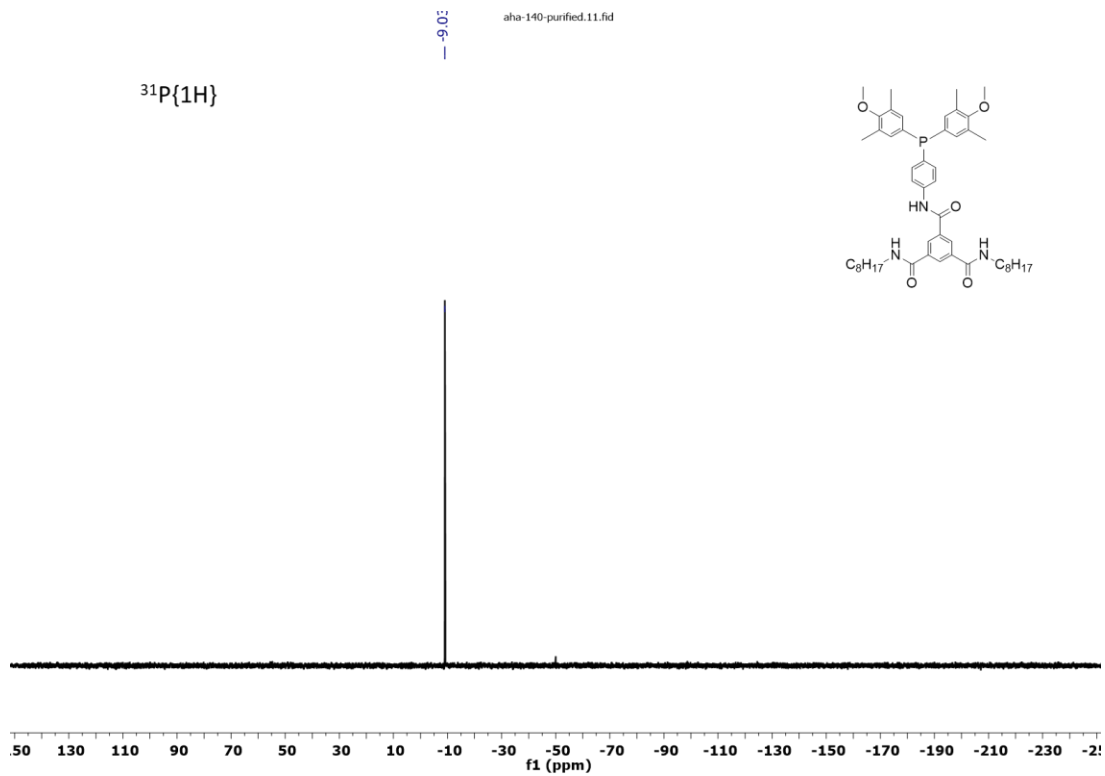


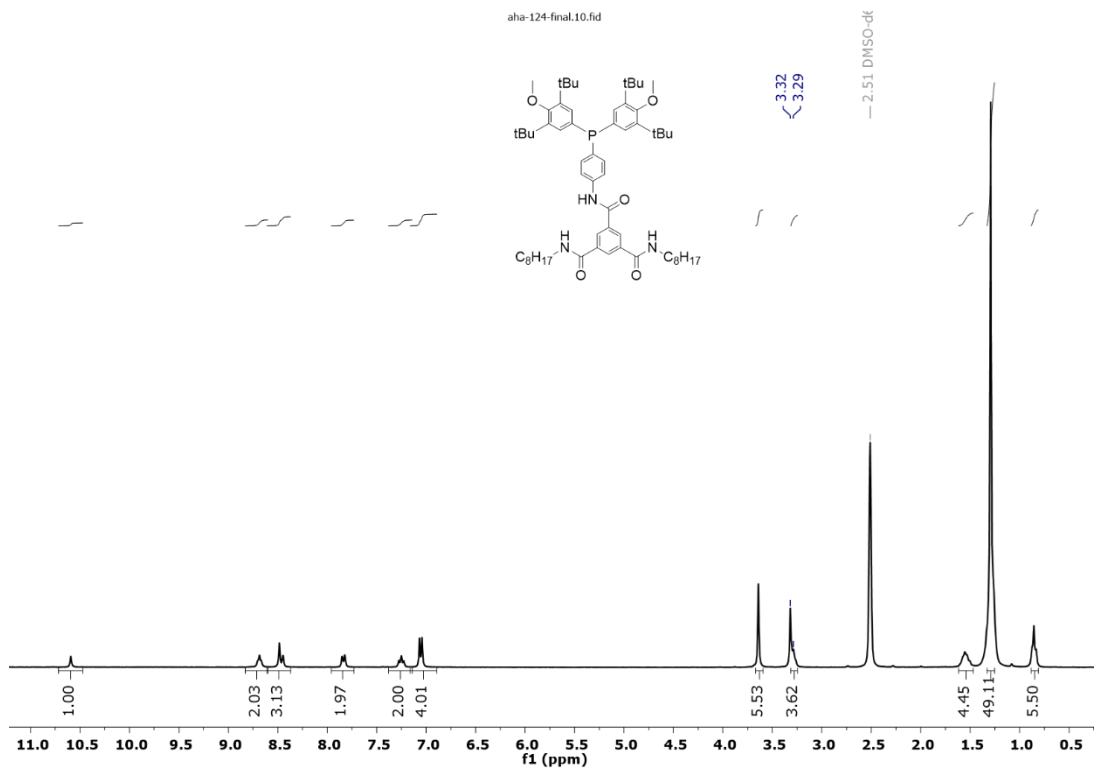
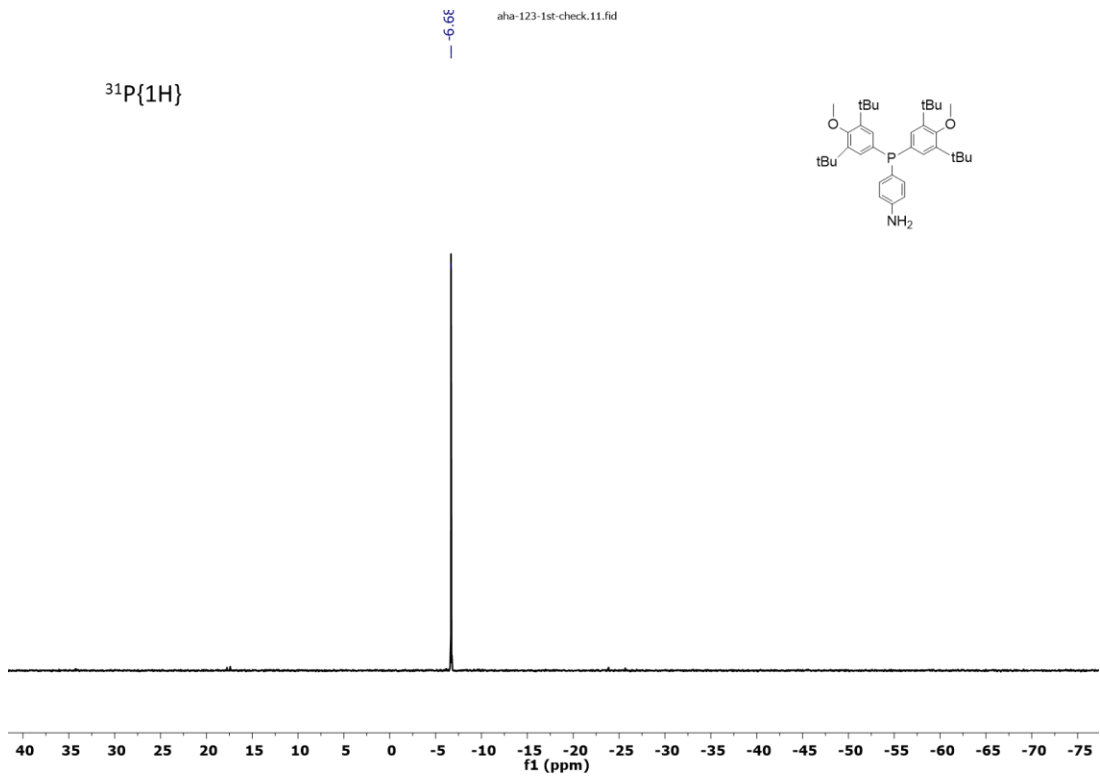


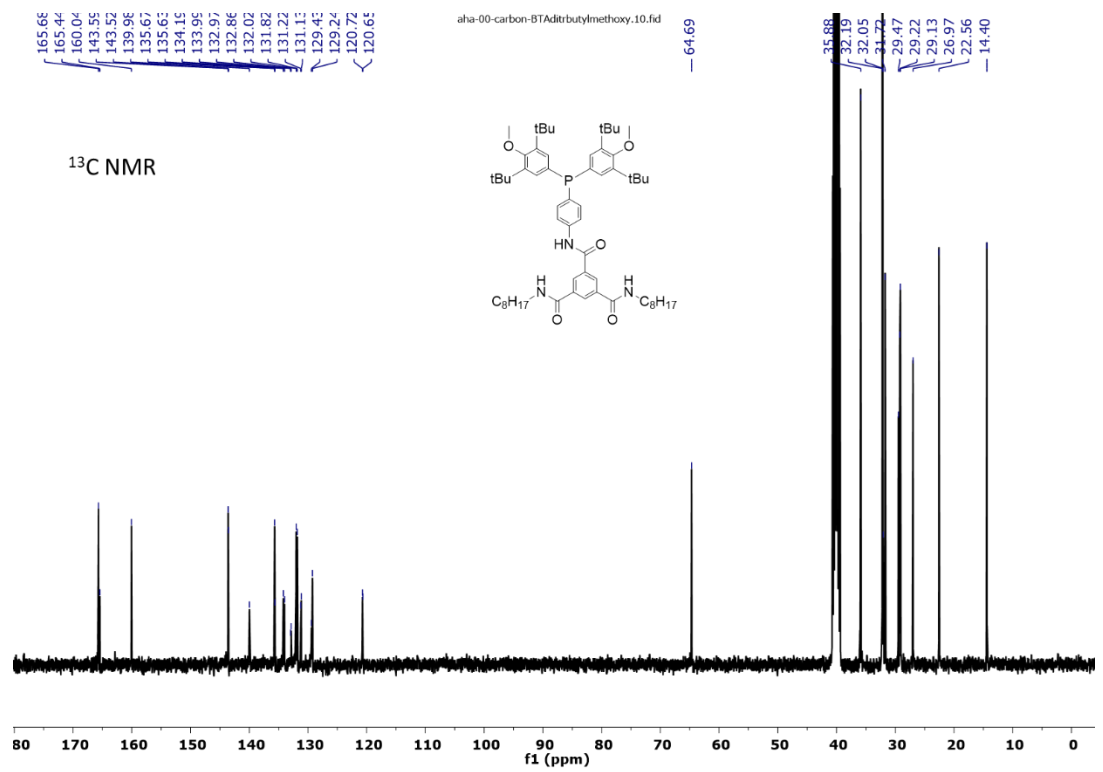
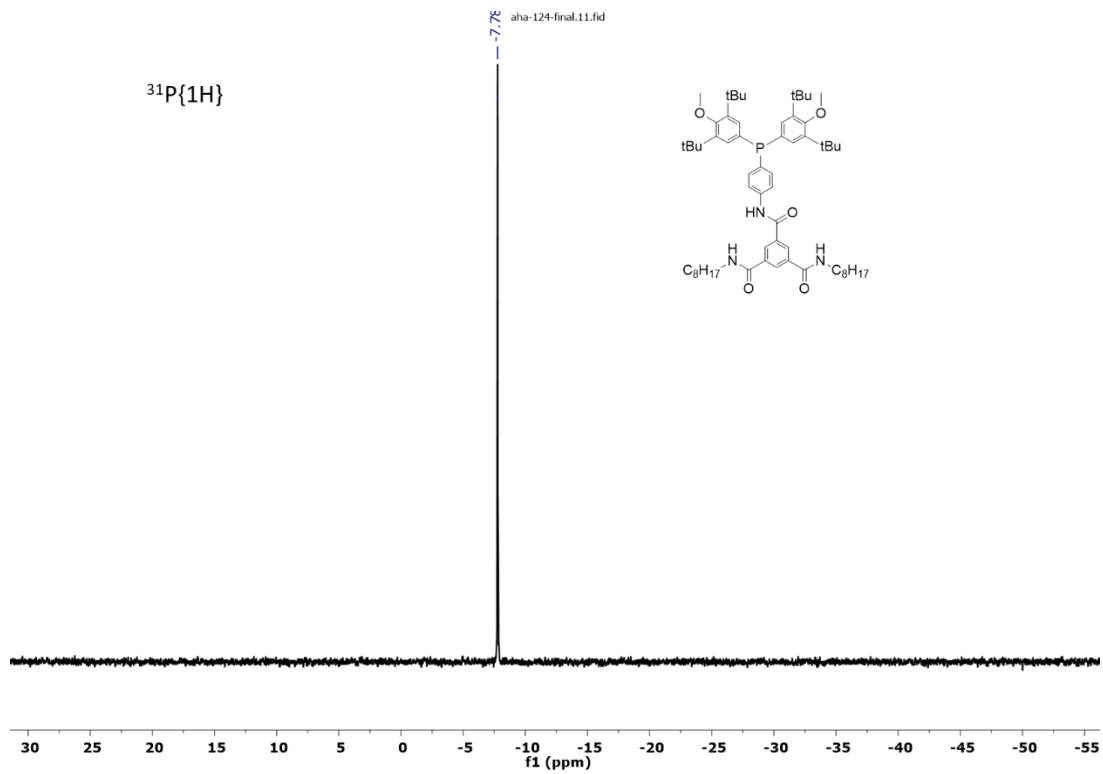


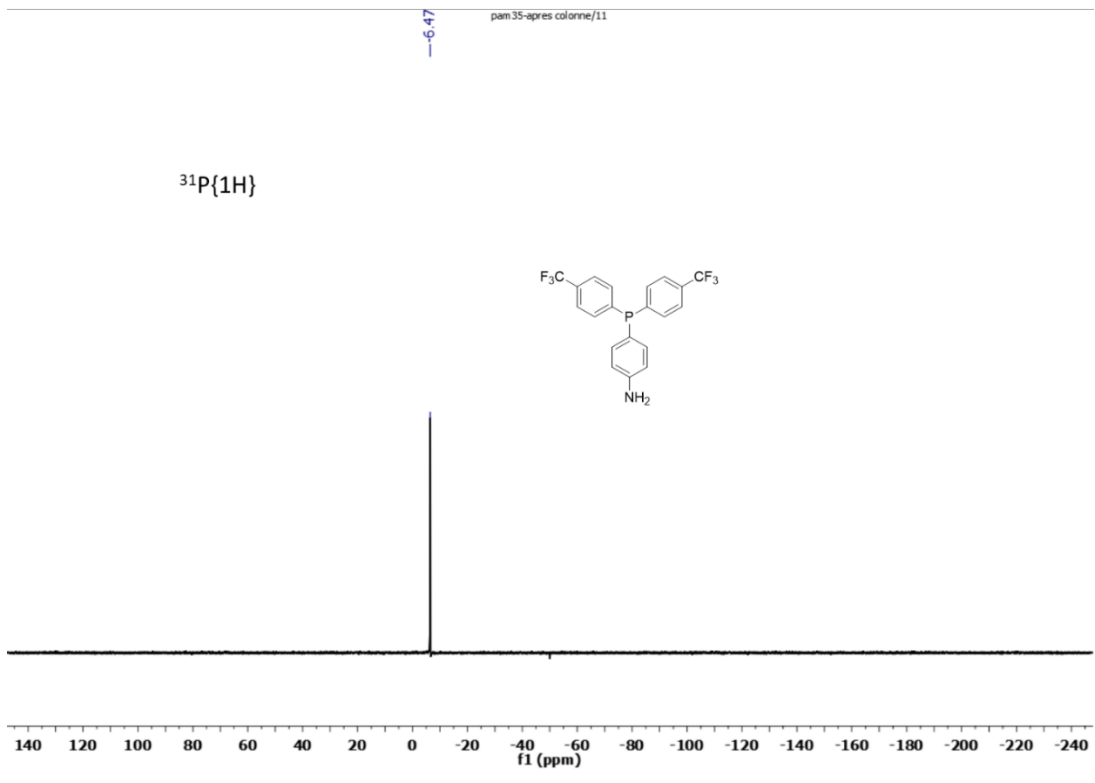
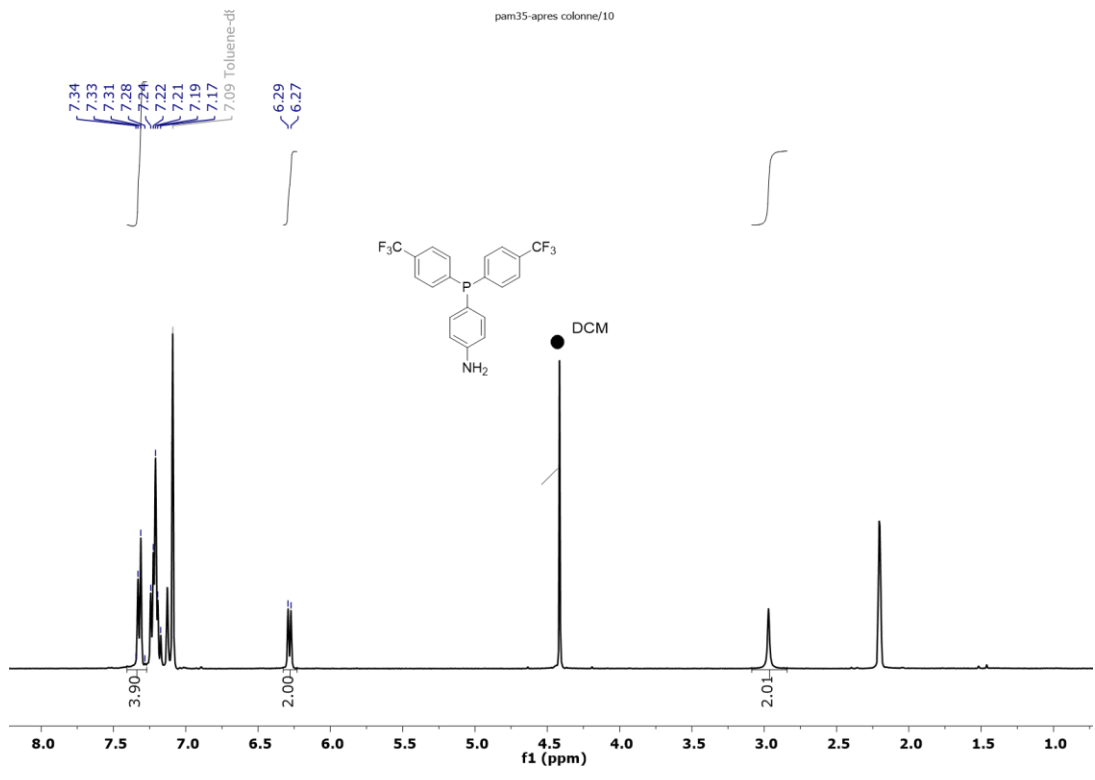


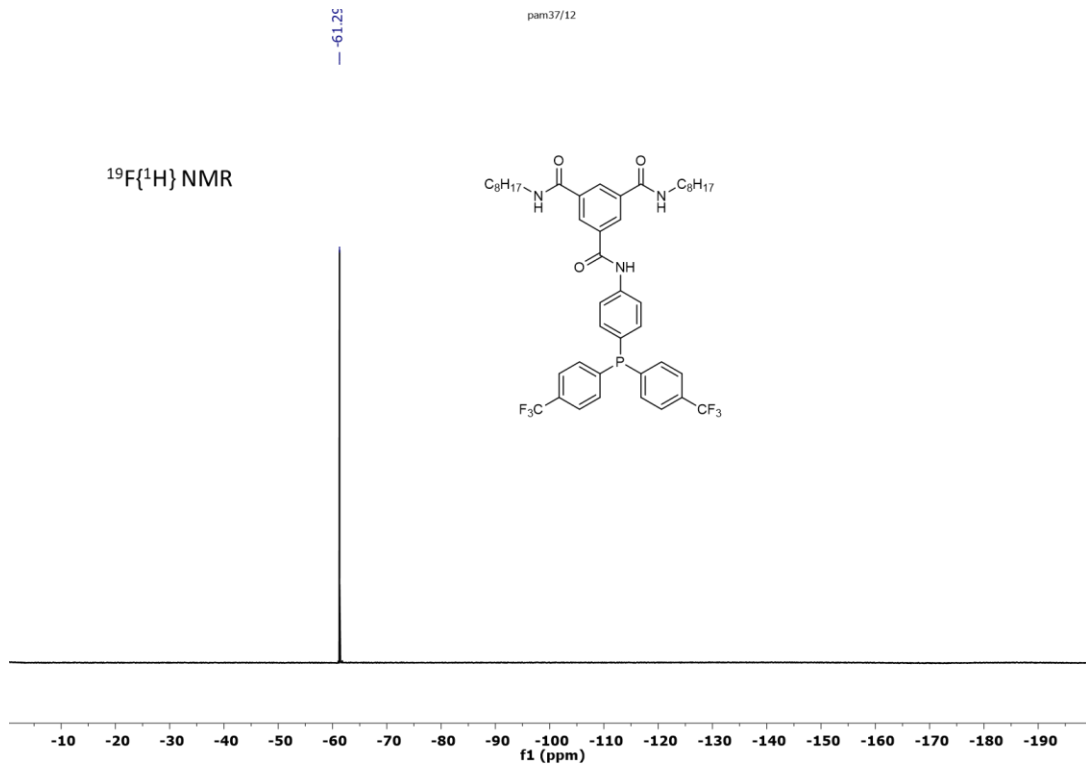
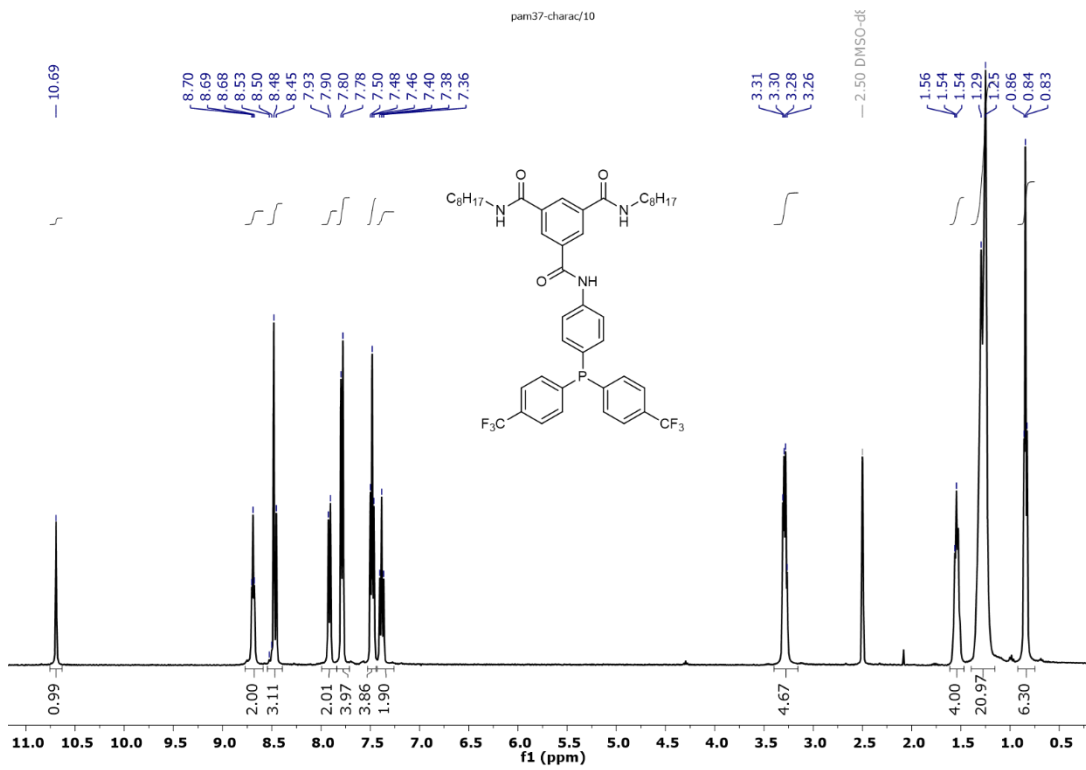








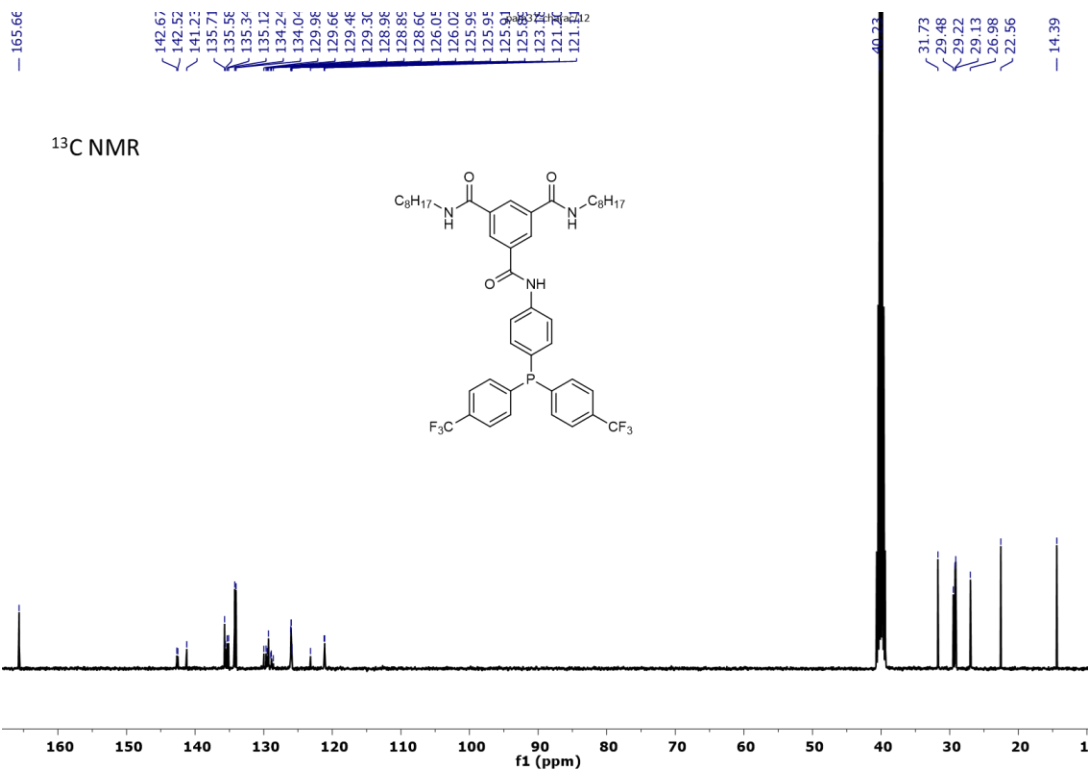
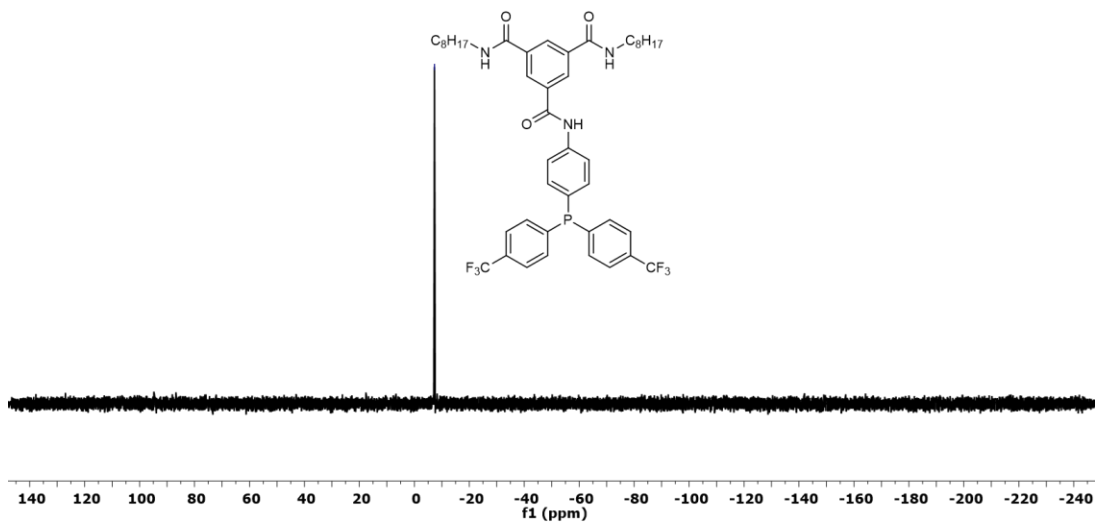


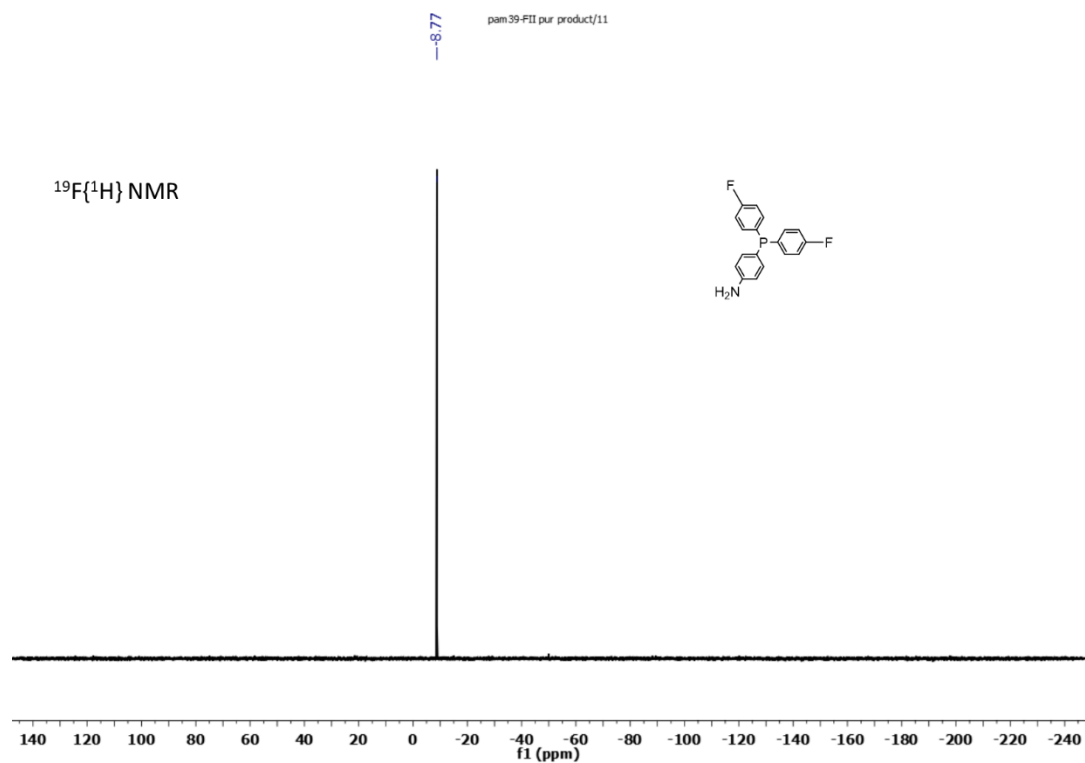
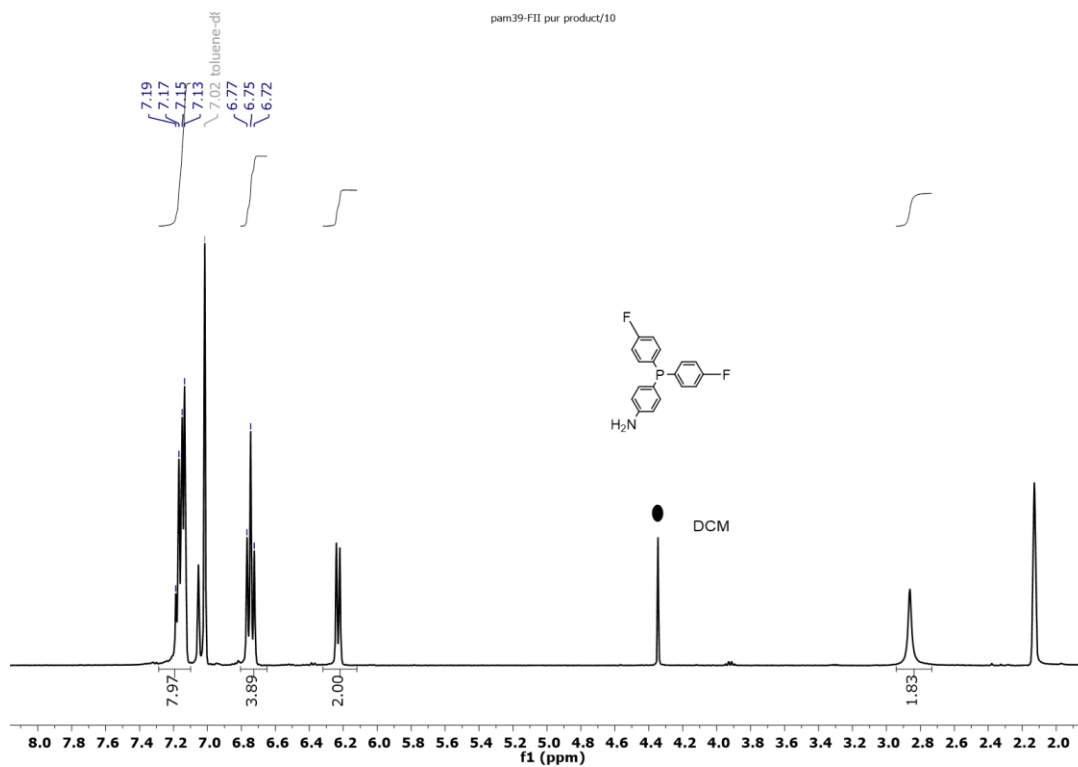


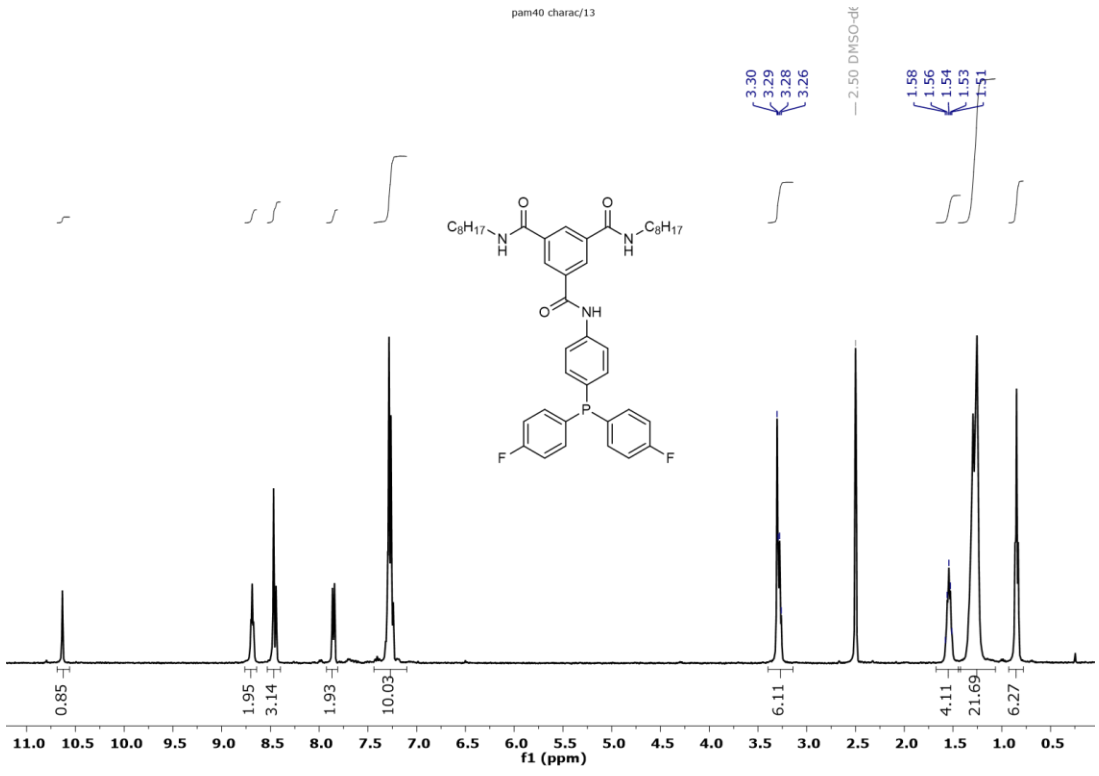
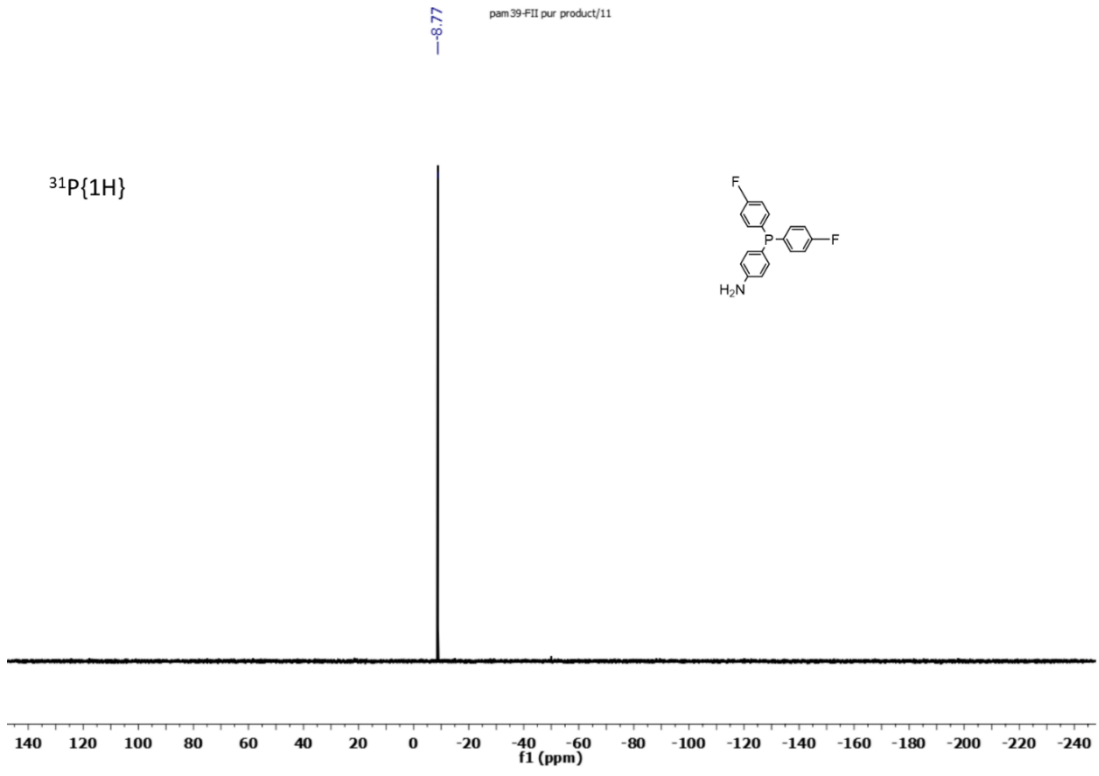
-7.32

pam37/11

$^{31}\text{P}\{^1\text{H}\}$



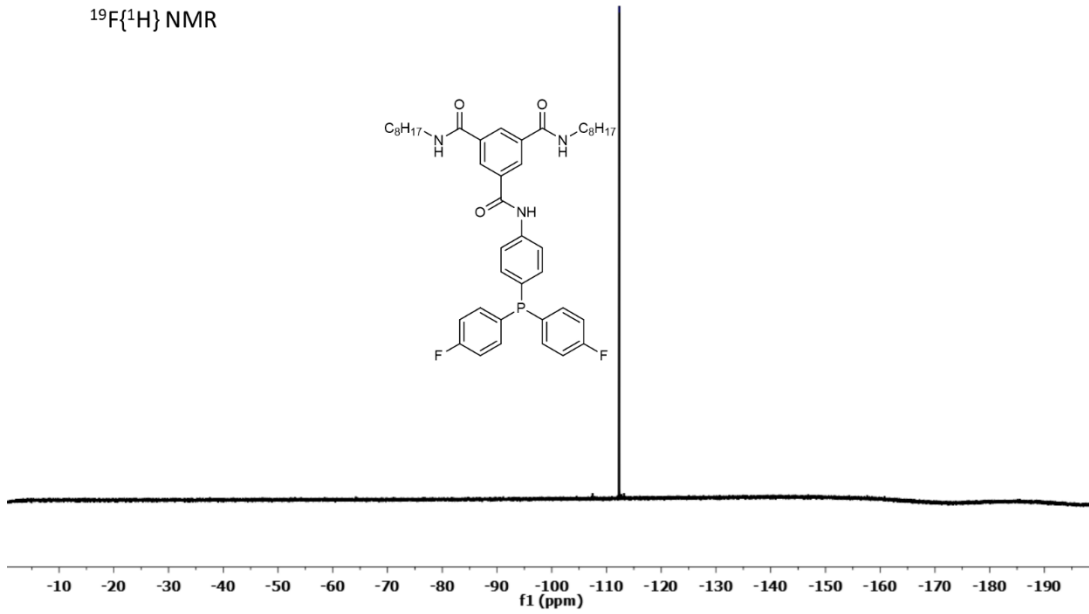
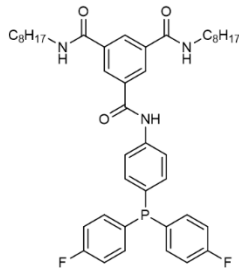




pan 40-FII/12

-112.33

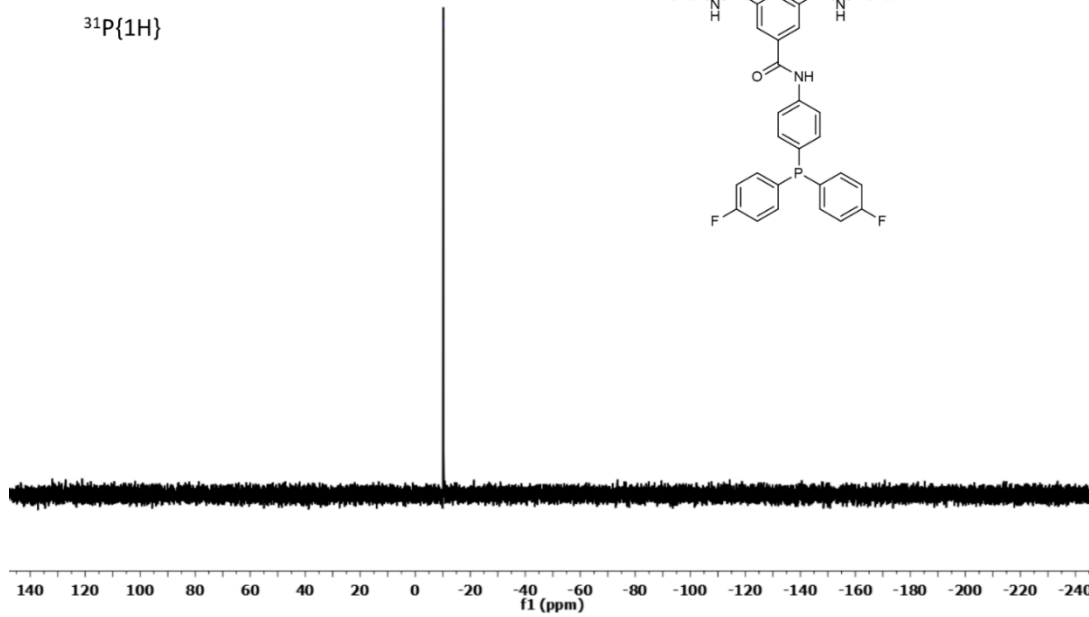
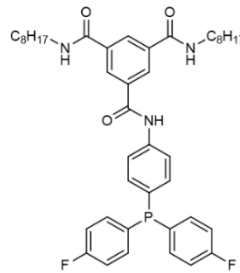
$^{19}\text{F}\{^1\text{H}\}$ NMR

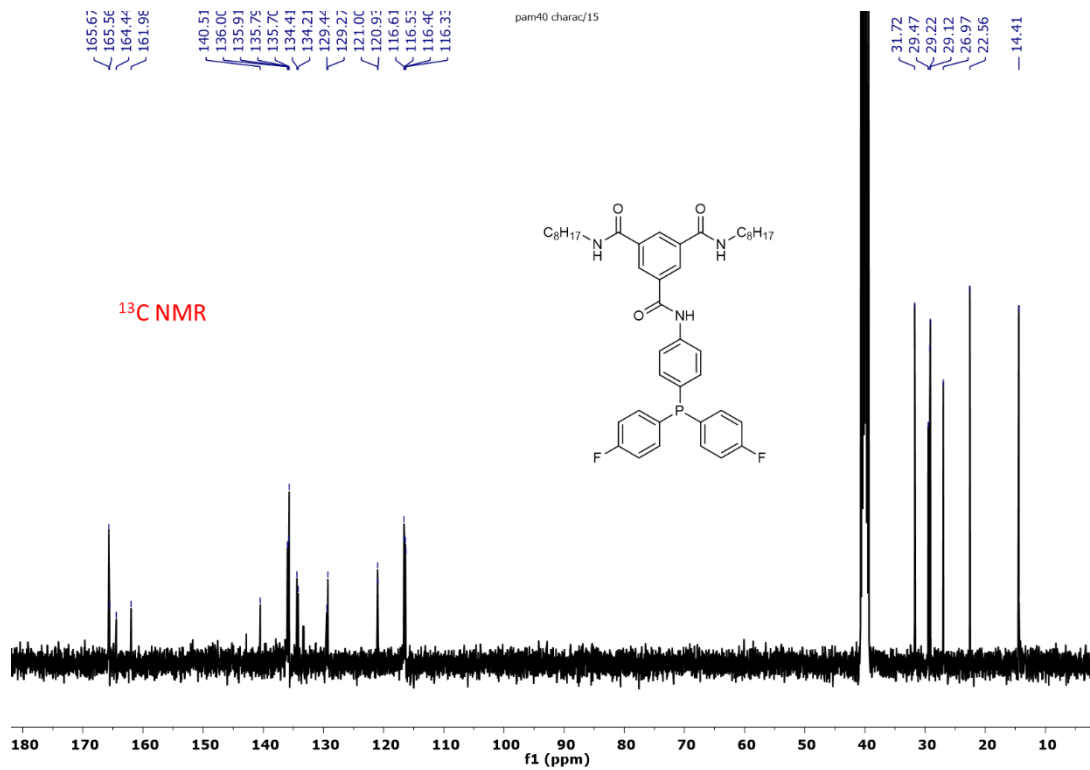


pan 40-FII/11

-10.15

$^{31}\text{P}\{^1\text{H}\}$





II.6.d. Selected chiral GC analyses:

Table II-6, Entry 1.

BTA-pPh₂, BTA (*S*)-Cha (0.06 mol%), $f_{\text{BTA}(\text{S})\text{-Cha}} = 0.5\%$, 293 K, no BTA cyclohex

0.5% ee

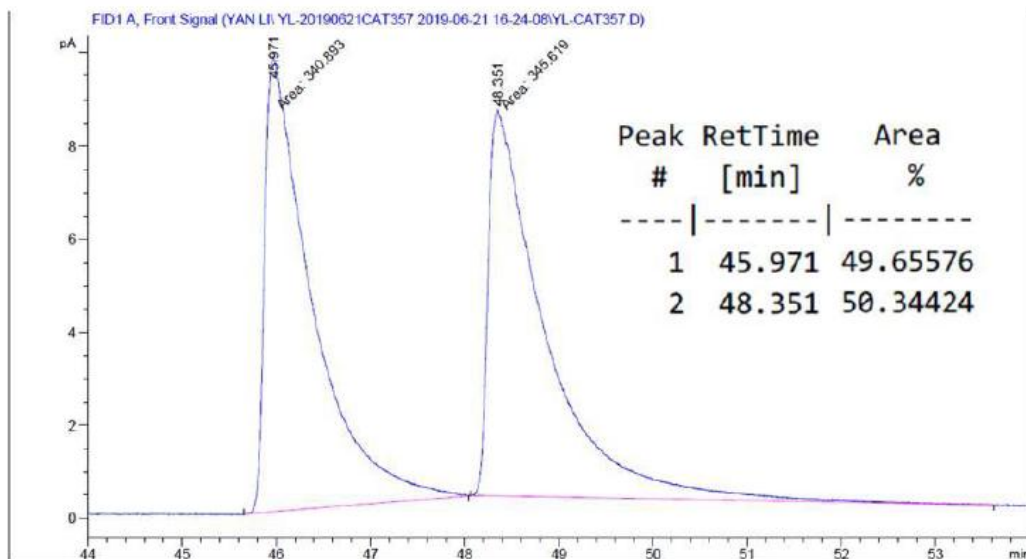


Table II-6, Entry 2.

BTA-pPh₂, BTA (*S*)-Cha (0.06 mol%), $f_{\text{BTA}(\text{S})\text{-Cha}} = 0.25\%$, 293 K, with BTA cyclohex

-50.4% ee (*R*)

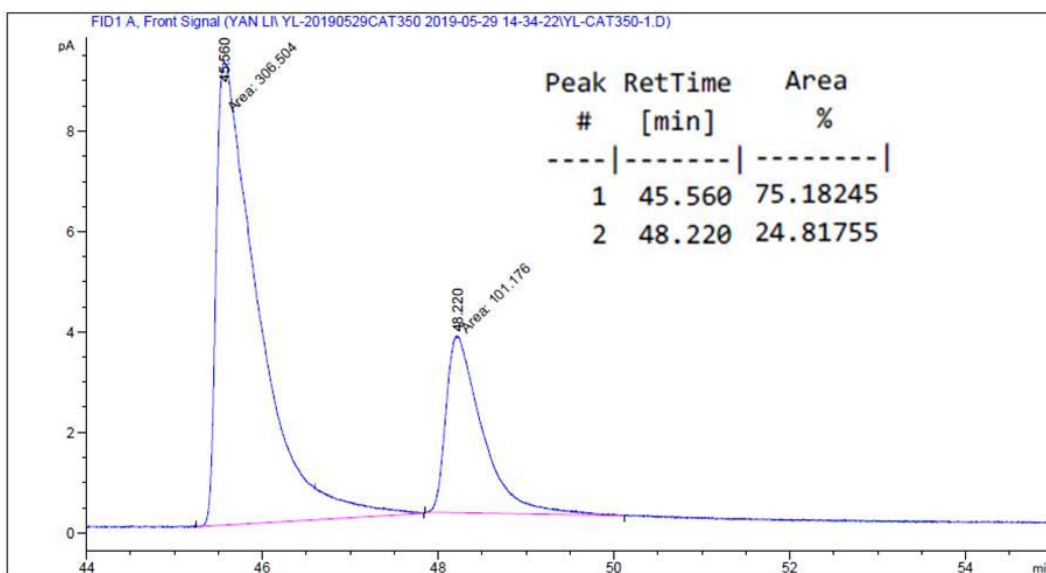


Table II-7, Entry 3.

BTA-P(Xylyl)2, BTA (S)-Cha (0.06 mol%), $f_{\text{BTA (S)-Cha}} = 0.5\%$, 200 K, no BTA cyclohex

-2.5% ee (R)

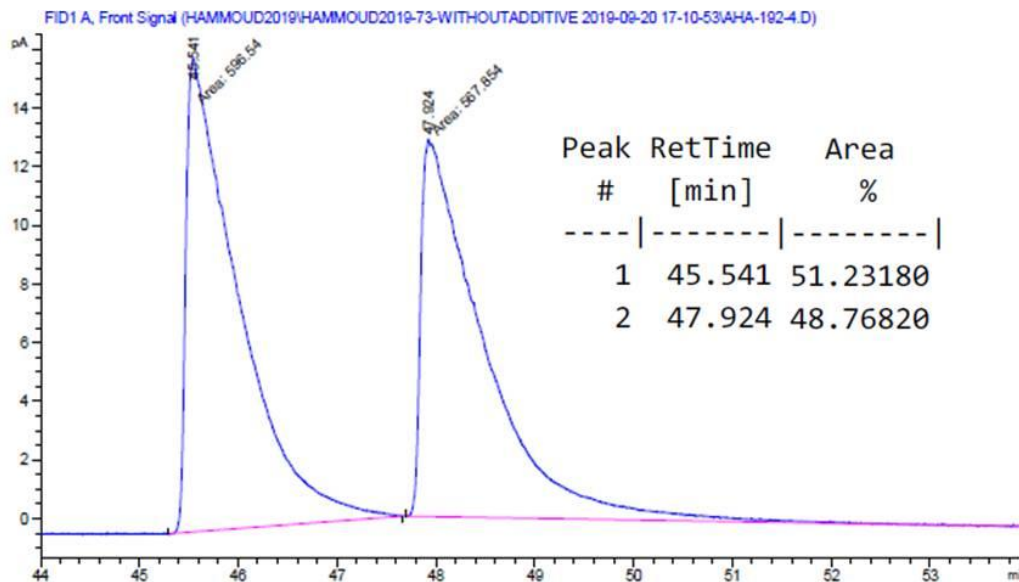


Table II-7, Entry 4

BTA-P(Xylyl)2, BTA (S)-Cha (0.06 mol%), $f_{\text{BTA (S)-Cha}} = 0.25\%$, 200 K, with BTA cyclohex

-90% ee (R).

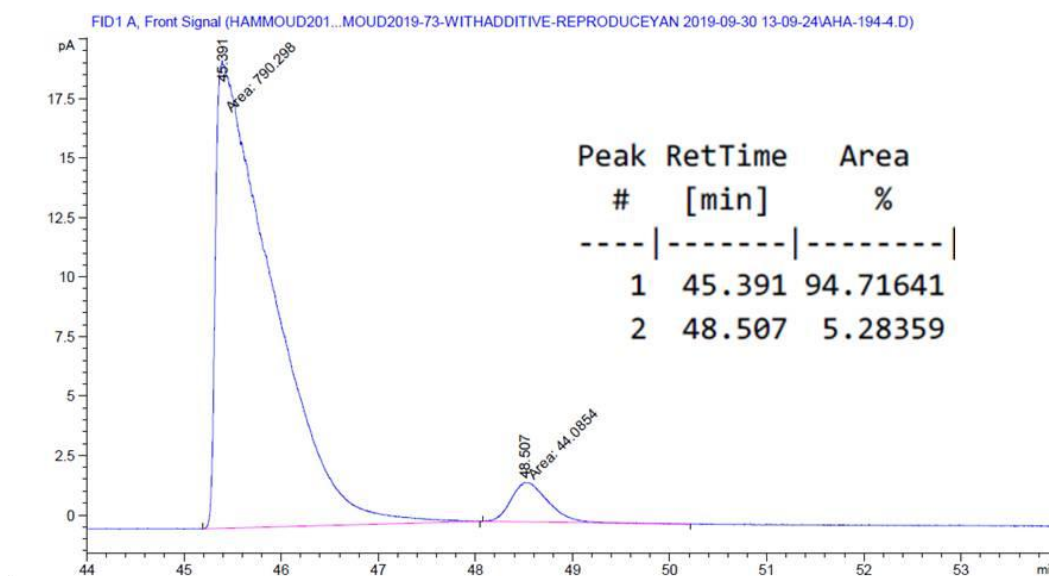


Table II-7, Entry 5

BTA-P(Xylyl)2, BTA (R)-Cha (0.06 mol%), $f_{\text{BTA (R)-Cha}} = 0.25\%$, 200 K, with BTA cyclohex

91% ee (S)

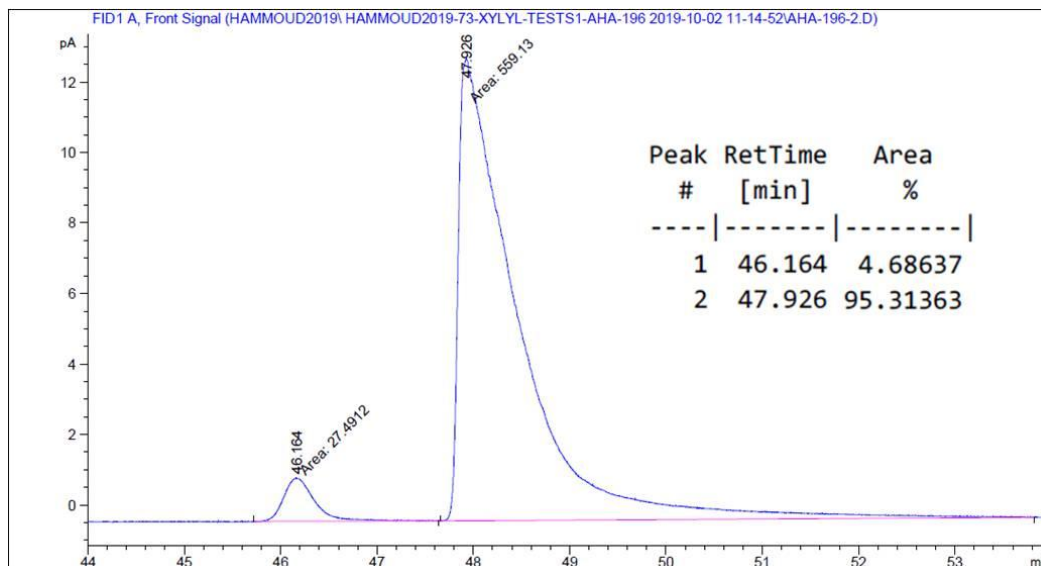
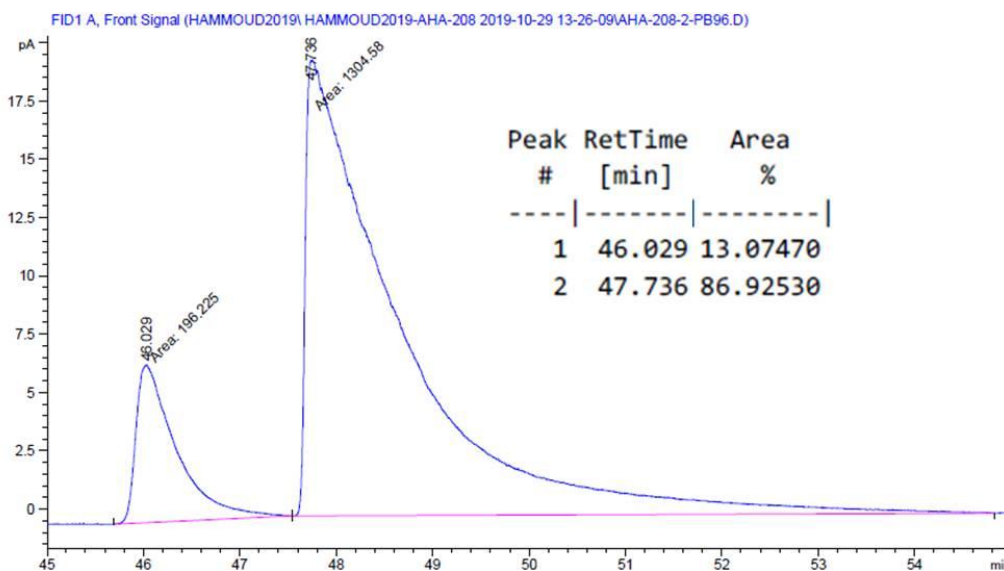


Table II-8, Entry 3

BTA-P(Xylyl)2, BTA (R)-Cha (75 ppm), $f_{\text{BTA (R)-Cha}} = 0.25\%$, 200 K, with BTA cyclohex

73.8% ee (S)



II.7. References.

- [1] J. M. Lehn, *Angew. Chem. Int. Ed. Engl.* **1990**, *29*, 1304–1319.
- [2] S. Cantekin, T. F. A. de Greef, A. R. A. Palmans, *Chem. Soc. Rev.* **2012**, *41*, 6125.
- [3] T. Curtius, *J. Für Prakt. Chem.* **1915**, *91*, 39–102.
- [4] M. Sidney, *Monomeric Compounds Comprising a Plurality of Vinyl Groups*, **1956**, US2774750A.
- [5] W. Ried, F.-J. Königstein, *Chem. Ber.* **1959**, *92*, 2532–2542.
- [6] M. P. Lightfoot, F. S. Mair, R. G. Pritchard, J. E. Warren, *Chem. Commun.* **1999**, 1945–1946.
- [7] P. J. M. Stals, J. F. Haveman, A. R. A. Palmans, A. P. H. J. Schenning, *J. Chem. Educ.* **2009**, *86*, 230.
- [8] S. Cantekin, H. M. M. ten Eikelder, A. J. Markvoort, M. A. J. Veld, P. A. Korevaar, M. M. Green, A. R. A. Palmans, E. W. Meijer, *Angew. Chem. Int. Ed.* **2012**, *51*, 6426–6431.
- [9] Y. Matsunaga, N. Miyajima, Y. Nakayasu, S. Sakai, M. Yonenaga, *Bull. Chem. Soc. Jpn.* **1988**, *61*, 207–210.
- [10] J. J. van Gorp, J. A. J. M. Vekemans, E. W. Meijer, *J. Am. Chem. Soc.* **2002**, *124*, 14759–14769.
- [11] A. R. A. Palmans, J. A. J. M. Vekemans, E. W. Meijer, A. R. A. Palmans, H. Kooijman, A. L. Spek, *Chem. Commun.* **1997**, *0*, 2247–2248.
- [12] L. Brunsveld, H. Zhang, M. Glasbeek, J. A. J. M. Vekemans, E. W. Meijer, *J. Am. Chem. Soc.* **2000**, *122*, 6175–6182.
- [13] R. van Hameren, P. Schön, A. M. van Buul, J. Hoogboom, S. V. Lazarenko, J. W. Gerritsen, H. Engelkamp, P. C. M. Christianen, H. A. Heus, J. C. Maan, T. Rasing, S. Speller, A. E. Rowan, J. A. A. W. Elemans, R. J. M. Nolte, *Science* **2006**, *314*, 1433–1436.
- [14] I. Paraschiv, M. Giesbers, B. van Lagen, F. C. Grozema, R. D. Abellon, L. D. A. Siebbeles, A. T. M. Marcelis, H. Zuilhof, E. J. R. Sudhölter, *Chem. Mater.* **2006**, *18*, 968–974.

- [15] J. van Herrikhuyzen, P. Jonkheijm, A. P. H. J. Schenning, E. W. Meijer, *Org. Biomol. Chem.* **2006**, *4*, 1539–1545.
- [16] B. Gong, C. Zheng, Y. Yan, *J. Chem. Crystallogr.* **1999**, *29*, 649–652.
- [17] K. P. van den Hout, R. Martín-Rapún, J. A. J. M. Vekemans, E. W. Meijer, *Chem. Eur. J.* **2007**, *13*, 8111–8123.
- [18] K. Matsuura, K. Murasato, N. Kimizuka, *J. Am. Chem. Soc.* **2005**, *127*, 10148–10149.
- [19] P. J. M. Stals, J. F. Haveman, R. Martín-Rapún, C. F. C. Fitié, A. R. A. Palmans, E. W. Meijer, *J. Mater. Chem.* **2009**, *19*, 124–130.
- [20] S. Lee, J.-S. Lee, C. H. Lee, Y.-S. Jung, J.-M. Kim, *Langmuir* **2011**, *27*, 1560–1564.
- [21] Y. Li, X. Caumes, M. Raynal, L. Bouteiller, *Chem. Commun.* **2019**, *55*, 2162–2165.
- [22] L. N. Neumann, M. B. Baker, C. M. A. Leenders, I. K. Voets, R. P. M. Lafleur, A. R. A. Palmans, E. W. Meijer, *Org. Biomol. Chem.* **2015**, *13*, 7711–7719.
- [23] M. Raynal, P. Ballester, A. Vidal-Ferran, P. W. N. M. van Leeuwen, *Chem Soc Rev* **2014**, *43*, 1660–1733.
- [24] J. M. Zimbron, X. Caumes, Y. Li, C. M. Thomas, M. Raynal, L. Bouteiller, *Angew. Chem. Int. Ed.* **2017**, *56*, 14016–14019.
- [25] A. Desmarchelier, X. Caumes, M. Raynal, A. Vidal-Ferran, P. W. N. M. van Leeuwen, L. Bouteiller, *J. Am. Chem. Soc.* **2016**, *138*, 4908–4916.
- [26] P. J. M. Stals, P. A. Korevaar, M. A. J. Gillissen, T. F. A. de Greef, C. F. C. Fitié, R. P. Sijbesma, A. R. A. Palmans, E. W. Meijer, *Angew. Chem Int. Ed.* **2012**, *124*, 11459–11463.
- [27] T. Mes, R. van der Weegen, A. R. A. Palmans, E. W. Meijer, *Angew. Chem.* **2011**, *123*, 5191–5195.
- [28] N. Hosono, M. A. J. Gillissen, Y. Li, S. S. Sheiko, A. R. A. Palmans, E. W. Meijer, *J. Am. Chem. Soc.* **2013**, *135*, 501–510.
- [29] O. Altintas, M. Artar, G. ter Huurne, I. K. Voets, A. R. A. Palmans, C. Barner-Kowollik, E. W. Meijer, *Macromolecules* **2015**, *48*, 8921–8932.

- [30] Y. Ogura, M. Artar, A. R. A. Palmans, M. Sawamoto, E. W. Meijer, T. Terashima, *Macromolecules* **2017**, *50*, 3215–3223.
- [31] J. Roosma, T. Mes, P. Leclère, A. R. A. Palmans, E. W. Meijer, *J. Am. Chem. Soc.* **2008**, *130*, 1120–1121.
- [32] T. Terashima, T. Mes, T. F. A. De Greef, M. A. J. Gillissen, P. Besenius, A. R. A. Palmans, E. W. Meijer, *J. Am. Chem. Soc.* **2011**, *133*, 4742–4745.
- [33] M. L. Ślęczkowski, E. W. Meijer, A. R. A. Palmans, *Macromol. Rapid Commun.* **2017**, *38*, 1700566.
- [34] M. García-Iglesias, B. F. M. de Waal, I. de Feijter, A. R. A. Palmans, E. W. Meijer, *Chem. – Eur. J.* **2015**, *21*, 377–385.
- [35] M. Raynal, F. Portier, P. W. N. M. van Leeuwen, L. Bouteiller, *J. Am. Chem. Soc.* **2013**, *135*, 17687–17690.
- [36] W. Zhang, D. Horoszewski, J. Decatur, C. Nuckolls, *J. Am. Chem. Soc.* **2003**, *125*, 4870–4873.
- [37] M. A. J. Veld, D. Haveman, A. R. A. Palmans, E. W. Meijer, *Soft Matter* **2011**, *7*, 524–531.
- [38] A. Desmarchelier, X. Caumes, M. Raynal, A. Vidal-Ferran, P. W. N. M. van Leeuwen, L. Bouteiller, *J. Am. Chem. Soc.* **2016**, *138*, 4908–4916.
- [39] X. Caumes, Hydrogen-Bonded Supramolecular Polymers as Dynamic Scaffolds for Catalysis, These de doctorat, Paris 6, **2016**.
- [40] S. G. Davies, *Organotransition Metal Chemistry: Applications to Organic Synthesis: Applications to Organic Synthesis*, Elsevier, **2013**.
- [41] G. Lu, R. Y. Liu, Y. Yang, C. Fang, D. S. Lambrecht, S. L. Buchwald, P. Liu, *J. Am. Chem. Soc.* **2017**, *139*, 16548–16555.
- [42] A. A. Thomas, K. Speck, I. Kevlishvili, Z. Lu, P. Liu, S. L. Buchwald, *J. Am. Chem. Soc.* **2018**, *140*, 13976–13984.

- [43] Y. Xi, B. Su, X. Qi, S. Pedram, P. Liu, J. F. Hartwig, *J. Am. Chem. Soc.* **2020**, *142*, 18213–18222.
- [44] D. Gelman, L. Jiang, S. L. Buchwald, *Org. Lett.* **2003**, *5*, 2315–2318.
- [45] O. Herd, A. Heßler, M. Hingst, M. Tepper, O. Stelzer, *J. Organomet. Chem.* **1996**, *522*, 69–76.
- [46] P. W. N. M. van Leeuwen, D. Rivillo, M. Raynal, Z. Freixa, *J. Am. Chem. Soc.* **2011**, *133*, 18562–18565.
- [47] M. Jin, M. Nakamura, *Chem. Lett.* **2013**, *42*, 1035–1037.
- [48] G. C. Lloyd-Jones, N. P. Taylor, *Chem. – Eur. J.* **2015**, *21*, 5423–5428.
- [49] S. Ganss, B. Breit, *Angew. Chem. Int. Ed Engl.* **2016**, *55*, 9738–9742.
- [50] T. Sawano, K. Ou, T. Nishimura, T. Hayashi, *J. Org. Chem.* **2013**, *78*, 8986–8993.
- [51] T. Liu, X. Sun, L. Wu, *Adv. Synth. Catal.* **2018**, *360*, 2005–2012.
- [52] Y. Li, X. Caumes, M. Raynal, L. Bouteiller, *Chem. Commun.* **2019**, *55*, 2162–2165.
- [53] M. A. Martínez-Aguirre, Y. Li, N. Vanthuyne, L. Bouteiller, M. Raynal, *Angew. Chem. Int. Ed.* **n.d.**, *n/a*, DOI <https://doi.org/10.1002/anie.202012457>.
- [54] A. Desmarchelier, M. Raynal, P. Brocorens, N. Vanthuyne, L. Bouteiller, *Chem. Commun.* **2015**, *51*, 7397–7400.
- [55] Y. Li, Switchable and Chirally-Amplified Helices Formed by Hydrogen-Bonded Supramolecular Polymers for Asymmetric Catalysis, PhD thesis, Sorbonne Université, **2019**.
- [56] Y. Li, A. Hammoud, L. Bouteiller, M. Raynal, *J. Am. Chem. Soc.* **2020**, *142*, 5676–5688.
- [57] T. W. Anderson, J. K. M. Sanders, G. D. Pantoş, *Org. Biomol. Chem.* **2010**, *8*, 4274–4280.
- [58] A. Desmarchelier, B. G. Alvarenga, X. Caumes, L. Dubreucq, C. Troufflard, M. Tessier, N. Vanthuyne, J. Idé, T. Maistriaux, D. Beljonne, P. Brocorens, R. Lazzaroni, M. Raynal, L. Bouteiller, *Soft Matter* **2016**, *12*, 7824–7838.

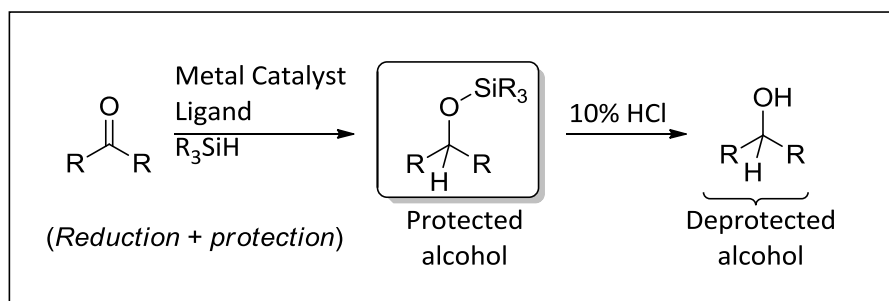
Chapter III Copper-catalyzed hydro-functionalization reactions with sergeants-and-soldiers type helical BTA catalysts : Hydroamination of styrene and cascade hydrosilylation/hydroamination of enone derivatives.

Abstract: A set of BTA ligands combined with **BTA Leu** as chiral co-monomer was evaluated in the asymmetric hydroamination of styrene and in the cascade hydrosilylation/hydroamination reaction of enone derivatives. Dramatic difference in catalytic rate, catalyst stability and product selectivity were observed for the hydroamination of styrene as a function of the nature of the BTA ligand. A set of parameters (copper source, temperature) was examined to optimize the best catalytic system, notably with the aim of minimizing the side reactions related to the vinyl bond reduction and the vinyl bond oligo/polymerization. The combination of **BTA-P(DTF)₂**, Cu(II)-i-butyrate and **BTA Leu** provided the hydroamination product in 60% yield and 67% *ee*. Different vinyl enone derivatives were screened for the cascade reaction. With α,β -enones, 1,4-reduction appeared to be very rapid with our BTA catalyst. As a result, the fully reduced product was obtained, which prevented hydroamination to occur. With α,γ -enones, the corresponding alcohol was obtained in very low yield (6%).

III.1. Introduction.

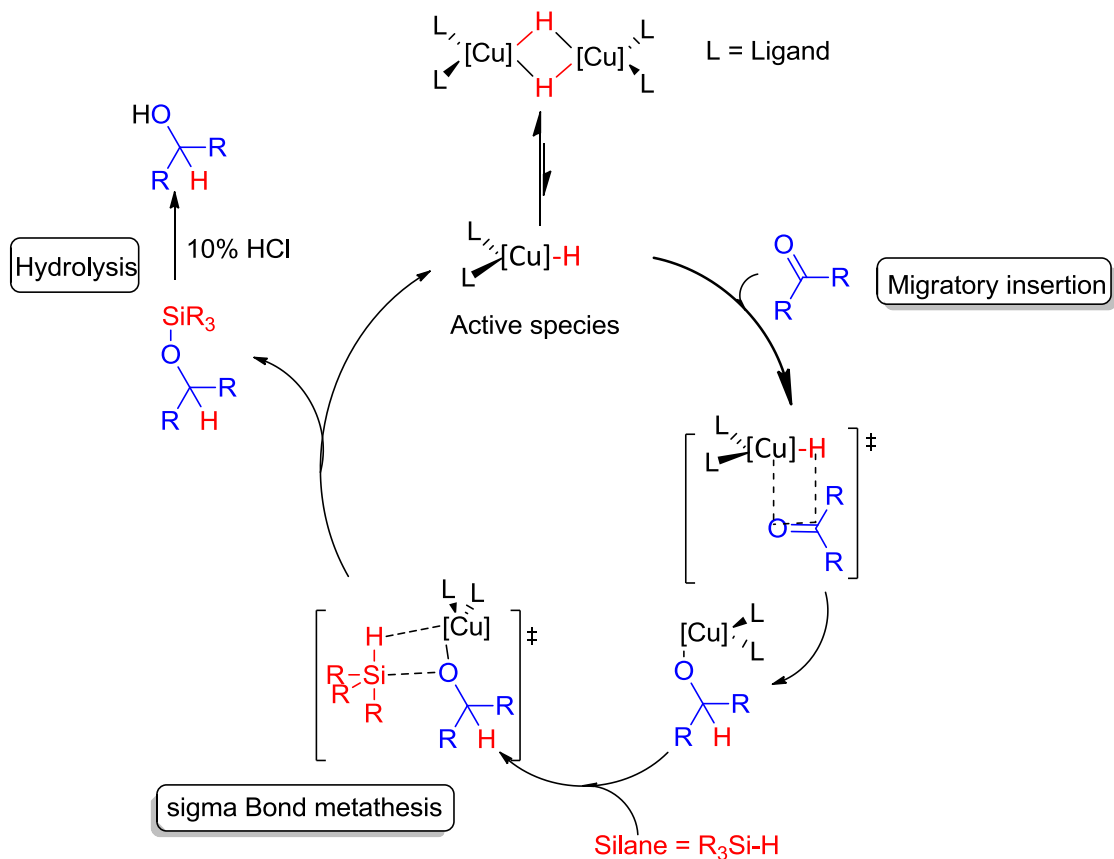
III.1.a. Hydrosilylation of unsaturated substrates by phosphine copper hydride catalysts.

Chiral secondary alcohols are important intermediates in organic synthesis towards biologically active molecules, agrochemicals, fragrance, and flavors. Obtaining the alcohol functionality through the reduction of a carbonyl moiety of either an aldehyde or a ketone via a hydride transfer process is considered as a fundamental transformation in organic synthesis^[1,2]. The reduction of many carbonyl compounds have been achieved successfully through transition-metal catalysis via hydrogenation or hydrosilylation^[1,2]. Depending on the nature of the substrate, hydrogenation reactions might require high pressure or elevated temperature to proceed in a good yield. In addition to that, if the reaction is part of a multistep synthesis, the resulting free alcohol frequently requires protection prior to the next synthetic step. Hydrosilylation reaction might appear as an efficient alternative under very mild reaction conditions for which both the reduction and the protection steps are performed simultaneously (Scheme III-1).



Scheme III-1 A catalytic hydrosilylation process of a carbonyl moiety showing that the reduction and protection steps are performed in a single step, to form the protected alcohol as organosilicon species.

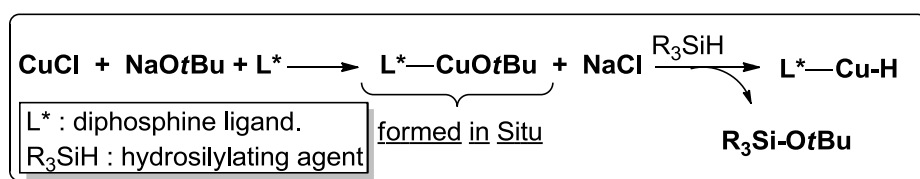
The first catalytic hydrosilylation systems for reduction of carbonyl compounds were reported in the early 1970s^[3-5] and consisted of rhodium-based catalysts. Traditionally, the catalytic hydrosilylation of the carbonyl functionality was performed with precious, and expensive metals such as Re, Rh, and Ru to Ir^[6-13]. Since then, efforts were devoted to replace these systems with more efficient ones based on cheaper or more abundant metals such as titanium^[14-17], iron^[18-23], manganese^[24-26], zinc^[27,28], and copper.



Scheme III-2 General catalytic cycle of CuH-catalyzed hydrosilylation of carbonyl compounds.

The first asymmetric hydrosilylation of carbonyl compounds based on diphosphine copper catalyst was reported in 1984^[29], by means of mixtures of Cu(I) compounds and optically active diphosphine ligands. As a result, hydrosilylated product of acetophenone was obtained in low optical purity ranging between 10 and 40% *ee*. It was not before the beginning of this century that very efficient diphosphine copper catalytic systems were developed for this reaction^[30-34]. The active catalytic species formed in situ was postulated to be a monomeric copper(I) hydride

species^[34]. Hydrocupration which occurs by a migratory insertion of the Cu-H bond into the carbonyl functionality is the enantio-determining step. Sigma bond metathesis between the alkoxy copper intermediate and the silane yields the alkoxy silane and regenerates the Cu-H catalyst. After reaction completion, the alkoxy silane is hydrolyzed into the desired alcohol (Scheme III-2). Lipshutz and coworkers described the formation of the Cu-H species in a system combining a catalytic quantity of [CuCl]/NaOtBu/diphosphine and a stoichiometric quantity of hydrosilylating agent that goes through trans-metalation with an in situ formed Cu-OtBu complex^[35–38] (Scheme III-3).



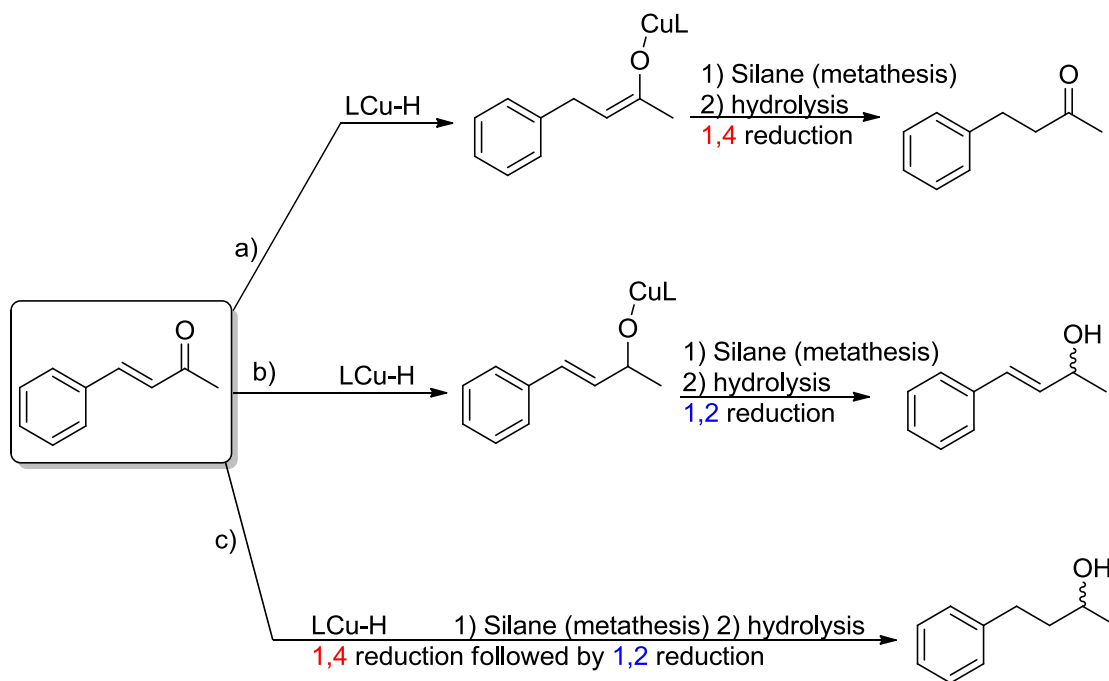
Scheme III-3 In situ generation of L-CuH species.

During that time, Carreira and co-workers^[39], as well as Riant and co-workers^[40–43], reported CuF₂ systems as interesting precursors to copper hydride. Other air and moisture-stable copper(II) salts, such as [Cu(OAc)₂·H₂O], in combination with inexpensive and readily available diphosphines such as **BINAP** have been efficiently used to catalyze the hydrosilylation of various ketones^[44,45]. On the one hand, very efficient molecular catalysts embedding diphosphine ligands (eg. **DTBM-SEGPHOS**^[35], **Xyl-P-Phos**^[46]) have been developed for the hydrosilylation of acetophenone and aryl/alkyl ketones as well as more elaborated substrates. On the other hand, very efficient supramolecular catalysts embedding phosphine containing BTA ligands have been developed by our group for the asymmetric hydrosilylation of 4-nitroacetophenone and 4-phenylacetophenone^[47–50].

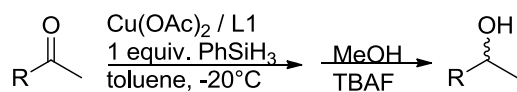
III.1.b. Regioselectivity issues in hydrosilylation reactions.

Enone derivatives are particularly interesting substrates for implementing our hydrosilylation/hydroamination cascade reaction. However, regioselectivity issues are commonly encountered during the reduction of this class of substrates. For example, in the case of α,β -enones, the hydrosilylation might generate the α,β -reduced ketone or the corresponding α,β -vinyl alcohol (Scheme III-4a, and 4b), depending on whether a 1,4-reduction

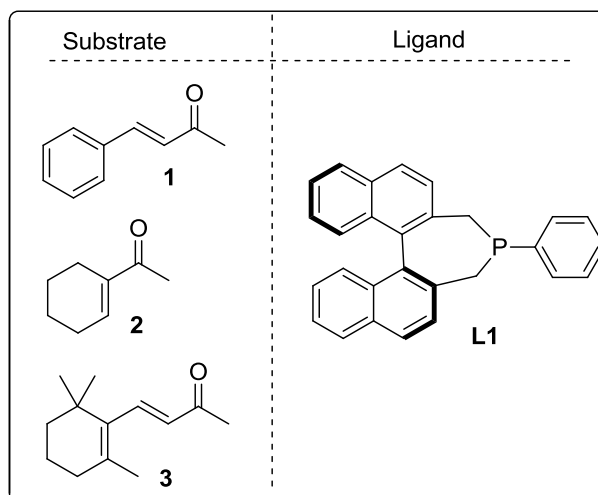
or 1,2-reduction pathway is followed, respectively^[51,52]. Likewise, both reactions can react to yield the α,β -reduced alcohol (Scheme III-4c).



Scheme III-4 Illustration of different pathways that could be encountered for benzylideneacetone in presence of copper hydride species. a) 1,4 reduction, leading to the reduction of the vinyl moiety. b) 1,2 reduction. c) 1,4 reduction followed by 1,2 reduction.

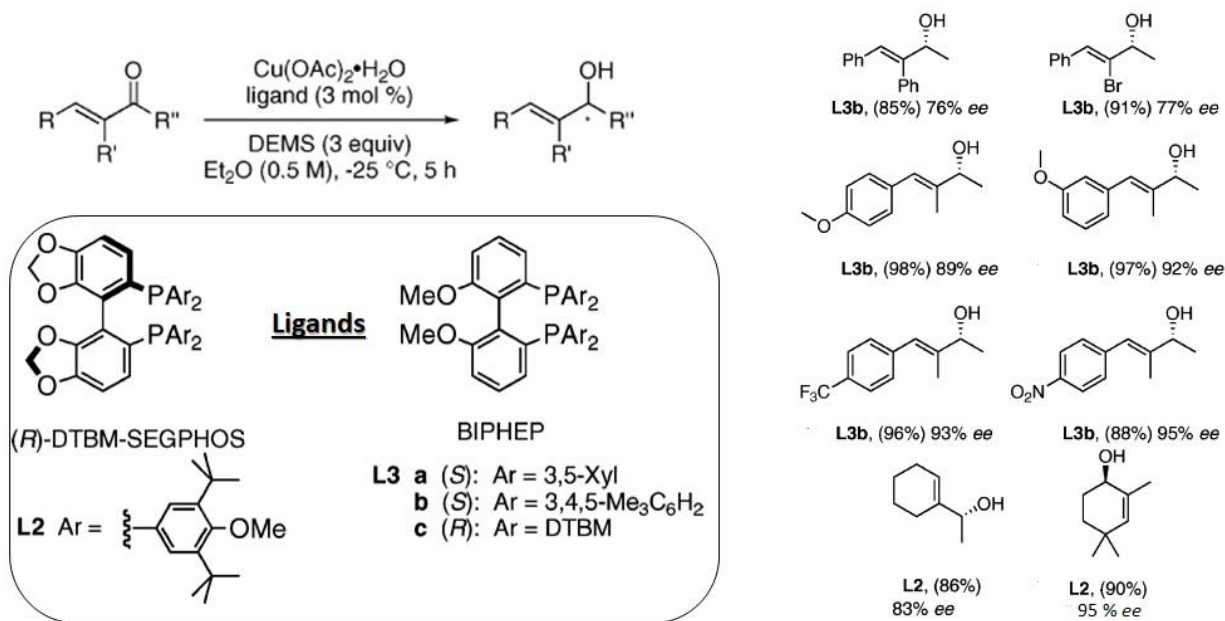


Substrate	Yield (%)	ee (%)
1	C-C(O) 10%	-
	C=C(OH) 22%	60%
	C-C(OH) 24%	28%
2	C=C(OH) 82%	96%
3	C=C(OH) 92%	84%



Scheme III-5 Left: Conditions for copper catalyzed hydrosilylation of α,β -enones: substrate (1 mmol), copper acetate (3 mol%), L1 (6 mol%), PhSiH_3 (1 equiv.), toluene (1 mL), 5h, -20°C . Right: structures of substrates (1, 2, and 3), and ligand L1 (4-phenyl-4,5-dihydro-3H-dinaphtho[2,1-c;1',2'-e]phosphepine). Adapted from reference^[53].

The regioselectivity is substrate-dependent as shown by Beller and co-workers^[53] for the hydrosilylation of various enones with chiral monodentate binaphthophosphine ligands. They found a poor regioselectivity for benzylideneacetone **1** whilst for the same catalyst, a high 1,2-addition selectivity was found for cyclohexenylethanone **2** and substrate **3** (Scheme III-5). There is an inherent mechanistic preference for initial d- π^* complexation of the Cu(I) to alkene which makes 1,4-addition the preferred pathway for most enone substrates. Lipshutz^[54] and co-workers discovered the possibility of favoring the 1,2 reduction pathway by playing both on the nature of the substrate (α -substitution) and the ligand (DTBM-SEGPHOS **L2** vs BIHEP **L3**, Scheme III-6). A range of α -substituted unsaturated ketones was hydrosilylated regioselectively and enantioselectively with different BIPHEP based ligands (Scheme III-6). Optimal yields were obtained at -25°C probably because the 1,4-reduction pathway was minimized at this temperature.



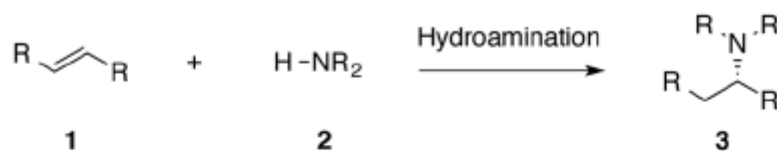
Scheme III-6 CuH-catalyzed asymmetric 1,2-reductions of α -substituted enones. Reactions were carried out on a 0.25 mmol scale in 0.5 mL of Et₂O. Isolated yields after column chromatography are given in parentheses. The reported *ee*'s were determined by chiral HPLC or GC analyses. Adapted from reference^[54].

Thus, competition between 1,2- and 1,4-reduction can be predictably controlled by altering electronic and steric properties of the catalytic system and the substrate^[54].

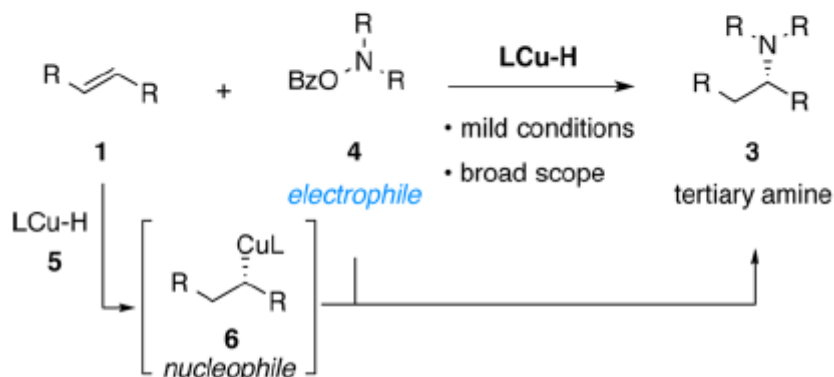
III.1.c. Asymmetric copper catalyzed hydroamination for the preparation of chiral amines.

Chiral amines are widespread structural motifs found in many pharmaceutical agents, natural products, and catalysts for asymmetric synthesis. For this reason, general and selective approaches for their preparation have long been chased^[55]. Methodologies using resolution^[56] or chiral auxiliaries^[57] have been put in place as reliable ways to obtain chiral amines. Important efforts have also been devoted to the development of catalytic asymmetric methods. Most of these methods are based on asymmetric reduction of imine, enamine, or enamide intermediates^[58–61]. Other approaches, such as asymmetric allylation of amine nucleophiles^[62] and direct C-H bond insertion by a nitrenoid species^[63] are considered as important alternatives. Asymmetric hydroamination^[64–69], described as the stereoselective addition of a hydrogen atom and an amino group directly across a double bond, is considered as an efficient and attractive approach for the preparation of chiral amines. Usually, a traditional hydroamination reaction involves the direct association of an alkene **1** with a primary or secondary amine nucleophile **2** in the presence of a catalyst (Scheme III-7a). Building on the intriguing reactivity of copper(I) hydride diphosphine complexes^[70,71], the groups of Miura^[72–76] and Buchwald^[77–79] independently reported an “umpolung” approach toward asymmetric hydroamination (Scheme III-7b). The mechanism was ascertained with **DTBM-SEGPHOS** ligand by means of kinetic and computational studies^[80]. The alkyl copper intermediate **6** (Scheme III-7b) which is formed through a hydrocupration step between olefin **1** and copper hydride species **5**, reacts with a suitable amine electrophile **4** to yield the enantioenriched tertiary amine **3**. This approach has been utilized for the preparation of chiral tertiary alkylamines from styrene derivatives^[81], 1,1-disubstituted alkenes^[82], vinylsilanes^[83], and alkynes^[84]. Independently, Miura and co-workers have reported a similar approach for the hydroamination of styrene derivatives^[85] and strained internal alkenes^[86]. The reaction delivers branched and linear amines when conducted from vinyl arenes or linear alkenes, respectively. To broaden the scope of the reaction, Buchwald and coworkers^[87] optimized this method to become more applicable including a wide range of alkenes and alkynes, including simple alkenes such as trans-2-butene which was hydroaminated enantioselectively^[87].

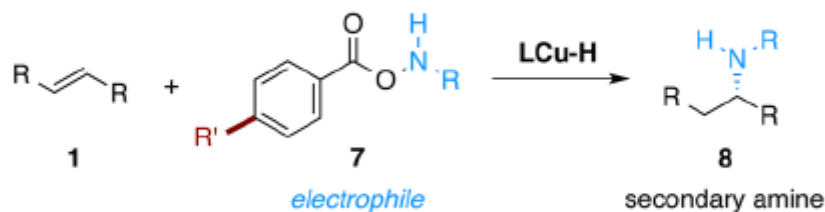
a) Traditional hydroamination



b) CuH catalyzed hydroamination: synthesis of chiral tertiary amines



c) synthesis of chiral secondary amines



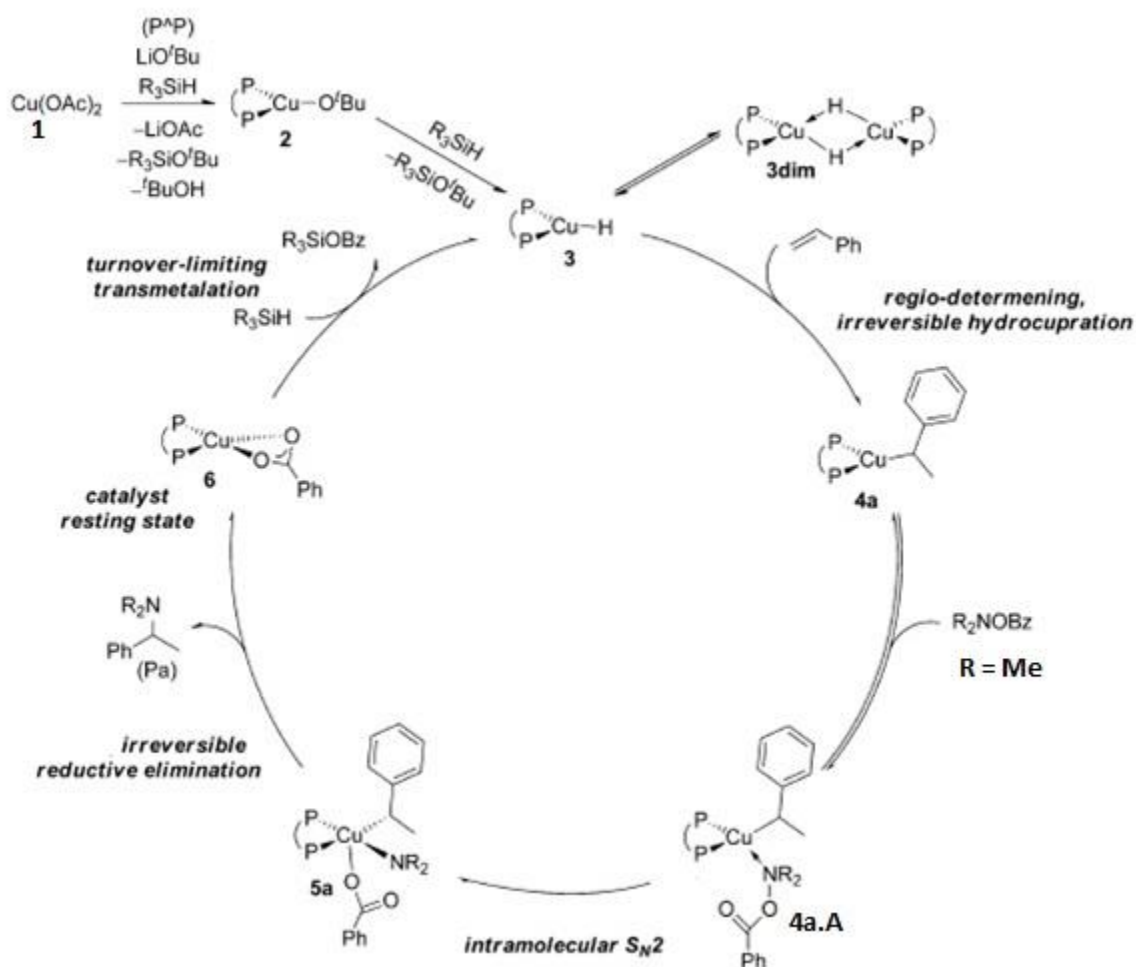
R' = H : generally poor yields

R' = NMe₂: broad substrate scope, good yields

Scheme III-7 Hydroamination approaches towards chiral amines^[84]

It was found that PPh₃ addition into the catalytic mixture is crucial to increase the stability and activity of the catalyst. A new catalytic system called *CuCatmix*^[78] was generated, which allows catalytic reactions to be carried under air, providing the hydroaminated styrene in 91% yield with high *ee* (up 95%) in less than 30 minutes. Furthermore, additional optimizations were applied by the same group^[88] which allowed the direct preparation of chiral secondary amines from mono-alkylamine electrophiles (Scheme III-7c). Thus, a copper-catalyzed hydroamination process was developed for generating chiral, branched secondary amines **8** from styrene derivatives. This process relies on a key element represented by the design and use of a more

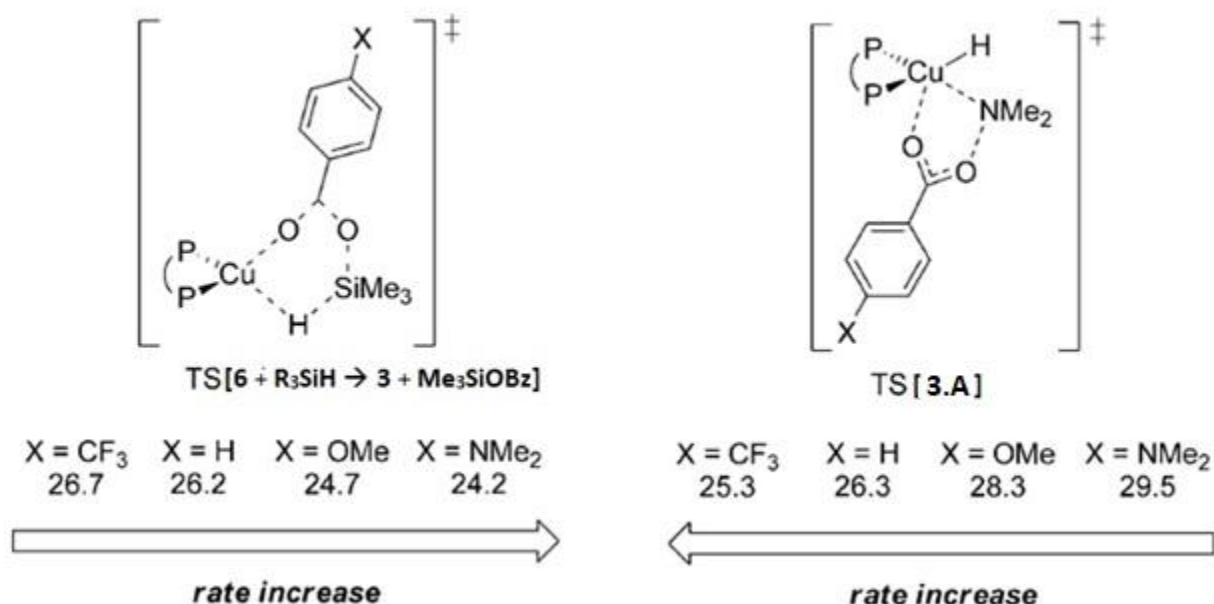
electron rich amine electrophile **7**. This modification reduces the nonproductive direct reduction of the amine electrophile by the phosphine copper hydride species^[88] which was also investigated by Tobisch^[89] (vide infra). A full mechanistic pathways for CuH-catalyzed hydroamination of styrene with 1,2-bis(diphenylphosphino)-benzene as ligand has been proposed by Tobisch^[89] (Scheme III-8).



Scheme III-8 Proposed catalytic cycle for CuH-catalyzed hydroamination of vinylarenes with amine electrophiles in the presence of a hydrosilane source^[89].

An energetically smooth and downhill sequence of steps transforms the starting copper acetate precursor **1** into the catalytically active $\{\text{P}^{\text{A}}\text{P}\}\text{Cu}(\text{I})$ hydride **3**, which is in equilibrium with its thermodynamically prevalent dimer **3dim**. First, a migratory insertion step takes place between the active Cu-H species **3** and the C=C bond of styrene. Hence, an irreversible hydrocupration

which is regio-determining occurs prior to the turnover-limiting transmetalation structure. The interception of the generated $\{P^*P\}Cu(I)$ benzyl **4a** with amine electrophile **Me₂NOBz (A)** produces the branched tertiary (Markovnikov) amine product **Pa** and $\{P^*P\}Cu(I)$ benzoate **6**. This transformation consists of a two-step process, comprising an intramolecular S_N2 displacement of the benzoate leaving group to give the highly reactive $\{P^*P\}Cu(III)$ intermediate **5a** from which **Pa** and **6** are generated upon rapid and strongly downhill reductive elimination. The formed **6** is found as the most stable species of the catalytic cycle, and corresponds to the catalyst resting state. The regeneration of catalytically active species **3** from **6** through transmetalation with **R₃SiH** is the turnover-limiting step. It is worth mentioning that a similar picture regarding hydrocupration and transmetalation steps has emerged from an experimental study by the Buchwald group on a **DTBM-SEGPHOS**-based Cu(I) catalyst^[78].



Scheme III-9 Kinetic demands for turnover-limiting regeneration of **3** from **6** (left), and for the undesired S_N2 N-O bond cleavage at adduct **3.A** (right) of the $\{P^*P\}Cu(I)$ hydride for several electronically modified amine-O-benzoates^[89].

In addition, the energy profile for two crucial steps: i) the turnover-limiting transmetalation [**6** + **R₃SiH** → **3** + **Me₃SiOBz**], and ii) the undesired intramolecular S_N2 substitution of the benzoate leaving group at **3.A**, which leads to performance-limiting consumption of a molar equivalent of

amine electrophile, has been re-evaluated for para-phenyl substituted O-benzoyl-N,N-dimethyl-hydroxylamines featuring electron-withdrawing ($X=CF_3$) or electron-releasing ($X=OMe$, NMe_2) groups^[89] (Scheme III-9). Accordingly, it was shown that the electronic modulation of the amine electrophile could act contrarily upon the two rival steps, such as more electron-rich amine electrophiles are expected to react faster in the transmetalation step, and thus generate copper $\{P^{\wedge}P\}Cu(I)$ hydride **3** easily, while slow reaction rates were detected for the intramolecular S_N2 substitution for [**3.A**], which in turn limits the amine electrophile decomposition.

Lastly, it is important to note that similar phosphine copper hydride species (notably the ones derived from **DTBM-SEGPHOS** and **Ph-BPE** ligands) have been found to be very efficient ligands not only for hydroamination but also for a large number of other hydro-functionalization reactions of alkenes^[90–94].

III.1.d. Content of this chapter.

High levels of chemo/regio/enantio-selectivity will be necessary for both steps of planned cascade reaction. For this reason, it was essential to probe the efficiency of BTA helical catalyst in the hydroamination reaction of styrene. The latter was selected because its hydroamination by copper catalytic systems has been widely reported in literature^[74,95,96]. This evaluation will shed light on the activity of the supramolecular catalyst in catalyzing hydroamination reaction, and on the optimized conditions required for obtaining a stable catalytic system able to provide high levels of enantioselectivity. The optimized conditions will be considered for the evaluation of different “enone” substrates in a cascade copper-catalyzed hydrosilylation/hydroamination process. Preliminary results will be introduced concerning the effect of both catalytic system and the substrate structure on the outcome of the copper-catalyzed reaction.

III.2. Copper-catalyzed hydroamination of styrene with sergeants-and-soldiers type helical BTA catalysts.

It has been shown that the combination of **BTA-pPPH2** and a suitable enantiopure co-monomer provided significant level of enantioselectivity in the copper-catalyzed hydrosilylation of acetophenone derivatives^[47,48,97]. Herein, we will probe the ability of mixtures between various achiral BTA ligands and the enantiopure co-monomer **BTA Leu** to promote the hydroamination

of styrene. This will constitute the first step towards our objective to engage the BTA co-assemblies in a hydrosilylation/hydroamination cascade process.

III.2.a. Probing the stability of the co-assemblies.

Preliminary characterization of the co-assemblies formed between the different BTA ligands synthesized in **Chapter II** and **BTA Leu** indicate that long one-dimensional co-assemblies are formed in toluene in the case of **BTA-pPPh₂**, **BTA-P(DTF)₂**, **BTA-P(Xylyl)₂** with similar degree of incorporation of **BTA Leu** (20<fs<30%).

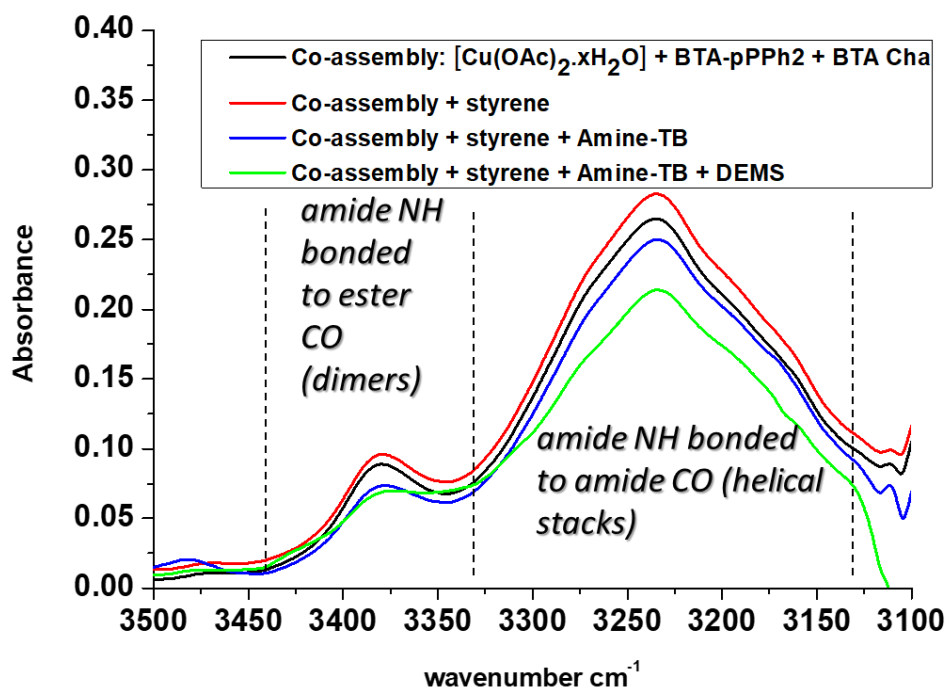


Figure III-1 Black: FT-IR analyses of the co-assembly of **BTA-pPPh₂** (52.7 mM), [CuOAc.xH₂O] (26.4 mM) and **BTA (S)-Cha** (54.3 mM) in toluene at room temperature. Red: after addition of 1.0 equiv. of styrene (0.29 M), blue: after addition of 1.0 equiv. of styrene (0.29 M) and of 1.2 equiv. of amine-TB (0.34 M), green: after addition of 1.0 equiv. of styrene (0.29 M), of 1.2 equiv. of amine-TB (0.34 M) and of 2.0 equiv. of DEMS (0,57 M).

Accordingly, these ligands have been selected for screening in the hydroamination (HA) of styrene. Any difference in the catalytic performance will thus be ascribed to the nature of the different aryl (Ar) groups connected to the P atom of the different BTA ligands. For the purpose of probing the influence of the position of electron-withdrawing groups on the catalytic ability

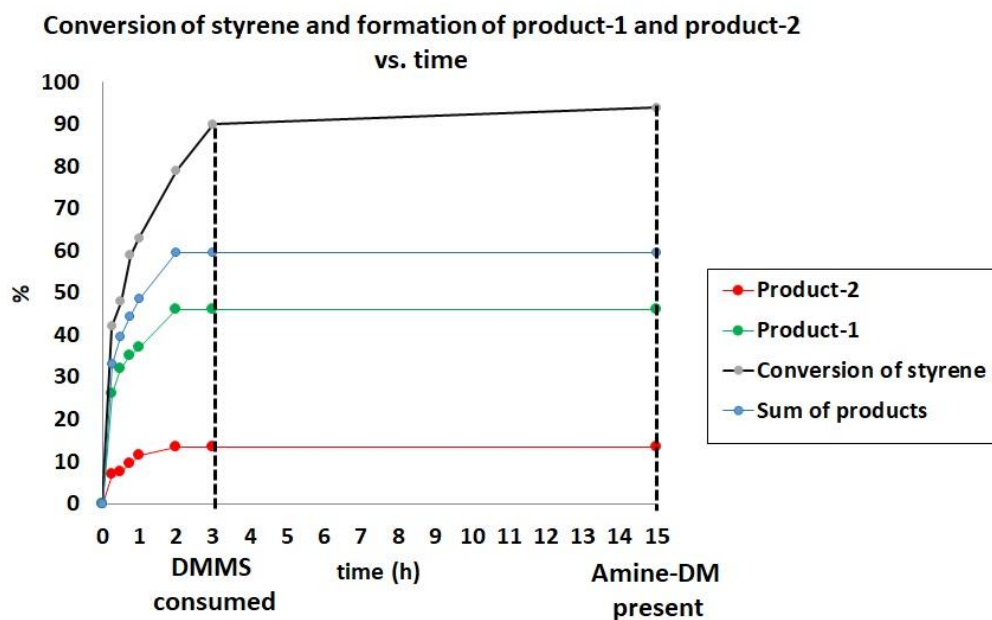
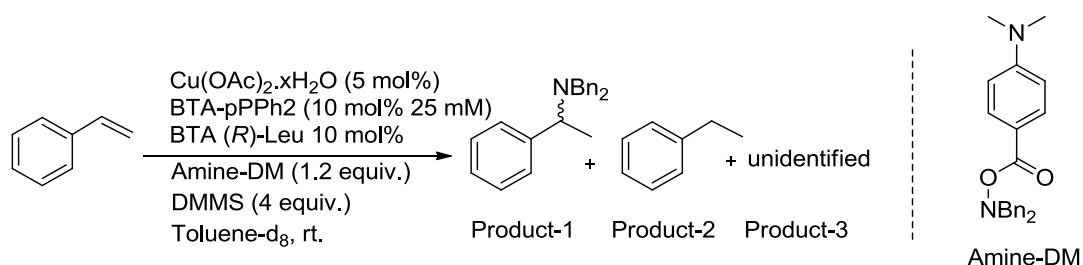
of these ligands, **BTA-P(PhF)2** and **BTA-(MTF)2** will also be tested (EWG groups are attached on 4-position of the aryl instead of the 3- and 5-positions for **BTA-P(DTF)2**).

It is important to check whether styrene, amine electrophile, and amine product are hydrogen bond competitors of the helical co-assemblies. FT-IR analyses were thus performed to probe the nature of hydrogen-bond network and its evaluation after addition of reactants and formation of the product. This study was performed on a mixture composed of $[\text{Cu}(\text{OAc})_2 \cdot x\text{H}_2\text{O}]$ coordinated to **BTA-pPPh2**, and **BTA (S)-Cha** co-monomer in toluene. The initial helical co-assemblies are long ($\text{DP}_n > 500$) contain *ca.* 60% of **BTA-pPPh2** and 40% of **BTA (S)-Cha**^[98]. As represented in Figure III-1, the addition of styrene, DEMS or amine-TB (N,N-dibenzyl-O-pivaloylhydroxylamine) has no significant effect on the structure of the co-assemblies. The bands at 3380 cm^{-1} and 3240 cm^{-1} corresponding to amide NH bonded to ester C=O (dimers) and amide NH bonded to amide C=O (stacks) respectively, do not experience any significant changes. The lower intensity of the band at 3240 cm^{-1} after addition of the silane might be related to some precipitation of the formed copper hydride complex. Neither the reagents nor the amine product N,N-dibenzyl-1-phenylethylamine (See Annex: subsection **III.4.b.i**, Figure S.III-1) affect significantly the nature of the co-assemblies. It is expected that the co-assemblies with other BTA ligands screened in this chapter have similar stabilities.

III.2.b. BTA-pPPh2 as ligand for the copper-catalyzed HA of styrene.

Preliminary screening studies were performed in order to determine if copper-based **BTA-pPPh2** helical supramolecular catalysts are active and selective in the hydroamination of styrene. Herein, we will discuss the activity of the supramolecular BTA catalyst based on the consumption of styrene, the catalyst chemoselectivity based on the nature of products formed throughout the process, and the enantiopurity of the amine product. Copper complexes of the BTA ligand were always prepared according to the following method: the BTA ligand and the copper source were mixed in THF, a solvent in which copper source is soluble, and BTAs are present under the form of monomers. Then THF solvent was removed and replaced by toluene, a solvent which promotes the assembly of BTAs into helical supramolecular polymers. Mixtures between **BTA-pPPh2** and an enantiopure co-monomer **BTA (R)-Leu** in 1:1 ratio were evaluated in presence of DMMS (4 equiv.) as silane reagent, and amine-DM (4-

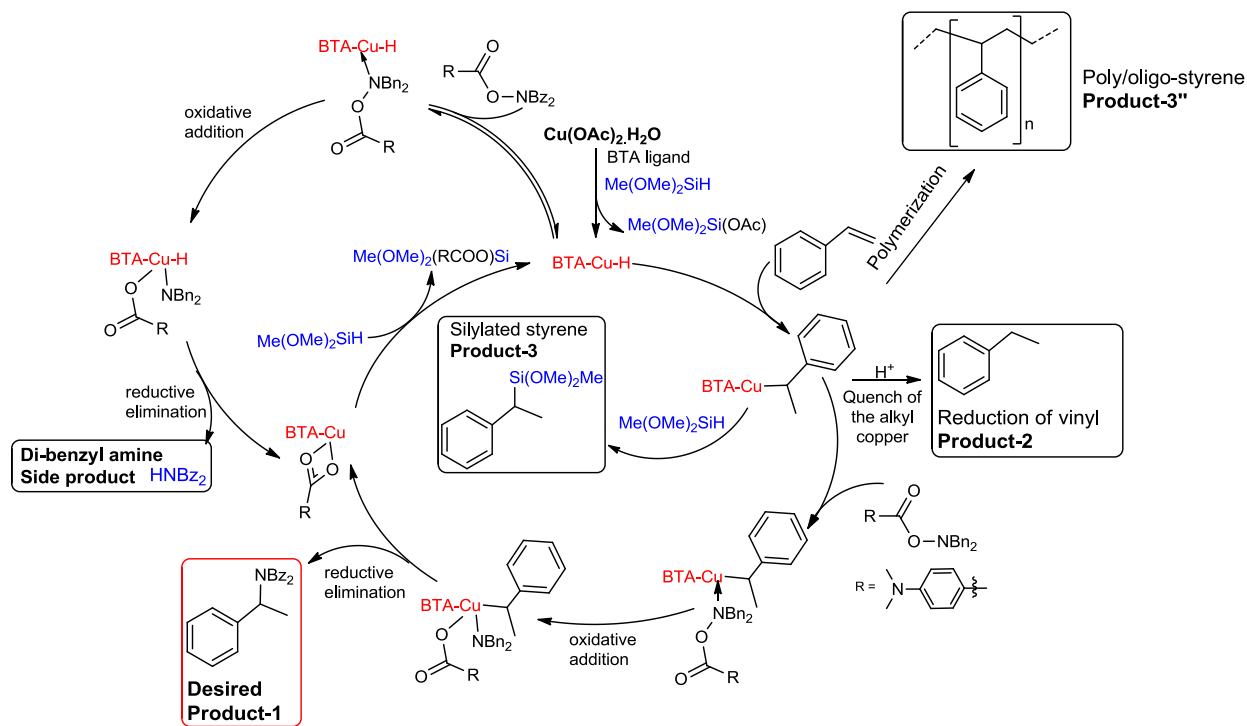
((dibenzylamino)oxy)carbonyl)-N,N-dimethylaniline) as amine electrophile. ^1H NMR spectroscopy in presence of an internal standard (1,3,5-trimethoxybenzene) in toluene- d_8 was used to track the consumption of styrene, amine electrophile, silane, and formation of products. HPLC was used to determine the enantiomeric excess (*ee*) of the formed chiral amine. For the reaction scheme, conditions and plots of reactant consumption and product formation, see Scheme III-10. For NMR spectra, see the Annex (subsection III.4.b.ii, Figure S.III-2, and S.III-3)



Scheme III-10 Reaction conditions : Styrene (0.15 mmol, 1 equiv.), Cu(OAc)₂.xH₂O (5 mol%), BTA-pPPh₂ (10 mol%), BTA (*R*)-Leu (10 mol%), DMMS (0.6 mmol, 4.0 eq), amine-DM (0.18 mmol, 1.2 equiv.), toluene-*d*₈ (600 μ L). Evolution was tracked by ^1H NMR in presence of IS: 1,3,5-trimethoxybenzene (0.15 mmol, 1 equiv.).

According to Scheme III-10, most of the styrene was consumed after 3 h (black line). The yield in the amine product ((*N,N*-dibenzyl-1-phenylethanamine) **product-1** increases from 32% after 15 minutes to its maximal value (46%) after 2 h (green line). The measured *ee* obtained for

product-1 is *ca.* 25% (determined for the reaction performed with DEMS as silane reagent, a similar value is expected with DMMS). Another product was formed throughout the process, which was identified as ethylbenzene **product-2** by ^1H NMR analysis. Maximum yield of **product-2** (14%) was reached after 2 h of stirring (red line, Scheme III-10). **Product-2** is likely formed by protonation of the electron-rich alkoxy copper intermediate, most probably by water molecules present as coordinative species of the Cu precursor or introduced unintentionally in toluene (Scheme III-11). The total yield of identified products (**product-1** + **product-2**) is of almost 60% after 2 h, which is lower than the total amount of styrene consumed over the same period (*ca.* 95%) (blue line, Scheme III-10). This indicates that styrene was converted to another unknown side product (**product-3**). It was also noticed that after 3 h of stirring all DMMS was totally consumed, despite being engaged in significant excess (4 equiv.). This explains why the plot in Scheme III-10 for **product-1** formation is not indicative of an overall zero-order process in substrate^[78]. Conversely, a proportion of amine-DM was found to be unreacted after 2 h. However, it was also noted that a part of amine-DM was decomposed into dibenzylamine most likely through the unwanted reduction of amine-DM by the copper hydride catalyst (Scheme III-11).



Scheme III-11 Proposed catalytic cycle that explains the formation of different products observed throughout the catalytic hydroamination process of styrene.

Two additional “control” experiments were performed to better understand these observations. The same catalytic experiment was conducted but in absence of the substrates (styrene and amine-DM). For NMR spectra, see the Annex (subsection **III.4.b.ii**, Figure S.III-4). It was found that DMMS was almost fully consumed after 2 h, most likely by a side reaction involving the copper hydride species. The second control experiment was made in presence of styrene but not amine-DM. Again, here a significant fraction of styrene was found to be consumed, with **product-2** being the main but not unique generated product (See Annex, subsection **III.4.b.ii**, Figure S.III-5 and S.III-6). This implies that **product-3** also forms which can be either an oligomer/polymer of styrene or the hydrosilylation product of styrene (Scheme III-11). The latter could be formed by metathesis reaction between the alkyl copper intermediate and the silane reagent as found by Buchwald and coworkers with **(S,S)-Ph-BPE** ligand^[99]. However, no trace of the characteristic methine signal at ≈ 5 ppm is found in the crude ^1H NMR spectra. This led us to postulate that **product-3** most likely corresponds to

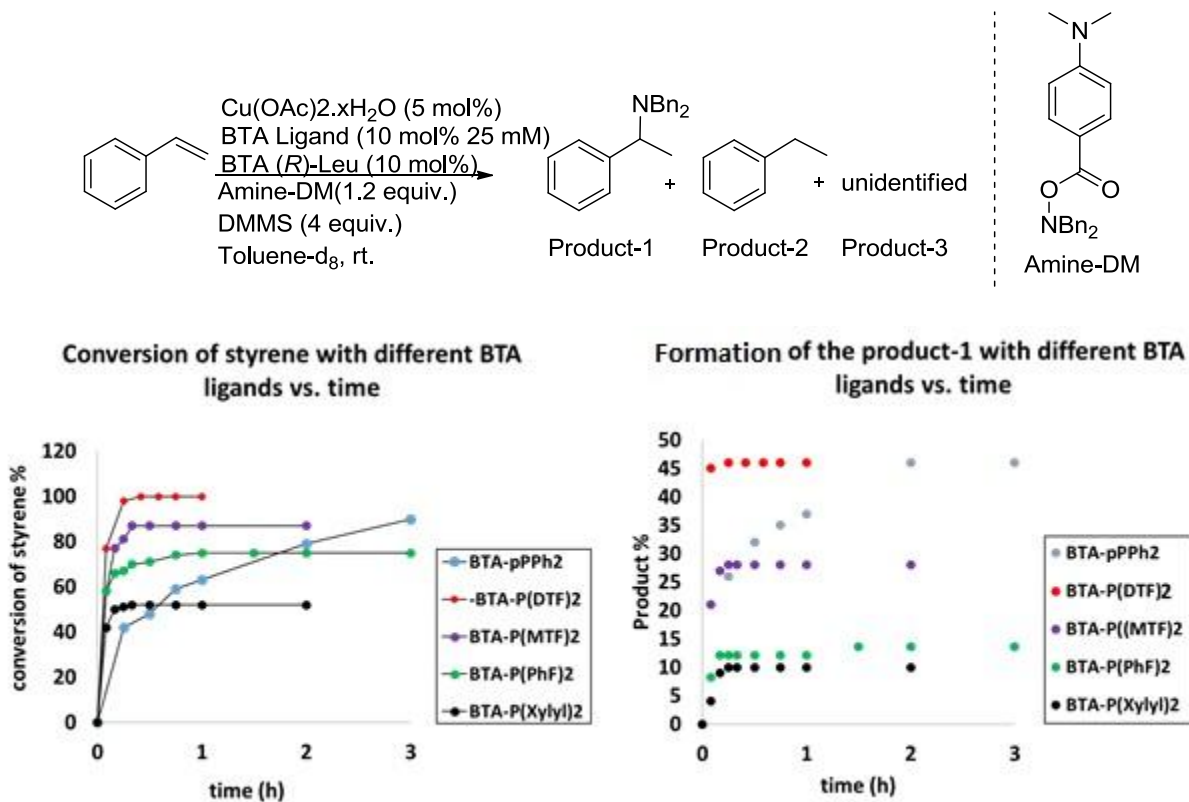
oligomer/polymer⁶ generated upon activation of styrene by the copper complex. It is unknown if this oligo/polymerization process is specific to our BTA helical catalyst or also occurs to some extent with conventional phosphine ligands.

Thus, as shown in Scheme III-10, the limited yield in **product-1** for the **BTA-P(Ph)₂/BTA Leu** system comes from a chemoselectivity issue. There are several competitive reactions, which preclude the vinyl moiety to react exclusively with the electrophile amine.

⁶ No signal that can be clearly attributed to these species has been detected in the crude NMR spectra.

III.2.c. Screening of different BTA ligands with $[\text{Cu}(\text{OAc})_2 \cdot x\text{H}_2\text{O}]$ as metal precursor in the HA of styrene.

Further investigations were performed in order to determine the effect of BTA ligand structure on the activity, chemoselectivity and enantioselectivity of the catalyst. For this purpose, the different BTA ligands, **BTA-pPPh₂**, **BTA-P(DTF)₂**, **BTA-P(Xylyl)₂**, **BTA-P(MTF)₂**, and **BTA-P(PhF)₂** were tested under the same reaction conditions. For the reaction scheme, conditions, and plots of reactant consumption and product formation, see Scheme III-12. For NMR spectra (See Annex, subsection **III.4.b.ii**, Figure S.III-7, S.III-8, S.III-9, and S.III-10).



Scheme III-12 Conditions: Styrene (0.15 mmol, 1 equiv.), $\text{Cu}(\text{OAc})_2 \cdot x\text{H}_2\text{O}$ (5 mol%), BTA ligand (10 mol%), BTA (*R*)-Leu (10 mol%), DMMS (0.6 mmol, 4.0 eq), amine-DM (0.18 mmol, 1.2 eq), toluene- d_8 (600 μL). Evolution was tracked by ^1H NMR in presence of IS: 1,3,5-trimethoxybenzene (0.15 mmol, 1 equiv.).

The plots in Scheme III-12 show that all the newly tested BTA ligands are as active as or more active than **BTA-pPPh₂**. The activity of three of the ligands, **BTA-P(Xylyl)₂**, **BTA-P(MTF)₂**, and **BTA-P(PhF)₂**, levels off before reaching full consumption of styrene. Upon closer observation of the crude ^1H NMR spectra, it is difficult to determine whether this erosion of the activity is

related to the consumption of DMMS or the deactivation of the catalyst^[100]. The comparison of the different BTA catalysts is better illustrated by data compiled in Table III-1.

Most notably, with the use of **BTA-P(DTF)2**, a 10-fold initial-rate enhancement was observed relatively to **BTA-pPPPh2** (entries 1, and 4, Table III-1). Employing other BTA ligands, such as **BTA-P(PhF)2**, and **BTA-P(MTF)2**, resulted in a slightly increased reaction rate relatively to **BTA-pPPPh2** (entries 2, and 3, Table III-1), whereas the use of **BTA-P(Xylyl)2** lowered the rate (entry 5, Table III-1). In overall, the best-performing ligand is **BTA-P(DTF)2**. It largely outperforms all ligands when considering all the criteria: in reaction rate, chemoselectivity, and enantioselectivity (entry 4, Table III-1). The consumption in styrene is related to the electronic nature of the BTA ligands: the more electron-poor being the more active.

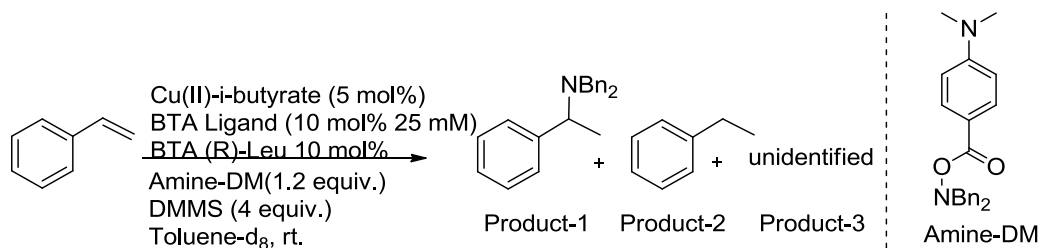
Entry	Ligand	Time	Conv. (%)	Yield P-1 (%)	Chemo-selectivity ^[a]	Rate (M/min)	Relative rate ^[b]	ee ^[c] (%)
1	BTA-pPPPh2	2h	79	46	0.58	$2,32 \times 10^{-3}$	1	25
2	BTA-P(PhF)2	1h30	75	14	0.19	$3,25 \times 10^{-3}$	1.4	10
3	BTA-P(MTF)2	15 mins	87	28	0.32	$7,5 \times 10^{-3}$	3.2	3
4	BTA-P(DTF)2	15 mins	100	46	0.46	$22,5 \times 10^{-3}$	9.7	69
5	BTA-P(Xylyl)2	15 mins	52	10	0.19	$1,85 \times 10^{-3}$	0.8	51

Table III-1 Comparison of reactivity, chemoselectivity, and enantioselectivity between systems. Yield of product-2 ranges between 8%-13% for all entries. [a] Chemoselectivity= yield of product-1/conversion of styrene, [b] Relative rate=(rate of BTA ligand/rate_{BTA-pPPPh2}). [c] % ee determined by chiral HPLC analysis.

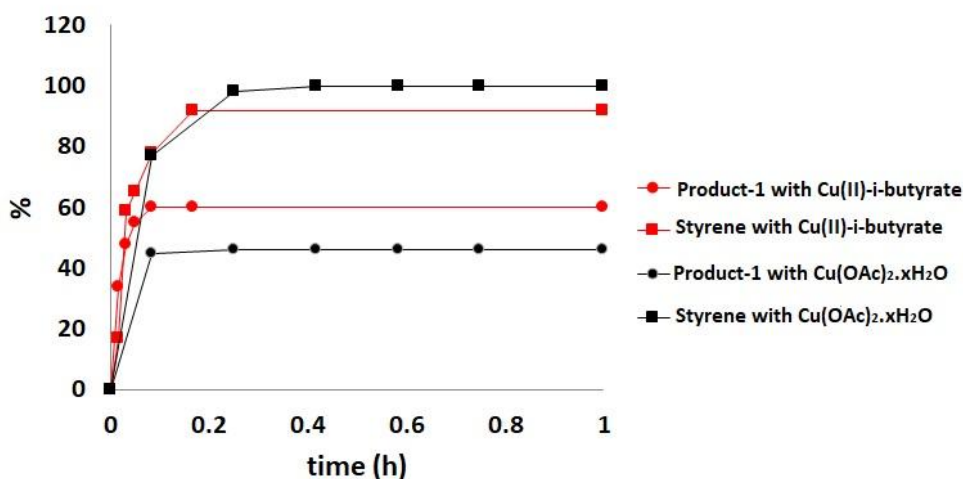
The importance of the nature of the ligand on the chemoselectivity of the reaction is more difficult to establish since both electron-rich and electron-poor ligands such as **BTA-P(PhF)2** and **BTA-P(Xylyl)2**, respectively, exhibit poor chemoselectivity (entries 2, and 5, Table III-1). However, our study unambiguously reveals the crucial importance of the position of the substituents on the aryl groups of the BTA ligand on the enantioselectivity of the hydroamination reaction. The enantioselectivity increases in the following order: BTA ligand with *meta*-substituents > non-substituted BTA > BTA with *para*-substituent. The positive influence of the substituents at the *meta* position of the PAr₂ group is assumed to come from favorable through space ligand-substrate interactions, *i.e.* dispersion^[90,101]. Clearly, the BTA ligand structure has a huge effect on the efficiency of the catalytic system.

III.2.d. Optimization for BTA-P(DTF)2 ligand: Cu(OAc)₂·H₂O versus Cu(II)-i-butyrate as a metal precursor.

Further investigations were performed in order to determine the effect of the copper precursor on the performance of the best performing ligand. For this purpose, Cu(II)-i-butyrate was selected to be tested with the BTA-P(DTF)2/BTA Leu mixture. For the reaction scheme and conditions, and plots of reactant consumption and product formation, see Scheme III-13. For catalytic results see Table III-2. For NMR spectra (See Annex, subsection III.4.b.ii, Figure S.III-11).



Conversion of styrene and the formation of product-1 vs time



Scheme III-13 Conditions: Styrene (0.15 mmol, 1 equiv.), Cu(II)-i-butyrate (5 mol%), BTA ligand (10 mol%), BTA (*R*)-Leu (10 mol%), DMMS (0.6 mmol, 4.0 eq), amine-DM (0.18 mmol, 1.2 eq), toluene-d₈ (600 μ L). Evolution was tracked by ¹H NMR in presence of IS: 1,3,5-trimethoxybenzene (0.15 mmol, 1 equiv.).

We were pleased to see that changing the copper source from Cu(OAc)₂·xH₂O to Cu(II)-i-butyrate increases the chemoselectivity of the reaction without altering the rate of conversion of styrene and the enantioselectivity. In addition, the overall rate with Cu(II)-i-butyrate is

increased 2-fold relative to $\text{Cu}(\text{OAc})_2 \cdot x\text{H}_2\text{O}$. It is assumed that in presence of $\text{Cu}(\text{II})$ -i-butyrate, the oligo/polymerization of styrene is reduced at the expense of the formation of the amine **product-1**. Reasonable yield (65%) and enantioselectivity (67%) were reached under these conditions (Table III-2).

Cu source	Time	Conv. (%)	Yield P-1(%)	Chemo-selectivity ^[a]	Rate M/min	Relative rate ^[b] M/min	ee(%) ^[c]
$\text{Cu}(\text{OAc})_2 \cdot x\text{H}_2\text{O}$	15 mins	100	46	0.46	$22,5 \times 10^{-3}$	1	65
$\text{Cu}(\text{II})$ -i-butyrate	15 mins	92%	60%	0.60	$52,67 \times 10^{-3}$	2.34	67

Table III-2 Comparison of reactivity, chemoselectivity, and enantioselectivity between both systems [a] Chemoselectivity= Yield product-1/conversion of styrene, [b] Relative rate (rate/rate _{$\text{Cu}(\text{II})$ -i-butyrate}). [c]. % ee determined by HPLC analysis.

III.3. Hydrosilylation/hydroamination cascade process on “enone” substrates.

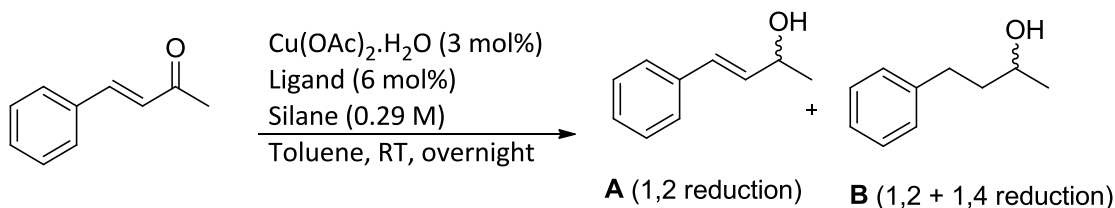
III.3.a. Hydrosilylation of benzylideneacetone, and cascade of (*E*)-3-methyl-4-phenylbut-3-en-2-one.

α,β enones have been selected by Buchwald for the synthesis of amino alcohols via a cascade copper-catalyzed hydrosilylation/hydroamination^[102]. Buchwald was able to obtain the analogous amino alcohols from a variety of different α,β enones in yields ranging from 60% to 80%. It was thus appealing to test these substrates with the BTA helical catalysts. Some of these experiments were performed before establishing that **BTA-P(DTF)2/BTA Leu** mixture as the best performing mixture for HA of styrene, and thus other ligand/**BTA Leu** mixtures were employed.

We first evaluated the BTA helical catalyst in the hydrosilylation (HS) of benzylidenacetone. For this purpose, different conditions have been probed: 1) the nature of the ligand, 2) the temperature, and 3) the nature of the silane reagent used. For reaction scheme, and catalytic results, see Table III-3. For selected ¹H NMR data (see Annex, subsection **III.4.b.iii**, Figure S.III-12).

We first tested the fate of the reaction with commercial ligand, **DTBM-(R)-SEGPHOS**. At room temperature, the yield of the desired allyl alcohol **A** was low (18%), relatively to the fully reduced **B** (55%) (entry 1, Table III-3). For the purpose of disfavoring the undesired 1,4

reduction pathway, the reaction was carried out at lower temperature (-60°C), *i.e.* the temperature used by Buchwald and co-workers^[102] for the HS step of the cascade reaction. At lower temperature, the yield of the desired allyl alcohol **A** was increased to 52%, and that of the fully reduced compound **B** decreased to 35% (entry 2, Table III-3). Clearly, with **DTBM-(R)-SEGPPOS**, reaction temperature has a huge influence on the reaction outcome by partially suppressing the unwanted reduction of the vinyl function.



Entry	Ligand	Temperature °C	Silane	Conversion %	Yield ^[a] of A	Yield ^[a] of B
1	DTBM-(R)-SEGPPOS ^[b]	RT	PhSiH ₃	73%	18%	55%
2	DTBM-(R)-SEGPPOS ^[b]	-60 °C	PhSiH ₃	87%	52%	35%
3	BTA-pPPh2	RT	PhSiH ₃	96%	22%	70%
4	BTA-pPPh2	-60 °C	PhSiH ₃	100%	24%	70%
5	BTA-pPPh2	-60 °C	DEMS	90%	5%	31%
6	BTA-P(Xylyl)2	-60 °C	DEMS	94%	20%	18%
7	BTA-P(Xylyl)2	-60 °C	PhSiH ₃	100%	30%	70%

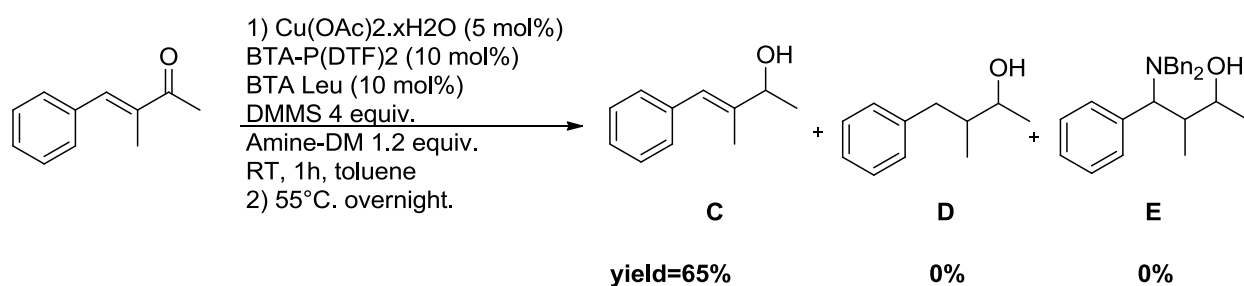
Table III-3 Conditions: benzylidenacetone (0.17 mmole, 1.0 eq), Cu(OAc)₂·xH₂O (3 mol%), **ligand** (6 mol%), silane (2.0 eq), toluene (300 μL). [a] Yield estimated by ¹H NMR according to an internal standard (DMA), [b] THF is used as a solvent.

This result is somewhat in agreement with the literature for which a yield of 76% was reported after the cascade reaction (the difference might come from the different silane source). With **BTA-pPPh2**, the desired allylic alcohol **A** was obtained in 22% yield at room temperature, concomitantly with a huge amount of fully reduced **B** (70%) (entry 3, Table III-3). Lowering the temperature has no positive influence on the chemoselectivity of the reaction (entries 4, Table III-3). The effect of the silane reagent was also evaluated and it was found that the yield in allylic alcohol **A** dropped to 5% with DEMS instead of PhSiH₃ (entry 5, Table III-3). Since both DEMS and PhSiH₃ show high consumption of benzylidenacetone, this result indicates that the reaction with DEMS generated more by-products. The effect of BTA ligand was also evaluated by replacing **BTA-pPPh2** with **BTA-P(Xylyl)2**, in presence of two different silanes (DEMS, and

PhSiH₃) at -60°C (entries 6, and 7, Table III-3). The yield in allylic alcohol **A** was increased to 30% when **BTA-P(Xylyl)2** and PhSiH₃ were used, but again the fully reduced **B** was the major product (70%).

The propensity of the BTA helical catalysts to reduce both functions is a severe limitation towards engaging this substrate into the second hydroamination step. Accordingly, the cascade reaction was not attempted on that substrate. However, further investigations will be carried out notably by testing the influence of **BTA-P(DTF)2/BTA Leu** mixture and the amount of silane on the fate of this catalytic reaction.

It was shown above (subsection **III.1.b**, Scheme III-6) that methyl substituents on α position of the keto group could prevent the 1,4-reduction pathway. For this purpose, (*E*)-3-methyl-4-phenylbut-3-en-2-one was selected to be probed in the cascade process using a catalytic system composed of Cu(OAc)₂.xH₂O/**BTA-P(DTF)2/BTA Leu** in presence of DMMS as silane reagent, and amine-DM as amine electrophile. The reaction was carried out at RT for 1h, then temperature was elevated to 55°C for overnight. For reaction scheme and catalytic results see Scheme III-14.



Scheme III-14 Conditions: (*E*)-3-methyl-4-phenylbut-3-en-2-one (0.25 mmole, 1.0 eq), Cu(OAc)₂.xH₂O (5 mol%), **BTA-P(DTF)2** (10 mol%), BTA (*R*)-Leu (10 mol%), DMMS (4.0 eq), amine-DM (1.2 equiv.), toluene (800 μ L). Yield estimated by ¹H NMR according to an internal standard: 1,3,5-trimethoxybenzene.

The allyl alcohol **C** was detected in 65% yield, while no traces of the fully reduced **D** were detected under these conditions. Although the 1,4 reduction appears to be completely suppressed by α -methylation, no traces of the amino alcohol **E** were detected by ¹H NMR analysis. Further investigations will be carried out for probing different copper sources,

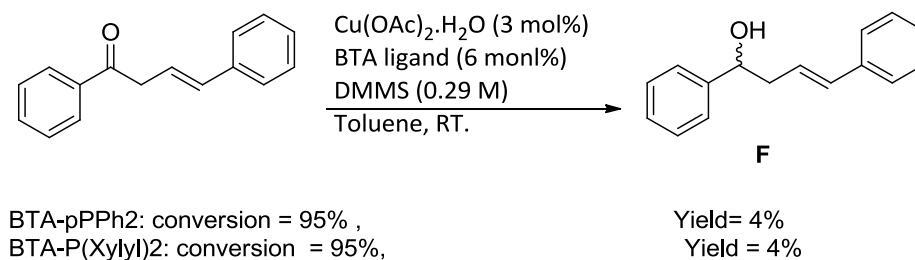
solvents, and HA reaction temperature for the cascade on (*E*)-3-methyl-4-phenylbut-3-en-2-one.

III.3.b. Evaluation of hydrosilylation and cascade reaction on (*E*)-1,4-diphenylbut-3-en-1-one and derivatives.

To suppress the undesired reduction of the vinyl function, we envisaged to add a carbon atom between both functionalities to break down the conjugation. For this purpose, α,γ -enone substrates were selected.

Two different BTA ligands (**BTA-pPPh2** and **BTA-P(Xylyl)2**) were selected for evaluating the hydrosilylation reaction on (*E*)-1,4-diphenylbut-3-en-1-one at RT in presence of DMMS as silane reagent. For reaction conditions and catalytic results see Scheme III-15. For selected ^1H NMR data (see Annex, subsection **III.4.b.iii**, Figure S.III-13)

The conversions were high but yields in the desired α,γ -alcohol **F** were very low, *ca.* 4%, in both cases. This low yield could be attributed to unidentified side reactions, since no peaks for the fully reduced were detected.

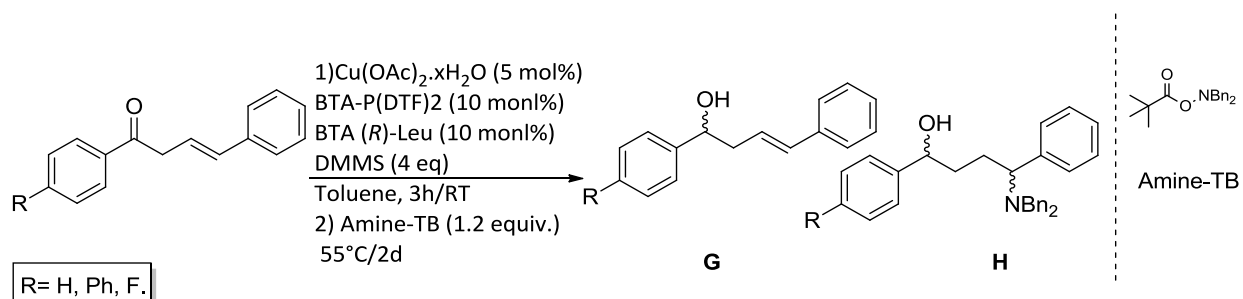


Scheme III-15 Conditions: (*E*)-1,4-diphenylbut-3-en-1-one (0.17 mmole, 1eq), $\text{Cu(OAc)}_2\cdot\text{H}_2\text{O}$ (3 mol%), BTA **ligand** (6 mol%), DMMS (2.0 eq), toluene (590 μL). Yields were estimated by ^1H NMR according to an IS (DMA).

A combination of **BTA-P(DTF)2** and **BTA (R)-Leu** was evaluated in the cascade hydrosilylation/hydroamination reaction of unaltered and substituted α,γ -enone substrates. The latter compounds contain a fluorine atom or a phenyl moiety at the *para* position of the benzyl ring. The hydrosilylation step was carried out at room temperature for 3 hours, followed by hydroamination which was expected to take place after the addition of amine-TB at elevated temperature (55° C) for 2 days. The reaction outcome was analyzed by ^1H NMR analysis. For

reaction scheme catalytic results see Table III-4. For selected ^1H NMR data (see Annex, subsection III.4.b.iii, Figure S.III-14)

Only the α,γ -alcohol **G** was detected in the crude ^1H NMR mixture. The reason why the hydroamination did not occur for this substrate is unclear. It can be due to the inherent reactivity of the double bond (β -methyl substituted styrenes are expected to be less reactive than non-substituted styrene), but additional control experiments are required notably to control whether the silane was consumed totally or not during the HS step.



Entry	Substrate	Conversion (%)	Alcohol - G	Amino alcohol- H
1	R = H	100%	detected	Not detected
2	R = F	100%	detected	Not detected
3	R = Ph	100%	detected	Not detected

Table III-4 Conditions: substrate (0.25 mmole, 1eq), $\text{Cu}(\text{OAc})_2 \cdot x\text{H}_2\text{O}$ (5 mol%), BTA-P(DTF) $_2$ (10 mol%), BTA (R)-Leu (10 mol%), DMMS (2.0 eq), amine-TB (1.3 eq), toluene (800 μL).

III.4. Conclusion.

Mixtures between an intrinsically achiral BTA ligand and an enantiopure ester BTA co-monomer provided good selectivity in the copper-catalyzed hydroamination of styrene. The following optimized conditions allowed to reach 67% *ee*, and 60% yield of the obtained amine **product-1** when the reaction is conducted at room temperature in toluene: $\text{Cu}(\text{II})$ -i-butyrate as the copper source, **BTA-P(DTF) $_2$** as the ligand, **BTA Leu** as the co-monomer, DMMS as the silane source, and amine-DM as an amine transfer reagent. In addition, high catalytic activity was recorded, and styrene was almost fully consumed throughout the process. The moderate yield obtained for the amine **product-1** could be attributed to the two following main factors: **1)** Undesired conversion of styrene into ethylbenzene via the reduction of the vinyl moiety in presence of

protic species ,and **2**) Oligo or polymerization of styrene throughout the process. Rapid consumption of the silane during the process was also observed which justifies using a significant excess of this reagent. Further investigations will be carried out in order to optimize reaction conditions and improve the yield of the reaction.

On the other hand, different “enone” substrates were screened for hydrosilylation or cascade reaction with BTA helical catalyst. With the α,β -enones, the main issue encountered was related to the regioselectivity of the catalyst, and 1,4 reduction was the preferred mode of reduction. Further investigations will be carried for probing **BTA-P(DTF)2** ligand in hydrosilylation of α,β enones. Considering α,γ -enones: poor yields in the desired alcohol were found. It was impossible to proceed further with this kind of substrate due to the low yield obtained. Additional control experiments are required notably to figure out the reasons behind the observed low yields.

III.5. Annex.

Materials preparation and methods.

1-(4-fluorophenyl)ethenone, benzaldehyde, acetophenone, 1-([1,1'-biphenyl]-4-yl)ethenone, phenyl acetylene, (*E*)-3-methyl-4-phenylbut-3-en-2-one, *t*BuOK, DEMS, DMMS, PhSiH₃, [Cu(OAc)₂·H₂O], and Cu(II)*i*-butyrate were purchased from Alfa Aesar and Sigma Aldrich and used as received. 4-(((dibenzylamino)oxy)carbonyl)-*N,N*-dimethylaniline, *N,N*-dibenzyl-*O*-pivaloylhydroxylamine were synthesized according to the reported procedures^[78,88], and the obtained characterization data were in agreement with the reported ones. **BTA (S)-Leu** and **BTA (R)-Leu** co-monomers used in this study have been purified by preparative HPLC. Dried solvents were obtained from an SPS solvent purification system (IT-Inc). NMR spectra were recorder on a Bruker Advance 400, or 300 spectrometer and calibrated to the residual solvent peak: CDCl₃ (¹H: 7.26 ppm; ¹³C: 77.16 ppm). Peaks are reported with their corresponding multiplicity (s: singlet; br s: broad singlet, d: doublet, t: triplet; q: quartet) and integration, and respective *J* coupling constants are given in Hertz. Unless otherwise noted, chromatography-grade solvents were used as received. All inert atmosphere reactions were carried out under an argon atmosphere with standard Schlenk-line techniques.

HPLC analyses: **N,N-dibenzyl-1-phenylethanamine (Product-1)**. The optical purity was determined by HPLC analysis: OD-H column, flow rate: 0.6mL/min, 98:2 hexane/iso-propanol, $\lambda=230$ nm, retention time for 1st enantiomer = 6.72 min, retention time for 2nd enantiomer = 8.08 min.

Fourier-Transform Infrared (FT-IR) analyses: FT-IR measurements were performed on a Nicolet iS10 spectrometer. Solution spectra were measured in CaF₂ cells by adjusting the pathlength (0.5 mm) to the concentration and were corrected for air, solvent and cell absorption.

III.5.a. General experimental procedure for catalysis.

Hydroamination of styrene in toluene-d₈ (Scheme III-10, III-12, and III-13).

An oven-dried test tube was loaded with Copper metal source (5 mol%, 7.5 μ mol) and BTA ligand (10 mol%, 0.015 mmol) in dry THF (500 μ L). The solvent was removed by rotatory evaporation and the test tube was put under vacuum (1.10^{-3} mbar) for 1h. Then Styrene (0.15 mmole, 17 μ L, 1 equiv.) was added before flushing the tube with argon for 10 seconds. **BTA leu** (0.015 mmol, 16mg), and internal standard: 1,3,5-trimethoxybenzene (0.15 mmol, 25mg, 1 equiv.) were added as solids. Deuterated toluene-d₈ (*ca.* for volume of 570 μ L) is added and the mixture was stirred for 15 mins at room temperature. The reaction was started by the addition of DMMS (0.6 mmol, 63.72 mg). Conversion of substrate and product yield were monitored by ¹H NMR by taking aliquots after each time interval. When reaction was completed, HCl (10%, 400 μ L) was added and the mixture was stirred 30 min (until the solution becomes translucent). Then, the products were extracted with Et₂O (3x1 mL). The solvent was removed by rotatory evaporation and the residue was taken up in DCM and passed through a silica plug eluting with DCM. The solvents were evaporated and the resulting product was analyzed by ¹H NMR and HPLC.

Hydrosilylation of benzylidenacetone, (Table III-3).

An oven-dried test tube was loaded with Cu(OAc)₂.xH₂O (3 mol%, 1 mg.) and BTA ligand (6 mol%) in dry THF (500 μ L). The solvent was removed by rotatory evaporation and the test tube was put under vacuum (1.10^{-3} mbar) for 1h. Then benzylidenacetone (0.17 mmole, 24 mg, 1 equiv.) in 300 μ L toluene was added before flushing the tube with argon for 10 seconds. The

reaction was started by the addition of DMMS (0.34 mmol, 63 mg, 2 equiv.). The mixture was stirred for overnight at room temperature. When reaction was completed, HCl (10%, 400 μ L) was added and the mixture was stirred 30 min (until the solution becomes translucent). Then, the products were extracted with Et₂O (3x1 mL). The solvent was removed by rotatory evaporation. Conversion of substrate and yield of product were estimated by ¹H NMR analysis of the crude mixture according to an internal standard (DMA).

Cascade reaction of α,β - and α,γ -enones (Scheme III-14, and Table III-4) .

An oven-dried test tube was loaded with Copper metal source (5 mol%) and **BTA-P(DTF)2** ligand (10 mol%, 24 mg) in dry THF (500 μ L). The solvent was removed by rotatory evaporation and the test tube was put under vacuum (1.10^{-3} mbar) for 1 hour. **BTA leu** (10 mol%, 26 mg), and internal standard (trimethoxy benzene) were added as solids. The substrate (0.25 mmol) was added in dry toluene (0.8 mL). The reaction was left to stir, and gently heated by a heat gun until few bubbles are seen. The reaction mixture was kept to cool down to RT. The reaction was started by addition of DMMS (2.0 equiv. for α,β -enones, and 4.0 equiv. for α,γ -enones) via micro pipette under argon. The resulting mixture was stirred at room temperature (RT) for the desired time until the color changed from blue to dark yellow, and it was kept for stirring at RT for almost 1h. Then amine electrophile was added (0.33 mmol, 1.3 eq) and kept stirring at 55°C for 2 days. A saturated solution of NH₄F in MeOH (3 mL) was added and the mixture was stirred at RT for 10 mins, followed by addition of a saturated aqueous solution of Na₂CO₃ (3 mL) and ethyl acetate (3 mL). The phases were separated and the aqueous layer was extracted with ethyl acetate (2 x 3 mL). The solvent was evaporated under rotary evaporation and reduced under vacuum. Conversion of substrate and yield of product were estimated by ¹H NMR analysis of the crude mixture according to an internal standard (DMA).

III.5.b. Supplementary figures.

III.5.b.i. FT-IR analysis.

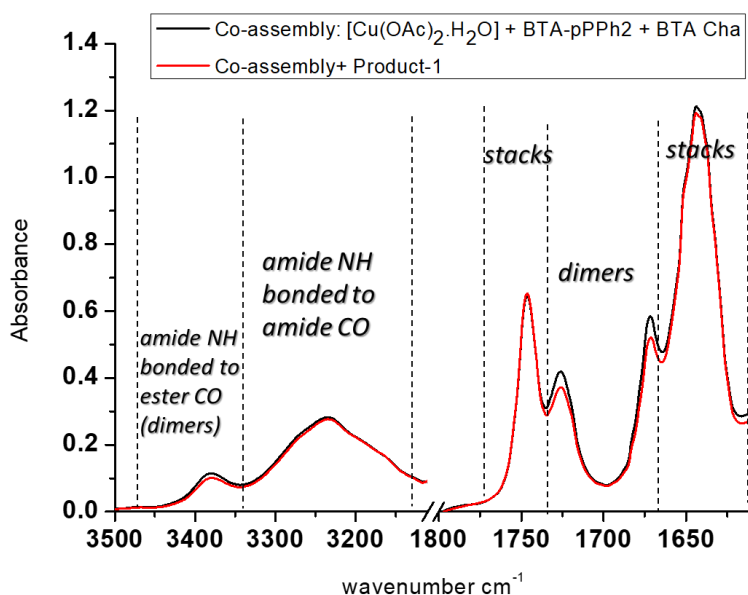


Figure S.III-1 FT-IR analyses of the co-assembly composed of **BTA-P(Ph)₂** (52.7 mM) coordinated to [CuOAc.H₂O] (26.35 mM) and **BTA (S)-Cha** (54.3 mM) in toluene at room temperature. Black line: before addition of N,N-dibenzyl-1-phenylethanamine **product-1**. Red: after addition of 1eq of **product-1**.

Interpretation: The same FT-IR spectra is obtained after addition of **product-1** into the co-assembly. Thus, N,N-dibenzyl-1-phenylethanamine (**product-1**) is not a hydrogen bond competitor, and its formation during the catalytic process does not affect the co-assembly.

III.5.b.ii. ^1H NMR analysis of the kinetic study of styrene Hydroamination in toluene- d_8 .

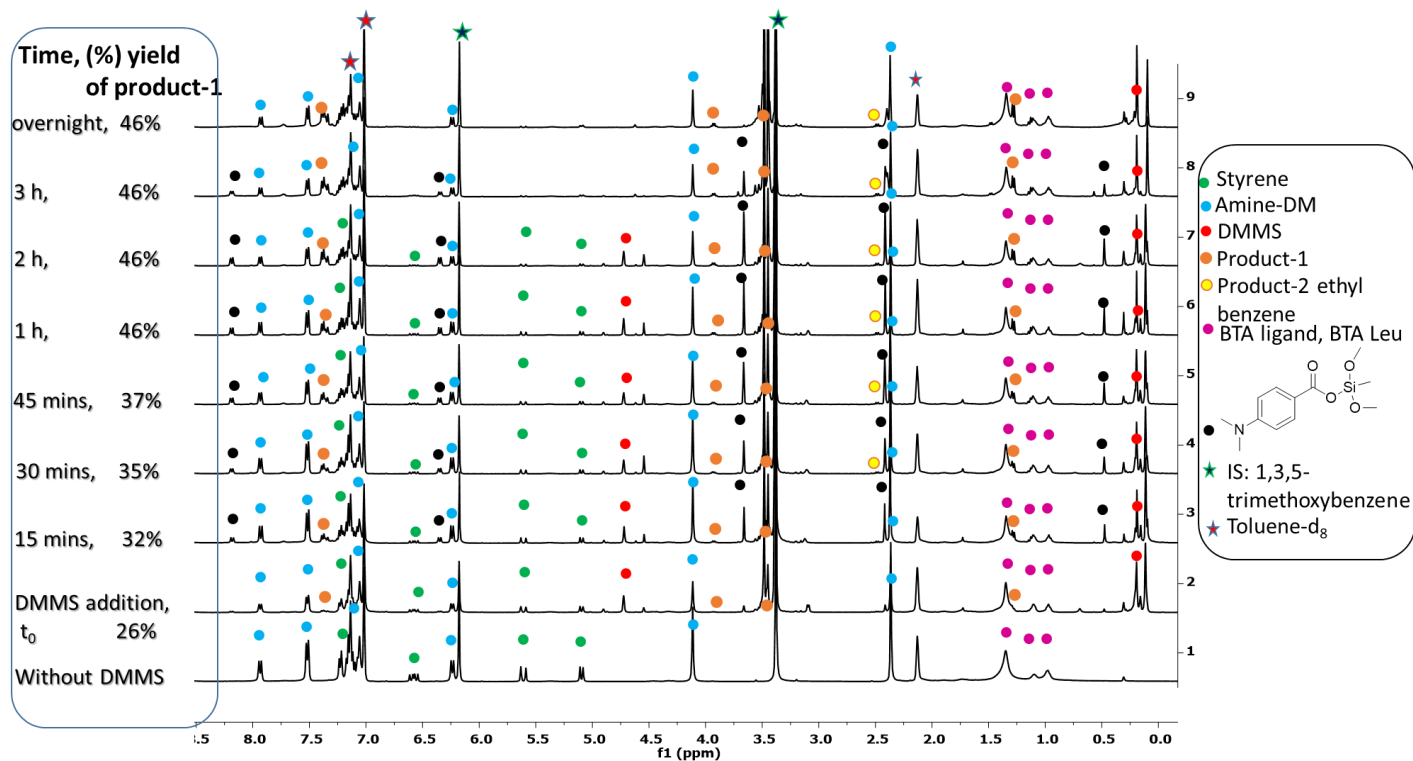


Figure S.III-2 Reaction conditions: Styrene (0.15 mmol), $\text{Cu}(\text{OAc})_2 \cdot x\text{H}_2\text{O}$ (5 mol%), **BTA-pPPH2** (10 mol%), BTA (*R*)-Leu (10 mol%), DMMS (4.0 eq), amine-DM (1.2 eq), toluene- d_8 (600 μL). Evolution was tracked by ^1H NMR in presence of IS: 1,3,5-trimethoxybenzene. **Study of Scheme III-10.**

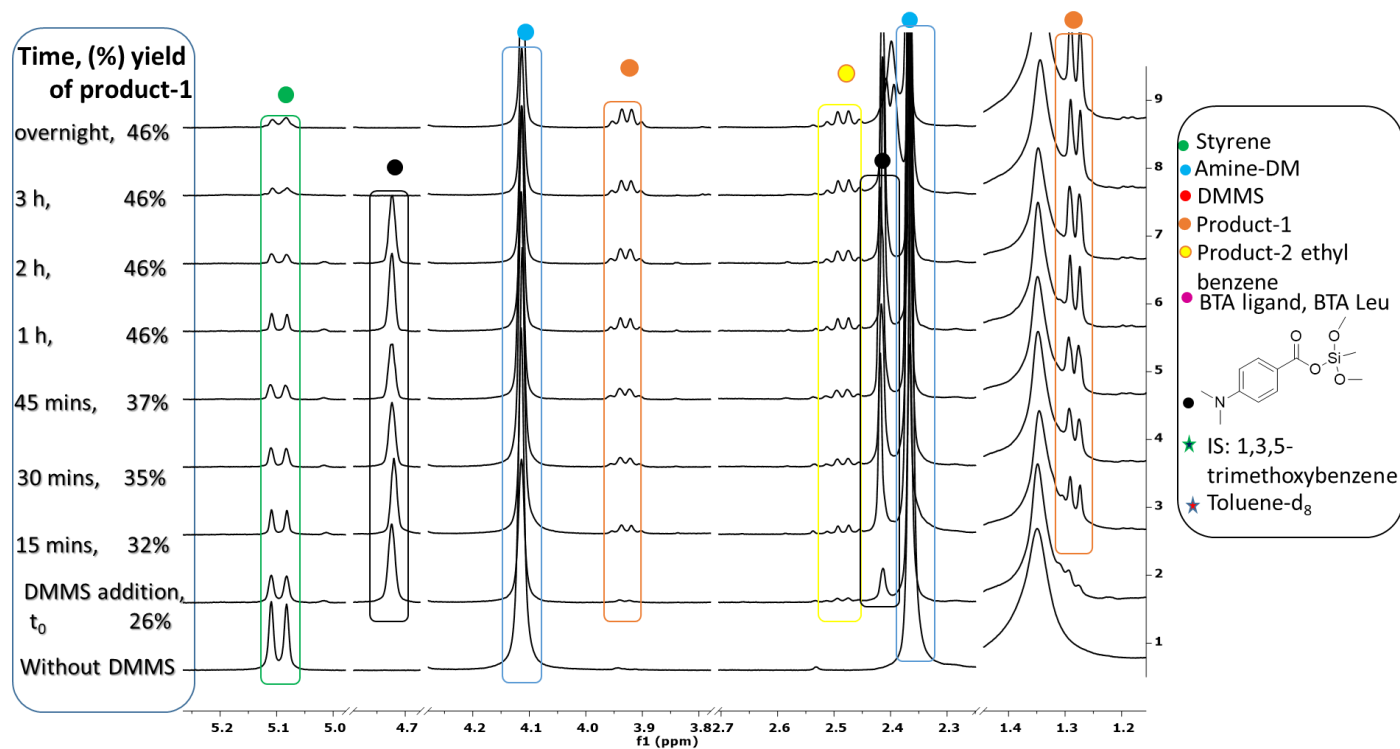


Figure S.III-3 Reaction conditions: Styrene (0.15 mmol), $\text{Cu}(\text{OAc})_2 \cdot x\text{H}_2\text{O}$ (5 mol%), **BTA-pPPH2** (10 mol%), BTA (*R*)-Leu (10 mol%), DMMS (4.0 eq), amine-DM (1.2 eq), toluene- d_8 (600 μL). Evolution was tracked by ^1H NMR in presence of IS: 1,3,5-trimethoxybenzene. [Study of Scheme III-10 \(Zoom in between 1.2-5.2 ppm\)](#).

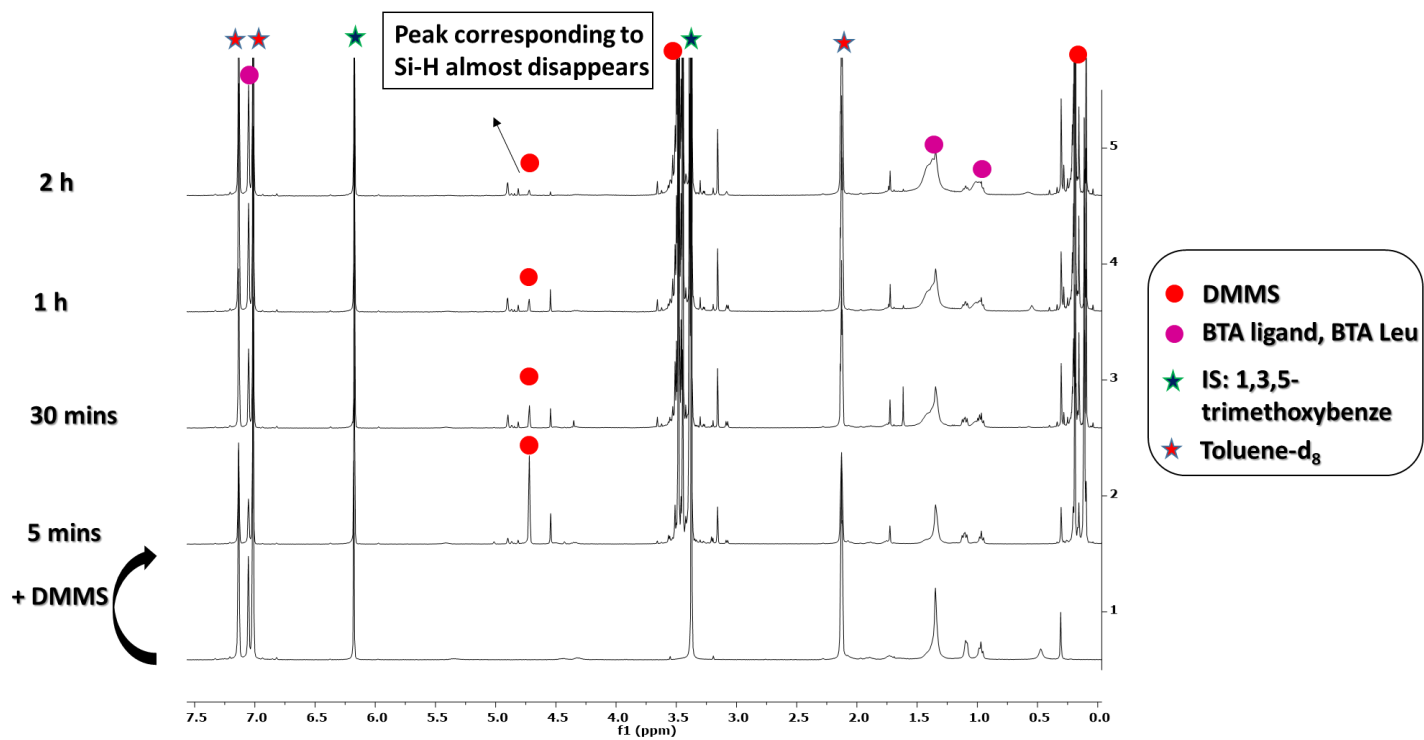


Figure S.III-4 Reaction conditions: $\text{Cu}(\text{OAc})_2 \cdot x\text{H}_2\text{O}$ (5 mol%), **BTA-pPPh2** (10 mol%), BTA (*R*)-Leu (10 mol%), DMMS (4.0 eq), toluene-d₈ (600 μL). Evolution was tracked by ¹H NMR in presence of IS: 1,3,5-trimethoxybenzene. [Study of Scheme III-10 \(control experiment 1\)](#).

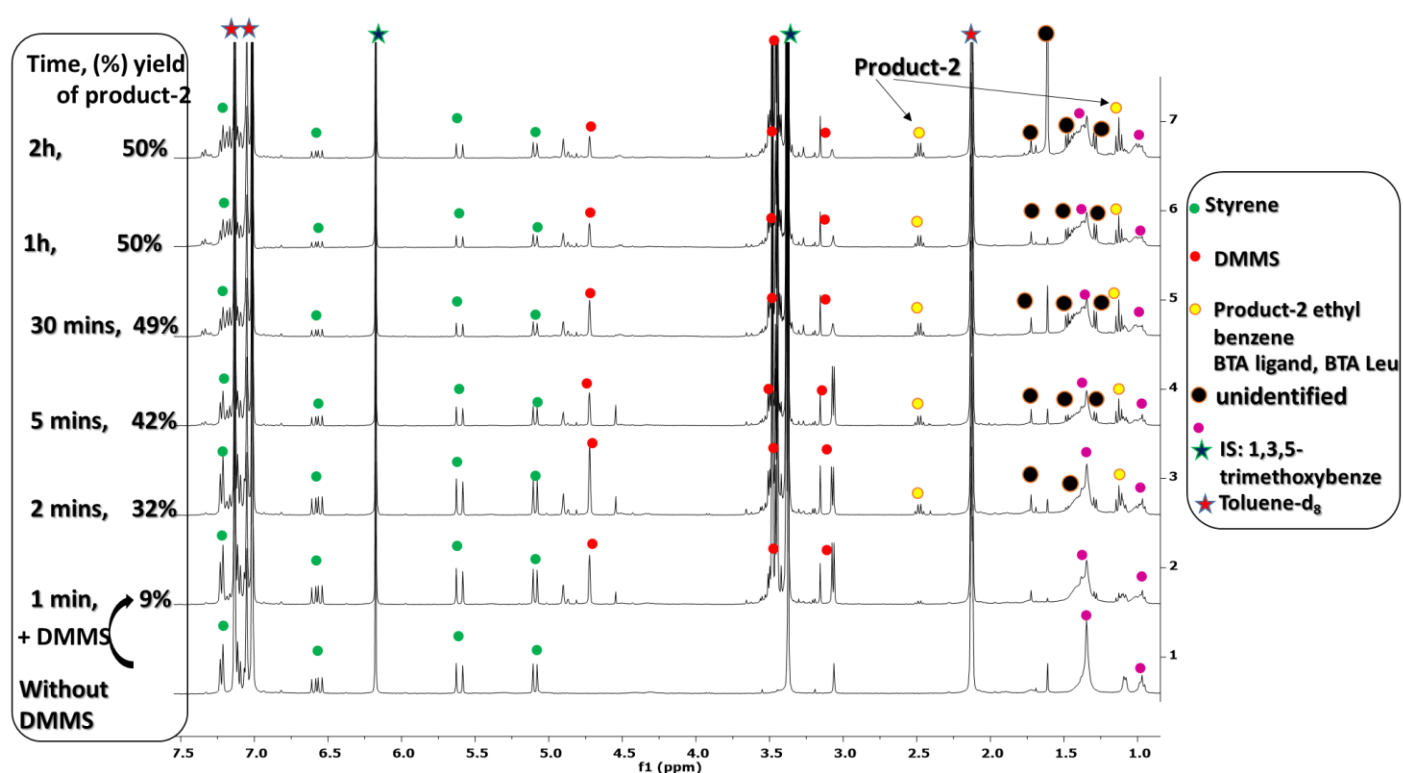


Figure S.III-5 Reaction conditions: Styrene (0.15 mmol), $\text{Cu}(\text{OAc})_2 \cdot x\text{H}_2\text{O}$ (5 mol%), **BTA-pPPH2** (10 mol%), BTA (*R*)-Leu (10 mol%), DMMS (4.0 eq), toluene- d_8 (600 μL). Evolution was tracked by ^1H NMR in presence of IS: 1,3,5-trimethoxybenzene. [Study of Scheme III-10 \(control experiment 2\)](#).

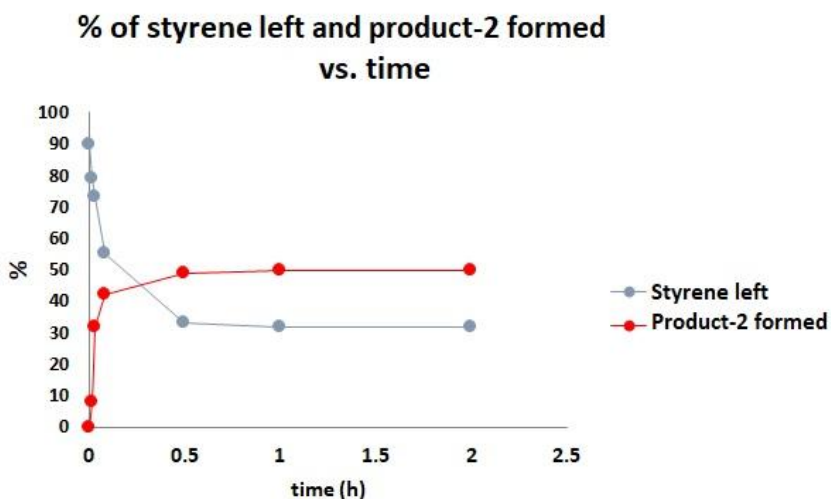


Figure S.III-6 Variation of styrene left and product-2 formed as function of time. [Study of Scheme III-10 \(control experiment 2\)](#).

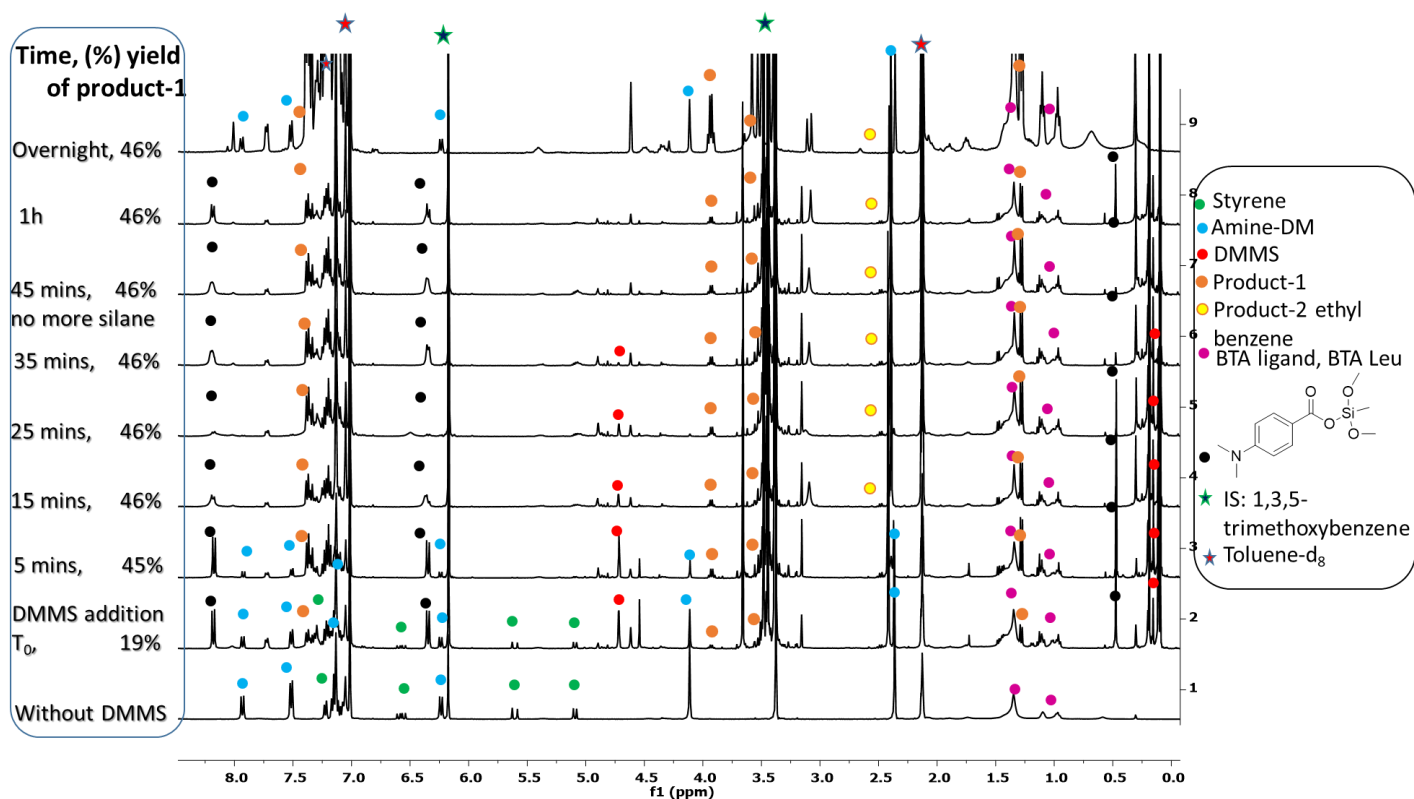


Figure S.III-7 Reaction conditions: Styrene (0.15 mmol), Cu(OAc)₂·H₂O (5 mol%), **BTA-P(DTF)2** (10 mol%), BTA (*R*)-Leu (10 mol%), DMMS (4.0 equiv.), amine-DM (1.2 equiv.), toluene-d₈ (600 μL). Evolution was tracked by ¹H NMR in presence of IS: 1,3,5-trimethoxybenzene. [Study of Scheme III-12.](#)

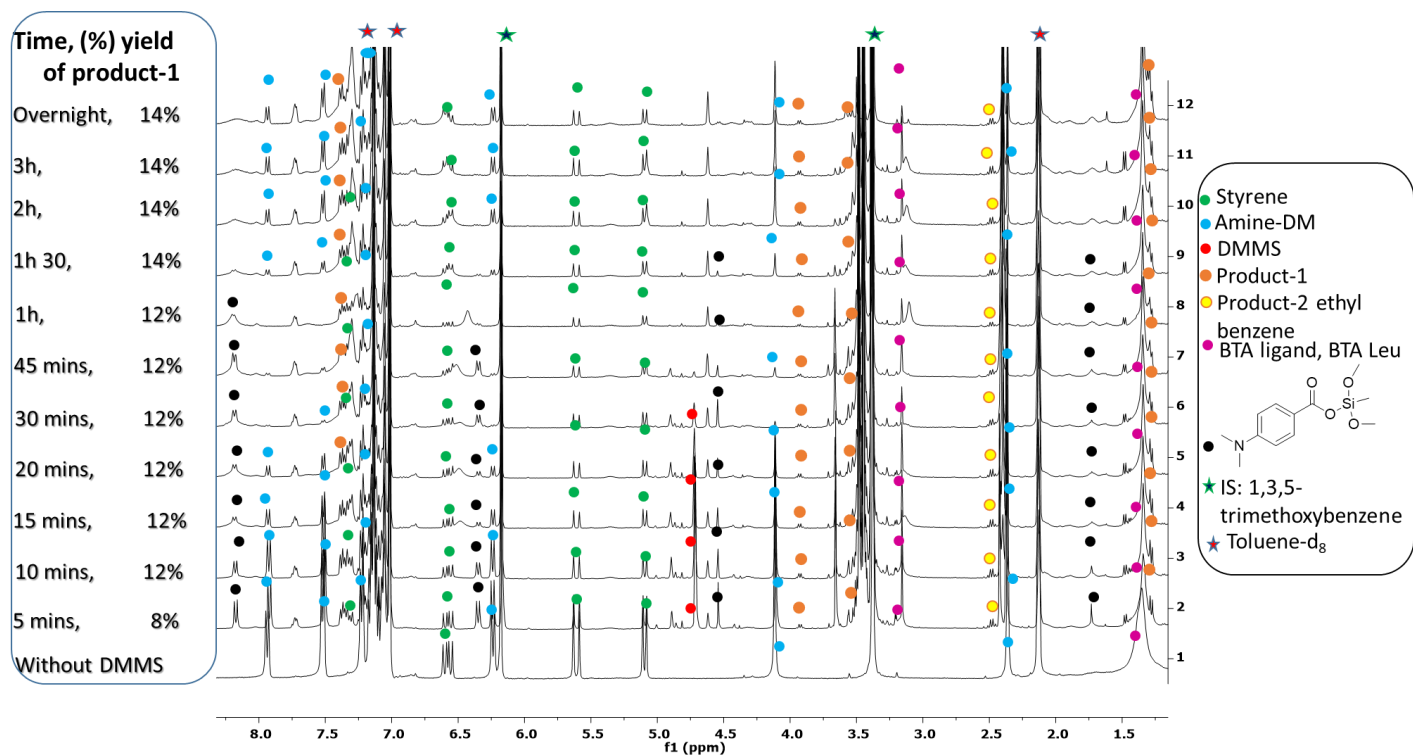


Figure S.III-8 Reaction conditions: Styrene (0.15 mmol), Cu(OAc)₂·H₂O (5 mol%), BTA-P(PhF)₂ (10 mol%), BTA (*R*)-Leu (10 mol%), DMMS (4.0 equiv.), amine-DM (1.2 equiv.), toluene-d₈ (600 μL). Evolution was tracked by ¹H NMR in presence of IS: 1,3,5-trimethoxybenzene. [Study of Scheme III-12.](#)

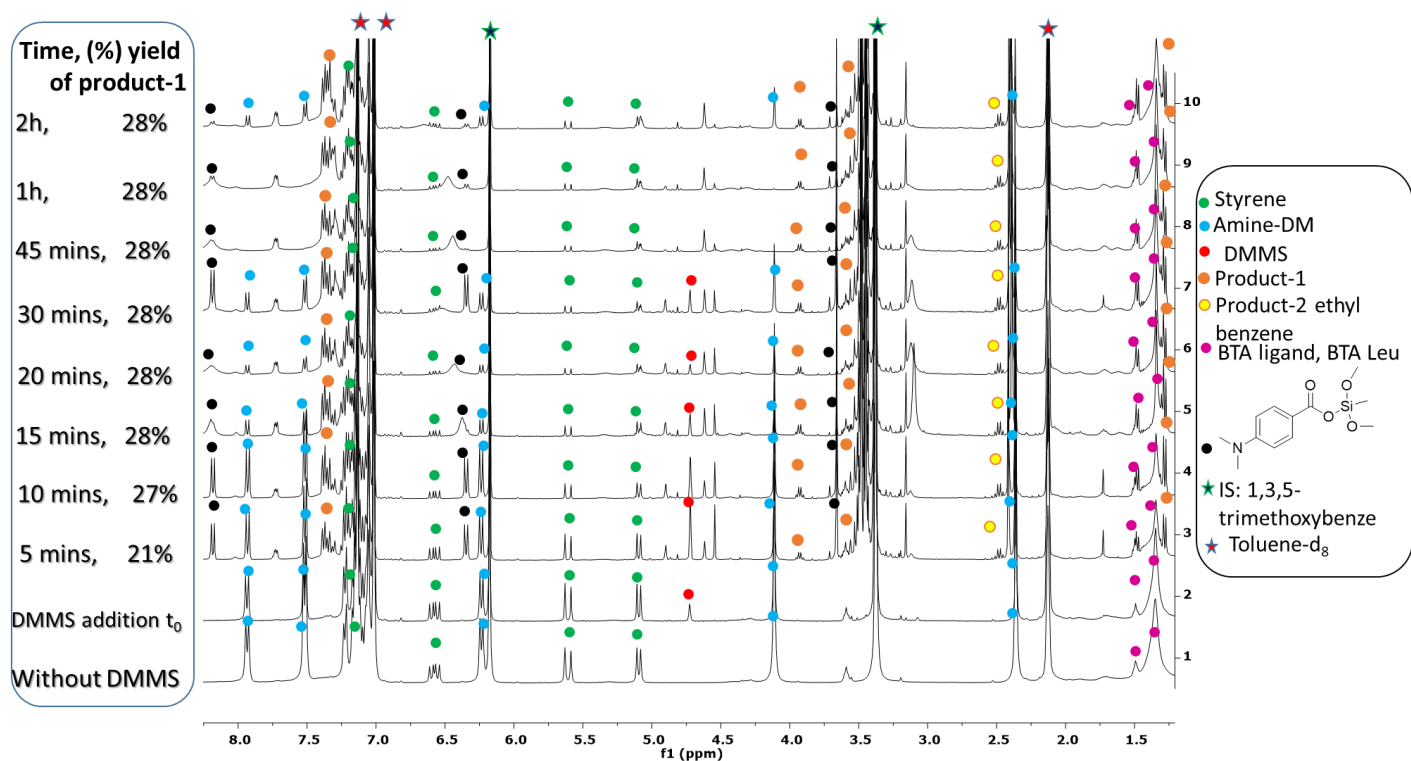


Figure S.III-9 Reaction conditions: Styrene (0.15 mmol), $\text{Cu}(\text{OAc})_2 \cdot \text{H}_2\text{O}$ (5 mol%), **BTA-P(MTF)2** (10 mol%), BTA (*R*)-Leu (10 mol%), DMMS (4.0 equiv.), amine-DM (1.2 equiv.), toluene- d_8 (600 μL). Evolution was tracked by ^1H NMR in presence of IS: 1,3,5-trimethoxybenzene. [Study of Scheme III-12.](#)

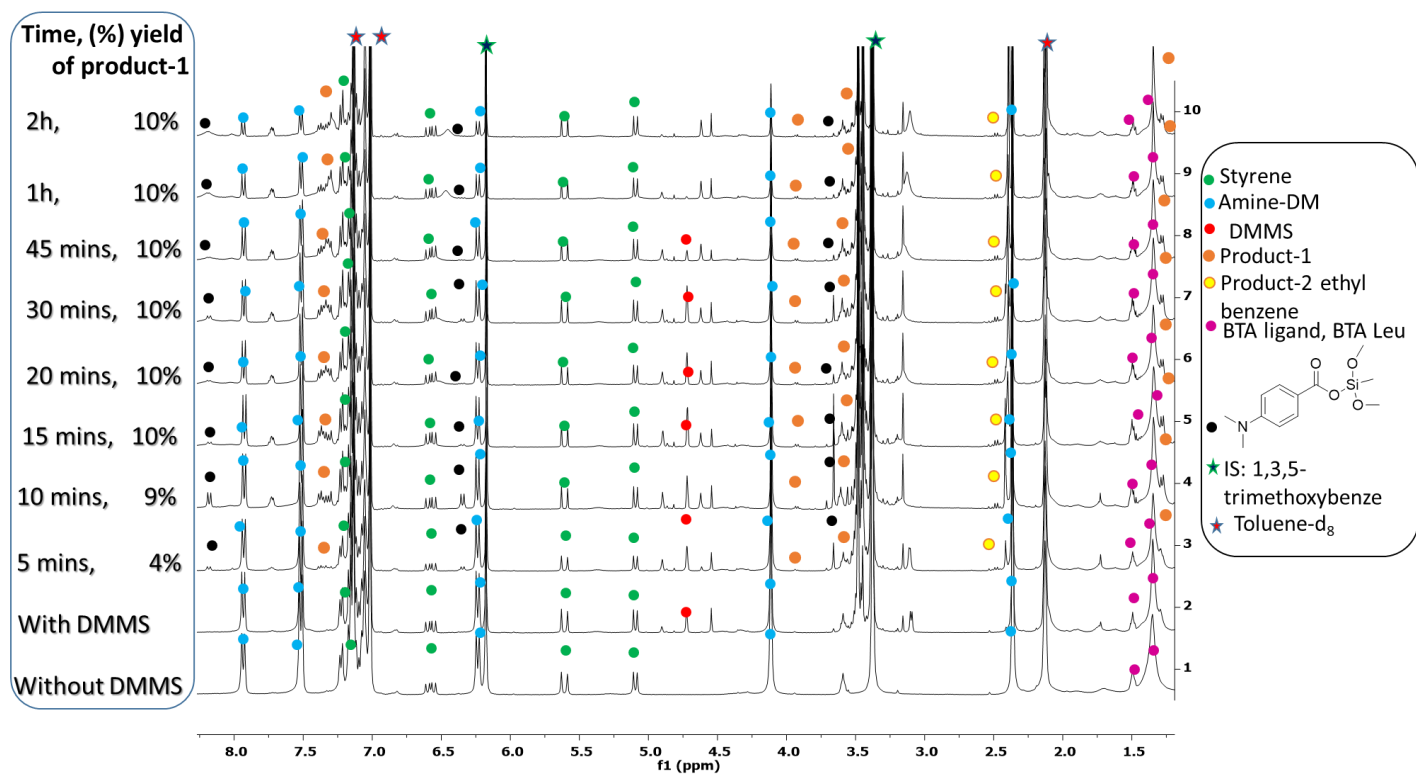


Figure S.III-10 Conditions: Styrene (0.15 mmol), Cu(OAc)₂·H₂O (5 mol%), **BTA-P(Xylyl)2** (10 mol%), BTA (*R*)-Leu (10 mol%), DMMS (4.0 equiv.), amine-DM (1.2 equiv.), toluene-d₈ (600 μL). Evolution was tracked by ¹H NMR in presence of IS: 1,3,5-trimethoxybenzene. [Study of Scheme III-12.](#)

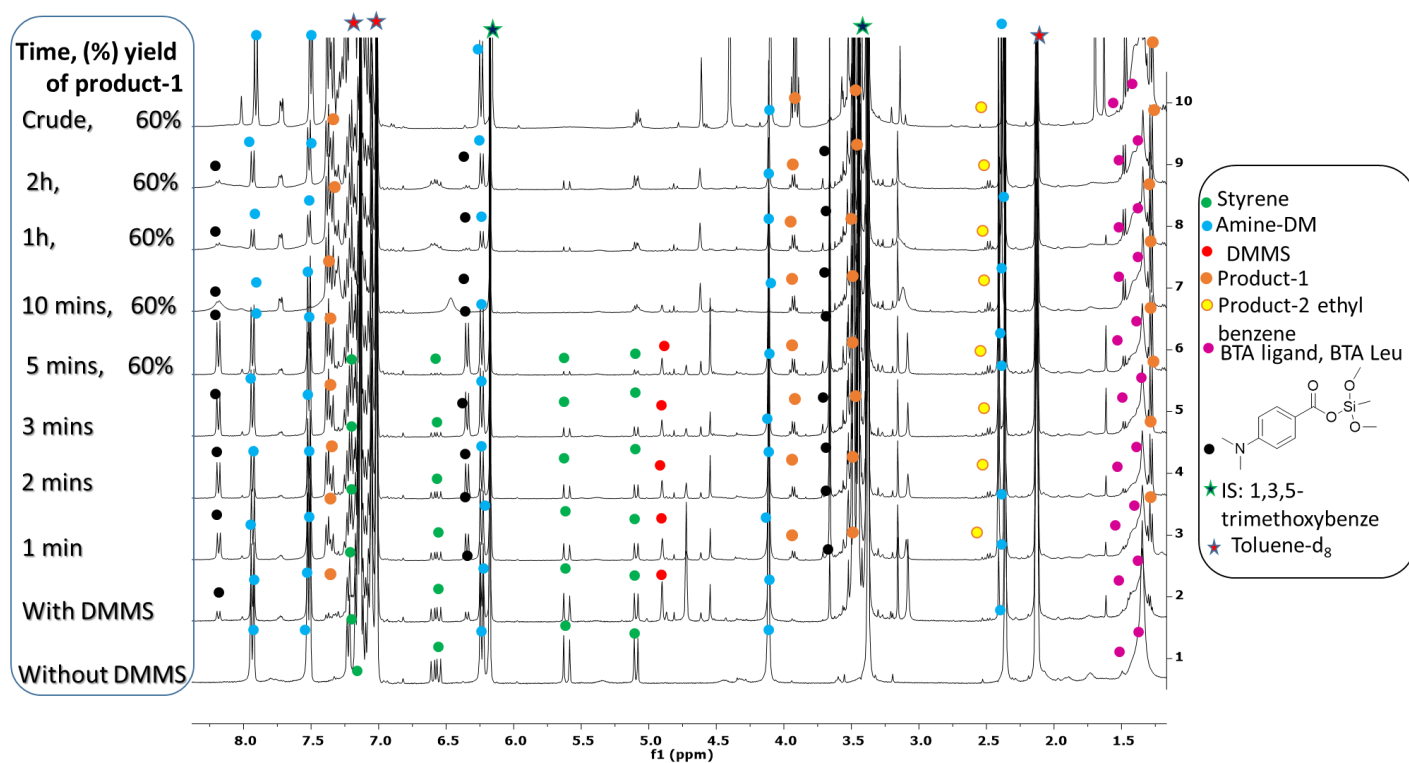


Figure S.III-11 Conditions: Styrene (0.15 mmol), Cu(II)-i)butyrate (5 mol%), **BTA-P(DTF)2** (10 mol%), BTA (*R*)-Leu (10 mol%), DMMS (4.0 equiv.), amine-DM (1.2 equiv.), toluene-d₈ (600 μ L). Evolution was tracked by ¹H NMR in presence of IS: 1,3,5-trimethoxybenzene. [Study of Table III-2.](#)

III.5.b.iii. ^1H NMR analysis of hydrosilylation and cascade of enone derivatives in CDCl_3 .

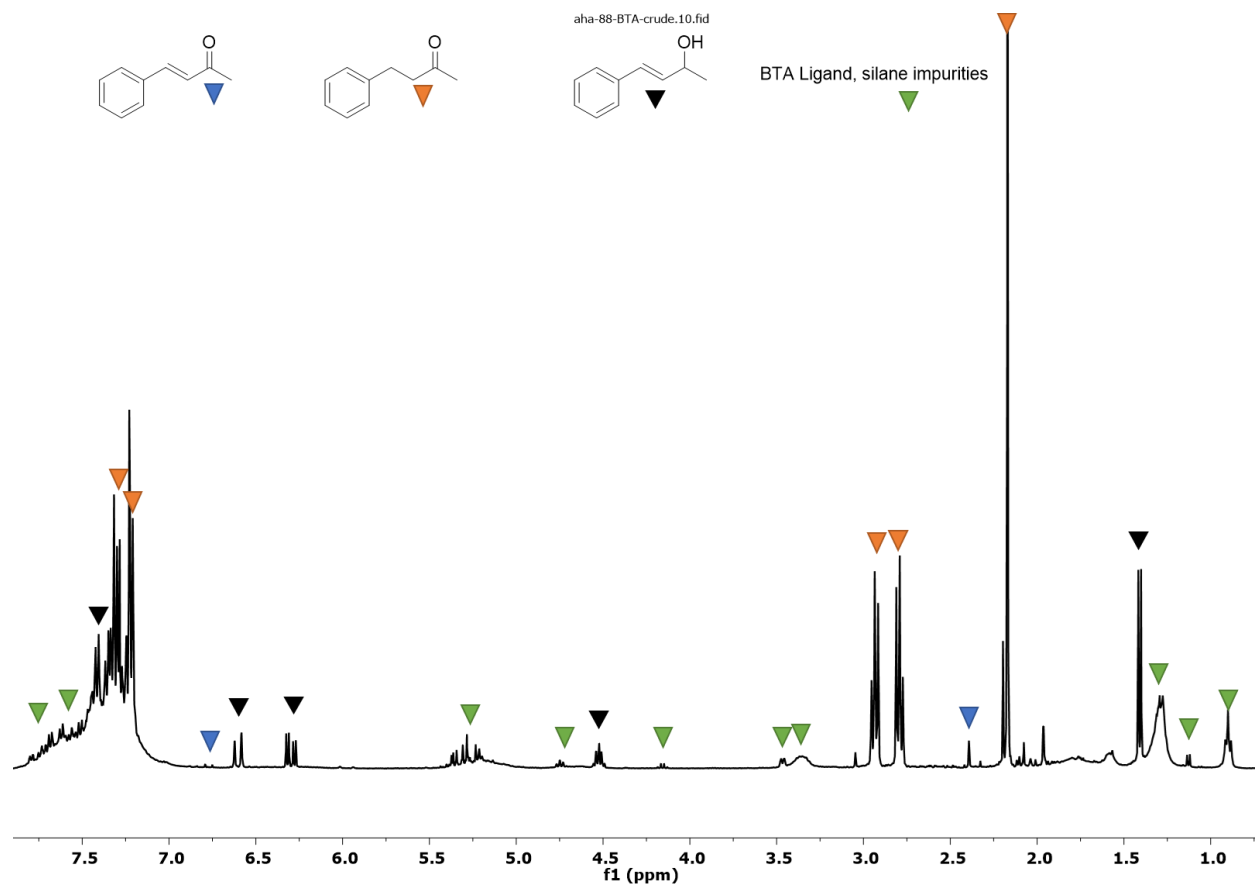


Figure S.III-12 Conditions: benzylidenacetone (0.17 mmole, 1.0 eq), $\text{Cu}(\text{OAc})_2 \cdot x\text{H}_2\text{O}$ (3 mol%), **BTA-pPPh₂** (6 mol%), PhSiH_3 (2.0 eq). **Entry 3, Table III-3.**

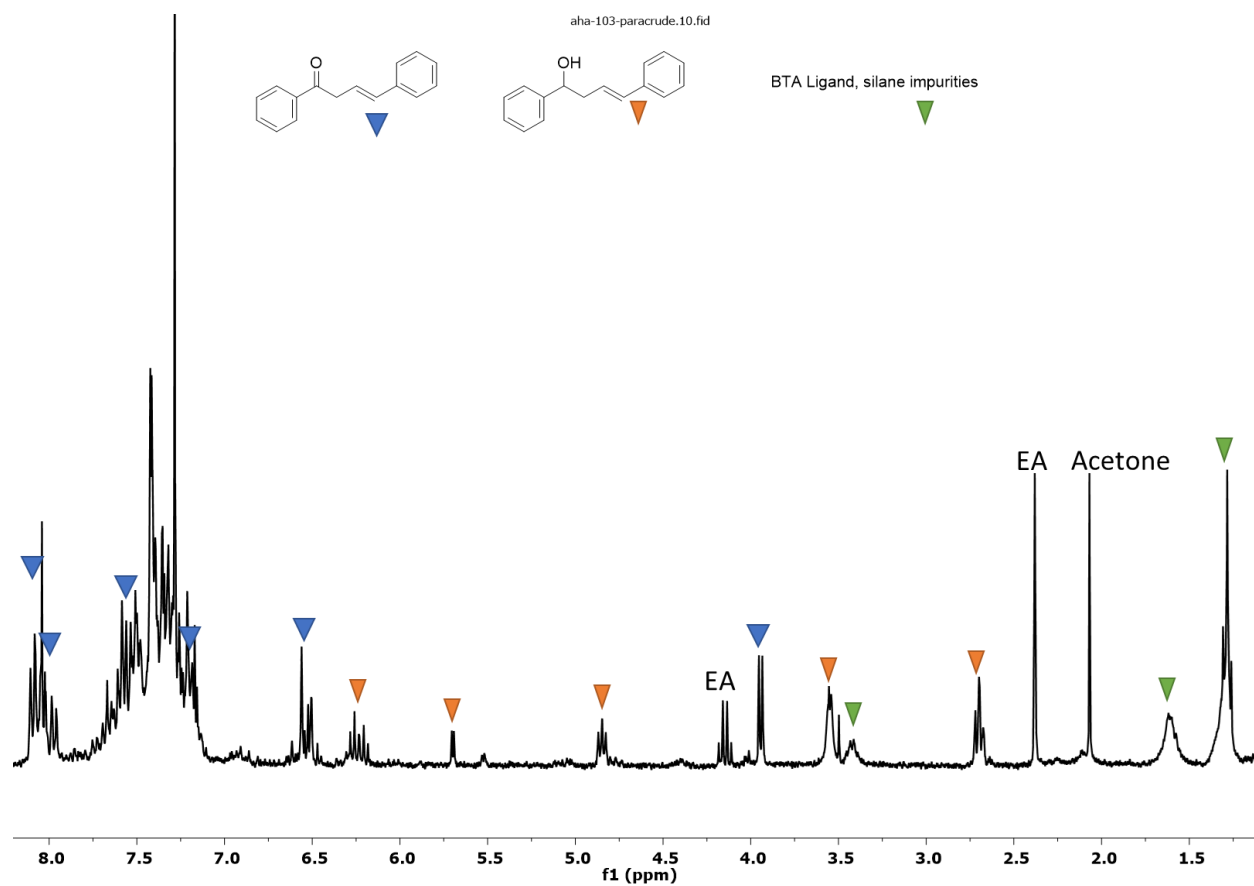


Figure S.III-13 Conditions: (E)-1,4-diphenylbut-3-en-1-one (0.17 mmole, 1eq), $\text{Cu}(\text{OAc})_2 \cdot \text{H}_2\text{O}$ (3 mol%), **BTA-pPPH2** (6 mol%), DMMS (2.0 eq). **Study of Scheme III-15.**

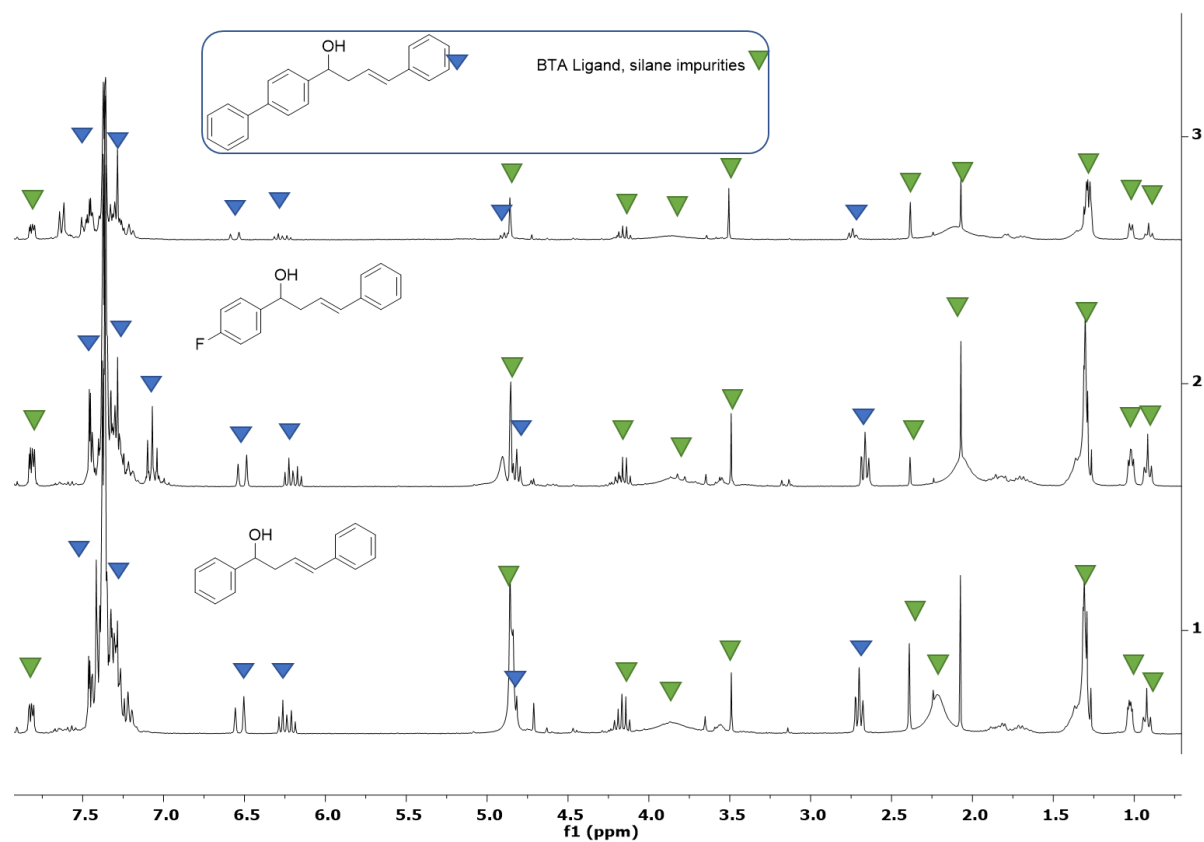
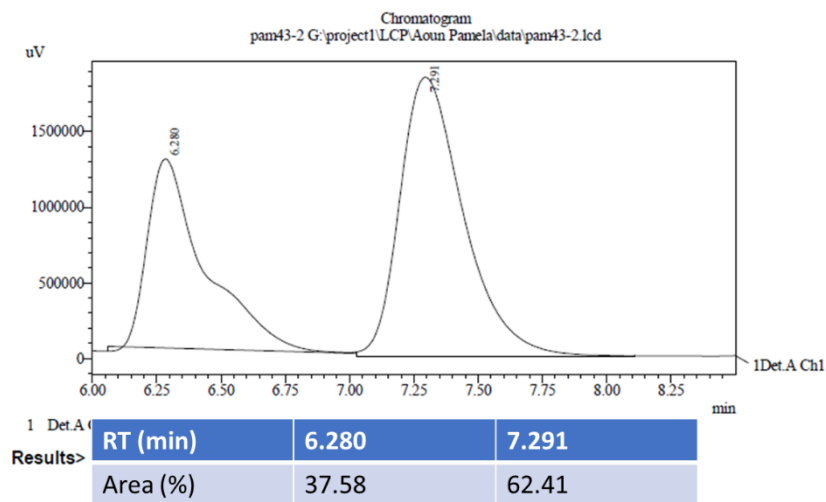


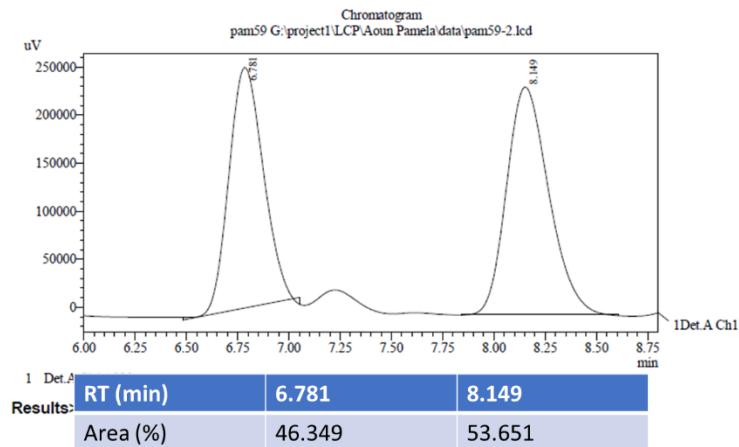
Figure S.III-14 Conditions: substrate (0.25 mmole, 1eq), Cu(OAc)₂·xH₂O (5 mol%), BTA-P(DTF)₂ (10 mol%), BTA (*R*)-Leu (10 mol%), DMMS (2.0 eq), amine-TB (1.3 eq). [Study of Table III-4](#).

III.5.c. Selected HPLC traces.

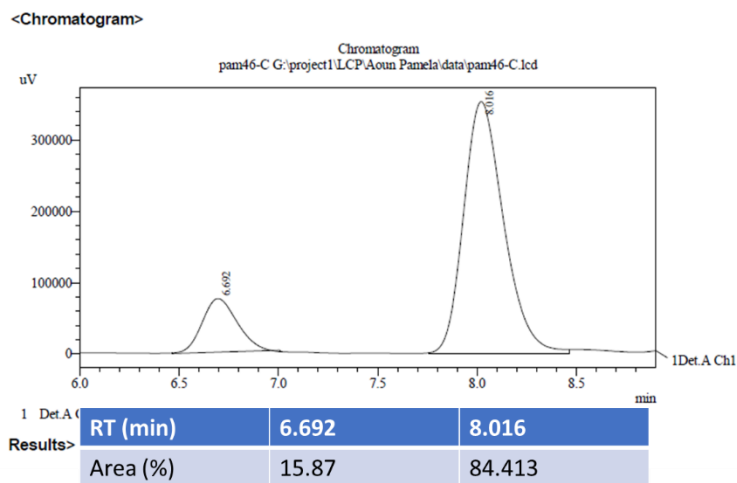
Entry 1, Table III-1. Cu(OAc)₂·xH₂O, BTA-pPPh₂, BTA (*R*)-Leu, toluene-d₈, ee= 25%.



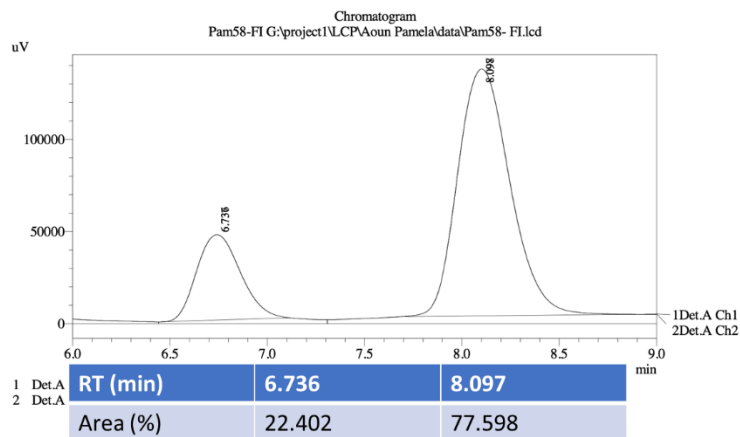
Entry 3, Table III-1. $\text{Cu}(\text{OAc})_2 \cdot x\text{H}_2\text{O}$, BTA-P(MTF)2 ,BTA (R)-Leu, toluene- d_8 . ee= 3%.



Entry 4, Table III-1. $\text{Cu}(\text{OAc})_2 \cdot x\text{H}_2\text{O}$, BTA-P(DTF)2 ,BTA (R)-Leu, toluene- d_8 . ee= 69%.



Entry 5, Table III-1. $\text{Cu}(\text{OAc})_2 \cdot x\text{H}_2\text{O}$, BTA-P(Xyllyl)2 ,BTA (R)-Leu, toluene- d_8 . ee= 55%.



III.5.d. Synthesis of substrates.

Benzylidenacetone. To a mixture of benzyl aldehyde (0.1 mol, 10.2 mL, 1 equiv.), acetone (0.27 mol, 20 mL, 2.69 equiv.) in H₂O (40 mL) and 5% NaOH aqueous solution (0.01 mol, 8 mL) was slowly added, and then the reaction was heated to 40 °C. Once the starting material was consumed, acetone was removed under reduced pressure. The aqueous phase was extracted with ethylacetate (3 x 50 mL), and the combined organic layers were dried over anhydrous Na₂SO₄. After removal of the solvent, the crude mixture was purified by flash column chromatography over silica column (PE : Ethyl acetate / 10:1), to obtain the product (11.66 g, 80% yield) as a yellow liquid. ¹H-NMR (300 MHz): δ (ppm) 7.55-7.50 (m, 3H), 7.40-7.39 (m, 3H), 6.72 (d, J= 16.3 Hz, 1H), 2.38 (s, 3H).

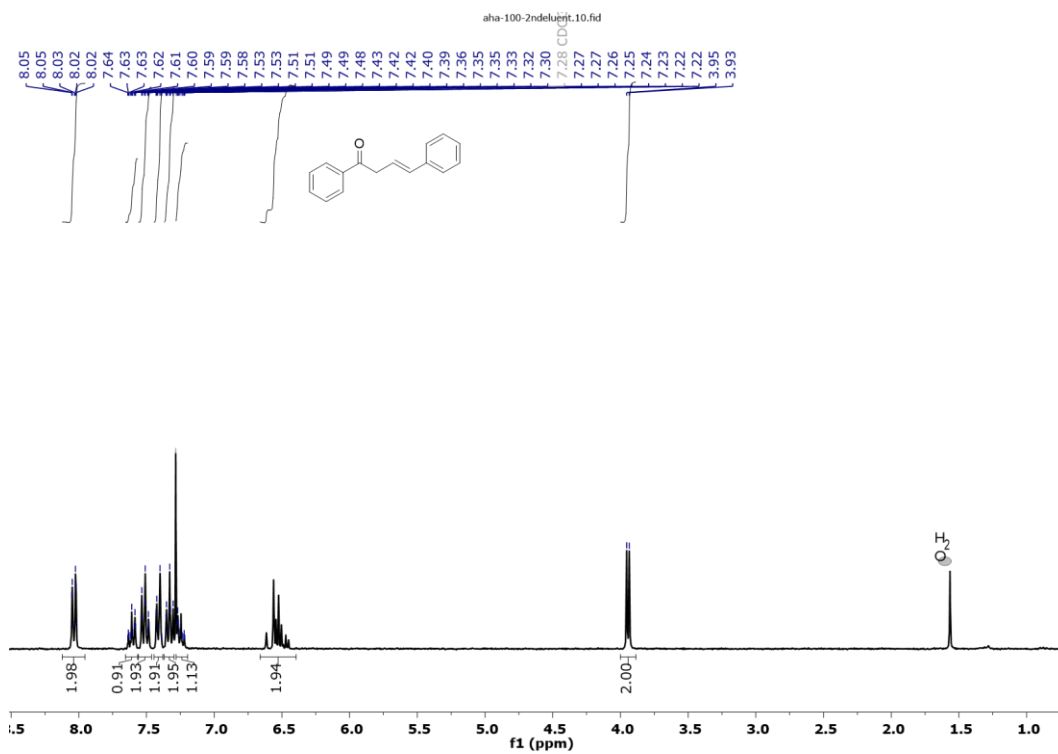
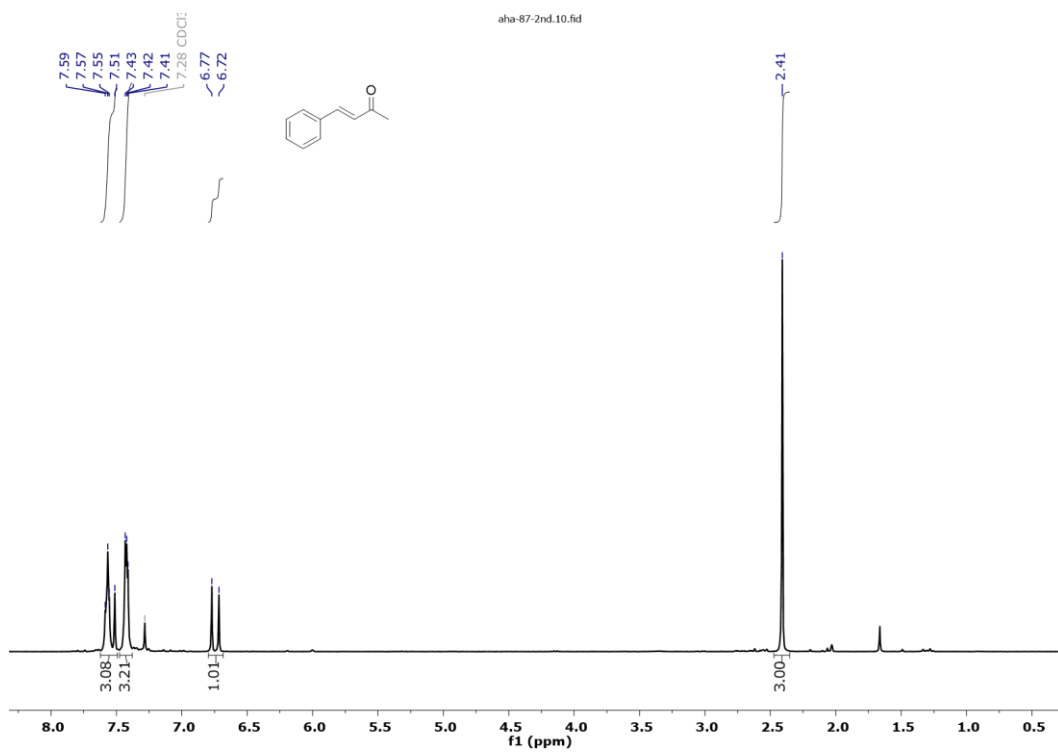
(E)-1,4-diphenylbut-3-en-1-one. A mixture of acetophenone (5.0 mmol, 0.6 mL, 1 equiv.), phenyl acetylene (5.0 mmol, 0.51 g, 1 equiv.), KOtBu (5.0 mmol, 0.56 g, 1 equiv.) in DMSO (36 mL) was heated to 100°C and stirred for 30 mins. The reaction was cooled to room temperature, diluted with 30 mL H₂O, neutralized with saturated NH₄Cl and extracted with ethyl acetate. The organic extract was washed with H₂O, and dried with MgSO₄. After filtration the solvent was evaporated under reduced pressure, and the crude mixture was purified by flash column chromatography over silica column (hexane : ethylacetate / 90:10), to obtain the product as white powder (1.11 g, 32%). ¹H-NMR (300 MHz): δ (ppm) 8.05-8.02 (m, 2H), 7.64-7.57 (m, 1H), 7.55-7.47 (m, 2H), 7.44-7.38 (m, 2H), 7.37-7.21 (m, 3H), 6.63-6.44 (m, 2H), 3.94 (d, J= 5.8 Hz, 1H).

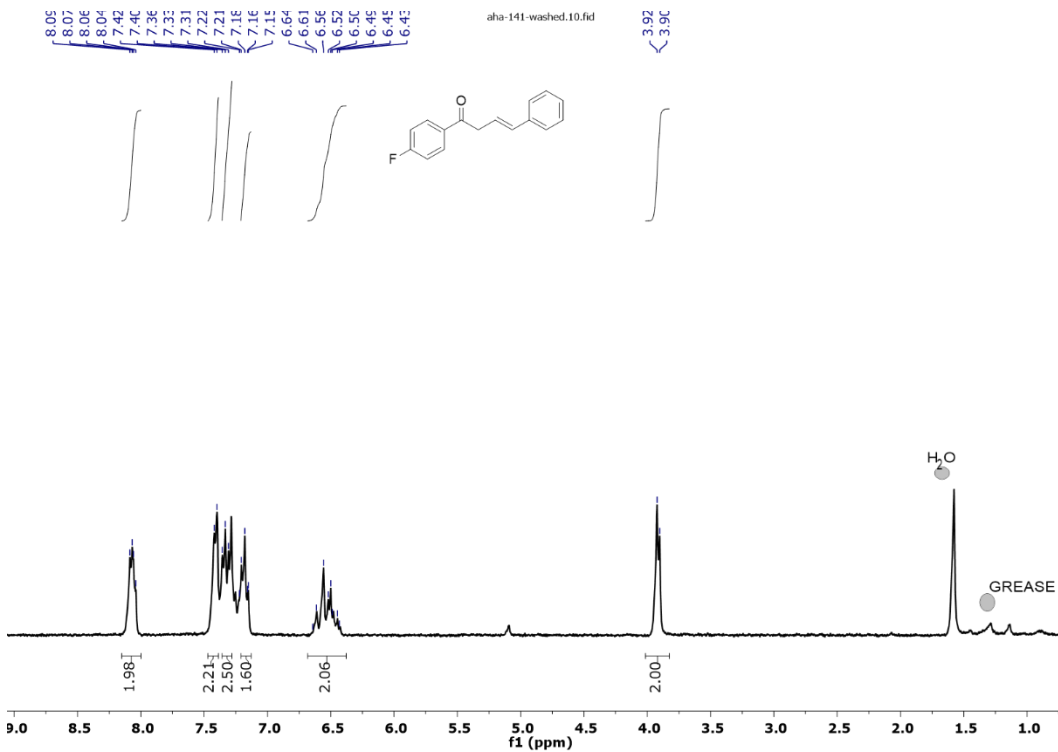
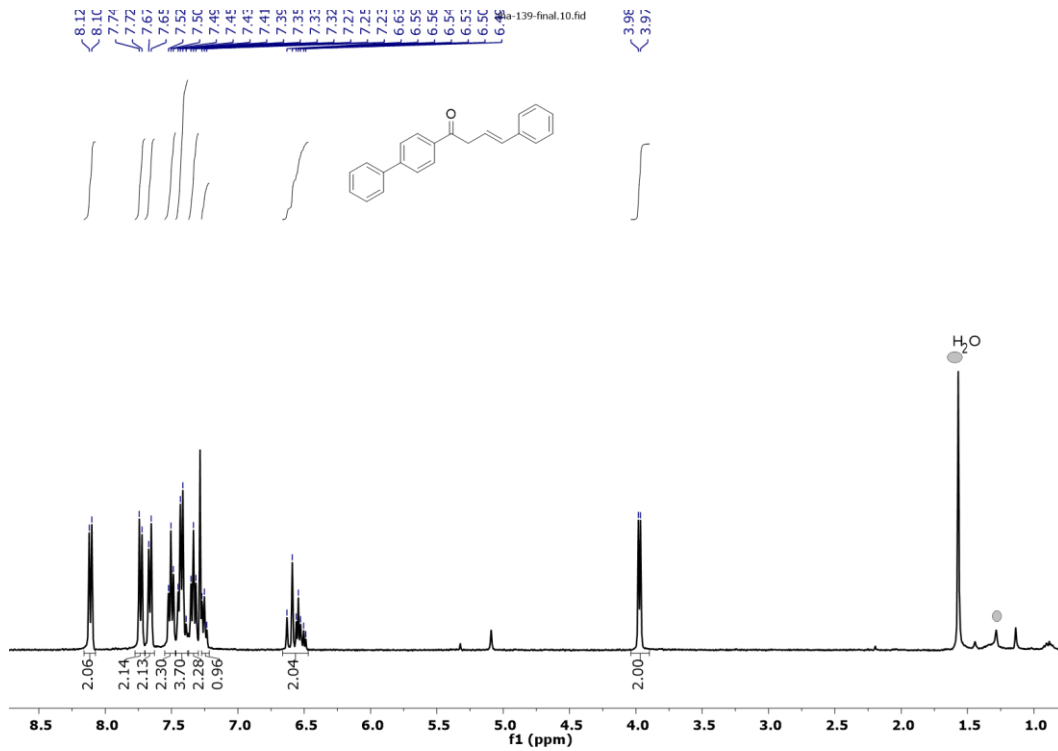
(E)-1-([1,1'-biphenyl]-4-yl)-4-phenylbut-3-en-1-one. A mixture of 1-([1,1'-biphenyl]-4-yl)ethanone (5.0 mmol, 0.98 g, 1.0 equiv.), phenyl acetylene (5.0 mmol, 0.51 g, 1.0 equiv.) and KOtBu (5.0 mmol, 0.56 g, 1.0 equiv.) in DMSO (12 mL) was heated to 100 °C and stirred for 30 mins. The reaction mixture was cooled to room temperature and was diluted with H₂O (12 mL), neutralized with a saturated aqueous solution of NH₄Cl, and extracted with ethyl acetate. The organic extract was washed with H₂O and dried with MgSO₄. After filtration the solvent was evaporated under reduced pressure and the crude mixture was purified by flash column chromatography over silica column (eluent hexane : ethyl acetate / 90:10) to yield the product as white powder (0.39 g, 26%). ¹H-NMR (300 MHz): δ 8.11 (ppm) (d, J = 8.0 Hz, 2H), 7.73 (d, J =

8.0 Hz, 2H), 7.66 (d, $J = 7.7$ Hz, 1H), 7.50 (t, $J = 7.5$ Hz, 2H), 7.47-7.39 (m, 4H), 7.33 (t, $J = 7.5$ Hz, 2H), 7.29-7.22 (m, 1H), 6.67-6.45 (m, 2H), 3.97 (d, $J = 6.3$ Hz, 2H).

(E)-1-(4-fluorophenyl)-4-phenylbut-3-en-1-one. A mixture of 1-(4-fluorophenyl)ethanone (5.0 mmol, 0.6 mL, 1.0 equiv), phenyl acetylene (5.0 mmol, 0.51 g, 1.0 equiv) and KO t -Bu (5.0 mmol, 0.56 g, 1.0 equiv) in DMSO (12 mL) was heated to 100 °C and stirred for 30 mins. The reaction mixture was cooled to room temperature and was diluted with H₂O (12 mL), neutralized with a saturated aqueous solution of NH₄Cl, and extracted with ethyl acetate. The organic extract was washed with H₂O and dried with MgSO₄. After filtration the solvent was evaporated under reduced pressure and the crude mixture was purified by flash column chromatography over silica column (eluent hexane : ethyl acetate / 90:10) to yield the product as white powder (0.07 g, 6%). ¹H-NMR (300 MHz): δ (ppm) 8.09-8.04 (m, 2H), 7.48-7.39 (m, 2H), 7.36-7.25 (m, 3H), 7.20-7.14 (m, 2H), 6.66-6.39 (m, 2H), 3.91 (d, $J = 6.1$ Hz, 1H).

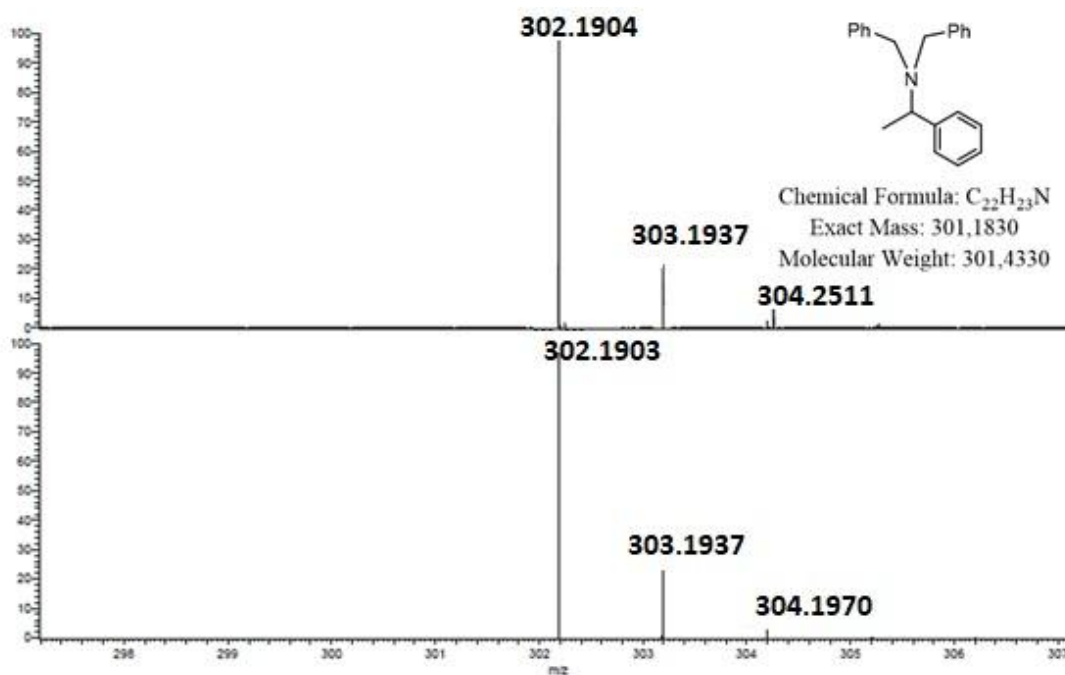
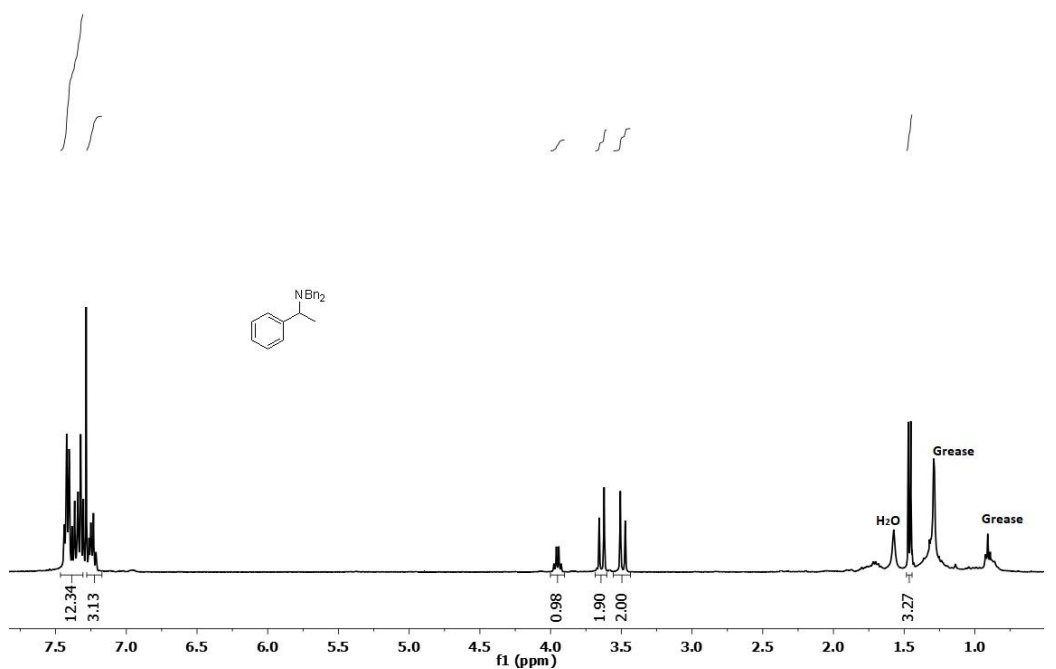
III.5.e. ^1H NMR of substrates.





III.5.f. ^1H NMR and HRMS of Product-1.

N,N-dibenzyl-1-phenylethanamine. ^1H NMR (300 MHz, CDCl_3) δ (ppm) 7.44-7.21 (m, 15H), 3.96 (q, 1H), 3.64 (d, 2H), 3.49 (d, 2H), 1.46 (d, 3H). HRMS (ESI, m/z): Calculated for $\text{C}_{22}\text{H}_{23}\text{N}$, $[\text{M}+\text{H}]^+$: 302.4330, found: 302.1904.



III.6. References.

- [1] E. N. Jacobsen, A. Pfaltz, H. Yamamoto, Eds. *Comprehensive Asymmetric Catalysis*, Springer-Verlag, Berlin Heidelberg, **1999**.
- [2] E. J. Corey, C. J. Helal, *Angew. Chem. Int. Ed.* **1998**, *37*, 1986–2012.
- [3] W. Dumont, J. C. Poulin, D. T. Phat, H. B. Kagan, *J. Am. Chem. Soc.* **1973**, *95*, 8295–8299.
- [4] I. Ojima, M. Nihonyanagi, Y. Nagai, *J. Chem. Soc. Chem. Commun.* **1972**, 938a–938a.
- [5] N. Langlois, T.-P. Dang, H. B. Kagan, *Tetrahedron Lett.* **1973**, *14*, 4865–4868.
- [6] G. Du, M. M. Abu-Omar, *Organometallics* **2006**, *25*, 4920–4923.
- [7] E. A. Ison, E. R. Trivedi, R. A. Corbin, M. M. Abu-Omar, *J. Am. Chem. Soc.* **2005**, *127*, 15374–15375.
- [8] K. A. Nolin, J. R. Krumper, M. D. Pluth, R. G. Bergman, F. D. Toste, *J. Am. Chem. Soc.* **2007**, *129*, 14684–14696.
- [9] H. Nishiyama, H. Sakaguchi, T. Nakamura, M. Horihata, M. Kondo, K. Itoh, *Organometallics* **1989**, *8*, 846–848.
- [10] B. Tao, G. C. Fu, *Angew. Chem. Int. Ed.* **2002**, *41*, 3892–3894.
- [11] M. Sawamura, R. Kuwano, Y. Ito, *Angew. Chem. Int. Ed. Engl.* **1994**, *33*, 111–113.
- [12] Y. Nishibayashi, K. Segawa, J. D. Singh, S. Fukuzawa, K. Ohe, S. Uemura, *Organometallics* **1996**, *15*, 370–379.
- [13] A. R. Chianese, R. H. Crabtree, *Organometallics* **2005**, *24*, 4432–4436.
- [14] T. Nakano, Y. Nagai, *Chem. Lett.* **1988**, *17*, 481–484.
- [15] M. Bandini, F. Bernardi, A. Bottoni, P. G. Cozzi, G. P. Miscione, A. Umani-Ronchi, *Eur. J. Org. Chem.* **2003**, *2003*, 2972–2984.
- [16] M. B. Carter, B. Schiott, A. Gutierrez, S. L. Buchwald, *J. Am. Chem. Soc.* **1994**, *116*, 11667–11670.
- [17] J. Yun, S. L. Buchwald, *J. Am. Chem. Soc.* **1999**, *121*, 5640–5644.
- [18] E. Buitrago, L. Zani, H. Adolfsson, *Appl. Organomet. Chem.* **2011**, *25*, 748–752.
- [19] D. Bézier, F. Jiang, T. Roisnel, J.-B. Sortais, C. Darcel, *Eur. J. Inorg. Chem.* **2012**, *2012*, 1333–1337.
- [20] D. Addis, N. Shaikh, S. Zhou, S. Das, K. Junge, M. Beller, *Chem. – Asian J.* **2010**, *5*, 1687–1691.

- [21] H. Nishiyama, A. Furuta, *Chem. Commun.* **2007**, 760–762.
- [22] R. H. Morris, *Chem. Soc. Rev.* **2009**, *38*, 2282–2291.
- [23] T. Bleith, H. Wadepohl, L. H. Gade, *J. Am. Chem. Soc.* **2015**, *137*, 2456–2459.
- [24] S. U. Son, S.-J. Paik, I. S. Lee, Y.-A. Lee, Y. K. Chung, W. K. Seok, H. N. Lee, *Organometallics* **1999**, *18*, 4114–4118.
- [25] V. Yempally, A. Shahbaz, W. Y. Fan, S. T. Madrahimov, A. A. Bengali, *Inorganics* **2020**, *8*, 61.
- [26] M. DiBiase Cavanaugh, B. T. Gregg, A. R. Cutler, *Organometallics* **1996**, *15*, 2764–2769.
- [27] H. Mimoun, J. Y. de Saint Laumer, L. Giannini, R. Scopelliti, C. Floriani, *J. Am. Chem. Soc.* **1999**, *121*, 6158–6166.
- [28] T. Ohkuma, S. Hashiguchi, R. Noyori, *J. Org. Chem.* **1994**, *59*, 217–221.
- [29] H. Brunner, W. Miehl, *J. Organomet. Chem.* **1984**, *275*, c17–c21.
- [30] S. Sirol, J. Courmarcel, N. Mostefai, O. Riant, *Org. Lett.* **2001**, *3*, 4111–4113.
- [31] B. H. Lipshutz, W. Chrisman, K. Noson, *J. Organomet. Chem.* **2001**, *624*, 367–371.
- [32] J. T. Issenhuth, S. Dagonne, S. Bellemin-Laponnaz, *Adv. Synth. Catal.* **2006**, *348*, 1991–1994.
- [33] C. Deutsch, N. Krause, *Chem. Rev.* **2008**, *108*, 2916–2927.
- [34] O. Riant, in *PATAI Chem. Funct. Groups*, American Cancer Society, **2011**.
- [35] B. H. Lipshutz, K. Noson, W. Chrisman, A. Lower, *J. Am. Chem. Soc.* **2003**, *125*, 8779–8789.
- [36] B. H. Lipshutz, A. Lower, K. Noson, *Org. Lett.* **2002**, *4*, 4045–4048.
- [37] B. H. Lipshutz, B. A. Frieman, *Angew. Chem. Int. Ed.* **2005**, *44*, 6253–6253.
- [38] B. H. Lipshutz, B. A. Frieman, *Angew. Chem. Int. Ed Engl.* **2005**, *44*, 6345–6348.
- [39] C. Czekelius, E. M. Carreira, *Org. Lett.* **2004**, *6*, 4575–4577.
- [40] N. Mostefai, S. Sirol, J. Courmarcel, O. Riant, *Synthesis* **2007**, *2007*, 1265–1271.
- [41] S. Sirol, J. Courmarcel, N. Mostefai, O. Riant, *Org. Lett.* **2001**, *3*, 4111–4113.
- [42] J. Courmarcel, N. Mostefai, S. Sirol, S. Choppin, O. Riant, *Isr. J. Chem.* **2001**, *41*, 231–240.
- [43] O. Riant, N. Mostefai, J. Courmarcel, *Synthesis* **2004**, *2004*, 2943–2958.

- [44] B. A. Baker, Ž. V. Bošković, B. H. Lipshutz, *Org. Lett.* **2008**, *10*, 289–292.
- [45] D. Lee, J. Yun, *Tetrahedron Lett.* **2004**, *45*, 5415–5417.
- [46] J. Wu, J.-X. Ji, A. S. C. Chan, *Proc. Natl. Acad. Sci.* **2005**, *102*, 3570–3575.
- [47] Y. Li, A. Hammoud, L. Bouteiller, M. Raynal, *J. Am. Chem. Soc.* **2020**, *142*, 5676–5688.
- [48] J. M. Zimbron, X. Caumes, Y. Li, C. M. Thomas, M. Raynal, L. Bouteiller, *Angew. Chem. Int. Ed.* **2017**, *56*, 14016–14019.
- [49] M. Raynal, P. Ballester, A. Vidal-Ferran, P. W. N. M. van Leeuwen, *Chem Soc Rev* **2014**, *43*, 1660–1733.
- [50] M. Raynal, F. Portier, P. W. N. M. van Leeuwen, L. Bouteiller, *J. Am. Chem. Soc.* **2013**, *135*, 17687–17690.
- [51] A. V. Malkov, *Angew. Chem. Int. Ed.* **2010**, *49*, 9814–9815.
- [52] A. J. Jordan, G. Lalic, J. P. Sadighi, *Chem. Rev.* **2016**, *116*, 8318–8372.
- [53] K. Junge, B. Wendt, D. Addis, S. Zhou, S. Das, M. Beller, *Chem. – Eur. J.* **2010**, *16*, 68–73.
- [54] R. Moser, Ž. V. Bošković, C. S. Crowe, B. H. Lipshutz, *J. Am. Chem. Soc.* **2010**, *132*, 7852–7853.
- [55] T. C. Nugent, *Chiral Amine Synthesis: Methods, Developments and Applications*, John Wiley & Sons, **2010**.
- [56] N. Turner, M. Truppo, **2010**, DOI 10.1002/9783527629541.CH14.
- [57] M. T. Robak, M. A. Herbage, J. A. Ellman, *Chem. Rev.* **2010**, *110*, 3600–3740.
- [58] D. Parmar, E. Sugiono, S. Raja, M. Rueping, *Chem. Rev.* **2014**, *114*, 9047–9153.
- [59] T. C. Nugent, M. El-Shazly, *Adv. Synth. Catal.* **2010**, *352*, 753–819.
- [60] J.-H. Xie, S.-F. Zhu, Q.-L. Zhou, *Chem. Rev.* **2011**, *111*, 1713–1760.
- [61] M. Yus, J. C. González-Gómez, F. Foubelo, *Chem. Rev.* **2011**, *111*, 7774–7854.
- [62] M. Johannsen, K. A. Jørgensen, *Chem. Rev.* **1998**, *98*, 1689–1708.
- [63] P. Müller, C. Fruit, *Chem. Rev.* **2003**, *103*, 2905–2920.
- [64] L. Huang, M. Arndt, K. Gooßen, H. Heydt, L. J. Gooßen, *Chem. Rev.* **2015**, *115*, 2596–2697.
- [65] T. E. Müller, K. C. Hultsch, M. Yus, F. Foubelo, M. Tada, *Chem. Rev.* **2008**, *108*, 3795–3892.

- [66] T. E. Müller, M. Beller, *Chem. Rev.* **1998**, *98*, 675–704.
- [67] J. F. Hartwig, *Pure Appl. Chem.* **2004**, *76*, 507–516.
- [68] S. Hong, T. J. Marks, *Acc. Chem. Res.* **2004**, *37*, 673–686.
- [69] M. Beller, J. Seayad, A. Tillack, H. Jiao, *Angew. Chem. Int. Ed.* **2004**, *43*, 3368–3398.
- [70] D. H. Appella, Y. Moritani, R. Shintani, E. M. Ferreira, S. L. Buchwald, *J. Am. Chem. Soc.* **1999**, *121*, 9473–9474.
- [71] G. Hughes, M. Kimura, S. L. Buchwald, *J. Am. Chem. Soc.* **2003**, *125*, 11253–11258.
- [72] D. Nishikawa, K. Hirano, M. Miura, *J. Am. Chem. Soc.* **2015**, *137*, 15620–15623.
- [73] Y. Miki, K. Hirano, T. Satoh, M. Miura, *Org. Lett.* **2014**, *16*, 1498–1501.
- [74] Y. Miki, K. Hirano, T. Satoh, M. Miura, *Angew. Chem. Int. Ed.* **2013**, *52*, 10830–10834.
- [75] T. Takata, D. Nishikawa, K. Hirano, M. Miura, *Chem. – Eur. J.* **2018**, *24*, 10975–10978.
- [76] T. Takata, K. Hirano, M. Miura, *Org. Lett.* **2019**, *21*, 4284–4288.
- [77] S. Zhu, N. Niljianskul, S. L. Buchwald, *J. Am. Chem. Soc.* **2013**, *135*, 15746–15749.
- [78] J. S. Bandar, M. T. Pirnot, S. L. Buchwald, *J. Am. Chem. Soc.* **2015**, *137*, 14812–14818.
- [79] G. Lu, R. Y. Liu, Y. Yang, C. Fang, D. S. Lambrecht, S. L. Buchwald, P. Liu, *J. Am. Chem. Soc.* **2017**, *139*, 16548–16555.
- [80] E. R. Strieter, B. Bhayana, S. L. Buchwald, *J. Am. Chem. Soc.* **2009**, *131*, 78–88.
- [81] S. Zhu, N. Niljianskul, S. L. Buchwald, *J. Am. Chem. Soc.* **2013**, *135*, 15746–15749.
- [82] S. Zhu, S. L. Buchwald, *J. Am. Chem. Soc.* **2014**, *136*, 15913–15916.
- [83] N. Niljianskul, S. Zhu, S. L. Buchwald, *Angew. Chem. Int. Ed.* **2015**, *54*, 1638–1641.
- [84] S.-L. Shi, S. L. Buchwald, *Nat. Chem.* **2015**, *7*, 38–44.
- [85] Y. Miki, K. Hirano, T. Satoh, M. Miura, *Angew. Chem. Int. Ed.* **2013**, *52*, 10830–10834.
- [86] Y. Miki, K. Hirano, T. Satoh, M. Miura, *Org. Lett.* **2014**, *16*, 1498–1501.
- [87] Y. Yang, S.-L. Shi, D. Niu, P. Liu, S. L. Buchwald, *Science* **2015**, *349*, 62–66.
- [88] D. Niu, S. L. Buchwald, *J. Am. Chem. Soc.* **2015**, *137*, 9716–9721.
- [89] S. Tobisch, *Chem. – Eur. J.* **2016**, *22*, 8290–8300.
- [90] Y. Xi, B. Su, X. Qi, S. Pedram, P. Liu, J. F. Hartwig, *J. Am. Chem. Soc.* **2020**, *142*, 18213–18222.

- [91] W. J. Jang, S. M. Song, J. H. Moon, J. Y. Lee, J. Yun, *J. Am. Chem. Soc.* **2017**, *139*, 13660–13663.
- [92] G. J. P. Perry, T. Jia, D. J. Procter, *ACS Catal.* **2020**, *10*, 1485–1499.
- [93] X. Feng, H. Jeon, J. Yun, *Angew. Chem.* **2013**, *125*, 4081–4084.
- [94] H. Wang, S. L. Buchwald, in *Org. React.*, American Cancer Society, **2019**, pp. 121–206.
- [95] S. Tobisch, *Chem. – Eur. J.* **2016**, *22*, 8290–8300.
- [96] Y. Yang, I. B. Perry, S. L. Buchwald, *J. Am. Chem. Soc.* **2016**, *138*, 9787–9790.
- [97] Y. Li, X. Caumes, M. Raynal, L. Bouteiller, *Chem. Commun.* **2019**, *55*, 2162–2165.
- [98] Y. Li, X. Caumes, M. Raynal, L. Bouteiller, *Chem. Commun.* **2019**, *55*, 2162–2165.
- [99] M. W. Gribble, M. T. Pirnot, J. S. Bandar, R. Y. Liu, S. L. Buchwald, *J. Am. Chem. Soc.* **2017**, *139*, 2192–2195.
- [100] G. J. P. Britovsek, *Angew. Chem. Int. Ed.* **2012**, *51*, 1518–1518.
- [101] A. A. Thomas, K. Speck, I. Kevlishvili, Z. Lu, P. Liu, S. L. Buchwald, *J. Am. Chem. Soc.* **2018**, *140*, 13976–13984.
- [102] S.-L. Shi, Z. L. Wong, S. L. Buchwald, *Nature* **2016**, *532*, 353–356.

Chapter IV : Enantio and diastereoselective cascade reaction with supramolecular and chirally-amplified helical catalyst: towards stereodivergency.

Abstract: The stereodivergent approach is implemented for the hydrosilylation/hydroamination cascade reaction of vinyl acetophenone derivatives. Investigations indicate that hydroamination only proceeds for **3-VPnone** substrate. Optimization of the cascade reaction identified Cu(II)-*i*-butyrate and MCH as the best metal precursor and solvent, respectively. Under these conditions, the amino alcohol product **3-APnol** is obtained with 85% yield, 93% *ee* and a *dr* of 2.8. For the non-switchable experiments, the two stereoisomers were obtained with convenient yields, excellent enantioselectivities, and moderate *dr*. However, all tested selectivity-switching experiments failed to produce the expected stereoisomer with a decent stereoselectivity. Actually, the switch was always partial, *i.e.* that a mixture was obtained which contains the desired stereoisomer as well as the one formed in absence of stereochemical switch.

IV.1. Introduction.

Predictable enantio-divergent catalysis has been well explored and described in the literature according to different approaches which rely on the utilization of asymmetric switchable catalysts. On the one hand, these catalysts were able to switch between two enantiomeric states by adapting different strategies^[1-14] to provide both enantiomers of the catalytic product with high levels of enantioselectivity^[15-17]. On the other hand, these catalysts have not been implemented in asymmetric cascade reactions for the formation of products embedding multiple stereogenic centers notably because of their chiral inversion power being hampered or drastically reduced in truly one-pot conditions (see **Chapter I**). The only known example for achieving predictable stereodivergency in cascade reactions relies on two catalysts anchored to the same molecular machine^[18]. Our aim is to implement a predictable stereodivergent method with a single catalyst. A switchable helical BTA catalyst will be engaged in an asymmetric hydrosilylation/hydroamination cascade process with the aim of producing all possible amino-alcohol stereoisomers in a one-pot reaction from vinyl ketone derivatives (Figure IV-1). The configuration of the consecutively formed stereogenic centers will be controlled by the handedness of the supramolecular helices, which in turn depends on the relative proportion of the enantiopure BTA co-monomers present in the helices (ester BTAs). The composition is tuned by simple addition of the desired amount of BTA co-monomers, which thanks to the diluted MR effect, provides an effective switch between the two directions of the helices. According to the investigations described in **Chapter III** we selected vinyl acetophenone derivatives as a family of substrates (Table IV-1) to be probed in a cascade reaction by our copper-catalyzed helical BTA catalysts. Vinyl acetophenone derivatives are interesting for evaluation in the cascade process because of their modular structure. First, these compounds are easily synthesized in one step according to a procedure published by Brown and co-workers^[19]. Second, it is expected that the two functions will react independently, *i.e.* the first created stereogenic center will not affect the catalytic outcome of the second reaction.

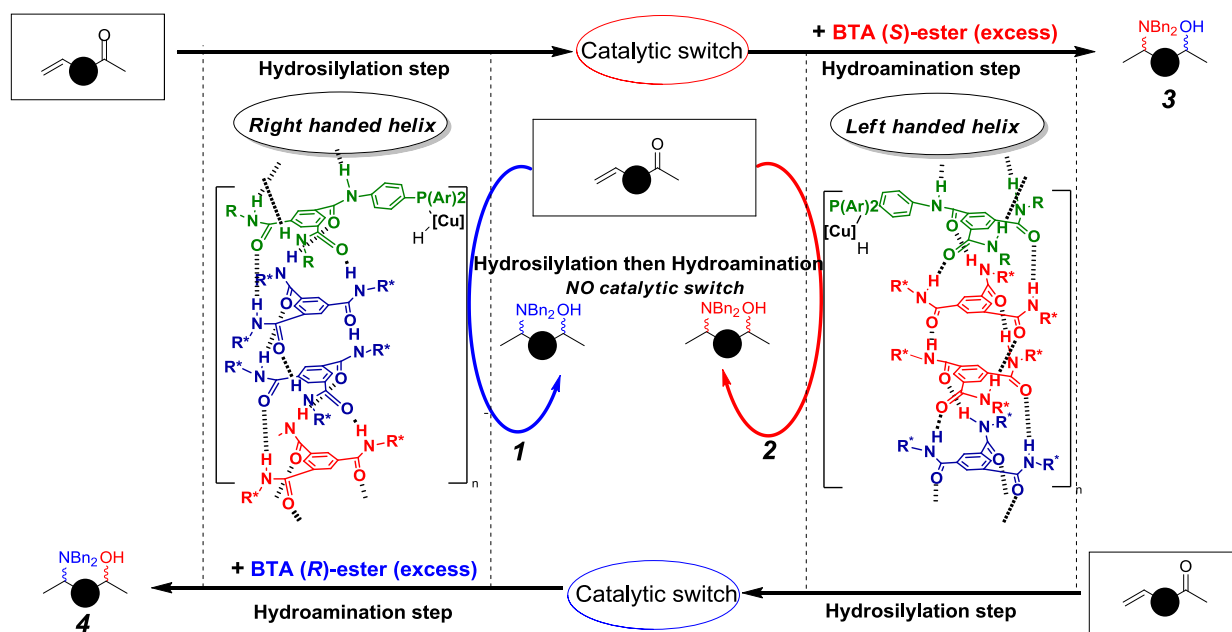
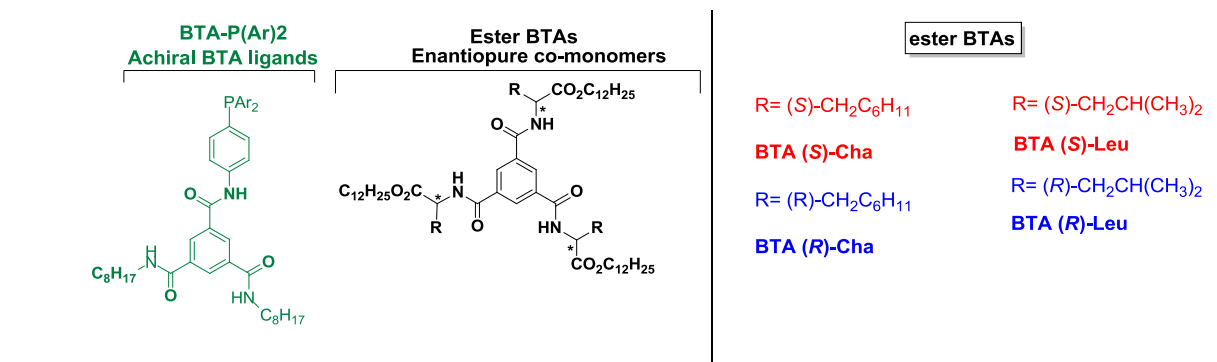


Figure IV-1 Above : Chemical structure of achiral BTA ligands, and chiral BTA co-monomers (BTA esters). Below: Different pathways followed to access all possible stereoisomers of amino alcohols from the copper-catalyzed hydrosilylation/hydroamination cascade reaction conducted from vinyl ketones. Two stereoisomers should be obtained without applying the catalytic switch, the other 2 stereoisomers should be obtained by applying the catalytic switch by adding an excess amount of the opposite chiral co-monomer. Hydrosilylation of the carbonyl function is the first step, and hydroamination on the vinyl moiety is the second step of the cascade reaction.

Finally, this class of substrates has not been investigated in asymmetric catalysis despite the resulting amino alcohols being interesting synthons for the construction of pharmaceutically relevant structures^[20].

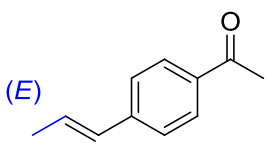
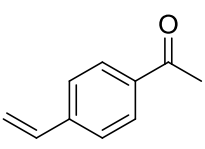
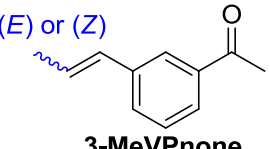
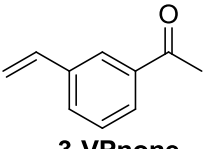
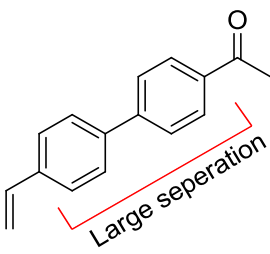
(a) vinyl acetophenone derivatives	(b) Increase the distance between functionalities
<div style="display: flex; justify-content: space-around; align-items: center;"> <div style="text-align: center;">  <p>(E) 4-E-MeVPnone</p> </div> <div style="text-align: center;">  <p>4-VPnone</p> </div> </div> <div style="display: flex; justify-content: space-around; align-items: center; margin-top: 20px;"> <div style="text-align: center;">  <p>(E) or (Z) 3-MeVPnone</p> </div> <div style="text-align: center;">  <p>3-VPnone</p> </div> </div>	 <p>4-VBPnone</p>

Table IV-1 Identifying two main categories (a, and b) of the selected vinyl acetophenone derivatives. (a) both functionalities are separated by one phenyl ring, and a methyl group is inserted on the vinyl moiety, (b) Increasing the distance between both functionalities. These substrates will be evaluated for the copper-catalyzed cascade process by our helical system.

The first objective is to achieve high levels of enantioselectivity for both reaction steps (hydrosilylation/hydroamination), in order to get one major stereoisomer in acceptable yield. Once the stereoisomers that do not require any inversion of the catalyst's enantiomeric state will be obtained (Figure IV-1, **1 & 2**), one can then identify three challenges to access the other two stereoisomers (Figure IV-1, **3 & 4**):

- (i) Substrate functionalities (vinyl, and carbonyl) must react sequentially not concomitantly. It can be anticipated that reaction conditions will be helpful to achieve this goal. These conditions include reaction temperature, knowing that hydrosilylation reactions are able to proceed at low temperatures, while hydroamination reactions usually require higher reaction temperatures. Time and order of addition of the reactants are additional factors that can be considered to control the chemo-selectivity of the catalytic system.

- (ii) Chirality amplification of the supramolecular helices must be at work in the BTA helical catalysts. It is essential that helical BTA catalysts embedding mixture of optically-pure monomers provide optimal levels of product stereoselectivity
- (iii) The stereochemical switch must be fast: *i.e.* the handedness of the helices must be inverted rapidly during the catalytic process.

Our effort towards accessing the four stereoisomers of the amino alcohol formed by a cascade copper-catalyzed hydrosilylation/hydroamination reaction of vinyl acetophenone derivatives is summarized in this chapter.

IV.2. Hydrosilylation of different vinyl acetophenone derivatives with supramolecular helical BTA catalysts.

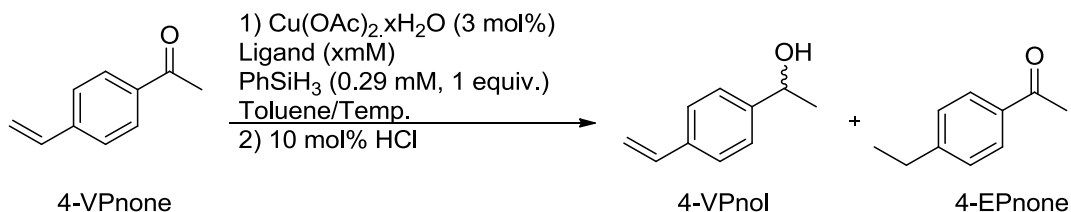
Selecting the best substrate for evaluation in the cascade reaction requires studying each catalytic step alone. For this purpose, hydrosilylation step was first evaluated alone for each substrate under different reaction conditions. These conditions included testing different BTA ligands, BTA esters, metal precursors, silane reagents and varying the reaction temperature . For all investigations, the catalytic system was prepared as followed: BTA ligand and copper source were dissolved in THF, a solvent in which BTA molecules are dissociated which facilitates the formation of the copper coordination complex. Then, THF was removed under vacuum and replaced by an apolar solvent (toluene or methylcyclohexane), a solvent which promotes the assembly of BTA molecules into hydrogen-bonded helical stacks.

All vinyl acetophenone substrates (Table IV-1) were synthesized according to the same procedure, and obtained in yields ranging between 40% and 70%, except for **4-VBPnone** (13% yield). All these substrates were characterized by NMR analyses (see Annex subsection **IV.8.j**) and stored under at low temperature to prevent their polymerization.

Preliminary FT-IR studies (Figure S.IV-1, Annex) were also conducted with the aim of probing the stability of BTA co-assemblies in presence of **3-VPnone**. BTA system composed of **BTA-pPPh2** coordinated to $[Cu(OAc)_2 \cdot xH_2O]$ was selected, and the results surmised that **3-VPnone** does not significantly modify the helical assemblies formed. Selected NMR and HPLC spectra are presented in the (Annex, subsections: **IV.8.h**, and **IV.8.i**)

IV.2.a. Hydrosilylation of 4-VPnone and 4-E-MeVPnone.

4-VPnone. Different parameters were studied for the hydrosilylation reaction: i) Nature of ligand: DTBM-(*R*)-Segphos was chosen as ligand to represent the molecular covalent system, and thus to compare its reactivity with the supramolecular system, ii) ligand concentration, and iii) reaction temperature. Experiments were carried out overnight in toluene in presence of PhSiH₃ as silane reagent. The reaction scheme and catalytic results are shown in Table IV-2.



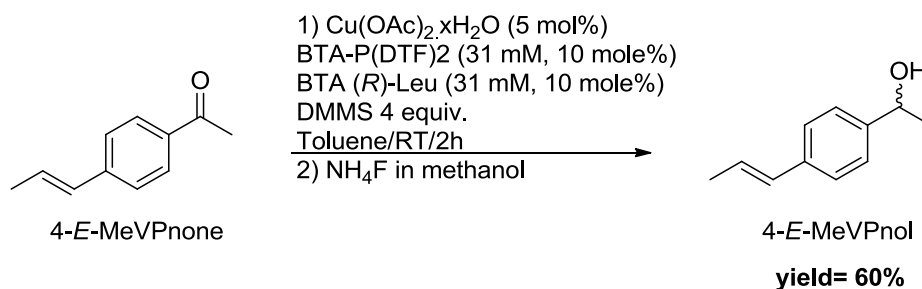
Entry	Ligand	[Ligand]	Temperature	Observation
1	DTBM-(<i>R</i>)-Segphos ^[a]	16.9 mM	RT	Gel, no 4-VPnol
2	DTBM-(<i>R</i>)-Segphos	16.9 mM	RT	Gel, no 4-VPnol
3	DTBM-(<i>R</i>)-Segphos	8.45 mM	RT	Gel, no 4-VPnol
4	DTBM-(<i>R</i>)-Segphos	8.45 mM	-60°C	Gel, no 4-VPnol
5	BTA-pPPh2	16.9 mM	RT	4-VPnol (traces)/4-EPnone
6	BTA-pPPh2	16.9 mM	-60°C	4-VPnol (traces)/4-EPnone

Table IV-2 Conditions : 4-VPnone (0.17 mmole, 1eq), Cu(OAc)₂.xH₂O (3 mol%), PhSiH₃ (1.0 eq), toluene (500 μL). [a] Reaction performed in THF.

Surprisingly, with DTBM-(*R*)-Segphos, the solution immediately turned into a strong yellow gel after the addition of phenyl silane, which prevents stirring (Figure S.IV-2, Annex). The same observation was found when THF was replaced by toluene (entry 2, Table IV-2), or when the ligand concentration (entry 3, Table IV-2), or reaction temperature were lowered (entry 4, Table IV-2). No traces of 4-VPnol as well as other products could be identified by ¹H NMR spectroscopy. We attributed this behavior to polymerization of the vinyl function, a side reaction that probably also occurs during the hydroamination of styrene with the BTA catalyst (Chapter II) but appears to be exacerbated with 4-VPnone. Unlike, DTBM-(*R*)-Segphos, no gel formation was detected with BTA-pPPh2 as ligand (entries 5 and 6, Table IV-2) but only traces of 4-VPnol were found by ¹H NMR spectroscopy. Signals attributed to 4-EPnone were detected

in larger amount which seems to indicate that for this substrate vinyl reduction is preferred over ketone reduction. We then investigated whether the polymerization reaction can be suppressed by adding a methyl group to the vinyl function.

Preliminary investigations were carried out with **4-E-MeVPnone**. For this purpose, **BTA-P(DTF)2** has been selected as a BTA ligand in presence of DMMS as silane reagent, and **BTA (R)-Leu** as chiral co-monomer in toluene at RT for 2 hours. For reaction scheme and catalytic results see Scheme IV-1.



Scheme IV-1 Conditions : **4-E-MeVPnone** (0.25 mmole, 1eq), Cu(OAc)₂.xH₂O (5 mol%), BTA-P(DTF)₂ (10 mol%), BTA (R)-Leu (10 mol%), DMMS (4.0 eq), toluene (800 μL). Yield was estimated according to an internal standard by ¹H NMR (DMA).

The desired product **4-E-MeVPnol**⁷ was obtained with 60% yield, and full conversion of substrate was noticed. Interestingly, no side product was detected. It is likely that polymerization also occurs to some extent but it was not detected. Thus, addition of methyl group on the vinyl moiety increased the stability of the substrate against polymerization or unfavored reduction.

IV.2.b. Hydrosilylation of 3-VPnone and 3-MeVPnone.

IV.2.b.i. Substrate : 3-VPnone

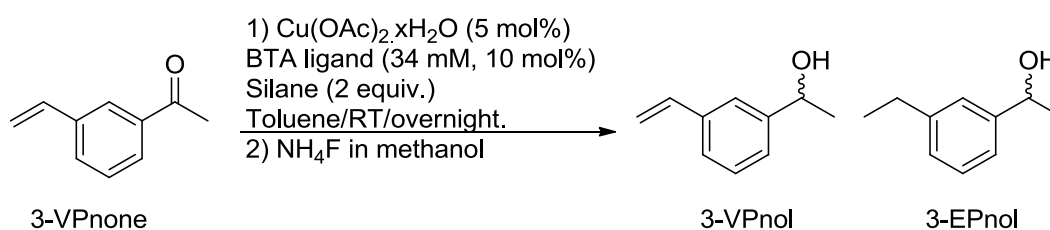
Preliminary screening studies were performed in order to determine if copper based BTA helical supramolecular catalysts were able to catalyze the hydrosilylation of **3-VPnone**. For this purpose, different BTA families were tested under different conditions, in order to see the effect of ligand structure on the efficiency of the catalytic reaction. Also, mixtures between the achiral BTA ligand and an enantiopure comonomer (**BTA Leu** or **BTA Cha**) in 1:1 ratio were

⁷ ee for **4-E-MeVPnol** was not determined since the product was engaged in the hydroamination step (HA) without further purification (see section IV.3.c)

evaluated, in order to see if their helical co-assemblies are able to transfer efficiently their chirality to copper catalytic centers.

1) Evaluation of the hydrosilylation step in absence of chiral co-monomer.

Firstly, different BTA ligands and silane reagents were screened. All reactions were carried out overnight at room temperature in toluene. For reaction scheme and catalytic conditions see Table IV-3. Very low yields in **3-VPnol** (1-6%) were obtained with all our BTA ligands except for **BTA-P(DTF)2** (entry 6, Table IV-3) for which a 32% yield in **3-VPnol** was obtained. **3-EPnol** was detected to a similar extent (2-6%) for all BTA ligands.



Entry	Ligand / Silane	Conversion % ^[a]	Yield 3-VPnol % ^[a]	Yield 3-EPnol % ^[a]
1	BTA-pPPh2 / PhSiH ₃	70%	6%	6%
2	BTA-pPPh2 / DMMS	67%	1%	0%
3	BTA-pPPh2 / DEMS	75%	2%	4%
4	BTA-P(Xyllyl)2 / DEMS	92%	2%	1%
5	BTA-P(DTBM)2 / DEMS	78%	5%	4%
6	BTA-P(DTF)2 / DEMS	83%	32%	3%
7	BTA-BPPH / DEMS	75%	9%	3%
8	BTA-P(Tolyl)2 / DEMS	90%	2%	1%
9	BTA-P(DMM)2 / DEMS	92%	2%	2%
10	DTBM-(R)-Segphos ^[b] / DEMS	100%	50%	11%

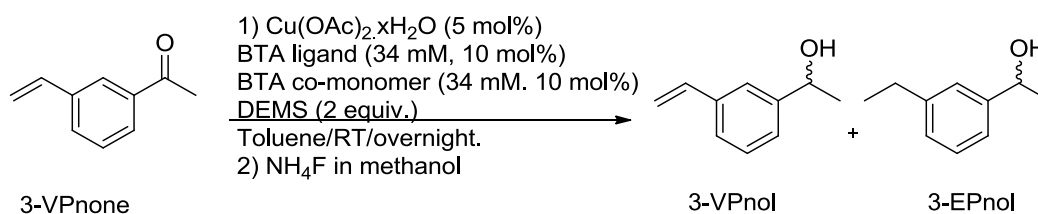
Table IV-3 Conditions : **3-VPnone** (0.17 mmole, 1.0 equiv.), Cu(OAc)₂.xH₂O (5 mol%) , BTA Ligand (10 mol%), Silane (2.0 equiv.), toluene (500 μL). [a] Conversion and yield were estimated according to an internal standard by ¹H NMR (DMA). [b] Reaction is carried out in THF (500 μL).

The formation of **3-EPnol** likely occurs through the reaction of alkyl copper intermediate with a protic species as mentioned in the previous chapter for styrene (**Chapter III**). Better but not maximal yield (50%) was obtained with **DTBM-(R)-Segphos** (entry 10, Table IV-3), which indicates that even for this ligand the reduction (11% yield of **3-EPnol**) and polymerization

reactions of the vinyl bond are not suppressed. We speculated this low yield is in part due to solubility issues, especially for the **copper-BTA-P(DTF)2** complex which appears to be moderately soluble in toluene. For this purpose, we decided to reinvestigate these systems in presence of a chiral BTA co-monomer which is supposed to both improve the solubility of the catalyst and provide a chiral bias for the catalytic reaction.

2) Evaluation of the hydrosilylation step in the presence of chiral co-monomer.

The same ligands were tested again in presence of **BTA Leu** or **BTA Cha** as an enantiopure BTA co-monomers and DEMS as a silane reagent. For reaction scheme and catalytic conditions see Table IV-4.



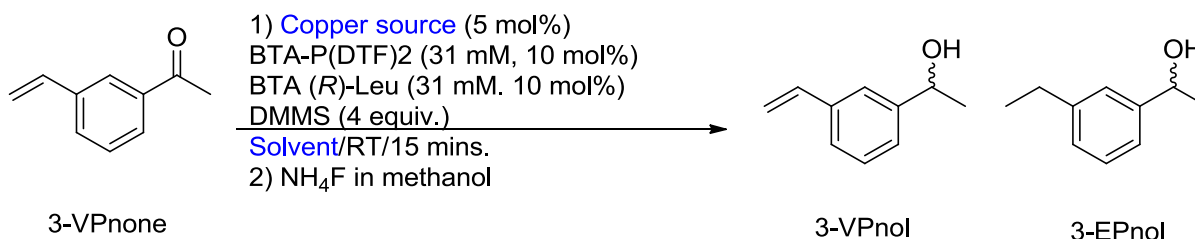
Entry	BTA ligand	Co-monomer	Conversion % ^[a]	Yield of 3-VPnol % ^[a]	Yield of 3-EPnol % ^[a]	ee % ^[b]
1	BTA-pPPh2	BTA (R)-Leu	98%	5%	6%	Nd
2	BTA-P(Xylyl)2	BTA (R)-Leu	87%	20%	19%	Nd
3	BTA-P(DTBM)2	BTA (R)-Leu	72%	15%	17%	Nd
4	BTA-P(DTF)2	BTA (R)-Leu	100%	38%	3%	81%
5	BTA-P(DTF)2	BTA (S)-Cha	100%	40%	6%	-76%
6	BTA-P(DTF)2 ^[c]	BTA (R)-Leu	66%	50%	16%	78%
7	BTA-BPPh	BTA (R)-Leu	40%	7%	3%	Nd
8	BTA-P(Tolyl)2	BTA (R)-Leu	27%	3%	traces	Nd

Table IV-4 Conditions : **3-VPnone** (0.17 mmole, 1eq), Cu(OAc)₂.xH₂O (5 mol%) , BTA Ligand (10 mol%), BTA co-monomer (10 mol%), DEMS (2.0 eq), toluene (500 μL). [a] Conversion and yield were estimated according to an internal standard by ¹H NMR (DMA). [b] % ee determined by HPLC, conditions. [c] Reaction carried out at -40°C with **BTA leu** as co-monomer. Nd= not determined.

Reaction yields and substrate conversions were slightly improved when a BTA co-monomer was added. Substrate conversion reached 100% and yield of desired alcohol increased up to 40% with the mixture composed of **BTA-P(DTF)2** and **BTA (S)-Cha** (entries 4, and 5 Table IV-4). **EPnol**

was again observed to some extent. Lowering the reaction temperature to -40°C with **BTA-P(DTF)2** decreases the conversion (66%) but suppresses the polymerization reaction since **3-VPnol** (50%) and **3-EPnol** (16%) account for all formed products (entry 6, Table IV-4). Interesting *ee* values were obtained with **BTA-P(DTF)2**: slightly higher *ee* was obtained with **BTA (R)-Leu** (81%) compared to **BTA Cha** (76%) co-monomer (entries 4, and 5 Table IV-4).

The temperature does not have a significant effect on the *ee* value obtained with the **BTA-P(DTF)2/BTA Leu** mixture. Therefore, the formed helical co-assemblies are able to transfer efficiently their chirality to copper catalytic centers. Considering the encouraging result obtained with **BTA-P(DTF)2/BTA (R)-Leu** system, it was interesting to check whether better yields could be obtained with different metal precursors and solvent. For this purpose, we selected Cu(II)-i-butyrate and methylcyclohexane (MCH) as new parameters to be tested with **BTA-P(DTF)2/BTA (R)-Leu** mixture in presence of DMMS as silane reagent. For reaction scheme and catalytic results see Table IV-5.



Entry	Metal precursor	Solvent	Conversion % ^[a]	Yield of 3-VPnol % ^[a]	Yield of 3-EPnol % ^[a]	<i>ee</i> % ^[b]
1	$\text{Cu}(\text{OAc})_2 \cdot x\text{H}_2\text{O}$	Toluene	100%	41 %	3%	81%
2	Cu(II)-i-butyrate	Toluene	100%	60%	3%	65%
3	$\text{Cu}(\text{OAc})_2 \cdot x\text{H}_2\text{O}$	MCH	100%	62%	10%	59%
4	Cu(II)-i-butyrate	MCH	100%	76%	6%	58%

Table IV-5 Conditions : **3-Vpnone** (0.17 mmole, 1 equiv.), Copper source (5 mol%), BTA-P(DTF)2 (10 mol%), BTA (R)-Leu (10 mol%), DMMS (4.0 eq), solvent (500 μL). [a] Conversion and yield were estimated according to an internal standard by ^1H NMR (trimethoxybenzene). [b] % *ee* determined by HPLC.

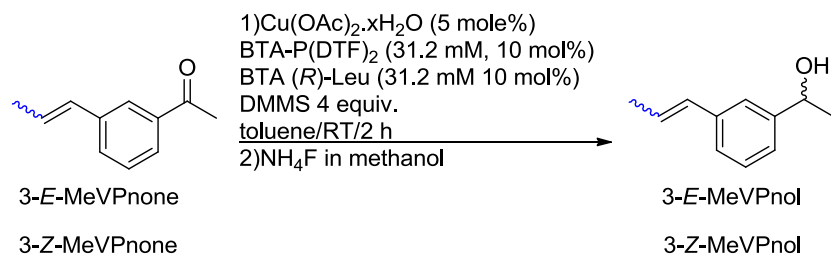
Yields of **3-VPnol** were improved by *ca.* 20% in both solvents when Cu(II)-i-butyrate was utilized instead of $\text{Cu}(\text{OAc})_2 \cdot x\text{H}_2\text{O}$ (compare entry 2 to 1, and 3 to 4, Table IV-5), but *ee* values were *ca.* 20% lower with Cu(II)-i-butyrate and MCH (compare entry 2 to 1, and 3 to 4, Table IV-5).

Reactions carried out in MCH yielded **3-VPnol** with higher yields than in toluene (compare entry 3 to 1, and 4 to 1, Table IV-5) but at expense of a reduced selectivity for both copper sources.

The improved yields with Cu(II)-i-butyrate and MCH are consistent with the fact that side reactions (reduction and polymerization of the vinyl function) are minimized under these conditions, similarly to what is observed for the HA of styrene (**Chapter II**). It is important to note that with this improvement the maximal yield is of 76%. The lower enantioselectivity might be attributed to a slightly different environment of the copper center in MCH and when iso-butyrate anion is present in the coordination sphere. Anyway, the obtained results make it interesting to proceed with this substrate into the hydroamination reaction (see section **IV.3.a**).

IV.2.b.ii. Substrates : **3-E-MeVPnone** and **3-Z-MeVPnone**.

Anticipating that the **Z** stereoisomer will react faster in the hydrocupration step, we tested both the **Z** and **E** isomers of **3-MeVPnone**. For reaction scheme and catalytic results see Table IV-6.



Entry	Substrate	Conversion % ^[a]	Yield % ^[a]	ee % ^[b]
1	3- <i>E</i> -MeVPnone	100%	80%	84%
2	3- <i>Z</i> -MeVPnone	100%	65%	Nd.

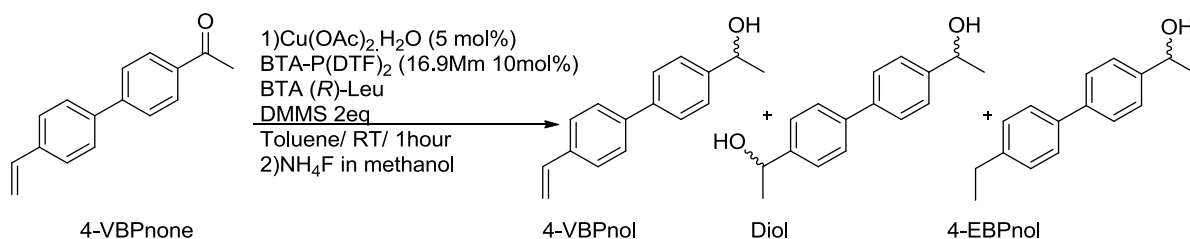
Table IV-6 Conditions : **3-MeVPnone** (0.25 mmole, 1eq), Cu(OAc)₂.xH₂O (5 mol%), BTA-P(DTF)₂ (10 mol%), BTA (*R*)-Leu (10 mol%), DMMS (4.0 eq), toluene (800 μL). [a] yield was estimated according to an internal standard by ¹H NMR (DMA). [b] % ee determined by chiral HPLC.

Hydrosilylation step worked very efficiently, **3-E-MeVPnol** was obtained with nearly 80% yield, and 84% ee (entry 1, Table IV-6). A lower yield was detected for **3-Z-MeVPnol** but this probably related to an uncertainty error of ±10% accompanied with ¹H NMR shimming in this specific case. The formation of the side product with the reduced vinyl function **3-MeEPnol** was not detected for both stereoisomers. This result was encouraging to select this substrate for the second step, *i.e.* hydroamination of the vinyl moiety (see section **IV.3.b**).

IV.2.c. Hydrosilylation of Substrate : 4-VBPnone.

Hydrosilylation of **4-VBPnone** was conducted with **BTA-P(DTF)2** and **BTA Leu** as BTA monomers and DMMS as silane reagent, at RT overnight in toluene. For reaction scheme and catalytic conditions see Table IV-7.

A very low yield of **4-VBPnol** was obtained (26%), which makes its isolation from the crude mixture impractical. By scrutinizing the ^1H NMR spectrum of the crude reaction mixture we were able to identify two side products: the product with both reduced ketone and vinyl functions (**4-EBPnol**) and more surprisingly 1,1'-([1,1'-biphenyl]-4,4'-diyl)diethanol (abbreviated as **Diol**, scheme of Table IV-7). The presence of the latter compound indicates that the vinyl function has been hydroxylated. This constitutes an unusual reactivity for the alkyl copper intermediate which might have been trapped by water or acetate anion present in the reaction medium. However, the low yield obtained for the hydrosilylation step prevents further investigation of this substrate in the cascade reaction.



Conversion of 4-VBPnone %^[a]	Yield of 4-VBPnol %^[a]	Yield of Diol%^[a]	Yield of 4-EBPnol%^[a]
98%	26%	15%	12%

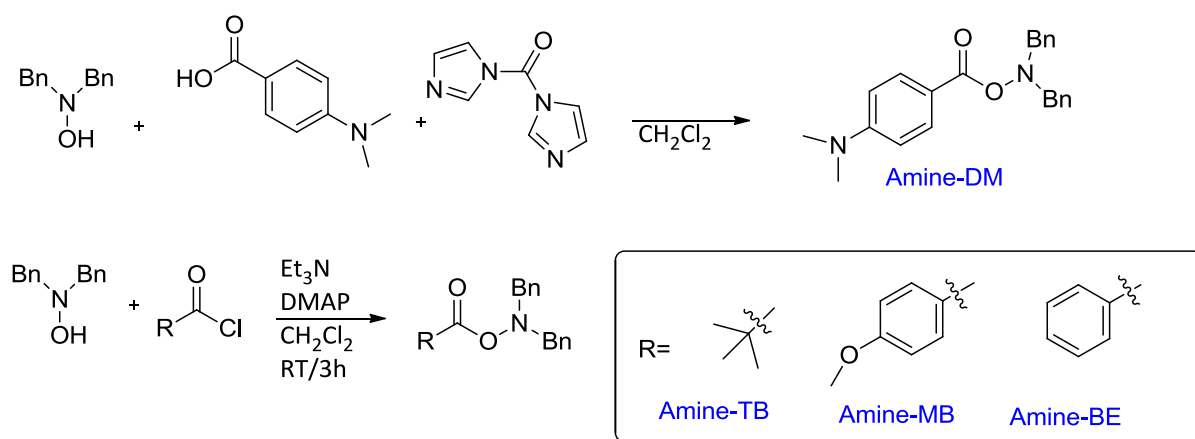
Table IV-7 Conditions : **4-VBPnone** (0.112 mmole, 1eq), $\text{Cu}(\text{OAc})_2 \cdot \text{xH}_2\text{O}$ (5 mol%), BTA-P(DTF)_2 (10 mol%), BTA (R)-Leu (10.1 mol%), DMMS (2.0 eq), toluene (500 μL). [a] yield was estimated according to an internal standard by ^1H NMR (DMA).

IV.2.d. Conclusion.

The hydrosilylation of **4-E-MeVPnone** and **3-VPnone** proceeds with decent yields and good enantioselectivities with helical co-assemblies composed of **BTA-P(DTF)2** and **BTA Leu** (or **BTA Cha**). Improvement of the reaction yield was made by using Cu(II)-i-butyrate and **MCH** instead of copper acetate and toluene.

IV.3. Preliminary tests for the cascade hydrosilylation/hydroamination reaction of 3-VPnone, 3-MeVPnone and 4-MeVPnone.

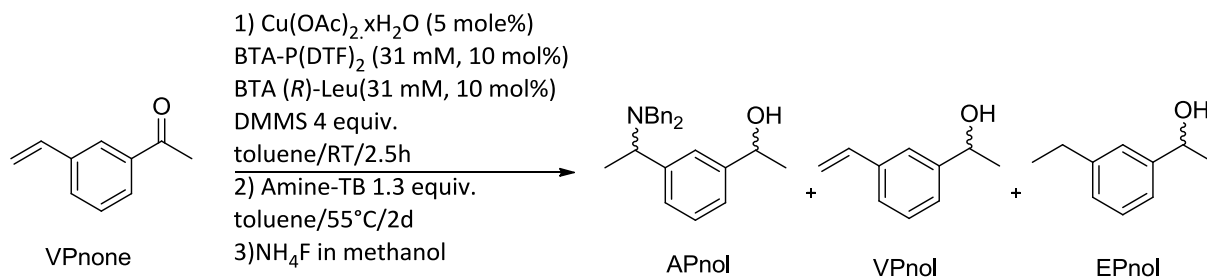
Our cascade reaction consists of two steps, a hydrosilylation followed by hydroamination. The latter reaction requires an amine electrophile. Different amine electrophiles were synthesized according to reported procedures^[21,22] (Scheme IV-2). The aim behind synthesizing different structures of amine electrophiles is to modulate their stability and reactivity. According to Buchwald and coworkers^[21], the more electron rich amine electrophiles are the less prone to direct reduction by the Cu-H species.



Scheme IV-2 Different amine electrophiles with different structures.

IV.3.a. Evaluation of the cascade process for 3-VPnone.

Hydrosilylation reaction was carried at RT (enantioselectivity of this step will be described as ee1) then the amine electrophile was added and the hydroamination reaction is carried out at 55°C (enantioselectivity of this step will be described as ee2/ee2' see Scheme IV-3). Initial conditions were set as follows: **BTA-P(DTF)2** and **BTA (R)-Leu** in equimolar amount, *i.e.* a fraction of sergeant in the assemblies equal to 0.5 (fs= 0.5 (R)), DMMS as the silane precursor, and pivaloyl amine (**Amine-TB**, 1.2 equiv.) as the amine electrophile.



Entry	Yield % of 3-APnol ^[a]	Yield % of 3-VPnol ^[a]	Yield % of 3-EPnol ^[a]	Major Si. ^[c] /%	ee _{tot} % / dr.	ee1/ee2/ee2' % ^[d]
1	31%	6%	6%	(-,+), 68 %	90 / 2.31	62 / 64/ 64

Table IV-8 Conditions : **3-VPnone** (0.5 mmole, 1eq), Cu(OAc)₂.xH₂O (5 mol%), BTA-P(DTF)₂ (10 mol%), BTA (*R*)-Leu (10 mol%), DMMS (4.0 eq), amine-TB (1.3 eq), toluene (500 μL). ee1: *ee* for hydrosilylation step, ee2: *ee* of hydroamination step, dr: diastereoisomeric ratio. [a] Yields estimated by ¹H NMR acc. to an IS (DMA). [c] Major stereoisomer is represented as (sign^{alcohol}, sign^{amino}). [d] With ee1 positive [negative] when the (-) enantiomer [(+)enantiomer, resp.] is in majority. With ee2 positive [negative] when the (+) enantiomer [(-)enantiomer, resp.] is in majority.

Yields were estimated according to an internal standard (DMA) by ¹H NMR, and *ee* values were determined by chiral HPLC. For reaction scheme and catalytic results see Table IV-8.

Using the supramolecular BTA catalyst, the desired amino alcohol **3-APnol** was obtained with 31% yield (entry 1, Table IV-8). Intermediate **3-VPnol** and side product **3-EPnol** were detected in similar amounts (6%). The combined yields of **3-APnol** and **3-VPnol** (37%) are in agreement with the yields in **3-VPnol** found in the aforementioned hydrosilylation experiments. This indicates that under these conditions the hydroamination of the vinyl bond occurs selectively. The next step was to determine the stereoselectivity of the cascade process. As no literature data exists for **3-APnol**, analytical and preparative HPLC experiments were first performed on **3-APnol** obtained from (*rac*)-BINAP in THF (30% yield). HPLC analyses indicated that all stereoisomers were obtained in virtually identical amounts (*ca.* 25%, Figure IV-2). As hydrosilylation and hydroamination had been realized consecutively, this is an indication that the stereo-discrimination process of the second step is independent of the configuration of the stereogenic center generated in the first step. Separation of the four stereoisomers by preparative HPLC allows to determine their relative configuration.

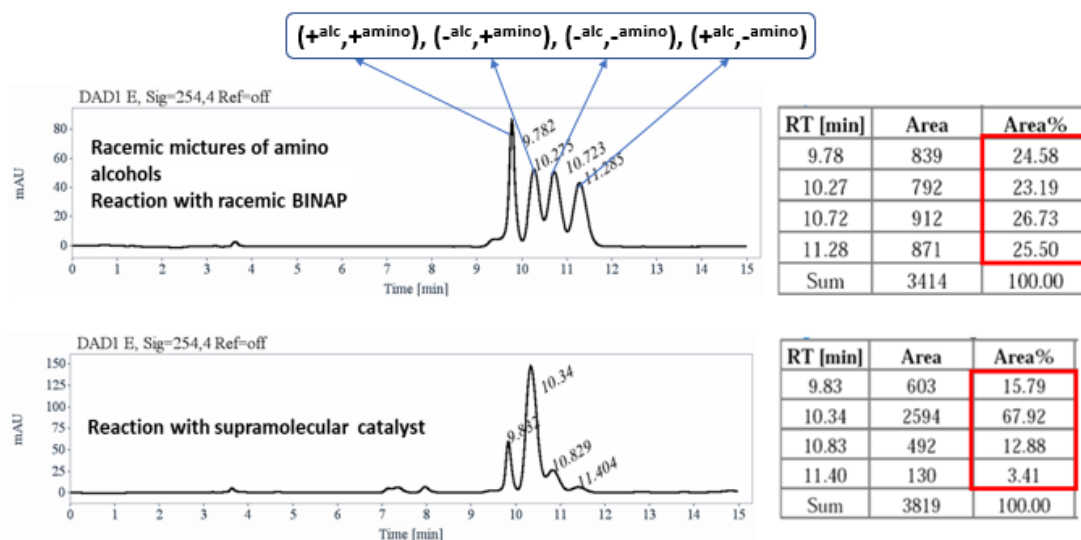
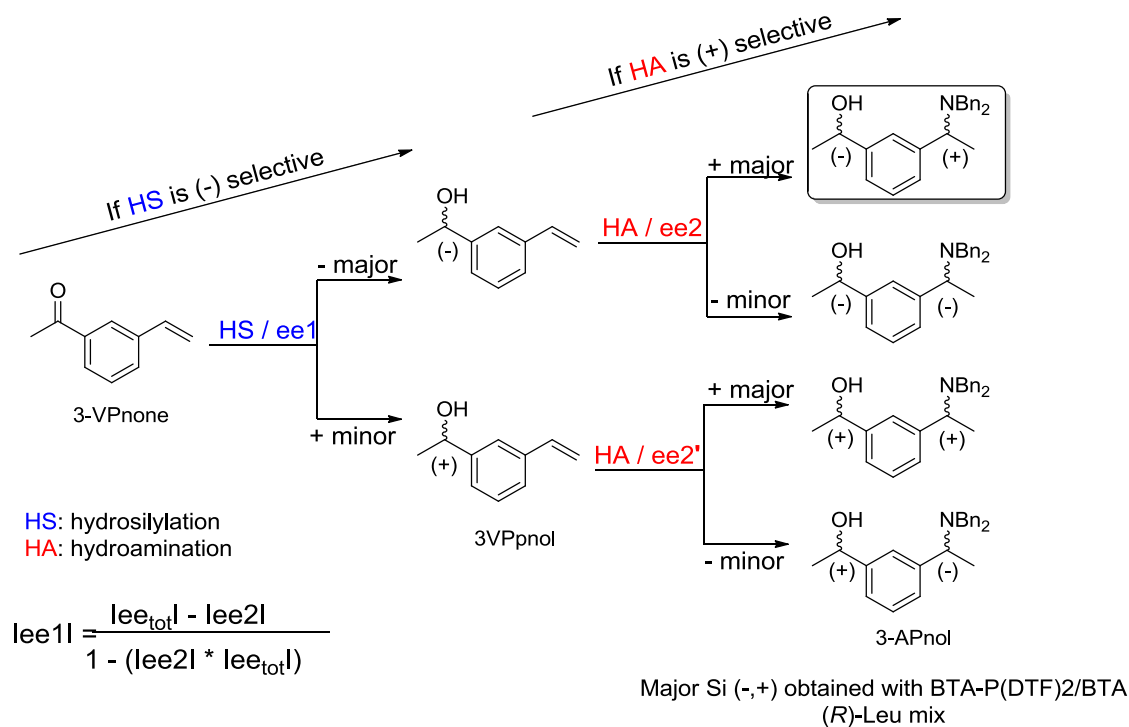


Figure IV-2 Above : Chiral HPLC trace of the racemic mixture of 3-APnol obtained from a reaction carried out with (*rac*)-BINAP ligand. Below: Chiral HPLC trace of 3-APnol obtained from a reaction carried out with supramolecular BTA catalyst (conditions of Table IV-8).



Scheme IV-3 Definition of ee1, ee2, ee2' and eetot regarding the formation of 3-APnol from 3-VPnone by a cascade hydrosilylation/hydroamination reaction.

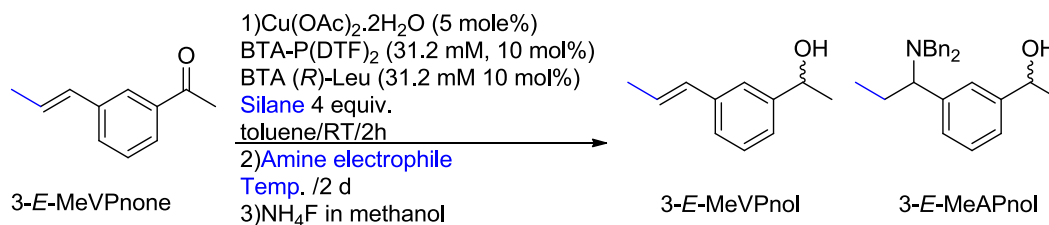
It is important to note that all stereoisomers exhibit identical NMR spectra and diastereomers cannot be separated by column chromatography by our hands (See Annex subsection: **IV.8.f**).

Thus, the stereoselectivity measured on the purified reaction mixture will reflect that truly obtained through the catalytic process. The absolute configuration has not been determined. However, with the help of experiments performed with catalysts of different configurations (*vide infra*, and Annex see subsection: **IV.8.f**), the four stereoisomers eluted with ChiralPak IG column can be attributed as follows: (+^{alc}, +^{amino}), (-^{alc}, +^{amino}), (-^{alc}, -^{amino}), and (+^{alc}, -^{amino}) where the first and second +/- signs correspond to the stereogenic centers connected to the alcohol and amine, respectively (Scheme IV-3). We were pleased to see that the reaction conducted with **BTA-P(DTF)2** and **BTA (R)-Leu** provided 68% of (-^{alc}, +^{amino}) as the major stereoisomer of **3-APnol**. It corresponds to an ee_{tot} and dr values of 90% and 2.31, respectively. ee₂ and ee_{2'}, from (-)-**VPnol** and (+)-**VPnol** respectively, can be directly extracted from the HPLC data and found to be both equal to 64%. The fact that these values are identical corroborates that the two steps of the cascade process are independent with our BTA helical catalyst. Then ee₁ was obtained according to the formula shown in Scheme IV-3 (see the Annex subsection: **IV.8.g** for more details). The determined value of 62% for ee₁ in the cascade process is slightly lower than the one determined from the hydrosilylation reaction under the same conditions (81% ee).

This preliminary result obtained with our two-component BTA system is highly interesting and promising. It showed the ability of our system to catalyze the two reactions in one pot. In addition, high ee_{tot} value was obtained when **BTA (R)-Leu** (fs= 0.5) was utilized as a chiral inducer. Further optimizations will be carried on this system for improving the yield of the reaction (*vide infra*).

IV.3.b. Evaluation of the cascade process on 3-E-MeVPnone and 3-Z-MeVPnone.

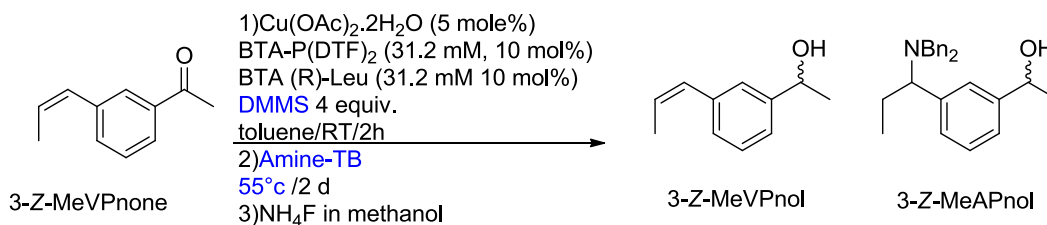
Knowing that the hydrosilylation of **3-E-MeVPnone** proceeds efficiently with our BTA system to yield 80% of **3-E-MeVPnol** with an ee of 84%, the cascade reaction was also assessed for this substrate. In this study, different parameters will be evaluated including the nature the amine electrophile, nature of the silane, and the hydroamination reaction temperature. Conversion was detected by ¹H NMR. For reaction scheme and catalytic results see Table IV-9.



Entry	Amine electrophile	Silane	HA	Conversion of	3-E-MeVPnol % ^[b]	3-E-MeAPnol
			Temperature °C	3-E-MeVPnone %		
1	Amine-TB	DMMS	55°C	100%	~ 80%	Not detected
2	Amine-BE	DMMS	55°C	100%	~ 80%	Not detected
3	Amine-MB	DMMS	55°C	100%	~ 80%	Not detected
4	Amine-DM	DMMS	55°C	100%	~ 80%	Not detected
5	Amine-DM	DEMS	55°C	100%	~ 80%	Not detected
6	Amine-DM	DEMS	80°C	100%	~ 80%	Not detected
7	Amine-DM	DEMS	90°C	100%	~ 80%	Not detected
8 ^[a]	Amine-DM	DEMS	55°C	100%	~ 80%	Not detected

Table IV-9 Conditions : **3-E-MeVPnone** (0.25 mmole, 1eq), Cu(OAc)₂·xH₂O (5 mol%), BTA-P(DTF)₂ (10 mol%), BTA (R)-Leu (10 mol%), Silane (4.0 eq), amine electrophile (1.2 eq), toluene (800 µL). [a] DTBM-(R)-Segphos is used as ligand, solvent: THF. [b] Yield estimated by ¹H NMR acc. to an IS (DMA).

Unfortunately, whatever the tested conditions, no amino alcohol **3-E-MeAPnol** was formed. Changing the nature of amine electrophile, the hydroamination reaction temperature, or the silane had no a significant effect on the final cascade process outcome. Only the intermediate alcohol, **3-E-MeVPnol**, was detected by ¹H NMR (up to 80% yield). Surprisingly, the reaction was not found to proceed neither with **DTBM-(R)-Segphos** ligand in THF (entry 8, Table IV-9). This high stability could be attributed to the configuration of the alkene (*trans*). For this reason, the cascade reaction was also evaluated with **3-Z-MeVPnone** but again no traces of amino alcohol **3-Z-MeAPnol**, was detected (Table IV-10).



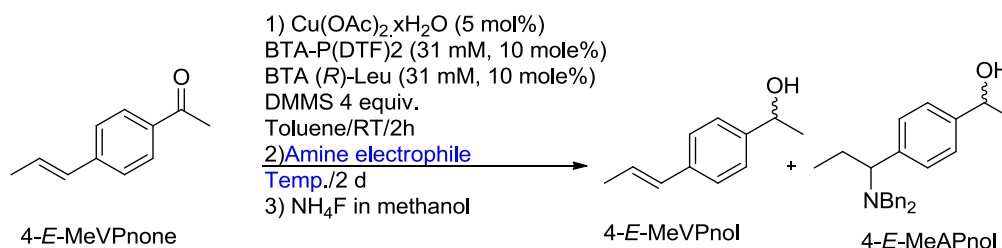
Entry	Conversion of 3-Z-MeVPnone %	3-Z-MeVPnol	3-Z-MeAPnol
1	100%	detected	Not detected

Table IV-10 Conditions : **3-Z-MeVPnone** (0.25 mmole, 1eq), Cu(OAc)₂·xH₂O (5 mol%), BTA-P(DTF)₂ (10 mol%), BTA (*R*)-Leu (10 mol%), DMMS (4.0 eq), amine-TB (1.2 eq), toluene (800 μL).

Modifying the alkene configuration did not really have an impact on the hydroamination reaction outcome. This might be due to a lower reactivity of the vinyl moiety. These substrates were not evaluated further.

IV.3.c. Evaluation of the cascade process for 4-*E*-MeVPnone.

Investigations were carried for **4-*E*-MeVPnone** as the hydrosilylation step with our system was found to proceed cleanly. Different conditions were tested including hydroamination reaction temperature, and nature of the amine electrophile. For catalytic results and reaction scheme see Table IV-11.



Entry	Amine	Hydroamination reaction temp. °C	Conversion %	4- <i>E</i> -MeVPnol	4- <i>E</i> -MeAPnol
1	Amine-TB	55°C	100%	detected	Not detected
2	Amine-DM	90°C	100%	detected	Not detected

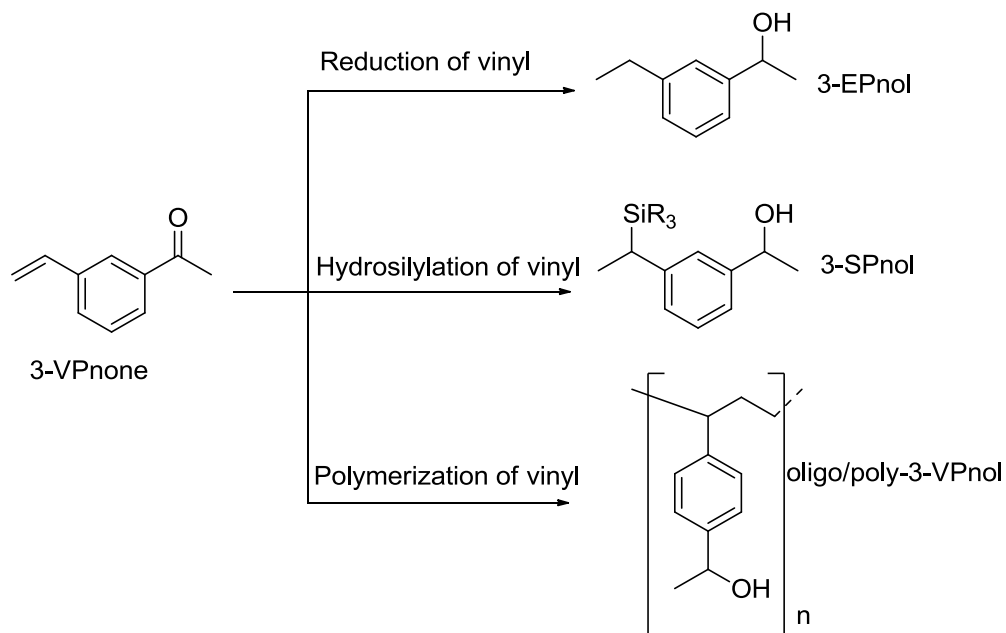
Table IV-11 Conditions : **4-*E*-MeVPnone** (0.25 mmole, 1eq), Cu(OAc)₂·xH₂O (5 mol%), BTA-P(DTF)₂ (10 mol%), BTA (*R*)-Leu (10 mol%), DMMS (4.0 eq), amine electrophile (1.2 eq), toluene (800 μL).

Hydroamination step did not proceed even at higher reaction temperatures, and with a more stable amine electrophile (entry 2, Table IV-11). The reason why the hydroamination of the β-

methyl styrene moieties in **3-MeVPnone** and **4-MeVPnone** did not proceed is not clear to us and accordingly these substrates were not investigated further.

IV.4. Cascade hydrosilylation/hydroamination of 3-VPnone : optimization of reaction conditions.

Under the aforementioned conditions, the hydrosilylation/hydroamination cascade reaction from **3-VPnone** yields **3-APnol** with 31% (NMR yield). The isolated yield is of only 15% after purification over chromatography column. We assume that the low yield in general comes from: i) side reactions involving the vinyl moiety: its reduction (into **3-EPnol**, detected), its hydrosilylation (into **3-SPnol**) and/or its oligo/polymerization (into **oligo-poly-3-VPnol**) (Scheme IV-4).

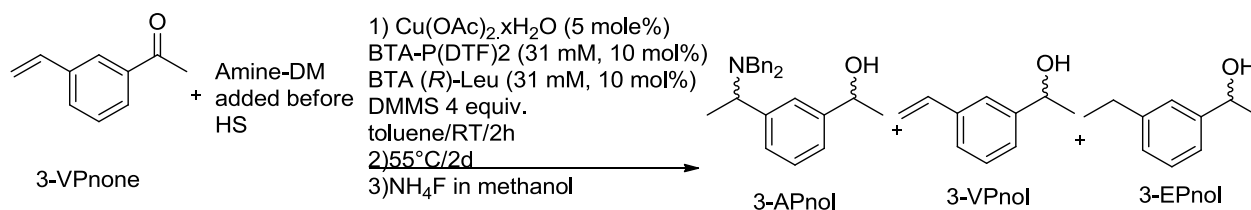


Scheme IV-4 Possible undesired pathways that could lower the yield of **3-APnol**.

The latter two reactions have already been surmised in the hydroamination of styrene (**Chapter III**) performed with BTA helical catalysts and happen to a certain extent during the hydrosilylation of **3-VPnone**. It was also found that the conversion was not completed since intermediate **3-VPnol** was detected. Several parameters were thus varied in order to increase the yield in **3-APnol**.

IV.4.a. Order of addition of the amine electrophile and influence of the reaction temperature.

In the aforementioned conditions, the amine electrophile was added into the catalytic mixture after stirring at RT for an interval time (1 h or 2 h). This procedure was followed for two main reasons. First, to prevent **3-VPnone** from reacting directly with amine electrophile, thus “mimicking” the conditions that will allow to switch the enantiomeric state of the catalyst in between the two steps of the catalytic process. Second, it is known that the amine electrophile decomposes in presence of copper hydride species, thus adding the amine electrophile after the first step is complete presumably limits its decomposition. On contrary, adding the amine electrophile must limit the extent of the side reactions involving the vinyl moiety. We thus compared experiments for which the amine electrophile was added before or after the hydrosilylation step and we tested the possibility of conducting both steps at room temperature. The evolution of reactants/product were tracked by ^1H NMR analysis. For reaction scheme and catalytic results see Table IV-12. The stereoselectivity of this reaction was not determined.



Order of amine addition	Yield of 3-APnol %^[a]	Yield of 3-VPnol %^[a]	Yield of 3-EPnol %^[a]
After HS step ^[b]	31%	6%	6%
Before HS step	60%	5%	traces

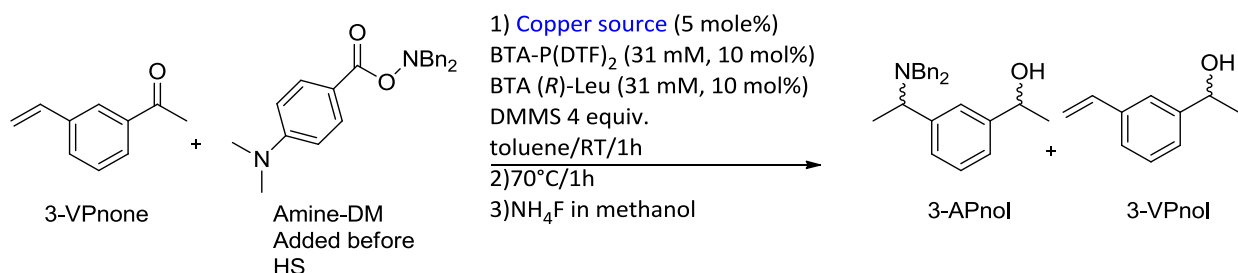
Table IV-12: Conditions : **3-VPnone** (0.5 mmole, 1eq), $\text{Cu}(\text{OAc})_2 \cdot x\text{H}_2\text{O}$ (5 mol%), BTA-P(DTF)2 (10 mol%), BTA (*R*)-Leu (10 mol%), DMMS (4.0 eq), amine-DM (1.3 eq), toluene (500 μL). [a] Yields estimated by ^1H NMR acc. to an IS (DMA). [b] Amine-TB was used instead of amine-DM.

Engaging the amine electrophile before the hydrosilylation step and performing the reaction at room temperature increased the yield of the cascade reaction to around 60% (Table IV-12). These conditions appear appealing for reactions which do not require switching the enantiomeric state of the catalyst. Accordingly, several parameters have been tested to avoid

any overlap between the two reactions of the cascade process. Further screening experiments were thus envisaged to maintain both a high reaction yield, and a high catalyst chemo-selectivity.

IV.4.b. Screening of different metal precursors.

Different copper sources could be used for binding the helical BTA pre-catalyst. For this purpose, different copper sources were selected: CuBr/NaOtBu^[23], CuF₂^[24,25], and Cu(II)-i-butyrate to see whether the nature of copper source would have an impact on the reaction outcome. We kept on following the new procedure which consists in engaging amine-DM at the beginning of the catalytic reaction. For catalytic results and reaction scheme see Table IV-13.



Entry	Copper source	Temp °C	Time	Conv. of 3-VPnone ^[a]	Yield of 3-APnol ^[a]	Yield of 3-VPnol ^[a]
1	Cu(OAc) ₂ .xH ₂ O	RT	1h	100%	— ^[b]	38%
2	CuBr/NaOtBu	RT	1h	51%	6%	0%
3	CuF ₂	RT	1h	0%	0%	0%
4	Cu(II)-i-butyrate	RT	1h	100%	22%	36%
5	CuBr/NaOtBu	70°C	1h	86%	0%	6%
6	CuF ₂	70°C	1h	20%	0%	0%
7	Cu(II)-i-butyrate	55°C	1h	100%	56%	27%
8	Cu(II)-i-butyrate	55°C	3h	100%	63%	28%

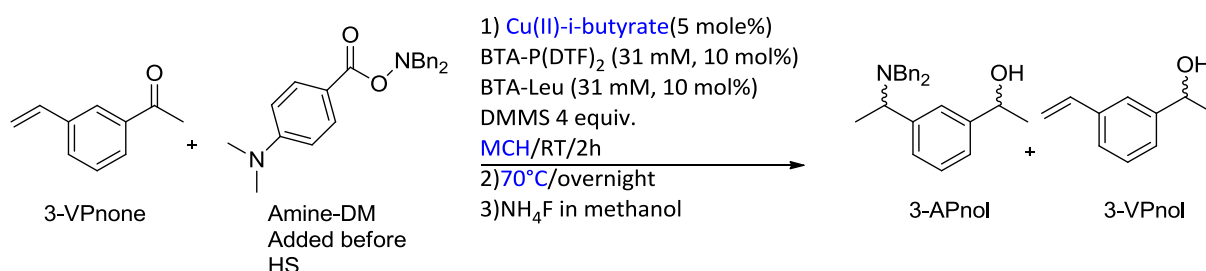
Table IV-13 Conditions : **3-VPnone** (0.5 mmole, 1eq), Copper source (5 mol%), BTA-P(DTF)₂ (10 mol%), BTA (*R*)-Leu (10 mol%), DMMS (4.0 eq), amine-DM (1.3 eq), toluene (500 μL). [a] Yields and conversions estimated by ¹H NMR acc. to an IS (1,3,5-trimethoxybenzene), [b] this experiment was performed without amine electrophile.

The reaction mixture was first left to stir for 1h at RT. At room temperature, far lower reactivity was observed for all tested copper sources relatively to Cu(OAc)₂.xH₂O, except for Cu(II)-i-butyrate. No conversion and modest conversions were observed for CuF₂ and CuBr/NaOtBu,

respectively (entries 2, and 3, Table IV-13). **3-APnol** was only detected for the latter Cu source (6%) (entry 2, Table IV-13). Full conversion was observed for Cu(II)-i-butyrate and interestingly **3-VPnol** predominates over **3-APnol** at room temperature, indicating the hydroamination occurs slowly at room temperature (entry 3, Table IV-13). Increasing the temperature (after stirring 1h at RT) led to an increase in the yield of **3-APnol** only for Cu(II)-i-butyrate (up to 63%) (entry 8, Table IV-13). Performing the reaction with Cu(II)-i-butyrate seems to have a positive impact on the yield of the reaction. It was thus decided to test further this effect in a different solvent, and at a higher hydroamination reaction temperature.

IV.4.c. Optimization of the conditions with Cu(II)-i-butyrate.

The cascade process was launched in methylcyclohexane (MCH) instead of toluene, for 1 h at RT, then the temperature was elevated to 70°C overnight. For reaction scheme and catalytic results see Table IV-14.



Entry	Initial cond.	Yield 3-APnol ^[a]	Yield 3-VPnol ^[a]	Major Si. ^[b] /%	ee _{tot} %/ dr.	ee1/ee2, ee2' ^[c]
1	F _S =0.5 (R)	84%	10%	(-,+), 70 %	93%/2.74	70%/67%/67%
2	F _S =0.5 (S)	84%	10%	(+,-), 69%	92%/2.58	-64%/-69%/-69%

Table IV-14 Conditions : **3-VPnone** (0.5 mmole, 1eq), Cu(II)-i-butyrate (5 mol%), BTA-P(DTF)₂ (10 mol%, 31 mM), fs: fraction of sergeant BTA Leu, DMMS (4.0 eq), amine-DM (1.3 eq), MCH (500 μL). ee1: ee for hydrosilylation step, ee2 and ee2': ee of hydroamination step, ee_{tot} : ee total for major stereoisomer, dr: diastereoisomeric ratio. [a] Yields estimated by ¹H NMR acc. to an IS (1,3,5-trimethoxybenzene). [b] Major stereoisomer is represented as (sign^{alcohol}, sign^{amino}). [c] With ee1 positive [negative] when the (-) enantiomer [(+)enantiomer, resp.] is in majority. With ee2 positive [negative] when the (+) enantiomer [(-)enantiomer, resp.] is in majority.

Under these conditions, the yield in **3-APnol** is increased to 84% (entries 1, and 2, Table IV-14). The combined yields of **3-APnol** and **3-VPnol** (94%) are consistent with a complete selectivity of the vinyl bond towards hydroamination, *i.e.* the aforementioned side reactions have been

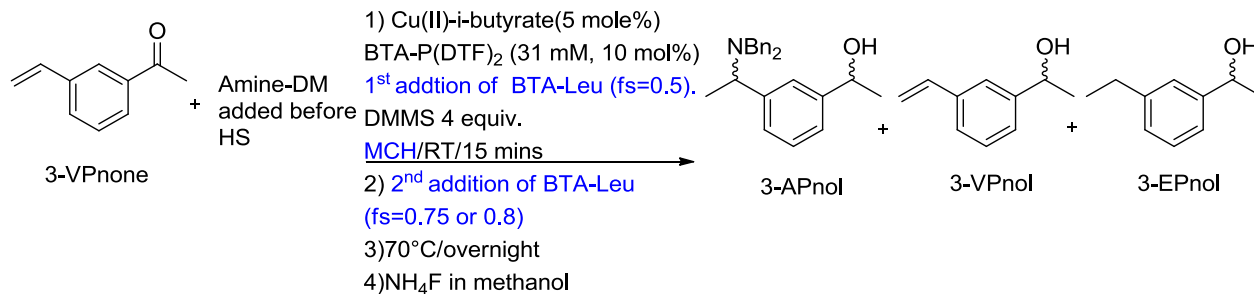
drastically minimized with **BTA (R)-Leu**. The (-,+) isomer represents 70% of the **3-APnol** which translates into $ee_{\text{tot}} = 93\%$ and dr: 2.74 (entry 1, Table IV-14). The first HS step proceeded with $ee_1 = 70\%$, and the second HA step with $ee_2 = 67\%$ (entry 1, Table IV-14). The stereoselectivity of the process under these conditions is similar to the other reported above with $\text{Cu}(\text{OAc})_2 \cdot x\text{H}_2\text{O}$ (Table IV-8). As expected, the reaction performed with **BTA (S)-Leu** yields the (+,-) stereoisomer with identical optical purity. Those conditions are considered optimal and will further be exploited to obtain selectively the (+,+) and (-,-) stereoisomers through inversion of the enantiomeric state in between the two steps of the cascade reaction.

IV.5. Applying the catalytic switch.

The optimized catalytic conditions mentioned in sub-section I.4.c were applied for performing the catalytic switch. Different experiments were launched using **Cu(II)-i-butyrate/BTA-P(DTF)2/BTA Leu** catalytic system for 15 mins at RT, then heated to 70°C overnight in MCH. Amine-DM was engaged at the beginning of the catalytic process. The yield obtained for **3-APnol** was estimated according to an IS (1,3,5-trimethoxy benzene) by ¹H NMR. For reaction scheme and catalytic results see Table IV-15.

With the aim of obtaining (-,-) as the major stereoisomer, the catalytic process was started with $fs=0.5(R)$, to provide (-)-**3-VPnol** and catalytic switch was then applied to end by $fs=0.75$ (33% *ee* for **BTA (S)-leu**) (entry 1, Table IV-15). Unfortunately, according to chiral HPLC separation, the major stereoisomer detected was (-,+) in 46% of the stereoisomer mixture, *i.e.* the major stereoisomer obtained with **BTA (R)-Leu** without performing switch. The fact that (-,+) is obtained as a major stereoisomer indicated that both steps have occurred in the same direction: indeed, *ee*₁ for HS step was = 68%, while *ee*₂ for HA step = 11%. The fact that *ee*₁ is similar to the aforementioned experiments indicates that the first step has occurred with homochiral helices. However, the value of *ee*₂ is lower than that expected even in absence of chirality amplification (*ca.* +35% *ee* for *ee*₂). This can be due to an incomplete incorporation of the added BTA enantiomer to achieve the stereochemical switch, and/or to the fact that the inversion of the handedness of the BTA helices was slower than the hydroamination reaction.

With the aim of potentially increasing the amount of BTA co-monomer incorporated, the amount of **BTA (R)-Leu** was increased in the second step to end by $fs=0.8$ [50% *ee* (R)]. The desired (+,+) stereoisomer was obtained as the major stereoisomer but with a modest content of 46% (entry 3, Table IV-15). For this experiment, the two steps actually proceed in opposite directions (*ee*₁= -67%, *ee*₂ = 11%) but the reached *ee*₂ is far lower than that expected even in absence of chirality amplification (-51% *ee*). The same reasons as above are suspected, incomplete incorporation and/or slow stereochemical switch.



Entry	Initial cond.	Final cond.	Yield 3-APnol ^[a]	Yield 3-VPnol ^[a]	Yield 3-EPnol ^[a]	Major Si. ^[b] / %	ee _{tot} %/ dr.	ee1/ee2, ee2' ^[c]
1	Fs=0.5 (R)	Fs=0.75 [33% ee (S)]	47%	10%	nd	(-,+), 46 %	74%/ 1.16	68%/11%/11%
2	Fs=0.5 (S)	Fs=0.75 [33% ee (R)]	69%	18%	nd	(+,-), 50 %	76%/ 1.32	-66%/-21%/-21%
3	Fs=0.5 (S)	Fs=0.8 [50% ee (R)]	44%	9%	nd	(+,+), 46 %	60%/ 0.87	-67%/11%/11%

Table IV-15 Conditions : **3-VPnone** (0.5 mmole, 1eq), Cu(II)-i-butyrate (5 mol%), BTA-P(DTF)₂ (10 mol%, 31 mM), fs: fraction of sergeant BTA Leu, DMMS (4.0 eq), amine-DM (1.3 eq), MCH (500 μ L). ee1: ee for hydrosilylation step, ee2: ee of hydroamination step, ee_{tot}: ee total for major stereoisomer. [a] Yields estimated by ¹H NMR acc. to an IS (1,3,5-trimethoxy benzene). [b] Major stereoisomer is represented as (sign^{alcohol}, sign^{amino}). [c] With ee1 positive [negative] when the (-) enantiomer [(+)enantiomer, resp.] is in majority. With ee2 positive [negative] when the (+) enantiomer [(-)enantiomer, resp.] is in majority.

IV.6. Probing the chirality amplification properties by Circular Dichroism.

IV.6.a. CD analyses for probing the diluted majority rule effects.

The aforementioned conditions complied the following requirements: i) convenient yields and selectivities with single enantiomeric state helical catalyst, ii) no overlap of the two steps of the cascade process. We next envisaged to test the chirality amplification properties of the BTA helical catalyst. As the chirally-switchable catalyst will be composed of a scalemic mixture of enantiopure co-monomers (**BTA (S/R)-Leu**) and of achiral **BTA-P(DTF)₂** ligand, the chirality amplification properties will be governed by: **i)** the ability of the major enantiomer to impose its chirality to the minor enantiomer and **ii)** the transfer of chirality from the scalemic mixture to

the achiral monomer. Such experiments, in which the enantiomeric monomers are mixed with achiral monomers, are called “diluted majority rule” experiments. BTA cyclohex was selected as an achiral additive because of its ability to dramatically enhance the chirality amplification properties of BTA assemblies as mentioned in **Chapter II**^[26].

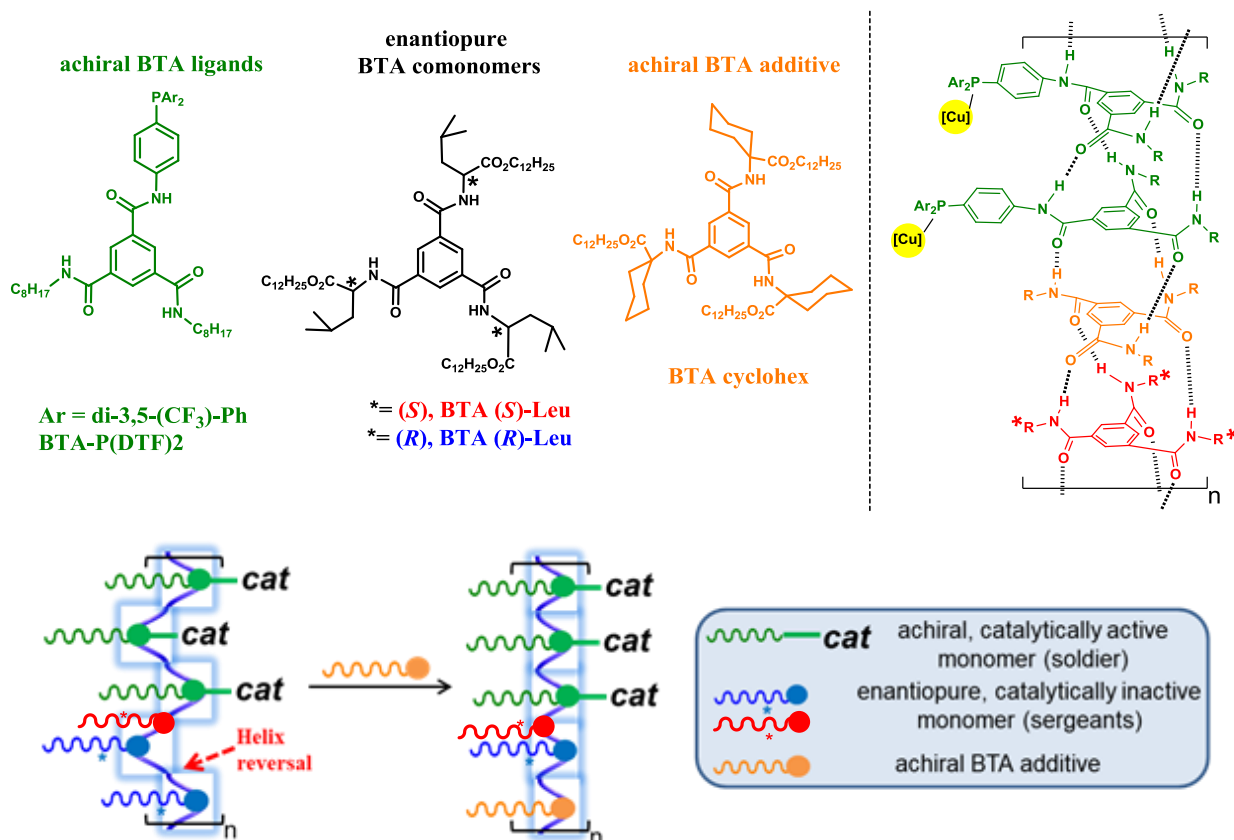


Figure IV-3 Above : Chemical structures of achiral BTA ligand BTA-P(DTF)2, chiral BTA comonomer BTA Leu, and achiral BTA additive BTA cyclohex. Below: schematic representation of the catalytic system with and without additive that shows the effect of BTA cyclohex in reducing the helix reversals and thus, rigidifying the assemblies.

In order to be as close as possible of the aforementioned optimized conditions, circular dichroism (CD) measurements were recorded with/without additive **BTA cyclohex** (31 mM) in two solvents (MCH and toluene) with **BTA-P(DTF)2** (31mM), **Cu(II)-i-butyrate** (15.6 mM) and **BTA Leu** (31 mM, $0 < ee < 100\%$) (Figure IV-3).

It is necessary to note that the Cotton effect centered at 280 nm is mainly attributed to **BTA-P(DTF)2** ligand, since both **BTA (R/S)-Leu** and **BTA cyclohex** show only very weak absorption in

this region. For CD analyses performed at lower BTA ligand concentration [5.8 mM], with and without additive: see the Annex (subsection IV.8.d).

IV.6.a.i. In MCH.

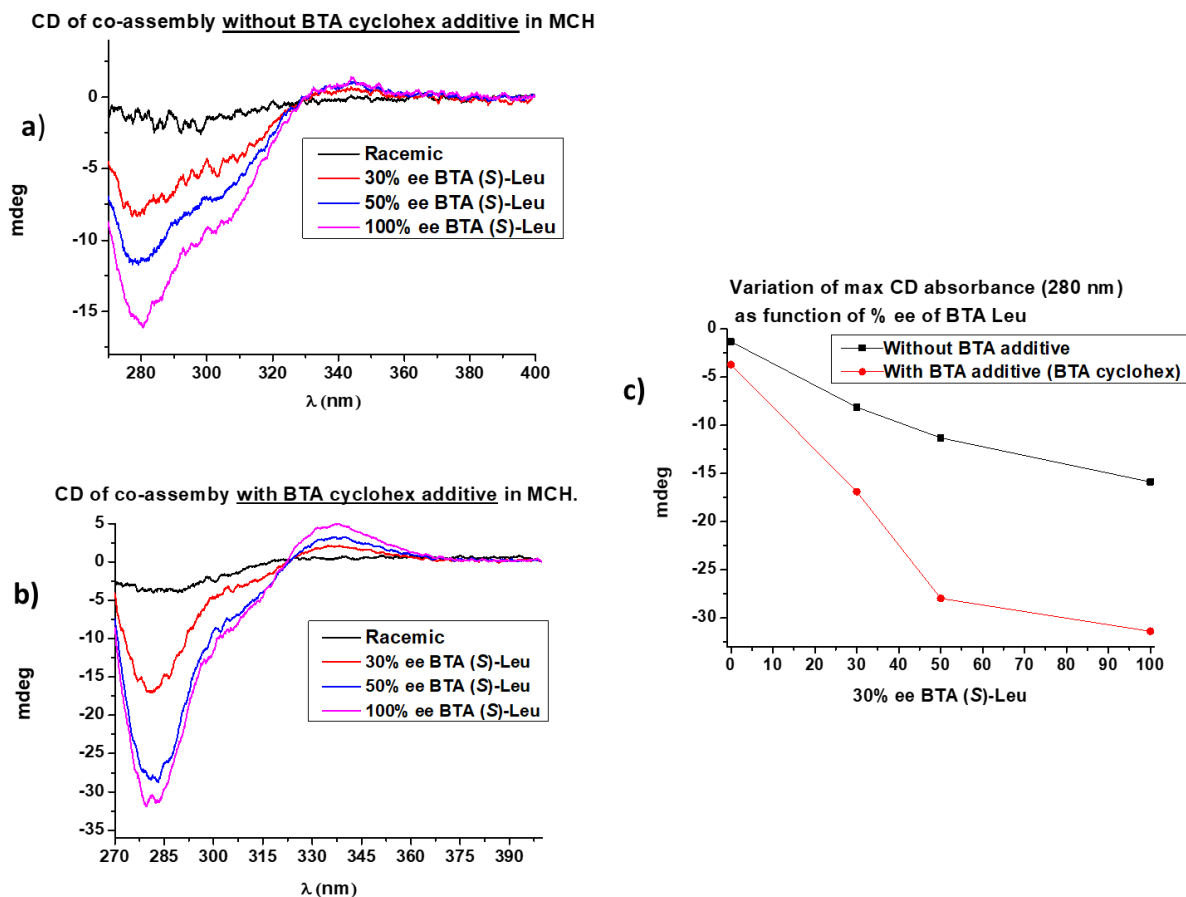


Figure IV-4 Spectra of the diluted majority-rules type experiments for two systems: a) BTA-P(DTF)₂ [31 Mm], Cu(II)-i-butyrate [15.6 mM], BTA Leu [31 mM] with variable ee in MCH, b) Same mixture in presence of BTA cyclohex [31 mM], c) Plot of the max CD absorption values (at $\lambda = 280$ nm) as function of % ee BTA (S)-Leu for both systems.

As shown in (Figure IV-4a, 4c black curve) for the mixture without additive, the negative CD Cotton effect at 280 nm increases linearly when the optical purity in **BTA Leu** increases. This indicates that no chirality amplification occurs in this system, *i.e.* that the optical purity of the BTA helices is proportional to the optical purity of **BTA Leu**. On contrary with additive **BTA cyclohex** (Figure IV-4b, 4c red curve), the negative CD cotton effect at 280 nm increases to

reach the optimal CD value with *ca.* 50% *ee* of **BTA (S)-Leu**⁸. The non-linear increase of the CD value⁹ indicates that chirality amplification occurs in this system. However, a scalemic excess superior to 50% *ee* is required to get the optimal value (Figure IV-4c red curve).

IV.6.a.ii. In toluene.

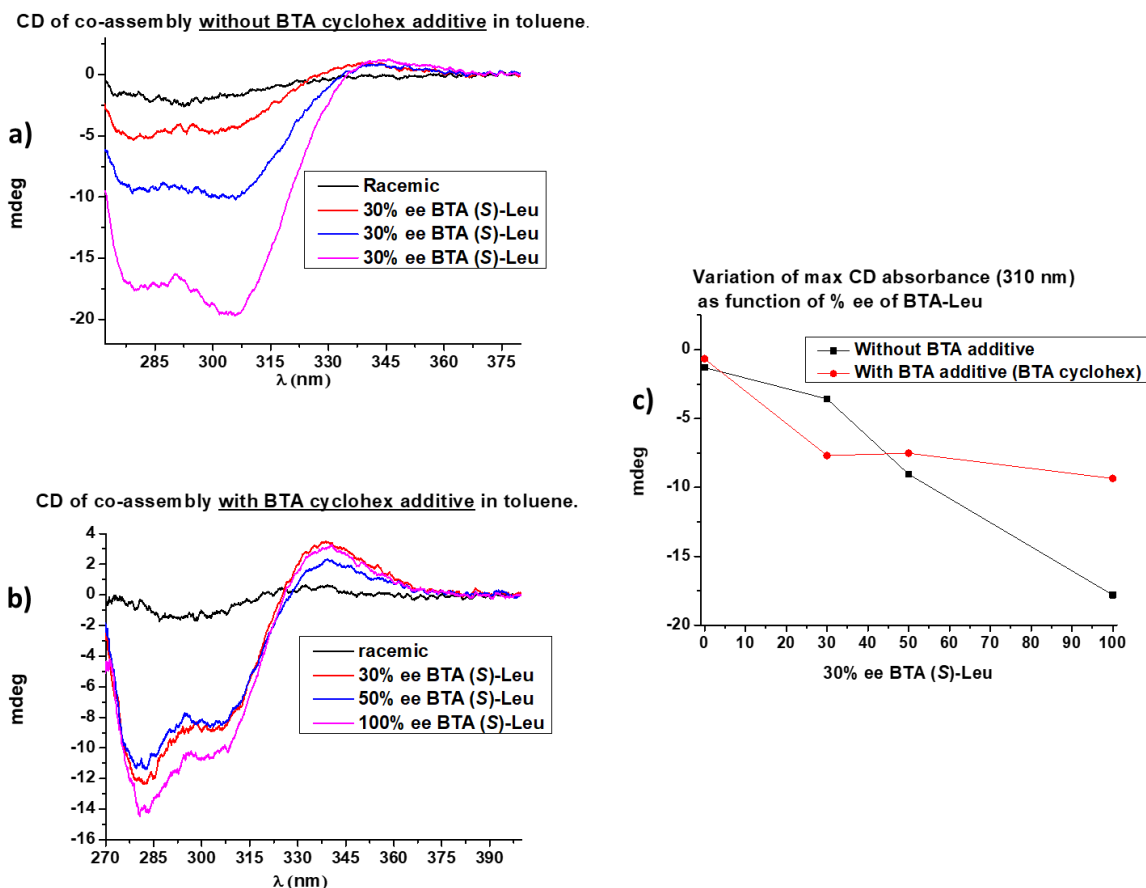


Figure IV-5 Spectra of the diluted majority-rules type experiments for two systems: a) BTA-P(DTF)₂ [31 mM], Cu(II)-i-butyrate [15.6 mM], BTA Leu [31 mM] with varied ee in toluene, b) Same mixture in presence of BTA cyclohex [31 mM], c) Plot of the CD values (at $\lambda = 280$ nm) as function of % ee BTA (S)-Leu for both systems.

CD analyses of the same mixture were performed in toluene instead of MCH. Again, a linear variation of the CD values was observed in the absence of the achiral additive which

⁸ No CD shape change is observed upon the addition of BTA cyclohex, which indicates no obvious change of the co-assembly structure upon incorporation of BTA-cyclohex

⁹ The difference in absolute CD values for different systems (with and without additive, MCH versus toluene) can't be interpreted satisfactorily and only the variation of the CD value as a function of the ee value in BTA Leu for the same system is discussed.

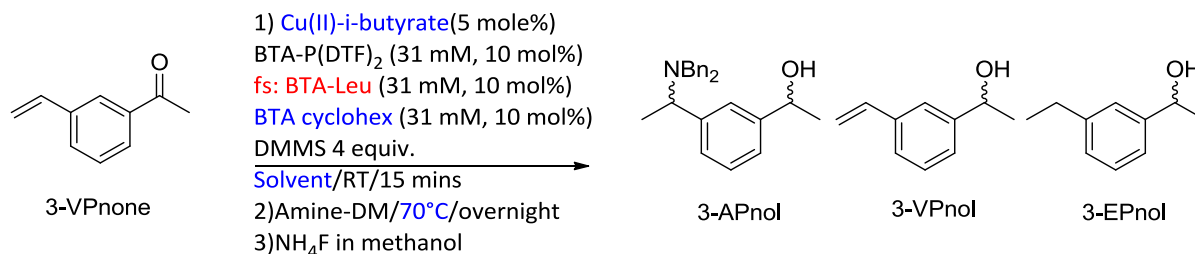
corresponds to a system with no chirality amplification properties (Figure IV-5c, black curve). In presence of BTA cyclohex (Figure IV-5b), the negative CD cotton effect at 280 nm increases to reach the optimal CD value with *ca.* 30% *ee* of **BTA (S)-Leu**. Thus, chirality amplification appears to be stronger in toluene compared to MCH¹⁰.

IV.6.b. Probing chirality amplification effects in catalysis in presence of BTA cyclohex as an additive.

According to CD analyses chirality amplification effects occur only when **BTA cyclohex** is present in the mixture. The aim of this study was thus to probe the influence of the additive on the aforementioned optimized conditions and to see whether optimal stereoselectivity can be reached with non-optimally pure catalytic mixtures, *i.e.* for scalemic mixtures of enantiopure chiral BTA co-monomers **(R/S)-BTA Leu**, and for catalytic mixtures embedding a lower fraction of sergeants. The cascade reaction was launched for 15 mins at RT, then the temperature was elevated to 70°C overnight. Despite the low possibility of having overlap between the two functions by using Cu(II)-i-butyrate system in MCH, we decided to prevent further this possibility by adding the electrophile amine after the HS step. Yield of **3-APnol** obtained was estimated according to an IS (1,3,5-trimethoxybenzene) by ¹H NMR. For reaction scheme and catalytic results see Table IV-16.

Initial conditions represent the fraction of sergeant present in each catalytic experiment, this fraction refers to the amount of chiral co-monomer **BTA Leu** over the total amount of **BTA-P(DTF)2 ligand + BTA Leu**. In all experiments, no catalytic switch was performed, thus the initial conditions and the final conditions are identical. As indicated in Table IV-16, yields for all experiments were lower than for the aforementioned optimized catalytic systems. It is probably ascribed to the fact that the amine electrophile was not engaged at the beginning and as such, side reactions occur during the hydrosilylation step. In addition, a negative influence of the additive (**BTA cyclohex**) on the yield of the reaction cannot be excluded.

¹⁰ The different shape of the CD bands in toluene versus MCH and for mixtures with and without additive suggests a subtle difference in the conformation of the PAr₂ units in the helices under these conditions.



Entry	Solv	Initial conditions	Yield 3-APnol ^[a]	Yield 3-VPnol ^[a]	Yield 3-EPnol ^[a]	Major S _i ^[b] /%	ee _{tot} % / dr.	ee1/ee2/ee2 ¹ [c]
1	tol	Fs=0.5 (R)	33%	21%	11%	(-,+), 74 %	94% / 3.02	68%/74%/74%
2	tol	Fs=0.2 (R)	35%	15%	10%	(-,+), 74%	96% / 3.45	67%/83%/83%
3	tol	Fs=0.5 [50% ee (S)]	32%	15%	10%	(+,-), 72%	94% / 2.90	-66%/-74%/-74%
4	MCH	Fs=0.5 (R)	50%	13%	9%	(-,+), 66%	91% / 2.30	52%/74%/74%
5 ^[d]	MCH	Fs=0.2 (R)	16%	21%	16%	(rac)	(rac)	close to (rac)
6	MCH	Fs=0.5 [50% ee (S)]	18%	26%	20%	(+,-), 64%	89% / 2.07	-50%/-70%/-70%

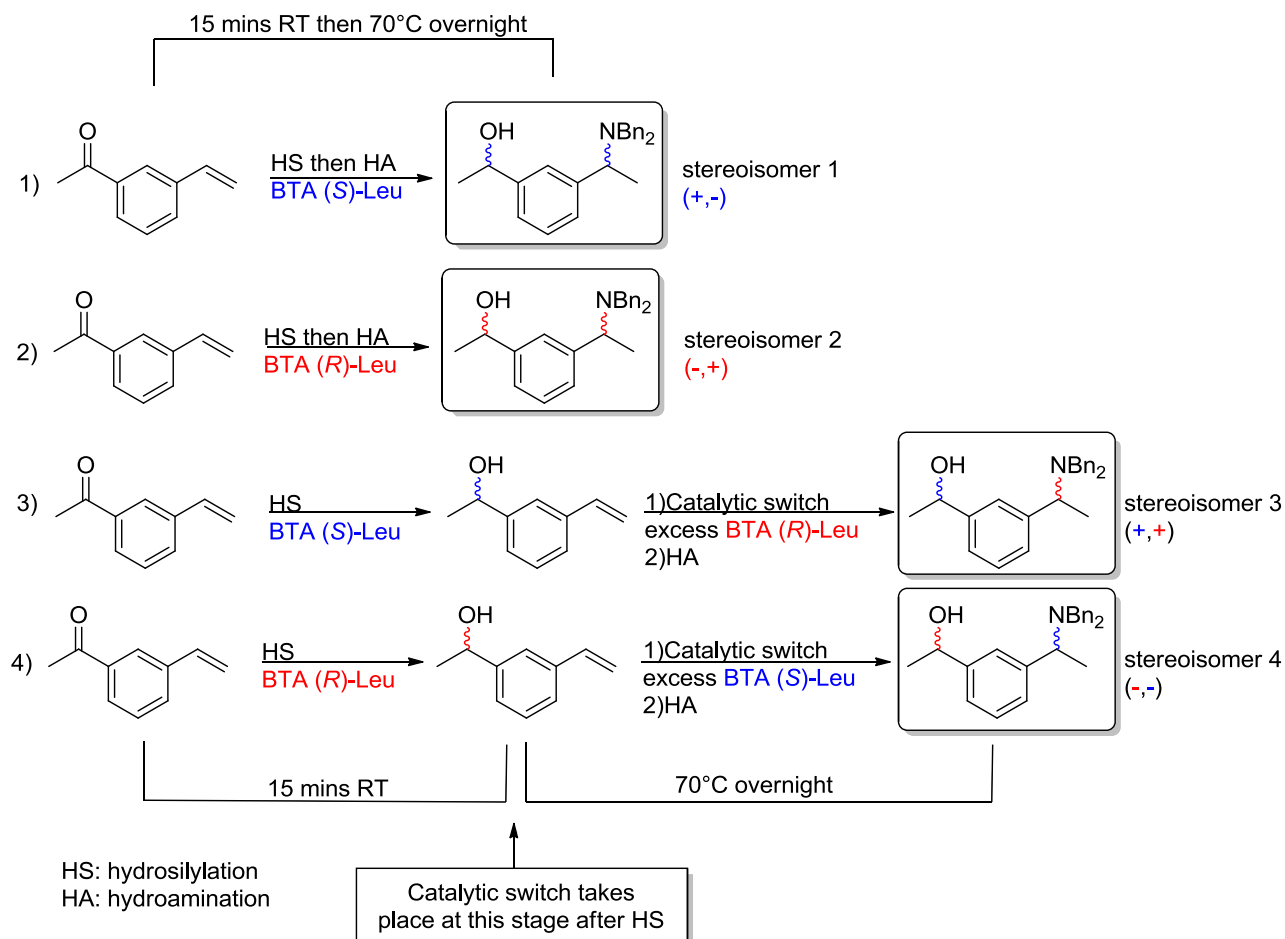
Table IV-16 Conditions : **3-VPnone** (0.5 mmole, 1eq), Cu(II)-i-butyrate (5 mol%), BTA-P(DTF)₂ (10 mol%, 31 mM), fs: fraction of sergeant BTA Leu, BTA cyclohex (10 mol%, 31 mM), DMMS (4.0 eq), amine-DM (1.3 eq), Solvent (500 μL). ee1: ee for hydrosilylation step, ee2: ee of hydroamination step, ee_{tot} : ee total for major stereoisomer, dr.: diastereoisomeric ratio. [a] Yields estimated by ¹H NMR acc. to an IS (1,3,5-trimethoxybenzene). [b] Major stereoisomer is represented as (sign^{alcohol}, sign^{amino}). [c] With ee1 positive [negative] when the (-) enantiomer [(+)enantiomer, resp.] is in majority. With ee2 positive [negative] when the (+) enantiomer [(-)enantiomer, resp.] is in majority. [d] ee_{tot} and dr. cannot be determined due to unclear HPLC separation.

However, **BTA cyclohex** has no negative impact on the stereoselectivity. Results in Table IV-16 shows that the stereoselectivity of the cascade reaction is slightly higher in toluene than in MCH, but reaction in both solvents produces the major enantiomer with > 64% which translates

into ee_{tot} values up to 96% in toluene and 91% in MCH. In toluene, the amount of **BTA Leu** can be decreased to 20% without eroding the selectivity (entry 2, Table IV-16). The result of the identical experiment in MCH cannot be ascertained (see Table caption [d]). Catalytic reactions performed with scalemic mixtures biased in favor of **BTA (S)-Leu** (50% *ee*) are very instructive. As expected, these experiments yield the same enantiomer than for reactions conducted with pure **BTA (S)-Leu**.

More interestingly, the stereoselectivity are virtually identical (compare entry 1 and 3 for toluene, and entry 4 and 6 for MCH, Table IV-16). This corroborates that the supramolecular helical BTA catalysts composed of **BTA-P(DTF)2** and **BTA Leu** exhibit significant chirality amplification in presence of **BTA cyclohex**.

IV.6.c. Probing the stereochemical switch capability of the catalyst.



Scheme IV-5 Illustration of the different paths for obtaining all possible stereoisomers with our switchable catalytic system.

Having demonstrated that significant level of stereoselectivity is achieved for mixtures of **BTA-P(DTF)2** and **BTA Leu** in experiments for which the handedness of the catalysts was not switched during the cascade reaction, it was then necessary to probe the possibility of inverting the handedness (and configuration) of the helical catalysts during the reaction. For the aim of obtaining all possible stereoisomers of **3-APnol**, opposite enantiomers of **BTA Leu** will be used either pure (Scheme IV-5, experiments 1 and 2) or as mixtures (Scheme IV-5, experiments 3 and 4). The objective is to switch the catalyst stereoselectivity after the hydrosilylation step.

This is supposed to be achieved by altering the composition of the co-assemblies during the catalysis by changing the nature of the major enantiomer of **BTA Leu** before and after the

hydrosilylation reaction. The experiments will be performed in presence of **BTA cyclohex** to ensure efficient amplification of chirality.

IV.6.c.i. Applying the catalytic switch in presence of BTA cyclohex additive.

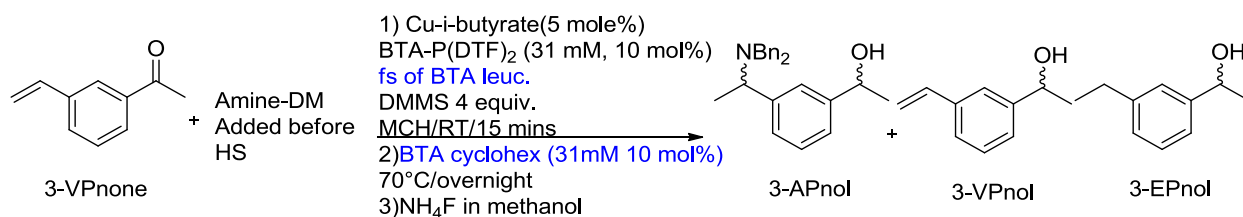
Different experiments were conducted using **Cu(II)-i-butyrate/BTA(PDTF)2/BTA Leu/BTA cyclohex** catalytic system . **BTA cyclohex** was added at the beginning of the catalytic process or in the second step while applying the catalytic switch. The yield obtained for **3-APnol** was estimated according to an IS (1,3,5-trimethoxy benzene) by ^1H NMR. For reaction scheme and catalytic results in MCH and toluene see Table IV-17 and IV-18, respectively.

1) In MCH.

For the experiment for which **BTA cyclohex** was added after the hydrosilylation step, concomitantly to **BTA (R)-Leu**, the major stereoisomer obtained was (+,-) with $ee_{\text{tot}}=73\%$ and dr: 1.42. (entry 2, Table IV-17). This stereoisomer is the one obtained with pure **BTA (S)-Leu** which indicates that both reactions proceeded in the same direction. The result here is even worse than the reaction performed in absence of the additive which furnished the expected stereoisomer, albeit with limited selectivity (entry 3, Table IV-15). Obviously **BTA cyclohex** added in the second step had a negative influence on the outcome of the reaction probably by impeding or slowing down the stereochemical inversion under the catalytic conditions. For experiment (entry 3, Table IV-17), the additive was present from the beginning and the composition of the system was changed from a low amount of pure **BTA (R)-Leu** ($fs=0.2$) to a scalemic mixture of **BTA Leu** biased in favor of **BTA (S)-Leu** ($fs= 0.5$, 50% *ee*).

The expected stereoisomer was obtained (+,+) but with an extremely low selectivity (32% *ee*) indicating that the catalytic outcome of this reaction is close to the racemic state. Here, both steps occur in different directions, both with limited enantioselectivities. The low value of ee_1 seems to indicate that no amplification of chirality through the S&S effect occurs in this system¹¹. The low value of ee_2 is probably related to the fact the stereochemical switch and the hydroamination reaction occurs concomitantly.

¹¹ This result seems consistent with the presence of a racemic mixture for the experiment corresponding to entry 5, Table IV-16 which was not ascertained because of the low quality of the HPLC trace.



Entry	Solv	Initial cond.	Final cond.	Yield of 3-APnol ^[a]	Major Si. ^[b] /%	ee _{tot} %/ dr.	ee1/ee2/ee2' ^[c]
1	MCH	Fs=0.5(S)	Id.	32%	(+,-), 72.17%	94%/2.90	-66%/-74%/- 74%
2	MCH	Fs=0.5(S)	Fs=0.8 [50% ee (R)]	44%	(+,-), 51%	73%/1.42	-54%/-32%/- 32%
3 ^[d]	MCH	Fs=0.2(R)	Fs=0.5 [50% ee (S)]	32%	(-,-), 34%	8%/0.95	13%/-21%/- 21%

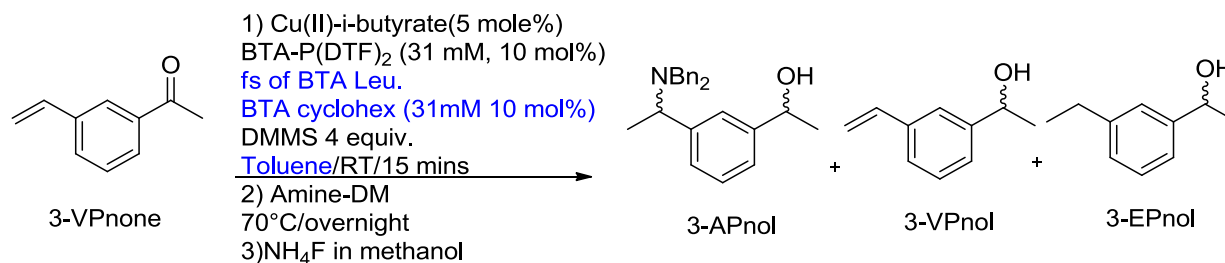
Table IV-17 Conditions : **3-VPnone** (0.5 mmole, 1eq), Cu(II)-i-butyrate (5 mol%), BTA-P(DTF)₂ (10 mol%), fs: fraction of sergeant BTA Leu, BTA cyclohex (10 mol%, 31 mM) DMMS (4.0 eq), amine-DM (1.3 eq), MCH (500 μ L). ee1: ee for hydrosilylation step, ee2: ee of hydroamination step, ee_{tot} : ee total for major stereoisomer. [a] Yields estimated by ¹H NMR acc. to an IS (1,3,5-trimethoxybenzene). [b] Major stereoisomer is represented as (sign^{alcohol}, sign^{amino}). [c] With ee1 positive [negative] when the (-) enantiomer [(+)enantiomer, resp.] is in majority. With ee2 positive [negative] when the (+) enantiomer [(-)enantiomer, resp.] is in majority. [d] BTA cyclohex added at the beginning of the catalytic process, while amine-DM added after HS.

2) In toluene.

Here we perform a catalytic experiment for which the initial and ending conditions were known to provide optimal selectivities.

As stated above, reactions conditions conducted in toluene with a lower fraction of **BTA Leu** or a scalemic mixture of **BTA Leu** (50% ee) provided the same selectivity than the homochiral helices (entry 1 and 2, Table IV-18). However, the result of selectivity switching experiment performed with these initial and ending conditions was disappointing. The desired major stereoisomer (-,-) was accessed but with a content of only 38% relatively to the other stereoisomers (entry 3, Table IV-18). ee1 of HS step reached 50% which is somewhat lower than the expected ee value (entry 1, Table IV-18), but more surprisingly the ee2 of the

hydroamination step was of 0%. Here, the low value of ee₂ can only be related to the fact that the stereochemical switch is slow relatively to the hydroamination step.



Conditions for switch:

Time of stirring after addition of opposite chiral BTA Leu, and before heating is estimated of 2 mins maximum

Entry	Solv	Initial cond.	Final cond.	Yield of 3-APnol ^[a]	Major Si. ^[b] /%	ee _{tot} %/ dr.	ee1/ee2/ee2' ^[c]
1	tol	Fs=0.2 (R)	id	35%	(-,+), 74%	96% / 3.45	67%/83%/83%
2	tol	Fs=0.5 [50% ee (S)]	id	32%	(+,-), 72%	94% / 2.90	-66%/-74%/-74%
3	tol	Fs=0.2(R)	Fs=0.5 [50% ee (S)]	44%	(-,-), 38%	50%/1.02	50%/0%/0%

Table IV-18 : Conditions : **3-VPnone** (0.5 mmole, 1eq), Cu(II)-i-butyrate (5 mol%), BTA-P(DTF)₂ (10 mol%), fs: fraction of sergeant BTA Leu, BTA cyclohex (10 mol%, 31 mM), DMMS (4.0 eq), amine-DM (1.3 eq), toluene (500 μ L). ee₁: ee for hydrosilylation step, ee₂: ee of hydroamination step, ee_{tot} : ee total for major stereoisomer, dr : diastereoisomeric ratio. [a] Yields estimated by ¹H NMR acc. to an IS (1,3,5-trimethoxybenzene). [b] Major stereoisomer is represented as (sign^{alcohol}, sign^{amino}). [c] With ee₁ positive [negative] when the (-) enantiomer [(+)enantiomer, resp.] is in majority. With ee₂ positive [negative] when the (+) enantiomer [(-)enantiomer, resp.] is in majority.

A period of 2 minutes was set after the addition of **BTA (S)-Leu** and before addition of amine-DM in order to trigger the stereochemical switch before the onset of the hydroamination reaction. The outcome of the catalytic reaction, ee₂ equals to zero, indicates that this time is not sufficient. This infers that stereochemical inversion was slow at room temperature. This seems to be a general trend of the selectivity-switching experiments presented in this chapter.

IV.7. Conclusion.

Different vinyl acetophenone derivatives were examined as substrates for a copper-catalyzed cascade hydroamination/hydrosilylation reaction in presence of supramolecular helical BTA co-

assemblies. The hydrosilylation proceeds very efficiently with the BTA mixture composed of **BTA-P(DTF)2/BTA Leu** ($f_s = 0.5$). Yields and enantioselectivities were moderate to good for **3-VPnone** and excellent for **4-MeVPnone** and **3-MeVPnone**. Investigation of the cascade reaction with these substrates indicates that hydroamination only proceeds for **3-VPnone**. Better yields were obtained when the amine electrophile was engaged at the beginning of the catalytic process as side reactions involving the vinyl moiety are minimized. Optimization of the cascade reaction for **3-VPnone** identified Cu(II)-i-butyrate, and MCH as the best metal precursor and solvent, respectively. Under these conditions, the amino alcohol product **3-APnol** is obtained with 85% yield, 93% ee_{tot} and a dr of 2.8. This translates into ee values for both the hydrosilylation and hydroamination step of *ca.* 65%. CD analyses revealed that chirality amplification effects are enhanced to useful extent only when **BTA cyclohex** is added to helical co-assemblies of **BTA-P(DTF)2** and **BTA Leu**. Chirality amplification effects were stronger in toluene, homochiral helices were generated with 30% ee of the desired **BTA Leu** co-monomer, while in MCH 50% ee was required. Catalytic experiments performed with a scalemic mixture of **BTA Leu** (50% ee) provided the same stereoselectivity as the optimized catalytic system which corroborates that chirality amplification is operative in the helical catalysts. Catalytic mixtures embedding a lower fraction of **BTA Leu** ($f_s = 0.2$) proceed efficiently in toluene but not in MCH.

Unfortunately, all tested selectivity-switching experiments failed to produce the expected stereoisomer with a decent stereoselectivity. Actually, the switch was always partial, *i.e.* a mixture was obtained which contains the desired stereoisomer as well as the one formed in absence of stereochemical switch. It was found that ee_2 of the hydroamination step was always lower than that expected. The main identified reason was that the stereochemical switch and the hydroamination occurs concomitantly. In the previously studied system^[27], composed of **BTAp-PPh2** and **BTA Cha** in toluene, the switch was fast (< 5 seconds). Here, it appears that the time afforded for the switch (2 minutes at room temperature) was not enough. Further investigations should be carried on for improving this stereochemical switch by finding better operating conditions, and by studying the time required for having efficient stereochemical switch with this supramolecular BTA catalyst. For this purpose, more CD analyses should be conducted on this catalytic system after different time intervals from the addition of the excess

amount of the desired **BTA Leu** co-monomer, to find the exact time need for having complete switch of the direction of the helices. Finally, the information gained from these CD experiments must be transferred to catalytic experiment. The final step of this project will be to test the scope of the substrates amenable to the hydrosilylation/hydroamination sequence of reaction.

IV.8. Annex.

IV.8.a. Materials preparation and methods.

4-(dimethylamino)benzoic acid, 4-methoxybenzoyl chloride, benzoyl chloride, pivaloyl chloride, 1-(3-bromophenyl)ethanone, 1-(4'-bromo-[1,1'-biphenyl]-4-yl)ethanone, 1-(4-bromophenyl)ethanone, di(1H-imidazol-1-yl)methanone, N,N-dibenzylhydroxylamine, potassium vinyltrifluoroborate, potassium (*Z*)-1-propene-1-trifluoroborate, potassium (*E*)-1-propene-1-trifluoroborate, DMAP, and triethylamine were obtained from Alfa Aesar, and Sigma-Aldrich, and used as received. DMMS, DEMS, PhSiH₃, [Cu(OAc)₂·H₂O], and Cu(II)-*i*-butyrate were purchased from Alfa Aesar. Cesium carbonate, and Ammonium fluoride were purchased from Fluorochem. 1-(3-vinylphenyl)ethenone (3-VPnone), and 1-(4-vinylphenyl)ethenone (4-VPnone) were synthesized according to a published procedure by Brown^[19], and 4-(((dibenzylamino)oxy)carbonyl)-N,N-dimethylaniline (Amine-DM), N,N-dibenzyl-O-(4-methoxybenzoyl)hydroxylamine (Amine-MB), N,N-dibenzyl-O-pivaloylhydroxylamine (Amine-TB), and O-benzoyl-N,N-dibenzylhydroxylamine (Amine-BE) were synthesized according to the reported procedures^[21,22], and all the obtained characterization data were in agreement with the reported ones. BTA (*S*)-Leu and BTA (*R*)-Leu co-monomers used in this study have been purified by preparative HPLC. Dried solvents were obtained from an SPS solvent purification system (IT-Inc). NMR spectra were recorder on a Bruker Advance 400, or 300 spectrometer and calibrated to the residual solvent peak: CDCl₃ (¹H: 7.26 ppm; ¹³C: 77.16 ppm). Peaks are reported with their corresponding multiplicity (s: singlet; br s: broad singlet, d: doublet, t: triplet; q: quartet) and integration, and respective *J* coupling constants are given in Hertz. Unless otherwise noted, chromatography-grade solvents were used as received. All inert atmosphere reactions were carried out under an argon atmosphere with standard Schlenk-line techniques.

Chiral HPLC analyses: 1-(3-vinylphenyl)ethanol (3-VPnol). The optical purity was determined by HPLC analysis: OD-H column, flow rate: 0.4ml/min, 95:5 hexane/iso-propanol, RT for 1st enantiomer= 8.52 min, RT for 2nd enantiomer= 9.01 min.

(E)-1-(3-(prop-1-en-1-yl)phenyl)ethanol (3-E-MeVPnol). The optical purity was determined by HPLC analysis: OD-H column, flow rate: 0.4ml/min, 95:5 hexane/iso-propanol, RT for 1st enantiomer= 8.266 min, RT for 2nd enantiomer= 11.227 min.

1-(3-(1-(dibenzylamino)ethyl)phenyl)ethanol (3-APnol). The optical purity was determined by chiral HPLC analysis: Chiralpak IG column, flowrate: 1mL/min, heptane/ethanol (98/2), 35°C, RT for 1st stereoisomer: 10.32 min, RT for 2nd stereoisomer: 11.036 min, RT for 3rd stereoisomer: 11.589 min, RT for 4th stereoisomer: 12.2 min. Analysis were performed in the Institute of Molecular sciences Marseille, Platform of chiral chromatography by Nicolas Vanthuyne.

Fourier-Transform Infrared (FT-IR) analyses: FT-IR measurements were performed on a Nicolet iS10 spectrometer. Solution spectra were measured in CaF₂ cells by adjusting the pathlength (0.1 mm or 0.01 mm) to the concentration and were corrected for air, solvent and cell absorption.

Circular dichroism (CD) analyses: CD measurements were performed on a Jasco J-1500 spectrometer equipped with a Peltier thermostated cell holder and Xe laser. Data were recorded at 20°C with the following parameters: 20 nm.min⁻¹ sweep rate, 0.1 nm data pitch, 2.0 nm bandwidth, and between 400 and 200 nm. Spectra were corrected for solvent and cell contribution. A 0.01 mm dismountable quartz cell, and 0.1 mm circular cell were used (pathlength adjusted to concentration). For all samples, LD contribution was negligible ($\Delta LD < 0.005$ dOD) and the shape of the CD signal was independent of the orientation of the quartz slide.

UV-Vis analyses: UV-Vis absorption spectra were extracted from CD on each of the above samples and obtained after correction of the absorption of air, solvent, and cell at the same temperature.

Exact mass measurements (HRMS): were obtained on TQ R30-10 HRMS spectrometer by ESI+ ionization and are reported in m/z for the major signal.

IV.8.b. General procedures for catalysis.

Hydrosilylation in toluene (Table IV-2, IV-3, IV-4, and IV-6). An oven-dried screw-cap reaction tube equipped with a magnetic stir bar is charged with $\text{Cu}(\text{OAc})_2 \cdot x\text{H}_2\text{O}$ ($8.5 \cdot 10^{-3}$ mmol, 1.7 mg, 0.05 equiv.) and **BTA-P(Ar)2** ligand (0.017 mmol, 0.1 equiv.) in 0.5 mL anhydrous THF, and kept stirring for 30 mins. Then solvent was removed under vacuum for 1h. The reaction tube was sealed with a screw-cap septum, then evacuated and backfilled with argon (this process was repeated a total of two times). Selected substrate (0.17 mmol, 1 equiv.) is dissolved in anhydrous toluene (0.5 mL) and added to the catalytic tube via syringe. BTA Leu or BTA Cha (0.017 mmol, 0.1 equiv.) is added as solid when reactions are carried out in presence of BTA co-monomer. The resulting mixture is stirred at RT for 15 mins until a homogenous solution is obtained, and heated gently by a heat gun until the appearance of small bubbles. The catalytic mixture is kept to cool down to room temperature, and the selected silane (0.34 mmol, 2 equiv.) is added and the reaction tube was sealed with a screw-cap septum, and then evacuated and backfilled with argon. The reaction was left stirring for the desired period of time. After completion, a saturated solution of NH_4F in MeOH (3 mL) is added and the mixture was stirred at RT for 10 min, followed by addition of a saturated aqueous solution of Na_2CO_3 (3 mL) and ethyl acetate (3 mL). The phases are separated and the aqueous layer is extracted with ethyl acetate (3 x 3 mL). The combined organic phases are dried over MgSO_4 and then filtered. The solvent was removed under rotavap, and then dried under vacuum. The crude mixture is purified over short silica column using ethyl acetate/hexane 13:87 as an eluent.

Hydrosilylation/hydroamination cascade reaction in toluene without switch: Addition of the amine electrophile after hydrosilylation (Tables 8, 9, 10, and 11). An oven-dried screw-cap reaction tube equipped with a magnetic stir bar was charged with a $\text{Cu}(\text{OAc})_2 \cdot x\text{H}_2\text{O}$ ($8.5 \cdot 10^{-3}$ mmol, 1.7 mg, 0.05 equiv.) and **BTA-P(Ar)2** ligand (0.017 mmol, 0.1 equiv.) in 0.5 mL anhydrous THF and kept stirring for 30 mins. Then solvent was removed under vacuum for 1 h. The reaction tube was sealed with a screw-cap septum, then evacuated and backfilled with argon (this process was repeated a total of two times). Selected substrate (0.17 mmol, 1 equiv.) is dissolved in 0.5 mL of toluene and added to the catalytic tube via syringe. BTA Leu (0.017 mmol, 18 mg, 0.1 equiv.) is added as solid. The resulting mixture was stirred at RT for 15 mins until a

homogenous solution is obtained, and heated gently by a heat gun until the appearance of small bubbles. The catalytic mixture is kept to cool down to room temperature, and DMMS (0.684 mmol, 98 μ l, 4 equiv.) is added and the reaction tube was sealed with a screw-cap septum, and then evacuated and backfilled with argon. The reaction is left stirring for the desired period of time. Amine electrophile (0.22 mmol, 80 mg, 1.3 equiv.) is added as a solid, and reaction temperature is elevated to (55°C, or 70°C), and left to stir overnight. After completion, the reaction mixture was allowed to cool to RT. A saturated solution of NH_4F in MeOH (3 mL) is added and the mixture was stirred at RT for 10 mins, followed by addition of a saturated aqueous solution of Na_2CO_3 (3 mL) and ethyl acetate (3 mL). The phases are separated and the aqueous layer is extracted with ethyl acetate (3 x 3 mL). The combined organic phases are dried over MgSO_4 and then filtered. The solvent was removed under rotavap, and then dried under vacuum. The crude mixture is purified over short silica column using DCM as an eluent. Yield is estimated by addition of an internal standard to the crude mixture by ^1H NMR.

Hydrosilylation/hydroamination cascade reaction in toluene without switch: screening of different copper sources (Table 13). An oven-dried screw-cap reaction tube equipped with a magnetic stir bar was charged with a Copper source (8.5×10^{-3} mmol, 0.05 equiv.) and **BTA-P(DTF)2** ligand (0.017 mmol, 16.3 mg, 0.1 equiv.) in 0.5 mL anhydrous THF and kept stirring for 30 mins. Then solvent was removed under vacuum for 1h. The reaction tube was sealed with a screw-cap septum, then evacuated and backfilled with argon (this process was repeated a total of two times). 1-(3-vinylphenyl)ethanone (0.17 mmol, 25 mg, 1 equiv.) is dissolved in anhydrous toluene (0.5 mL) and added to the catalytic tube via syringe. BTA Leu (0.017 mmol, 18 mg, 0.1 equiv.), amine-DM (0.22 mmole, 80 mg 1.3 equiv.) were added as solids. The resulting mixture was stirred at RT for 15 mins until a homogenous solution is obtained, and heated gently by a heat gun until the appearance of small bubbles. The catalytic mixture was kept to cool down to room temperature, and DMMS (0.34 mmol, 2 equiv.) is added and the reaction tube was sealed with a screw-cap septum, and then evacuated and backfilled with argon. The reaction is left stirring for 1h at RT (1h at RT, and then 1h at elevated temperature (55°C or 70°C) just for entries 5, 6, 7, and 8). After completion. A saturated solution of NH_4F in MeOH (3 mL) is added

and the mixture was stirred at rt for 10 mins, followed by addition of a saturated aqueous solution of Na₂CO₃ (3 mL) and ethyl acetate (3 mL). The phases are separated and the aqueous layer is extracted with ethyl acetate (3 x 3 mL). The combined organic phases are dried over MgSO₄ and then filtered. The solvent was removed under rotavap, and then dried under vacuum. The crude mixture is purified over short silica column using ethyl acetate/hexane 13:87 as an eluent. Yield is estimated by addition of an internal standard to the crude mixture by ¹H NMR.

Hydrosilylation/hydroamination cascade reaction without switch in MCH: Addition of the amine electrophile at the beginning with Cu(II)-i-butyrate (Table 14). An oven-dried screw-cap reaction tube equipped with a magnetic stir bar was charged with a Cu(II)-i-butyrate (8.5*10⁻³ mmol, 2mg, 0.05 equiv.) and **BTA-P(DTF)2** ligand (0.017 mmol, 16.5 mg, 0.1 equiv.) in 0.5 mL anhydrous THF and kept stirring for 30 mins. Then solvent was removed under vacuum for 1h. The reaction tube was sealed with a screw-cap septum, then evacuated and backfilled with argon (this process was repeated a total of two times). 1-(3-vinylphenyl)ethanone (0.17 mmol, 25 mg, 1 equiv.) is dissolved in 0.5 mL of MCH and added to the catalytic tube via syringe. BTA Leu (0.017 mmol, 18 mg, 0.1 equiv.), amine-DM (0.22 mmol, 80 mg, 1.3 equiv.) were added as a solid. The resulting mixture was stirred at RT for 15 mins until a homogenous solution is obtained, and heated gently by a heat gun until the appearance of small bubbles. The catalytic mixture is kept to cool down to room temperature, and DMMS (0.684 mmol, 98 µl, 4 equiv.) is added and the reaction tube was sealed with a screw-cap septum, and then evacuated and backfilled with argon. The reaction is left stirring for the desired period of time, and then reaction temperature is elevated to 70°C, and left to stir overnight. After completion, the reaction mixture was allowed to cool to room RT. A saturated solution of NH₄F in MeOH (3 mL) is added and the mixture was stirred at RT for 10 mins, followed by addition of a saturated aqueous solution of Na₂CO₃ (3 mL) and ethyl acetate (3 mL). The phases are separated and the aqueous layer is extracted with ethyl acetate (3 x 3 mL). The combined organic phases are dried over MgSO₄ and then filtered. The solvent was removed under rotavap, and then dried under vacuum. The crude mixture is purified over short silica column using DCM as an eluent. Yield is estimated by addition of an internal standard to the crude mixture by ¹H NMR.

Hydrosilylation/hydroamination cascade reaction without switch. Reaction in presence of BTA cyclohex, and amine electrophile added after HS (Table 16). An oven-dried screw-cap reaction tube equipped with a magnetic stir bar was charged with a Copper(II)-iso-butyrate (8.5×10^{-3} mmol, 2mg, 0.05 equiv.) and **BTA-P(DTF)2** ligand (0.017 mmol, 16.5 mg, 0.1 equiv.) in 0.5 mL anhydrous THF and kept stirring for 30 mins. Then solvent was removed under vacuum for 1 h. The reaction tube was sealed with a screw-cap septum, then evacuated and backfilled with argon (this process was repeated a total of two times). 1-(3-vinylphenyl)ethanone (0.17 mmol, 25 mg, 1 equiv.) is dissolved in 0.5 mL of (MCH or toluene) and added to the catalytic tube via syringe. BTA (*R*)-Leu (Fs=0.5/Fs=0.2 (*R*), or Fs=0.5 [50% *ee* (*S*)]), BTA cyclohex (0.0171 mmole, 18.6 mg, 0.1 equiv.) were added as a solid. The resulting mixture was stirred at RT for 15 min until a homogenous solution is obtained, and heated gently by a heat gun until the appearance of small bubbles. The catalytic mixture is kept to cool down to room temperature, and DMMS (0.684 mmol, 98 μ l, 4 equiv.) is added and the reaction tube was sealed with a screw-cap septum, and then evacuated and backfilled with argon. The reaction is left stirring for 15 mins at RT, then amine-DM (0.22 mmol, 80 mg, 1.3 equiv.) is added. Reaction temperature is elevated to 70°C, and left to stir overnight. After completion, the reaction mixture was allowed to cool to room RT. A saturated solution of NH₄F in MeOH (3 mL) is added and the mixture was stirred at RT for 10 min, followed by addition of a saturated aqueous solution of Na₂CO₃ (3 mL) and ethyl acetate (3 mL). The phases are separated and the aqueous layer is extracted with ethyl acetate (3 x 3 mL). The combined organic phases are dried over MgSO₄ and then filtered. The solvent was removed under rotavap, and then dried under vacuum. The crude mixture is purified over short silica column using DCM as an eluent. Yield is estimated by addition of an internal standard to the crude mixture by ¹H NMR.

Hydrosilylation/hydroamination cascade reaction with switch: in presence/absence of BTA cyclohex (Tables 17 and 18). An oven-dried screw-cap reaction tube equipped with a magnetic stir bar was charged with a Cu(II)-i-butyrate (8.5×10^{-3} mmol, 2mg, 0.05 equiv.) and **BTA-P(DTF)2** ligand (0.017 mmol, 16.5 mg, 0.1 equiv.) in 0.5 mL anhydrous THF and kept stirring for 30 mins. Then solvent was removed under vacuum for 1h. The reaction tube was sealed with a screw-cap septum, then evacuated and backfilled with argon (this process was repeated a total

of two times). 1-(3-vinylphenyl)ethanone (0.17 mmol, 25 mg, 1 equiv.) is dissolved in 0.5 mL of (*MCH* or *toluene*) and added to the catalytic tube via syringe. BTA (*R*)-Leu (*fs*= 0.2 or 0.5), amine-DM (0.22 mmol, 80 mg, 1.3 equiv.), BTA cyclohex (0.0171 mmole, 18.6 mg, 0.1 equiv.) were added as a solid. The resulting mixture was stirred at RT for 15 mins until a homogenous solution is obtained, and heated gently by a heat gun until the appearance of small bubbles. The catalytic mixture is kept to cool down to room temperature, and DMMS (0.684 mmol, 98 μ l, 4 equiv.) is added and the reaction tube was sealed with a screw-cap septum, and then evacuated and backfilled with argon. The reaction is left stirring for 15 mins at RT, then BTA (*S*)-Leu (*fs*= 0.5 or 0.8) is added. Reaction temperature is elevated to 70°C, and left to stir overnight. After completion, the reaction mixture was allowed to cool to room RT. A saturated solution of NH₄F in MeOH (3 mL) is added and the mixture was stirred at rt for 10 mins, followed by addition of a saturated aqueous solution of Na₂CO₃ (3 mL) and ethyl acetate (3 mL). The phases are separated and the aqueous layer is extracted with ethyl acetate (3 x 3 mL). The combined organic phases are dried over MgSO₄ and then filtered. The solvent was removed under rotavap, and then dried under vacuum. The crude mixture is purified over short silica column using DCM as an eluent. Yield is estimated by addition of an internal standard to the crude mixture by ¹H NMR.

IV.8.c. Preparation of solutions for CD analyses.

Diluted MR-type experiments with ([BTA-P(DTF)2]= 31 mM, and total concentration of [BTA leu]= 31 mM, and [BTA cyclohex]=31 mM if present (Figures IV-4, and IV-5)): a given amount of a stock solution prepared by mixing BTA-P(DTF)2 and Cu(II)-*i*-butyrate was divided in order to get Cu(II)-*i*-butyrate (0.00625 mmol, 1.48 mg) and BTA-P(DTF)2 (0.0125 mmol, 12 mg) in dry THF (500 μ l) in each vial. The mixture was stirred for 30 mins. The solvent was removed under vacuum and the tube was further put under vacuum (10⁻³ mbar) for 1h. A mixture of BTA (*S*)-Leu and BTA (*R*)-Leu co-monomers with the desired *ee* (0.0125 mmol, 13.2 mg in total) was added to vials, as well as BTA cyclohex (0.0125 mmol, 13.6 mg) when needed. Then *MCH* or *toluene* was added in order to get a total solvent volume is set to 0.8 mL. All solutions were pre-heated prior to analysis.

Diluted MR-type experiments with [BTA-P(DTF)2]= 31 mM, and total concentration of [BTA leu]= 31 mM, and [BTA Aib]=31 mM if present (Figure S.IV-3, and S.IV-4): a given amount of a stock solution prepared by mixing BTA-P(DTF)2 and Cu(II)-i-butyrate was divided in order to get Cu(II)-i-butyrate (0.00625 mmol, 1.48 mg) and BTA-P(DTF)2 (0.0125 mmol, 12 mg) in dry THF (500 μ L) in each vial. The mixture was stirred for 30 mins. The solvent was removed under vacuum and the tube was further put under vacuum (10^{-3} mbar) for 1h. A mixture of BTA (*S*)-Leu and BTA (*R*)-Leu co-monomers with the desired *ee* (0.0125 mmol, 13.2 mg in total) was added to vials, as well as BTA Aib (0.0125 mmol, 12.1 mg) when needed. The total solvent volume is set to 0.8 mL (MCH or Toluene).

Diluted MR-type experiments with [BTA-P(DTF)2]= 5.8 mM, and total concentration of [BTA leu]= 5.8 mM, and [BTA cyclohex]= 5.8 mM if present (Figure S.IV-5, S.IV-6, S.IV-8, S.IV9): a given amount of a stock solution prepared by mixing BTA-P(DTF)2 and Cu(II)-i-butyrate was divided in order to get Cu(II)-i-butyrate (0.0029 mmol, 0.68 mg) and BTA-P(DTF)2 (0.0058 mmol, 5.59 mg) in dry THF (500 μ L) in each vial. The mixture was stirred for 30 mins. The solvent was removed under vacuum and the tube was further put under vacuum (10^{-3} mbar) for 1h. A mixture of BTA (*S*)-Leu and BTA (*R*)-Leu co-monomers with the desired *ee* (0.0058 mmol, 6.12 mg in total) was added to vials, as well as BTA cyclohex (0.0058 mmol, 6.12 mg) when needed. The total solvent volume is set to 1 mL (MCH or Toluene).

Diluted MR-type experiments with [BTA-P(DTF)2]= 5.8 mM, and total concentration of [BTA leu]= 5.8 mM, and [BTA Aib]= 5.8 mM if present (Figure S.IV-7, and S.IV-10): a given amount of a stock solution prepared by mixing BTA-P(DTF)2 and Cu(II)-i-butyrate was divided in order to get Cu(II)-i-butyrate (0.0029 mmol, 0.68 mg) and BTA-P(DTF)2 (0.0058 mmol, 5.59 mg) in dry THF (500 μ L) in each vial. The mixture was stirred for 30 mins. The solvent was removed under vacuum and the tube was further put under vacuum (10^{-3} mbar) for 1h. A mixture of BTA (*S*)-Leu and BTA (*R*)-Leu co-monomers with the desired *ee* (0.0058 mmol, 6.12 mg in total) was added to vials, as well as BTA Aib (0.0058 mmol, 5.62 mg) when needed. The total solvent volume is set to 1 mL (MCH or toluene).

IV.8.d. Supplementary figures.

FT-IR analysis to check if (3-VPnone) is a hydrogen bond competitor.

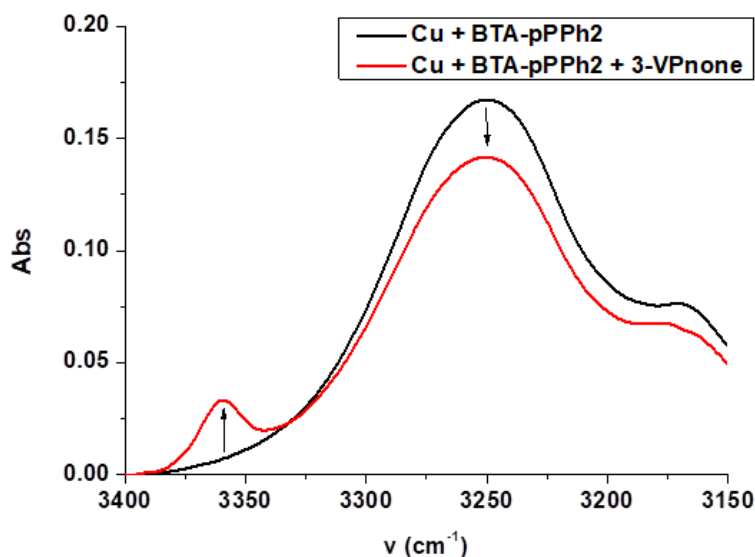


Figure S.IV-1 FT-IR analyses of the assembly of **BTA-pPPh2** (34 mM), with $\text{Cu}(\text{OAc})_2 \cdot x\text{H}_2\text{O}$ coordinated to **BTA-pPPh2** in toluene at room temperature. Black: before addition of 3-VPnone into helical BTA system, Red: after addition of 1eq of 3-VPnone into helical BTA system.

Interpretation: Before starting catalytic investigations, it was crucial to check if **3-VPnone** is a hydrogen bond competitor and whether it could impose a negative effect on the assembly formation of our helical BTA system. The most convenient way to probe this effect is to use FT-IR analysis to track the evolution of bonded amide and carbonyl functionalities of the BTA system before and after adding the substrate. The studied helical BTA system is composed of BTA ligand (**BTA-pPPh2**) coordinated to $\text{Cu}(\text{OAc})_2 \cdot x\text{H}_2\text{O}$ metal precursor. The addition of **3-VPnone** into helical BTA system composed of $\text{Cu}(\text{OAc})_2 \cdot x\text{H}_2\text{O}$ coordinated to **BTA-pPPh2** ligand in toluene provoked the formation of a small band at 3359 cm^{-1} which corresponds to free NH amide (out of stacks), and the band at 3249 cm^{-1} which corresponds to the bonded NH amide (Stacks) was slightly decreased. Thus, there is a small but not drastic effect of **3-VPnone** on the self-assemblies of **BTA-pPPh2** ligand.

Strong yellow gel obtained when DTBM-(*R*)-Segphos was employed as ligand (Table IV-2).



Figure S.IV-2 Strong yellow gel obtained after addition of silane reagent to the catalytic system composed of $\text{Cu}(\text{OAc})_2 \cdot x\text{H}_2\text{O}$ and DTBM-(*R*)-Segphos ligand.

CD analyses.

Spectra of the diluted majority-rules type experiments of a system composed of BTA-P(DTF)2

31 mM, Cu(II)-i-butyrate 15.6 mM, BTA Leu 31 mM in varied ee, and BTA Aib 31 mM in MCH.

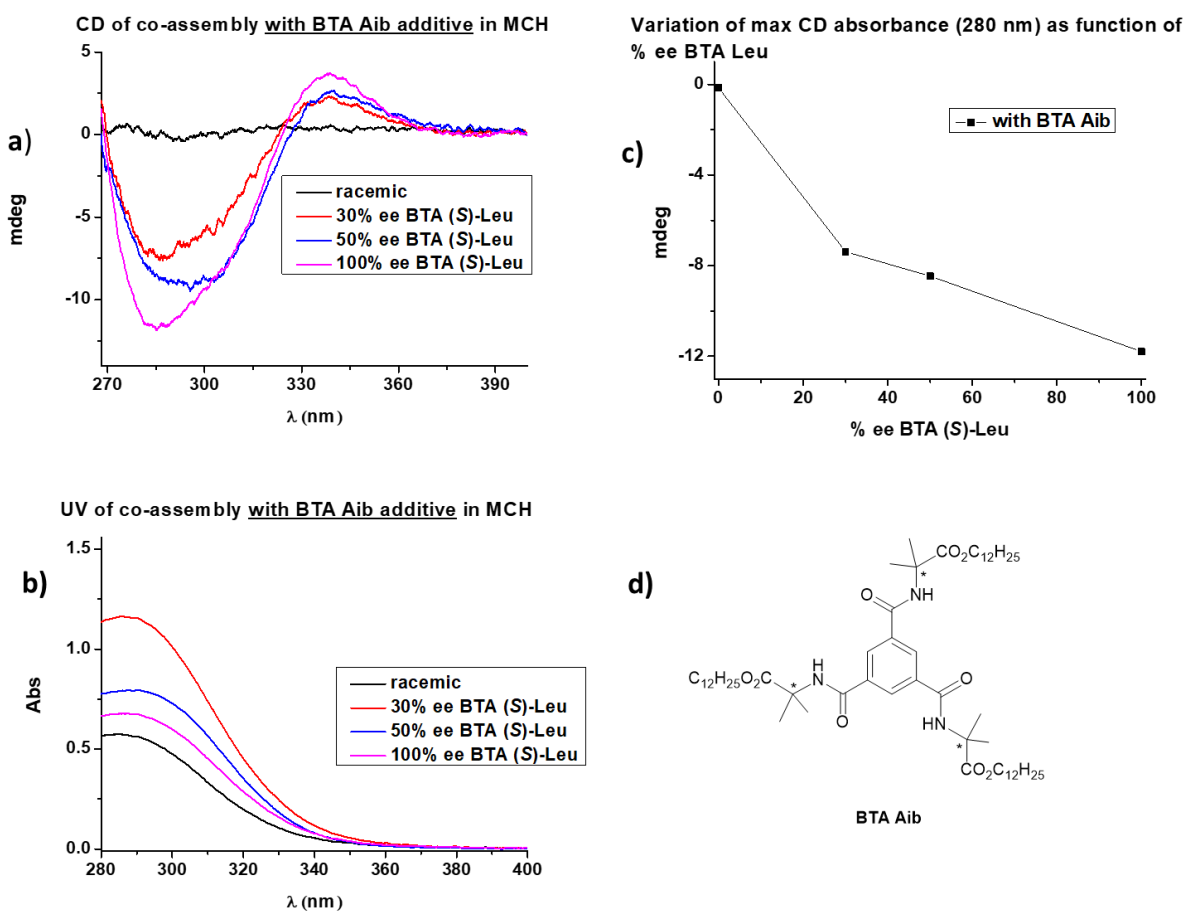


Figure S.IV-3 Spectra of the diluted majority-rules type experiments: a) CD spectra of a system composed of BTA-P(DTF)2 31 mM, Cu(II)-i-butyrate 15.6 mM, BTA Leu 31 mM in varied ee, and BTA Aib 31 mM in MCH, b) UV spectra, c) Variation of max CD absorbance as function of % ee BTA (S)-Leu, d) Structure of BTA Aib.

Interpretation: In presence of BTA Aib 31 mM as an additive in MCH, diluted MR effects are not significantly enhanced as observed for the experiments performed at constant concentration in [BTA-P(DTF)2]. As shown in (Figure S.IV-3a, d), the negative CD cotton effect at 280 nm increases almost linearly when the optical purity in BTA Leu increases. This indicates that no chirality amplification occurs in this system, *i.e.* that the optical purity of the BTA helices is proportional to the optical purity of BTA Leu.

Spectra of the diluted majority-rules type experiments: of a system composed of BTA-P(DTF)2 31 mM, Cu(II)-i-butyrate 15.6 mM, BTA Leu 31 mM in varied ee, and BTA Aib 31 mM in toluene.

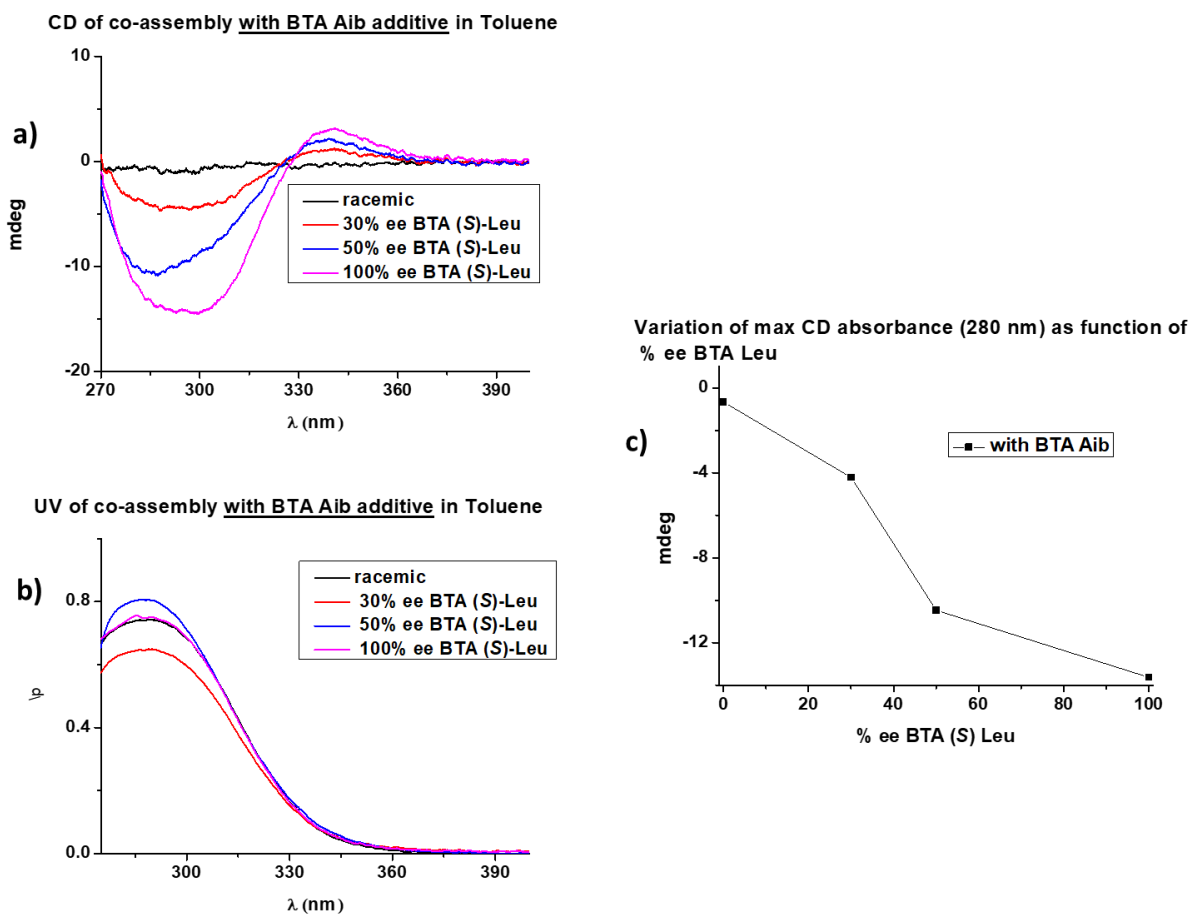


Figure S.IV-4 Spectra of the diluted majority-rules type experiments: a) CD spectra of a system composed of BTA-P(DTF)2 31 mM, Cu(II)-i-butyrate 15.6 mM, BTA Leu 31 mM in varied ee, and BTA Aib 31 mM in toluene, b) UV spectra, c) Variation of max CD absorbance (280 nm) as function of % ee BTA (S)-Leu.

Interpretation: In presence of BTA Aib 31 mM as an additive in Toluene, diluted MR effects are not significantly enhanced as observed for the experiments performed at constant concentration in [BTA-P(DTF)2]. As shown in (Figure S.IV-4a, c), the negative CD cotton effect at 280 nm increases almost linearly when the optical purity in BTA Leu increases. This indicates that no chirality amplification occurs in this system, *i.e.* that the optical purity of the BTA helices is proportional to the optical purity of BTA Leu.

Spectra of the diluted majority-rules type experiments of a system composed of BTA-P(DTF)2 5.8 mM, Cu(II)-i-butyrate 2.9 mM, BTA Leu 5.8 mM in varied ee in toluene.

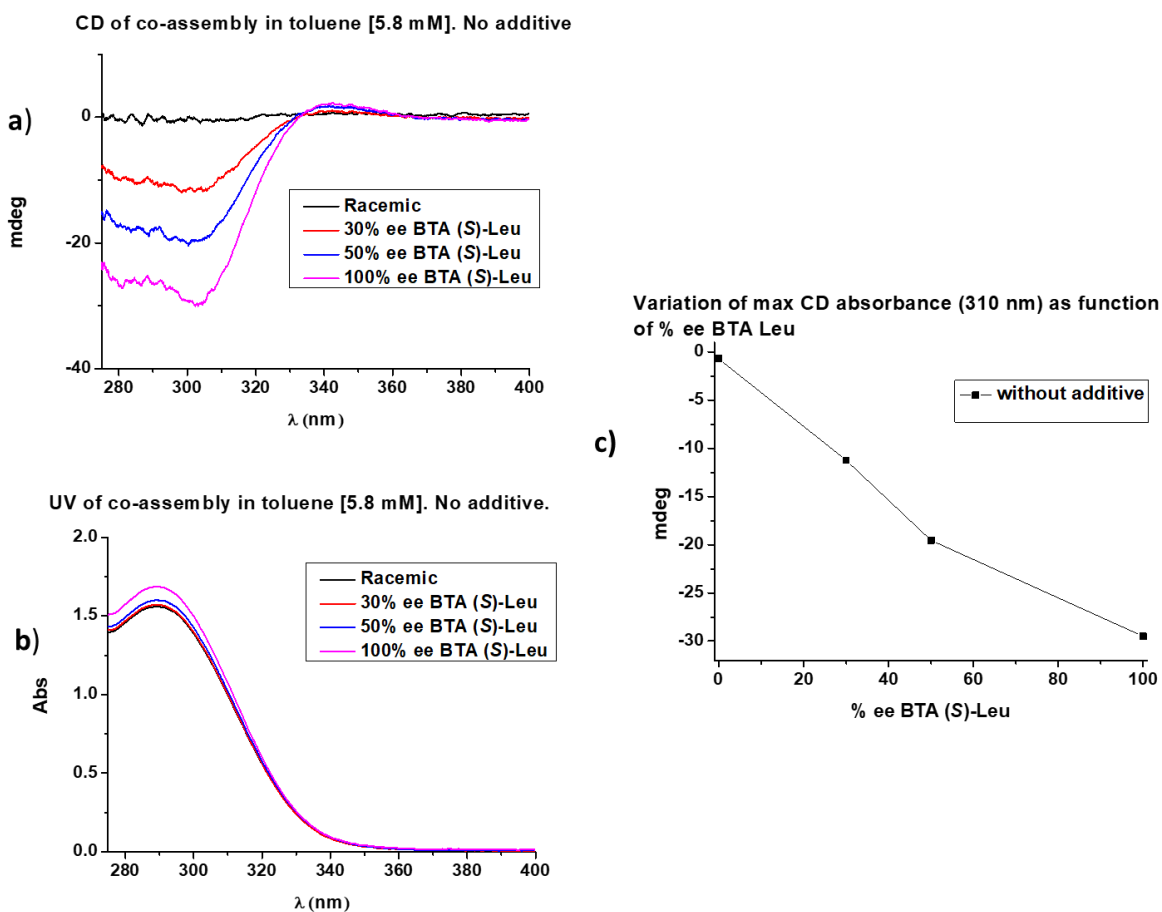


Figure S.IV-5 Spectra of the diluted majority-rules type experiments: a) CD spectra of a system composed of BTA-P(DTF)2 5.8 mM, Cu(II)-i-butyrate 2.9 mM, BTA Leu 5.8 mM in varied ee in toluene, b) UV spectra, c) Variation of max CD absorbance (310 nm) as function of % ee BTA (S)-Leu. No additive.

Interpretation: In absence of any additive in toluene, diluted MR effects are not significantly enhanced as observed for the experiments performed at constant concentration in [BTA-P(DTF)2] of 5.8 mM. Again, a linear variation of the CD values is observed in the absence of the achiral additive which corresponds to a system with no chirality amplification properties (Figure S.IV-5a, c).

Spectra of the diluted majority-rules type experiments of a system composed of **BTA-P(DTF)2** 5.8 mM, Cu(II)-i-butyrate 2.9 mM, BTA Leu 5.8 mM in varied *ee*, and BTA cyclohex 5.8 mM in toluene.

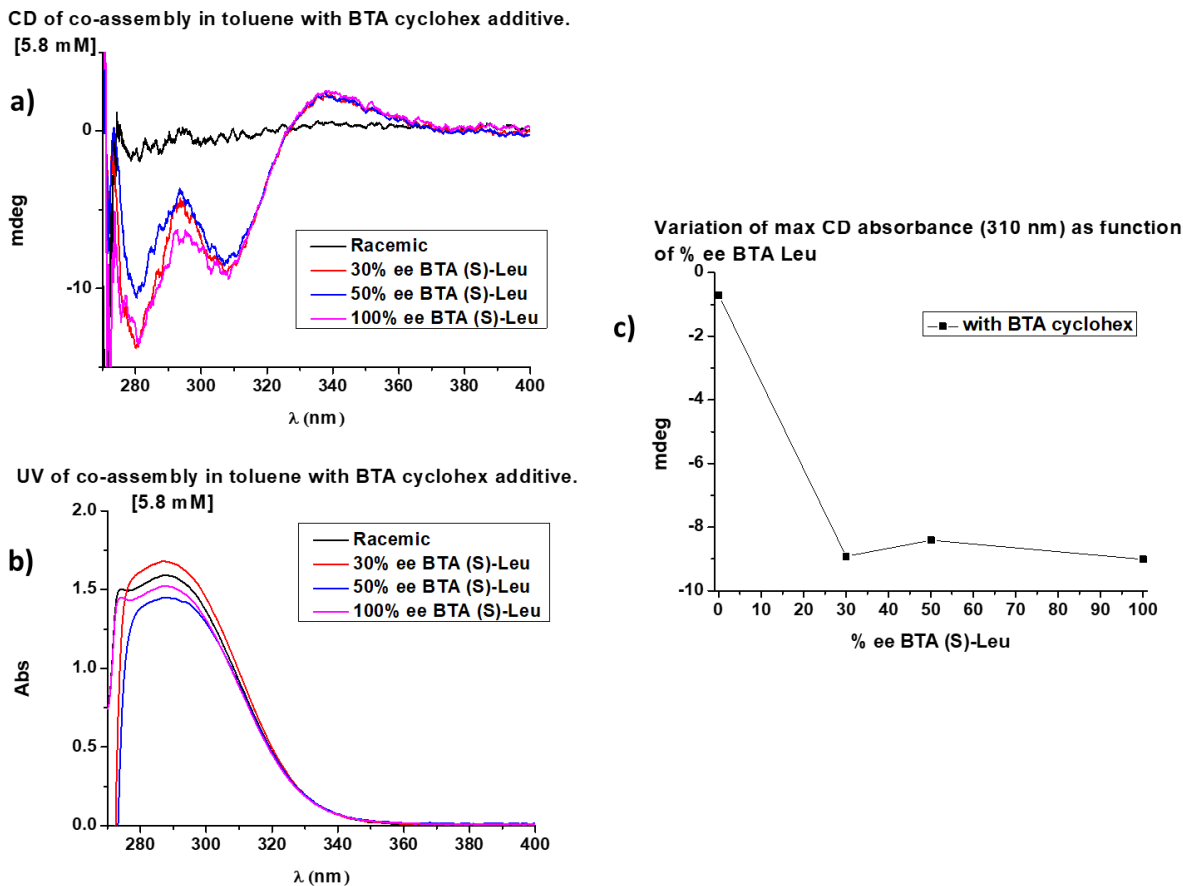


Figure S.IV-6 Spectra of the diluted majority-rules type experiments: a) CD spectra of a system composed of BTA-P(DTF)2 5.8 mM, Cu(II)-i-butyrate 2.9 mM, BTA Leu 5.8 mM in varied *ee*, and BTA cyclohex 5.8 mM in toluene, b) UV spectra, c) Variation of max CD absorbance (310 nm) as function of % *ee* BTA (S)-Leu.

Interpretation: In presence of BTA cyclohex 5.8 mM as an additive in toluene, diluted MR effects are enhanced as observed for the experiments performed at constant concentration in [BTA-P(DTF)2]. The negative CD cotton effect at 280 nm increases to reach the optimal CD value with *ca.* 30% *ee* of BTA (S)-Leu. The non-linear increase of the CD value indicates that chirality amplification occurs in this system. A scalemic excess equal to 33% *ee* is required to get the optimal value (Figure S.IV-6a, c).

Spectra of the diluted majority-rules type experiments of a system composed of BTA-P(DTF)2 5.8 mM, Cu(II)-i-butyrate 2.9 mM, BTA Leu 5.8 mM in varied *ee*, and BTA Aib 5.8 mM in toluene.

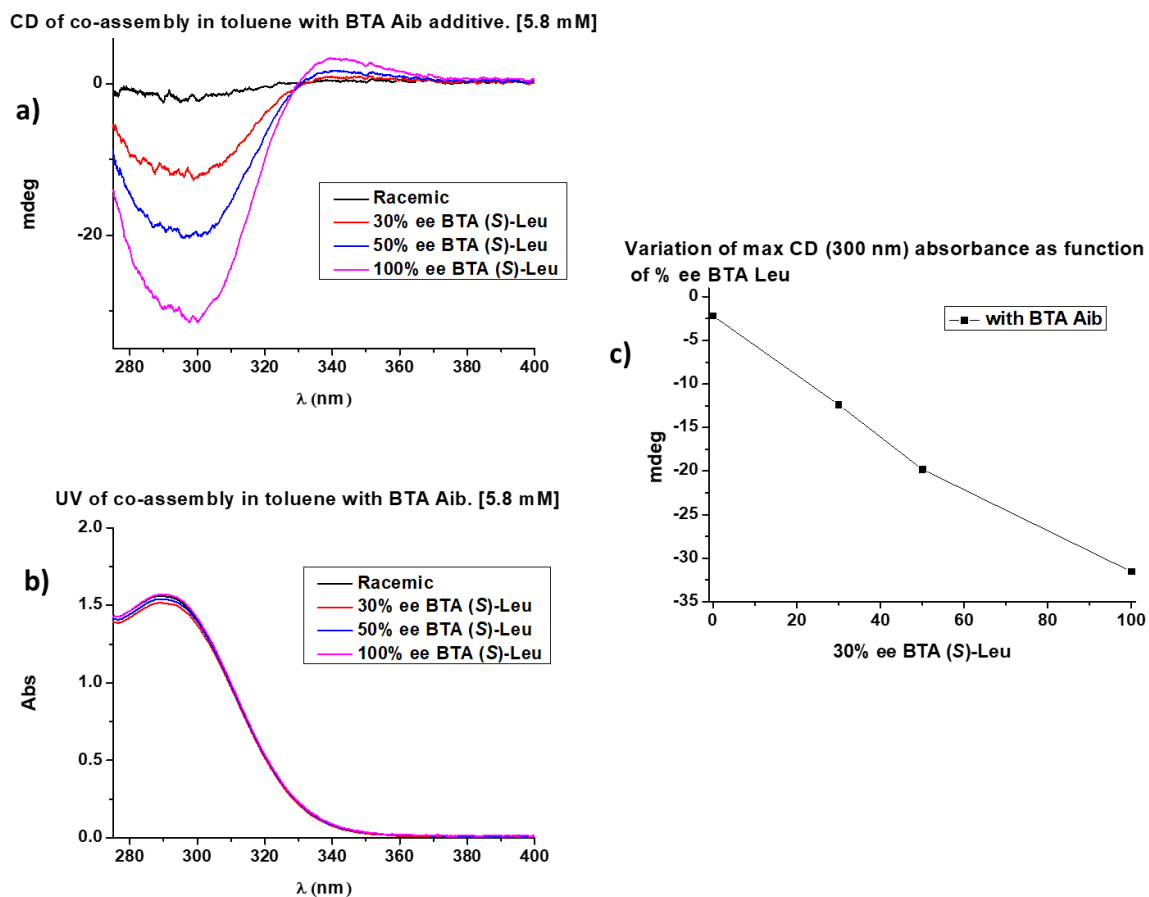


Figure S.IV-7 Spectra of the diluted majority-rules type experiments: a) CD spectra of a system composed of BTA-P(DTF)2 5.8 mM, Cu(II)-i-butyrate 2.9 mM, BTA Leu 5.8 mM in varied *ee*, and BTA Aib 5.8 mM in toluene, b) UV spectra, c) Variation of max CD absorbance (300 nm) as function of % *ee* BTA (S)-Leu.

Interpretation: In presence of BTA Aib 5.8 mM as an additive in toluene, diluted MR effects are not enhanced as observed for the experiments performed at constant concentration in [BTA-P(DTF)2]. Again, a linear variation of the CD values is observed in presence of BTA Aib additive, which corresponds to a system lacking chirality amplification properties(Figure S.IV-7a, c).

Spectra of the diluted majority-rules type experiments of a system composed of **BTA-P(DTF)2** 5.8 mM, Cu(II)-i-butyrate 2.9 mM, BTA Leu 5.8 mM in varied *ee* in MCH.

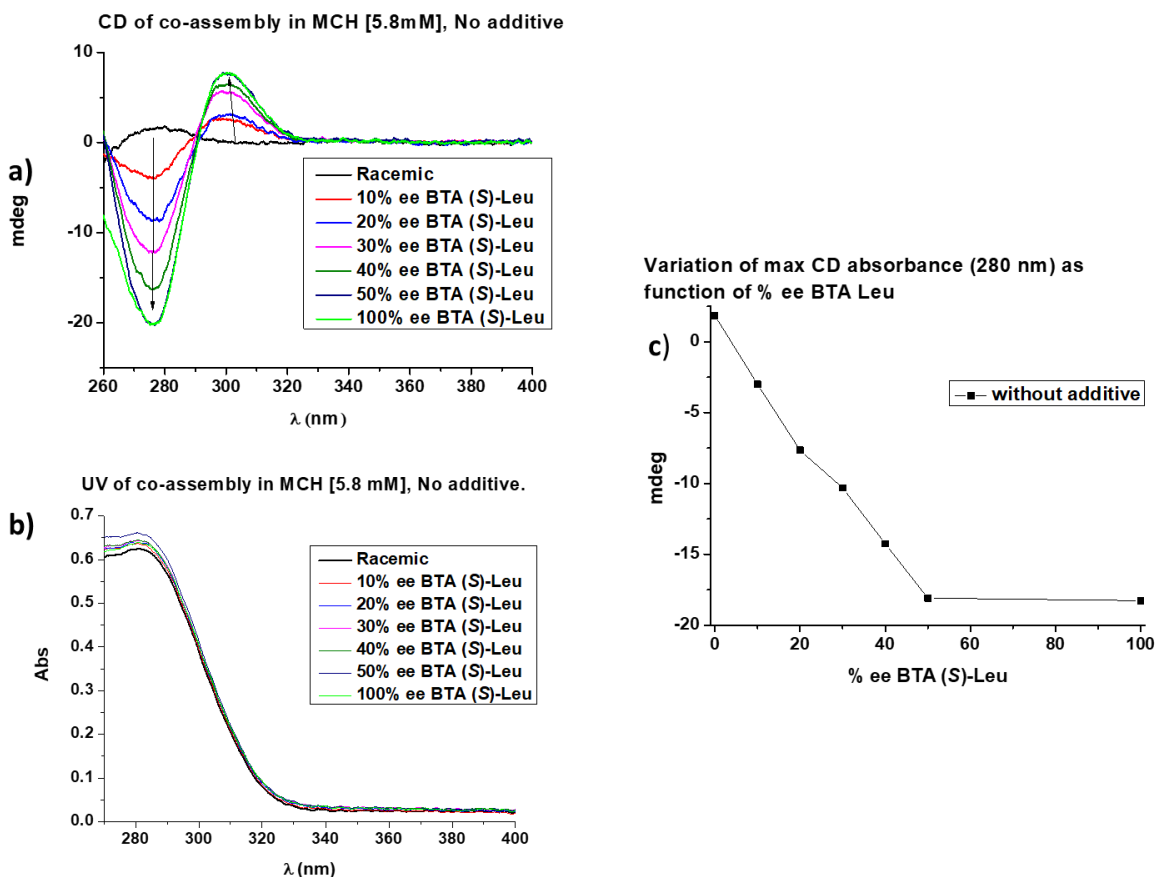


Figure S.IV-8 Spectra of the diluted majority-rules type experiments: a) CD spectra of a system composed of BTA-P(DTF)2 5.8 mM, Cu(II)-i-butyrate 2.9 mM, BTA Leu 5.8 mM in varied *ee* in MCH, c) Variation of max CD absorbance (280 nm) as function of % *ee* BTA (S)-Leu.

Interpretation: In absence of any additive in MCH, diluted MR effects observed for the experiments performed at constant concentration in [BTA-P(DTF)2] of 5.8 mM. The negative CD cotton effect at 280 nm increases to reach the optimal CD value with *ca.* 50% *ee* of BTA (S)-Leu. The non-linear increase of the CD value indicates that chirality amplification occurs in this system. A scalemic excess equal to 50% *ee* is required to get the optimal value (Figure S.IV-8a, c).

Spectra of the diluted majority-rules type experiments of a system composed of BTA-P(DTF)2 5.8 mM, Cu(II)-i-butyrate 2.9 mM, BTA Leu 5.8 mM in varied *ee*, BTA cyclohex 5.8 mM in MCH.

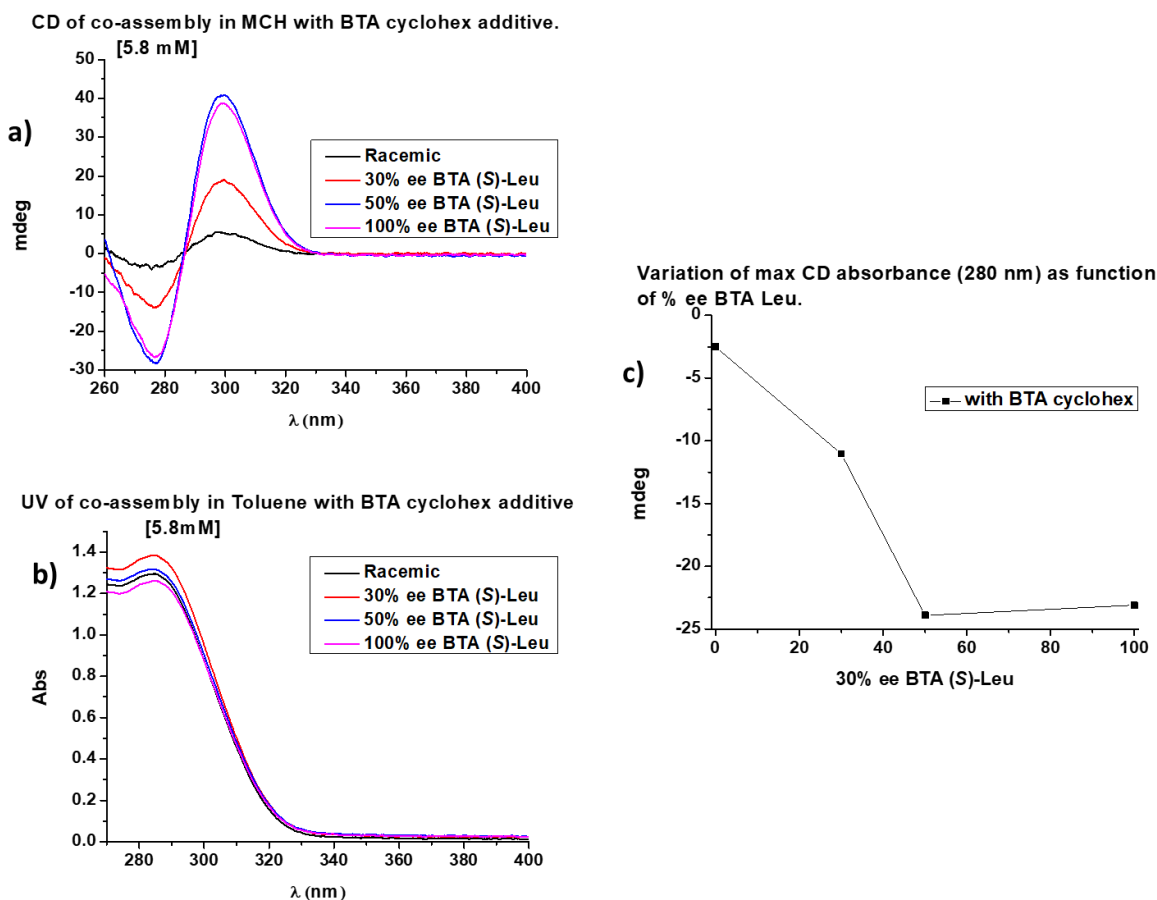


Figure S.IV-9 Spectra of the diluted majority-rules type experiments: a) CD spectra of a system composed of BTA-P(DTF)2 5.8 mM, Cu(II)-i-butyrate 2.9 mM, BTA Leu 5.8 mM in varied *ee*, BTA cyclohex 5.8 mM in MCH, c) Variation of max CD absorbance (280 nm) as function of % *ee* BTA (S)-Leu.

Interpretation: In presence of BTA cyclohex 5.8 mM as an additive in MCH, diluted MR effects are enhanced as observed for the experiments performed at constant concentration in [BTA-P(DTF)2]. The negative CD cotton effect at 280 nm increases to reach the optimal CD value with *ca.* 50% *ee* of BTA (S)-Leu. The non-linear increase of the CD value indicates that chirality amplification occurs in this system. A scalemic excess equal to 50% *ee* is required to get the optimal value (Figure S.IV-9a, c).

Spectra of the diluted majority-rules type experiments of a system composed of BTA-P(DTF)2 5.8 mM, Cu(II)-i-butyrate 2.9 mM, BTA Leu 5.8 mM in varied ee, BTA Aib 5.8 mM in MCH.

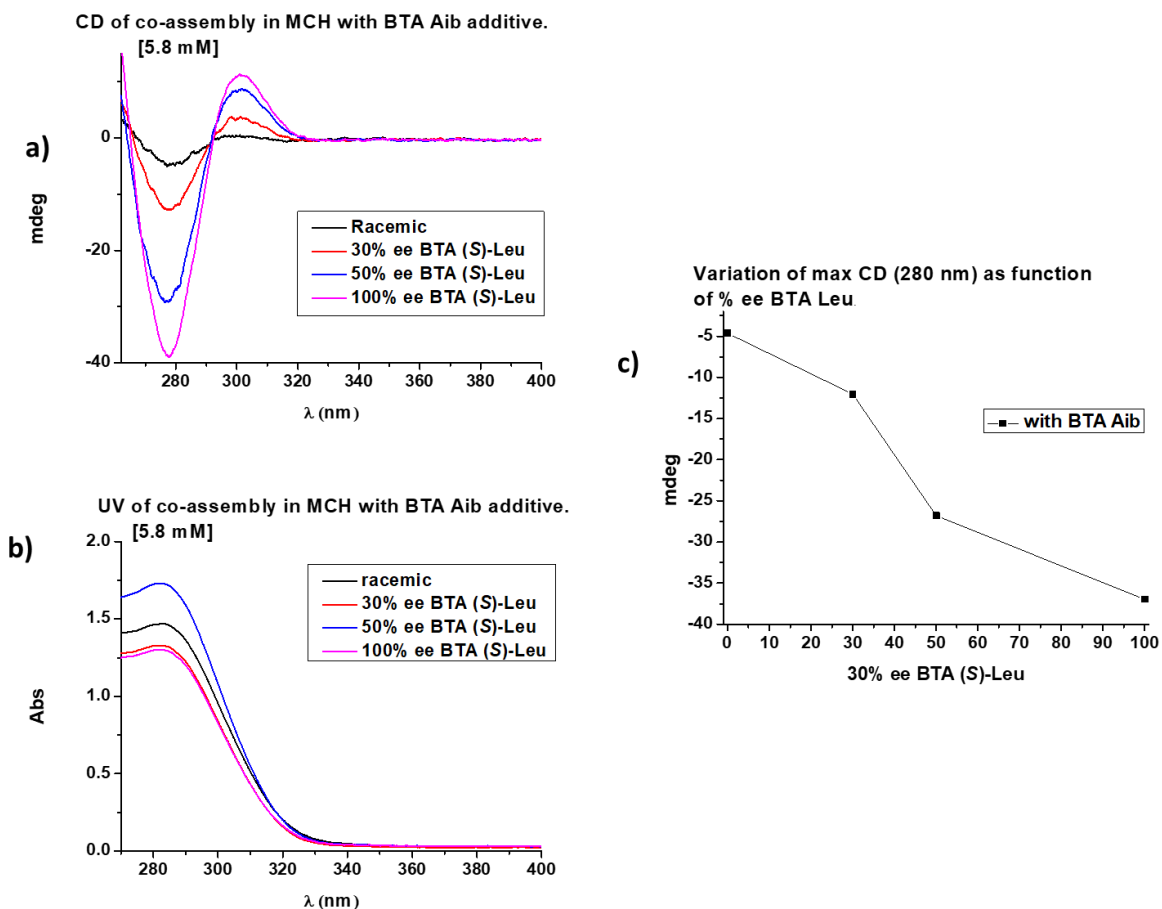


Figure S.IV-10 Spectra of the diluted majority-rules type experiments: a) CD spectra of a system composed of BTA-P(DTF)2 5.8 mM, Cu(II)-i-butyrate 2.9 mM, BTA Leu 5.8 mM in varied ee, BTA Aib 5.8 mM in MCH, c) Variation of max CD absorbance (280 nm) as function of % ee BTA (S)-Leu.

Interpretation: In presence of BTA Aib 5.8 mM as an additive in MCH, diluted MR effects are not significantly enhanced as observed for the experiments performed at constant concentration in [BTA-P(DTF)2]. Again, a linear variation of the CD values is observed in presence of BTA Aib as additive which corresponds to a system with no chirality amplification properties (Figure S.IV-10a, c).

IV.8.e. Synthesis of substrates.

(*E*)-1-(3-(prop-1-en-1-yl)phenyl)ethenone (**3-*E*-MeVPnone**). A solution of potassium (*E*)-1-propene-1-trifluoroborate (16.9 mmol, 2.5 g, 1.3 equiv.), PdCl₂ (0.26 mmole, 46 mg, 0.02 equiv.), PPh₃ (0.77 mmole, 0.2 g, 0.06 equiv.), Cs₂CO₃ (39 mmol, 13 g, 3 equiv.), and 1-(3-bromophenyl)ethanone (13.0 mmole, 1.7 mL, 1 equiv.) in THF/H₂O (9:1) (70 mL) was heated at 85 °C under argon atmosphere in a sealed tube. The reaction mixture was stirred at 85 °C for 22 h, then cooled to RT and diluted with H₂O (70 mL) followed by extraction with CH₂Cl₂ (50 mL X 3). The solvent was removed in vacuum, and the crude product was purified by flash chromatography over silica gel (PE/ethylacetate : 20/1) to give the desired product as a pale-yellow oil (1.5 g, 70% yield). ¹H NMR (300 MHz, CDCl₃) δ (ppm) 7.93 (t, 1H), 7.80 (d, 1H), 7.56 (d, 1H), 7.41 (t, 1H), 6.51-6.29 (m, 2H), 2.63 (s, 3H).

(*Z*)-1-(3-(prop-1-en-1-yl)phenyl)ethenone (**3-*Z*-MeVPnone**). A solution of Potassium (*Z*)-1-propene-1-trifluoroborate (16.89 mmol, 2.5 g, 1.3 equiv.), PdCl₂ (0.259 mmole, 46 mg, 0.02 equiv.), PPh₃ (0.77 mmole, 0.2 g, 0.06 equiv.), Cs₂CO₃ (38.97 mmol, 13 g, 3 equiv.), and 1-(3-bromophenyl)ethanone (12.99 mmole, 1.7 ml, 1 equiv.) in THF/H₂O (9:1) (70 mL) was heated at 85 °C under argon atmosphere in a sealed tube. The reaction mixture was stirred at 85 °C for 22 h, then cooled to RT and diluted with H₂O (70 mL) followed by extraction with CH₂Cl₂ (50 mL X 3). The solvent was removed in vacuum, and the crude product was purified by silica gel chromatography (PE/ethylacetate : 20/1) to give the desired product as pale-yellow oil (1.5g, 70% yield). ¹H NMR (300 MHz, CDCl₃) δ (ppm) 7.90 (s, 1H), 7.84 (d, 1H), 7.54-7.42 (m, 2H), 6.59 – 6.39 (m, 1H), 5.90 (dq, *J* = 11.6, 7.2 Hz, 1H), 2.64 (s, 3H).

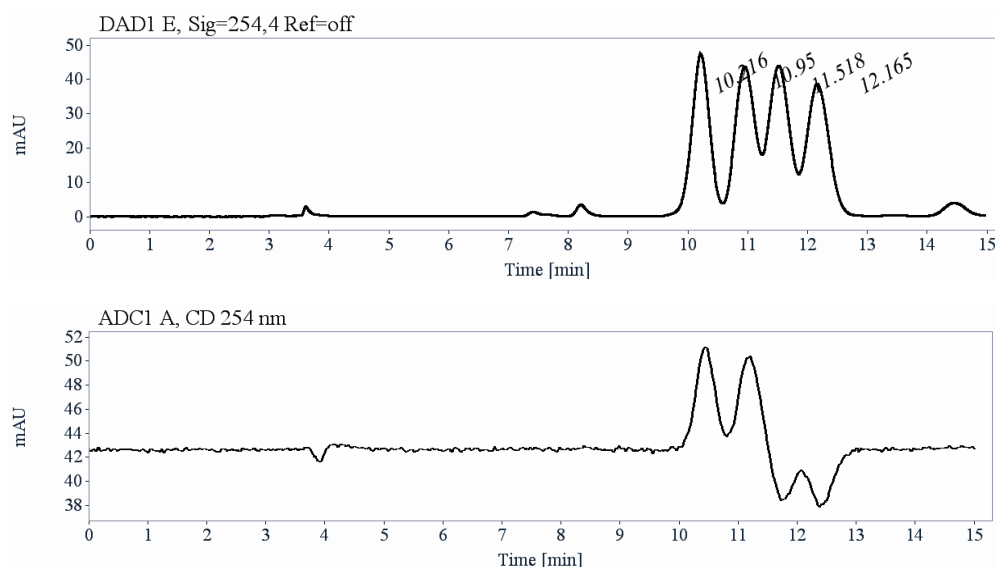
(*E*)-1-(4-(prop-1-en-1-yl)phenyl)ethenone (**4-*E*-MeVPnone**). A solution of Potassium (*E*)-1-propene-1-trifluoroborate (16.89 mmol, 2.5 g, 1.3 equiv.), PdCl₂ (0.259 mmole, 46 mg, 0.02 equiv.), PPh₃ (0.77 mmole, 0.2 g, 0.06 equiv.), Cs₂CO₃ (38.97 mmol, 13 g, 3 equiv.), and 1-(4-bromophenyl)ethanone (12.99 mmole, 1.7 ml, 1 equiv.) in THF/H₂O (9:1) (70 mL) was heated at 85 °C under argon atmosphere in a sealed tube. The reaction mixture was stirred at 85 °C for 22 h, then cooled to RT and diluted with H₂O (70 mL) followed by extraction with CH₂Cl₂ (50 mL X 3). The solvent was removed in vacuum, and the crude product was purified by silica gel chromatography (PE/ethylacetate : 20/1) to give the desired product as pale-yellow oil (1.2g,

60% yield). ^1H NMR (300 MHz, CDCl_3) δ (ppm) 7.91 (d, 2H), 7.42 (d, 2H), 6.50-6.34 (m, 2H), 2.60 (s, 3H).

1-(4'-vinyl-[1,1'-biphenyl]-4-yl)ethenone (4-VBPnone). A solution of Potassium vinyl trifluoroborate (11.19 mmol, 1.5 g, 1.3 equiv.), PdCl_2 (0.17 mmole, 30.1 mg, 0.02 equiv.), PPh_3 (0.516 mmole, 0.14 g, 0.06 equiv.), Cs_2CO_3 (38.97 mmol, 13 g, 3 equiv.), and 1-(4'-bromo-[1,1'-biphenyl]-4-yl)ethanone (8.6 mmole, 1.57 ml, 1 equiv.) in THF/ H_2O (9:1) (70 mL) was heated at 85 °C under argon atmosphere in a sealed tube. The reaction mixture was stirred at 85 °C for 22 h, then cooled to RT and diluted with H_2O (70 mL) followed by extraction with CH_2Cl_2 (50 mL X 3). The solvent was removed in vacuum, and the crude product was purified by silica gel chromatography (PE/ethylacetate : 20/1) to give the desired product as pale-yellow oil (25 mg, 13% yield). ^1H NMR (300 MHz, CDCl_3) δ (ppm) 8.06 (d, 2H), 7.73 (d, 2H), 7.64 (d,2H), 7.55 (d,2H), 6.80 (dd, $J = 17.6, 10.9$ Hz, 1H), 5.88 (d, $J = 18.4$ Hz 1H), 5.34 (d, $J = 10.9$ Hz, 1H), 2.66 (s, 3H).

IV.8.f. Analytical chiral HPLC separation for compound 3-APnol.

The sample is dissolved in a mixture of heptane/ethanol (98/2), injected on the chiral Chiralpak IG column, and detected with an UV detector at 254 nm. The flow-rate is 1 mL/min, Temp: 35°C.



RT [min]	Area	Area%	
10.22	894	23.78	1 st eluted on Chiralpak IG ($\alpha_D + 104$) (+, CD 254 nm)
10.95	911	24.25	2 nd eluted on Chiralpak IG ($\alpha_D + 68$) (+, CD 254 nm)
11.52	1003	26.69	3 rd eluted on Chiralpak IG ($\alpha_D - 104$) (-, CD 254 nm)
12.16	950	25.28	4 th eluted on Chiralpak IG ($\alpha_D - 68$) (-, CD 254 nm)
Sum	3758	100.00	

Preparative HPLC separation of all stereoisomers of 3-APnol.

The separation was done in three steps:

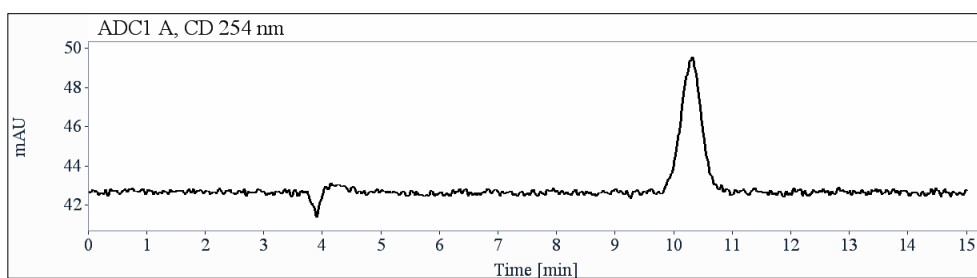
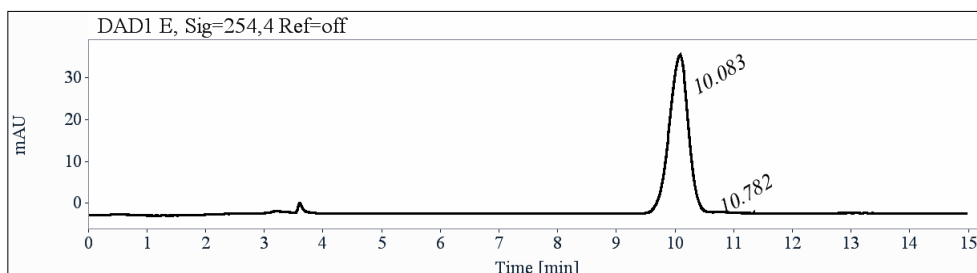
1- On Chiralpak AD-H (250 x 10 mm), hexane / Ethanol (97/3) as mobile phase, flow-rate = 5 mL/min, UV detection at 230 nm, to separate the (+)-isomers from the (-)-isomers.

2- On Lux-Cellulose-1 (250 x 10 mm), hexane / Isopropanol (95/5) as mobile phase, flow-rate = 5 mL/min, UV detection at 254 nm, to separate the isomer with $\alpha_D = +104$ from the isomer with $\alpha_D = +68$.

3- On Chiralpak AD-H (250 x 10 mm), hexane / Iso-propanol (95/5) as mobile phase, flow-rate = 5 mL/min, UV detection at 254 nm, to separate the isomer with $\alpha_D = -104$ from the isomer with $\alpha_D = -68$.

Collected isomers:

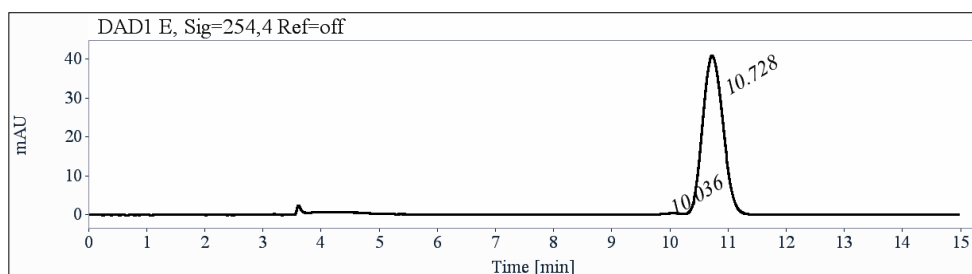
- 1st eluted on Chiralpak IG ($\alpha_D +104$): 10 mg of **(+,+)** isomer with de > 99% and ee > 99.5%,

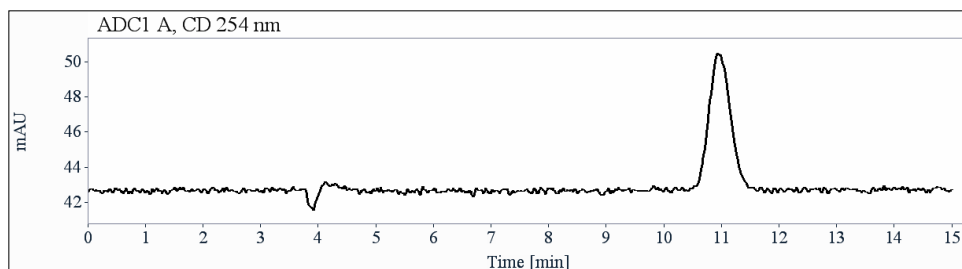


RT [min]	Area	Area%
10.08	864	99.04
10.78	8	0.96
Sum	873	100.00

Fraction: 2.3 mg with de > 96% and ee > 99.5%.

- 2nd eluted on Chiralpak IG ($\alpha_D + 68$): 15 mg of **(-,+)** isomer with de > 98.5% and ee > 99.5%

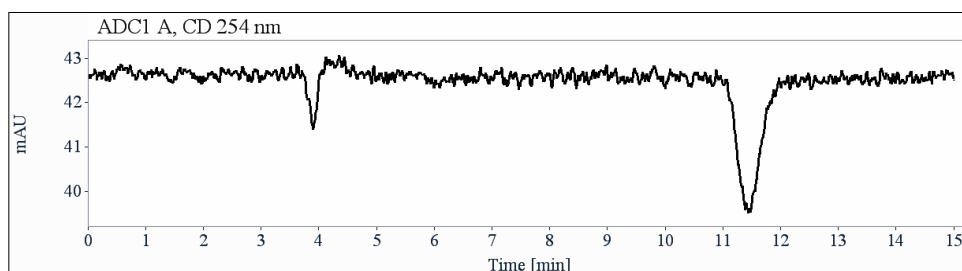
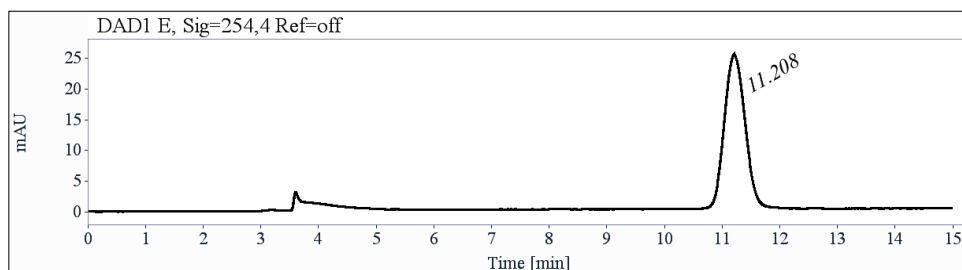




RT [min]	Area	Area%
10.04	9	0.87
10.73	999	99.13
Sum	1008	100.00

Fraction: 10 mg with de = 93.5% and ee > 99.5%.

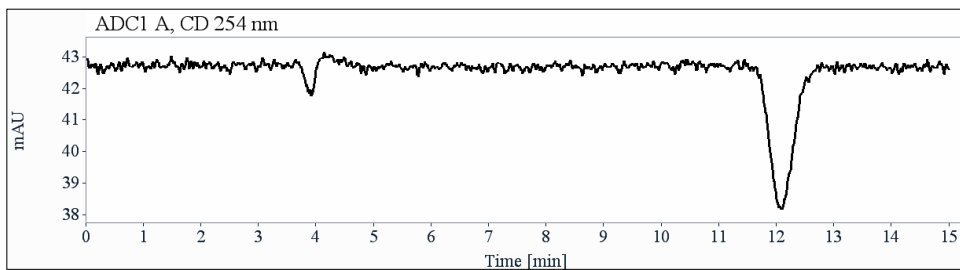
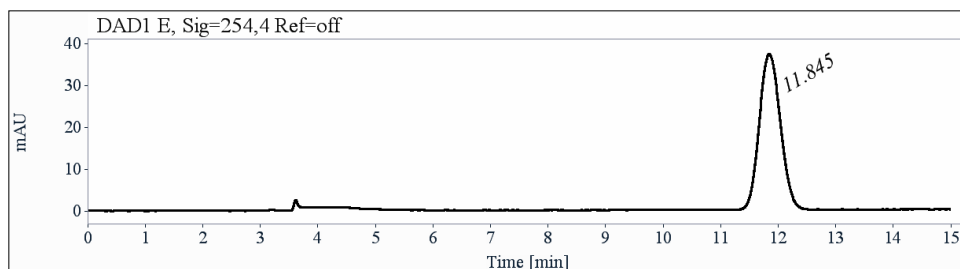
- 3rd eluted on Chiralpak IG (α_D - 104): 3.8 mg of (-,-) isomer with de > 99 % and ee > 99.5%



RT [min]	Area	Area%
11.21	632	100.00
Sum	632	100.00

Fraction: 11 mg with de > 98% and ee > 99.5%.

- 4th eluted on Chiralpak IG (α_D - 68): 11 mg of (+,-) isomer with de > 99.5% and ee > 99.5%



RT [min]	Area	Area%
11.85	950	100.00
Sum	950	100.00

Fraction: 1.2 mg with de > 98.5% and ee > 99.5%

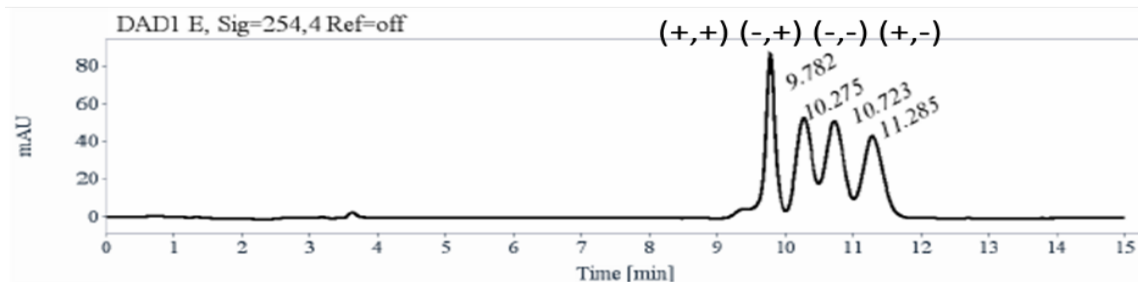
Optical rotations.

Optical rotations were measured on a Jasco P-2000 polarimeter with a halogen lamp (589, 578, 546, 436, 405 and 365 nm), in a 10 cm cell, thermostated at 25°C with a Peltier controlled cell holder.

λ (nm)	Amino-Alcohol (+,+) , first eluted on Chiralpak IG, $[\alpha]_{\lambda}^{25}$ (CH ₂ Cl ₂ , c =0.54)	Amino-Alcohol (-,-) , third eluted on Chiralpak IG, $[\alpha]_{\lambda}^{25}$ (CH ₂ Cl ₂ , c =0.55)
589	+ 104	- 104
578	+ 109	- 109
546	+ 127	- 127
436	+ 229	- 229
405	+ 289	- 289
365	+ 421	- 421

λ (nm)	Amino-Alcohol (-, +) , second eluted on Chiralpak IG, $[\alpha]_{\lambda}^{25}$ (CH ₂ Cl ₂ , c =0.5)	Amino-Alcohol (+,-) , fourth eluted on Chiralpak IG, $[\alpha]_{\lambda}^{25}$ (CH ₂ Cl ₂ , c =0.53)
589	+ 68	- 68
578	+ 71	- 71
546	+ 84	- 84
436	+ 156	- 156
405	+ 200	- 200
365	+ 300	- 300

Attribution of HPLC signals to stereoisomers



The different stereoisomers eluted from the ChiralPak IG can be attributed as follows: $(+^{alc}, +^{amino})$, $(-^{alc}, +^{amino})$, $(-^{alc}, -^{amino})$, and $(+^{alc}, -^{amino})$ where the first and second +/- signs correspond to the stereogenic centers connected to the alcohol and amine, respectively. This attribution was made possible according to:

- i) The aforementioned preparative chiral HPLC which allow the identification of the pair of enantiomers.
- ii) The catalytic experiments performed with catalysts of different configuration. **(+,+)** stereoisomer was obtained from the catalyst yielding **(+,-)** in absence of commutation for the second step, see e.g. (Table IV-15, entry 3) and **(-,-)** stereoisomer was obtained from the catalyst yielding **(-,+)** in absence of commutation for the second step, see e.g. (Table IV-17, entry 3).

Electronic Circular Dichroism and UV spectra.

ECD and UV spectra were measured on a JASCO J-815 spectrometer equipped with a JASCO Peltier cell holder PTC-423 to maintain the temperature at $25.0 \pm 0.2^\circ\text{C}$. A CD quartz cell of 1 mm of optical pathlength was used. The CD spectrometer was purged with nitrogen before recording each spectrum, which was baseline subtracted. The baseline was always measured for the same solvent and in the same cell as the samples. The spectra are presented without smoothing and further data processing.

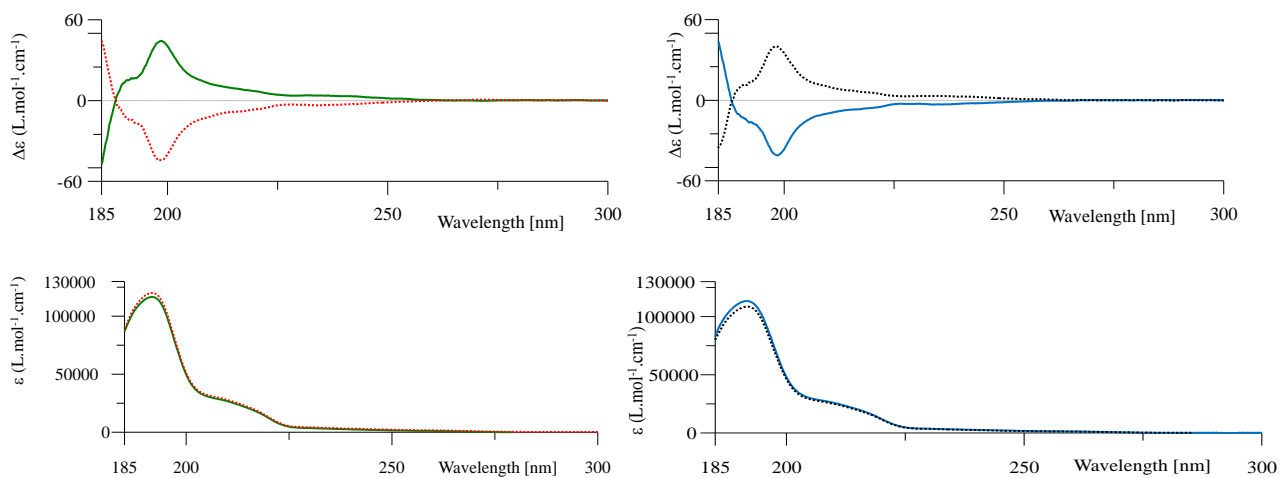
First eluted isomer on Chiralpak IG, $\alpha_D = +104$: green solid line, concentration = $0.165 \text{ mmol.L}^{-1}$ in acetonitrile.

Third eluted isomer on Chiralpak IG, $\alpha_D = -104$: red dotted line, concentration = $0.157 \text{ mmol.L}^{-1}$ in acetonitrile.

Second eluted isomer on Chiralpak IG, $\alpha_D = +68$: black dotted line, concentration = $0.179 \text{ mmol.L}^{-1}$ in acetonitrile.

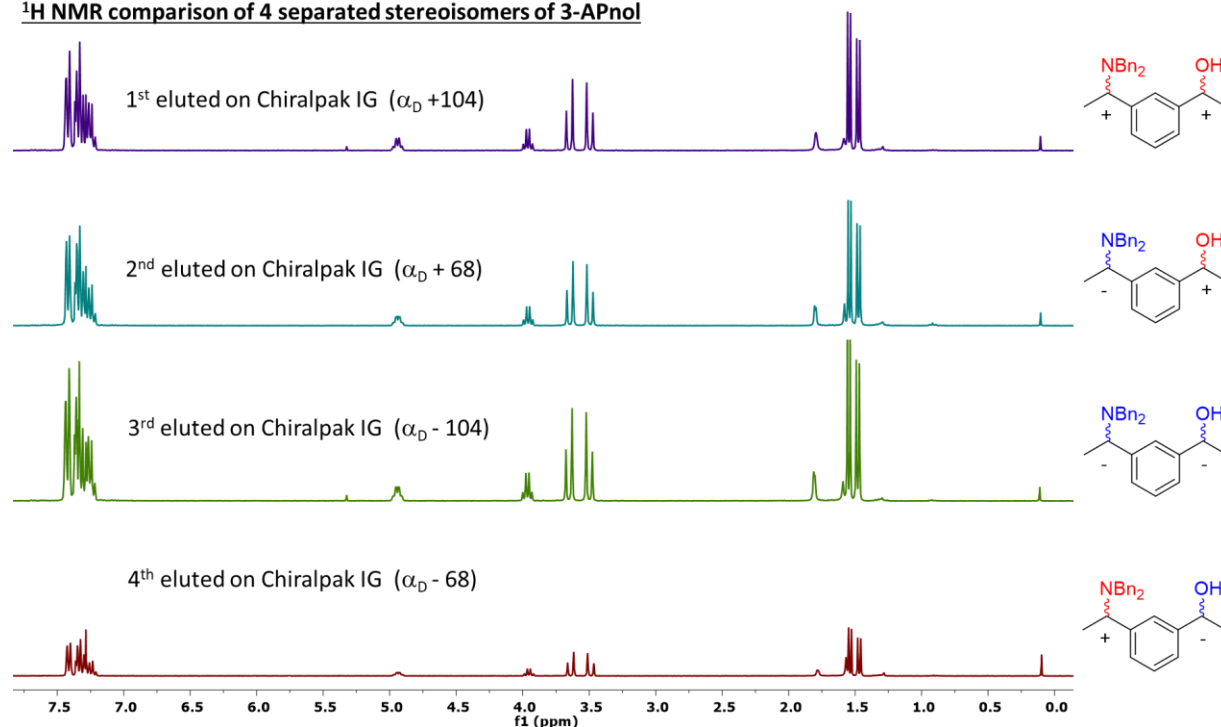
Fourth eluted isomer on Chiralpak IG, $\alpha_D = -68$: blue solid line, concentration = $0.145 \text{ mmol.L}^{-1}$ in acetonitrile.

Acquisition parameters: 0.1 nm as intervals, scanning speed 50 nm/min, band width 2 nm, and 3 accumulations per sample.



^1H NMR of separated fractions .

^1H NMR comparison of 4 separated stereoisomers of 3-APnol



According to ^1H NMR analyses, all **3-APnol** stereoisomers exhibited exactly the same ^1H NMR spectrum.

IV.8.g. Formulas for determining ee1, ee2, ee_{tot}, and dr.

The cascade reaction is composed of two reaction steps (HS and HA). Both steps are considered as independent, *i.e.* the first formed stereogenic center ($\text{C}^{\text{alcohol}}$) by HS has no influence on the reactivity and selectivity of the second step which yields the second stereogenic center (C^{amino}). ee1 represents the enantiomeric excess of the first alcohol intermediate formed, and ee2 the enantiomeric excess of the (C^{amino}) stereogenic center formed by HA. After HS, two enantiomers of **3-VPnol** are formed: (+)-**3-VPnol**, and (-)-**3-VPnol**. Those two enantiomers will undergo hydroamination to give the four possible stereoisomers of **3-APnol**. Enantioselectivity (ee2, ee2') and conversion of the HA step are assumed to be identical for (+)-**3-VPnol**, and (-)-**3-VPnol**. This hypothesis is supported by the fact that for mixed BTA catalytic systems composed of **BTA-P(DTF)2** and **BTA Leu** ee2 \approx ee2'.

If the major stereoisomer of **3-APnol** is (-,+), as in the case of the experiment conducted with **BTA-P(DTF)2** and **BTA (R)-Leu** mixture:

First step ee1 is in favor of (-)-3-VPnol:

$$\text{such as } ee1 = [(-)\text{-3-VPnol} - (+)\text{-3-VPnol}] / [(+)\text{-3-VPnol} + (-)\text{-3-VPnol}]$$

$$\text{Then: } (-)\text{-3-VPnol} = (1+ee1)/2.$$

The second step ee2 is in favor of (+)-C^{amino}:

$$\text{such as } ee2 = [(-,+)\text{-3-APnol} - (-,-)\text{-3-APnol}] / [(-,+)\text{-3-APnol} + (-,-)\text{-3-APnol}]$$

$$\text{and } ee2' = [(+,+)\text{-3-APnol} - (+,-)\text{-3-APnol}] / [(+,+)\text{-3-APnol} + (+,-)\text{-3-APnol}]$$

$$\text{With } (-)\text{-3-VPnol} = (-,+)\text{-3-APnol} + (-,-)\text{-3-APnol}$$

$$\text{such as } ee2 = [(-,+)\text{-3-APnol} - (-)\text{-3-VPnol} + (-,+)\text{-3-APnol}] / (-)\text{-3-VPnol},$$

$$ee2 = [2 \times (-,+)\text{-3-APnol} - (-)\text{-3-VPnol}] / (-)\text{-3-VPnol},$$

$$\text{and thus: } (-,+)\text{-3-APnol} = [ee2 \times (-)\text{-3-VPnol} + (-)\text{-3-VPnol}] / 2$$

which gives after combining the equations:

$$f(-,+) = \frac{(1+ee2) \times (1+ee1)}{4}$$

$$f(-,-) = \frac{(1-ee2) \times (1+ee1)}{4}$$

$$f(+,+) = \frac{(1+ee2) \times (1-ee1)}{4}$$

$$f(+,-) = \frac{(1-ee2) \times (1-ee1)}{4}$$

Here (-,+) is the major stereoisomer such as:

$$ee_{tot}(-,+) = \frac{(-,+) - (+,-)}{(-,+) + (+,-)} = \frac{ee1 + ee2}{1 + (ee2 \times ee1)}$$

ee2 is determined exp. so ee1 is deduced such as:

$$ee1 = \frac{ee_{tot}(-,+) - ee2}{1 - (ee2 \times ee_{tot}(-,+))}$$

$$dr = \frac{(-,+)+(+,-)}{(+,+)+(-,-)} = \frac{1 + (ee_2 \times ee_1)}{1 - (ee_2 \times ee_1)}$$

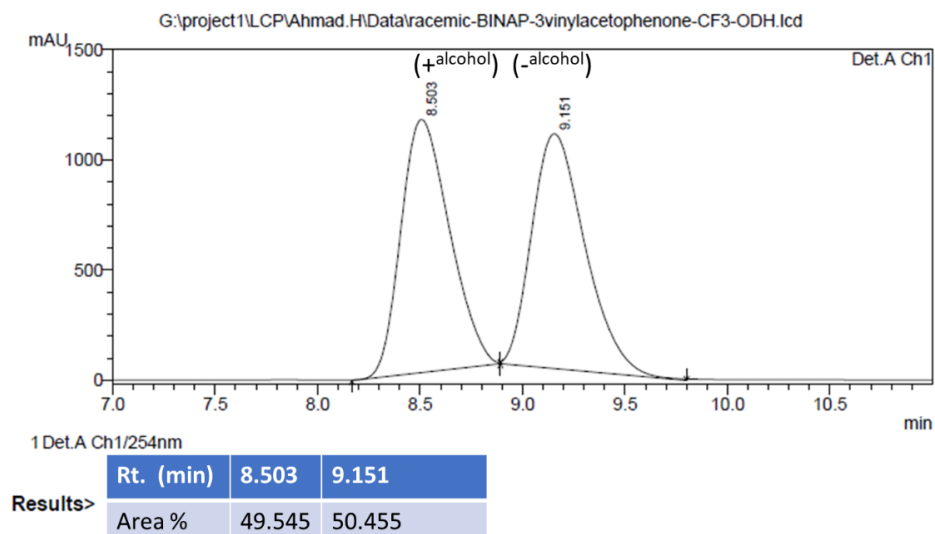
With ee1 positive [negative] when the (-) enantiomer [(+)enantiomer, resp.] is in majority.

With ee2 positive [negative] when the (+) enantiomer [(-)enantiomer, resp.] is in majority.

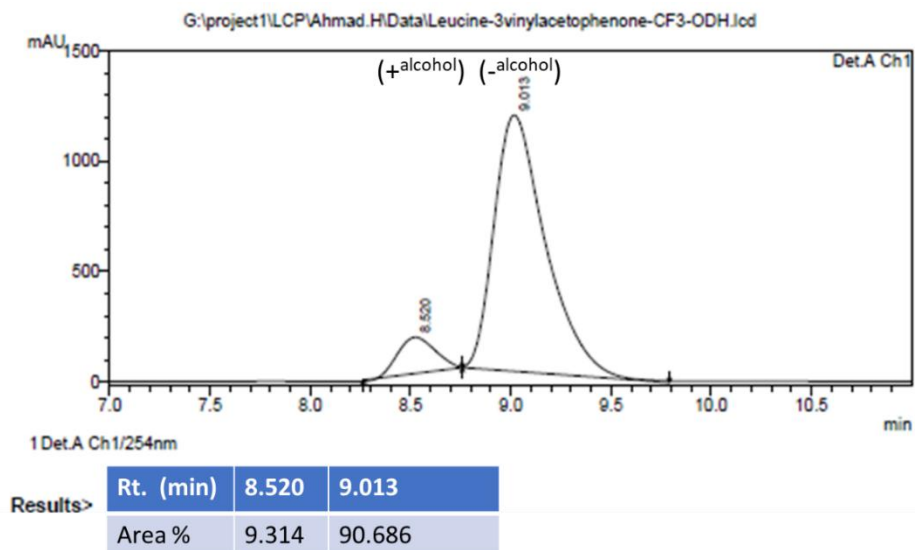
IV.8.h. Selected HPLC spectrums.

Selected HPLC spectrums of (3-VPnol)

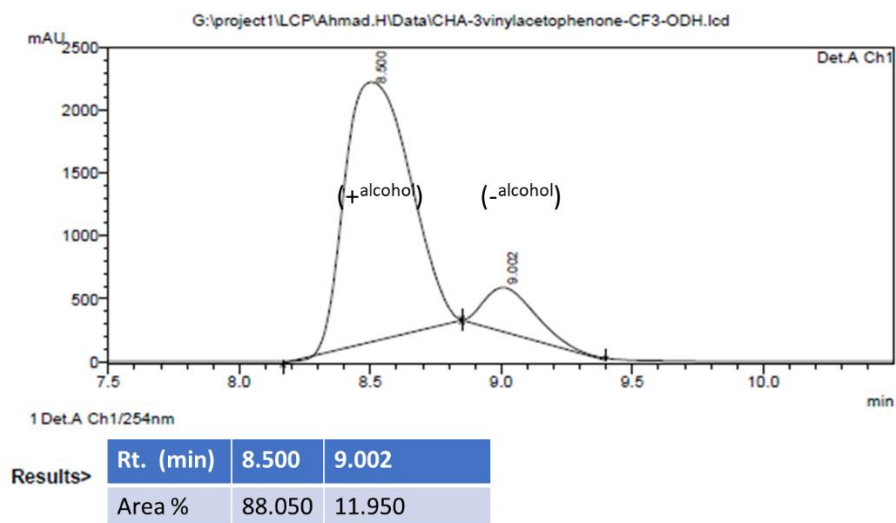
-Reference: Cu(OAc)₂.H₂O, Racemic BINAP, THF, ee: 0%.



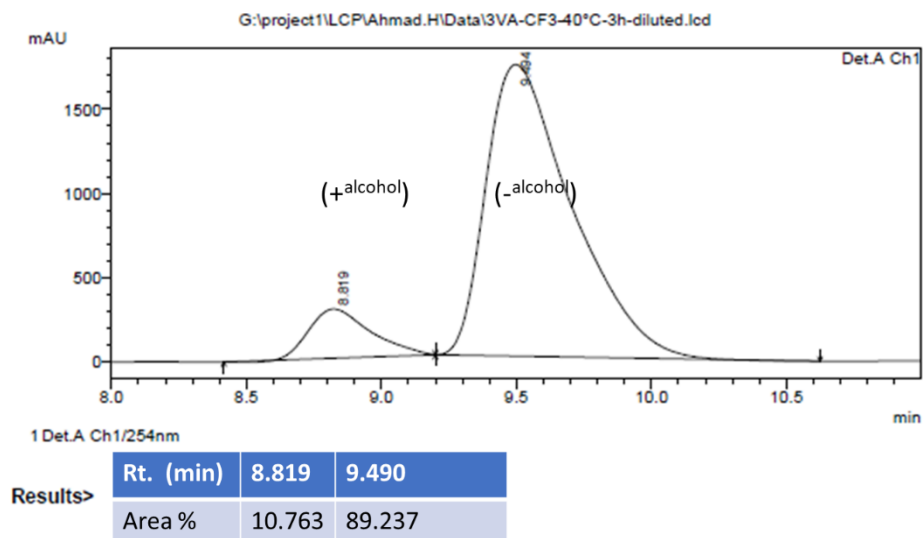
-Table IV-4, entry 4. Cu(OAc)₂.H₂O, BTA-P(DTF)₂, BTA (*R*)-Leu, fs=0.5%, toluene, ee: 81%.



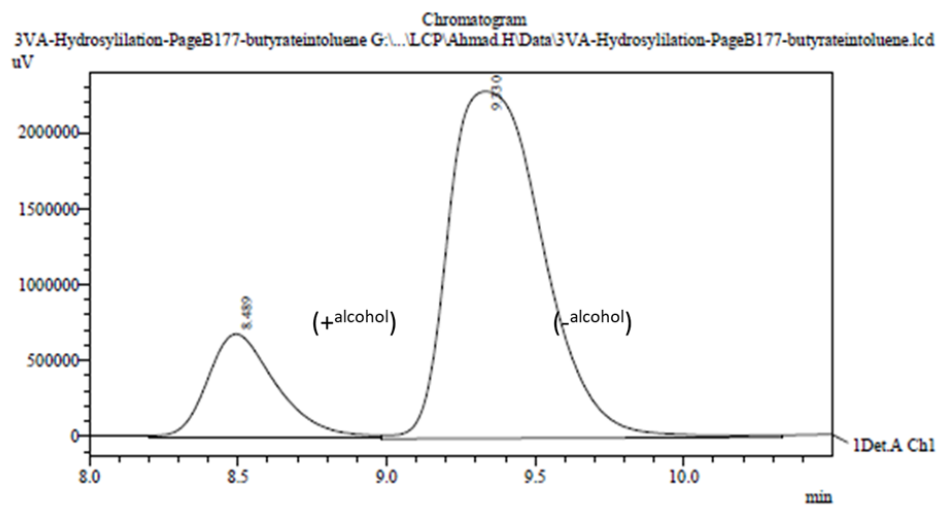
-Table IV-4, entry 5. $\text{Cu}(\text{OAc})_2 \cdot \text{H}_2\text{O}$, BTA-P(DTF)2, BTA (S)-Cha, fs=0.5%, toluene, ee: -76%.



-Table IV-4, entry 6. $\text{Cu}(\text{OAc})_2 \cdot \text{H}_2\text{O}$, BTA-P(DTF)2, BTA (R)-Leu, fs=0.5%, toluene, -40°C , ee: 78%.



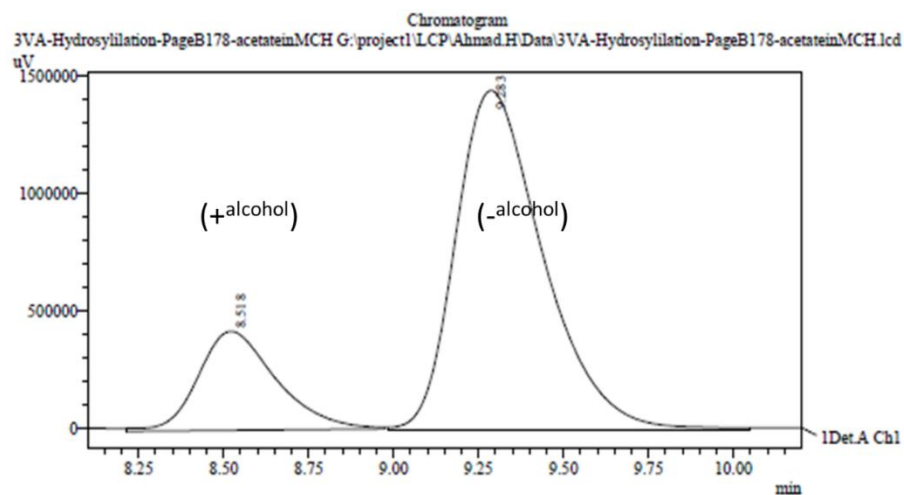
-Table IV-5, entry 2. Cu(II)-i-butyrate, BTA-P(DTF)2, BTA (*R*)-Leu, fs=0.5%, toluene, ee: 65%.



Results>

Rt. (min)	8.489	9.330
Area %	17.708	82.292

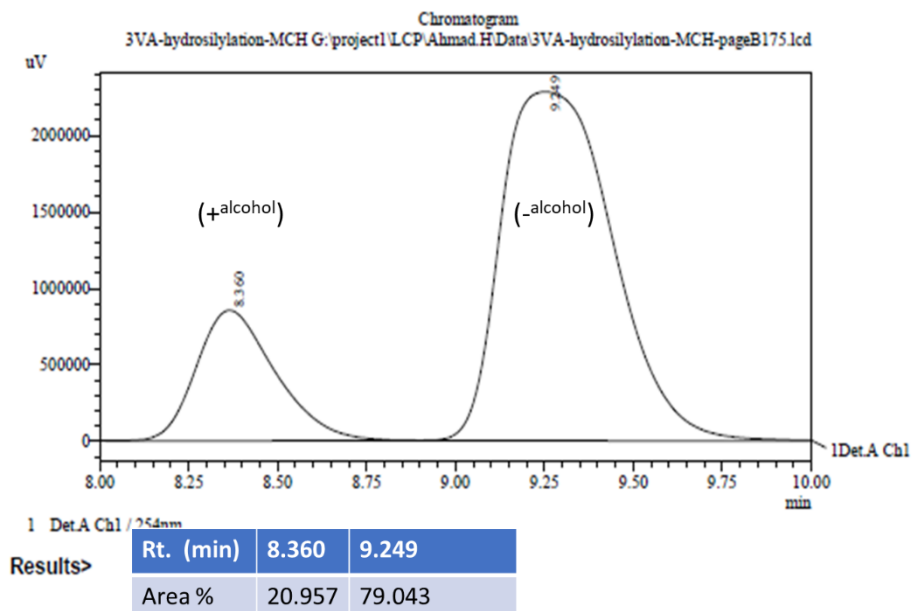
-Table IV-5, entry 3. Cu(OAc)₂·H₂O, BTA-P(DTF)2, BTA (*R*)-Leu, fs=0.5%, MCH, ee: 59%.



Results>

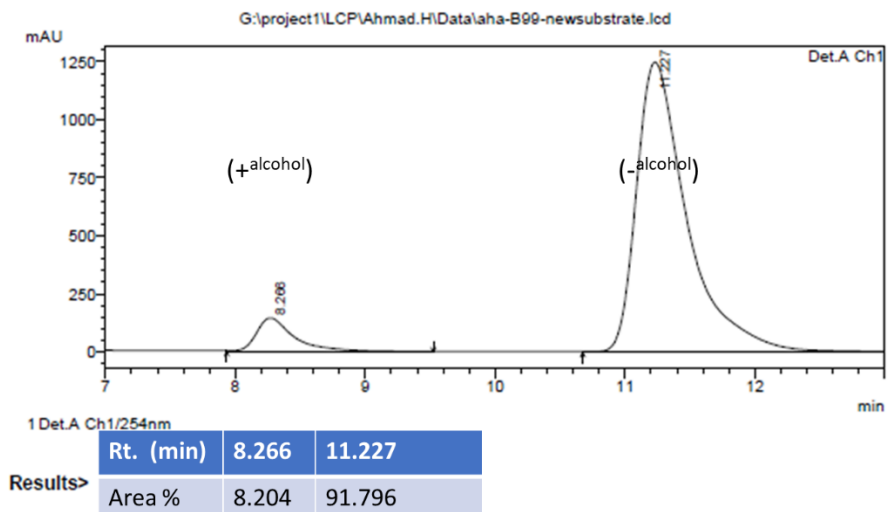
Rt. (min)	8.518	9.283
Area %	20.606	79.394

-Table IV-5, entry 4. Cu(II)-i-butyrate, BTA-P(DTF)2, BTA (*R*)-Leu, fs=0.5%, MCH, ee: 58%.



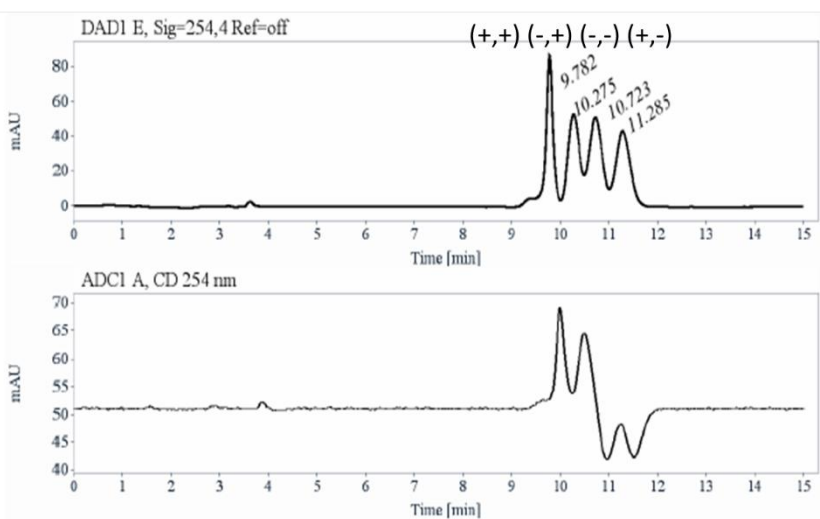
Selected HPLC spectrums of 3-E-MeVpnl

-Table IV-6, entry 1. $\text{Cu}(\text{OAc})_2 \cdot \text{H}_2\text{O}$, BTA-P(DTF)₂, BTA (*R*)-Leu, *fs*=0.5%, toluene, *ee*: 84%.



Selected chiral HPLC spectrums/CD detector of 3-APnl.

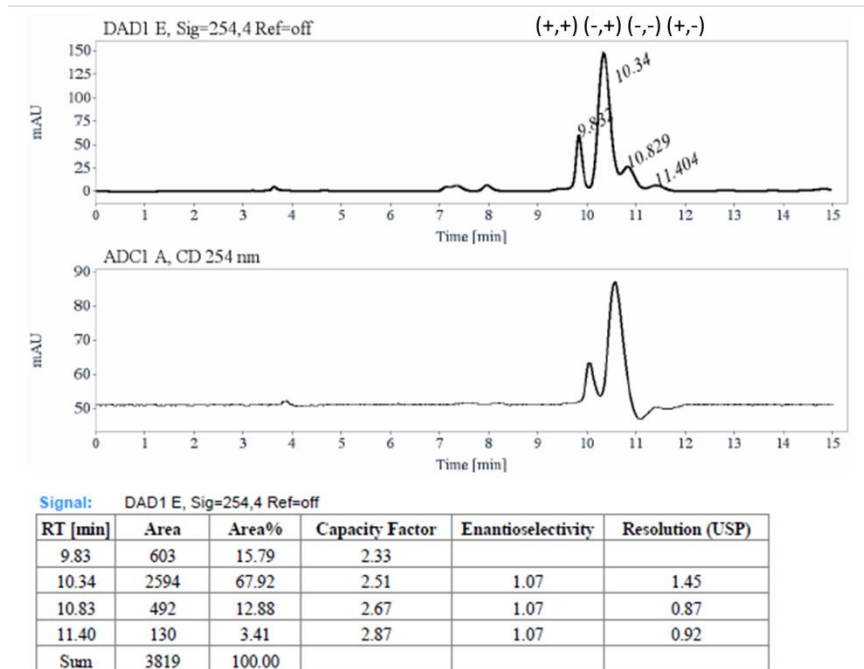
-Reference: $\text{Cu}(\text{OAc})_2 \cdot \text{H}_2\text{O}$, Racemic BINAP, THF, *eetot*: 0%, *dr*:1.



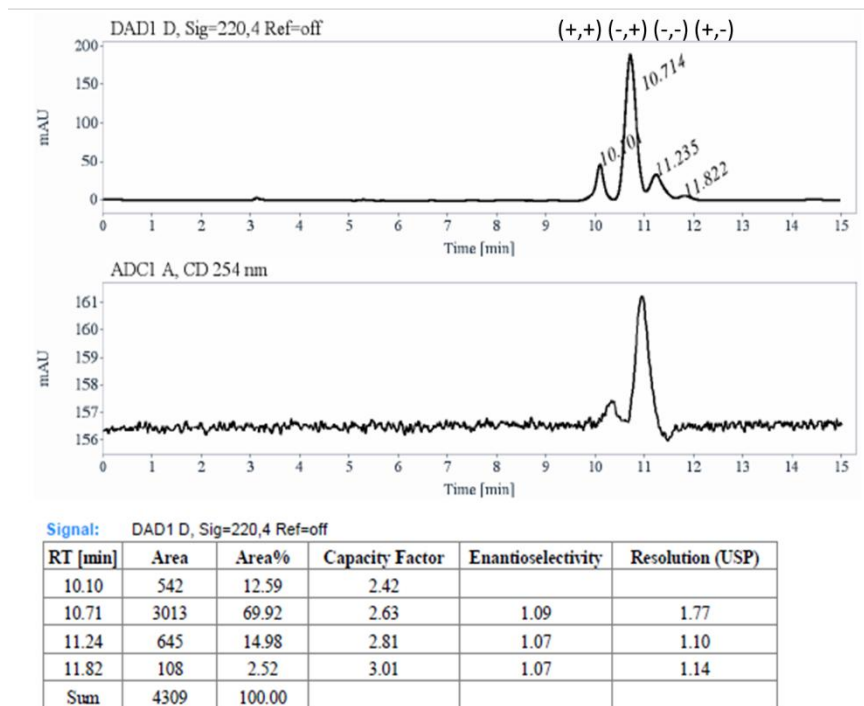
Signal: DAD1 E, Sig=254,4 Ref=off

RT [min]	Area	Area%	Capacity Factor	Enantioselectivity	Resolution (USP)
9.78	839	24.58	2.32		
10.27	792	23.19	2.48	1.07	1.46
10.72	912	26.73	2.64	1.06	0.94
11.28	871	25.50	2.83	1.07	1.05
Sum	3414	100.00			

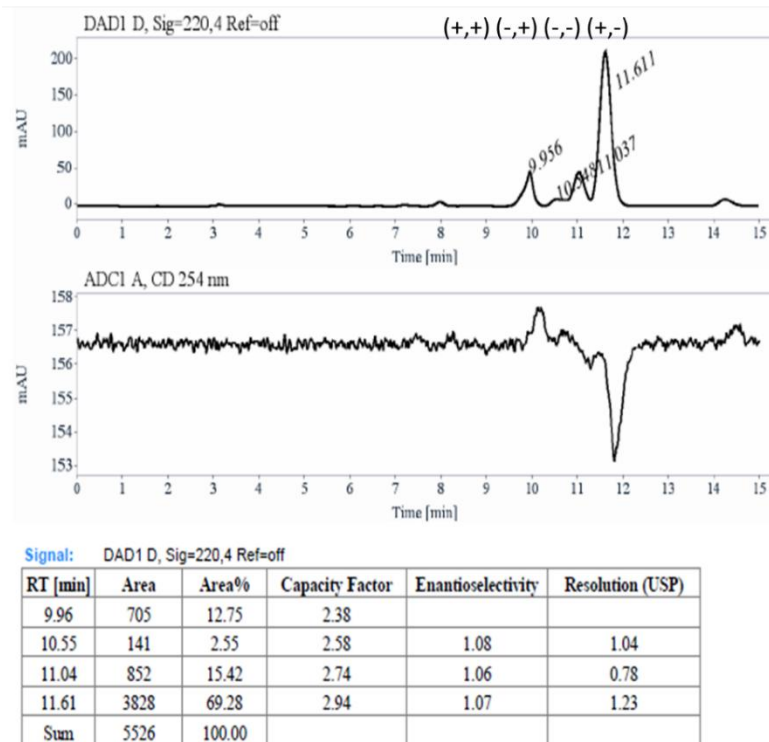
-Table IV-8, entry1. $\text{Cu}(\text{OAc})_2 \cdot \text{H}_2\text{O}$, BTA (*R*)-Leu, fs=0.5%, toluene, eetot: 90%, dr: 2.31.



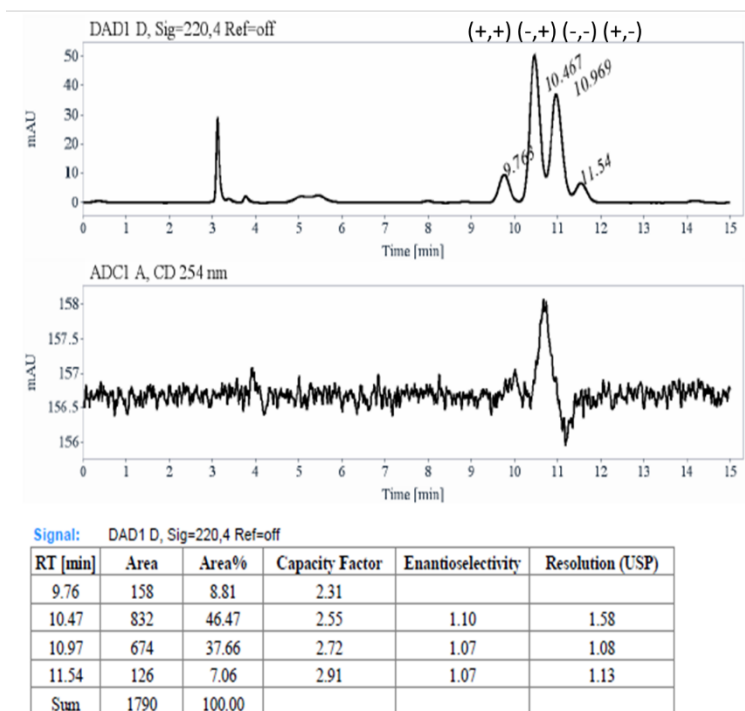
-Table IV-14, entry 1. $\text{Cu}(\text{II})$ -i-butyrate, BTA (*R*)-Leu, fs=0.5%, MCH, eetot: 93%, dr: 2.74.



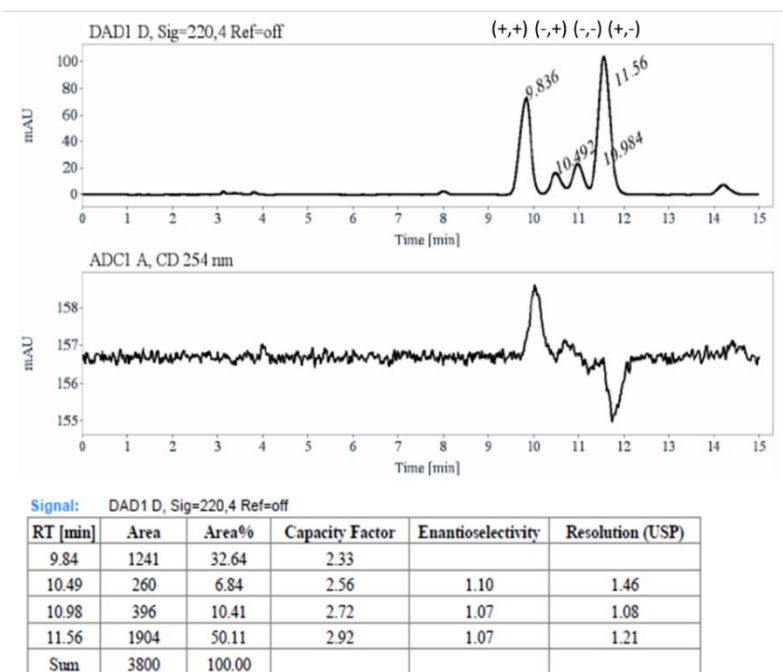
-Table IV-14, entry 2. Cu(II)-i-butyrate, BTA (S)-Leu, fs=0.5%, MCH, eetot: 92%, dr: 2.58.



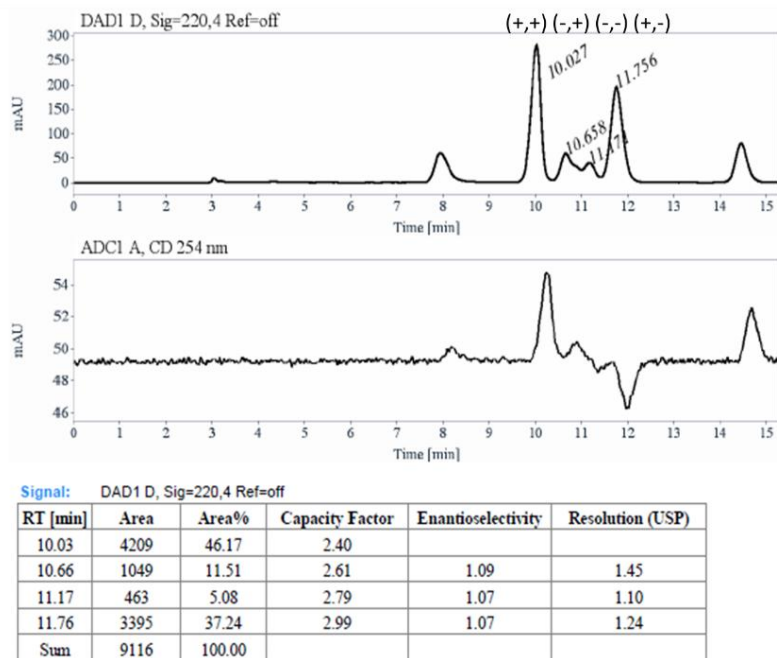
-Table IV-15, entry 1. Cu(II)-i-butyrate, BTA Leu, [fs=0.5% (R) then fs=0.75% (33% (S))], MCH, eetot: 74%, dr: 1.16.



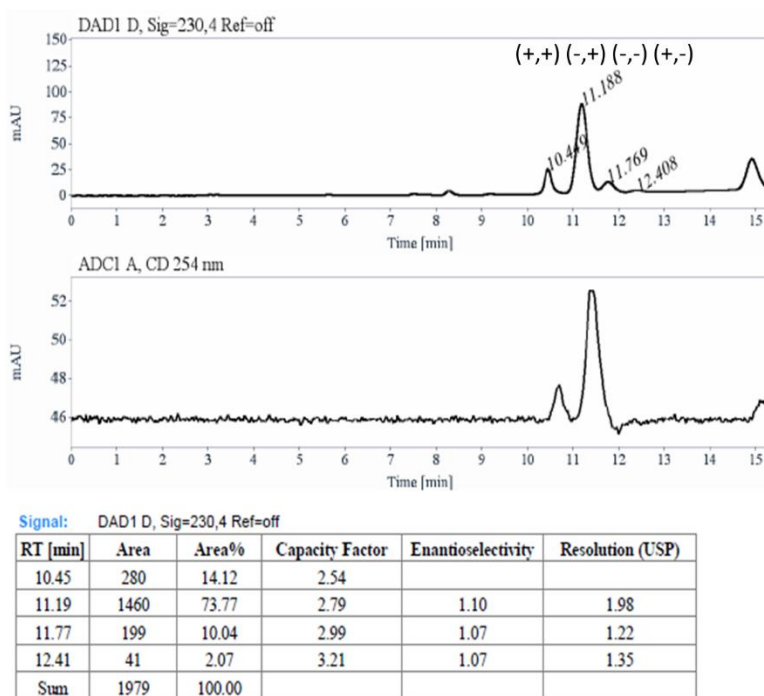
-Table IV-15, entry 2. Cu(II)-i-butyrate, BTA Leu, [fs=0.5% (S) then fs=0.75% (33% (R))], MCH, eetot: 76%, dr: 1.32.



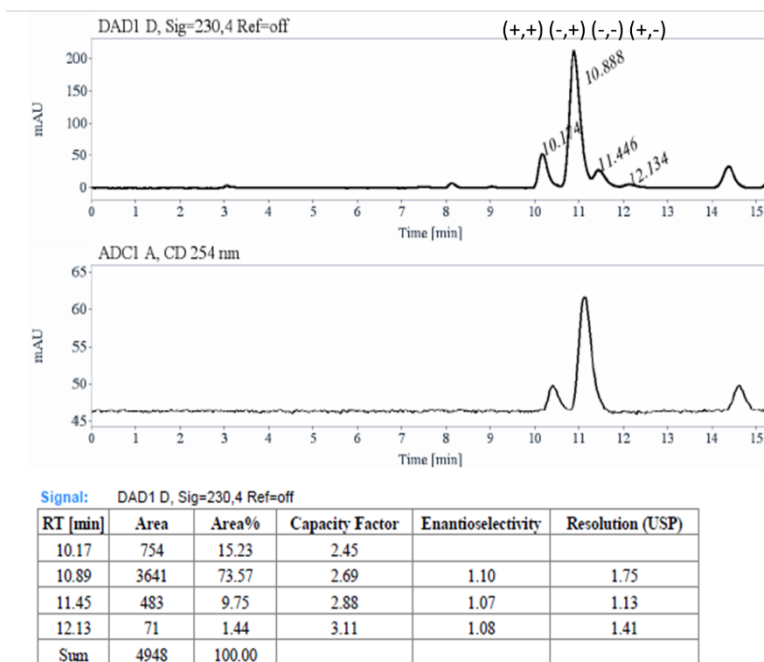
-Table IV-15, entry 3. Cu(II)-i-butyrate, BTA Leu, [fs=0.5% (S) then fs=0.8% (50% (R))], MCH, eetot: 60%, dr: 0.87.



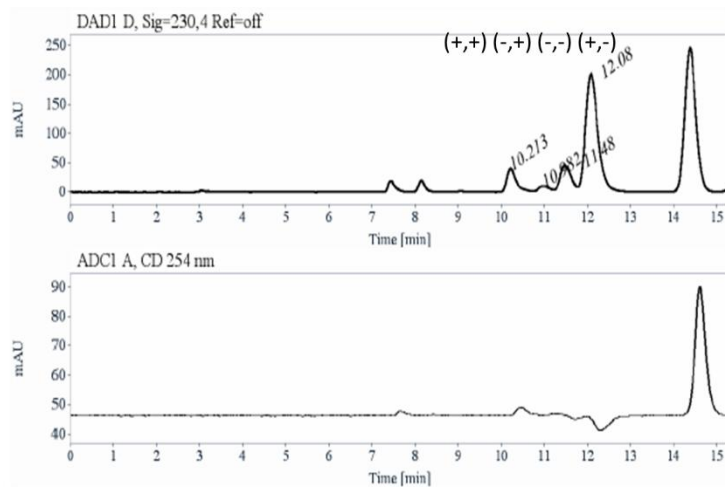
-Table IV-16, entry 1. Cu(II)-i-butyrate, BTA-P(DTF)2, BTA (*R*)-Leu, fs=0.5%, BTA cyclohex, toluene, eetos: 94%, dr: 3.02.



-Table IV-16, entry 2. Cu(II)-i-butyrate, BTA (*R*)-Leu, fs=0.2%, BTA cyclohex, toluene, eetos: 96%, dr: 3.45.



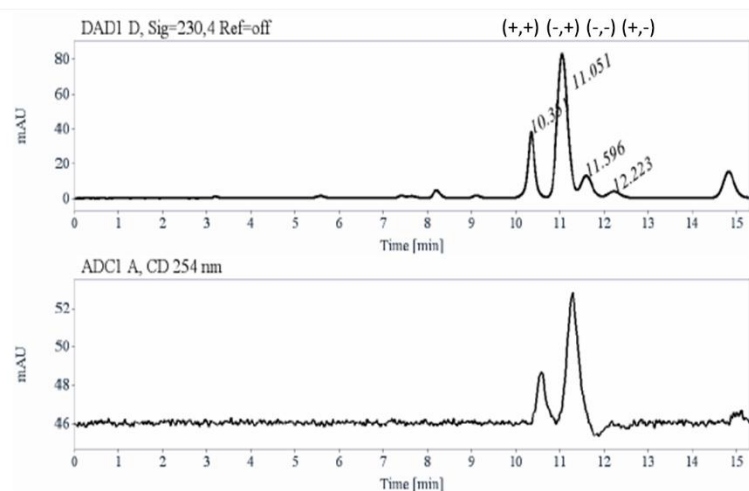
-Table IV-16, entry 3. Cu(II)-i-butyrate, BTA Leu, fs=0.5% [50% ee (S)], BTA cyclohex, toluene, eetot: 94%, dr: 2.90.



Signal: DAD1 D, Sig=230,4 Ref=off

RT [min]	Area	Area%	Capacity Factor	Enantioselectivity	Resolution (USP)
10.21	594	10.75	2.46		
10.98	157	2.84	2.72	1.11	1.87
11.48	788	14.24	2.89	1.06	1.08
12.08	3991	72.17	3.09	1.07	1.21
Sum	5529	100.00			

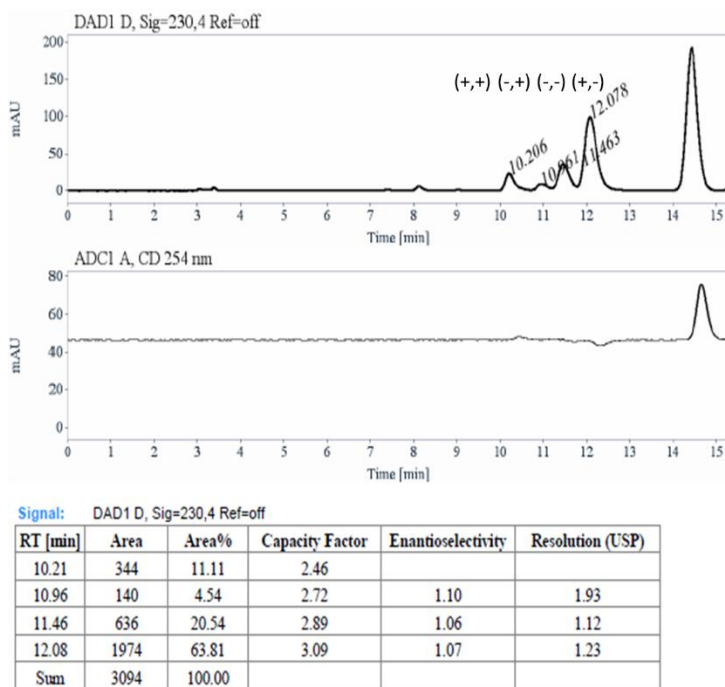
-Table IV-16, entry 4. Cu(II)-i-butyrate, BTA (R)-Leu, fs=0.5%, BTA cyclohex, MCH, eetot: 91%, dr: 2.30.



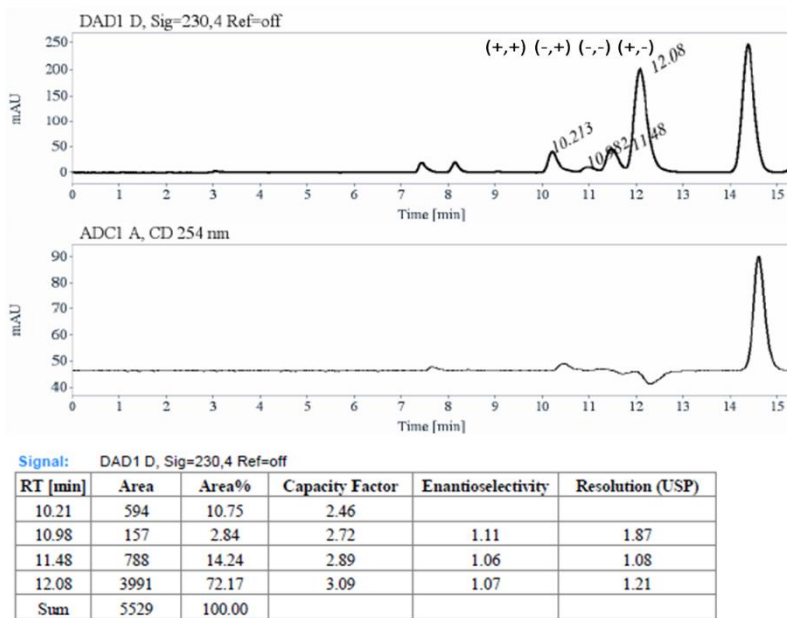
Signal: DAD1 D, Sig=230,4 Ref=off

RT [min]	Area	Area%	Capacity Factor	Enantioselectivity	Resolution (USP)
10.35	425	20.70	2.51		
11.05	1357	66.10	2.75	1.09	1.96
11.60	210	10.22	2.93	1.07	1.19
12.22	61	2.97	3.14	1.07	1.35
Sum	2053	100.00			

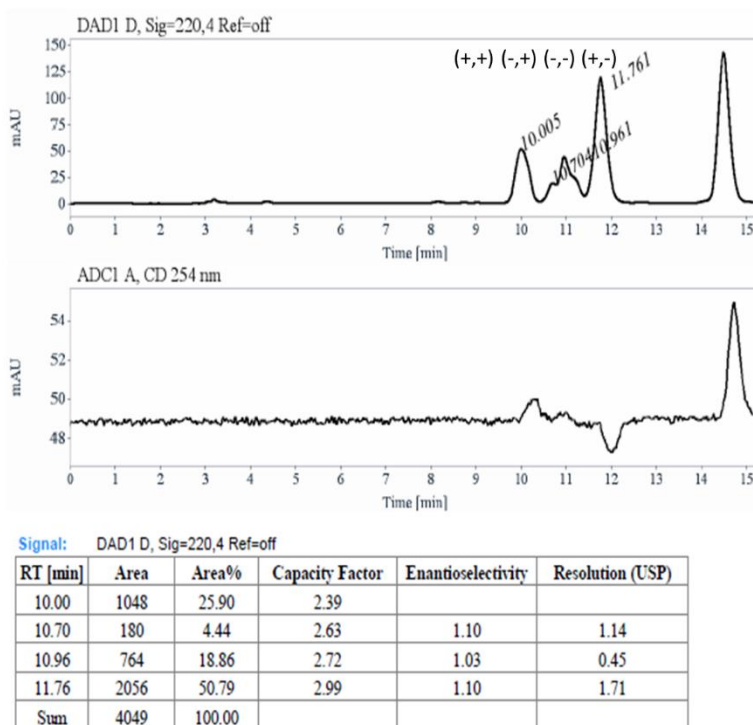
-Table IV-16, entry 6. Cu(II)-i-butyrate, BTA Leu, fs=0.5% [50% ee (S)], BTA cyclohex, MCH, eetot: 89%, dr: 2.07.



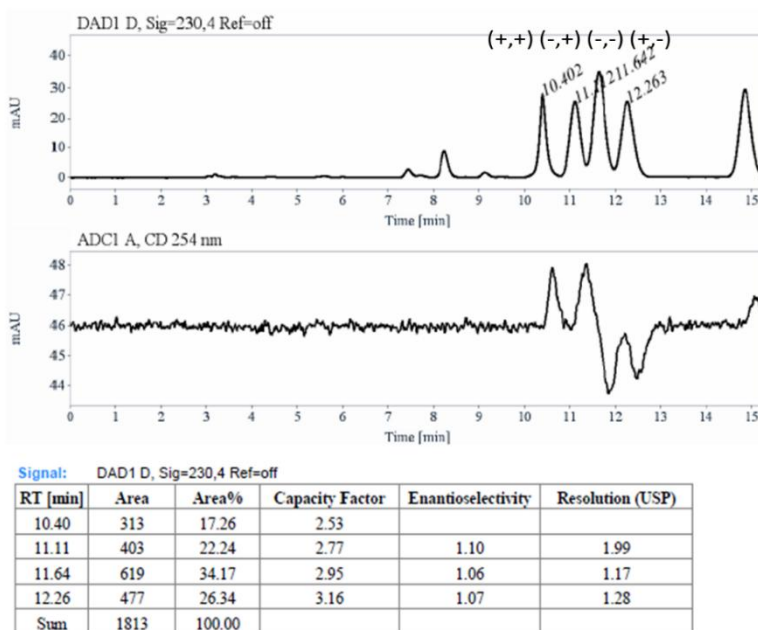
-Table IV-17, entry 1. Cu(II)-i-butyrate, BTA (S)-Leu, fs=0.5%, BTA cyclohex, MCH, eetot: 94%, dr: 2.90.



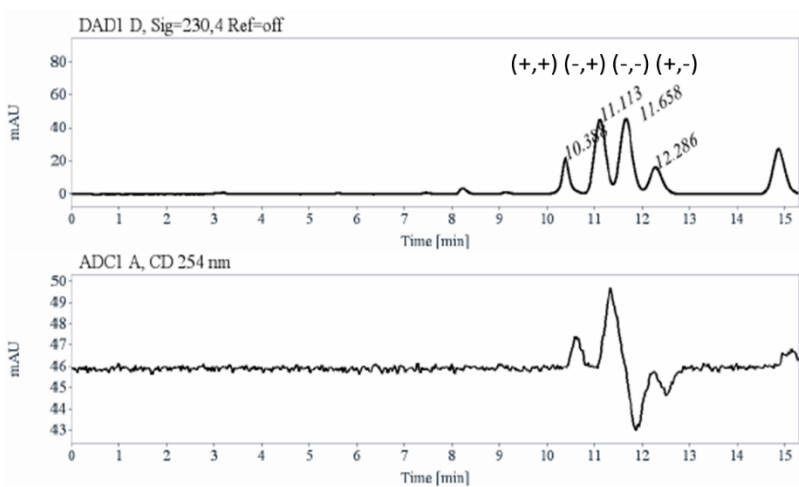
-Table IV-17, entry 2. Cu(II)-i-butyrate, BTA Leu, [fs=0.5%(S) then fs=0.8 (50% (R))], BTA cyclohex, MCH, eetot: 73%, dr: 1.42.



-Table IV-17, entry 3. Cu(II)-i-butyrate, BTA Leu, [fs=0.2%(R) then fs=0.5 (50% (S))], BTA cyclohex, MCH, eetot: 8%, dr: 0.95.



-Table IV-18, entry 3. Cu(II)-i-butyrate, BTA Leu, [fs=0.2%(R) then fs=0.5 (50% (S)), BTA cyclohex, Toluene, eetos: 50%, dr: 1.02.

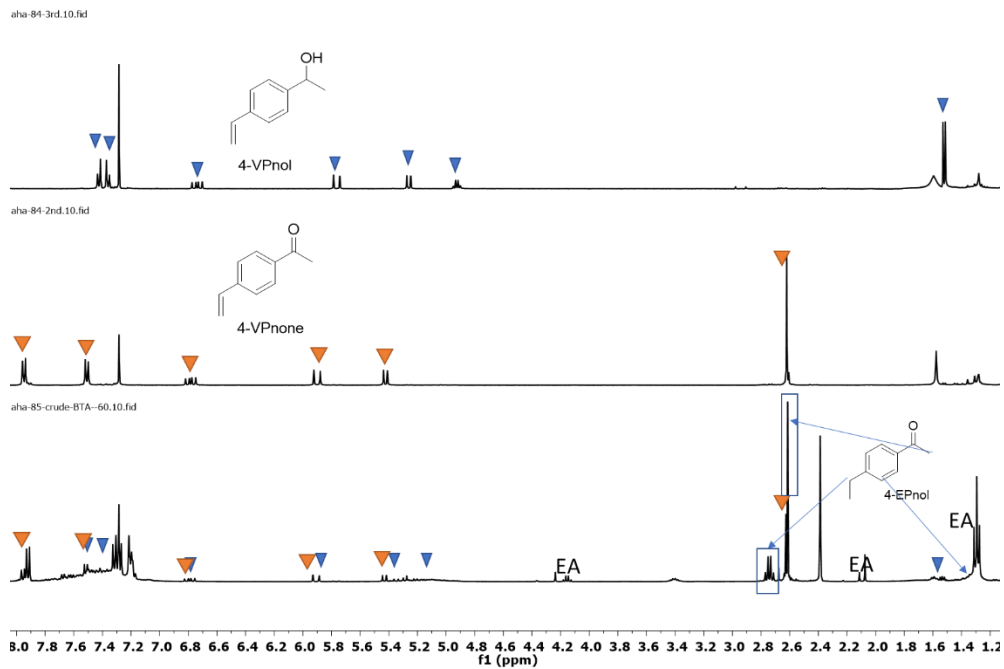


Signal: DAD1 D, Sig=230,4 Ref=off

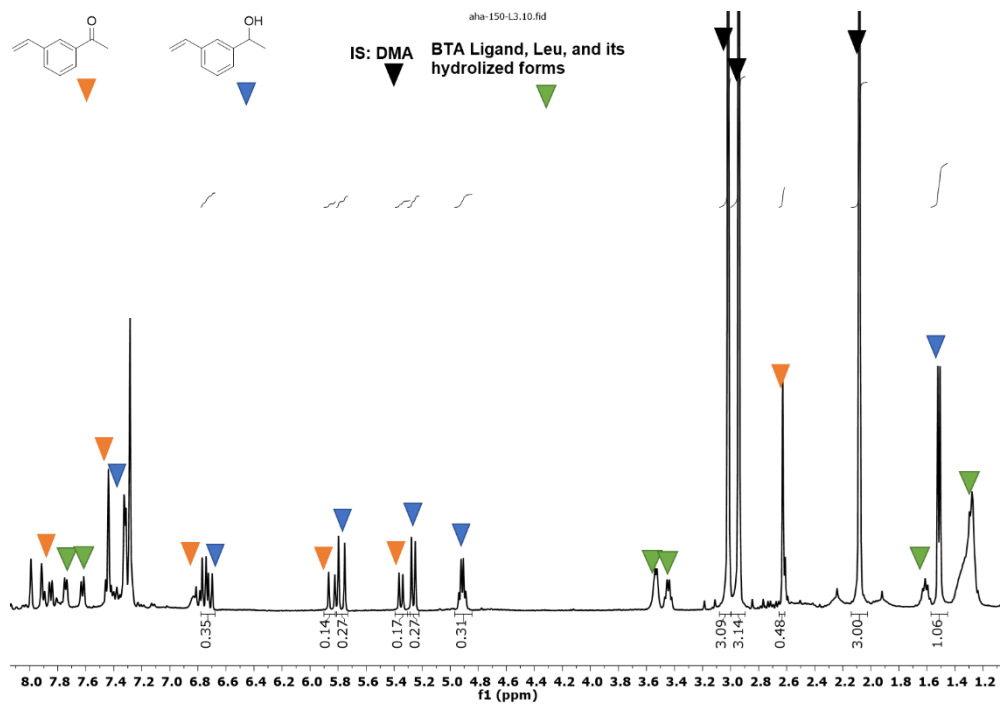
RT [min]	Area	Area%	Capacity Factor	Enantioselectivity	Resolution (USP)
10.39	248	12.63	2.52		
11.11	717	36.43	2.77	1.10	2.01
11.66	755	38.37	2.95	1.07	1.21
12.29	247	12.57	3.16	1.07	1.35
Sum	1967	100.00			

IV.8.i. Selected crude ^1H NMR analyses of some catalytic experiments in CDCl_3 .

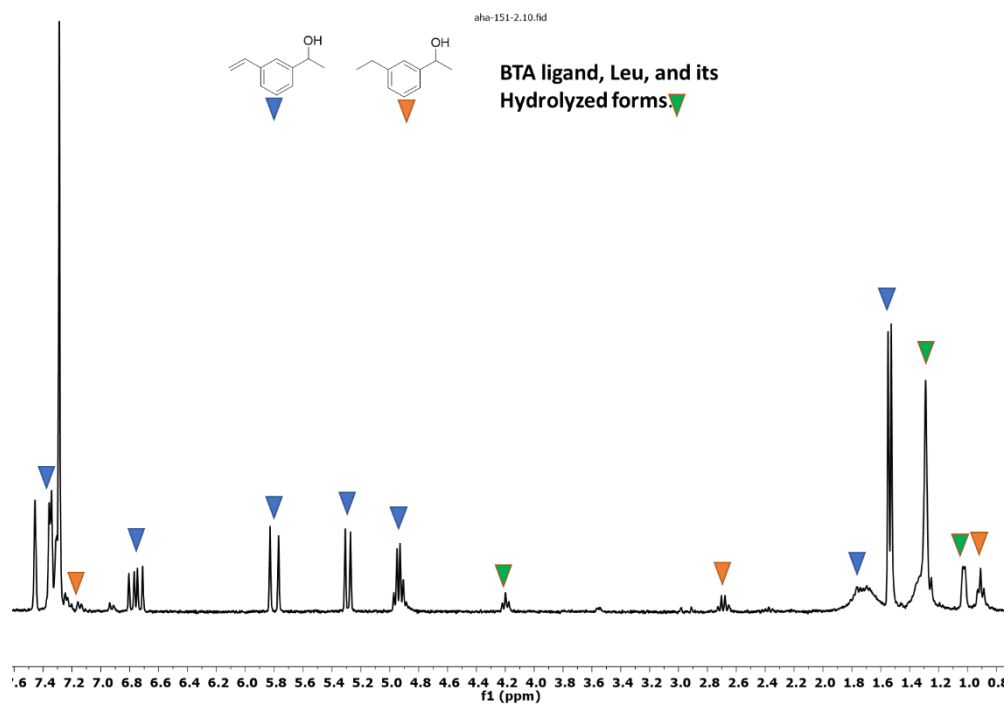
-Hydrosilylation of 4-VPnone, $\text{Cu}(\text{OAc})_2 \cdot x\text{H}_2\text{O}$, BTA-pPPh₂, toluene (entry 6, Table IV-2).



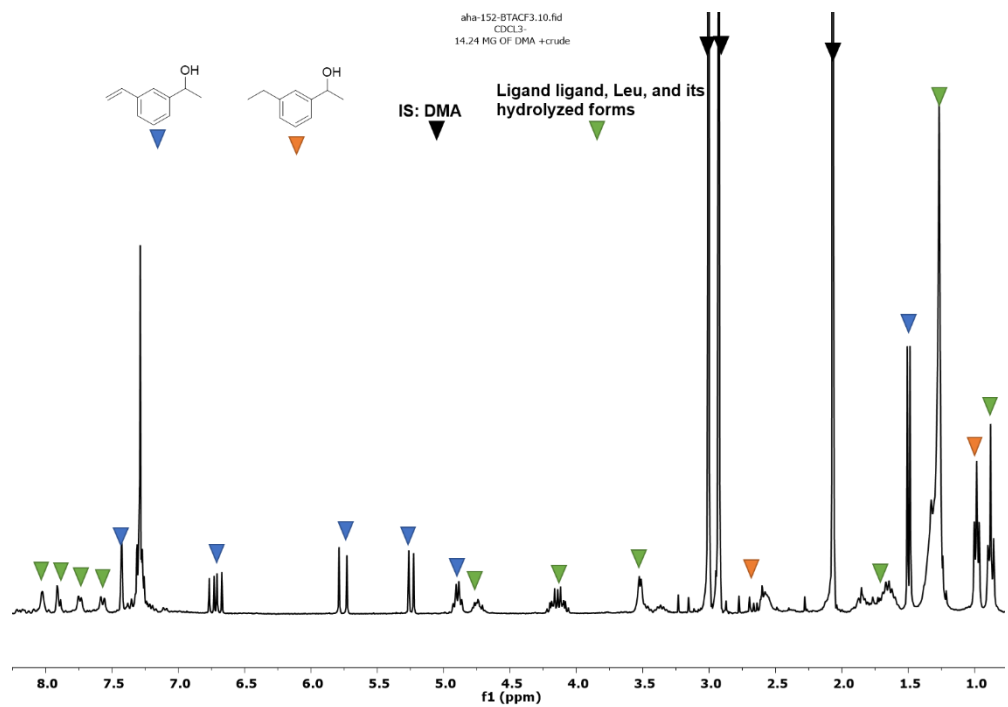
-Hydrosilylation of 3-VPnone, $\text{Cu}(\text{OAc})_2 \cdot x\text{H}_2\text{O}$, BTA-P(DTF)₂, DEMS, toluene (entry 6, Table IV-3).



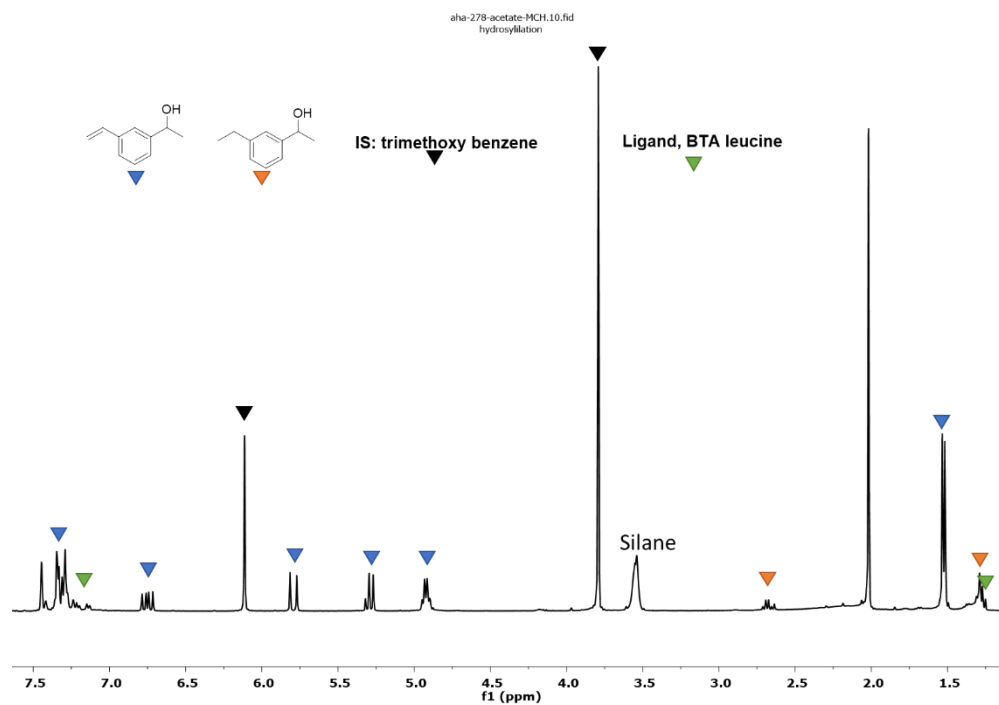
-Hydrosilylation of 3-VPnone, $\text{Cu}(\text{OAc})_2 \cdot x\text{H}_2\text{O}$, BTA-P(DTBM)2, BTA Leu, DEMS, toluene (entry 4, Table IV-4).



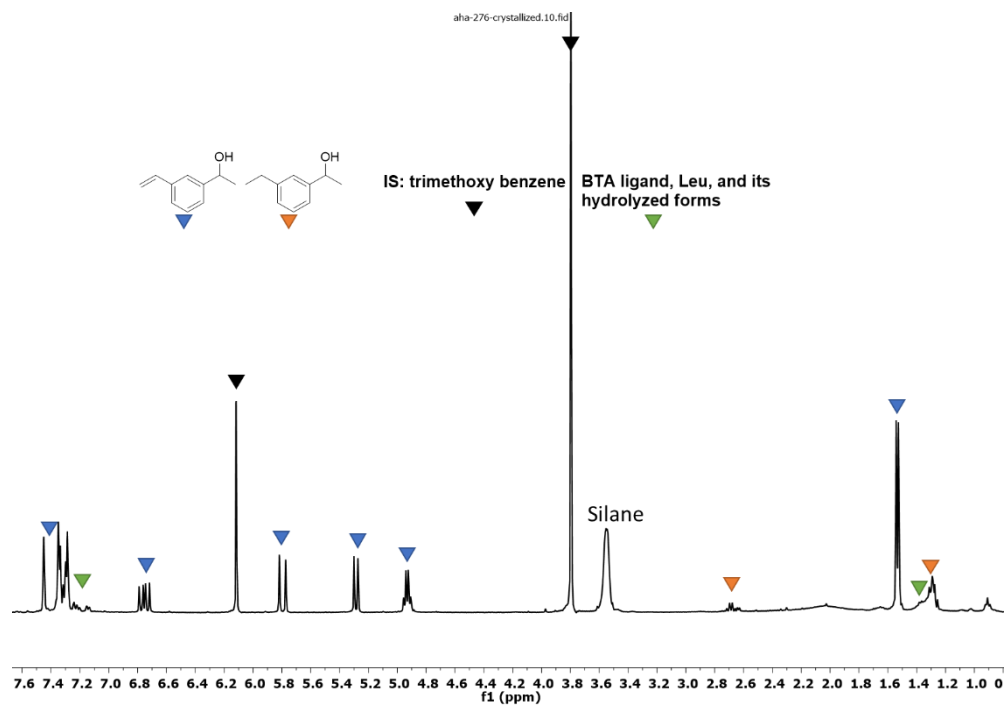
-Hydrosilylation of 3-VPnone, $\text{Cu}(\text{OAc})_2 \cdot x\text{H}_2\text{O}$, BTA-P(DTF)2, BTA (*R*)-Leu, DMMS, toluene (entry 1, Table IV-5).



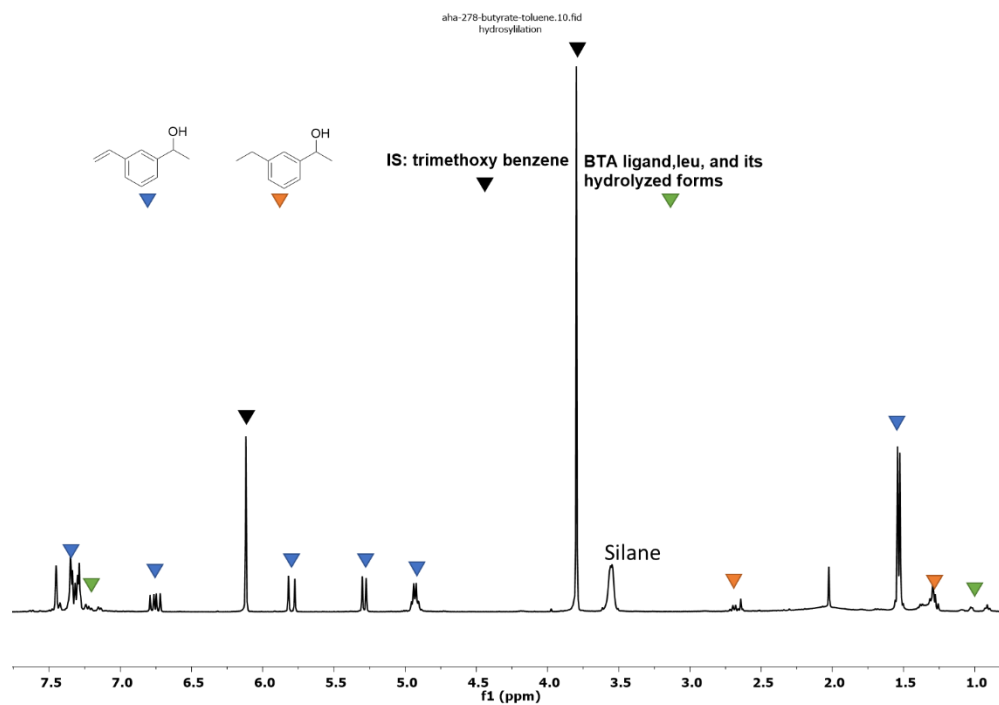
-Hydrosilylation of 3-VPnone, Cu(II)-i-butyrate, BTA-P(DTF)2, BTA (*R*)-Leu, DMMS, toluene (entry 2, Table IV-5) .



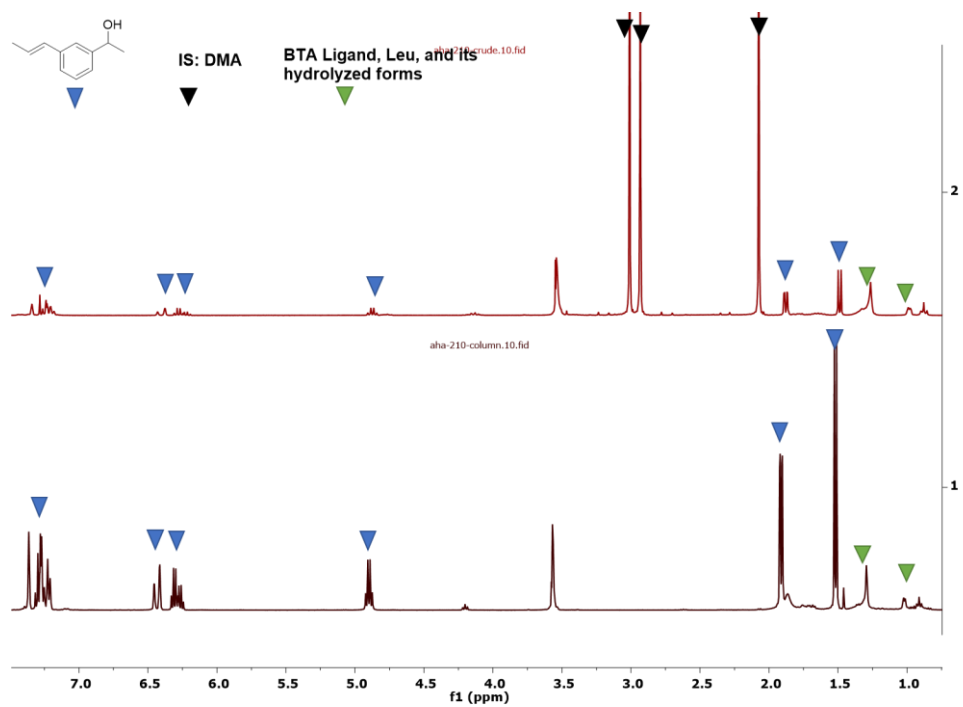
-Hydrosilylation of 3-VPnone, Cu(OAc)₂.xH₂O, BTA-P(DTF)2, BTA (*R*)-Leu, DMMS, MCH (entry 3, Table IV-5).



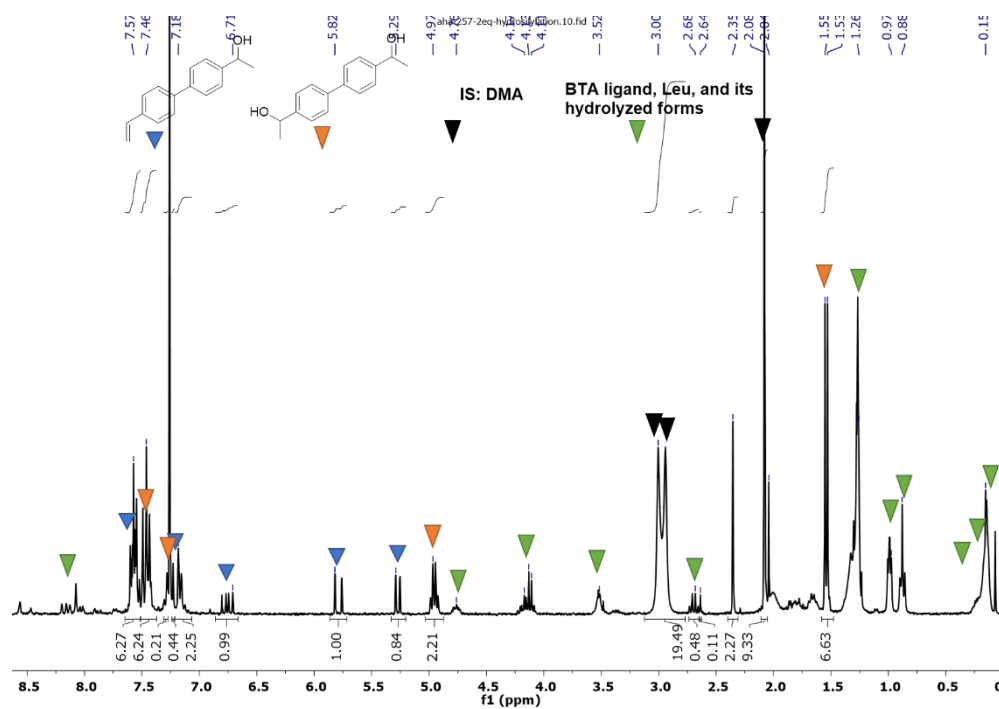
-Hydrosilylation of 3-VPnone, Cu(II)-i-butyrate, BTA-P(DTF)2, BTA (*R*)-Leu, DMMS, MCH (entry 4, Table IV-5).



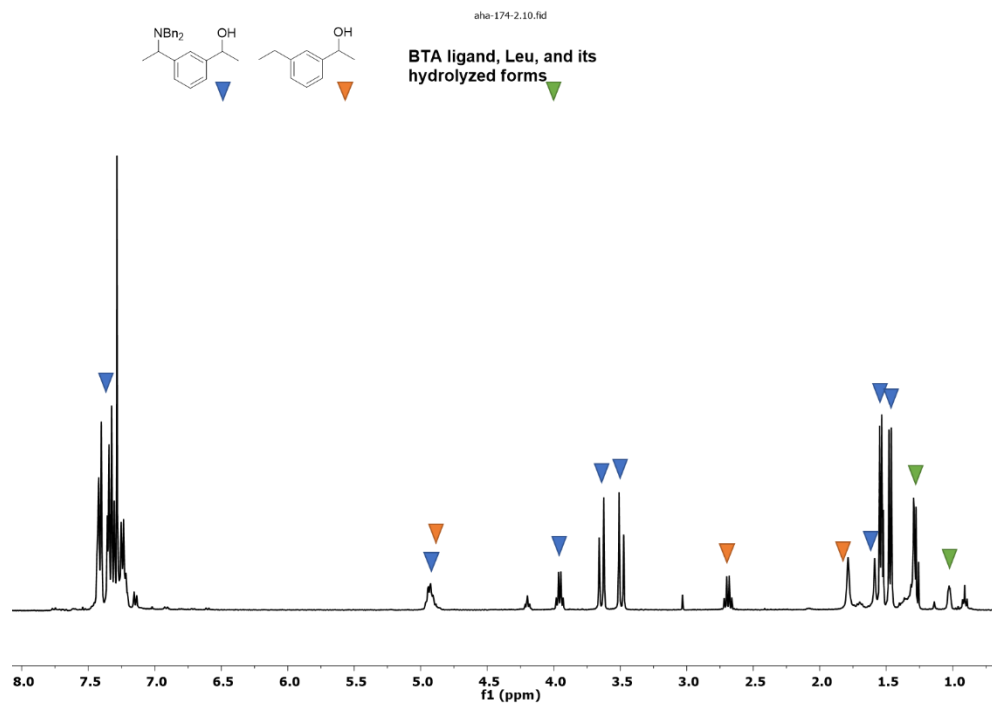
-Hydrosilylation of 3-MeVPnone, Cu(OAc)₂·xH₂O, BTA-P(DTF)2, BTA (*R*)-Leu, DMMS, toluene (entry 1, Table IV-6).



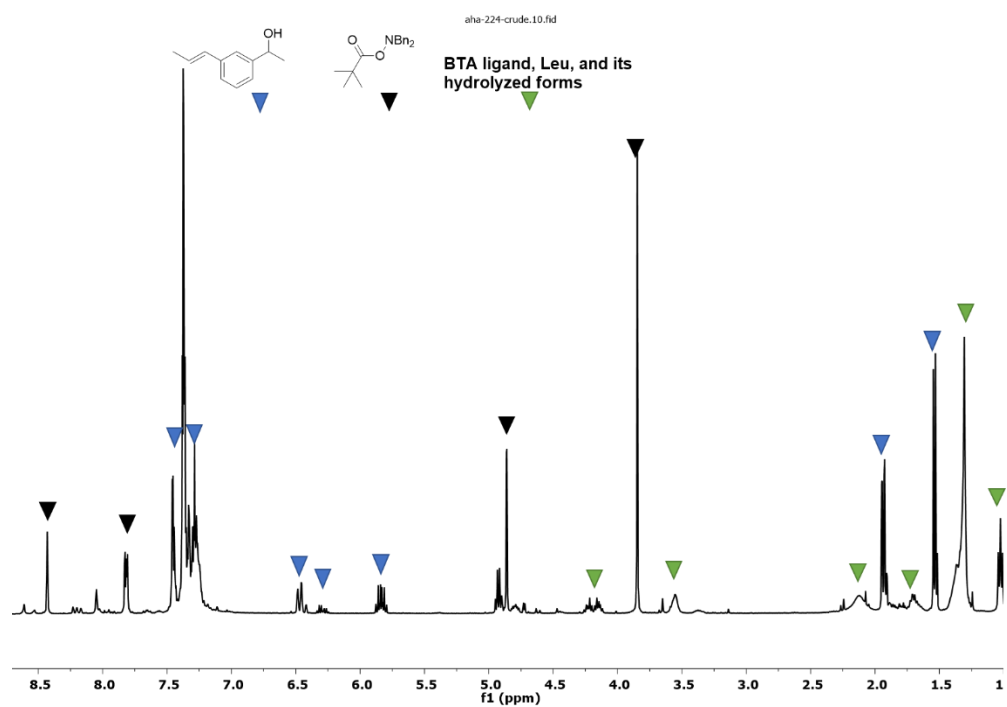
-Hydrosilylation of 4-VBPhone, $\text{Cu}(\text{OAc})_2 \cdot x\text{H}_2\text{O}$, BTA-P(DTF)2, BTA (*R*)-Leu, DMMS, toluene (Table IV-7).



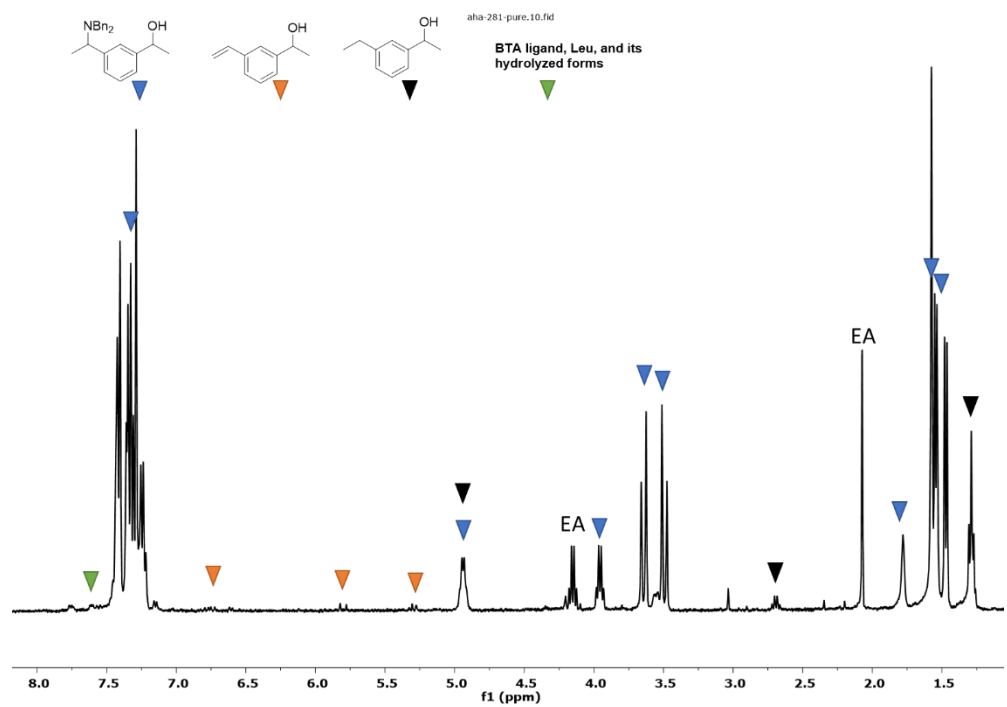
-Cascade on 3-VPnone, $\text{Cu}(\text{OAc})_2 \cdot x\text{H}_2\text{O}$, BTA-P(DTF)2, BTA (*R*)-Leu, DMMS, amine-TB, toluene (entry 1, Table IV-8).



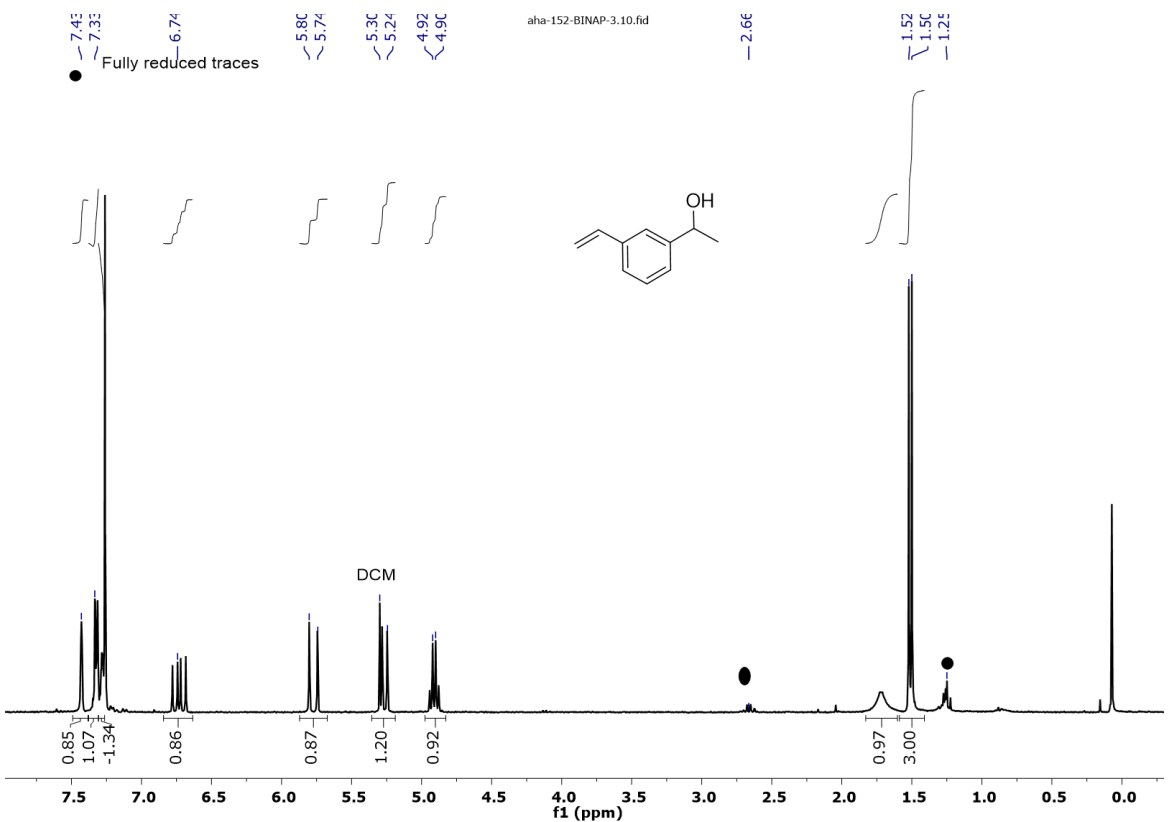
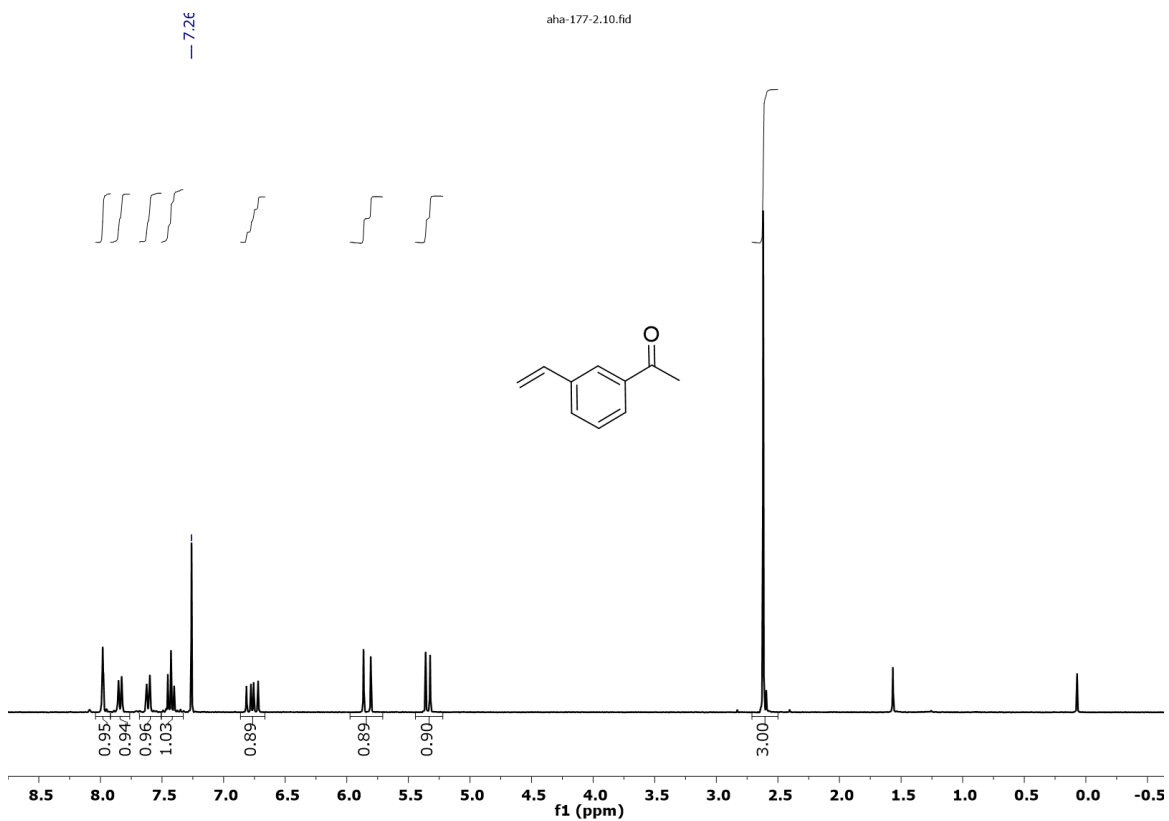
-Cascade on 3-*E*-MeVPnone, Cu(OAc)₂.xH₂O, BTA-P(DTF)2, BTA (*R*)-Leu, DMMS (4.0 eq), amine-TB, toluene (entry 1, Table IV-9).

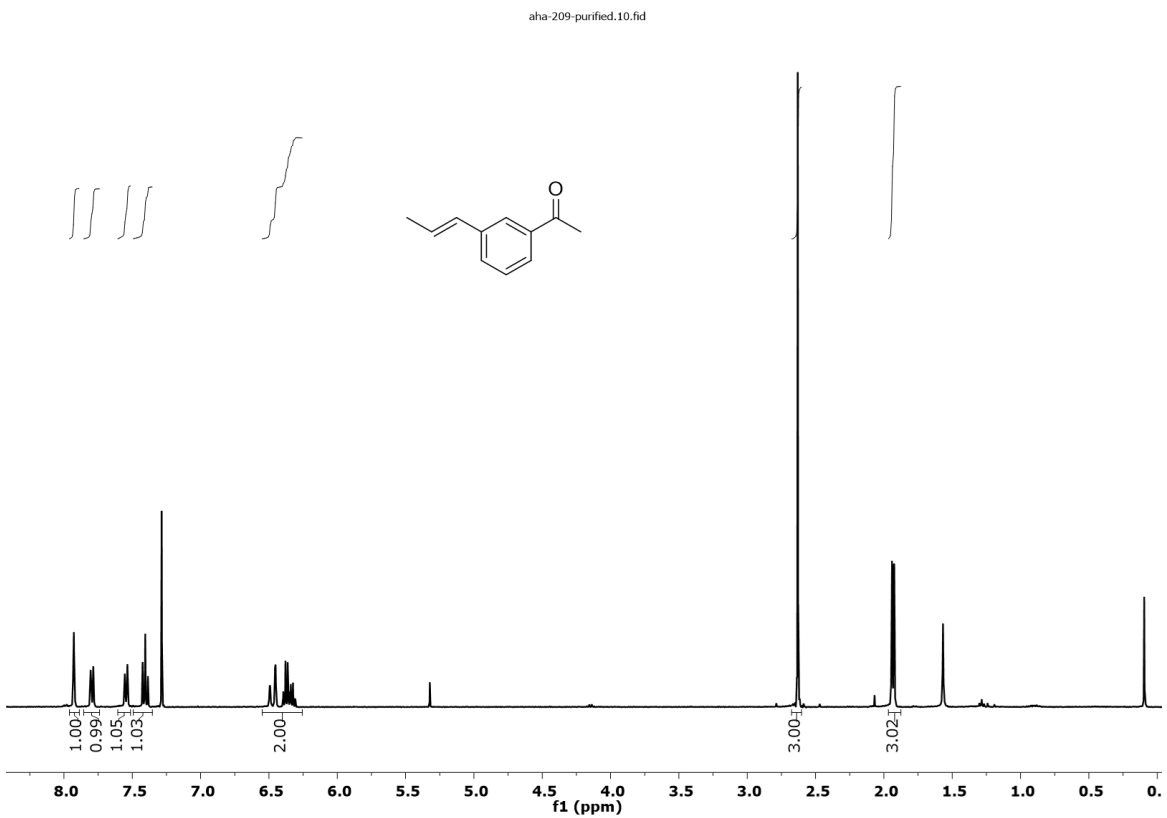
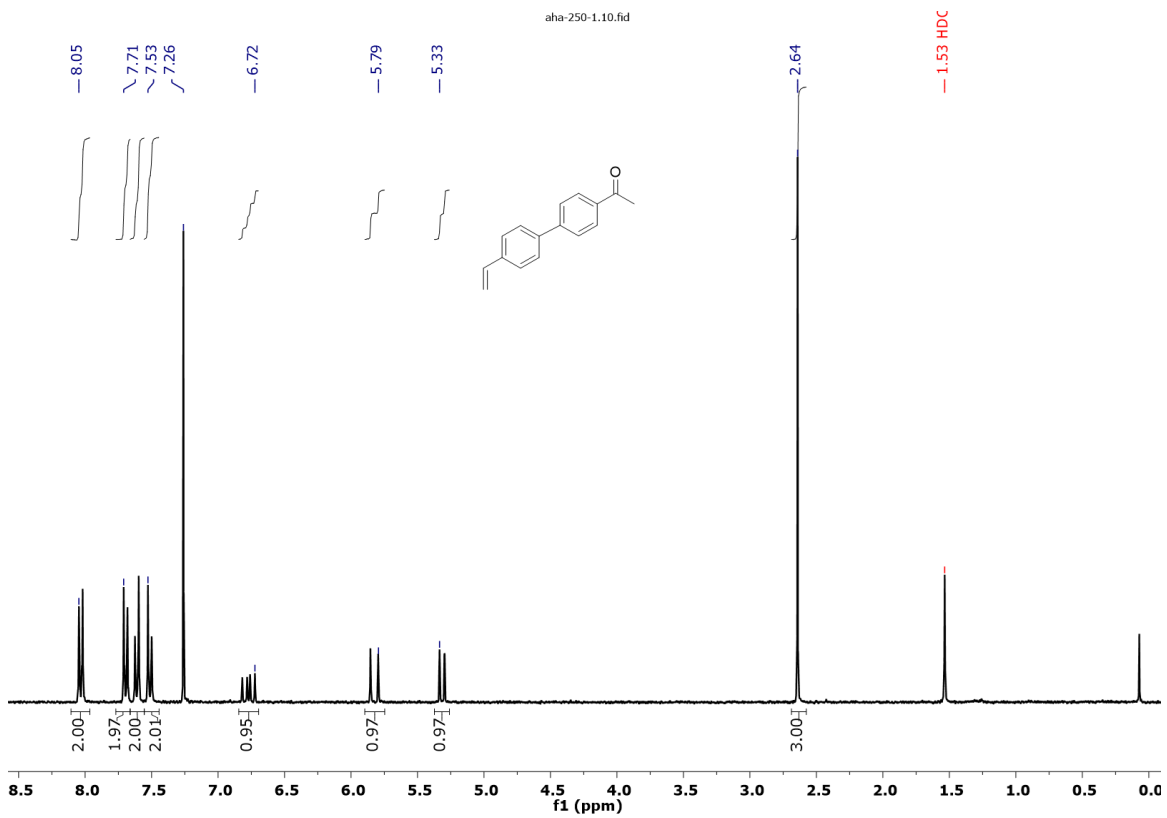


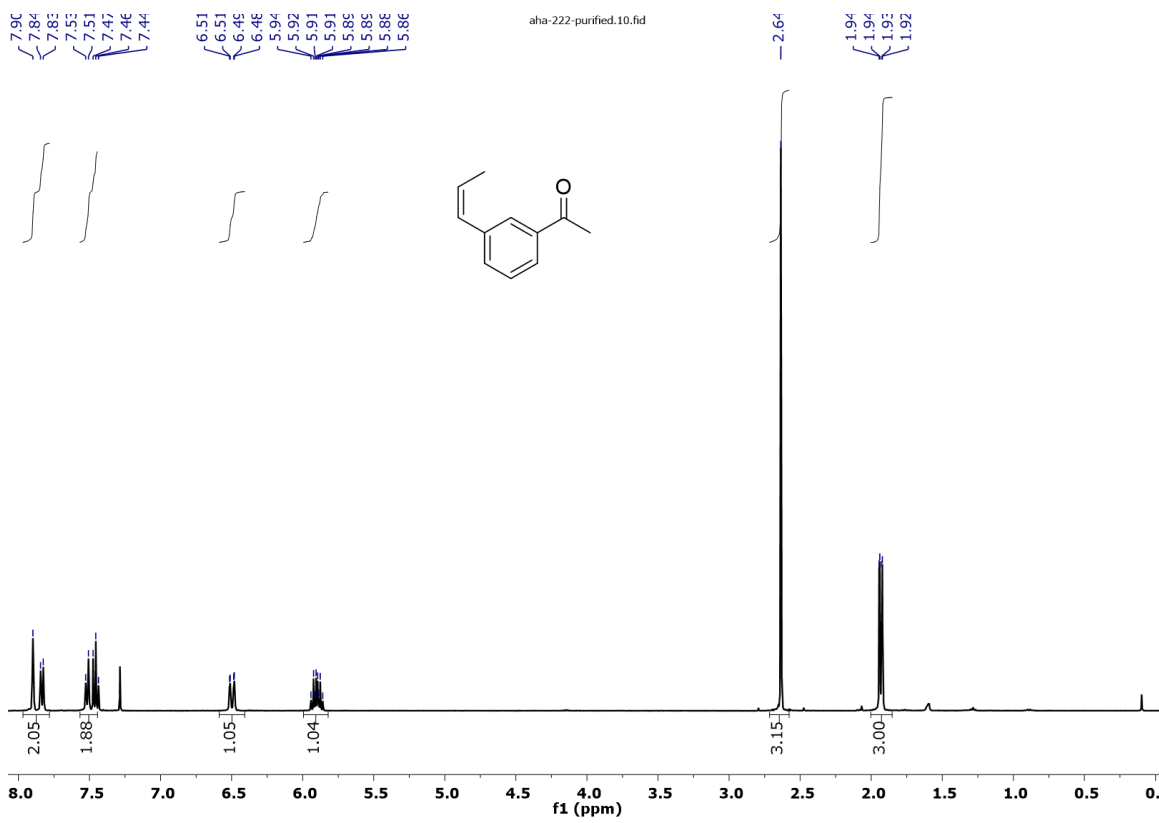
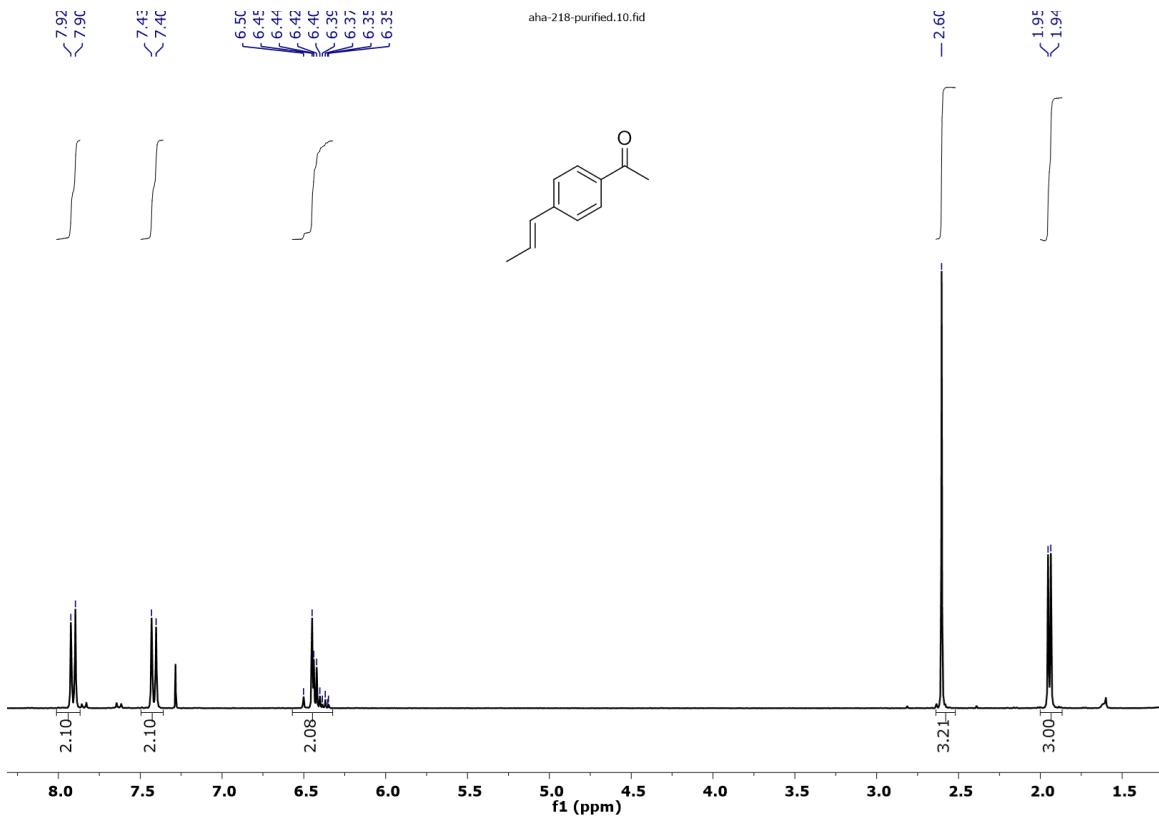
-Cascade on 3-VPnone, Cu(II)-*i*-butyrate, BTA-P(DTF)2, DMMS, amine-DM, MCH (entry 1, Table IV-14).



IV.8.j. ¹H NMR data of substrates.

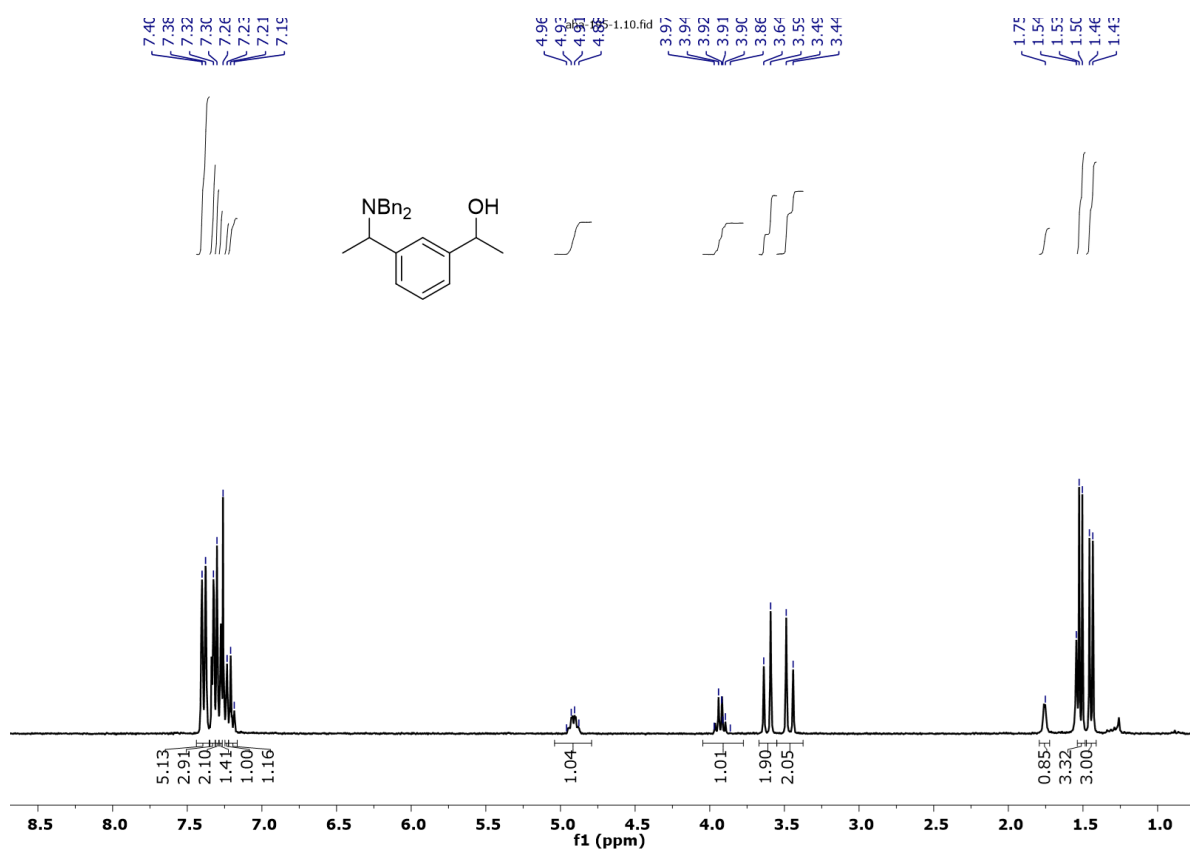


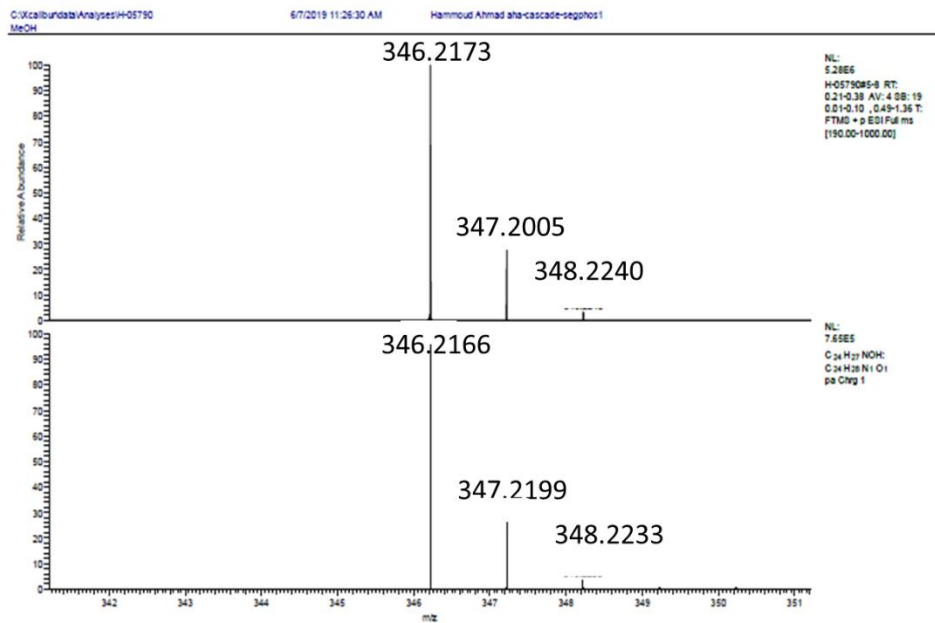
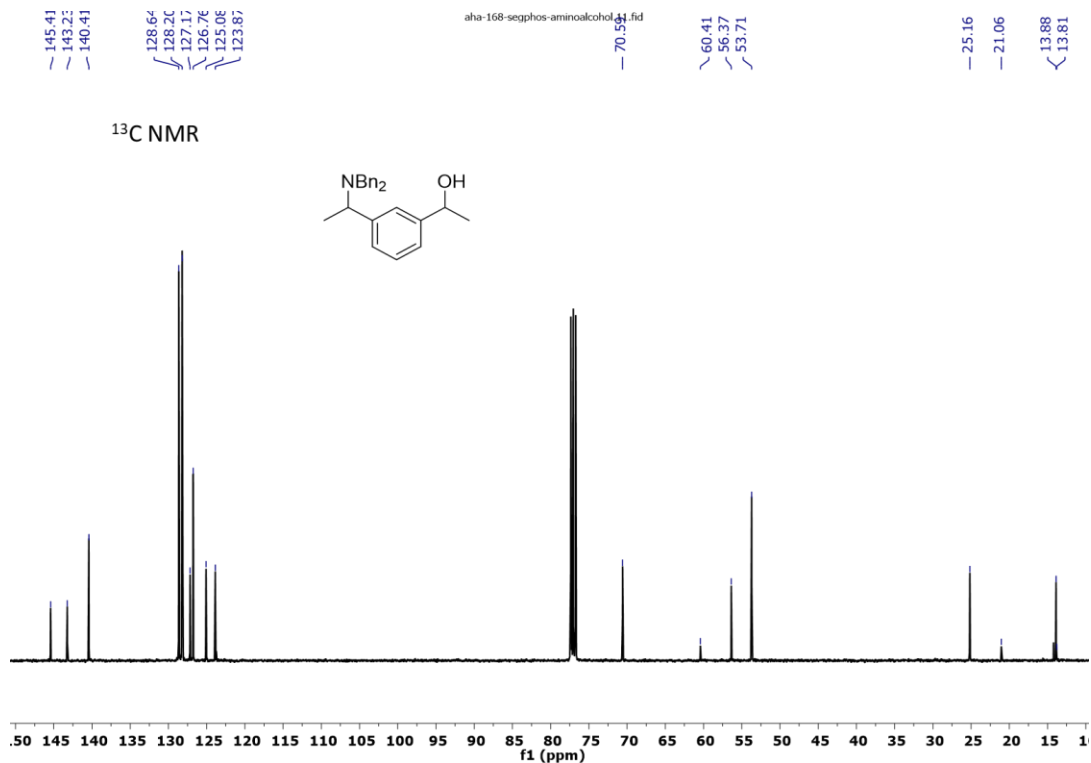




IV.8.k. ^1H NMR, ^{13}C NMR, and HRMS of 3-APnol:

1-(3-(1-(dibenzylamino)ethyl)phenyl)ethanol. ^1H NMR (300 MHz, CDCl_3) δ (ppm) 7.47-7.40 (m, 5H), 7.40-7.38 (m, 5H), 7.30-7.21 (m, 4H), 4.94 (q, 1H), 3.97 (q, 1H), 3.66 (d, 3H), 3.52 (d, 2H), 1.85 (bs, 1H), 1.54 (d, 3H), 1.47 (d, 3H). $^{13}\text{C}\{^1\text{H}\}$ NMR (CDCl_3) δ (ppm) 145.43, 143.25, 140.42, 128.66, 128.22, 127.19, 126.77, 125.09, 123.88, 70.59, 60.42, 56.38, 53.71, 25.17, 21.06, 14.22, 13.89. HRMS (ESI, m/z): Calculated for $\text{C}_{24}\text{H}_{27}\text{NO}$, $[\text{M}+\text{H}]^+$: 346.2173, found: 346.2173.





Erreur = 2.2 ppm ; Intensité Relative (%) 100

Calcul des masses monoisotopiques – 1.00728 Th (-H⁺).
–18.0338 Th (-NH₄⁺).
–22.98922 Th (-Na⁺).
–38.96316 Th (-K⁺).

IV.9. References

- [1] D. Sud, T. B. Norsten, N. R. Branda, *Angew. Chem. Int. Ed.* **2005**, *44*, 2019–2021.
- [2] C.-T. Chen, C.-C. Tsai, P.-K. Tsou, G.-T. Huang, C.-H. Yu, *Chem. Sci.* **2017**, *8*, 524–529.
- [3] D. Zhao, T. M. Neubauer, B. L. Feringa, *Nat Commun* **2015**, *6*, 6652.
- [4] J. Wang, B. L. Feringa, *Science* **2011**, *331*, 1429–1432.
- [5] M. Vlatković, L. Bernardi, E. Otten, B. L. Feringa, *Chem. Commun.* **2014**, *50*, 7773.
- [6] S. F. Pizzolato, P. Štacko, J. C. M. Kistemaker, T. van Leeuwen, E. Otten, B. L. Feringa, *J. Am. Chem. Soc.* **2018**, *140*, 17278–17289.
- [7] Y. Nagata, T. Nishikawa, M. Suginome, *J. Am. Chem. Soc.* **2014**, *136*, 15901–15904.
- [8] Y. Akai, T. Yamamoto, Y. Nagata, T. Ohmura, M. Suginome, *J. Am. Chem. Soc.* **2012**, *134*, 11092–11095.
- [9] T. Yamada, Y. Nagata, M. Suginome, *Chem. Commun.* **2010**, *46*, 4914.
- [10] S. Mortezaei, N. R. Catarineu, J. W. Canary, *Tetrahedron Letters* **2016**, *57*, 459–462.
- [11] S. Mortezaei, N. R. Catarineu, J. W. Canary, *J. Am. Chem. Soc.* **2012**, *134*, 8054–8057.
- [12] S. Mortezaei, N. R. Catarineu, X. Duan, C. Hu, J. W. Canary, *Chem. Sci.* **2015**, *6*, 5904–5912.
- [13] G. Storch, O. Trapp, *Angew. Chem. Int. Ed.* **2015**, *54*, 3580–3586.
- [14] S. Wang, J. Xiao, J. Li, H. Xiang, C. Wang, X. Chen, R. G. Carter, H. Yang, *Chem. Commun.* **2017**, *53*, 4441–4444.
- [15] S. Mortezaei, N. R. Catarineu, J. W. Canary, *Tetrahedron Letters* **2016**, *57*, 459–462.
- [16] A. Nojiri, N. Kumagai, M. Shibasaki, *J. Am. Chem. Soc.* **2009**, *131*, 3779–3784.
- [17] Y. Sohtome, T. Yamaguchi, S. Tanaka, K. Nagasawa, *Org. Biomol. Chem.* **2013**, *11*, 2780.
- [18] S. Kassem, A. T. L. Lee, D. A. Leigh, V. Marcos, L. I. Palmer, S. Pisano, *Nature* **2017**, *549*, 374–378.

- [19] G. A. Molander, A. R. Brown, *J. Org. Chem.* **2006**, *71*, 9681–9686.
- [20] J. Mou, H. Fang, Y. Liu, L. Shang, Q. Wang, L. Zhang, W. Xu, *Bioorganic & Medicinal Chemistry* **2010**, *18*, 887–895.
- [21] J. S. Bandar, M. T. Pirnot, S. L. Buchwald, *J. Am. Chem. Soc.* **2015**, *137*, 14812–14818.
- [22] L. Yu, P. Somfai, *Angew. Chem. Int. Ed.* **2019**, *58*, 8551–8555.
- [23] C. Deutsch, N. Krause, B. H. Lipshutz, *Chem. Rev.* **2008**, *108*, 2916–2927.
- [24] J. T. Issenhuth, S. Dagherne, S. Bellemin-Lapponnaz, *Adv. Synth. Catal.* **2006**, *348*, 1991–1994.
- [25] J. Courmarcel, N. Mostefai, S. Sirol, S. Choppin, O. Riant, *Israel Journal of Chemistry* **2001**, *41*, 231–240.
- [26] Y. Li, A. Hammoud, L. Bouteiller, M. Raynal, *J. Am. Chem. Soc.* **2020**, *142*, 5676–5688.
- [27] J. M. Zimbron, X. Caumes, Y. Li, C. M. Thomas, M. Raynal, L. Bouteiller, *Angew. Chem. Int. Ed.* **2017**, *56*, 14016–14019.

Conclusions.

The main objective of this thesis was to develop a stereodivergent approach by exploiting the dynamic properties of the switchable helical BTA catalysts in order to access all possible stereoisomers of an amino alcohol in a one pot manner. The concept can be summarized as follows: A cascade hydrosilylation/hydroamination process was targeted for which both steps are catalyzed by phosphine copper hydride catalysts located at the periphery of the supramolecular BTA helices. It has been well established prior to this work that the direction of the asymmetric reaction is dictated by the handedness of the helices. The helical catalysts are composed of an achiral BTA ligand (for metal binding) and of an enantiopure co-monomer (for inducing and amplifying the chirality). The composition of helical co-assemblies is tuned by simple addition of the desired amount of BTA co-monomers, which thanks to the diluted MR effect provides an effective switch between the two directions of the helices. It was thus envisaged that the configuration of the consecutively formed stereogenic centers will be controlled by the handedness of the supramolecular helices, by which tuning the relative proportion of the enantiopure BTA co-monomers present in the helices will allow to access all possible stereoisomers from a single catalyst.

In **Chapter II**, the syntheses of nine new phosphine-containing BTA ligands were disclosed. These newly designed BTA ligands differ from the previously employed **BTA-pPPh₂** ligand by the nature of the substituents present on the aryl groups attached to the phosphorous atom. These ligands present different electronic and steric properties. The design of these BTA ligands also considered the possible ligand substrate interactions which might arise in the transition state of the copper-catalyzed hydroamination reaction. Accordingly, electron-donating and electron-withdrawing groups were introduced at the 3- and 5- positions of the aryl groups. The general synthetic route was adopted according to a similar three-step synthetic procedure, which allowed obtaining the final BTA ligands on hundreds of mg or gram scale with a high level of purity except for **BTA-P(DMM)₂** and **BTA-P(Mesityl)₂**. Further optimization could be carried for improving the yields of those two ligands, either by optimizing purification conditions of

starting materials, or by modifying the reaction conditions for obtaining the corresponding starting materials and intermediates with a higher purity.

SANS data combined with FT-IR analyses showed the ability of **BTA-P(DTF)2**, **BTA-P(Xylyl)2** and **BTA-P(Tolyl)2** to co-assemble with **BTA Leu** into single rods of length > 200 Å whilst for **BTA-BPPH** both monomers co-assemble into aggregated rods. On contrary, only short stacks are detected for the mixture between **BTA-P(DTBM)2** and **BTA Leu**.

These newly designed BTA ligands were implemented in the copper-catalyzed hydrosilylation of 1-(4-nitrophenyl)ethenone in presence of very limited amount of **BTA Cha** as chiral co-monomer (0.5%). The BTA ligand structure had an important impact on the stereochemical outcome of this reaction. Significant selectivity was displayed (up to 90% *ee*) when **BTA-P(Xylyl)2** was employed in presence of BTA cyclohex in the catalytic mixture. This selectivity was significantly higher than that displayed by the reference ligand **BTA-pPPH2**, showcasing the importance of the substitution on the aryl groups attached to the P atom of the BTA ligands.

In **Chapter III**, a set of BTA ligands combined with **BTA Leu** as chiral co-monomer was evaluated in the asymmetric hydroamination of styrene and in the cascade hydrosilylation/hydroamination reaction of enone derivatives. Dramatic difference in catalytic rate, catalyst stability and product selectivity were observed for the hydroamination of styrene as function of the nature of the BTA ligand. A set of parameters (copper source, temperature) was examined to optimize the best catalytic system, notably with the aim of minimizing the side reactions related to the vinyl bond reduction and the vinyl bond oligo/polymerization. It was also noted that the silane reagent readily decomposed in presence of the phosphine-CuH catalyst and thus an excess of silane reagent is required to get convenient yields. The combination of **BTA-P(DTF)2**, Cu(II)-*i*-butyrate and **BTA Leu** provided the hydroamination product in 60% yield and 67% *ee*. Ethylbenzene was the only detected by-product (10%) under these conditions. Even though the yield of the reaction can probably be increased through further optimization, the enantioselectivity obtained for the hydroamination reaction appeared promising for implementation of the BTA helical catalysts in cascade reactions.

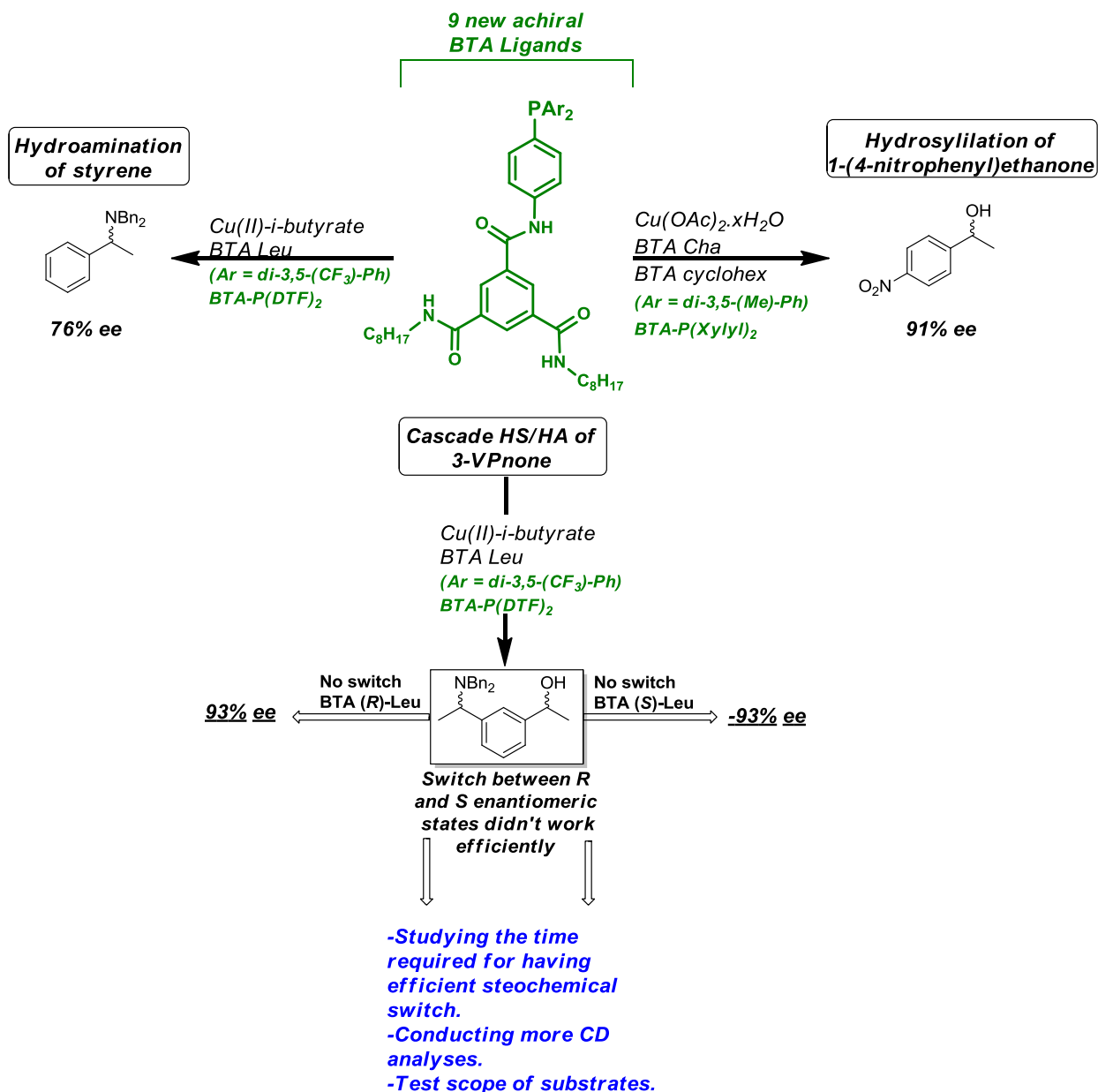
Different vinyl enone derivatives were screened for the cascade reaction. With α,β -enones, 1,4-reduction appeared to be very rapid with our BTA catalyst. As a result, the fully reduced

product was obtained, which prevented hydroamination to occur. With α,γ -enones, the corresponding alcohol was obtained in very low yield (6%).

In **Chapter IV**, the stereodivergent approach was implemented for the hydrosilylation/hydroamination cascade reaction of vinyl acetophenone derivatives. The hydrosilylation proceeds very efficiently with the BTA mixture composed of **BTA-P(DTF)2/BTA Leu** ($f_s=0.5$). Yields and enantioselectivities were moderate to good for **3-VPnone** and excellent for **4-MeVPnone** and **3-MeVPnone**. Investigation of the cascade reaction with these substrates indicates that hydroamination only proceeds for **3-VPnone**. Optimization of the cascade reaction identified Cu(II)-i-butyrate and MCH as the best metal precursor and solvent, respectively. Under these conditions, the amino alcohol product **3-APnol** is obtained with 85% yield, 93% *ee* and a dr of 2.8. This translates into *ee* value for both the hydrosilylation and hydroamination step of *ca.* 65%. With these optimal conditions for the non-switchable experiments, the two stereoisomers were obtained with convenient yields, excellent enantioselectivities, and moderate dr. CD analyses revealed that chirality amplification effects are enhanced to useful extent only when **BTA cyclohex** is added to helical co-assemblies of **BTA-P(DTF)2** and **BTA Leu**. Chirality amplification effects were stronger in toluene, homochiral helices were generated with a scalemic mixture of **BTA Leu** enantiomers biased to 30% *ee*, while in MCH 50% *ee* is required. Catalytic experiments performed with a scalemic mixture of **BTA Leu** (50% *ee*) provided the same stereoselectivity than the optimized catalytic system which corroborates that chirality amplification is operative in the helical catalysts. Catalytic mixtures embedding a lower fraction of **BTA Leu** ($f_s=0.2$) proceed efficiently in toluene but not in MCH.

Finally, selectivity-switching experiments were performed in a range of conditions: toluene or MCH as solvent, in presence or absence of **BTA cyclohex**, with **amine-DM** present from the beginning or added after the hydrosilylation step, and with different initial and ending compositions of the helical catalysts. Unfortunately, all tested selectivity-switching experiments failed to produce the expected stereoisomer with a decent stereoselectivity. Actually, the switch was always partial, *i.e.* that a mixture was obtained which contains the desired stereoisomer as well as the one formed in absence of stereochemical switch. In most cases, this

was attributed to the fact that the stereochemical switch and the hydroamination reaction occurs concomitantly. Further investigation will be needed to improve this stereochemical switch by finding better operating conditions. For this purpose, CD analysis must be helpful notably to determine the time required to have complete inversion of the handedness of the helical catalyst.



In conclusion, the synthesis of a new set of BTA ligands and its implementation in two different catalytic reactions allowed us to understand more precisely the mode of action of

supramolecular helical BTA catalysts. In addition, a huge progress has been achieved by demonstrating the ability of optimized BTA helical co-assemblies composed of a BTA ligand and an enantiopure co-monomer to promote hydroamination reaction and a catalytic hydrosilylation/hydroamination cascade reaction in presence of copper precursors. The corresponding products were obtained with convenient yields and enantioselectivities. Several steps towards the implementation of one-pot stereodivergent catalyst have also been made. Further investigations are necessary to improve the catalytic switch ability of the helical BTA catalysts and extend the scope of substrates amenable to the cascade reaction.

Resumé.

Un procédé stéréodivergent est le procédé qui permet d'accéder à n'importe quel stéréoisomère donné d'un produit avec plusieurs stéréocentres provenant du même ensemble de matières de départ. Cependant, la catalyse stéréodivergente en un seul pot au moyen d'un seul catalyseur n'a pas été réalisée malgré l'intérêt fondamental et les avantages pratiques d'une telle approche. Un système catalytique particulièrement intéressant dans ce contexte est celui récemment développé à partir d'assemblages hélicoïdaux BTA. Les catalyseurs supramoléculaires BTA hélicoïdaux sont constitués de plusieurs monomères complémentaires reliés entre eux par des liaisons hydrogène et des interactions aromatiques. Le ligand BTA et le monomère BTA énantiopur co-assemblent in situ pour produire un ligand hélicoïdal à une seule main et des niveaux élevés d'énantiosélectivité ont été obtenus dans des réactions d'hydrogénation catalysée au rhodium et d'hydrosilylation catalysée par le cuivre. La nature dynamique de ces assemblages supramoléculaires a également été exploitée pour concevoir un catalyseur asymétrique dynamique capable de changer sa sélectivité en temps réel en ajoutant un excès d'un comonomère chiral (Figure 0-1). Grâce aux propriétés d'amplification de chiralité présentes dans ce système, la configuration des sites catalytiques est presque totalement inversée bien que les assemblages soient composés d'un mélange de comonomères énantiopurs. L'application de ce système initial à la transformation d'un mélange 1:1 de deux substrats sert de preuve de principe pour le développement d'un catalyseur véritablement stéréodivergent. L'objectif de cette thèse est donc de développer une approche stéréodivergente en exploitant l'amplification de chiralité et les propriétés dynamiques des catalyseurs BTA hélicoïdaux commutables. Il a été montré qu'en présence de réactif silane, les catalyseurs au cuivre à base de BTA sont capables de générer des espèces d'hydrure de cuivre, capables de catalyser des réactions d'hydrosilylation. Deux réactions consécutives sont visées : l'hydrosilylation suivie de l'hydroamination. Les deux réactions nécessitent des espèces d'hydrure de cuivre pour se dérouler. Une réaction d'hydrosilylation / hydroamination en cascade sera ainsi mise en œuvre afin d'accéder à tous les stéréoisomères possibles d'un amino-alcool. Surtout, tous les stéréoisomères devraient être obtenus d'une manière unique qui n'a aucun précédent dans la littérature (Figure 0-2).

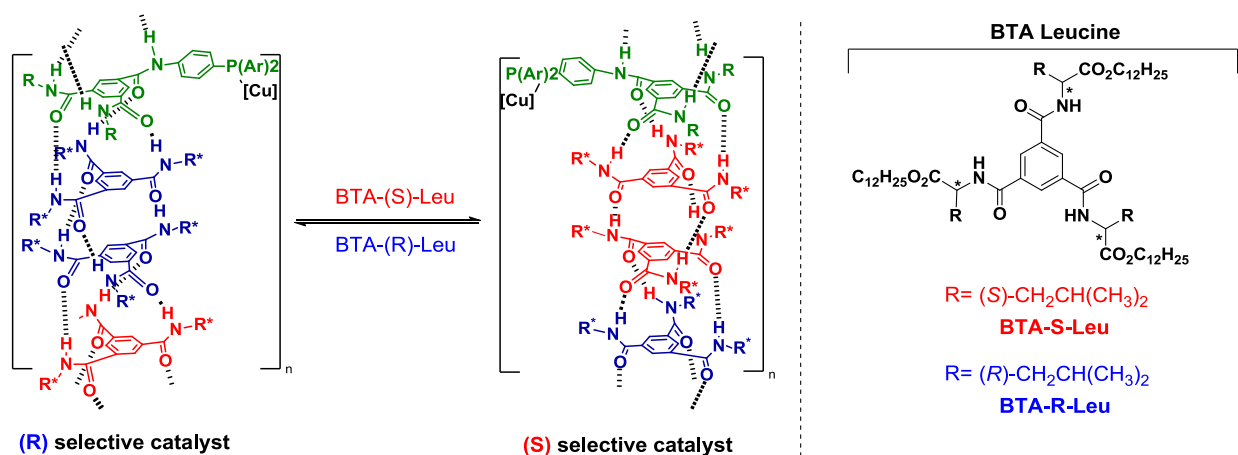


Figure 0-1 Contrôle en temps réel de l'énantiosélectivité affichée par le catalyseur hélicoïdal supramoléculaire.

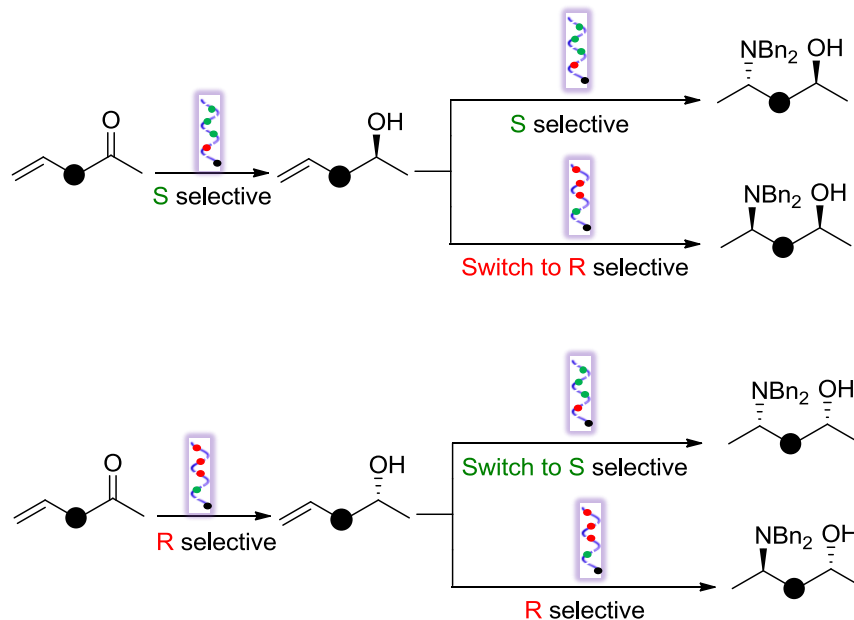
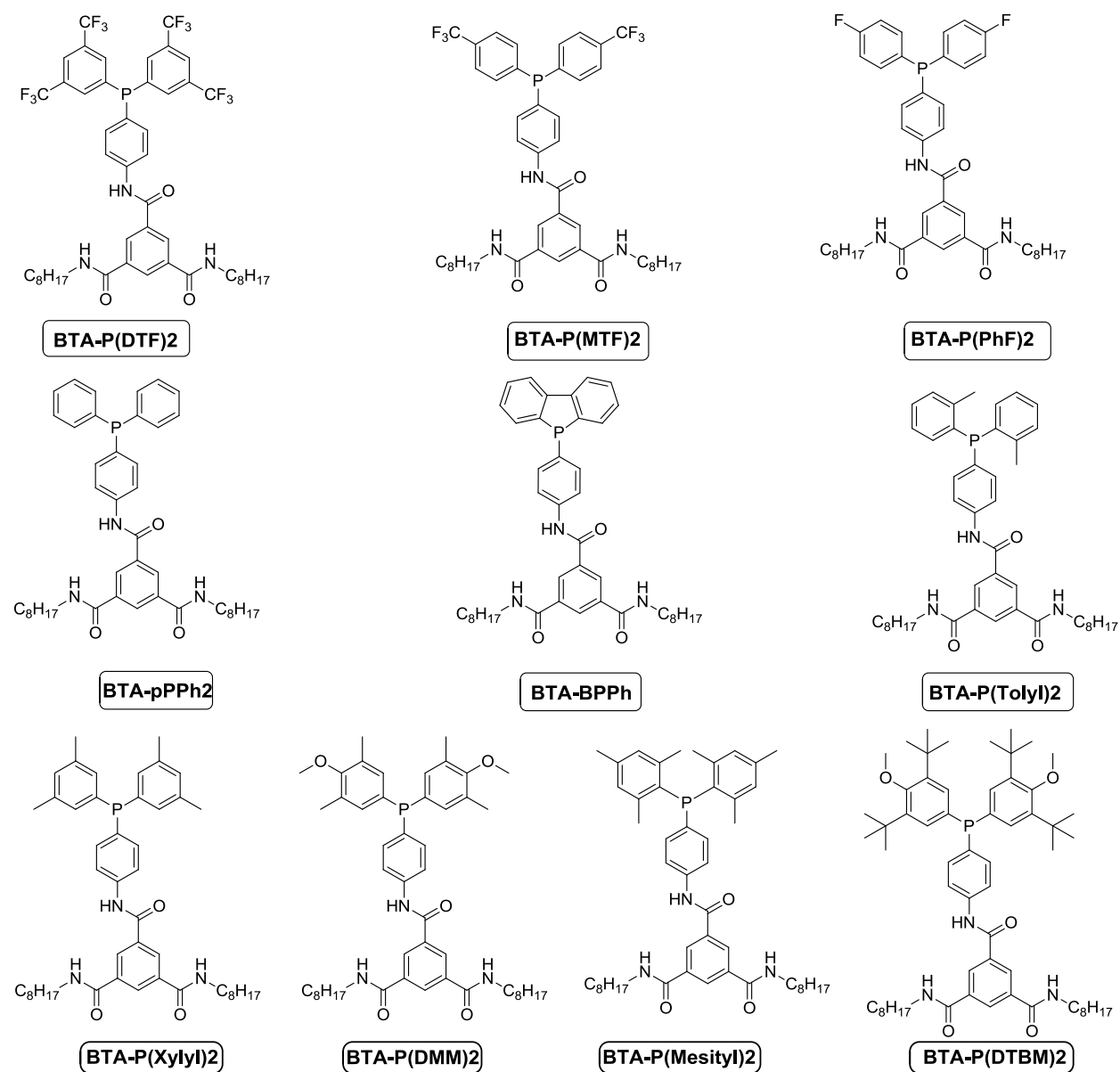


Figure 0-2 L'hydrure de cuivre en cascade a catalysé l'hydroxylation et l'hydroamination d'énones facilement disponibles.

Dans le **chapitre II**, la synthèse de neuf nouveaux ligands BTA contenant de la phosphine sera divulguée (Scheme 0-1) qui diffèrent du ligand BTA précédemment utilisé, **BTA-pPPP2** par la nature des substituants présents sur les groupes aryle attachés à l'atome de phosphore. Ces neuf ligands présentent des propriétés électroniques et stériques différentes. La conception de ces ligands BTA prend également en considération les interactions possibles de substrat ligand qui pourraient survenir dans l'état de transition de la réaction d'hydroamination catalysée par

le cuivre. En conséquence, des groupes donneurs et attracteurs d'électrons ont été introduits aux positions 3 et 5 du groupe aryle.



Scheme 0-1 Structure chimique des ligands BTA contenant de la phosphine nouvellement conçus.

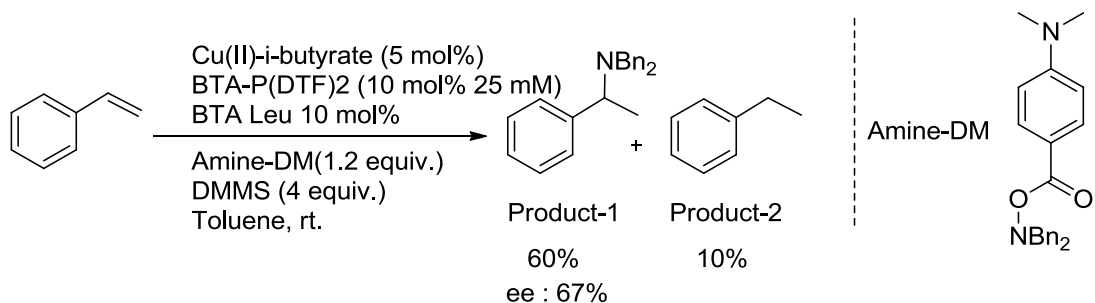
Ces neuf ligands BTA ont été synthétisés selon une procédure de synthèse similaire en trois étapes, et obtenus sur des centaines de mg ou une échelle de gramme avec une pureté élevée à l'exception du **BTA-P (DMM)2** et du **BTA-P (Mesityl)2**. Une optimisation supplémentaire pourrait être réalisée pour améliorer les rendements de ces deux ligands, soit en optimisant les

conditions de purification des matières de départ, soit en modifiant les conditions de réaction pour obtenir les matières de départ correspondantes et les intermédiaires avec une pureté plus élevée.

Les données SANS combinées aux analyses FT-IR ont montré la capacité de **BTA-P (DTF)2**, **BTA-P (Xylyl)2** et **BTA-P (Tolyl)2** à co-assembler avec **BTA Leu** en bâtonnets uniques de longueur > 200 Å tandis que pour le **BTA-BPPh**, les deux monomères se co-assemblent en tiges agrégées. Au contraire, seuls de courts empilements sont détectés pour le mélange entre **BTA-P(DTBM)2** et **BTA Leu**.

Ces ligands BTA nouvellement conçus ont été mis en œuvre dans l'hydrosilylation catalysée par le cuivre de la 1-(4-nitrophényl)éthénone en présence d'une quantité très limitée de **BTA Cha** comme co-monomère chiral (0,5%). La structure du ligand BTA a un impact important sur le résultat stéréochimique de cette réaction. Une sélectivité significative a été affichée (jusqu'à 90% ee) lorsque **BTA-P(Xylyl)2** a été utilisé lorsqu'un additif achiral est présent dans le mélange catalytique. Cette sélectivité est significativement supérieure à celle affichée par le ligand de référence, **BTA-pPPH2** mettant en évidence l'importance de la substitution sur les groupements aryles attachés à l'atome P des ligands BTA.

Dans le **chapitre III**, un ensemble de ligands BTA combinés avec **BTA Leu** en tant que comonomère chiral a été évalué dans l'hydroamination asymétrique du styrène et dans la réaction d'hydrosilylation / hydroamination en cascade de dérivés d'énone. Une différence dramatique de vitesse catalytique, de stabilité du catalyseur et de sélectivité du produit a été observée pour l'hydroamination du styrène en fonction de la nature du ligand BTA. Un ensemble de paramètres (source de cuivre, température) a été examiné pour optimiser le meilleur système catalytique, notamment dans le but de minimiser les réactions secondaires liées à la réduction de la liaison vinyle et à l'oligo / polymérisation de la liaison vinyle. Il a également été noté que le réactif silane se décomposait facilement en présence du catalyseur phosphine-CuH et qu'un excès de réactif silane est donc nécessaire pour obtenir des rendements convenables. La combinaison de **BTA-P(DTF)2**, de Cu(II)-i-butyrate et de **BTA Leu** fournit le produit d'hydroamination avec un rendement de 60% et 67% ee (Scheme 0-2). L'éthylbenzène était le seul sous-produit détecté (10%) dans ces conditions.



Scheme 0-2 Reaction conditions: Styrene (0.15 mmol), Cu(II)-i-butyrate (5 mol%), **BTA-P(DTF)2** (10 mol%), BTA Leu (10 mol%), DMMS (4.0 eq), amine-DM (1.2 eq), toluene- d_8 (600 mL).

Même si le rendement de la réaction peut probablement être augmenté grâce à une optimisation supplémentaire, l'énantiosélectivité obtenue pour la réaction d'hydroamination apparaît prometteuse pour la mise en œuvre des catalyseurs hélicoïdaux BTA dans des réactions en cascade. Différents substrats ont ainsi été criblés pour la réaction en cascade (Figure 0-3).

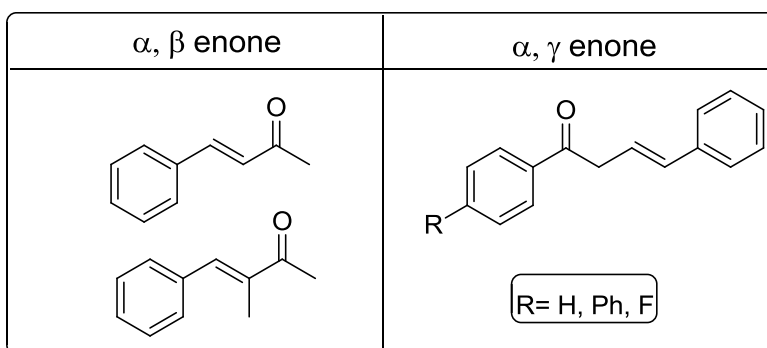
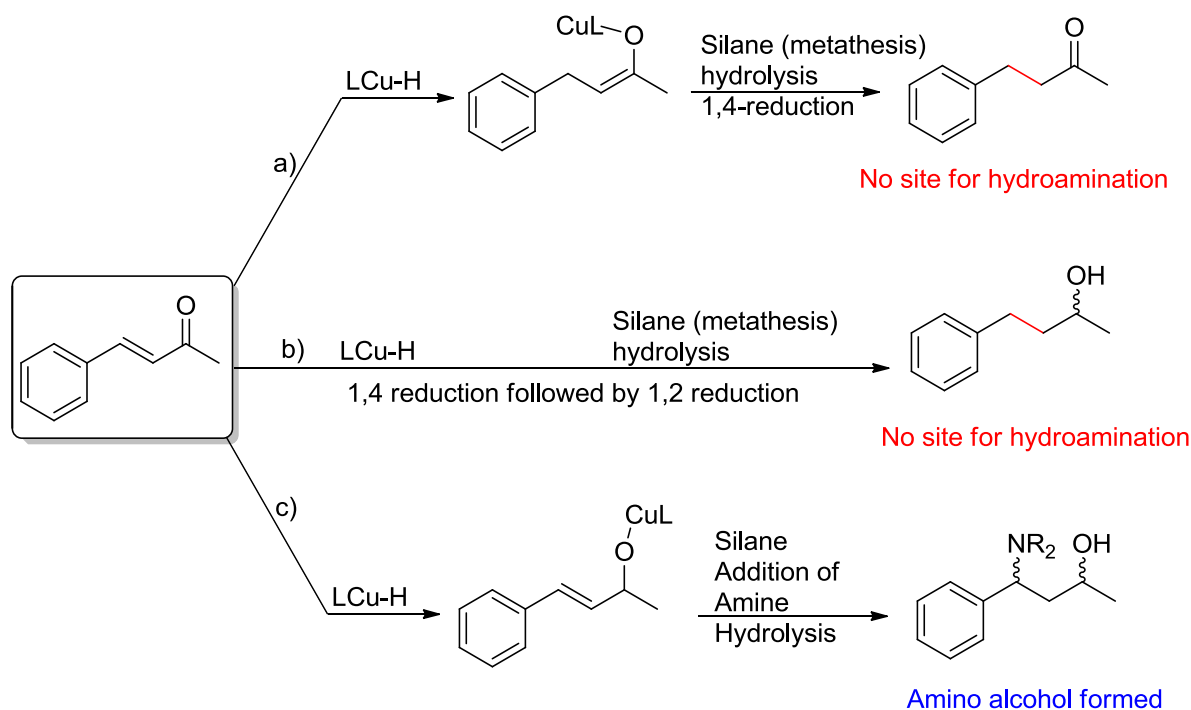


Figure 0-3 Substrats tamisés pour la réaction en cascade.

Avec les α , β -étones, la 1,4-réduction semble être très rapide avec notre catalyseur BTA. En conséquence, le produit entièrement réduit a été obtenu, ce qui a empêché l'hydroamination de se produire (Scheme 0-3). Avec les α , γ -étones, l'alcool correspondant a été obtenu avec un très faible rendement (6%).



Scheme 0-3 Une illustration de différentes voies pourrait être rencontrée pour la α,β -énone en présence d'espèces d'hydrure de cuivre. a) la 1,4-réduction est préférée à la 1,2-réduction, conduisant à la réduction de la fraction vinyle. b) Les réductions 1,4 et 1,2 se sont déroulées sur la même échelle de temps. c) La voie souhaitée pour laquelle la 1,2-réduction exclusive est suivie par l'hydroamination du vinyle.

Au **chapitre IV**, l'approche stéréodivergente a été mise en œuvre pour la réaction en cascade d'hydrosilylation / hydroamination de dérivés de vinylacétophénone (Figure 0-4). Il a été montré que l'insertion d'un groupe méthyle sur le fragment vinyle empêche la réaction d'hydroamination. Les meilleurs résultats pour le processus en cascade ont été obtenus avec la 3-VPnone, en utilisant un système catalytique composé de **BTA-P(DTF)₂**, Cu(II)-i-butyrate et **BTA Leu** dans du méthylcyclohexane (MCH).

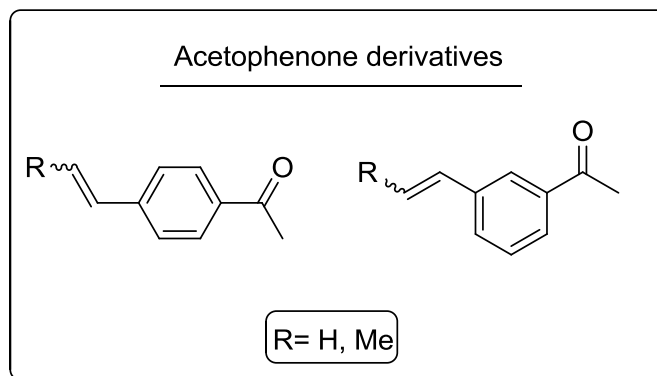
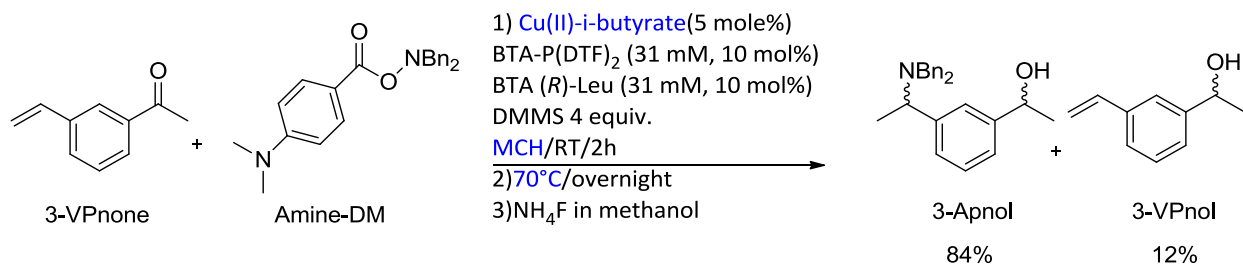


Figure 0-4 Substrats de vinyl acétophénone testés dans la réaction de cascade d'hydrosilylation / hydroamination.

L'hydrosilylation s'est déroulée à TA, et la conversion totale a été détectée après 15 minutes. L'hydroamination s'est déroulée en présence d'amine-DM à une température élevée jusqu'à 70 ° C. Le démarrage du processus catalytique avec du **BTA (R)-Leu** énantio pur fournit 70% de (-, +) comme stéréoisomère principal (Figure 0-5). Ce stéréoisomère majeur a été obtenu avec ee_{tot} = 93% et dr. : 2.74. La première étape HS s'est déroulée avec ee₁ = -70% et la deuxième étape HA avec ee₂ = -67% (Figure 0-5). Le rendement total de **3-APnol** a été considérablement amélioré pour atteindre 84%, et il ne restait que 12% de **3-VPnol** (Scheme 0-4). Une température de réaction plus élevée était nécessaire (70°C) pour initier complètement la réaction d'hydroamination avec un système à base de Cu(II)-i-butyrate. Ces conditions sont considérées comme optimales pour améliorer le rendement final de la réaction en cascade, et pourraient être utilisées pour obtenir tous les stéréoisomères possibles du **3-APnol**.



Scheme 0-4 Conditions **3-VPnone** (0,5 mmole, 1 eq), Cu(II)-i-butyrate (5 mol%), BTA-P(DTF) 2 (10 mol%), BTA (R)-Leu (10 mol%), DMMS (4,0 eq), amine-DM (1,3 eq), MCH (500 µL).

Ceci représente les conditions optimales pour les expériences non commutables puisque les deux stéréoisomères sont obtenus avec des rendements convenables, d'excellentes énantiosélectivités et un dr modéré.

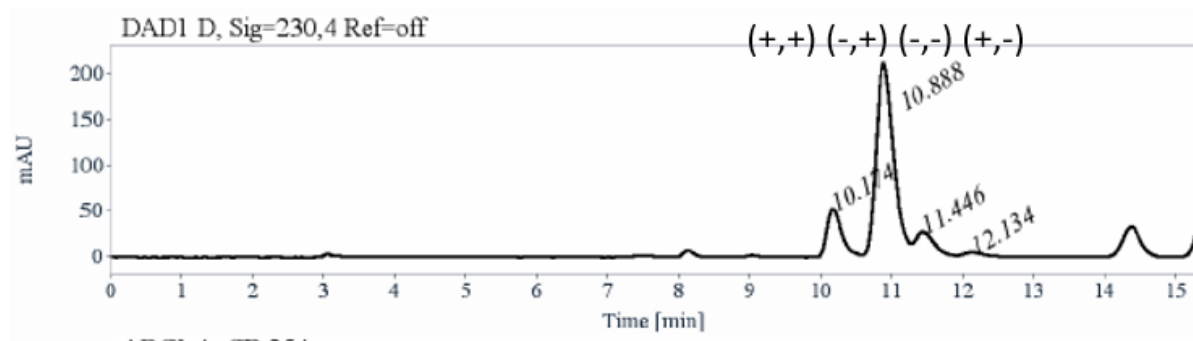


Figure 0-5 Traces HPLC de 3-APnol obtenues à partir du processus en cascade avec énantio pur BTA (R)-Leu.

Les analyses de CD (Figure 0-6) ont révélé que les effets d'amplification de la chiralité sont présents dans ce système uniquement si le **BTA cyclohex** (voir la Figure 0-7) est ajouté. Les effets d'amplification de la chiralité étaient plus forts dans le toluène, des hélices homochirales ont été générées avec un mélange scalemique d'énantiomères **BTA Leu** biaisé à 30% *ee*, tandis que dans MCH 50% *ee* est nécessaire.

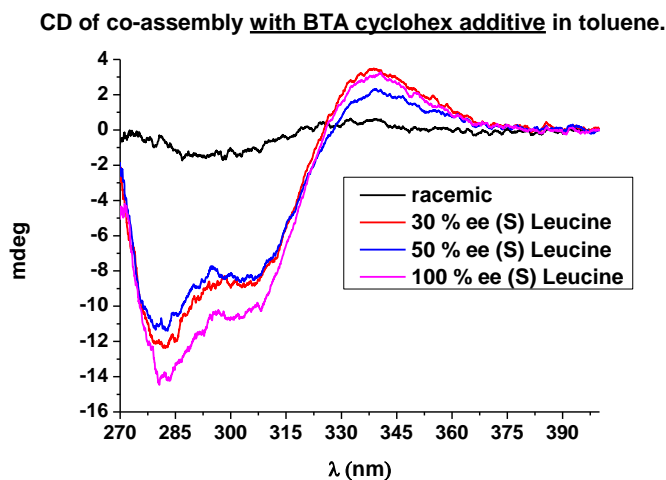


Figure 0-6 Spectre des expériences de type règles de majorité diluées pour deux systèmes: BTA-P (DTF)2 [31 mM], BTA cyclohex [31 mM], Cu(II)-i-butyrate [15,6 mM] et BTA Leu [31 mM] avec des *ee* dans le toluène

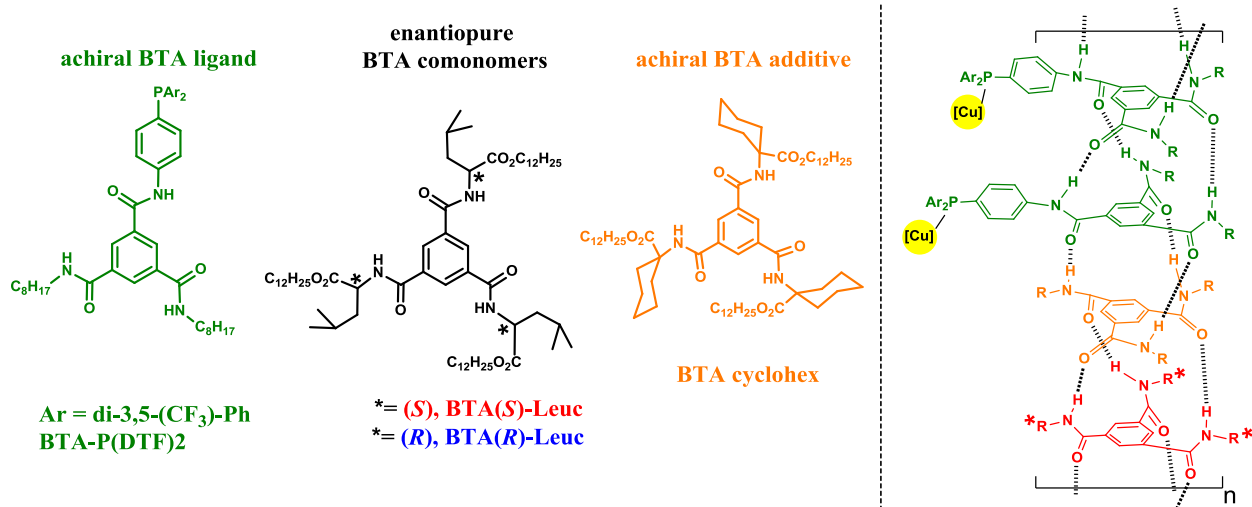


Figure 0-7 Représentation schématique du co-assemblage hélicoïdal formé en présence de l'additif achiral BTA cyclohex.

Lorsqu'il est appliqué à la catalyse, le mélange de type S & S avec seulement 20% de **BTA (S)-Leu** (Figure 0-8) et le mélange de type MR dilué avec **BTA Leu** à 50% *ee* en présence de BTA cyclohex présentent la même énantiosélectivité que celle affichée par le système initial composé d'une fraction plus élevée de monomères énantio-purs de **BTA Leu**.

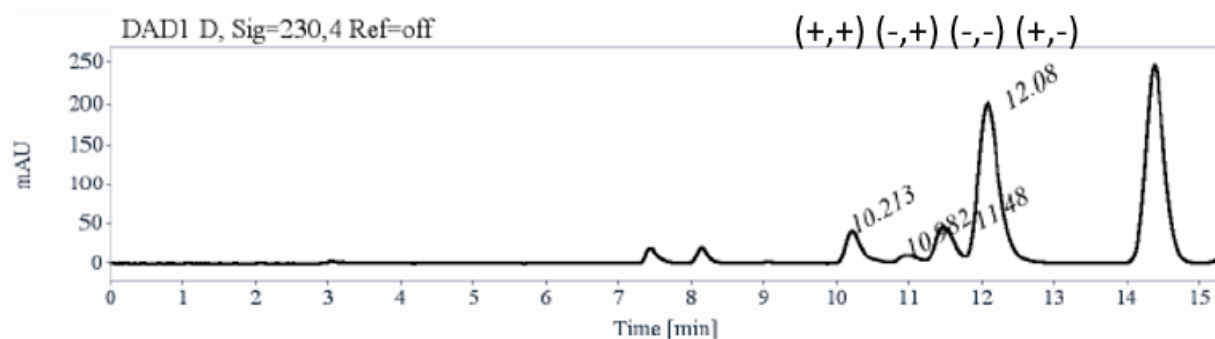


Figure 0-8 Les traces HPLC de 3-APnol obtenues à partir du processus en cascade avec le mélange de type S&S avec seulement 20% de BTA (S)-Leu en présence de BTA cyclohex présentent la même énantiosélectivité que celle affichée par le système initial composé d'une fraction plus élevée de BTA énantio-pur Monomères Leu.

C'est un résultat très encourageant car il indique que l'amplification de chiralité est opérationnelle dans ces catalyseurs hélicoïdaux. Enfin, des expériences de commutation de sélectivité ont été réalisées dans une gamme de conditions : toluène ou MCH comme solvant, en présence ou en l'absence de **BTA cyclohex**, avec amine-DM présente dès le début ou ajoutée

après l'étape d'hydrosilylation, et avec différentes compositions initiale et finale des catalyseurs hélicoïdaux. Malheureusement, le commutateur catalytique stéréochimique s'est avéré être partiel dans toutes ces conditions, c'est-à-dire que soit le stéréoisomère principal était le même que pour l'expérience non commutée, soit le stéréoisomère attendu a été obtenu avec une très faible sélectivité. Dans la plupart des cas, cela a été attribué au fait que l'interrupteur stéréochimique et la réaction d'hydroamination se produisent de manière concomitante. Des recherches supplémentaires seront nécessaires pour améliorer ce commutateur stéréochimique en trouvant de meilleures conditions de fonctionnement. A cet effet, l'analyse CD doit être utile notamment pour déterminer le temps nécessaire pour avoir une inversion complète de la propriété du catalyseur hélicoïdal.

En conclusion, la synthèse d'un nouvel ensemble de ligands BTA et sa mise en œuvre dans deux réactions catalytiques différentes nous ont permis de comprendre plus précisément le mode d'action des catalyseurs BTA hélicoïdaux supramoléculaires. De plus, un énorme progrès a été réalisé en démontrant la capacité de co-assemblages hélicoïdaux BTA optimisés composés d'un ligand BTA et d'un comonomère énantio-pur à favoriser une réaction d'hydroamination et une réaction en cascade catalytique d'hydrosilylation / hydroamination en présence de précurseurs de cuivre. Les produits correspondants ont été obtenus avec des rendements et des énantiosélectivités convenables. Plusieurs étapes vers la mise en œuvre d'un catalyseur stéréodivergent à un pot ont également été réalisées. Des recherches supplémentaires sont nécessaires pour améliorer la capacité de commutation catalytique des catalyseurs BTA hélicoïdaux et étendre la portée de la réaction en cascade.

Synthèse stéréodivergente au moyen de catalyseurs supramoléculaires amplifiés chiralement.

Résumé:

La catalyse supramoléculaire a émergé avec un tas de caractéristiques très intéressantes et attrayantes telles que la modularité, la réversibilité, la recyclabilité et les propriétés de réponse aux stimuli. Ces caractéristiques sont considérées comme des outils importants pour le développement de méthodes de synthèse efficaces et fiables, notamment dans le domaine de l'industrie pharmaceutique pour laquelle la configuration des médicaments dicte leur efficacité. Notamment, les voies de synthèse stéréo-divergentes sont vitales pour obtenir tous les stéréoisomères possibles d'un candidat médicament. Cependant, la catalyse stéréodivergente à un seul pot utilisant un seul catalyseur n'a pas été obtenue malgré l'intérêt fondamental et les avantages pratiques d'une telle approche. L'objectif de cette thèse est donc de développer une approche stéréodivergente en exploitant l'amplification de la chiralité et les propriétés dynamiques des catalyseurs BTA supramoléculaires hélicoïdaux commutables. Une réaction d'hydrosilylation / hydroamination en cascade sera ainsi mise en œuvre afin d'accéder à tous les stéréoisomères possibles d'un amino-alcool.

Mots clés: Polymères supramoléculaires, liaison hydrogène, BTA, catalyse homogène, catalyse supramoléculaire, catalyseur commutable, induction de chiralité, amplification de chiralité, cascade, hydrosilylation, hydroamination.

Stereodivergent synthesis by means of chirally-amplified supramolecular catalysts.

Abstract :

Supramolecular catalysis has emerged with a bunch of highly interesting and attractive features such as modularity, reversibility, recyclability, and stimuli-responsive properties. These features are considered as important tools for the development of efficient and reliable synthetic methods, especially in the domain of pharmaceutical industry for which the configuration of drugs dictates their efficiency. Notably, stereo-divergent synthetic routes are vital to obtain all possible stereoisomers of a drug candidate. However, one-pot stereodivergent catalysis using a single catalyst has not been achieved despite the fundamental interest and practical advantages of such an approach. The objective of this thesis is therefore to develop a stereodivergent approach by exploiting the amplification of chirality and the dynamic properties of switchable helical supramolecular BTA catalysts. A cascade hydrosilylation / hydroamination reaction will thus be implemented in order to access all the possible stereoisomers of an amino alcohol.

Keywords: Supramolecular polymers, hydrogen-bond, BTA, homogenous catalysis, supramolecular catalysis, switchable catalyst, chirality induction, chirality amplification, cascade, hydrosilylation, hydroamination.